# FILAMENTOUS BACTERIOPHAGE IN BIO/NANO/TECHNOLOGY, BACTERIAL PATHOGENESIS AND ECOLOGY

EDITED BY: Jasna Rakonjac, Bhabatosh Das and Ratmir Derda
PUBLISHED IN: Frontiers in Microbiology

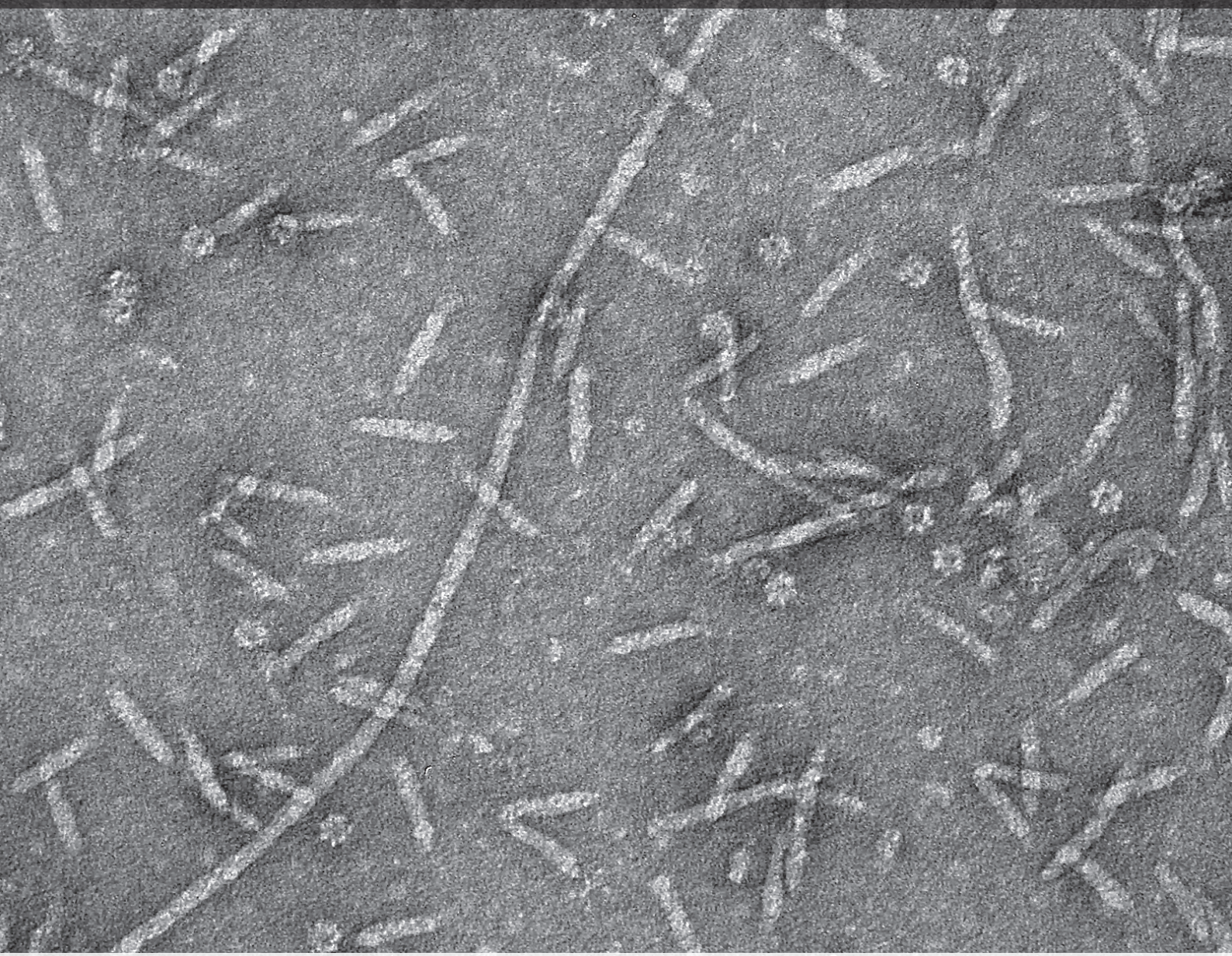

frontiers Research Topics

# frontiers



**ISSN 1664-8714**
**ISBN 978-2-88945-095-4**
**DOI 10.3389/978-2-88945-095-4**

## About Frontiers

Frontiers is more than just an open-access publisher of scholarly articles: it is a pioneering approach to the world of academia, radically improving the way scholarly research is managed. The grand vision of Frontiers is a world where all people have an equal opportunity to seek, share and generate knowledge. Frontiers provides immediate and permanent online open access to all its publications, but this alone is not enough to realize our grand goals.

## Frontiers Journal Series

The Frontiers Journal Series is a multi-tier and interdisciplinary set of open-access, online journals, promising a paradigm shift from the current review, selection and dissemination processes in academic publishing. All Frontiers journals are driven by researchers for researchers; therefore, they constitute a service to the scholarly community. At the same time, the Frontiers Journal Series operates on a revolutionary invention, the tiered publishing system, initially addressing specific communities of scholars, and gradually climbing up to broader public understanding, thus serving the interests of the lay society, too.

## Dedication to Quality

Each Frontiers article is a landmark of the highest quality, thanks to genuinely collaborative interactions between authors and review editors, who include some of the world's best academicians. Research must be certified by peers before entering a stream of knowledge that may eventually reach the public - and shape society; therefore, Frontiers only applies the most rigorous and unbiased reviews.
Frontiers revolutionizes research publishing by freely delivering the most outstanding research, evaluated with no bias from both the academic and social point of view.
By applying the most advanced information technologies, Frontiers is catapulting scholarly publishing into a new generation.

## What are Frontiers Research Topics?

Frontiers Research Topics are very popular trademarks of the Frontiers Journals Series: they are collections of at least ten articles, all centered on a particular subject. With their unique mix of varied contributions from Original Research to Review Articles, Frontiers Research Topics unify the most influential researchers, the latest key findings and historical advances in a hot research area! Find out more on how to host your own Frontiers Research Topic or contribute to one as an author by contacting the Frontiers Editorial Office: **researchtopics@frontiersin.org**

# FILAMENTOUS BACTERIOPHAGE IN BIO/NANO/TECHNOLOGY, BACTERIAL PATHOGENESIS AND ECOLOGY

Topic Editors:
**Jasna Rakonjac,** Massey University, New Zealand
**Bhabatosh Das,** NCR Biotech Science Cluster, India
**Ratmir Derda,** University of Alberta, Canada

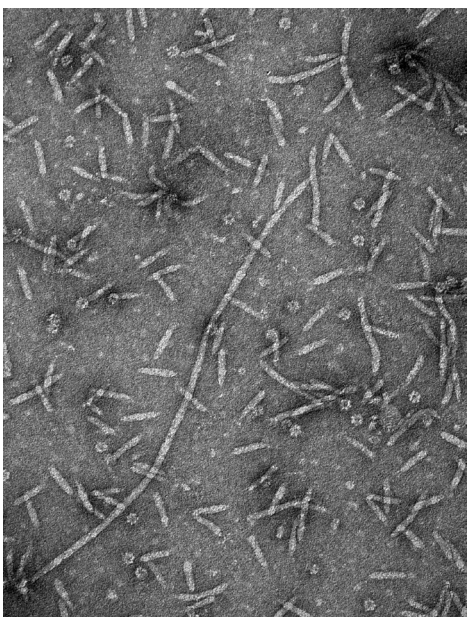

Transmission Electron Microscopy (TEM) image of a full-length filamentous phage f1 surrounded by short f1-derived nanorods displaying fibronectin-binding domain of the Sof protein from *Streptococcus pyogenes*. The rosette-like shapes with a 7-fold symmetry correspond to the GroEL chaperonin. The sample was prepared by Sadia Sattar and the micrograph was produced by Doug Hopcroft at the Manawatu Microscopy and Imaging Centre, Institute of Fundamental Sciences, Massey University, Palmerston North, New Zealand.

Filamentous phage (genus Inovirus) infect almost invariably Gram-negative bacteria. They are distinguished from all other bacteriophage not only by morphology, but also by the mode of their assembly, a secretion-like process that does not kill the host. "Classic" *Escherichia coli* filamentous phage Ff (f1, fd and M13) are used in display technology and bio/nano/technology, whereas filamentous phage in general have been put to use by their bacterial hosts for adaptation to environment, pathogenesis, biofilm formation, horizontal gene transfer and modulating genome stability.

Many filamentous phage have a "symbiotic" life style that is often manifested by inability to form plaques, preventing their identification by standard phage-hunting techniques; while the absence or very low sequence conservation between phage infecting different species often complicates their identification through bioinformatics. Nevertheless, the number of discovered filamentous phage is increasing rapidly, along with realization of their significance. "Temperate" filamentous phage whose genomes are integrated into the bacterial chromosome of pathogenic bacteria often modulate virulence of the host. The *Vibrio cholerae* phage CTXφ genome encodes cholera toxin, whereas many filamentous prophage influence virulence without encoding virulence factors. The nature of their effect on the bacterial pathogenicity and overall physiology is the next frontier in understanding intricate relationship between the filamentous phage and their hosts.

Phage display has been widely used as a combinatorial technology of choice for discovery of therapeutic antibodies and peptide leads that have been applied in the vaccine design, diagnostics and drug development or targeting over the past thirty years. Virion proteins of filamentous phage are integral membrane proteins prior to assembly; hence they are ideal for display of bacterial surface and secreted proteins. The use of this technology at the scale of microbial community has potential to identify host-interacting proteins of uncultivable or low-represented community members.

Recent applications of Ff filamentous phage extend into protein evolution, synthetic biology and nanotechnology. In many applications, phage serves as a monodisperse long-aspect nano-scaffold of well-defined shape. Chemical or chenetic modifications of this scaffold are used to introduce the necessary functionalities, such as fluorescent labels, ligands that target specific proteins, or peptides that promote formation of inorganic or organic nanostructures. We anticipate that the future holds development of new strategies for particle assembly, site-specific multi-functional modifications and improvement of existing modification strategies. These improvements will render the production of filamentous-phage-templated materials safe and affordable, allowing their applications outside of the laboratory.

**Citation:** Rakonjac, J., Das, B., Derda, R., eds. (2017). Filamentous Bacteriophage in Bio/Nano/Technology, Bacterial Pathogenesis and Ecology. Lausanne: Frontiers Media.
doi: 10.3389/978-2-88945-095-4

# Table of Contents

frontiers in Microbiology

EDITORIAL
published: 23 December 2016
doi: 10.3389/fmicb.2016.02109

# Editorial: Filamentous Bacteriophage in Bio/Nano/Technology, Bacterial Pathogenesis and Ecology

*Jasna Rakonjac*[1,2]*, *Bhabatosh Das*[3] *and Ratmir Derda*[4]

[1] Institute of Fundamental Sciences, Massey University, Palmerston North, New Zealand, [2] Maurice Wilkins Centre for Molecular Biodiscovery, The University of Auckland, Auckland, New Zealand, [3] Molecular Genetics Laboratory, Centre for Human Microbial Ecology, Translational Health Science and Technology Institute, NCR Biotech Science Cluster, Faridabad, India, [4] Department of Chemistry and Alberta Glycomics Centre, University of Alberta, Edmonton, Canada

**Keywords: filamentous bacteriophage, phage display, bionanotechnology, phage therapy, bacterial pathogenesis, biological nanorods, microbial communities, biofilms**

**Editorial on the Research Topic**

**Filamentous Bacteriophage in Bio/Nano/Technology, Bacterial Pathogenesis and Ecology**

## INTRODUCTION

Filamentous bacteriophage predominantly infect Gram-negative bacteria and make an important contribution to host physiology, ecology, and virulence, including production of deadly toxins, such as cholera toxin. The unique filamentous structure, small genome size (4–12 kbp), replicative and/or integrative mode of inheritance, simple cultivation, and easy genomic manipulation sparked considerable attention to this class of bacteriophage for a number of applications, including cloning, sequencing, recombinant protein expression, phage display technology, and nanotechnology. This book covers a range of topics that can be grouped into two themes: impact of diverse filamentous phage on their host bacteria (five chapters) and applications of *Escherichia coli* Ff phage (eight chapters).

## IMPACT OF DIVERSE FILAMENTOUS PHAGE ON THE HOST BACTERIA

Five articles explore diverse filamentous bacteriophage, including identification, replication, integration into the host chromosome, and effect on their bacterial host properties, such as growth rate, biofilm dynamics, and virulence.

Nagayoshi et al. describe the first fully sequenced hyperthermophilic filamentous phage, ΦOH3, discovered in geothermal water. This phage infects the thermophilic bacterium *Thermus thermophilus* HB8. Ahmad et al. identify and describe a novel filamentous phage isolated from soil. The phage, named XacF1, causes loss of virulence in *Xanthomonas axonopodis pv*. citri, the causative agent of citrus canker, and could potentially be used for treatment or prevention of this disease.

Both XacF1 and ΦOH3 replicate efficiently and form turbid plaques due to increase of the host generation time, but do not kill the host. Lack of the host killing is intrinsic to the secretion-like process of filamentous phage assembly and release, while the superinfection is prevented due to the blocking of primary and secondary host receptors by the production of phage-encoded receptor-binding protein pIII in the infected cells. One exception to these universally accepted rules

OPEN ACCESS

***Edited by:***
*Akio Adachi,*
*Tokushima University, Japan*

***Reviewed by:***
*Kevin A. Henry,*
*National Research Council (NRC), Canada*

***Correspondence:**
*Jasna Rakonjac*
*j.rakonjac@massey.ac.nz*

***Specialty section:***
*This article was submitted to Virology, a section of the journal Frontiers in Microbiology*

***Received:*** *03 November 2016*
***Accepted:*** *13 December 2016*
***Published:*** *23 December 2016*

***Citation:***
*Rakonjac J, Das B and Derda R (2016) Editorial: Filamentous Bacteriophage in Bio/Nano/Technology, Bacterial Pathogenesis and Ecology. Front. Microbiol. 7:2109. doi: 10.3389/fmicb.2016.02109*

is prophage Pf4 of *Pseudomonas aeruginosa* PAO1. This phage converts into a "superinfective" form within the mature *P. aeruginosa* biofilms, infecting and killing the surrounding prophage-containing cells. Here, Hui et al. identify a role of reactive oxygen or nitrogen species DNA-damaging activities in the formation of superinfective phage, providing a link to the observed high-frequency mutations in the gene encoding repressor of Pf4 phage replication in the mature *P. aeruginosa* biofilms.

In contrast to the phage described above, filamentous phage YpfΦ of the plague bacillus *Yersinia pestis* replicates poorly, yet allows better colonization of the mammalian host in comparison to the phage-free strain. Derbise and Carniel review the intertwined microevolution of *Y. pestis* and YpfΦ over the past 3000 years. Some peculiarities of this phage include its broad host spectrum, elusive host receptor(s), and hard-to-reconcile pattern of seemingly exclusively episomal or integrated states in closely related *Y. pestis* strains.

Most lysogenic filamentous phage rely on a host-encoded XerCD recombinase for integration into highly conserved *dif* sites of bacterial chromosomes; however the mechanisms of integration and prophage biology vary widely. Das reviews the integration mechanisms of three lysogenic filamentous vibriophage (CTXΦ, VGJΦ, and TLCΦ) into the *Vibrio cholerae* chromosomes. Variation in DNA sequences of *attP* sites in the phage genomes drives differences in the integration and excision mechanisms, which ultimately impact on the lysogen activation, prophage replication, and efficiency of phage production. This review therefore outlines how the *attP* sites in a filamentous phage can be used to predict integration/replication modes of filamentous prophage and conversely, how the engineered *attP* sites can be used to design novel types of chromosomally-integrated bacterial expression vectors.

## APPLICATIONS OF THE FF FILAMENTOUS PHAGE

Eight chapters in this book review or report recent applications and technological innovations involving Ff phage of *E. coli*, or derived particles. Phage display is the most prominent application of filamentous phage. It was developed on the shoulders of versatile cloning vectors derived from the *E. coli* Ff (F-pilus specific) filamentous phage (f1, fd, and M13), and knowledge about their life cycle. Combinatorial technologies including Ff phage display are based on a physical link of coding sequence to encoded protein displayed on the virus particle. Screening vast Ff display libraries for variants that bind a "bait" of interest has resulted over the past 25 years in identification of bioactive peptides or therapeutic recombinant antibodies. Two chapters, by Gagic et al. and Henry et al., review, respectively, phage display applications for discovery of microbial surface proteins (including vaccine targets) and non-traditional applications of phage particles as therapeutic biologics, vaccines carriers, or bioconjugation scaffolds.

A technology report (Tjhung et al.) addresses an issue that has plagued phage display libraries of proteins and peptides fused to the N-terminus of virion protein pIII, in that some peptide variants are more likely to be degraded than others. Recombinant phage encoding these degradable variants have advantage at amplification step over other library clones, due to more efficient pIII-mediated infection of the host, and may outcompete the true binders in the library screens. The authors demonstrate that this can be prevented by displaying peptides between the pIII N1 and N2 domains instead of display at the N-terminus. Given that N1 domain is essential for infection, amplification of recombinant phage clones depends on preservation of displayed peptide (and thereby retention of the N1 domain in the phage). This strategy eliminates those recombinant clones in the library whose displayed peptides are degraded. It is very likely that phage display between N1 and N2 domains of pIII will be taken up by many researchers in the future.

Two research reports describe novel applications of Ff-phage-derived particles in tumor targeting. Gillespie et al. describe a new approach for assembly of tumor-targeting drug-loaded liposomes, by enabling spontaneous insertion of cancer-cell-binding peptide-pVIII fusion protein. The insertion via pVIII hydrophobic core without damaging the liposome was achieved by applying a novel method for direct purification from the phage particles, using 2-propanol. This protocol greatly simplifies the assembly of cancer-targeting drug-loaded liposomes, allowing screening of multiple peptides for targeting efficiency and drug delivery. Dor-On and Solomon report brain tumor targeting by naked Ff phage (not displaying any brain-targeting peptides) in a mouse model of glioblastoma after intranasal application. Interestingly, particle-associated lipopolysaccharides may be the key to brain targeting and anti-tumor activity of Ff in this model.

Three reports describe applications of Ff phage as nanoparticles. Sattar et al. report development of a method to functionalize and efficiently produce extremely short Ff-derived particles (50 nm in length) that contain no genes or antibiotic markers. The authors show that the short particles perform better than the full-length phage of the same composition as diagnostic particles in lateral-flow diagnostic assays. In a short review, Bernard and Francis discuss modifications that are essential for applications of Ff phage as functionalized nanoparticles. These include chemical conjugation to organic molecules such as fluorophores, pigments, carbohydrates, or inorganic molecules. One fascinating property of filamentous phage is that they are liquid crystals at high concentrations. Review by Dogic gives a clear, biologist-friendly, and up-to-date account of the liquid crystalline properties filamentous phage and their applications in the soft matter physics.

## PERSPECTIVE

Future holds discovery of many novel filamentous phage. Some of these will likely be used as genetic tools for bacterial engineering, utilizing knowledge about their *attP* sites, integration, and replication. Many filamentous phage modulate bacterial pathogenicity, hence therapeutic interventions against pathogenic bacteria, based on known and novel filamentous bacteriophage, are eagerly anticipated. Filamentous phage of

innocuous bacteria other than currently used Ff (f1, fd, and M13) will find applications in biotechnology, biomedicine, and nanotechnology, allowing exploration of novel properties, with the aim of decreasing the production cost and environmental footprint. Upscaling and eliminating safety concerns (removal of antibiotic-resistance genes and ability to replicate) will allow transition of filamentous-phage-particle-based technology from the laboratory containment to the consumer. In parallel, filamentous-phage-derived particles of ever more imaginative functions or physical properties will be designed and assembled into advanced nanostructures and nanomachines.

## AUTHOR CONTRIBUTIONS

Manuscript was written by JR and BD; it was edited by all three authors.

## FUNDING

Funding to JR laboratory by Palmerston North Medical Research Foundation, Massey University, Institute of Fundamental Sciences, Anonymous Donor and the Maurice Wilkins Centre for Molecular Biodiscovery is gratefully acknowledged. Work in BD laboratory was funded by Department of Biotechnology, Govt. of India (Grant No. BT/MB/THSTI/HMC-SFC/2011). RD acknowledges funding from the Alberta Glycomics Centre.

## ACKNOWLEDGMENTS

JR wishes to especially acknowledge the pioneers of filamentous bacteriophage research, Marjorie Russel and Peter Model (Rockefeller University), for generously sharing their knowledge through discussions and advice, and for the gifts of filamentous phage and *E. coli* strain collections.

**Conflict of Interest Statement:** The authors declare that the research was conducted in the absence of any commercial or financial relationships that could be construed as a potential conflict of interest.

frontiers in Microbiology

ORIGINAL RESEARCH
published: 23 February 2016
doi: 10.3389/fmicb.2016.00050

# Physiological Properties and Genome Structure of the Hyperthermophilic Filamentous Phage φOH3 Which Infects *Thermus thermophilus* HB8

*Yuko Nagayoshi[1], Kenta Kumagae[1], Kazuki Mori[2], Kosuke Tashiro[2], Ayano Nakamura[1], Yasuhiro Fujino[3], Yasuaki Hiromasa[4], Takeo Iwamoto[5], Satoru Kuhara[2], Toshihisa Ohshima[6] and Katsumi Doi[1]**

[1] Faculty of Agriculture, Institute of Genetic Resources, Kyushu University, Fukuoka, Japan, [2] Department of Bioscience and Biotechnology, Faculty of Agriculture, Kyushu University, Fukuoka, Japan, [3] Faculty of Arts and Science, Kyushu University, Fukuoka, Japan, [4] Faculty of Agriculture, Attached Promotive Center for International Education and Research of Agriculture, Kyushu University, Fukuoka, Japan, [5] Core Research Facilities, Research Center for Medical Sciences, Jikei University School of Medicine, Tokyo, Japan, [6] Department of Biomedical Engineering, Faculty of Engineering, Osaka Institute of Technology, Osaka, Japan

OPEN ACCESS

**Edited by:**
*Bhabatosh Das, Translational Health Science and Technology Institute, India*

**Reviewed by:**
*Sukhendu Mandal, University of Calcutta, India*
*Paul T. Hamilton, North Carolina State University, USA*

***Correspondence:**
*Katsumi Doi*
*doi@agr.kyushu-u.ac.jp*

**Specialty section:**
*This article was submitted to Virology, a section of the journal Frontiers in Microbiology*

**Received:** *16 September 2015*
**Accepted:** *12 January 2016*
**Published:** *23 February 2016*

**Citation:**
*Nagayoshi Y, Kumagae K, Mori K, Tashiro K, Nakamura A, Fujino Y, Hiromasa Y, Iwamoto T, Kuhara S, Ohshima T and Doi K (2016) Physiological Properties and Genome Structure of the Hyperthermophilic Filamentous Phage φOH3 Which Infects Thermus thermophilus HB8 Front. Microbiol. 7:50. doi: 10.3389/fmicb.2016.00050*

A filamentous bacteriophage, φOH3, was isolated from hot spring sediment in Obama hot spring in Japan with the hyperthermophilic bacterium *Thermus thermophilus* HB8 as its host. Phage φOH3, which was classified into the *Inoviridae* family, consists of a flexible filamentous particle 830 nm long and 8 nm wide. φOH3 was stable at temperatures ranging from 70 to 90°C and at pHs ranging from 6 to 9. A one-step growth curve of the phage showed a 60-min latent period beginning immediately postinfection, followed by intracellular virus particle production during the subsequent 40 min. The released virion number of φOH3 was 109. During the latent period, both single stranded DNA (ssDNA) and the replicative form (RF) of phage DNA were multiplied from min 40 onward. During the release period, the copy numbers of both ssDNA and RF DNA increased sharply. The size of the φOH3 genome is 5688 bp, and eight putative open reading frames (ORFs) were annotated. These ORFs were encoded on the plus strand of RF DNA and showed no significant homology with any known phage genes, except ORF 5, which showed 60% identity with the gene VIII product of the *Thermus* filamentous phage PH75. All the ORFs were similar to predicted genes annotated in the *Thermus aquaticus* Y51MC23 and *Meiothermus timidus* DSM 17022 genomes at the amino acid sequence level. This is the first report of the whole genome structure and DNA multiplication of a filamentous *T. thermophilus* phage within its host cell.

**Keywords: hyperthermophilic phage, *Thermus thermophilus*, filamentous phage, *Inoviridae*, replicative form**

## INTRODUCTION

Thermophilic phages or viruses play extraordinarily important roles in the processes of evolution, biogeochemistry, ecology, and genetic exchange in extreme environments (Prangishvili et al., 2006). Among these phages, those that infect *Thermus* species have been extensively studied (Liu et al., 2009), and complete genome sequences have been reported for myoviruses YS40

(Naryshkina et al., 2006) and TMA (Tamakoshi et al., 2011); siphoviruses P23-45, P74-26 (Minakhin et al., 2008), TSP4 (Lin et al., 2010), and φIN93 (Matsushita and Yanase, 2009); and tectivirus P23-77 (Jalasvuori et al., 2009). As far as we know, however, no genome information has been reported for a filamentous phage that infects *Thermus* species.

Filamentous phages belong to the *Inoviridae* family. As reported by Ackermann (Ackermann, 2007), phages belonging to this family are far fewer in number than tailed phages. The inovirus virions contain a circular, positive sense, single-stranded DNA (ssDNA) genome within a helical array composed of thousands of copies of the major capsid protein. As a result of this structural arrangement, inoviruses are flexible filaments about 7 nm in diameter. Inoviruses infect both gram-negative and gram-positive bacteria (Day, 2012), but are unusual among bacteriophages in that they do not lyse their host cells when new phage particles are produced. Instead, new virions are packaged at the cell surface and extruded (Rakonjac et al., 1999; Marvin et al., 2014). These virions contain ssDNA that typically enters new hosts via pili on the cell surface (Stassen et al., 1994). Once inside the host, inoviruses persist in a circular, double-stranded replicative form (RF); alternatively, they can integrate into the host chromosome through the actions of phage-encoded transposases (Kawai et al., 2005) and host-encoded XerC/D (Huber and Waldor, 2002; Hassan et al., 2010), which normally resolves chromosome dimers. Production of new phage ssDNA can then proceed via rolling-circle replication from the RF. The genomes of inoviruses are composed of modules that encode proteins involved in genome replication, virion structure and assembly, and regulation (Campos et al., 2010). Like many other phages, inoviruses can undergo extensive recombination, often picking up new genes in the process, so that they may act as important vectors for gene transfer among hosts (Davis and Waldor, 2003; Faruque et al., 2005).

Phage PH75 is the only reported inovirus isolated from *T. thermophiles* HB8 (Yu et al., 1996). Although structural analysis of its coat proteins has been carried out (Pederson et al., 2001; Overman et al., 2004; Tsuboi et al., 2005), to our knowledge there is no reported genome information for phage PH75. Thirty-six species of inovirus listed by International Committee on Taxonomy of Viruses (ICTV) have been isolated from enterobacteria and the *Pseudomonas*, *Vibrio,* and *Xanthomonas* species. Among them, the genomes of the enterobacteria phages fd (Beck et al., 1978), f1 (Hill and Petersen, 1982), Ike (Peeters et al., 1985), and M13 (van Wezenbeek et al., 1980); the *Propionibacterium* phage B5 (Chopin et al., 2002); *Pseudomonas* phages Pf1 (Hill et al., 1991) and Pf3 (Luiten et al., 1985); and *Vibrio* phages VCYφ (Xue et al., 2012); and *Yersinia* phage Ypfφ (Derbise and Carniel, 2014) have all been completely sequenced. Because all of these filamentous phages infect mesophilic bacteria, comparison of the genome of a hyperthermophilic *Thermus* inovirus and the aforementioned mesophilic inoviruses may provide important insight into the diversity, evolution, and ecology of bacteriophages. In particular, it may shed light on the features that confer thermostability to the phage proteins encoded by its genomic DNA.

In this report, we characterize phage φOH3, a filamentous phage infecting *T. thermophiles* HB8, including its temperature, pH and salt tolerances, as well as its host range, one-step growth curve and replicative behavior in host cells. We also report the structure of the φOH3 genome the first example from a *Thermus* filamentous phage.

## MATERIALS AND METHODS

### Geothermal Water Sample

The hot spring water samples from which φOH3 was isolated were collected from the Obama hot spring, Nagasaki, Japan (32°43′25″N, 130°12′50″E, 75°C).

### Bacterial Strains, Media, and Growth Conditions

*Thermus thermophilus* HB8 (Oshima and Imahori, 1971) was used as the host strain for phage φOH3 in this study. *T. thermophilus* strains AT-62 (Saiki et al., 1972), HB27 (Oshima and Imahori, 1971), TMY (Fujino et al., 2008), and Fiji3 A.1 (Saul et al., 1993) as well as *Thermus aquaticus* YT-1 (Brock and Freeze, 1969), *Meiothermus ruber* strain 21 (Loginova and Egorova, 1975), and *Geobacillus kaustophilus* NBRC 102445 (Priest et al., 1988) were also used as indicators. *T. thermophilus* strains were cultivated in HB8 broth (Sakaki and Oshima, 1975) at 70°C with shaking at 180 rpm. Castenholz medium (Nold and Ward, 1995) was used for cultivation of *T. aquaticus* YT-1 and *M. ruber* strain 21 at 70 and 55°C, respectively. *G. kaustophilus* NBRC 102445 was cultivated in Nutrient broth (Nissui Pharmaceutical, Japan) at 55°C with shaking at 180 rpm.

Plasmid pUC18 was used for cloning and analysis of the nucleotide sequence of the φOH3 genome. *Escherichia coli* DH5α was grown in Luria-Bertani (LB) medium at 37°C (Sambrook and Russell, 2001). When required, 50 μg/ml ampicillin was added. SM buffer [100 mM NaCl, 8 mM $MgSO_4$ $7H_2O$, 50 mM Tris-HCl (pH 7.5), and 0.002% (w/v) gelatin] was used for storage and dilution of phage particles (Sambrook and Russell, 2001).

### Isolation and Purification of Phage

A geothermal water sample was added to an equal volume of HB8 broth for an enrichment culture. After cultivation (70°C, 180 rpm, 2 days), the culture was centrifuged (6000 × g, 10 min, 4°C) to remove bacterial cells and debris, after which and the supernatant was passed through a nitrocellulose filter with 0.45 μm pores (Advantec, Japan). The filtrate was then added to an equal amount of double strength HB8 broth supplemented with 10 mM $CaCl_2$ and inoculated with a log-phase host culture ($OD_{660}$ = 0.4). The phage was assayed using the soft agar overlap technique (Adams et al., 1959). After overnight incubation (70°C), typical plaques were suspended in SM buffer and purified through 10 rounds of single-plaque isolation.

### Transmission Electron Microscopy

Phage morphology was determined using transmission electron microscopy to observe negatively stained preparations (Luo et al.,

2012). One drop containing approximately $10^{12}$ PFU/ml freshly prepared purified phage solution was applied to the surface of a Formver-coated grid (200 mesh copper grid), negatively stained with 2% (wt/vol.) phosphotungstic acid (pH 7.2), and then examined using an Hitachi H-7500 transmission electron microscope operated at 80 kV (Hitachi High-Technologies Corp., Japan).

## Host Range Determination

The host range of the phage was investigated using the spot test (Shirling and Speer, 1967) against five *T. thermophilus* strains (HB8, HB27, AT62, TMY, and Fiji3 A.1) as well as *T. aquaticus* YT-1, *M. ruber* 21, and *G. kaustophilus*. Incubation temperatures were set with optimum temperatures for each strain.

## Heat, pH, and Saline Stability

All plaque assays were performed using a 0.8% TM agar overlay on 2.0% TM agar. Plaque development occurred within 1 day, and assays were conducted in triplicate. Thermal, pH and salt stabilities were tested as described previously (Lin et al., 2011) with modification. Briefly, to examine of thermal stability, phage stocks ($1.0 \times 10^7$ PFU/ml in SM buffer) were incubated separately for 60 min at 50, 60, 80, and 90°C. The phage titer was then evaluated using the double-layer method with early log phase *T. thermophilus* HB8 cells at a multiplicity of infection (MOI) of 1. For pH stability, $1.0 \times 10^7$ PFU/ml phage solution was added into modified TM broth (pH values were adjusted from 3 to 11) and then incubated for 24 h at 20∼70°C. To asses salt stability, sodium chloride was dissolved to 0, 0.1, 0.5, 1.0, or 3.0 M with phage lysates ($1.0 \times 10^7$ PFU/ml), and the mixture was incubated for 24 h at 20∼70°C. The resultant phage solutions were diluted to $1.0 \times 10^4$ PFU with TM broth and then used to infect HB8 cells at a MOI of 0.1. The plates were then incubated overnight at 70°C before examination for the presence of plaques.

## One-Step Growth Curve

A one-step growth curve was constructed as previously described (Pajunen et al., 2000) with some modifications. An early-exponential-phase culture (10 ml) of *T. thermophilus* HB8 ($OD_{660}$ = 0.4) was harvested by centrifugation and resuspended in 1 ml of fresh TM broth ($10^8$ CFU/ml). φOH3 was added to the HB8 suspension at a MOI of 10 and allowed to adsorb for 15 min at 70°C. Thereafter, the mixture was washed with an equal volume of fresh TM broth. This manipulation was repeated three times to remove any free phage particles. After centrifugation, the pelleted cells were resuspended in 100 ml of fresh TM broth and incubated for 2 h at 70°C while shaking. During the incubation, samples were taken at 10-min intervals and immediately centrifuged, after which the supernatants were plated on TM agar to determine the phage titer. Number of released virion was calculated as the ratio of the final count of liberated phage particles to the initial number of infected bacterial cells during the latent period like as burst size of lytic phage (Adams et al., 1959).

## Extraction and Purification of Phage Genomic DNA

φOH3 genomic DNA was obtained from its host cells using a Cica Geneus Plasmid Prep Kit (KANTO CHEMICAL, Japan) with continuous extraction every 10 min after infection. Extracted DNA samples were separated using 0.8% agarose gel electrophoresis, and then ssDNA and RF DNA were visualized using acridine orange staining (Mayor and Hill, 1961; McMaster and Carmichael, 1977). Determination of the copy number of ssDNA and RF DNA within the φOH3 genome was done using ImageJ ver 1.48 (http://rsb.info.nih.gov/ij/) by comparing the intensities of their fluorescent signals. The peak areas of both the ssDNA and RF signal were quantified and used to calculate the copy number. To purify RF DNA, the plasmid-like genomes were isolated from 5-ml samples of *T. thermophilus* HB8 after cultivation for 80 min. The φOH3 genomic DNA was then separated on 1.0% agarose gels, and the bands corresponding to the RF DNA were excised and purified using a MinElute Gel Extraction Kit (QIAGEN GmbH, Germany).

## Genome Characterization

RF DNA was digested using *Hin*d III, *Kpn* I, or *Pst* I, after which the resultant φOH3 RF fragments were inserted into separate pUC18 vectors. Each recombinant plasmid was then used to transform *E. coli* DH5α competent cells. Nucleotide sequencing of the plasmids was accomplished through primer walking using a BigDye Terminator v3.1 Cycle Sequencing Kit (Life Technologies, CA, USA). Sequences were determined using an Applied Biosysytems Gene Analyzer 3130xl (Life Technologies). The sequence of the φOH3 genome was also obtained by pyrosequencing performed with a 454 Genome Sequencer FLX system (Roche, Schweiz) as described previously (Doi et al., 2013). Open reading frames (ORFs) were predicted using a combination of MiGAP and GENETYX ver. 15 (GENETYX, Japan). Translated ORFs were analyzed through blastp, PsiBlast, rpsblast, and hhpred searches.

## DNA Blot Analysis

To confirm that ORFs were located on the plus strand, DNA blot analysis was carried out as described by Liu et al. (2012). Non-denatured DNA samples were separated on a 1.0% agarose gel and then transferred to a nylon membrane (Amersham Hybond-N+; GE Healthcare, UK) through capillary action. The probes corresponding to each strand of RF DNA in the blotting experiments were prepared using DIG Northern Starter Kit (Roche). The DNA probe used in the Southern blotting experiments was a 294-bp DNA fragment derived from ORF2, which was prepared by PCR. The primer set used for the PCR was derived from the coding region of ORF2 and is as follows: orf2-f (5′-ATGAAGGTTTTGGTTCTAGGAGT-3′) and orf2-r (5′-TCACGCCTTGACCTCCT-3′). The amplified ORF2 gene was inserted into the pTA2 vector (TOYOBO, Japan), and the resultant plasmid was digested with *Hin*d III or *Pst* I, after which the linearized plasmid served as the template for RNA transcription catalyzed using T3 or T7 RNA polymerase. Hybridization of each RNA product, RNA probe-1and -2, to the

phage DNA and detection were carried out according to the manufacturer's instructions.

## Structural Protein Identification by Mass Spectroscopy

To analyze φOH3 virion proteins, phage solution ($10^{10}$ pfu/ml) was concentrated with Amicon Ultra-15 filter (NMWL 50000; Merck Millipore, Germany) and then purified using DISMIC membrane filter (0.45 mm; ADVANTEC, Japan). The purified phage particles were mixed with lysis buffer (62.5 mM Tris-HCl, pH 6.8, containing 5% 2-mercaptoethanol, 2% sodium dodecyl sulfate, 10% glycerol, and 0.01% bromophenol blue) and boiled for 10 min. The prepared proteins were then separated by electrophoresis on precast Tricine-SDS 15% polyacrylamide gels (e-PAGEL E-T/R15S; ATTO Corporation, Japan).

## In-Gel Digestion

Excised gel pieces were de-stained with acetonitrile solution. After the gel plugs were dried, 400 ng of sequencing-grade trypsin (Trypsin Gold, Promega, Madison, WI) in 20 μl of 25 mM ammonium bicarbonate were added and incubated for 12 h at 37°C. Selected gel plugs were also treated with chymotrypsin. Digested peptides were recovered from the gel plugs using 50 μl of 50% acetonitrile in 5% formic acid (FA) for 30 min at 25°C. The extracted peptides were concentrated in a speed vacuum concentrator and added to 20 μl of 5% acetonitrile in 0.1% FA.

## Protein Identification

A Nano-HPLC system (nanoADVANCE, Bruker Michrom., Billerica, MA) was used to identify proteins automatically using a micro-column switching device coupled to an autosampler and a nanogradient generator. Peptide solution (5 μl) was loaded onto a C18 reversed-phase capillary column (100 μm ID × 30 cm, Zaplous α X Pep C18: AMR, Tokyo, Japan) in conjunction with a Magic C18AQ trapping column (300 μm ID × 10 mm, Bruker). The peptides were separated using a nanoflow linear acetonitrile gradient of buffer A (0.1% FA) and buffer B (0.1% FA, 99.9% acetonitrile), going from 5 to 45% buffer B over 50 min at a flow rate of 500 nl/min. The column was then washed in 95% buffer B for 5 min. Hystar 3.2 system-control software (Bruker Daltonics Inc., Billerica, MA) was used to control the entire process. The eluted peptides were ionized through a CaptiveSpray source (Bruker Daltonics) and introduced into a Maxis 3G Q-TOF mass spectrometer (Bruker Daltonics Inc., Billerica, MA) set up in a data-dependent MS/MS mode to acquire full scans (m/z acquisition range from 50 to 2200 Da). The four most intense peaks in any full scan were selected as precursor ions and fragmented using collision energy. MS/MS spectra were interpreted and peak lists were generated using DataAnalysis 4.1 and Biotools 3.2.

## Bioinformatics

The filtered data were searched on the Mascot 2.2 server (Matrix Science) using the NCBInr (NCBI 20150627) custom genome sequence and custom expected protein databases for φOH3. The custom φOH3 genome sequence database was created by dividing every 2000 sequences from the φOH3 genome sequence (LC035386). Fixed modification was set on cysteine with carbamidomethylation. Variable modification was based on methionine with oxidation and asparagine/glutamine with deamidation. Maximum missed cleavage was set to 2 and limited to trypsin cleavage sites. Precursor mass tolerance (MS) and fragment mass tolerance (MS/MS) were set to 100 ppm and ± 0.6 Da, respectively. Positive protein identifications using a threshold of 0.05 were used. Peptides scoring <20 were automatically rejected, ensuring all protein identifications were based on the reliable peptide identifications.

## Nucleotide Sequence Accession Number

The genome sequence of φOH3 has been deposited in GenBank with accession number LC035386.

# RESULTS

## Isolation and Morphology of φOH3

Large numbers of plaques were formed from the enrichment culture of a geothermal water sample using *T. thermophilus* HB8 as the host. One of them, φOH3, formed turbid plaques 0.5–1.1 mm in diameter on the lawn of *T. thermophilus* HB8 after incubation for 12 h at 70°C. Transmission electron microscopy and negative staining revealed the morphology of φOH3 to consist of flexible filaments, approximately 8 nm wide and 830 nm long (**Figure 1**). On that basis, phage φOH3 was classified as a member of the family *Inoviridae*.

## Host Range of φOH3

The infectivity of phage φOH3 was examined using various thermophilic bacteria, including *T. thermophilus* HB8, *T. thermophilus* HB27, *T. thermophilus* AT62, *T. thermophilus* TMY, *T. thermophilus* Fiji3 A.1, *T. aquaticus* YT-1, *M. ruber* strain 21, and *G. kaustophilus* NBRC 102445. Phage φOH3 formed an inhibitory zone only on *T. thermophilus* HB8.

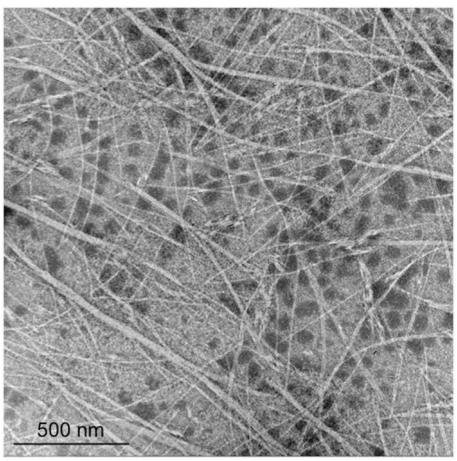


**FIGURE 1 | Morphology of phage φOH3.** Shown are transmission electron micrographs of inovirus φOH3 negatively stained with 2% (wt/vol) potassium phosphotungstate (pH 7.0). The scale bar is 500 nm.

## Heat, pH, and Salt Tolerance

Thermostability assays showed that phage φOH3 was most stable at 70°C. After incubation for 1 h at 80 or 90°C, the φOH3 survival fraction dramatically decreased to 59.2 and 6.5%, respectively (**Figure 2A**), and the phage was completely inactivated at 100°C (data not shown). φOH3 was most stable at pH 7.0 and was sensitive to both acidic and alkali pHs (**Figure 2B**). At lower or higher pHs, phage survival decreased substantially. For example, when the pH was lower than 3.0 or higher than 9.0, the phage survival fraction was reduced to 4 and 32.7%, respectively.

Phage φOH3 was stable in NaCl at concentrations ranging from 0 to 1 M. (**Figure 2C**), and was most stable in SM buffer, which contains 0.5 M NaCl. In solution containing 3M NaCl, the phage survival fraction was only 1.1%. In the complete absence of NaCl, the survival fraction was reduced to 60%.

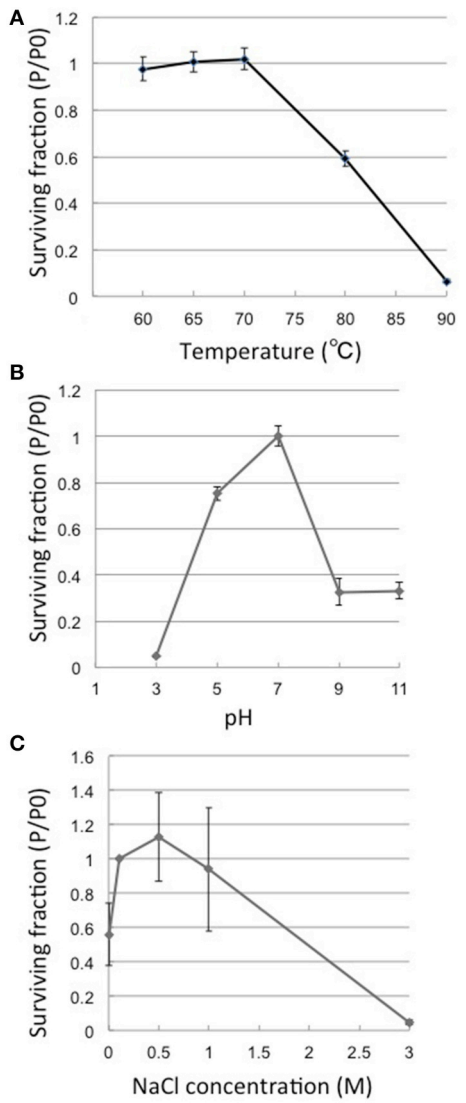


**FIGURE 2 | Heat, pH and salt stability of φOH3.** Surviving fractions (P/P0) are plotted, where P0 is the φOH3 initial titer, and P is the mean titer from triplicate assays after incubation for 1 h at the indicated temperature **(A)**, 24 h at the indicated pH **(B),** or 24 h at the indicated NaCl concentration **(C)**.

## Phage Particle Propagation and Genome Replication

The one-step growth curve for phage φOH3 showed the latent period and release period to be 60 and 40 min, respectively (**Figure 3A**). The phage adsorption fraction was 90.0%, and 109 phage particles were released from each infected cell, on average. Agarose gel electrophoresis showed that the φOH3 genome was present in HB8 cells as both RF DNA and ssDNA (**Figure 3B**). While changes in the copy number of RF DNA were detected 40–80 min after infection, changes in ssDNA copy number increased sharply after 50 min. Overall, the intracellular DNA concentrations increased in proportion to the duration of cultivation. Because the copy number of the cryptic plasmid pTT8 (9328 bp) of *T. thermophilus* HB8 remained constant at 8 throughout the latent and release periods (Hishinuma et al., 1978; Takayama et al., 2004), we were able to use it as an internal standard and determine that the copy numbers of the RF DNA and ssDNA comprising the φOH3 genome were roughly 30 and 16, respectively, 80 min after infection.

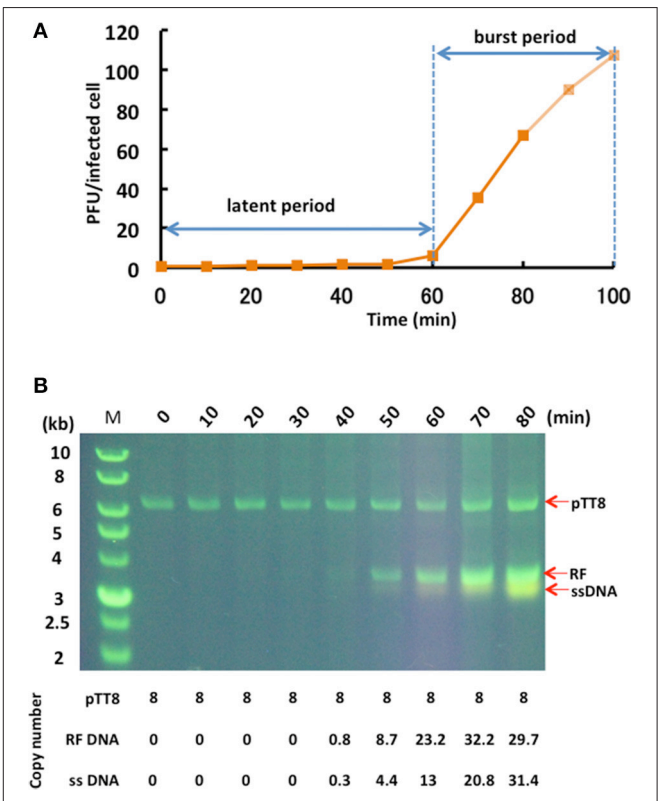


**FIGURE 3 | Propagation of φOH3 in *T. thermophilus* HB8. (A)** One-step growth curve of φOH3. **(B)** Agarose gel electrophoresis of phage φOH3 genomic DNA. The φOH3 genome was extracted with alkaline lysis after the indicated cultivation periods. Double stranded RF DNA and ssDNA were distinguished by acrydine orange staining. Corresponding estimated copy numbers of pTT8 (Takayama et al., 2004), RF DNA, and ssDNA of φOH3 are shown under the gels.

## Phage Genome Analysis

The genome of φOH3 consists of 5688 base pairs (bp) with a G+C content of 58.03%, which is significantly lower than the 69.52% of its host strain, *T. thermophilus* HB8 (NCBI RefSeq accession number: NC_006461; **Figure 4**). Southern hybridization using oligoprobes designed from each strand of the RF sequence showed that the φOH3 genome was single stranded (**Figure 5**). Using MiGAP pipeline, six ORFs longer than 100 bp were predicted from the sequence of the plus strand, which was revealed by Southern hybridization. In addition, two small ORFs (<100 bp) were predicted based on comparative genome analysis (**Table 1**). These eight putative ORFs had no significant homology with any phage genes registered in databases at the nucleotide sequence level. On the other hand, the amino acid sequence of the ORF V product showed 60% identity with P8, the major coat protein of phage PH75 (Pederson et al., 2001; **Figure 6**), while the amino acid sequences of the other putative ORF products showed similarities to putative uncharacterized proteins encoded in the *T. aquaticus* Y51MC23, *Meiothermus timidus* DSM 17022 and *Thermus* sp. genomes (GenBank accession numbers: ABVK00000000, ARDL00000000, and JTJB00000000; **Table 1**). Based on comparisons with the

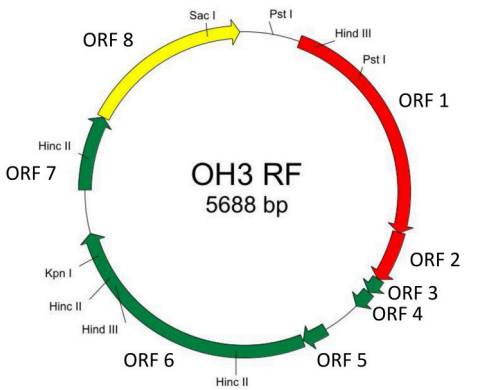


**FIGURE 4 | Genetic map of φOH3 RF DNA.** Predicted ORFs are indicated by arrows. Arrow colors show putative gene functions as follows: replication, red; structure, green; assembly, yellow. Since the conserved domain of Zot was detected in the ORF8 product, ORF8 might function for phage assembly.

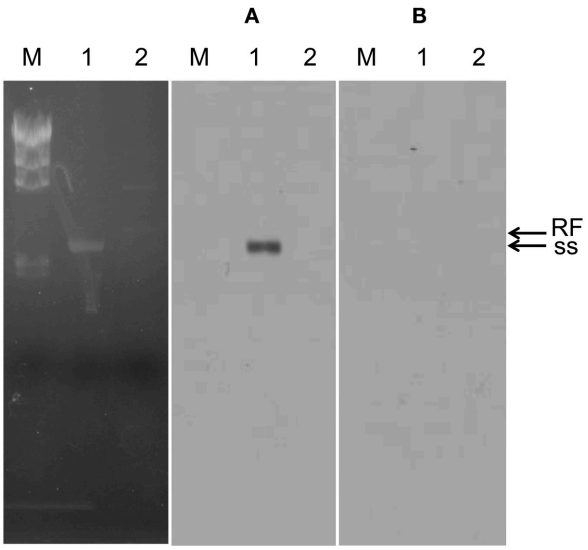


**FIGURE 5 | Southern blot confirming the plus strand of phage φOH3.** Lanes: M, lambda -*Hin*d III marker; 1, φOH3 ssDNA; 2, φOH3 RF DNA. **(A)** RNA probe-1, which was transcribed by T7 RNA polymerase (antisense strand of ORF2). **(B)** RNA probe-2, which were transcribed by T3 RNA polymerase (sense strand of ORF2). Bands corresponding to ss DNA or RF DNA are indicted with arrows.

**TABLE 1 | Protein-encoding region predicted in the φOH3 genome and their relationship to amino acid sequences from the databases.**

| ORF no. | Position (5′→3′) | Corresponding gene in M13 | Putative protein function | Homologous protein | Identity | *e*-value | Accession no. |
|---|---|---|---|---|---|---|---|
| 1 | 319–1659 | II | RF replication Endonuclease | Hypothetical protein (*Thermus aquaticus* Y51MC23) | 54% | $9e^{-146}$ | WP_003044556.1 |
| | | | | Hypothetical protein (*Thermus* sp. 2.9) | 55% | $2e^{-145}$ | WP_039459567.1 |
| 2 | 1656–1949 | V | Single-strand DNA binding protein | Hypothetical protein (*Thermus aquaticus* Y51MC23) | 51% | $4e^{-21}$ | WP_003044553.1 |
| | | | | Hypothetical protein (*Meiothermus timidus* DSM 17022) | 41% | $9e^{-15}$ | WP_018467932.1 |
| 3 | 1946–2038 | VII | Minor coat protein | Hypothetical protein (*Thermus aquaticus* Y51MC23) | 62% | $5e^{-04}$ | EED10729.1 |
| 4 | 2039–2143 | IX | Minor coat protein | Hypothetical protein (*Thermus aquaticus* Y51MC23) | 68% | $4e^{-06}$ | EED10728.1 |
| 5 | 2363–2503 | VIII | Major coat protein | Hypothetical protein (*Meiothermus timidus* DSM 17022) | 64% | 0.016 | WP_018467931.1 |
| | | | | Hypothetical protein (*Thermus* sp. 2.9) | 65% | 0.063 | WP_039459577.1 |
| | | | | Hypothetical protein (*Thermus aquaticus* Y51MC23) | 61% | 1.4 | EED10727.1 |
| 6 | 2507–4027 | III | Adsorption protein | Hypothetical protein (*Thermus aquaticus* Y51MC23) | 50% | $6e^{-136}$ | EED10726.1 |
| 7 | 4277–4705 | VI | Minor coat protein | Hypothetical protein (*Thermus* sp. 2.9) | 61% | $6e^{-43}$ | WP_039459592.1 |
| | | | | Hypothetical protein (*Thermus filiformis* ATCC 43280) | 59% | $5e^{-36}$ | WP_038066844.1 |
| | | | | Hypothetical protein (*Thermus aquaticus* Y51MC23) | 52% | $4e^{-29}$ | WP_003046233.1 |
| 8 | 4705–5661 | IV | Morphogenesis | Hypothetical protein (*Thermus* sp. 2.9) | 86% | $5e^{-177}$ | WP_039459711.1 |
| | | | | Hypothetical protein (*Thermus aquaticus* Y51MC23) | 81% | $4e^{-150}$ | WP_003046231.1 |
| | | | | Hypothetical protein (*Meiothermus timidus* DSM 17022) | 76% | $1e^{-149}$ | WP_018467929.1 |

| Phage | | | | | Identity |
|---|---|---|---|---|---|
| φOH3 | ORF5 | 1 | VEFDAGAIVSTVQNYILAIAGAGVALLGLTIGLSAAWRYAKKFLKG | 46 | |
| PH75 | 1hgv | 1 | MDFNPSEVASQVTNYIQAIAAAGVGVLALAIGLSAAWKYAKRFLKG | 46 | 60% |
| Pf3 | Pf3_2 | 7 | ---DVTGQLTAVQADITTIGGAIIVLAAVVLGIR--WIKAQFF--- | 44 | 30% |
| M13 | VIII | 36 | ------SLQASATEYIGYAWAMVVVIVGATIGIKLFKKFTSK---- | 71 | 22% |

**FIGURE 6 | Comparison of the amino acid sequences of ORF5 product (φOH3), 1hgv (PH75), Pf3_2 (Pf3), and g8p (M13).** Identical and similar amino acid residues are indicated in red and blue, respectively. Hyphens represent gaps in the alignment.

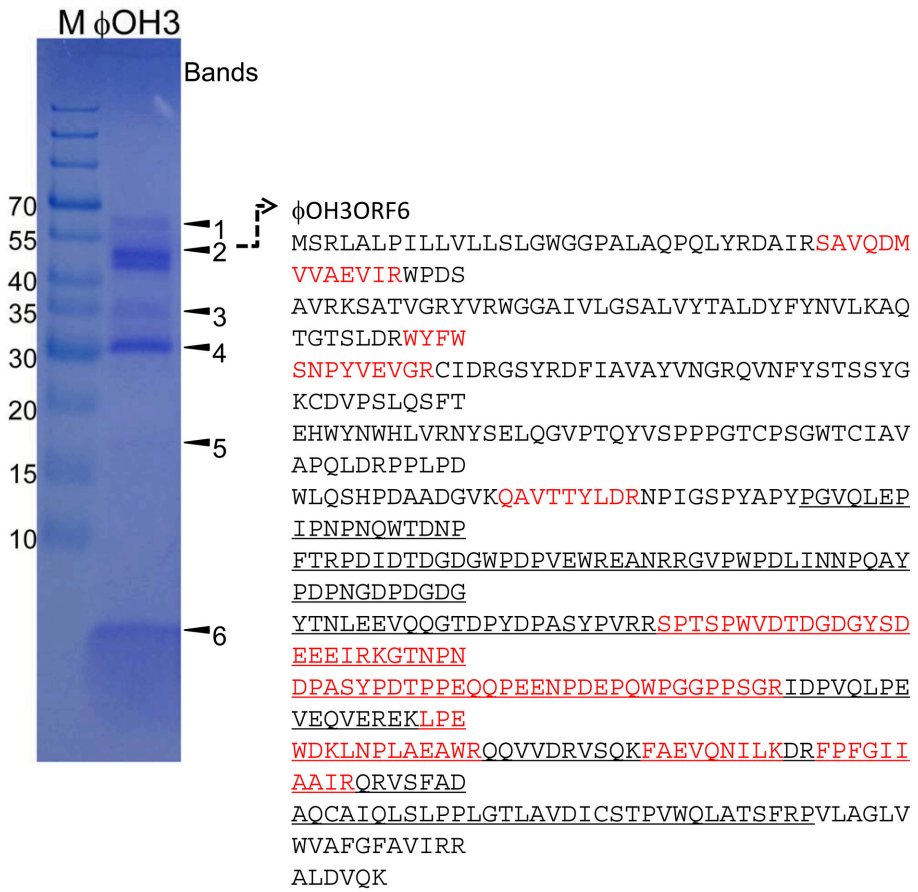


**FIGURE 7 | SDS-PAGE of proteins from purified φOH3 virions staining with Coomassie brilliant blue R250.** The numbers indicate the bands excised for mass spectrometric analysis (Supplemental Tables 1, 2). The left lane contains protein molecular mass markers (kDa). Red colored and underlined characters indicate matched peptides and domain of DNA translocase FtsK (PRK10263).

genomes of these strains, ORFs 3 and 4 were presumed to be situated between ORFs 2 and 5. A conserved domain of Zonula occludens toxin (Zot) (Koonin, 1992) was detected in the N-terminal region (A.A. 1–197) of the ORF8 product. Although gene localization within φOH3 is similar to that in M13, fd, B5, and Pf3, four other filamentous phages, there are no genes homologous to gene I encoding the assembly protein in the φOH3 genome.

## Protein Analysis of φOH3

Purified phage particles were analyzed using SDS-PAGE (**Figure 7**). Six major bands with estimated molecular masses of 60, 55, 35, 30, 17, and 5 kDa, respectively, were found. The bands were then subjected to bioinformatics analysis using the bacteria sequence databases of NCBInr, which showed that all the protein bands included proteins from *Thermus thermophiles* (Supplemental Table 1). With a custom φOH3 database, analysis using six-frame translation showed that the peptides from the 55 kDa band matched the sequence region of the φOH3ORF 6 sequence (Supplemental Table 2 and **Figure 7**). No other significant matches were found with six-frame translation of the DNA database. Nine unique peptides were matched against the φOH3ORF 6 sequence, giving 27% total sequence coverage (matched 136 A.A./total 506 A.A.). With a Blastp search,

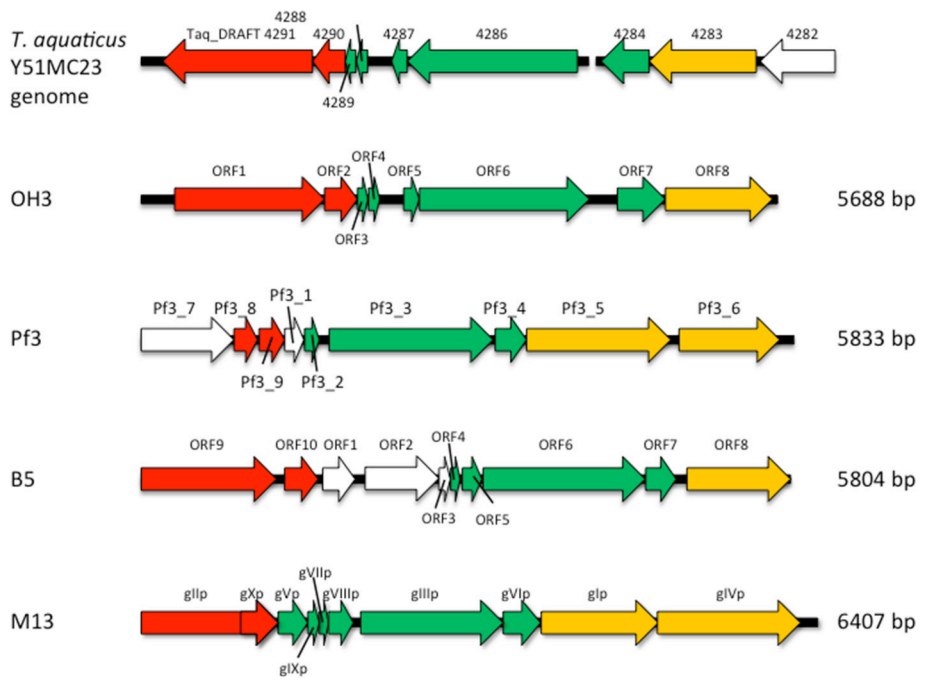


**FIGURE 8 | Comparison of the genome organization of phage φOH3 with that of the phage Pf3, B5, M13, and *T. aquaticus* Y51MC23 genomes.** Open reading frames with similar functions are indicated using the same color scheme used in **Figure 4**. White arrows show regions encoding hypothetical proteins with unknown functions.

we found that the φOH3ORF 6 sequence includes the DNA translocase FtsK domain structure (PRK10263) and shows 50% identity with the hypothetical protein TaqDRAFT_4286 (*Thermus aquaticus* Y51MC23, gb|EED10726.1|). The peptides from 5 kDa band were also covered from the sequence of φOH3ORF5 (Supplemental Table 2 and **Figure 7**). Initial proteomics analysis using trypsin digestion failed to identify the protein. Since the cleavage sites of trypsin in φOH3ORF5 sequence are only located at the C-terminal region, possible tryptic fragments are expected to be 38 amino acids or longer. Proteomics analysis, especially high throughput measurement, is not efficient at obtaining sequence information from peptides that are more than 30 residues long. Sequences of three uniques chymotryptic bands were detected. However, these mascot scores were insignificant.

## DISCUSSION

We have shown that the filamentous phage φOH3 infects the hyperthermophilic bacterium *T. thermophilus* HB8. To date, several kinds of *Thermus* phages belonging to the *Mioviridae*, *Siphoviridae*, *Tectiviridae,* and *Inoviridae* families have been isolated and characterized (Yu et al., 2006). φOH3 appears to be a *Thermus* filamentous phage belonging to the family *Inoviridae*. PH75 is another filamentous phage that infects *T. thermophilus* HB8. Although the physiological characteristics of pVIII, the major coat protein in PH75, have been investigated using Raman and UV-resonance Raman spectroscopy (Overman et al., 2004; Tsuboi et al., 2005), there is presently no information on the PH75 genome sequence in any database, as far as we know. Detailed characteristics of this phage also have never been published. Consequently, biological characterization and genome analysis of a thermophilic filamentous phage could provide new information for virology, physiology, nanotechnology, and so on.

Thermostability assays showed that φOH3 was most stable at 70°C, which is similar to the optimal temperature for φYS40, but is higher than that for phages TSP4 (most stable at 60°C), MMP17 (most stable at 55–60°C), and GVE1 (most stable at 60°C), whose hosts are *T. thermophilus* HB8 (φOH3 and φYS40), *Thermus* TC4 (TSP4), *Meiothermus* TG17 (MMP17), and *Geobacillus* sp. E26323 (GVE1), respectively. The high thermostability of φOH3 may reflect the growth temperature of the host bacterium *T. thermophilus* HB8 rather than its filamentous morphology. The pH stability of φOH3 resembled that of MMP17 but was less than that of TSP4. In addition, Sakaki and Oshima reported that φYS40 is sensitive to high concentrations of salt (NaCl) (1975). Like φYS40, φOH3 was inactivated in the presence of 3 M NaCl. The dominant ions in the Obama hot spring waters from which φOH3 was isolated are Cl and Na, with concentrations ranging from 0.06 to 0.37 M and 0.04 to 0.31 M, respectively (Saibi and Ehara, 2010). From these results, it appears that the temperature, pH and NaCl sensitivity of phage φOH3 reflect its taxonomic position and/or geographic origin.

In the life cycle of Inoviruses, injection of the phage ssDNA through bacterial membranes into the cytoplasm is carried out after pilus-mediated adsorption of the phage onto its host cell. Thereafter, the host polymerase converts the ssDNA into

covalently closed double-stranded DNA, which is the replicative form. In φOH3, it takes the host polymerase at least 40 min to convert the ssDNA to RF DNA (**Figure 3B**). Finally, newly generated plus ssDNA strands are converted into new RF DNA molecules. It is noteworthy that the release period was initiated simultaneously with ssDNA replication, that continuous replication of both ssDNA and RF DNA is observed throughout the release period, and that plasmid pTT8 replication was unaffected by the phage DNA replication.

Nucleotide analysis of the φOH3 genome showed it to be 5688 bp in size, which is approximately the same as other filamentous phages such as Pf3 (5833 bp), B5 (5804 bp), and M13 (6407 bp; **Figure 8**). Although BLASTn revealed no homologous genes within the φOH3 genome, BLASTx revealed significant homology with predicted genes in the genomes of *T. aquaticus* Y51MC23 and *M. timidus* DSM 17022 (**Figure 8**). It thus appears that φOH3-like phages are able to infect *T. aquaticus* or *Meiothermus* species and that these phage genomes are integrated into their host chromosomes. No genes encoding an integrase or transposase are present in the φOH3 genome. Because the homologous genes are located on discrete contigs in each strain, the φOH3-related genes may be defective phages or traces of phage integration. Phage φOH3 could not infect either *T. aquaticus* or *Meiothermus* species (data not shown), and no hybridized bands were detected in the *T. aquaticus* YT-1 or *M. timidus* DSM 17022 genome using φOH3 DNA as a probe (data not shown), though ssDNA or RF DNA from φOH3 or a homolog could be transformed to these species with their natural competency. The amino acid sequence of the ORF 5 product shows high similarity (60%) to 1 hgv of phage PH75, but low similarity (<30%) to major coat proteins from other filamentous phages, such as Pf3_2 from Pf3 or protein VIII from M13. It seems likely the structural differentiation arose for the hyperthermostability of the φOH3 and PH75 virions (Tsuboi et al., 2005; Russel and Model, 2006).

Because nearly all the ORFs in the φOH3 genome are annotated as similar to other predicted genes with unknown function, we applied ESI-MS/MS and nano LC-MS/MS to identify the phage structural proteins. Because of difficulty for purification with ultracentrifugation, we selected to concentrate the phage particles using MS analysis enabled experimental examination of structural proteins and confirmed the genome-based gene predictions (Lavigne et al., 2009). Peptide sequences of the ORF 6 product could be detected with ESI-MS/MS. We cloned all the predicted ORFs in *E. coli* and examined the properties and localization of the gene products. These results will be reported elsewhere in the near future. Further comparative study of the thermophilic filamentous phage φOH3 will shed light not only on the mechanism underlying the thermostability of the proteins but also on mechanisms of gene evolution and transfer in a geothermal environment.

## AUTHOR CONTRIBUTIONS

The work presented here was carried out in collaboration between all authors. KD and TO defined the research theme. KD, YN, AN, and YF designed methods and experiments, carried out the virological experiments, analyzed the data, interpreted the results, and wrote the paper. KM, KT, and SK co-designed and analyzed DNA sequencing experiments, and co-worked on associated data collection and their interpretation. YH and TI co-designed protein analysis and ESI-MS/MS experiments, discussed analyses, interpretation, and presentation. All authors have contributed to, seen and approved the manuscript.

## FUNDING

This work was partly funded by JSPS KAKENHI No. 24658083, 26292182, and JST A-STEP No. 15650473.

## ACKNOWLEDGMENTS

We thank H. W. Ackermann, A. Ichinose, and M. Sakaguchi for advice on electron microscopic analysis, and K. Yamaguchi for helpful advice on Mascot analysis.

## SUPPLEMENTARY MATERIAL

The Supplementary Material for this article can be found online at: http://journal.frontiersin.org/article/10.3389/fmicb.2016.00050

## REFERENCES

Ackermann, H. W. (2007). 5500 Phages examined in the electron microscope. *Arch. Virol.* 152, 227–243. doi: 10.1007/s00705-006-0849-1

Adams, M. H., Anderson, E., and Kellenberger, E. (1959). *Bacteriophages*. New York, NY: Interscience publishers.

Beck, E., Sommer, R., Auerswald, E. A., Kurz, C., Zink, B., Osterburg, G., et al. (1978). Nucleotide sequence of bacteriophage fd DNA. *Nucleic Acids Res.* 5, 4495–4503. doi: 10.1093/nar/5.12.4495

Brock, T. D., and Freeze, H. (1969). *Thermus aquaticus* gen. n. and sp. n., a non-sporulating extreme thermophile. *J. Bacteriol.* 98, 289–297.

Campos, J., Martínez, E., Izquierdo, Y., and Fando, R. (2010). VEJφ, a novel filamentous phage of *Vibrio cholerae* able to transduce the cholera toxin genes. *Microbiology* 156, 108–115. doi: 10.1099/mic.0.032235-0

Chopin, M. C., Rouault, A., Ehrlich, S. D., and Gautier, M. (2002). Filamentous phage active on the gram-positive bacterium *Propionibacterium freudenreichii*. *J. Bacteriol.* 184, 2030–2033. doi: 10.1128/JB.184.7.2030-2033.2002

Davis, B. M., and Waldor, M. K. (2003). Filamentous phages linked to virulence of *Vibrio cholerae*. *Curr. Opin. Microbiol.* 6, 35–42. doi: 10.1016/S1369-5274(02)00005-X

Day, L. A. (2012). "Family inoviridae," in *Virus Taxonomy: Ninth Report of the International Committee for the Taxonomy of Viruses*, eds A. M. Q. King, M. J. Adams, E. B. Carstens, and E. J. Lefkowitz (Amsterdam: Elsevier Academic Press), 375–383.

Derbise, A., and Carniel, E. (2014). YpfΦ: a filamentous phage acquired by *Yersinia pestis*. *Front. Microbiol.* 5:701. doi: 10.3389/fmicb.2014.00701

Doi, K., Mori, K., Martono, H., Nagayoshi, Y., Fujino, Y., Tashiro, K., et al. (2013). Draft genome sequence of *Geobacillus kaustophilus* GBlys, a lysogenic

strain with bacteriophage φOH2. *Genome Announc.* 1, e00634–e00613. doi: 10.1128/genomeA.00634-13

Faruque, S. M., Bin Naser, I., Fujihara, K., Diraphat, P., Chowdhury, N., Kamruzzaman, M., et al. (2005). Genomic sequence and receptor for the *Vibrio cholerae* phage KSF-1φ: evolutionary divergence among filamentous vibriophages mediating lateral gene transfer. *J. Bacteriol.* 187, 4095–4103. doi: 10.1128/JB.187.12.4095-4103.2005

Fujino, Y., Kawatsu, R., Inagaki, F., Umeda, A., Yokoyama, T., Okaue, Y., et al. (2008). *Thermus thermophilus* TMY isolated from silica scale taken from a geothermal power plant. *J. Appl. Microbiol.* 104, 70–78. doi: 10.1111/j.1365-2672.2007.03528.x

Hassan, F., Kamruzzaman, M., Mekalanos, J. J., and Faruque, S. M. (2010). Satellite phage TLCφ enables toxigenic conversion by CTX phage through dif site alteration. *Nature* 467, 982–985. doi: 10.1038/nature09469

Hill, D. F., and Petersen, G. B. (1982). Nucleotide sequence of bacteriophage f1 DNA. *J. Virol.* 44, 32–46.

Hill, D. F., Short, N. J., Perham, R. N., and Petersen, G. B. (1991). DNA sequence of the filamentous bacteriophage Pf1. *J. Mol. Biol.* 218, 349–364. doi: 10.1016/0022-2836(91)90717-K

Hishinuma, F., Tanaka, T., and Sakaguchi, K. (1978). Isolation of extrachromosomal deoxyribonucleic acids from extremely thermophilic bacteria. *J. Gen. Microbiol.* 104, 193–199. doi: 10.1099/00221287-104-2-193

Huber, K. E., and Waldor, M. K. (2002). Filamentous phage integration requires the host recombinases XerC and XerD. *Nature* 417, 656–659. doi: 10.1038/nature00782

Jalasvuori, M., Jaatinen, S. T., Laurinavicius, S., Ahola-Iivarinen, E., Kalkkinen, N., Bamford, D. H., et al. (2009). The closest relatives of icosahedral viruses of thermophilic bacteria are among viruses and plasmids of the halophilic archaea. *J. Virol.* 83, 9388–9397. doi: 10.1128/JVI.00869-09

Kawai, M., Uchiyama, I., and Kobayashi, I. (2005). Genome comparison *in silico* in *Neisseria* suggests integration of filamentous bacteriophages by their own transposase. *DNA Res.* 12, 389–401. doi: 10.1093/dnares/dsi021

Koonin, E. V. (1992). The second cholera toxin, Zot, and its plasmid-encoded and phage-encoded homologues constitute a group of putative ATPases with an altered purine NTP-binding motif. *FEBS Lett.* 312, 3–6. doi: 10.1016/0014-5793(92)81398-6

Lavigne, R., Ceyssens, P. J., and Robben, J. (2009). Phage proteomics: applications of mass spectrometry. *Methods Mol. Biol.* 502, 239–251. doi: 10.1007/978-1-60327-565-1_14

Lin, L., Han, J., Ji, X., Hong, W., Huang, L., and Wei, Y. (2011). Isolation and characterization of a new bacteriophage MMP17 from *Meiothermus*. *Extremophiles* 15, 253–258. doi: 10.1007/s00792-010-0354-z

Lin, L., Hong, W., Ji, X., Han, J., Huang, L., and Wei, Y. (2010). Isolation and characterization of an extremely long tail *Thermus* bacteriophage from Tengchong hot springs in China. *J. Basic Microbiol.* 50, 452–456. doi: 10.1002/jobm.201000116

Liu, B., Zhou, F., Wu, S., Xu, Y., and Zhang, X. (2009). Genomic and proteomic characterization of a thermophilic *Geobacillus* bacteriophage GBSV1. *Res. Microbiol.* 160, 166–171. doi: 10.1016/j.resmic.2008.12.005

Liu, J., Liu, Q., Shen, P., and Huang, Y. P. (2012). Isolation and characterization of a novel filamentous phage from *Stenotrophomonas maltophilia*. *Arch. Virol.* 157, 1643–1650. doi: 10.1007/s00705-012-1305-z

Loginova, L. G., and Egorova, L. A. (1975). *Thermus ruber* obligate thermophilic bacteria in the thermal springs of Kamchatka. *Mikrobiologiia* 44, 661–665.

Luiten, R. G., Putterman, D. G., Schoenmakers, J. G., Konings, R. N., and Day, L. A. (1985). Nucleotide sequence of the genome of Pf3, an IncP-1 plasmid-specific filamentous bacteriophage of *Pseudomonas aeruginosa*. *J. Virol.* 56, 268–276.

Luo, C. H., Chiou, P. Y., Yang, C. Y., and Lin, N. T. (2012). Genome, integration, and transduction of a novel temperate phage of *Helicobacter pylori*. *J. Virol.* 86, 8781–8792. doi: 10.1128/JVI.00446-12

Marvin, D. A., Symmons, M. F., and Straus, S. K. (2014). Structure and assembly of filamentous bacteriophages. *Prog. Biophys. Mol. Biol.* 114, 80–122. doi: 10.1016/j.pbiomolbio.2014.02.003

Matsushita, I., and Yanase, H. (2009). The genomic structure of *Thermus* bacteriophage φIN93. *J. Biochem.* 146, 775–785. doi: 10.1093/jb/mvp125

Mayor, H. D., and Hill, N. O. (1961). Acridine orange staining of a single-stranded DNA bacteriophage. *Virology* 14, 264–266. doi: 10.1016/0042-6822(61)90202-1

McMaster, G. K., and Carmichael, G. G. (1977). Analysis of single- and double-stranded nucleic acids on polyacrylamide and agarose gels by using glyoxal and acridine orange. *Proc. Natl. Acad. Sci. U.S.A.* 74, 4835–4838. doi: 10.1073/pnas.74.11.4835

Minakhin, L., Goel, M., Berdygulova, Z., Ramanculov, E., Florens, L., Glazko, G., et al. (2008). Genome comparison and proteomic characterization of *Thermus thermophilus* bacteriophages P23-45 and P74-26: siphoviruses with triplex-forming sequences and the longest known tails. *J. Mol. Biol.* 378, 468–480. doi: 10.1016/j.jmb.2008.02.018

Naryshkina, T., Liu, J., Florens, L., Florens, L., Swanson, S. K., Pavlov, A. R., et al. (2006). *Thermus thermophilus* bacteriophage φYS40 genome and proteomic characterization of virions. *J. Mol. Biol.* 364, 667–677. doi: 10.1016/j.jmb.2006.08.087

Nold, S. C., and Ward, D. M. (1995). Diverse *Thermus* species inhabit a single hot spring microbial mat. *Syst. Appl. Microbiol.* 18, 274–278. doi: 10.1016/S0723-2020(11)80398-X

Oshima, T., and Imahori, K. (1971). Isolation of an extreme thermophile and thermostability of its transfer ribonucleic acid and ribosomes. *J. Gen. Appl. Microbiol.* 17, 513–517. doi: 10.2323/jgam.17.513

Overman, S. A., Kristensen, D. M., Bondre, P., Hewitt, B., and Thomas, G. J. Jr. (2004). Effects of virion and salt concentrations on the Raman signatures of filamentous phages fd, Pf1, Pf3, and PH75. *Biochemistry* 43, 13129–13136. doi: 10.1021/bi0485023

Pajunen, M., Kiljunen, S., and Skurnik, M. (2000). Bacteriophage phiYeO3-12, specific for *Yersinia enterocolitica* serotype O:3, is related to coliphages T3 and T7. *J. Bacteriol.* 182, 5114–5120. doi: 10.1128/JB.182.18.5114-5120.2000

Pederson, D. M., Welsh, L. C., Marvin, D. A., Sampson, M., Perham, R. N., Yu, M., et al. (2001). The protein capsid of filamentous bacteriophage PH75 from *Thermus thermophilus*. *J. Mol. Biol.* 309, 401–421. doi: 10.1006/jmbi.2001.4685

Peeters, B. P., Peters, R. M., Schoenmakers, J. G., and Konings, R. N. (1985). Nucleotide sequence and genetic organization of the genome of the N-specific filamentous bacteriophage IKe. Comparison with the genome of the F-specific filamentous phages M13, fd and f1. *J. Mol. Biol.* 181, 27–39. doi: 10.1016/0022-2836(85)90322-5

Prangishvili, D., Forterre, P., and Garrett, R. A. (2006). Viruses of the Archaea: a unifying view. *Nat. Rev. Microbiol.* 4, 837–848. doi: 10.1038/nrmicro1527

Priest, F. G., Goodfellow, M., and Todd, C. (1988). A numerical classification of the genus *Bacillus*. *J. Gen. Microbiol.* 134, 1847–1882. doi: 10.1099/00221287-134-7-1847

Rakonjac, J., Feng, J-N., and Model, P. (1999). Filamentous phage are released from the bacterial membrane by a two-step mechanism involving a short C-terminal fragment of pIII. *J. Mol. Biol.* 289, 1253–1265.

Russel, M., and Model, P. (2006). "Filamentous phage," in *The Bacteriophages, 2nd Edn.*, eds R. C. Calendar and S. T. Abedon (New York, NY: Oxford University Press), 146–160.

Saibi, H., and Ehara, S. (2010). Temperature and chemical changes in the fluids of the Obama geothermal field (SW Japan) in response to field utilization. *Geothermics* 39, 228–241. doi: 10.1016/j.geothermics.2010.06.005

Saiki, T., Kimura, R., and Arima, K. (1972). Isolation and characterization of extremely thermophilic bacteria from hot springs. *Agric. Biol. Chem.* 34, 2357–2366. doi: 10.1271/bbb1961.36.2357

Sakaki, Y., and Oshima, T. (1975). Isolation and characterization of a bacteriophage infectious to an extreme thermophile, *Thermus thermophilus* HB8. *J. Virol.* 15, 1449–1453.

Sambrook, J., and Russell, D. (2001). *Molecular Cloning: A Laboratory Manual, 3rd Edn.* Harbor, CA: Cold Spring Harbor Laboratory Press.

Saul, D. J., Rodrigo, A. G., Reeves, R. A., Williams, L. C., Borges, K. M., Morgan, H. W., et al. (1993). Phylogeny of twenty *Thermus* isolates constructed from 16S rRNA gene sequence data. *Int. J. Syst. Bacteriol.* 43, 754–760. doi: 10.1099/00207713-43-4-754

Shirling, E. B., and Speer, M. (1967). Spot test method for rapid serological grouping of streptomycete bacteriophages. *Appl. Microbiol.* 15, 456–457.

Stassen, A. P., Folmer, R. H., Hilbers, C. W., and Konings, R. N. (1994). Single-stranded DNA binding protein encoded by the filamentous bacteriophage M13: structural and functional characteristics. *Mol. Biol. Rep*. 20, 109–127. doi: 10.1007/BF00990543

Takayama, G., Kosuge, T., Maseda, H., Nakamura, A., and Hoshino, T. (2004). Nucleotide sequence of the cryptic plasmid pTT8 from *Thermus thermophilus* HB8 and isolation and characterization of its high-copy-number mutant. *Plasmid* 51, 227–237. doi: 10.1016/j.plasmid.2004.01.003

Tamakoshi, M., Murakami, A., Sugisawa, M., Tsuneizumi, K., Takeda, S., Saheki, T., et al. (2011). Genomic and proteomic characterization of the large Myoviridae bacteriophage φTMA of the extreme thermophile *Thermus thermophilus*. *Bacteriophage* 1, 152–164. doi: 10.4161/bact.1.3.16712

Tsuboi, M., Benevides, J. M., Bondre, P., and Thomas, G. J. Jr. (2005). Structural details of the thermophilic filamentous bacteriophage PH75 determined by polarized Raman microspectroscopy. *Biochemistry* 44, 4861–4869. doi: 10.1021/bi0479306

van Wezenbeek, P. M., Hulsebos, T. J., and Schoenmakers, J. G. (1980). Nucleotide sequence of the filamentous bacteriophage M13 DNA genome: comparison with phage fd. *Gene* 11, 129–148. doi: 10.1016/0378-1119(80)90093-1

Xue, H., Xu, Y., Boucher, Y., and Polz, M. F. (2012). High frequency of a novel filamentous phage, VCYφ, within an environmental *Vibrio cholerae* population. *Appl. Environ. Microbiol.* 78, 28–33. doi: 10.1128/AEM.06297-11

Yu, M. X., Slater, M. R., and Ackermann, H. W. (2006). Isolation and characterization of *Thermus* bacteriophages. *Arch. Virol.* 151, 663–679. doi: 10.1007/s00705-005-0667-x

Yu, M. X., Slater, M. R., Shultz, J. W., and Ackermann, H. W. (1996). "Isolation and characterization of thermus bacteriophages," *Abstracts of the Xth International Congress of Virology*, Vol. 106 (Jerusalem).

**Conflict of Interest Statement:** The authors declare that the research was conducted in the absence of any commercial or financial relationships that could be construed as a potential conflict of interest.

frontiers in
MICROBIOLOGY

ORIGINAL RESEARCH ARTICLE
published: 01 July 2014
doi: 10.3389/fmicb.2014.00321

# The filamentous phage XacF1 causes loss of virulence in *Xanthomonas axonopodis* pv. *citri*, the causative agent of citrus canker disease

**Abdelmonim Ali Ahmad[1], Ahmed Askora[1,2], Takeru Kawasaki[1], Makoto Fujie[1] and Takashi Yamada[1]***

[1] Department of Molecular Biotechnology, Graduate School of Advanced Sciences of Matter, Hiroshima University, Higashi-Hiroshima, Japan
[2] Department of Microbiology, Faculty of Science, Zagazig University, Zagazig, Sharkia, Egypt

**Edited by:**
*Jasna Rakonjac, Massey University, New Zealand*

**Reviewed by:**
*Bhabatosh Das, Translational Health Science and Technology Institute, India*
*Anne Derbise, Pasteur Institut, France*

***Correspondence:**
*Takashi Yamada, Department of Molecular Biotechnology, Graduate School of Advanced Sciences of Matter, Hiroshima University, 1-3-1 Kagamiyama, Higashi-Hiroshima 739-8530, Japan*
*e-mail: tayamad@hiroshima-u.ac.jp*

In this study, filamentous phage XacF1, which can infect *Xanthomonas axonopodis* pv. *citri* (*Xac*) strains, was isolated and characterized. Electron microscopy showed that XacF1 is a member of the family *Inoviridae* and is about 600 nm long. The genome of XacF1 is 7325 nucleotides in size, containing 13 predicted open reading frames (ORFs), some of which showed significant homology to Ff-like phage proteins such as ORF1 (pII), ORF2 (pV), ORF6 (pIII), and ORF8 (pVI). XacF1 showed a relatively wide host range, infecting seven out of 11 strains tested in this study. Frequently, XacF1 was found to be integrated into the genome of *Xac* strains. This integration occurred at the host *dif* site (*att*B) and was mediated by the host XerC/D recombination system. The *att*P sequence was identical to that of *Xanthomonas* phage Cf1c. Interestingly, infection by XacF1 phage caused several physiological changes to the bacterial host cells, including lower levels of extracellular polysaccharide production, reduced motility, slower growth rate, and a dramatic reduction in virulence. In particular, the reduction in virulence suggested possible utilization of XacF1 as a biological control agent against citrus canker disease.

**Keywords: filamentous phage, loss of virulence, citrus canker, biocontrol**

## INTRODUCTION

*Xanthomonas axonopodis* pv. *citri*, *Xac* (syn. *Xanthomonas campestris* pv. *citri*), is the causative agent of Asiatic citrus canker disease (ACC), one of the most serious citrus plant diseases in the world (Civerolo, 1984; Graham et al., 2004). Under natural conditions, the bacterium can invade all aboveground parts of plants, entering through natural openings and wounds (Brunings and Gabriel, 2003; Vojnov et al., 2010). A characteristic symptoms include raised corky lesions surrounded by a water or oil-soaked margin on leaves, stems, and fruits, including defoliation, twigs dieback, general tree decline, blemished fruit, and premature fruit drop in severely infected trees (Graham et al., 2004). Management of ACC relies on an integrated approach that includes: (1) replacement of susceptible citrus species with resistant ones; (2) production of disease-free nursery stock; (3) reduction of pathogen spread by establishing windbreaks and fences around groves; (4) preventative copper sprays; and (5) application of insecticide to control Asian leafminer. Because of the limited effectiveness of the current integrated management strategies, citrus canker disease continues to be an economically serious problem for field-grown crops worldwide (Balogh et al., 2010). Hence, alternative control methods are necessary.

Bacteriophages have recently been evaluated for controlling a number of phytobacteria and are now commercially available for some diseases (Balogh et al., 2010). The use of phages for disease control is a fast expanding area of plant protection, with great potential to replace existing chemical control measures. Bacteriophages have been used effectively for controlling several diseases caused by *Xanthomonas* species, including, peach bacterial spot, caused by *X. campestris* pv. *pruni*, geranium bacterial blight, caused by *X. campestris* pv. *pelargonii*, tomato bacterial spot caused by *Xanthomonas euvesicatoria* and *Xanthomonas perforans*, and onion leaf blight caused by *X. axonopodis* pv. *allii* (Flaherty et al., 2000; Balogh et al., 2003; Obradovic et al., 2004, 2005; Lang et al., 2007). Major challenges of agricultural use of phages arise from the inherent diversity of target bacteria, high probability of resistance development, and weak phage persistence in the plant environment (Balogh et al., 2008, 2010). Very recently, utilization of filamentous phages as a disease management strategy has been investigated, and application will likely increase in the future (Askora et al., 2009; Addy et al., 2012). The filamentous ϕRSM phages have dramatic effects on the virulence of *Ralstonia solanacearum*. Infection of *R. solanacearum* cells with ϕRSM3 decreased their growth rate, twitching motility, movement in tomato plant stems, extracellular polysaccharide (EPS) production, and *phcA* expression, resulting in loss of virulence (Addy et al., 2012). This strategy using filamentous phage might be expanded to control various diseases, including citrus canker disease. In contrast to lytic phages, filamentous phages do not kill the host cells but establish a persistent association between the host and the phage (Askora et al., 2009; Addy et al., 2012). This is an advantage of filamentous phages to solve the problem of bacteriophages easily inactivated by sunlight UV irradiation (Balogh et al., 2010).

In the current study, we isolated and characterized a novel filamentous phage and showed that changes occurred at a cellular level in *X. axonopodis* pv. *citri* strains following infection. This filamentous phage might be a unique biological agent for use against bacterial citrus canker disease.

## MATERIALS AND METHODS

### BACTERIAL STRAINS AND GROWTH CONDITIONS

Ministry of Agriculture, Forestry, and Fisheries (MAFF) strains of *X. axonopodis* pv. *citri, Xac* (**Table 1**) were obtained from the National Institute of Agrobiological Sciences, Japan. Strain KC33 was obtained from the National Institute of Fruit Tree Science, the National Agriculture and Food Research Organization, Japan. All strains were stored at −80°C in 0.8% nutrient broth (NB) (BBL, Becton Dickinson and Co., Cockeysville, MD, USA) supplemented with 30% (v/v) glycerol. The strains were grown on nutrient agar (NA) medium (Difco, BBLBD, Cockeysville, MD, USA) at 28°C. For preparation of bacterial suspension, *Xac* strains were cultured for 24 h at 28°C with shaking at 220 rpm in NB medium.

For time course experiments, phage-infected and uninfected cells were grown overnight in 5 mL of NB media. Then, 0.5 mL of the cell suspensions ($10^8$ cfu/mL) were transferred into 100-mL flasks containing 30 mL of NB medium. Cultures were grown at 28°C with agitation at 200 rpm, and $OD_{600\,nm}$ measurements were taken every 3 h over the course of 48 h using a spectrophotometer. Three replicates were included at each time point. The experiments were repeated twice (Li and Wang, 2011).

### BACTERIOPHAGE ISOLATION, PURIFICATION, AND CHARACTERIZATION

The presence of filamentous phages in collected soil samples from cropping fields in Japan was detected by the spot test and plaque-forming assay technique (Yamada et al., 2007). Approximately 10 g of soil was placed in a sterile 50 mL conical centrifuge tube that then was filled to the top with tap water, and allowed to stand for 20 min with periodic inversions. The tubes were then centrifuged at 15,000 × g for 20 min and the supernatant was passed through a membrane filter (0.45-μm pore size) (Millipore Corp., Bedford, MA, USA). One-hundred-microliter aliquots of the soil filtrate were subjected to spot test and plaque-forming assay with strains of *Xac* (**Table 1**) as host on NB plates containing 1.5% (w/v) agar. Phages were propagated and purified from single-plaque isolates. An overnight culture of bacteria grown in NB medium (1 mL) was diluted 100-fold with 100 mL of fresh NB medium in a 500 mL flask. To collect a sufficient amount of phage particles, a total of 2 L of bacterial culture was grown. When the cultures reached an $OD_{600}$ of 0.2, bacteriophage was added at a multiplicity of infection (moi) of 0.001–1.0. After further growth for 12–24 h, the cells were removed by centrifugation in a Hitachi Himac CR21E centrifuge with an R12A2 rotor at 8000 × g for 15 min at 4°C. The supernatant was passed through a 0.45-μm-pore membrane filter followed by precipitation of the phage particles in the presence of 0.5 M NaCl and 5% (v/v) polyethylene glycol 6000 (Kanto Chemical Co., Tokyo, Japan). The pellet was collected by centrifugation in a Hitachi Himac CR21E centrifuge with an RPR20-2 rotor at 15 000 × g for 30 min at 4°C, and was dissolved in SM buffer [50 mM Tris/HCl at pH 7.5, 100 mM NaCl, 10 mM $MgSO_4$ and 0.01% gelatin (w/v)]. Phages were stored at 4°C in complete darkness. Phage titers were determined by serial dilution and subsequent plaque-forming assays (Yamada et al., 2007). The purified phage [$10^{13}$ pfu/mL was stained with sodium phosphotungstate prior to observation in a Hitachi H600A electron microscope, according to the methods of Dykstra (1993)].

**Table 1 | Bacterial strains used in this study[a].**

| Strain | Host (Citrus species) | XacF1 sensitivity | Source |
|---|---|---|---|
| ***X.axonopodis* pv. *citri*** | | | |
| MAFF 301077 | *C. limon* | − | NIAS[b] |
| MAFF 301080 | *C. sinensis* | + | NIAS |
| MAFF 311130 | *C. iyo* | − | NIAS |
| MAFF 302102 | *Citrus* sp. | + | NIAS |
| MAFF 673001 | *C. natsudaidai* | + | NIAS |
| MAFF 673010 | *Citrus* sp. | + | NIAS |
| MAFF 673011 | *C. limon* | − | NIAS |
| MAFF 673013 | *Citrus* sp. | + | NIAS |
| MAFF 673018 | *Citrus* sp. | + | NIAS |
| MAFF 673021 | *C. limon* | − | NIAS |
| KC33 | *C. iyo* | + | Shiotani et al., 2007 |
| Phages | | | |
| XacF1 | | | This study |

[a] *All strains originated in Japan.*

[b] *NIAS, National Institute of Agrobiological sciences, Japan.*

### PHAGE SUSCEPTIBILITY AND ADSORPTION ASSAYS

The phage susceptibility assays were based on a standard agar overlay method with dilution series of phage preparations (Yamada et al., 2007; Ahmad et al., 2014). Small turbid plaques, typical of Ff-phages, always appeared at reasonable frequencies depending on input phage titers (usually 300–600 pfu/plate), if the bacterial strain was sensitive to the phage. No spontaneous phages (induced prophages) appeared from either strain tested under usual plaque assay conditions. In the phage adsorption assay, exponentially growing cells ($OD_{600}$ 0.1) of the test strain were mixed with XacF1 phage at moi of 0.1, and the mixture was incubated for 0 min (no adsorption) and 30 min at 28°C to allow binding of the phage to the cell surface. Following centrifugation at 15,000 × g for 5 min at 4°C in a Sakuma SS-1500 microcentrifuge (Sakuma Seisakusho, Tokyo, Japan), the phage titer in the supernatant was determined by a standard plaque assay with the indicator strain (MAFF301080). *Escherichia coli* JM109 was used as a negative control.

### DNA ISOLATION AND MANIPULATION

Standard molecular biological techniques for DNA isolation, digestion with restriction enzymes and other nucleases, and construction of recombinant DNAs were followed, according to Sambrook and Russell (2001). Phage DNA was isolated

from the purified phage particles by phenol extraction. In some cases, extrachromosomal DNA was isolated from phage-infected *Xac* cells by the minipreparation method (Ausubel et al., 1995). Replicative-form (RF) DNA for sequencing was isolated from host bacterial cells infected with XacF1 phage, treated with S1 nuclease, and then shotgun-sequenced by Hokkaido System Science Co. (Sapporo, Japan) using a Roche GS Junior Sequence System. The draft assembly of the obtained sequences was assembled using GS *De novo* Assembler v2.6. The analyzed sequences corresponded to 156 times the final genome size of XacF1 (7325 bp). Computer-aided analysis of the nucleotide sequence data was performed using DNASIS v3.6 (Hitachi Software Engineering Co., Tokyo, Japan). Potential ORFs larger than 80 bp were identified using the online program ORF Finder (http://www.ncbi.nlm.nih.gov/gorf/gorf.html) and the DNASIS program. Sequence alignment was performed using the ClustalW (Larkin et al., 2007) program. To assign possible functions to the ORFs, DDBJ/EMBL/GenBank databases were searched using the FASTA, FASTX, BLASTN, and BLASTX programs (Altschul et al., 1997).

#### DETERMINATION OF *att*L AND *att*R SEQUENCES IN *Xac* MAFF673010

Chromosomal DNA was extracted from *Xac* MAFF673010 after infection with XacF1 and subjected to PCR to amplify fragments containing left and right attachment sites (*att*L and *att*R). The *att*L was amplified using a 29-base forward primer, 5′-TGC GAT CGA GCA GCT TCC CAG TTG GCG AT-3′ (primer P1) and a 30-base reverse primer, 5′-TTC GAT GGT CAC GGT GCC TGT AGT AGA GGC-3′ (primer P2), while *att*R was amplified using a 30-base forward primer, 5′-ATA ATT TGC TTG ACA CCG TGC GCA AGT CGT 3′ (primer P3) and a 28-base reverse primer, 5′-CCT TGA CCG TCA GGG ACT GCA TCA GCC T-3′ (primer P4). The primer sequences were based on the *dif* (*att*B) region sequence of *Xanthomonas citri* subsp. citri Aw12879 (DDBJ accession no. CP003778.1). The PCR products were purified from an agarose gel and subjected to sequencing.

#### SOUTHERN HYBRIDIZATION

Genomic DNA from bacterial cells was prepared by the minipreparation method according to Ausubel et al. (1995). Following digestion with restriction enzyme *Hin*cII, DNA fragments were separated by agarose gel electrophoresis, blotted onto a nylon membrane (Piodyne; Pall Gelman Laboratory, Closter, NJ, USA), hybridized with a probe (the entire XacF1 DNA digested by *Eco*RI), labeled with fluorescein (Gene Images Random Prime labeling kit; Amersham Biosciences, Uppsala, Sweden), and detected with a Gene Images CDP-Star detection module (Amersham Biosciences). Hybridization was performed in buffer containing 5× SSC (0.75 M NaCl, 0.075 M sodium citrate), 0.1% (w/v) sodium dodecyl sulfate (SDS), 5% liquid block, and 5% (w/v) dextran sulfate for 16 h at 65°C. The filter was washed at 60°C in 1× SSC and 0.1% (w/v) SDS for 15 min and then in 0.5× SSC and 0.1% (w/v) SDS for 15 min with agitation, according to the manufacturer's protocol. The hybridization signals were detected by exposing X-ray film (RX-U; Fuji Film, Tokyo, Japan) to the filter.

#### EPS ASSAY

EPS in bacterial culture supernatants was determined quantitatively as described previously (Guo et al., 2010). Briefly, bacterial strains were grown in NB supplemented with 2% (w/v) D-glucose for 24 h at 28°C with shaking at 200 rpm. A 10-mL portion of the culture was collected, and the cells were removed by centrifugation (5000 × g for 20 min). The supernatant was mixed with three volumes of 99% ethanol and the mixture was kept at 4°C for 30 min. To determine the dry weights of EPS, the precipitated EPS was collected by centrifugation and dried at 55°C overnight prior to measurement. Three replicates were used for each strain and the test was repeated three times.

#### MOTILITY ASSAY

Swimming and swarming motilities were examined on NB containing 0.3% (w/v) and 0.7% (w/v) agar (Difco, Franklin Lakes, NJ, USA), respectively. Overnight cultures of bacteria grown in NB were centrifuged at 8000 × g for 2 min at 4°C, washed twice with $ddH_2O$, and resuspended in $ddH_2O$ ($OD_{600} = 1.0$). Two microliters of the suspension were spotted onto NA plates (diameter, 90 mm; containing 20 mL of NA) and incubated at 28°C. The migration zones were measured, and used to evaluate the motility of *Xac* cells (Li and Wang, 2011; Addy et al., 2012). For twitching motility assays, overnight bacterial culture in NB were centrifuged at 8000 × g for 2 min at 4°C, washed twice with $ddH_2O$, resuspended in $ddH_2O$ ($OD_{600} = 1.0$), and spotted on minimal medium (MM) plates (Addy et al., 2012). Plates were incubated at 28°C, and the morphology of the colony edge was observed under a light microscope (100× magnification).

#### PATHOGENICITY ASSAY

After careful washing with tap water, immature fully expanded lemon leaves were sterilized by soaking for 2 min in sodium hypochlorite, followed by rinsing in sterilized water. Leaves were placed on the surface of filter paper with abaxial surfaces facing upwards. Lemon leaves were inoculated with bacterial suspension of *Xac* phage-uninfected and phage-infected strains ($10^8$ cfu/mL in sterile water) using an infiltration or a needle pricking method. The infiltration method was conducted by pushing a needleless syringe containing the bacterial suspension against the surface of a citrus leaf supported by a finger on the opposite side of the leaf. The treated areas were immediately marked following inoculation (Chen et al., 2012). Needle-prick inoculation was performed by pricking the leaves, and droplets (10 μL) of bacterial suspensions were applied to each inoculation site. In both methods, the inoculated leaves were covered with a plastic bag for 48 h to facilitate the infection. Leaves were incubated in a growth chamber at 28°C with a photoperiod of 12 h light and 12 h dark for 4 weeks (Verniére et al., 1998; Li and Wang, 2011; Malamud et al., 2012).

#### PHAGE STABILITY TEST

We used *Xac* strain MAFF301080 because it was free from a XacF1 sequence in the genome. After infection with XacF1, a single colony was isolated and confirmed for its production of phage particles, the presence of XacF1 DNA in the cells by miniprep, and no integration of XacF1 DNA in the chromosome by PCR with a primer set of chromosomal sequences, 5′-ACT CGC TTT

GCA TGA AAT TCG CTA GCG AT-3′ (forward) and 5′-TTC GAT GGT CAC GGT GCC TGT AGT AGA GGC (reverse). After cultivation in NB at 28°C for several generations, random colonies spread on NA plates were picked and subjected to plaque assay, miniprep for XacF1 DNA, and PCR to detect lysogeny with the same primers as above.

### *Nucleotide sequence accession number*

The sequence of the XacF1 genome has been deposited in the DDBJ under accession no. AB910602.

## RESULTS

### ISOLATION, MORPHOLOGY, AND HOST RANGE OF XacF1

A total of 20 phages were isolated from soil samples collected from citrus fields in Japan using a plaque assay on *Xac* strains (see Experimental Procedures), one of which formed small and turbid plaques (designated XacF1). A single plaque of this phage was picked for propagation, purification, and further experiments. Electron micrographs using highly purified phage particles ($10^{13}$ pfu/mL) showed that XacF1 virions have typical filamentous phage features, with a long fibrous shape approximately 600 nm in length (**Figure 1A**). To determine the host range of the phage, *Xac* strains infecting different citrus species were tested for phage susceptibility (**Table 1**). The host range of the XacF1 phage was relatively wide, infecting 7 out of 11 *Xac* strains tested in this study (**Table 1**).

### NUCLEOTIDE SEQUENCE AND GENOMIC ORGANIZATION OF XacF1

The genomic DNA of XacF1 was obtained as a replicative form (RF) from MAFF301080 as a host. XacF1 phage genomic DNA was digested using several restriction enzymes; *Eco*RI digestion produced a single band corresponding to approximately 7.3 kb on an agarose gel (**Figure 1B**, lane 4). The genomic DNA isolated from phage particles was completely digested by S1 nuclease treatment (data not shown), suggesting that the XacF1 genome is a circular single stranded DNA, like those of all other filamentous phages.

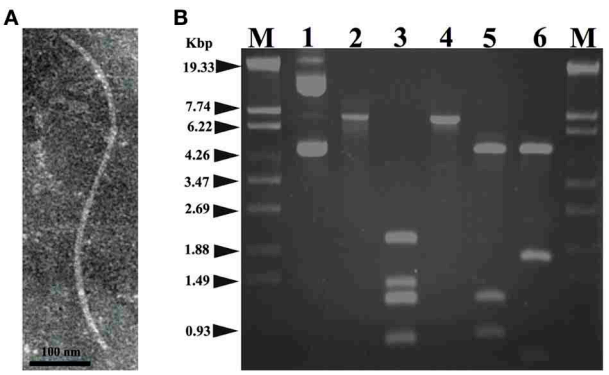


**FIGURE 1 | (A)** Morphology of the XacF1 phage. The purified particles of XacF1 were negatively stained with phosphotungstate and examined by transmission electron microscopy. A filamentous structure was observed (approximately 600 nm in length). **(B)** Restriction patterns of the replicative form of the XacF1 genomic DNA. Lanes: 1, undigested XacF1 DNA (RF); 2, digested with S1 nuclease; 3, *Hin*cII; 4, *Eco*RI; 5, *Eco*RV; 6, *Cla*I; M, λ *Sty*I marker.

To determine the entire nucleotide sequence of XacF1, DNA was shotgun-sequenced. The results showed that the complete genome was 7325 nucleotides long, with a G+C content of 57.8%, which was significantly lower than that of the host genome (i.e., 64.7% for strain 306, accession no. NC_003919). There were 13 putative open reading frames (ORFs), of which 11 were located on the same strand and two were on the opposite strand (**Table 2** and **Figure 2**). When databases were searched for sequences homologous to the XacF1 DNA sequence using BLAST and BLASTX programs, nine ORFs showed high similarity to ORFs previously reported for other filamentous phages, especially to ORFs of *X. campestris* pv. *citri* phage Cf1c (Kuo et al., 1991) (accession no. NC_001396), *X. campestris* pv. *vesicatoria* Cf1 phage (YP_364205.1), and *X. campestris* pv. *campestris* phi-Lf phage (X70328) (**Table 2**). XacF1 ORFs could be arranged in a similar modular structure to that of previously characterized filamentous phages of the Ff group (Model and Russel, 1988; Marvin, 1998), as shown in **Figure 2**. Within the putative replication module (**Figure 2**), we identified ORF1 and ORF2. The peptide encoded by ORF1 was homologous to filamentous phage phi-Lf replication initiation protein II (98% amino acid sequence identity) (**Table 2**). This gene encodes the pII protein, which is necessary for rolling-circle replication of phage genomes (Model and Russel, 1988). The deduced amino acid sequence encoded by ORF2 was homologous to peptides that mapped at the same position as the ssDNA binding protein (gV gene) of Ff phages, and its size was similar to that of this binding protein (**Figure 2** and **Table 2**). Within the putative structural module of XacF1, we predicted five ORFs. ORF3 showed similarity to a hypothetical *Xanthomonas* protein (**Table 2**), with 32% amino acid sequence identity to a transmembrane motif (WP_005416529), supporting the hypothesis that ORF3 belongs to the module of structural genes (**Figure 2**). Moreover, ORF4, ORF5, and ORF7 (**Figure 2** and **Table 2**) were the same size and in the same position as genes encoding the coat proteins of Ff phages. Another possible ORF included in this module was ORF6 (with similarity to coat protein Cf1c phage cp3, Kuo et al., 1991), which was similar in both size and location to *gIII* of the Ff phage. *gIII* encodes *p*III, a minor coat protein that recognizes and interacts with receptors and coreceptors on the host cells (Armstrong et al., 1981; Lubkowski et al., 1999; Heilpern and Waldor, 2003) (**Figure 2** and **Table 2**). It also showed 28% amino acid sequence identity to phage adsorption protein of *Xanthomonas citri* subsp. *citri* (YP_007649573). Therefore, ORF6 could be a homolog of g*III* in XacF1. In the third putative module of XacF1, the assembly module, we found that ORF8 showed the highest homology to the cp4 protein of Cf1c phage (**Figure 2** and **Table 2**), and to the zot protein of *Xanthomonas vesicatoria* (WP_005997731), with 59% amino acid sequence identity. Also, based on its size and position, it seems that ORF8 is a homolog of *p*I. XacF1 does not encode a *p*IV homolog, hence like many filamentous phages it must use a host encoded *p*IV homolog, outer membrane protein of the secretin family. Interestingly, we found that ORF12 might encode a regulator gene similar to those found in several filamentous phages, because amino acids encoded by this ORF exhibited similarity

**Table 2 | Predicted ORFs found in the XacF1 genome.**

| Coding sequence | Strand | Position 5′–3′ | GC content (%) | Length of protein (aa) | Molecular mass (Kda) | Amino acid sequence identity/ similarity to best homologs (no. of amino acid identical; % identity) | *E*-value | Accession no. |
|---|---|---|---|---|---|---|---|---|
| ORF1 | + | 1–1080 | 57.7 | 360 | 40.5 | Filamentous phage phiLf replication initiation protein II (340; 98) | 0.0 | YP_005637352 |
| ORF2 | + | 1077–1373 | 57.3 | 99 | 9.1 | V protein *Xanthomonas* phage Cf1c (73; 99) | 2e-46 | NP_536673 |
| ORF3 | + | 1405–1605 | 51.4 | 67 | 7.2 | Hypothetical protein- *Xanthomonas* (65; 98) | 2e-40 | WP_010378728 |
| ORF4 | + | 1611–1868 | 60.5 | 62 | 8.4 | B coat protein- *Xanthomonas* phage Cf1c (62; 100) | 6e-33 | Q38618 |
| ORF5 | + | 1928–1995 | 55 | 23 | 5.9 | No significant similarity | – | |
| ORF6 | + | 1996–3474 | 55.8 | 493 | 51.7 | A coat protein- *Xanthomonas* phage Cf1c (383; 96) | 0.0 | Q38619 |
| ORF7 | + | 3474–3791 | 54.2 | 106 | 11.5 | Hypothetical protein- *Xanthomonas campestris* (103; 98) | 5e-67 | WP_010378725 |
| ORF8 | + | 3788–4954 | 59.0 | 389 | 42.8 | Hypothetical protein Cf1cp4- *Xanthomonas* phage Cf1c (388; 100) | 0.0 | NP_040477 |
| ORF9 | + | 4954–5601 | 59.4 | 216 | 23.5 | Hypothetical protein Cf1cp5- *Xanthomonas* phage Cf1c (214; 99) | 4e-148 | NP_536676 |
| ORF10 | + | 5617–6009 | 56.6 | 131 | 14.4 | Hypothetical protein Cf1cp6- *Xanthomonas* phage Cf1c (130; 100) | 4e-88 | NP_536677 |
| ORF11 | – | 6047–6430 | 59.7 | 128 | 14.4 | Hypothetical protein Cf1cp7- *Xanthomonas* phage Cf1c (127; 100) | 1e-86 | NP_536678 |
| ORF12 | – | 6427–6885 | 57.6 | 153 | 16.4 | - Filamentous phage Cf1 protein- *Xanthomonas campestris* pv. *vesicatoria* str. 85-10 (146; 90) | 3e-88 | YP_364205 |
| | | | | | | - 18.2K protein- *Xanthomonas* phage Cf1c (164; 99) | 5e-113 | NP_536679 |
| ORF13 | + | 7015–7203 | 54.8 | 63 | 6.8 | Hypothetical protein- *Xanthomonas axonopodis* (59; 95) | 6e-32 | WP_017171337 |

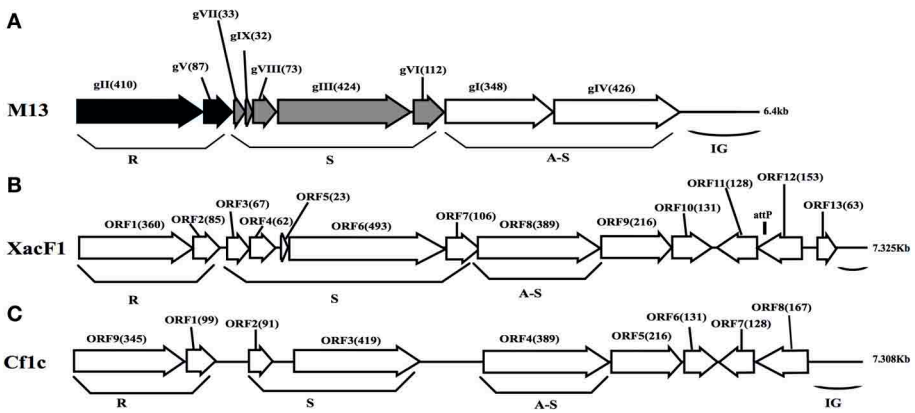


**FIGURE 2 | Genomic organization of bacteriophage XacF1.** Linear genomic maps of *E. coli* phage M13 **(A)**, XacF1 **(B)**, and Cf1c **(C)** are compared. Arrows oriented in the direction of transcription represent ORFs or genes. The functional modules for replication (R), structure (S), and assembly-secretion (A-S) are indicated according to the M13 model (Marvin, 1998). Map for Cf1c was drawn according to the genomic sequence (accession no. NC_001396, Kuo et al., 1991). ORF sizes (in amino acids) are in parentheses. IG (intergenic region), and *att*P are also shown.

to several putative transcriptional regulators and DNA-binding helix-turn-helix proteins of phages (e.g., Cp8 of *X. campestris* pv. *citri* phage Cf1c (99% amino acid identity) (Shieh et al., 1991); phage repressor of *Vibrio parahaemolyticus* V-223/04, exhibiting 45% amino acid identity, EVU16279, *E*-value = 0.71). ORFs 9, 10, 11, and 13 had homology to hypothetical proteins of phages and bacteria, but did not appear to belong to any of the previously described modules.

### XacF1 USES HOST XerCD RECOMBINASES TO INTEGRATE INTO THE *XANTHOMONAS* GENOME

Homology searches of the DDBJ/EMBL/GenBank databases for the XacF1 sequence revealed similar sequences in the genomes of some *Xanthomonas* species. This result suggested possible integration of this kind of phage into the host genome. To test this possibility, we performed genomic Southern blot analysis of 11 strains of *Xac* using a XacF1 DNA probe. The results, shown in **Figure 3A**, indicated that eight of the 11 strains contained hybridizing bands and, among them, seven strains showed similar hybridization patterns with variations in signal intensity. Therefore, XacF1 likely has a lysogenic cycle and integrates frequently into the host genome. Regarding the integration mechanism of XacF1, we could not find any genes or ORFs that encode a phage integrase in the genome (**Table 2**). In several cases, involvement of the host recombination system by XerC/D in integration of filamentous phages into host genomes has been established, including *Vibrio cholerae* phage CTXϕ (Huber and Waldor, 2002; Das et al., 2011). In CTXϕ integration, the *dif* site of the host genome (*att*B) forms a recombination complex with *dif*-like sequences on the phage genome (*att*P) (Val et al., 2005). We therefore looked for a possible *dif*-like sequence for *att*P on the XacF1 sequence and found a 15-bp *dif* core sequence of

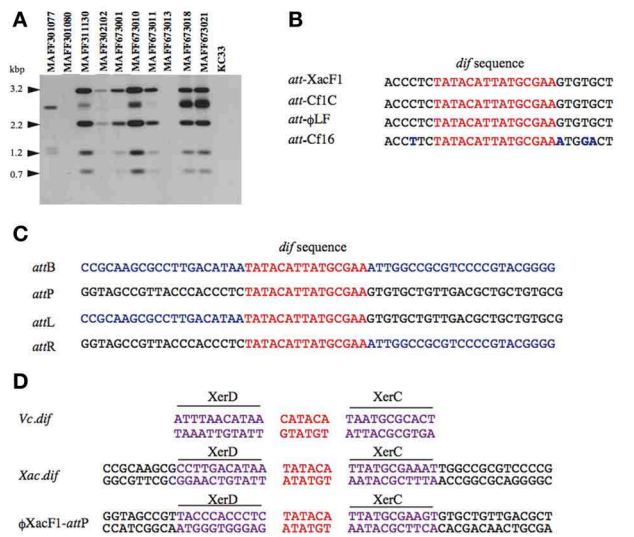


**FIGURE 3 | Site specific integration of XacF1 DNA into the chromosome of *Xac*. (A)** Southern blot hybridization analysis showing integration of the XacF1 phage into *Xac* host chromosomes. Genomic DNA of *X. axonopodis* pv. *citri* strains was digested with *Hin*cII and hybridized with a probe (the entire XacF1 phage genomic DNA digested with *Eco*RI). **(B)** The *att*P sequence indicated for XacF1 is compared with *att*P sequences (putative in some cases) of filamentous phages, including Cf1c (accession no. NC_001396), Cf16-v1 (M23621), and Lf (X70328) phages of *X. campestris*. The *dif* core sequences are shown in red. Changed nucleotides are shown in blue. **(C)** Alignment of *att* sequences in the XacF1 integration system. The *att*L and *att*R sequences were determined for a lysogenic strain newly established with *Xac* MAFF673010 infected with XacF1. The *att*B sequence (*dif*) of *X. axonopodis* pv. *citri* 306 was obtained from the genome database (accession no. AE008923.1, Jalan et al., 2011). Common 15 bases are shown in red and chromosomal sequences are in blue. **(D)** Putative XerC, XerD binding sites of the XacF1 system are compared with those of *Vibrio cholerae dif*1.

5′-TAT ACA TTA TGC GAA (XacF1 positions 6504–6518). This sequence showed a high degree of homology to *att*P sequences of phages Cf1c (accession no. NC_001396) (Kuo et al., 1991), Cf16-v1 (M23621), ϕLf (X70328), CTXϕ (AΦ220606), and ϕVGJ (AY242528) (**Figure 3B**). It was also reported that Cf1c, Cf1t, Cf16v1, and ϕLf phages of *X. campestris* use the XerCD recombinases of their host to integrate into the *dif* locus of the bacterial genome (Campos et al., 2003; de Mello Varani et al., 2008; Askora et al., 2012; Das et al., 2013). These results suggested that the filamentous phage XacF1 uses the host XerC/D system for integration into the host genome. To confirm this, we obtained both *att*L and *att*R fragments by PCR from newly established XacF1-lysogenic cells of *X. axonopodis* pv. *citri* strain MAFF673010. The *att*L and *att*R sequences are aligned with XacF1 *att*P and *dif* of *X. axonopodis* pv. *citri* strain 306 (accession no. AE008923.1, Jalan et al., 2011) in **Figure 3C**. From these results, we predicted XerCD binding sites according to Das et al. (2011) as shown in **Figure 3D**. However, XacF1 *att*P is located within the coding region of ORF12, so following integration into *att*B of the host chromosome, ORF12 may be split into two portions. This change in ORF12 may affect XacF1 functions because ORF12 encodes a possible phage regulator, as described above.

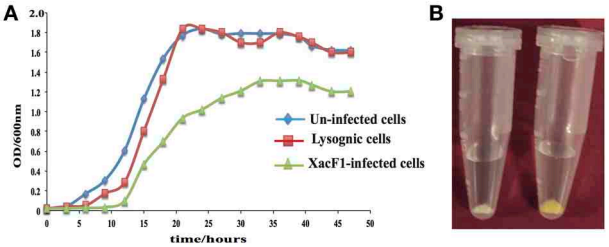


**FIGURE 4 | (A)** Effects of XacF1 infection on the growth of *X. axonopodis* pv. *citri* (MAFF301080). **(B)** Effects of XacF1 infection on EPS production. The pellet of uninfected *Xac* MAFF301080 cells (right) was yellow, while the pellet of XacF1-infected cells (left) was white, indicating a defect in xanthan production.

### EFFECTS OF XacF1 INFECTION ON THE GROWTH RATE OF *X. AXONOPODIS* PV. *CITRI*

Unlike other bacterial viruses, the Ff phages do not kill their hosts, but establish a persistent coexistence in which new virions are continually released (Model and Russel, 1988). Because of this non-lytic mode of viral replication, it is possible to grow high-titer cultures of the virus. Similarly, infection by XacF1 did not cause lysis of host cells, but established a persistent association between the host and phage, releasing phage particles from the growing host cells. Although cells infected with XacF1 could continue to grow and divide indefinitely, the process caused the infected cells to grow at a significantly lower rate than uninfected cells (**Figure 4A**).

### EFFECT OF XacF1 INFECTION ON HOST EPS PRODUCTION

EPS production was compared between uninfected and XacF1-infected cells of strain MAFF301080. The XacF1-infected cells used in this experiment were confirmed to be free from prophage by plaque assay of the culture supernatant, Southern hybridization (**Figure 3A**), and PCR. The amount of EPS produced by the infected cells was significantly lower than that of the wild-type cells. We observed that following centrifugation, the culture pellets of the infected cells turned white, reflecting a low production of xanthan, which is the major component of EPS and is responsible for the yellow color of *Xanthomona*s culture in the media (**Figure 4B**). Our prediction was confirmed by an EPS quantitation assay, which showed that the XacF1-infected cells had significantly lower EPS production (0.6 mg/ $10^{10}$ cfu) than uninfected cells (3.35 mg/ $10^{10}$ cfu).

### EFFECT OF XacF1 INFECTION ON HOST MOTILITY

Swimming, swarming, and twitching motilities of uninfected and XacF1-infected cells of strain MAFF301080 were compared. A significant reduction in swimming and swarming motility was observed in XacF1-infected cells (**Figures 5A–D**). When visualized with a microscope, the colony margin of uninfected cells had a highly irregular shape, indicating proficient twitching motility, whereas the colony edge of XacF1-infected cells was smooth (**Figure 5E**), suggesting a decrease or loss of twitching motility. Because twitching motility is the surface movement associated with type IV pili (Marques et al., 2002; Meng et al., 2005),

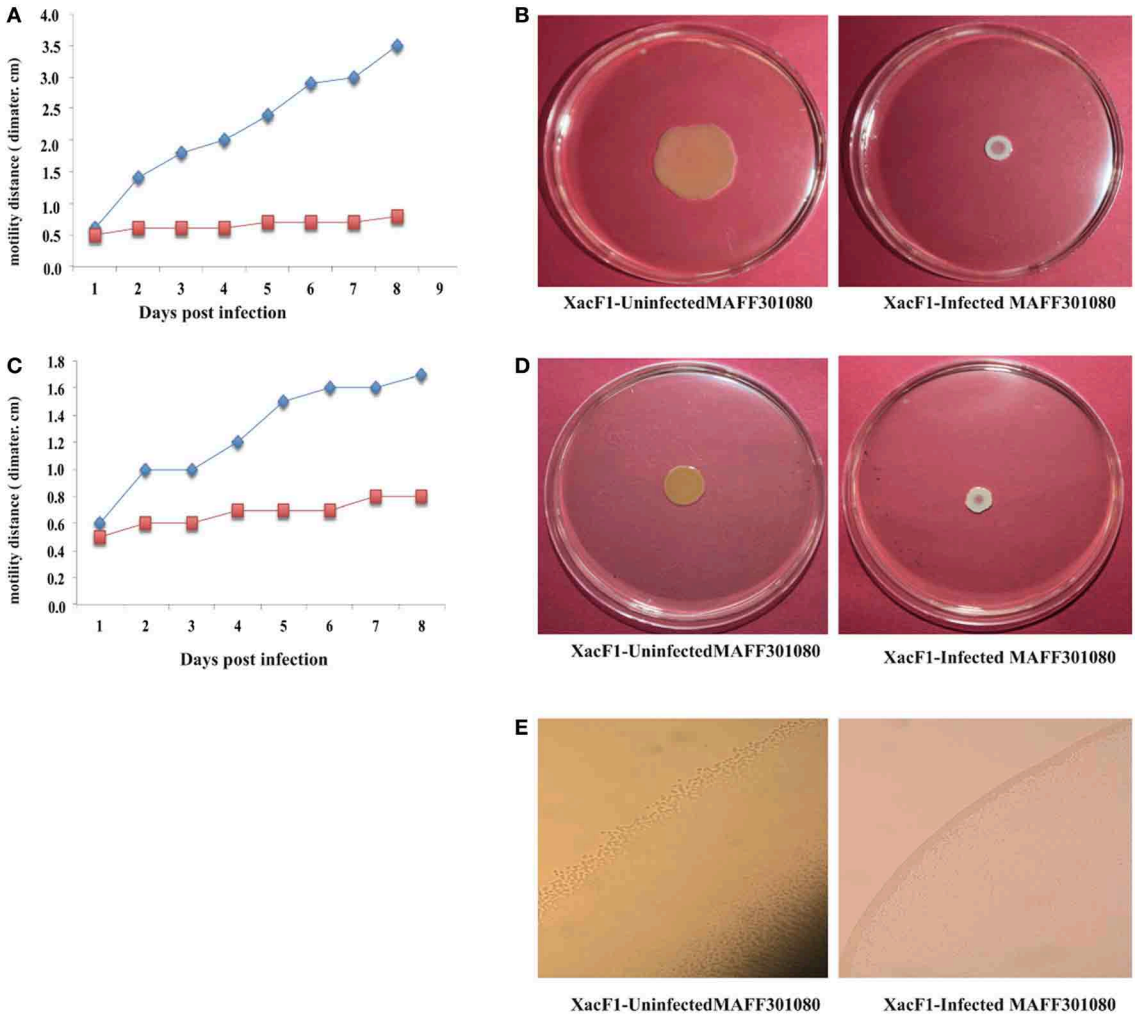


**FIGURE 5 | Impact of XacF1 infection on the motility of *Xac* MAFF301080 cells.** Two microliters of bacterial solution [$10^8$ colony forming units (CFU)/mL] were inoculated in the swimming assay [0.3% (w/v) agar] **(A,B)**, swarming assay [0.7% (w/v) agar] **(C,D)**, and twitching motility assay (minimal agar medium) **(E)**. The movement of bacterial cells was photographed 5 and 8 days post-inoculation (dpi) on the swimming and swarming plates, respectively. Twitching motility of bacteria was observed under a microscope 5 dpi on the twitching plates.

XacF1 infection may have affected the type IV pilus structures and/or functions of the host cells. We examined whether cell surface structural components were affected by XacF1 infection. Cell surface structure proteins were prepared by passing bacterial cells through a hypodermic needle, separated by SDS-PAGE, and compared between XacF1-infected and uninfected cells. XacF1-infected cells had considerably decreased levels of PilA, the major component of type IV pili, and decreased levels of FilC, flagellin (Supplemental Figure S1).

### EFFECTS OF XacF1 INFECTION ON VIRULENCE OF *X. AXONOPODIS* PV. *CITRI*

Wild-type cells of strain MAFF301080 caused infection symptoms 4 days post-infection, and formed clear cankers 1 week post-inoculation (**Figure 6A**). Starting from 2 weeks post-infection, the lesion became brown in color and its center became raised and spongy or corky, typical canker symptoms (Graham et al., 2004) that reflected the aggressive virulence of this strain. In contrast, the symptoms of XacF1-infected MAFF301080 cells were relatively weak, and no mature canker symptoms were observed up to 4 weeks post-infection, except for marginal lesions formed around the pricking site (**Figure 6A**). To be more precise, we measured lesion size (**Figure 6B**), which showed that in uninfected cells, the lesions were large with a smooth center, spongy raised top, and their distribution around the infected area reached more than 6.5 mm in width 4 weeks post-infection. In contrast, the lesions formed by XacF1-infected cells remained weak and dry, and they did not expand more than 1 mm in width. Another inoculation method, in which we infiltrated the bacterial suspension into the lemon leaves, showed that XacF1-uninfected MAFF301080 cells incurred water soaking at the inoculation site 3 days post-infection, and then an erumpent tissue reaction was obvious 1 week after inoculation. The erumpent tissue expanded to an aggressive canker area on both sides of the leaf, and then

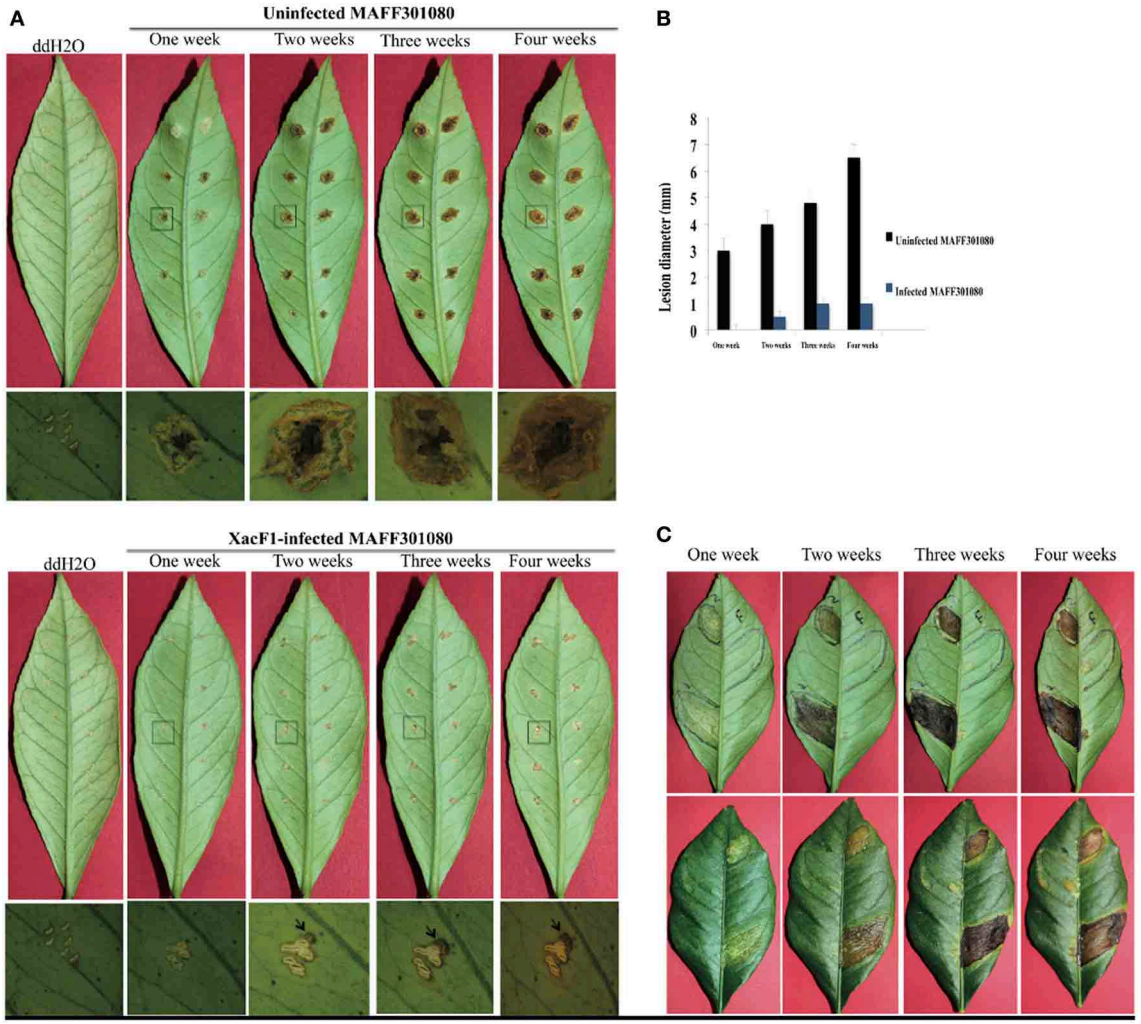


**FIGURE 6 | Lesions on detached lemon leaves inoculated with cells of *Xac* MAFF301080. (A)** Canker symptoms that had developed on leaves 1, 2, 3, and 4 weeks post-infection by the needle-pricking method. Leaves were inoculated with uninfected cells (upper panels) or XacF1-infected cells (lower panels). Leaf areas shown by a square were examined by photomicroscopy and the microscopic images are shown under each corresponding leaf. Characteristic canker lesions occurred with uninfected cells, while no obvious cankers developed on XacF1-infected cells. **(B)** Comparison of the size of lesions formed on lemon leaves. **(C)** Lesions formed on lemon leaves by infiltration of bacterial cells. Uninfected MAFF301080 cells were applied to two areas of the leaf (left half of the abaxial side), and XacF1-infected cells were similarly applied to the right side (upper panels). Lesions on the axial side are also shown in lower panels. Lesions on both lower and upper surfaces of leaves inoculated with the uninfected cells showed severe symptoms, expanding with time. No lesions formed on either surface of the leaves infected with XacF1-infected cells.

the lesions became dark and decayed with a yellow halo at the inoculation site 4 weeks post-infection (**Figure 6C**). However, in XacF1-infected cells, a slight water-soaking area on the leaf surface was only visible 2 weeks after inoculation, and weak canker symptoms could be seen 4 weeks post-infection. In all cases, leaves inoculated with $ddH_2O$ showed no canker symptoms.

## DISCUSSION

In this study, we isolated and characterized a filamentous phage, named XacF1, that infects *X. axonopodis* pv. *citri* strains. The isolated phage had a relatively wide range of host bacterial strains. Of particular interest, this study showed that along with the phage infection, the infected cells had decreased ability to form citrus cankers and a loss of virulence. We demonstrated that the canker symptoms of XacF1-infected lemon leaves were dramatically mitigated up to 4 weeks post-infection using both pricking and infiltration methods of inoculation (**Figures 6A–C**). The significant reduction in EPS (xanthan) production caused by XacF1 phage could be one of the reasons for such a dramatic decrease in canker formation. Virulence of numerous phytopathogenic bacteria, particularly various *Xanthomonas* species, is correlated with their ability to produce EPS (Dolph et al., 1988; Bellemann and Geider, 1992; Kao et al., 1992; Chou et al., 1997; Katzen et al., 1998; Dharmapuri and Sonti, 1999; Yu et al., 1999; Kemp et al., 2004). The multiple functions of EPS in virulence include protection of bacteria from toxic plant compounds, reduction

of bacterial contact with plant cells to minimize host defense responses, promotion of bacterial multiplication by prolonging water soaking of tissues, and supporting invasion or systemic colonization of bacterial cells (Denny, 1999). Another possible role of EPS is to confer epiphytic fitness. It was previously suggested that EPS functions during both epiphytic and pathogenic phases of infection in *X. campestris* pv. *campestris* (Poplawsky and Chun, 1998; Rigano et al., 2007). As significant differences in virulence were observed between wild-type and xanthan-deficient mutant strains of other *Xanthomonas* species, Dunger et al. (2007) proposed that in citrus canker, xanthan supports epiphytic survival in citrus canker, but is not required for colonizing nearby tissue. Without xanthan the bacteria were unable to retain water and could not withstand abiotic stress and, thus, could not survive on the leaf surface. Therefore, xanthan works in two ways: to enhance bacterial virulence and to block the host defense. The drastic reduction in host EPS production caused by XacF1 infection may explain why the XacF1-infected cells showed dramatically decreased virulence.

Another major finding is the significant reduction in the swimming, swarming, and twitching motilities of *Xac* cells following infection by XacF1. Bacteria use a variety of motility mechanisms to colonize host tissues. These mechanisms include flagella-dependent swimming and swarming for movement in liquid surfaces, and flagella-independent twitching, gliding, and sliding for movement on solid surfaces (O'Toole and Kolter, 1998; Mattick, 2002; Harshey, 2003). Recent reports propose that bacterial adhesion and motility are required in the initial stages of *Xac* biofilm formation, whereas lipopolysaccharide and EPS play important roles in the establishment of mature biofilms (Li and Wang, 2011). The reduction in motility of XacF1-infected cells may be because filamentous phages such as XacF1 assemble on the host cell membrane and protrude from the cell surface, and so the nature of the host cell surface may change drastically during phage production (Addy et al., 2012). As shown in Supplemental Figure S1, XacF1-infected cells had considerably decreased levels of PilA, the major component of type IV pili.

Frequent protrusion of XacF1 particles from the infected cell surface may somehow compete with the formation of type four pili (Tfp). As reported by Kang et al. (2002), Tfp is responsible for twitching motility and adherence to multiple surfaces and is required for virulence. Interestingly, ORF 9 of the XacF1 phage (**Table 2**) showed significant homology to a TraX family protein (H8FlE6, *E*-value = 1e-70) and a putative F pilin acetylation protein (Q3BsT0, *E*-value = 4e-70), involved in pilus modification. Therefore, the loss of virulence in the XacF1-infected cells seems to be, at least partly, caused by the reduction or modification of Tfp formation and decrease in swimming, swarming, and twitching motilities.

Several works have described the use of phages for control of bacterial citrus canker caused by *X. campestris* pv. *citri* (Balogh et al., 2010). In those cases, the bacteriophages used for foliar plant diseases interacted with the target bacteria on the leaf surface, the phylloplane. The phylloplane is a constantly changing environment: there are changes in temperature, sunlight irradiation, leaf moisture, relative humidity, osmotic pressure, pH, microbial flora, and, in the case of agricultural plants, chemical compounds (Jones et al., 2012). These factors may be harmful to bacteriophages to varying extents. Sunlight irradiation, especially in the UVA and -B range, is mainly responsible for eliminating bacteriophages within hours of application (Jones et al., 2012). To avoid quick inactivation of XacF1, we propose the application of XacF1-infected cells instead of XacF1 phage alone. The XacF1-infected cells can grow and continue to produce infectious phage, so the XacF1 phage may serve as an efficient long-lasting tool to control citrus canker by decreasing the virulence of the pathogen. Concerning the stability of XacF1-infected cells, we observed relatively high stability of "a free phage state" in the infected cells. After several bacterial generations, 100% cells contained XacF1 and more than 70% of them were at the state of producing free phages without integration into the host chromosome (confirmed by PCR) (data not shown). Even if once prophage states were established, we observed frequent spontaneous excision and production of phage particles.

Another possible way to use XacF1 for biological control may be given as a phage cocktail with other lytic phages, such as Cp1 and Cp2, originating from Japan, which can infect more than 97% of *Xac* strains and was recently characterized by Ahmad et al. (2014).

## ACKNOWLEDGMENT

This study was supported in part by a Japanese Society for the Promotion of Science KAKENHI grant 25.03086 to Ahmed Askora.

## SUPPLEMENTARY MATERIAL

The Supplementary Material for this article can be found online at: http://www.frontiersin.org/journal/10.3389/fmicb.2014.00321/abstract

## REFERENCES

Addy, H. S., Askora, A., Kawasaki, T., Fujie, M., and Yamada, T. (2012). Loss of Virulence of the phytopathogen *Ralstonia solanacearum* through infection by ϕRSM filamentous Phages. *Phytopathology* 102, 469–477. doi: 10.1094/PHYTO-11-11-0319-R

Ahmad, A. A., Ogawa, M., Kawasaki, T., Fujie, M., and Yamada, T. (2014). Characterization of bacteriophages Cp1 and Cp2, the strain typing agents for *Xanthomonas axonopodis* pv. *citri*. *Appl. Environ. Microbiol.* 80, 77–85. doi: 10.1128/AEM.02310-13

Altschul, S. F., Madden, T. L., Schaffer, A. A., Zhang, Z., Miller, W., and Lipman, D. J. (1997). Gapped BLAST and PSI-BLAST: a new generation of protein database search programs. *Nucleic Acids Res.* 25, 3389–3402. doi: 10.1093/nar/25.17.3389

Armstrong, J., Perharm, R. N., and Walker, J. E. (1981). Domain structure of bacteriophage fd adsorption protein. *FEBS Lett.* 135, 167–172. doi: 10.1016/0014-5793(81)80969-6

Askora, A., Abdel-Haliem, M. E., and Yamada, T. (2012). Site-specific recombination systems in filamentous phages. *Mol. Genet. Genomics* 287, 525–530. doi: 10.1007/s00438-012-0700-1

Askora, A., Kawasaki, T., Usami, S., Fujie, M., and Yamada, T. (2009). Host recognition and integration of filamentous phage ϕRSM in the phytopathogen, *Ralstonia solanacearum*. *Virology* 384, 69–76. doi: 10.1016/j.virol.2008.11.007

Ausubel, F., Brent, R., Kjngston, R. E., Moore, D. D., Seidman, J. G., Smith, J. A., et al. (1995). *Short Protocols in Molecular Biology*. 3rd Edn. Hoboken, NJ: John Wiley & Sons, Inc.

Balogh, B., Canteros, B. I., Stall, R. E., and Jones, J. B. (2008). Control of citrus canker and citrus bacterial Spot with Bacteriophages. *Plant Dis.* 92, 1048–1052. doi: 10.1094/PDIS-92-7-1048

Balogh, B., Jones, J. B., Iriarte, F. B., and Momol, M. T. (2010). Phage therapy for plant disease control. *Curr. Pharm. Biotechnol*. 11, 48–57. doi: 10.2174/138920110790725302

Balogh, B., Jones, J. B., Momol, M. T., Olson, S. M., Obradovic, A., King, P., et al. (2003). Improved efficacy of newly formulated bacteriophages for management of bacterial spot on tomato. *Plant Dis*. 87, 949–954. doi: 10.1094/PDIS.2003.87.8.949

Bellemann, P., and Geider, K. (1992). Localization of transposon insertions in pathogenicity mutants of *Erwinia amylovora* and their biochemical characterization. *J. Gen. Microbiol.* 138, 931–940. doi: 10.1099/00221287-138-5-931

Brunings, A., and Gabriel, D. (2003). *Xanthomonas citri*: breaking the surface. *Mol. Plant Pathol*. 4, 141–157. doi: 10.1046/j.1364-3703.2003.00163.x

Campos, J., Martinez, E., Suzarte, E., Rodriguez, B. L., Marrero, K., Silva, Y., et al. (2003). VGJϕ, a novel wlamentous phage of *Vibrio cholerae*, integrates into the same chromosomal site as CTXϕ. *J. Bacteriol.* 185, 5685–5696. doi: 10.1128/JB.185.19.5685-5696.2003

Chen, P. S., Wang, L. Y., Chen, Y. J., Tzeng, K. C., Chang, S. C., Chung, K. R., et al. (2012). Understanding cellular defence in kumquat and calamondin to citrus canker caused by *Xanthomonas citri* subsp. *citri. Physiol. Mol. Plant Pathol*. 79, 1–12. doi: 10.1016/j.pmpp.2012.03.001

Chou, F. L., Chou, H. C., Lin, Y. S., Yang, B. Y., Lin, N. T., Weng, S. F., et al. (1997). The *Xanthomonas campestris gum*D gene required for synthesis of xanthan gum is involved in normal pigmentation and virulence in causing Black rot. *Biochem. Biophys. Res. Commun.* 233, 265–269. doi: 10.1006/bbrc.1997.6365

Civerolo, E. (1984). Bacterial canker disease of citrus. *J. Rio Grande Valley Hort. Soc*. 37, 127–146.

Das, B., Bischerour, J., and Barre, F. X. (2011). VGJϕ integration and excision mechanisms contribute to the genetic diversity of *Vibrio cholerae* epidemic strains. *Proc. Natl. Acad. Sci. U.S.A.* 108, 2516–2521. doi: 10.1073/pnas.1017061108

Das, B., Martiìnez, E., Midonet, C., and Barre, F. X. (2013). Integrative mobile elements exploiting Xer recombination. *Trends Microbiol*. 1, 23–30. doi: 10.1016/j.tim.2012.10.003

de Mello Varani, A., Souza, R. C., Nakaya, H. I., de Lima, W. C., de Almeid, P., Watabnabe-Kitajima, E., et al. (2008). Origins of the *Xylella fastidiosa* prophage-like regions and their impact in genome differentiation. *PLoS ONE* 3:e4059. doi: 10.1371/journal.pone.0004059

Denny, T. P. (1999). Autoregulator-dependent control of extracellular polysaccharide production in phytopathogenic bacteria. *Eur. J. Plant Pathol.* 105, 417–430. doi: 10.1023/A:1008767931666

Dharmapuri, S., and Sonti, R. V. (1999). A transposon insertion in the gumG homologue of *Xanthomonas oryzae* pv. *oryzae* causes loss of extracellular polysaccharide production and virulence. *FEMS Microbiol. Lett*. 179, 53–59. doi: 10.1111/j.1574-6968.1999.tb08707.x

Dolph, P. J., Majerczak, D. R., and Coplin, D. L. (1988). Characterization of a gene cluster for exopolysaccharide biosynthesis and virulence in *Erwinia stewartii*. *J. Bacteriol*. 170, 865–871.

Dunger, G., Relling, V. M., Tondo, M. L., Barreras, M., Ielpi, L., Orellano, E. G., et al. (2007). Xanthan is not essential for pathogenicity in citrus canker but contributes to Xanthomonas epiphytic survival. *Arch. Microbiol.* 188, 127–135. doi: 10.1007/s00203-007-0227-8

Dykstra, M. J. (1993). *A Manual of Applied Technique for Biological Electron Microscopy*. New York, NY: Plenum Press. doi: 10.1007/978-1-4684-0010-6

Flaherty, J. E., Jones, J. B., Harbaugh, B. K., Somodi, G. C., and Jackson, L. E. (2000). Control of bacterial spot on tomato in the greenhouse and field with H-mutant bacteriophages. *HortScience* 35, 882–884.

Graham, J. H., Gottwald, T. R., Cubero, J., and Achor, D. S. (2004). *Xanthomonas axonopodi*s pv. *citri*: factors affecting successful eradication of citrus canker. *Mol. Plant Pathol*. 5, 1–15. doi: 10.1046/j.1364-3703.2004.00197.x

Guo, Y., Sagaram, U. S., Kim, J. S., and Wang, N. (2010). Requirement of the galU gene for polysaccharide production by and pathogenicity and growth in planta of *Xanthomonas citri* subsp. *citri. Appl. Environ. Microbiol*. 76, 2234–2242. doi: 10.1128/AEM.02897-09

Harshey, R. M. (2003). Bacterial motility on a surface: many ways to a common goal. *Annu. Rev. Microbiol.* 57, 249–273. doi: 10.1146/annurev.micro.57.030502.091014

Heilpern, A. J., and Waldor, M. K. (2003). pIIICTX, a predicted CTX phi minor coat protein, can expand the host range of coliphage fd to include *Vibrio cholerae*. *J. Bacteriol.* 185, 1037–1044. doi: 10.1128/JB.185.3.1037-1044.2003

Huber, K. E., and Waldor, M. K. (2002). Filamentous phage integration requires the host recombinases XerC and XerD. *Nature* 417, 656–659. doi: 10.1038/nature00782

Jalan, N., Aritua, V., Kumar, D., Yu, F., Jones, J. B., Graham, J. H., et al. (2011). Comparative genomic analysis of *Xanthomonas axonopodis* pv. *citrumelo* F1, which causes citrus bacterial spot disease and related strains provides insights into virulence and host specificity. *J. Bacteriol.* 14, 6342–6357. doi: 10.1128/JB.05777-11

Jones, J. B., Vallad, G. E., Iriarte, F. B., Obradovic, A., Wernsing, M. H., Jackson, L. E., et al. (2012). Considerations for using bacteriophages for plant disease control. *Bacteriophage* 2, 208–214. doi: 10.4161/bact.23857

Kang, Y., Liu, H., Genin, S., Schell, M. A., and Denny, T. P. (2002). *Ralstonia solanacearum* requires type 4 pili to adhere to multiple surfaces and for natural transformation and virulence. *Mol. Microbiol*. 46, 427–437. doi: 10.1046/j.1365-2958.2002.03187.x

Kao, C. C., Barlow, E., and Sequeira. L. (1992). Extracellular polysaccharide is required for wild-type virulence of *Pseudomonas solanacearum. J. Bacteriol.* 174, 1068–1071.

Katzen, F., Ferreiro, D., Oddo, C., Ielmini, M. V., Becker, A., Puhler, A., et al. (1998). *Xanthomonas campestris* pv. *campestris* gum mutants: effects on xanthan biosynthesis and plant virulence. *J. Bacteriol.* 180, 1607–1617.

Kemp, B. P., Horne, J., Bryant, A., and Cooper, R. M. (2004). *Xanthomonas axonopodis* pv. *manihotis gum*D gene is essential for EPS production and pathogenicity and enhances epiphytic survival on cassava (Manihotesculenta). *Physiol. Mol. Plant Pathol*. 64, 209–218. doi: 10.1016/j.pmpp.2004.08.007

Kuo, T. T., Tan, M. S., Su, M. T., and Yang, M. K. (1991). Complete nucleotide sequence of filamentous phage Cf1c from *Xanthomonas campestris* pv. *citri. Nucleic Acids Res*. 19, 2498. doi: 10.1093/nar/19.9.2498

Lang, J. M., Gent, D. H., and Schwartz, H. F. (2007). Management of *Xanthomonas* leaf blight of onion with bacteriophages and a plant activator. *Plant Dis*. 91, 871–878. doi: 10.1094/PDIS-91-7-0871

Larkin, M. A., Blackshields, G., Brown, N. P., Chenna, R., McGettigan, P. A., McWilliam, H., et al. (2007). Clustal W and Clustal X version 2.0. *Bioinformatics* 23, 2947–2948. doi: 10.1093/bioinformatics/btm404

Li, J., and Wang, N. (2011). The *wxac*O gene of *Xanthomonas citri* ssp. *citri* encodes a protein with a role in lipopolysaccharide biosynthesis, biofilm formation, stress tolerance and virulence. *Mol. Plant. Pathol.* 1, 381–396. doi: 10.1111/j.1364-3703.2010.00681.x

Lubkowski, J., Hennecke, F., Puckthun, A., and Wlodawer. A. (1999). Filamentous phage infection: crystal structure of g3p in complex with its coreceptor, the C-terminal domain of TolA. *Structure* 7, 711–722. doi: 10.1016/S0969-2126(99)80092-6

Malamud, F., Conforte, V. P., Rigano, L. A., Castagnaro, A. P., Marano, M. R., Morais do Amaral, A., et al. (2012). *hrpM* is involved in glucan biosynthesis, biofilm formation and pathogenicity in *Xanthomonas citri* ssp. *citri. Mol. Plant Pathol.* 13, 1010–1018. doi: 10.1111/j.1364-3703.2012.00809.x

Marques, L. L. R., Ceri, H., Manfio, G. P., Reid, D. M., and Olsen, M. E. (2002). Characterization of biofilm formation by *Xylella fastidiosa in vitro*. *Plant Dis*. 86, 633–638. doi: 10.1094/PDIS.2002.86.6.633

Marvin, D. A. (1998). Filamentous phage structure, infection and assymply. *Curr. Opin. Struct. Biol*. 8, 150–158. doi: 10.1016/S0959-440X(98)80032-8

Mattick, J. S. (2002). Type IV pili and twitching motility. *Annu. Rev. Microbiol*. 56, 289–314. doi: 10.1146/annurev.micro.56.012302.160938

Meng, Y., Li, Y., Galvani, C. D., Hao, G., Turner, J. N., Burr, T. J., et al. (2005). Upstream migration of *Xylella fastidiosa* via pilus-driven twitching motility. *J. Bacteriol.* 187, 5560–5567. doi: 10.1128/JB.187.16.5560-5567.2005

Model, P., and Russel, M. (1988). "Filamentous bacteriophage," in *The Bacteriophages,* Vol. 2, ed R. Calendar (New York, NY: Plenum Publishing Corporation), 375–456.

Obradovic, A., Jones, J. B., Momol, M. T., Balogh, B., and Olson, S. M. (2004). Management of tomato bacterial spot in the field by foliar applications of bacteriophages and SAR inducers. *Plant Dis*. 88, 736–740. doi: 10.1094/PDIS.2004.88.7.736

Obradovic, A., Jones, J. B., Momol, M. T., Olson, S. M., Jackson, L. E., Balogh, B., et al. (2005). Integration of biological control agents and systemic acquired resistance inducers against bacterial spot on tomato. *Plant Dis*. 89, 712–716. doi: 10.1094/PD-89-0712

O'Toole, G. A., and Kolter, R. (1998). Flagellar and twitching motility are necessary for *Pseudomonas aeruginosa* biofilm development. *Mol. Microbiol.* 30, 295–304. doi: 10.1046/j.1365-2958.1998.01062.x

Poplawsky, A. R., and Chun, W. (1998). *Xanthomonas campestris* pv. *campestris* requires a functional *pigB* for epiphytic survival and host infection. *Mol. Plant Microbe. Interact.* 11, 466–475. doi: 10.1094/MPMI.1998.11.6.466

Rigano, L. A., Payette, C., Brouillard, G., Marano, M. R., Abramowicz, L., Torres, P. S., et al. (2007). Bacterial cyclic beta-(1,2)-glucan acts in systemic suppression of plant immune responses. *Plant Cell* 19, 2077–2089. doi: 10.1105/tpc.106.047944

Sambrook, J., and Russell, D. W. (2001). *Molecular Cloning: A Laboratory Manual.* 3rd Edn. Cold Spring Harbor, NY: Cold Spring Harbor Laboratory Press.

Shieh, G. J., Charng, Y. C., Yang, B. C., Jenn, T., Bau, H. J., and Kuo, T. T. (1991). Identification and nucleotide sequence analysis of an open reading frame involved in high-frequency conversion of turbid to clear plaque mutants of filamentous phage Cf1t. *Virology* 185, 316–322. doi: 10.1016/0042-6822(91)90779-B

Shiotani, H., Fujikawa, T., Ishihara, H., Tsuyumu, S., and Ozaki, K. (2007). A pthA homolog from Xanthomonas axonopodis pv. citri responsible for host-specific suppression of virulence. *J. Bacteriol.* 189, 3271–3279. doi: 10.1128/JB.01790-06

Val, M. E., Bouvier, M., Campos, J., Sherratt, D., Cornet, F., Mazel, D., et al. (2005). The single-stranded genome of phage CTX is the form used for integration into the genome of *Vibrio cholerae*. *Mol. Cell* 19, 559–565. doi: 10.1016/j.molcel.2005.07.002

Verniére, C., Hartung, J. S., Pruvost, O. P., Civerolo, E. L., Alvarez, A. M., Maestri, P. et al. (1998). Characterization of phenotypically distinct strains of *Xanthomonas axonopodis* pv. *citri* from Southwest Asia. *Eur. J. Plant Pathol.* 104, 477–487. doi: 10.1023/A:1008676508688

Vojnov, A. A., Morais do Amaral, A., Dow, J. M., Castagnaro, A. P., and Marano, M. R. (2010). Bacteria causing important diseases of citrus utilise distinct modes of pathogenesis to attack a common host. *Appl. Microbiol. Biotechnol.* 87, 467–477. doi: 10.1007/s00253-010-2631-2

Yamada, T., Kawasaki, T., Nagata, S., Fujiwara, A., Usami, S., and Fujie, M. (2007). New bacteriophages that infect the phytopathogen *Ralstonia solanacearum*. *Microbiology* 153, 2630–2639. doi: 10.1099/mic.0.2006/001453-0

Yu, J., Penaloza-Vazquez, A., Chakrabarty, A. M., and Bender, C. L. (1999). Involvement of the exopolysaccharide alginate in the virulence and epiphytic fitness of *Pseudomonas syringae* pv. *syringae. Mol. Microbiol.* 33, 712–720. doi: 10.1046/j.1365-2958.1999.01516.x

**Conflict of Interest Statement:** The authors declare that the research was conducted in the absence of any commercial or financial relationships that could be construed as a potential conflict of interest.

*Received: 31 March 2014; accepted: 11 June 2014; published online: 01 July 2014.*
*Citation: Ahmad AA, Askora A, Kawasaki T, Fujie M and Yamada T (2014) The filamentous phage XacF1 causes loss of virulence in Xanthomonas axonopodis pv. citri, the causative agent of citrus canker disease. Front. Microbiol.* ***5****:321. doi: 10.3389/fmicb.2014.00321*
*This article was submitted to Virology, a section of the journal Frontiers in Microbiology.*

frontiers in
MICROBIOLOGY

ORIGINAL RESEARCH ARTICLE
published: 02 December 2014
doi: 10.3389/fmicb.2014.00654

# Environmental cues and genes involved in establishment of the superinfective Pf4 phage of *Pseudomonas aeruginosa*

***Janice G. K. Hui[1], Anne Mai-Prochnow[1†], Staffan Kjelleberg[1,2], Diane McDougald[1,2] and Scott A. Rice[1,2]****

[1] The Centre for Marine Bio-Innovation and the School of Biotechnology and Biomolecular Sciences, The University of New South Wales, Sydney, NSW, Australia
[2] The Singapore Centre on Environmental Life Sciences Engineering and The School of Biological Sciences, Nanyang Technological University, Singapore, Republic of Singapore

***Edited by:***
*Jasna Rakonjac, Massey University, New Zealand*

***Reviewed by:***
*Dahlene N. Fusco, Massachusetts General Hospital, USA*
*Grzegorz Wegrzyn, University of Gdansk, Poland*

***Correspondence:**
*Scott A. Rice, The Singapore Centre on Environmental Life Sciences Engineering and The School of Biological Sciences, Nanyang Technological University, 60 Nanyang Drive, Singapore, SBS-01N-27, Republic of Singapore*
*e-mail: rscott@ntu.edu.sg*

**†Present address:**
*Anne Mai-Prochnow, Commonwealth Science and Industrial Research Organisation Manufacturing Flagship, P.O. Box 218, Lindfield, NSW 2070, Australia*

Biofilm development in *Pseudomonas aeruginosa* is in part dependent on a filamentous phage, Pf4, which contributes to biofilm maturation, cell death, dispersal and variant formation, e.g., small colony variants (SCVs). These biofilm phenotypes correlate with the conversion of the Pf4 phage into a superinfection (SI) variant that reinfects and kills the prophage carrying host, in contrast to other filamentous phage that normally replicate without killing their host. Here we have investigated the physiological cues and genes that may be responsible for this conversion. Flow through biofilms typically developed SI phage approximately days 4 or 5 of development and corresponded with dispersal. Starvation for carbon or nitrogen did not lead to the development of SI phage. In contrast, exposure of the biofilm to nitric oxide, $H_2O_2$ or the DNA damaging agent, mitomycin C, showed a trend of increased numbers of SI phage, suggesting that reactive oxygen or nitrogen species (RONS) played a role in the formation of SI phage. In support of this, mutation of *oxyR*, the major oxidative stress regulator in *P. aeruginosa*, resulted in higher level of and earlier superinfection compared to the wild-type (WT). Similarly, inactivation of *mutS*, a DNA mismatch repair gene, resulted in the early appearance of the SI phage and this was four log higher than the WT. In contrast, loss of *recA*, which is important for DNA repair and the SOS response, also resulted in a delayed and decreased production of SI phage. Treatments or mutations that increased superinfection also correlated with an increase in the production of morphotypic variants. The results suggest that the accumulation of RONS by the biofilm may result in DNA lesions in the Pf4 phage, leading to the formation of SI phage, which subsequently selects for morphotypic variants, such as SCVs.

**Keywords:** ***Pseudomonas aeruginosa*, Inovirus, filamentous phage, superinfection, biofilm, variants, oxidative stress**

## INTRODUCTION

It is increasingly accepted that biofilms, or surface-attached communities, account for the majority of bacteria in the environment and that planktonic cells may be more relevant for the dissemination of cells between biofilm habitats (McDougald et al., 2012). This shift in understanding has driven a substantial amount of research focused on understanding how and why bacteria make biofilms and while there are some commonalities, not surprisingly, the regulation of biofilm development is quite complex. Indeed, biofilm formation by *Pseudomonas aeruginosa*, one of the most intensively studied biofilm-forming bacteria, has been suggested to involve around 10% of its genomic potential (Whiteley et al., 2001; Hentzer et al., 2005; Manos et al., 2008). Biofilm development has been shown to be affected by nutrient conditions, and to involve quorum sensing, adhesion proteins, and proteins involved in the turnover of c-di-GMP. Additionally, it has been shown that an endogenous prophage, Pf4, also plays an important role in biofilm development, stress tolerance, dispersal, the formation of morphotypic variants and virulence (Rice et al., 2009).

The Pf4 phage, which has a genome comprised of 12 Kbp, is a member of the Inoviridae and is closely related to ssDNA phage such as M13 and fd. Such phage are continuously secreted by the bacterial host without cell lysis. The effect of the Pf4 phage on biofilm development and variant formation is linked to the establishment of a superinfection (SI) variant of the Pf4 phage. The SI phage are able to form plaques on the wild-type (WT) host, which is otherwise immune to reinfection by the non-SI phage (Rice et al., 2009). Additionally, we have recently shown through deep sequencing of the biofilm dispersal population that the phage accumulates mutations at a significantly higher frequency than the rest of the PAO1 genome, suggesting that superinfection is linked to mutations in the Pf4 prophage (McElroy et al., 2014). Because the formation of the SI phage is an integral part of the biofilm development life-cycle, it is likely that the establishment of the SI phenotype is the result of biofilm-specific physiology and gene expression. However, the specific conditions that lead to SI are currently not known.

Biofilms consist of a stratified population, where cells in different parts of the biofilm exhibit varied physiologies due to differences in nutrient gradients, oxygen gradients, signaling molecules and the accumulation of metabolic products. For example, oxygen gradients can be formed by the failure of

oxygen to penetrate through the biofilm as oxygen is respired by the upper layer of cells (Stewart and Franklin, 2008). Similarly, it has been demonstrated that a gradient of nutrients is established, where the high concentration present in the bulk phase is rapidly depleted in the deeper or thicker parts of the biofilm (Zhang et al., 1995; Stewart, 2003). This can result in the reduction of nutrient availability and causes stress to the biofilm cells leading to nutrient starvation in the biofilm's interior. Conversely, there is a higher concentration of metabolic by-products in the interior of the biofilm compared to the cells in the upper layer of the biofilm, where such waste products may freely diffuse away from the biofilm into the bulk solution.

The accumulation of waste products such as reactive oxygen and nitrogen species (RONS) in biofilms leads to oxidative and nitroxidative stress (Webb et al., 2003; Barraud et al., 2006). For example, aerobic bacteria generate high concentrations of electrons during redox reactions, especially during respiration. These reactions also are partly responsible for the release of different species of oxygen (Cabiscol et al., 2000). This results in the build up of ROS and can lead to DNA damage, protein carbonylation, cofactor degradation, and lipid peroxidation. Therefore, bacteria are dependent on oxidative stress defense systems to mitigate the accumulation of oxygen and oxygen derivatives, e.g., hydrogen peroxide ($H_2O_2$), superoxide anions ($O^{2-}$) and hydroxyl radicals ($OH^-$). Bacteria counteract oxidative stress by expressing enzymes to detoxify ROS and repair damage (Storz and Imlay, 1999; Vinckx et al., 2010). This again supports the observation that bacteria in the biofilm interior differ from those on the exterior surface not only in general physiology, but also in terms of gene expression. Therefore, it is anticipated that stress responses play important roles in host defense to constantly changing environments similar to that observed in biofilms. In *P. aeruginosa,* the OxyR transcriptional regulator is the key global regulator of the oxidative stress response, regulating 56 genes (Wei et al., 2012), including *katA, katB, ahpB, ahpCF, sodA,* and *sodB*. In addition, it was recently shown that OxyR binds to the Pf4 phage genome (Wei et al., 2012) and, therefore, may play an important role in phage production during conditions of oxidative stress.

DNA damage can be repaired through a number of pathways, including the methyl directed mismatch repair (MMR) and the RecA recombination repair systems. The MMR corrects errors that occur during DNA replication and is a key factor in minimizing mutations during replication (Modrich, 1991). RecA acts as a recombinase and facilitates translesion synthesis during DNA repair as well as facilitating the cleavage of the LexA repressor during the SOS response (Cox, 2007). Interestingly, RecA has been linked to the conversion of lambda phage from lysogeny into lytic replication. Given their role in DNA repair and the observation that the phage accumulates a significant number of mutations at the time of dispersal (McElroy et al., 2014), DNA repair systems may play important roles in the formation of the SI phage.

Here, the physiological triggers that lead to mutations and hence SI and variant formation were determined, and the role of DNA repair systems in formation of the SI Pf4 phage investigated. Multiple inducers were tested, including starvation for different key nutrients, oxidative stress, exposure to $H_2O_2$ and mitomycin C. The induced DNA damage from $H_2O_2$ and mitomycin C resulted in increased occurrence of SI. Similarly, mutational inactivation of the oxidative stress response regulator, OxyR as well as the inactivation of the MMR response via mutation of *mutS* gene, resulted in earlier phage production and a higher titer of the SI Pf4 phage. Interestingly, loss of RecA resulted in a decrease in the formation of SI phage suggesting that recombination may be important in this process.

## MATERIALS AND METHODS

### BACTERIAL STRAINS AND CULTURE CONDITIONS

All *P. aeruginosa* strains (**Table 1**) were cultured in Bertani (1951) medium supplemented with 1% (w/v) NaCl (LB10) or in M9 minimal medium containing: 48 mM $NaHPO_4$, 22 mM $KH_2PO_4$, 9 mM NaCl, 19 mM $NH_4Cl$, 2 ml $MgSO_4$, 100 μM $CaCl_2$, supplemented with 15 mM glucose (M9 complete medium). Strains were maintained on LB10 agar (1.5% w/v agar) plates and incubated overnight at 37°C. Liquid cultures were incubated overnight at 37°C with shaking (200 rpm).

### BIOFILM EXPERIMENTS

#### *Planktonic cultures*

Planktonic cultures were cultivated in 15 ml centrifuge tubes (Falcon) in M9 complete medium and incubated overnight at 37°C with shaking at 200 rpm for 24 h. For stress conditions, 1 mL was collected, centrifuged at 10,000 × *g* for 3 min and the supernatant was discarded. Starvation was induced by replacing M9 complete medium with a solution of M9 salts without glucose (carbon starvation) or without ammonium chloride (nitrogen starvation) as medium for 3 days. Cultures were exposed to nitric oxide (NO) by supplementing the M9 complete medium with the NO donor sodium nitroprusside (SNP; Sigma Aldrich) at 10 μM, 100 μM, and 1 mM for 3 days. Oxidative stress was induced by supplementing M9 complete medium with 100 μM, 1 mM and 10 mM $H_2O_2$ (Biorad) for 3 days. Mitomycin C (Sigma Aldrich) was added to M9 complete medium at 3, 30 and 150 μM to induce DNA damage and cultures were treated for 3 days. All treatments were performed as biological triplicates and were compared to cultures maintained in M9 complete medium. The samples were collected daily to determine the phage titre.

**Table 1 | List of *Pseudomonas aeruginosa* strains used in this study.**

| Strain | Reference |
|---|---|
| PAO1 WT | Laboratory stock |
| PAO1 ΔPf4 | Rice et al. (2009) |
| PAO1 SCV2 | This study |
| PAO1 Δ*mutS* | Jacobs et al. (2003) |
| PAO1 Δ*recA* | Jacobs et al. (2003) |
| PAO1 Δ*oxyR* | Wei et al. (2012) |

### Batch biofilms

Batch biofilms were cultivated in tissue culture treated 24 well microtiter plates (Falcon). Briefly, overnight cultures grown in M9 complete medium were diluted 1:100 and 1 ml of the diluted culture was inoculated into each well. Biofilms were formed for 1 d before being treated. Carbon and nitrogen starvation treatments were performed as above and the biofilms were incubated for a further 3 days. Biofilms were exposed to NO, $H_2O_2$ and Mitomycin C as described above and incubated for a further 3 d at 37°C with shaking at 80 rpm. Medium and treatments were replaced daily and at the same time, 1 mL of the biofilm supernatant was harvested to determine plaque forming units (PFUs, see below). All treatments were performed as biological triplicates and were compared to biofilms maintained in M9 complete medium.

### Continuous-culture biofilm

Biofilms were established in silicone tubing (inner diameter 2.64 ± 0.28 mm and outer diameter 4.88 ± 0.28 mm; Silastic® laboratory tubing). Overnight cultures grown in M9 medium were diluted 1:100 and 2 ml of the diluted culture was inoculated into the tubing using a syringe with a 15G needle, and the bacteria were allowed to attach to the tubing under conditions of no flow for 1 h at room temperature. After the attachment phase, M9 complete medium was pumped through the tubing at a flow rate of 6 ml/h at room temperature. Biofilms were allowed to form for 2 days before treatment. Carbon and nitrogen starvation was induced as above and starvation medium was supplied to the biofilm for 5 days. Similarly, biofilms were exposed to NO by supplementing the M9 complete medium with 1 mM SNP for 5 days. $H_2O_2$ (10 mM) and mitomycin C were added to the M9 complete medium and fed to the biofilm for 5 days. All treatments were performed as biological triplicates and were compared to biofilms maintained in M9 complete medium. The samples were collected daily for CFU and PFU counts.

### CFU counts and morphological variants from the biofilm effluent

CFUs and the numbers of variants were obtained by collecting 5 ml of the biofilm effluent on days 2–7. Serial dilutions were spread plated onto LB10 agar. The plates were incubated overnight for at least 12 h at 37°C. The plates were incubated for additional 12 h at room temperature to facilitate observation of morphotypic variants.

### Phage assays

The supernatant was tested for SI phage using a modified version of the top-layer agar method previously described (Eisenstark, 1967). Briefly, bacterial lawns of either the WT PA01 (SI phage) or the Pf4 mutant (total phage) were prepared by mixing 500 μl of an overnight culture, grown in M9 complete medium, with 5 ml of 0.8% (w/v) molten LB10 agar at 55°C. The mixture was poured onto a LB10 agar. The biofilm effluent was centrifuged at 13,000 × *g* for 5 min and filtered through a 0.22 μm filter (Millipore Millex GP) to obtain cell-free supernatant. The supernatant was serially diluted and 10 μl drops were spotted onto the bacterial lawns, air-dried and incubated overnight at 37°C to observe and quantify plaque formation.

## RESULTS

In *P. aeruginosa* PAO1 biofilms, the lysogenic Pf4 prophage converts into its SI form during the dispersal phase and can be detected by the ability of the SI phage to form plaques on lawns of the WT *P. aeruginosa*. This indicates that the SI phage can infect and kill *P. aeruginosa*, which is otherwise resistant to reinfection by the WT Pf4 phage. This is accompanied by the appearance of small colony variants (SCVs) in the dispersal population. To determine the physiological or genetic factors involved in the formation of SI, strains and chemical treatments associated with DNA damage or spontaneous mutation, including *mutS*, *recA*, *oxyR* mutants, $H_2O_2$, mitomycin C, and the NO donor SNP were tested. To facilitate testing a wide range of treatments and conditions, experiments were performed on planktonic and batch biofilms for higher throughput. While the planktonic cultures produced SI phage, their appearance was inconsistent (data not shown) and indeed, the control cultures displayed a random pattern of SI induction. When the same treatments were tested on batch grown biofilms, no SI was observed, even after 3 days of cultivation (data not shown). The control biofilms also showed no SI, suggesting that batch biofilms in microtiter plates, over the 3 days tested, do not replicate flow cell conditions sufficiently to allow for the formation of the SI phage.

Since neither planktonic nor batch biofilms resulted in reproducible patterns of SI induction, subsequent experiments were conducted in flow through biofilms. The control biofilm produced SI phage on days 4 at $9.7 \times 10^4$ PFU/ml (**Figure 1**). The number of SI phage increased exponentially to days 6, reaching a maximum of $7 \times 10^9$ PFU/ml before a slight decline on days 7. The nutrient starved (carbon or nitrogen) biofilms were observed to disperse within 24 h of treatment. This was accompanied by a dramatic decrease in the overall phage titre as observed on the Pf4 lawn, most likely due to the loss of biomass through dispersal (data not shown). These results are in agreement with previous work showing that starvation induces biofilm dispersal (Huynh et al., 2012). Therefore, these experiments were not repeated.

When the continuous culture biofilms were exposed to 10 mM of $H_2O_2$ starting from days 2, the SI phage appeared on days 4 at $4.68 \times 10^7$ PFU/ml and increased throughout the duration of the experiment reaching a maximum of $3.65 \times 10^{10}$ PFU/ml on days 7. PAO1 biofilms treated with the NO donor SNP, had $9.12 \times 10^7$ PFU/ml in the biofilm effluent on days 4. The number of PFU/ml increased on days 5 and 6, reaching a maximum of $8.10 \times 10^9$ PFU/ml on days 6 and decreased on days 7 to $2.14 \times 10^9$ PFU/ml. This pattern of change in PFU numbers observed from the SNP treated biofilms was also observed when the biofilm was exposed to DNA damaging agent, mitomycin C (**Figure 1**). There was an exponential increase in PFUs starting on days 4 of $3.4 \times 10^7$ PFU/ml that reached a plateau on days 6 at $1.9 \times 10^{10}$ PFU/ml and subsequently declined on days 7 to $5.6 \times 10^9$ PFU/ml. While the results were not statistically significant (two-way ANOVA), the trends, seen in multiple experiments, suggest that DNA damaging agents or NO exposure may play a role in the formation of SI phage. Further, there was a two-log difference on days 4 for all of the treatments relative to the control, suggesting

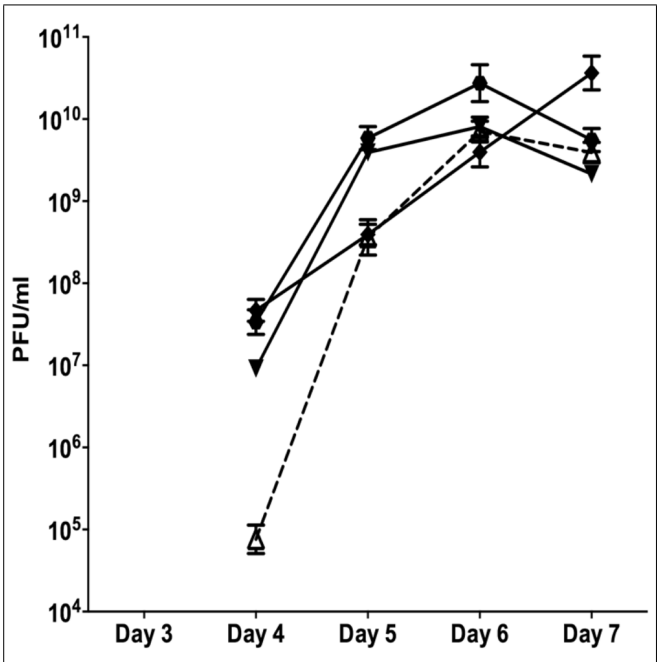


**FIGURE 1 | The appearance of SI Pf4 phage during biofilm development of PAO1 wild-type (WT; open triangle with dotted line), PAO1 treated with mitomycin C (hexagon), PAO1 treated with $H_2O_2$ (diamond) and PAO1 treated with SNP (inverted triangle).** The SI Pf4 phage was detected via the plaque assay with the PAO1 WT as the target lawn. Data represent the means of three independent experiments and error bars show SE of the mean.

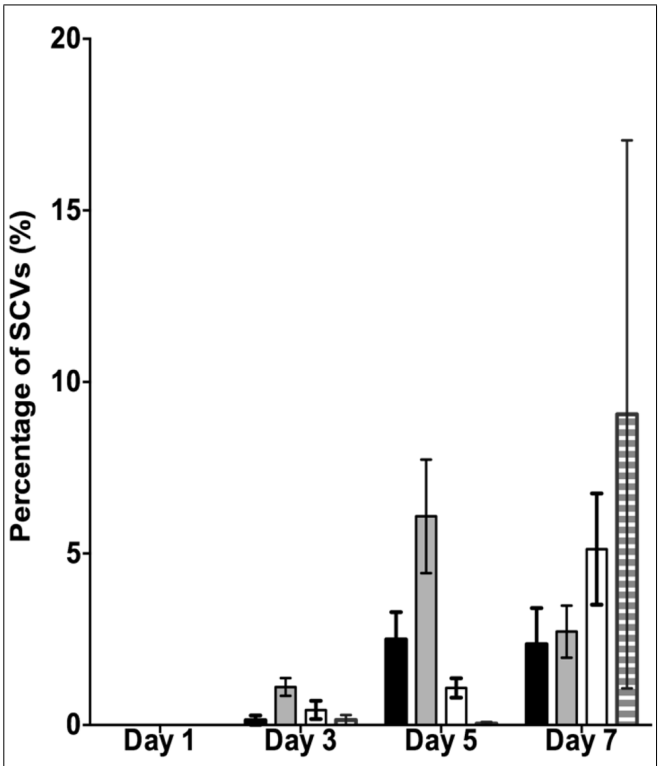


**FIGURE 2 | The percentage of small colony variants (SCVs) from the PAO1 biofilm untreated (black bars), treated with 150 μM of mitomycin C (gray bars), treated with 10 mM of $H_2O_2$ (white bars) and treated with 1 mM of SNP (striped bars).** Data represent the means and SE of the mean of three experiments.

that these treatments have an effect on the titre of the SI phage even though they did not induce the earlier production of SI phage.

It has previously been shown that SI Pf4 phage can induce the formation of SCVs (Rice et al., 2009). Therefore, the effluents from the biofilms treated with mitomycin C, $H_2O_2$ and SNP were plated to quantify the number of SCVs relative to the untreated control biofilms (**Figure 2**). The effluent of biofilms exposed to mitomycin C consisted of 1.1% SCVs on days 3 and increased to 6.1% SCVs on days 5. In comparison, the untreated PAO1 biofilm effluent consisted of less than 1% of SCVs on days 3 and 2.5 and 2.4% of SCVs on days 5 and 7, respectively. The DNA damaging agent mitomycin C induced the highest frequency of SCVs over the first 5 days, peaking at 7.5%. In contrast, exposure to $H_2O_2$ and SNP had a lesser effect. For example, there were $<$ 1% SCVs on days 3 from the biofilm exposed to $H_2O_2$, which increased on days 5 and 7, reaching 5.1% SCVs on days 7. Similarly, the biofilm exposed to SNP had less than 1% of SCVs from days 3, reaching its maximum of 9.1% of SCVs on days 7. In comparison to the untreated PAO1 biofilm, there was a two and fourfold increase in SCVs from the biofilm effluent on days 7 for the $H_2O_2$ and SNP treated biofilms, respectively. While the results were not statistically significant when averaged across the three independent experiments ($p > 0.05$, two-way ANOVA), the trend of more SCVs in the treated biofilms relative to the controls was consistent across multiple experiments.

The data presented above (**Figures 1** and **2**) suggests that oxidative stress (exposure to $H_2O_2$ and SNP) and DNA damage (exposure to mitomycin C) may lead to the development of the SI phage, resulting in the appearance of SCVs. Oxidative stress in *P. aeruginosa* is primarily controlled by the transcriptional regulator, OxyR (Storz and Imlay, 1999). This protein changes in conformation upon exposure to oxidative stress, allowing it to bind to specific promoters to control their expression. Therefore, to investigate the role of the global transcriptional regulator, OxyR, in the conversion of the Pf4 phage into its SI form during biofilm development, the *oxyR* mutant biofilm was compared with the PAO1 WT biofilm. The *oxyR* mutant biofilm showed early conversion of the SI Pf4 phage on days 4 as compared to the PAO1 WT biofilm, which produced SI phage on days 5 in these experiments (**Figure 3**). On days 4 for the *oxyR* mutant biofilm, there were $1.2 \times 10^3$ PFU/ml detected in the biofilm effluent, and the number increased to $8.1 \times 10^9$ PFU/ml on days 5. The *oxyR* mutant biofilm was also observed to have a higher percentage of SCVs during the late stages of biofilm development (**Figure 4**). The PAO1 WT biofilm generated 1.3% SCVs on days 6 and 1.9% on days 7 in comparison to 16.7% and 7.6% of SCVs from the *oxyR* mutant biofilm on days 6 and 7, respectively. The difference between the two biofilms was statistically significant on days 6, with more than 10-fold difference in SCVs. The same trend was observed in the three independent experiments; therefore it is highly likely that

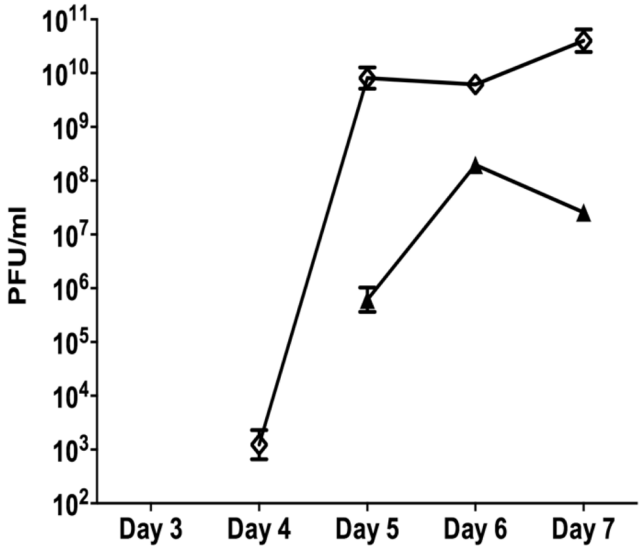


**FIGURE 3 | The role of OxyR in the development of superinfection (SI).** Biofilm effluents from the PAO1 WT (triangle) and *oxyR* mutant (diamond) were screened for the appearance of the SI Pf4 phage, using the soft agar overlay method with the PAO1 WT as the target lawn. Data are the means and SEM of three independent experiments. Note that error bars are present for all data points, but may be too small to visualize on the graph.

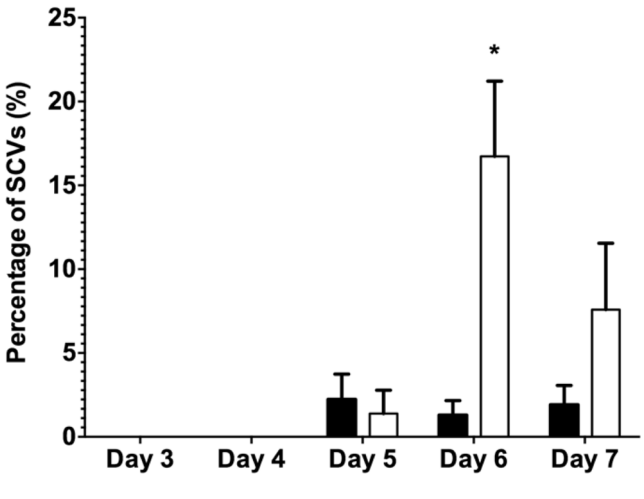


**FIGURE 4 | The percentage of SCVs from the dispersal population of the PAO1 WT biofilm (black bars) and the PAO1 *oxyR* mutant biofilm (white bars).** Colony forming units were determined from biofilm effluents for phenotypic variants from the biofilms. Data represent the means of three experiments and error bars show SE of the mean. (*) indicates a statistically significant difference when compared to PAO1 WT at 95% confidence interval with two-way ANOVA with a Sidak's post test.

OxyR plays an important role in the conversion to the SI and the appearance of SCVs.

The early appearance and increased number of SI phage observed for the *oxyR* mutant further supports the possibility that oxidative stress and DNA damage are associated with this conversion. Bacteria have evolved a number of mechanisms to repair damaged DNA and two of the most important mechanisms are the MMR system and the RecA recombination system. To mimic the loss of a functional repair system, a *mutS* mutant biofilm was compared to the PAO1 WT biofilm. The *mutS* mutant biofilm produced $6.5 \times 10^4$ PFU/ml of SI phage on days 3 compared to the PAO1 WT biofilm where conversion did not occur until days 5 (**Figure 5**). Additionally, on days 5 the *mutS* mutant produced significantly ($P < 0.01$) more phage ($4.3 \times 10^{12}$ PFU/ml) than the WT ($9.8 \times 10^7$ PFU/ml). The number of PFU from the *mutS* mutant biofilm decreased to $4.6 \times 10^9$ PFU/ml on days 9 and 11. In contrast, the *recA* mutant showed a substantial reduction in the number of SI phage ($4.7 \times 10^6$ PFU/ml) compared to the PAO1 WT biofilm, with Pf4 phage conversion occurring on days 5 of biofilm development (**Figure 5**). Indeed, the number of SI phage observed in the biofilm effluent for the *recA* mutant was approximately one log lower than the WT at all time points tested. This suggests that loss of repair increases the appearance of SI and that the formation of SI phage may also be partially dependent on RecA-mediated recombination activity.

When comparing the dispersal variants from the biofilms, SCVs were observed from the *mutS* mutant biofilm from days 1 onward and peaked on days 5 at 6.1% SCVs, which was statistically significantly different ($P < 0.05$) to the WT biofilm with 2.5% of SCVs on days 5 (**Figure 6**). While the number of SCV's was higher for the *mutS* mutant on days 1–5, the percentage of SCVs produced by the *mutS* mutant was similar to the WT from days 7 onward. In contrast, the percentage of SCVs observed in the effluent of the *recA* mutant biofilm was not statistically different from the WT for days 1–3. However, from days 7 onward, the *recA* mutant generated

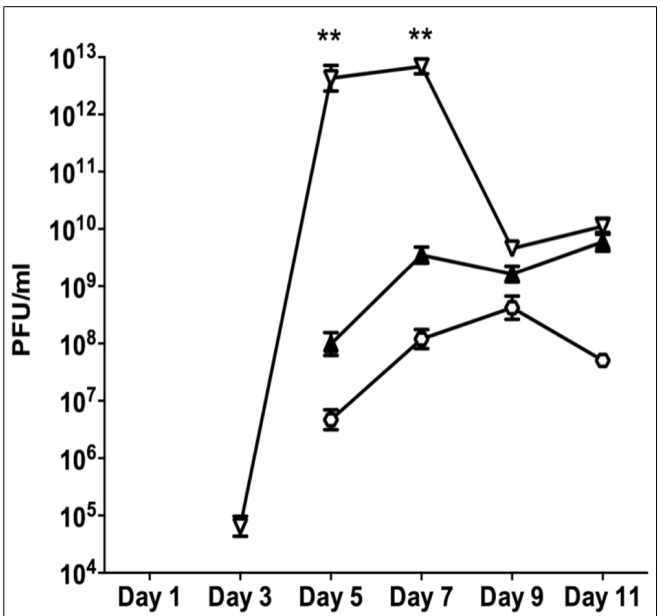


**FIGURE 5 | The appearance of the SI Pf4 phage during biofilm development for PAO1 (closed triangle), the *mutS* mutant (inverted triangle) and the *recA* mutant (hexagon).** Data are the means of three independent experiments and the error bars show SE of the mean. (**) indicates a statistically significant difference compared to PAO1 WT at the 99% confidence interval as determined using a one-way ANOVA.

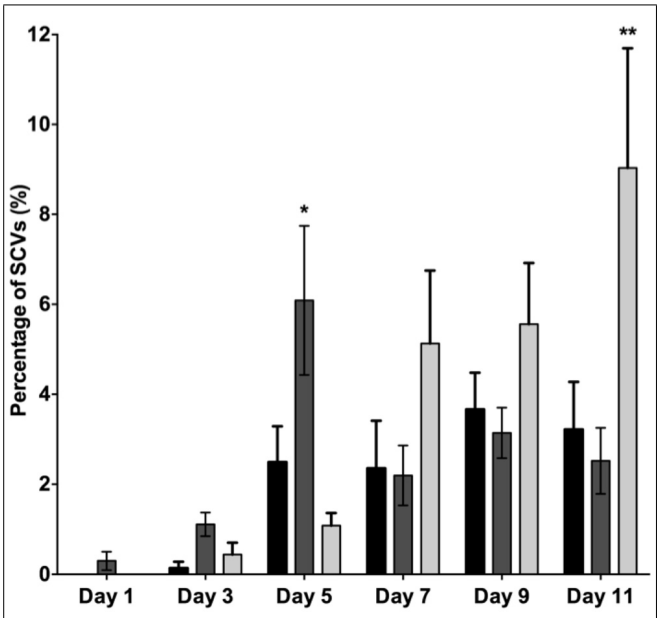


**FIGURE 6 | The percentage of SCVs in the biofilm dispersal population for PAO1 WT (black bars), the *mutS* mutant (dark gray) and the *recA* mutant (light gray).** Data are means of three experiments and the error bars indicate SE of the mean. (*) and (**) indicate a statistically significant difference when compared to PAO1 WT at 95 and 99% confidence intervals respectively, as determined by using a one-way ANOVA.

significantly more SCVs than the WT and the *mutS* mutant. For example, on days 11 the *recA* mutant produced 9% SCVs, representing a statistically significant difference ($P < 0.01$) compared to the WT at 3.2% SCVs. These data suggest that the appearance of the SI phage correlates with the onset of detection of the SCV's in biofilm effluent but does not correlate with the titre of the SI phage. For example, the *recA* mutant produced less SI phage, but significantly more SCVs than either the WT or the *mutS* mutant (**Figure 6**), which produced >four log more phage than the *recA* mutant from days 7 to 11 (**Figure 5**).

## DISCUSSION

It was previously shown that growth in a biofilm leads to the formation of a SI variant of the Pf4 phage (Rice et al., 2009). While biofilm dispersal has previously been linked to nutrient starvation and the accumulation of NO (Sauer et al., 2004; Barraud et al., 2006; Huynh et al., 2012), the specific metabolic or stress conditions that lead to the establishment of the SI phage has not been determined. The results presented here strongly suggest that SI conversion is linked to a dysfunctional oxidative stress response and the MMR system. This is supported by the results showing that chemical treatments that are linked with either DNA damage (mitomycin C) or oxidative stress ($H_2O_2$ and SNP) also result in increased or early development of SI. Oxidative stress is a consequence of the build up of RONS as a result of endogenous by-products that accumulate during aerobic metabolism and/or upon external exposure to ROS, such as the oxidative burst of immune cells. Aerobic bacteria naturally generate high concentrations of electrons and multiple oxygen species through oxidative phosphorylation and respiration. This results in the build up of ROS such as $H_2O_2$, $O^{2-}$ and hydroxyl radical ($OH^-$; Henle and Linn, 1997; Storz and Imlay, 1999). It has been shown that ROS and RONS accumulate within microcolonies of the biofilm leading to cell death (Barraud et al., 2006) and that microcolonies within the biofilms are hot spots for the accumulation of mutants (Conibear et al., 2009). While bacterial cells are constantly exposed to intracellularly generated ROS, they are also exposed to exogeneous ROS generated by other microorganisms which can either be used to eliminate competitors or can be released by immune cells to kill invading pathogens (Klotz and Hutcheson, 1992; Brunder et al., 1996). For example, the release of superoxides by the phagocyte NADPH oxidase is a host defense mechanism used by macrophages against pathogens (Miller and Britigan, 1997; Babior, 1999; Janssen et al., 2003).

Hydrogen peroxide can freely diffuse across cellular membranes, making it a lethal antimicrobial as it causes DNA damage through strand breakage (Ananthaswamy and Eisenstark, 1977), deoxynucleotide base damage (Rhaese and Freese, 1968), deoxynucleotide base release (Ward and Kuo, 1976) and DNA cross-linking (Massie et al., 1972). It has previously been shown that the rate of damage caused by $OH^-$, the product of $H_2O_2$ degradation via the Fenton reaction, is greater than damage caused by $H_2O_2$, as $OH^-$ have a greater ability to bind to DNA (Ananthaswamy and Eisenstark, 1977; Ward et al., 1987). The fact that $OH^-$ are more damaging, could explain the observation that $H_2O_2$ had a relatively minor effect on the biofilm compared to the loss of the OxyR regulator (*oxyR* mutant biofilm), which acts in response to combinations of RONS. Exposure to $H_2O_2$ gives rise to oxidative stress, however, bacterial cells harbor repair mechanisms that repair DNA damage and produce enzymes to scavenge and remove $H_2O_2$ (Ma and Eaton, 1992). Therefore, $H_2O_2$ may induce the expression of SI phage by a few hours because it has limited capacity to damage the cell in comparison to the loss of OxyR. In the case of the OxyR mutant, the SI phage was induced a day earlier than in the PAO1 WT biofilm which may reflect the broader role of OxyR in controlling the global oxidative stress response.

It was determined that OxyR of *P. aeruginosa* binds to multiple sites in the genome (Wei et al., 2012). Interestingly, one of those sites is the intergenic region between PA0716 and PA0717 genes of the Pf4 genome. The binding region lies within the ORF of the repressor *c* gene of the prophage genome. This suggests that interactions of the OxyR protein with the Pf4 phage genome are important in SI conversion and overall control of phage production. One possible mechanism is that the OxyR normally binds to the repressor C promoter and represses gene expression. When the repressor C acquires mutations, these may prevent binding of the OxyR to the phage genome leading to overproduction of the phage particles. Binding assays of the OxyR to the repressor *c* gene and/or competition binding between OxyR and repressor C may elucidate the role of OxyR in SI phage conversion and the interactions between the OxyR regulator and the prophage. Deep sequencing data of the *P. aeruginosa* dispersal population and associated phage indicates that there is a high frequency of mutations in the *repC* gene and the upstream promoter region,

while there are no other mutations in the phage genome (McElroy et al., 2014).

Inactivation of the MMR system is associated with the highly mutable state, called hypermutation. For example, *P. aeruginosa* CF isolates have been shown to lack the *mutS* and *mutY* genes of the MMR system leading to the hypermutatable phenotype (Oliver et al., 2000). The *mutS* protein plays an important role in recognizing mismatches and initiates the repair by association with other Mut proteins, the loss of this protein will completely arrest the MMR system. Our results suggest that loss of a functional MMR system leads to early conversion of the SI phage and higher SCV numbers. This supports the possibility that mutations in the genome lead to the conversion of the SI phage and that this process is linked to DNA damage via oxidative stress and requires active MMR functions to reduce conversion to the SI phage.

The mutations could arise in either the prophage genome, the replicative form (RF) or in the ssDNA phage genome as it is replicated for packing into phage particles. In the latter two cases, the mutated RF or phage genome (after conversion into dsDNA) could be introduced into the prophage locus via recombination. The loss of RecA leads to a decrease in the SI Pf4 phage in the biofilm, suggesting that RecA is required for the conversion to the SI phage. RecA plays roles in both the induction of the SOS response and in recombination based DNA repair (Schlacher and Goodman, 2007) and it is not clear from the data presented here, which function of RecA is associated with the formation of the SI phage. It is possible that the mutations resulting in SI Pf4 occur during phage replication and that the mutated phage genome is recombined with the genomic prophage, resulting in fixation of the mutation in the bacterial host, although this is yet to be experimentally determined.

*Pseudomonas aeruginosa* biofilms have been shown to generate genetic diversity by producing phenotypic variants with a variety of functions such as the production of pyomelanin for protection against oxidative stress (Boles et al., 2004), loss of flagellar and twitching motility for enhanced adherence to surfaces (Deziel et al., 2001), and increased tolerance against antibiotic treatment (Drenkard and Ausubel, 2002). These adaptive phenotypes are important for the survival and the fitness of bacteria. However, deep sequencing data (McElroy et al., 2014) suggest that there are a limited number of mutations in the host genome outside of the phage region. This could suggest that instead of frequent random mutations, the conversion of the Pf4 phage to its SI form may drive the formation of the phenotypic variants observed from the biofilm through an as yet unknown mechanism. Genetic variation is important for the increased stress and antimicrobial tolerance of *P. aeruginosa* biofilms (Boles et al., 2004) and the formation of SI phage has been shown to increase variant formation. Therefore, the process of SI formation could have negative treatment implications, where SI leads to the increased number of resistant variants during chronic, biofilm related infections.

## CONCLUSION

The conversion into the SI Pf4 phage coincided with the appearance of SCVs from the dispersal population of the PAO1 biofilm. In the work presented here, formation of the SI phage appears to be correlated with a functional MMR system and the oxidative stress response mediated by OxyR. Further, the results presented here suggest that high levels of either DNA damaging agents or ROS can induce the SI phenotypes. Therefore, it is likely that during biofilm maturation, high concentrations of RONS accumulate due to endogenous metabolism, overwhelming the ability of the host to detoxify DNA damaging molecules, leading to the accumulation of mutations. The nucleotide composition of the repressor *c* gene may predispose it to acquire single nucleotide polymorphisms at frequencies higher than the host genome and such mutations disrupt or change the immunity function of the repressor C protein, allowing the mutant phage to subsequently reinfect hosts with WT immunity functions. This would lead to strong selection pressure in the biofilm for variants that are resistant to the SI (and additionally carry the SI Pf4 phage) that subsequently persist. The SI phage, through an unknown mechanism, also drives changes in the morphology of the SI host. Therefore, it is of interest to understand how SI results in morphotypic variation, the involvement of the repressor *c* gene and the mechanism by which OxyR controls SI.

## AUTHOR CONTRIBUTIONS

Janice G. K. Hui designed and performed experiments, contributed to the interpretation of results, wrote the manuscript and approved the final version for publication; Anne Mai-Prochnow, Staffan Kjelleberg, Diane McDougald, and Scott A. Rice designed experiments, contributed to the interpretation of results, wrote the manuscript and approved the final version for publication.

## ACKNOWLEDGMENTS

Funding support (Scott A. Rice and Diane McDougald) was provided by the Australian Research Council (DP110104525), the Centre for Marine Bio-Innovation and the Singapore Centre on Environmental Life Sciences Engineering.

## REFERENCES

Ananthaswamy, H. N., and Eisenstark, A. (1977). Repair of hydrogen peroxide-induced single-strand breaks in *Escherichia coli* deoxyribonucleic acid. *J. Bacteriol.* 130, 187–191.

Babior, B. M. (1999). NADPH oxidase. *Blood* 93, 1464–1476.

Barraud, N., Hassett, D. J., Hwang, S.-H., Rice, S. A., Kjelleberg, S., and Webb, J. S. (2006). Involvement of nitric oxide in biofilm dispersal of *Pseudomonas aeruginosa*. *J. Bacteriol.* 188, 7344–7353. doi: 10.1128/JB.00779-06

Bertani, G. (1951). Studies on lysogenesis. *J. Bacteriol.* 62, 293–300.

Boles, B. R., Thoendel, M., and Singh, P. K. (2004). Self-generated diversity produces "insurance effects" in biofilm communities. *Proc. Natl. Acad. Sci. U.S.A.* 101, 16630–16635. doi: 10.1073/pnas.0407460101

Brunder, W., Schmidt, H., and Karch, H. (1996). KatP, a novel catalase-peroxidase encoded by the large plasmid of enterohaemorrhagic *Escherichia coli* O157:H7. *Microbiology* 142, 3305–3315. doi: 10.1099/13500872-142-11-3305

Cabiscol, E., Tamarit, J., and Ros, J. (2000). Oxidative stress in bacteria and protein damage by reactive oxygen species. *Int. Microbiol.* 3, 3–8. doi: 10.1042/BJ20061131

Conibear, T. C. R., Collins, S. L., and Webb, J. S. (2009). Role of mutation in *Pseudomonas aeruginosa* biofilm development. *PLoS ONE* 4:e6289. doi: 10.1371/journal.pone.0006289

Cox, M. M. (2007). Regulation of bacterial RecA protein function. *Crit. Rev. Biochem. Mol. Biol.* 42, 41–63. doi: 10.1080/10409230701260258

Deziel, E., Comeau, Y., and Villemur, R. (2001). Initiation of biofilm formation by *Pseudomonas aeruginosa* 57RP correlates with emergence of hyperpiliated and highly adherent phenotypic variants deficient in swimming, swarming, and

twitching motilities. *J. Bacteriol.* 183, 1195–1204. doi: 10.1128/JB.183.4.1195-1204.2001

Drenkard, E., and Ausubel, F. M. (2002). *Pseudomonas* biofilm formation and antibiotic resistance are linked to phenotypic variation. *Nature* 416, 740–743. doi: 10.1038/416740a

Eisenstark, A. (1967). *Bacteriophage Techniques: Methods in Virology*. New York, NY: Academic Press.

Henle, E. S., and Linn, S. (1997). Formation, prevention, and repair of DNA damage by iron/hydrogen peroxide. *J. Biol. Chem.* 272, 19095–19098. doi: 10.1074/jbc.272.31.19095

Hentzer, M., Eberl, L., and Givskov, M. (2005). Transcriptome analysis of *Pseudomonas aeruginosa* biofilm development: anaerobic respiration and iron limitation. *Biofilms* 2, 37–61. doi: 10.1017/S1479050505001699

Huynh, T. T., Mcdougald, D., Klebensberger, J., Al Qarni, B., Barraud, N., Rice, S. A., et al. (2012). Glucose starvation-induced dispersal of Pseudomonas aeruginosa biofilms is cAMP and energy dependent. *PLoS ONE* 7:e42874. doi: 10.1371/journal.pone.0042874

Jacobs, M. A., Alwood, A., Thaipisuttikul, I., Spencer, D., Haugen, E., Ernst, S., et al. (2003). Comprehensive transposon mutant library of *Pseudomonas aeruginosa*. *Proc. Natl. Acad. Sci. U.S.A.* 100, 14339–14344. doi: 10.1073/pnas.2036282100

Janssen, R. T., Van Der Straaten, T., Van Diepen, A., and Van Dissel, J. T. (2003). Responses to reactive oxygen intermediates and virulence of *Salmonella typhimurium*. *Microbes Infect.* 5, 527–534. doi: 10.1016/S1286-4579(03)00069-8

Klotz, M. G., and Hutcheson, S. W. (1992). Multiple periplasmic catalases in phytopathogenic strains of *Pseudomonas syringae*. *Appl. Environ. Microbiol.* 58, 2468–2473.

Ma, M., and Eaton, J. W. (1992). Multicellular oxidant defense in unicellular organisms. *Proc. Natl. Acad. Sci. U.S.A.* 89, 7924–7928. doi: 10.1073/pnas.89.17.7924

Manos, J., Arthur, J., Rose, B., Tingpej, P., Fung, C., Curtis, M., et al. (2008). Transcriptome analyses and biofilm-forming characteristics of a clonal *Pseudomonas aeruginosa* from the cystic fibrosis lung. *J. Med. Microbiol.* 57, 1454–1465. doi: 10.1099/jmm.0.2008/005009-0

Massie, H. R., Samis, H. V., and Baird, M. B. (1972). The kinetics of degradation of DNA and RNA by hydrogen peroxide. *Biochim. Biophys. Acta* 272, 539–548. doi: 10.1016/0005-2787(72)90509-6

McDougald, D., Rice, S. A., Barraud, N., Steinberg, P. D., and Kjelleberg, S. (2012). Should we stay or should we go: Mechanisms and ecological consequences for bacterial dispersal from biofilms. *Nat. Rev. Microbiol.* 10, 39–50. doi: 10.1038/nrmicro2695

McElroy, K., Hui, J., Woo, J. K. K., Luk, A., Webb, J. S., Kjelleberg, S., et al. (2014). Strain-specific, parallel evolution drives short-term diversification during *Pseudomonas aeruginosa* biofilm formation. *Proc. Natl. Acad. Sci. U.S.A.* 111, E1419–E1427. doi: 10.1073/pnas.1314340111

Miller, R. A., and Britigan, B. E. (1997). Role of oxidants in microbial pathophysiology. *Clin. Microbiol. Rev.* 10, 1–18.

Modrich, P. (1991). Mechanisms and biological effects of mismatch repair. *Annu. Rev. Genet.* 25, 229–253. doi: 10.1146/annurev.ge.25.120191.001305

Oliver, A., Canton, R., Campo, P., Baquero, F., and Blazquez, J. (2000). High frequency of hypermutable *Pseudomonas aeruginosa* in cystic fibrosis lung infection. *Science* 288, 1251–1253. doi: 10.1126/science.288.5469.1251

Rhaese, H. J., and Freese, E. (1968). Chemical analysis of DNA alterations I. Base liberation and backbone breakage of DNA and oligodeoxyadenylic acid by hydrogen peroxide and hydroxylamine. *Biochim. Biophys. Acta* 155, 476–490. doi: 10.1016/0005-2787(68)90193-7

Rice, S. A., Tan, C. H., Mikkelsen, P. J., Kung, V., Woo, J., Tay, M., et al. (2009). The biofilm life cycle and virulence of *Pseudomonas aeruginosa* are dependent on a filamentous prophage. *ISME J.* 3, 271–282. doi: 10.1038/ismej.2008.109

Sauer, K., Cullen, M. C., Rickard, A. H., Zeef, L. A. H., Davies, D. G., and Gilbert, P. (2004). Characterization of nutrient-induced dispersion in *Pseudomonas aeruginosa* PAO1 biofilm. *J. Bacteriol.* 186, 7312–7326. doi: 10.1128/JB.186.21.7312-7326.2004

Schlacher, K., and Goodman, M. F. (2007). Lessons from 50 years of SOS DNA-damage-induced mutagenesis. *Nat. Rev.* 8, 587–594. doi: 10.1038/nrm2198

Stewart, P. S. (2003). Diffusion in biofilms. *J. Bacteriol.* 185, 1485–1491. doi: 10.1128/JB.185.5.1485-1491.2003

Stewart, P. S., and Franklin, M. J. (2008). Physiological heterogeneity in biofilms. *Nat. Rev. Microbiol.* 6, 199–210. doi: 10.1038/nrmicro1838

Storz, G., and Imlay, J. A. (1999). Oxidative stress. *Curr. Opin. Microbiol.* 2, 188–194. doi: 10.1016/S1369-5274(99)80033-2

Vinckx, T., Wei, Q., Matthijs, S., and Cornelis, P. (2010). The *Pseudomonas aeruginosa* oxidative stress regulator oxyR influences production of pyocyanin and rhamnolipids: protective role of pyocyanin. *Microbiology* 156, 678–686. doi: 10.1099/mic.0.031971-0

Ward, J. F., Evans, J. W., Limoli, C. L., and Calalbro-Jones, P. M. (1987). Radiation and hydrogen peroxide induced free radical damage to DNA. *Br. J. Cancer* 8, 105–112.

Ward, J. F., and Kuo, I. (1976). Strand breaks, base release, and postirradiation changes in DNA γ-irradiated in dilute ozygen saturated aqueous solution. *Radiat. Res.* 66, 485–498.

Webb, J. S., Thompson, L. S., James, S., Charlton, T., Tolker-Nielsen, T., Koch, B., et al. (2003). Cell death in *Pseudomonas aeruginosa* biofilm development. *J. Bacteriol.* 185, 4585–4592. doi: 10.1128/JB.185.15.4585-4592.2003

Wei, Q., Le Minh, P. N., Dötsch, A., Hildebrand, F., Panmanee, W., Elfarash, A., et al. (2012). Global regulation of gene expression by OxyR in an important human opportunistic pathogen. *Nucleic. Acids Res.* 40, 4320–4333. doi: 10.1093/nar/gks017

Whiteley, M., Bangera, M. G., Bumgarner, R. E., Parsek, M. R., Teitzel, G. M., Lory, S., et al. (2001). Gene expression in *Pseudomonas aeruginosa* biofilms. *Nature* 413, 860–864. doi: 10.1038/35101627

Zhang, T., Fu, Y., and Biship, P. (1995). Competition for substrate and space in biofilms. *Water Environ. Res.* 67, 992–1003. doi: 10.2175/106143095X133220

**Conflict of Interest Statement:** The authors declare that the research was conducted in the absence of any commercial or financial relationships that could be construed as a potential conflict of interest.

*Received: 11 August 2014; accepted: 13 November 2014; published online: 02 December 2014.*

*Citation: Hui JGK, Mai-Prochnow A, Kjelleberg S, McDougald D and Rice SA (2014) Environmental cues and genes involved in establishment of the superinfective Pf4 phage of Pseudomonas aeruginosa. Front. Microbiol.* ***5****:654. doi: 10.3389/fmicb.2014.00654*

*This article was submitted to Virology, a section of the journal Frontiers in Microbiology.*

frontiers in
MICROBIOLOGY

MINI REVIEW ARTICLE
published: 15 December 2014
doi: 10.3389/fmicb.2014.00701

# YpfΦ: a filamentous phage acquired by *Yersinia pestis*

***Anne Derbise* and Elisabeth Carniel***

*Yersinia Research Unit, Department of Microbiology, Institut Pasteur, Paris, France*

***Edited by:***
*Bhabatosh Das, Translational Health Science and Technology Institute, India*

***Reviewed by:***
*Jasna Rakonjac, Massey University, New Zealand*
*François-Xavier Barre, CNRS, France*

****Correspondence:***
*Anne Derbise, Yersinia Research Unit, Department of Microbiology, Institut Pasteur, 28 rue du Dr. Roux, 75724 Paris Cedex 15, France*
*e-mail: aderbise@pasteur.fr*

*Yersinia pestis*, the plague bacillus, has an exceptional pathogenicity for humans. The plague bacillus emerged very recently (≈3,000 years ago) from the enteropathogen *Y. pseudotuberculosis*. Early after its emergence, *Y. pestis* became infected by a filamentous phage named YpfΦ. During the microevolution of the plague bacillus, the phage remained in the various lineages as an unstable extrachromosomal element. However, in the sub branch that caused the third plague pandemic, YpfΦ integrated itself into the bacterial chromosome to become a stable prophage. The genome of this phage has the same genetic organization as that of other filamentous phages such as the *Vibrio cholerae* CTXΦ phage, and shares high sequence identity with the CUS-1 filamentous phage of a high-virulence *Escherichia coli* K1 clone. In addition to genes involved in phage physiology, YpfΦ carries at each extremity of its genome two open reading frames with no predicted functions. This filamentous phage confers some selective properties to *Y. pestis* during the infectious process, which may explain why it was conserved during *Y. pestis* microevolution, despite its instability as an extrachromosomal element in most branches.

**Keywords: filamentous bacteriophage, plague, *Yersinia pestis***

## INTRODUCTION

*Yersinia pestis*, one of the most dangerous bacterial pathogens of humans, is the causative agent of plague, a zoonotic disease transmitted from animals to humans by fleabites. After injection into the dermis, the bacteria migrate to the draining lymph node, where they cause the pathognomonic bubo. Bubonic plague, the most common clinical form, is fatal in less than a week in 40–70% of the patients if left untreated. Pneumonic plague, the second most common form of the disease, results from human-to-human transmission of the bacillus by aerosols, and is systematically and rapidly lethal if effective antibiotic therapy is not delivered before or at the onset of symptoms. Despite considerable progress in plague prevention and cure, this infection has not been eradicated. Natural plague foci still persist in numerous countries in Africa, Asia, and the Americas. Several genetic elements conferring virulence properties have been horizontally acquired by *Y. pestis*. This includes three plasmids: (i) pYV, which encodes a type III secretion system and toxins that subvert the defenses of the mammalian hosts, (ii) pFra, a large replicon which codes for a capsule that confers some resistance to the antibacterial activity of macrophages, and (iii) pPla, whose main product (Pla) is an important virulence factor that has protease and plasminogen activator activities. Another horizontally acquired element is the High Pathogenicity Island which allows *Y. pestis* to utilize the host iron and to cause septicemia. The most recently described mobile element is a filamentous phage, named YpfΦ that plays a role in the capacity of the plague bacillus to multiply and disseminate in mice (Derbise et al., 2007). The purpose of this review is to present the current knowledge about YpfΦ and to discuss its impact on the plague bacillus physiology.

## CHARACTERISTICS OF YpfΦ

YpfΦ forms filamentous particles that are secreted by the *Y. pestis* cells into the culture supernatant without affecting bacterial growth or lyzing the cells. Low titers of phages are produced in standard *in vitro* growth conditions. YpfΦ has a filamentous virion 1,200 nm in length and 8 nm in diameter, which contains a circular positive single strand DNA molecule (**Figure 1A**). The phage has the capacity under laboratory conditions to infect the three pathogenic *Yersinia* species (*Y. pestis* and the enteropathogens *Y. pseudotuberculosis* and *Y. enterocolitica*). The phage infectivity rates, determined with an antibiotic tagged version of YpfΦ range from $<2 \times 10^{-9}$ to $10^{-1}$ depending on the isolates. *Y. pestis* strains are the most susceptible to a YpfΦ infection (99% of the strains), followed by *Y. enterocolitica* (50% of the strains), while only 30% of the *Y. pseudotuberculosis* strains are infected. The infectivity spectrum of YpfΦ is not restricted to *Yersinia* since *Escherichia coli* strains (TOP10, ECOR31) were also successfully transduced with YpfΦ.

No YpfΦ receptor on the bacterial surface has been identified yet. Deletion of genes encoding pili-like structures (*pilA*, *psaA*) that were potential candidate receptors did not affect the susceptibility of *Y. pestis* to YpfΦ (Chouikha et al., 2010). It could be possible that YpfΦ uses several receptor molecules at the bacterial surface, a hypothesis that is supported by the wide host range of this phage. Many filamentous phages use the TolQAR complex as a membrane receptor for entry into the recipient cell. Since TolQAR is highly conserved in Gram negative bacteria (Click and Webster, 1997; Heilpern and Waldor, 2000), it could serve as a secondary receptor for YpfΦ entry (Russel et al., 1988).

## ORIGIN AND DISTRIBUTION OF YpfΦ

*Yersinia pestis* is a clonal species that emerged recently from *Y. pseudotuberculosis*, a much less virulent bacterium (Achtman et al., 1999). Molecular phylogenetic studies combined with whole genome sequencing showed that after its divergence from *Y. pseudotuberculosis*, *Y. pestis* evolved along one branch (branch 0), before the split into two main branches (1 and 2) and several sub

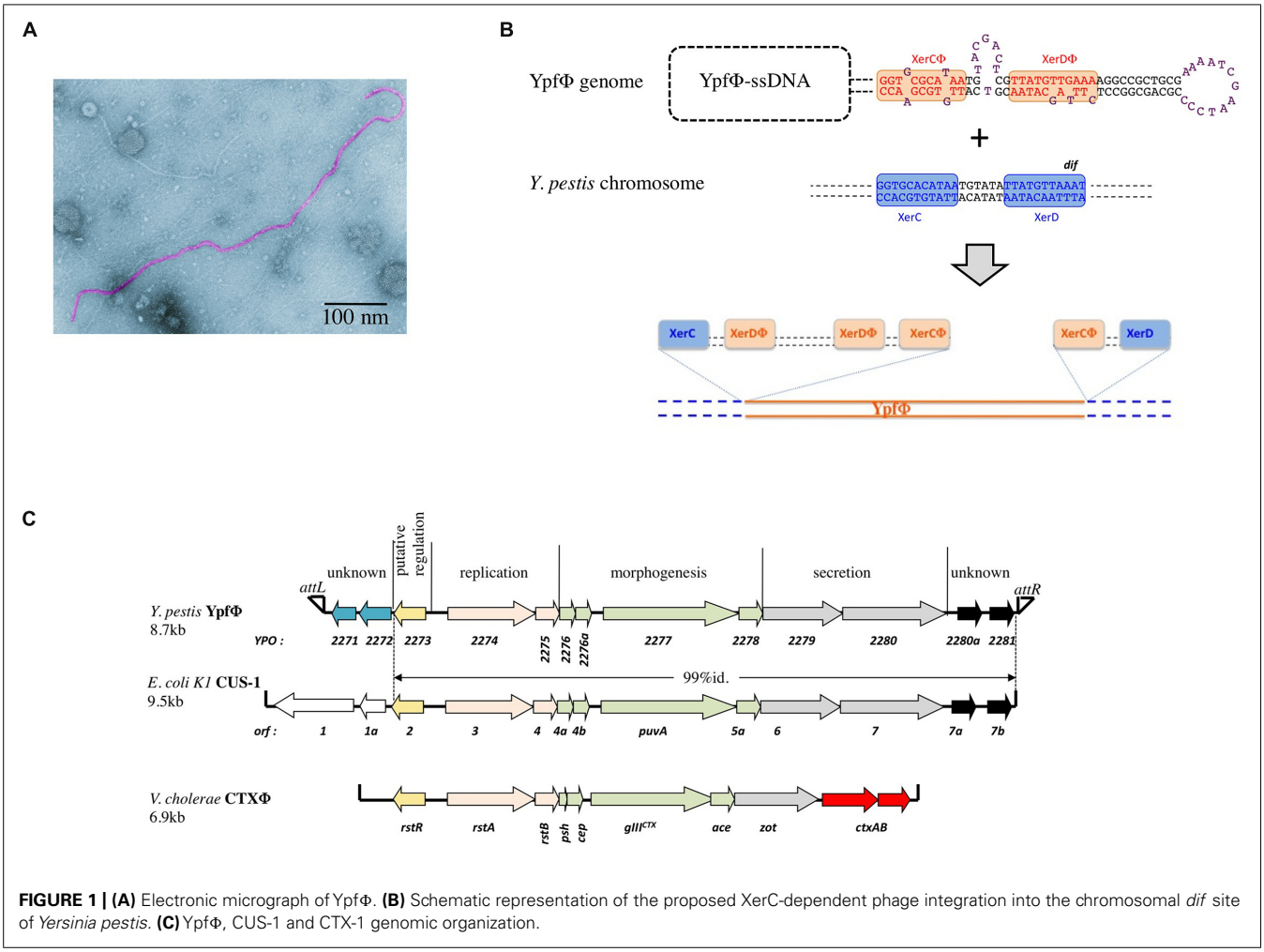


**FIGURE 1 | (A)** Electronic micrograph of YpfΦ. **(B)** Schematic representation of the proposed XerC-dependent phage integration into the chromosomal *dif* site of *Yersinia pestis*. **(C)** YpfΦ, CUS-1 and CTX-1 genomic organization.

branches (**Figure 2**; Achtman et al., 2004). The YpfΦ prophage genome was initially identified in a comparative study of the genomes of one strain each of *Y. pestis* and *Y. pseudotuberculosis*. An analysis of an extensive set of isolates showed that the phage is systematically absent from *Y. pseudotuberculosis*. In *Y. pestis*, the phage is present in isolates from the three main phylogenetic branches, suggesting its acquisition early after *Y. pestis* emergence (Derbise et al., 2007). However, YpfΦ was not detected in all *Y. pestis* isolates. The phage is systematically present in strains from sub branch 1.ORI (**Figure 2**). This branch corresponds to the *Y. pestis* isolates that caused the third plague pandemic and that are found in most plague foci worldwide today. In the other sub branches YpfΦ is detected in some isolates only. Furthermore, only a portion of the bacterial cells that were found to be phage-positive harbors the phage genome (Derbise et al., 2007; Li et al., 2008). This indicates that YpfΦ is not stably maintained in the non-1.ORI branches and that the phage is easily lost upon *Y. pestis* subcultures *in vitro*. The capacity to stabilize the phage genome in the bacterial chromosome as a prophage is thus a property that was acquired late during *Y. pestis* evolution, and only in the third pandemic lineage.

## LOCATION OF YpfΦ GENOME IN THE BACTERIAL CELL

In sub branch 1.ORI, YpfΦ is present mostly as an integrated prophage although extrachromosomal forms are also detected. As observed for several other filamentous prophages (Gonzalez et al., 2002; Huber and Waldor, 2002) YpfΦ integrates its genome into the chromosomal *dif* site of the host bacterium. *dif* is a recombinational locus used by the XerCD recombinases of the bacterial host to resolve chromosome dimers (Das et al., 2013). YpfΦ insertion reconstitutes an intact *dif* site at the 3′ extremity of the prophage sequence (**Figure 1B**). Sequence analysis of the YpfΦ encapsidated genome indicates the presence of a potential pair of binding sites for XerC and XerD in inverted orientations (**Figure 1B**). Similarly to the *Vibrio cholerae* filamentous phage CTXΦ such structure may constitute a XerCD substrate for recombination with the bacterial *dif* site, leading to the integration of the phage genome into the host chromosome (**Figure 1B**; Val et al., 2005). In the *Y. pestis* chromosome, the YpfΦ genome forms tandem repeats of two to four copies. Although two copies is the predominant form, more copies can be detected in the same bacterial population, suggesting constant and dynamic rearrangements between tandem repeats. Variations in the number of tandem repeats may also result from continuous excision by homologous

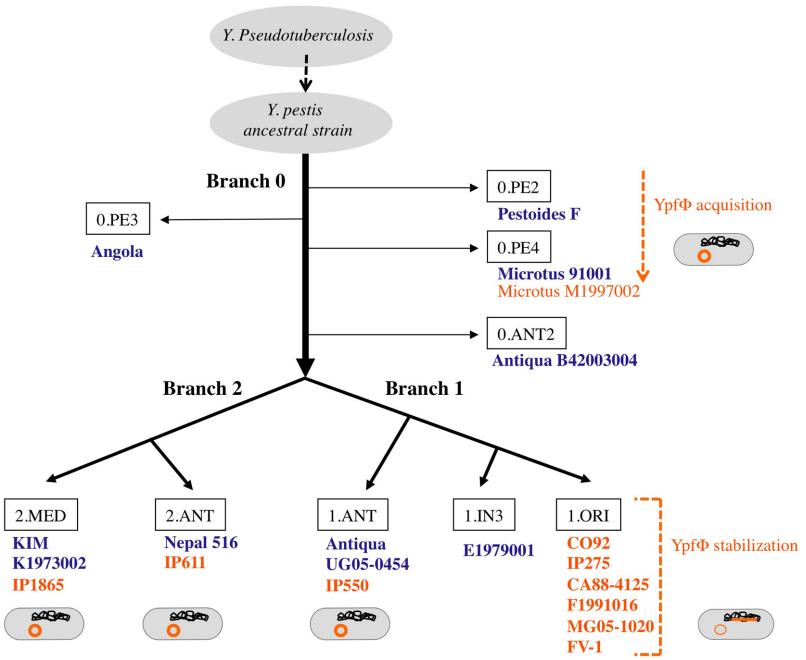


**FIGURE 2 | Microevolution tree of *Y. pestis*.** Strains in which no YpfΦ was identified in the sequenced genome are indicated in blue. Strains from which a phage genome was detected by PCR and/or sequencing are indicated in orange. The location of the phage genome within the bacterial cell is schematized in orange.

recombination of some copies and insertion of extrachromosomal phage genomes. Supporting this hypothesis is the recent demonstration that EndoIII, a DNA glycosylase/lyase, serves as a co-factor facilitating the integration of CTXΦ ssDNA into the *V. cholerae* chromosomal *dif* site and increasing the number of tandem repeats (Bischerour et al., 2012). Since *Y. pestis* harbors in its genome a homologue to EndoIII, this protein may promote multiple successive integration events leading to the generation of YpfΦ tandem repeats.

In the phage-positive *Y. pestis* strains that belong to phylogenetic branches other than 1.ORI, the phage genome is present as an extrachromosomal replicon only. The difference in location, as compared with the 1.ORI strains, is not due to differences in phage properties since the YpfΦ nucleotide sequence is 100% identical in all *Y. pestis* isolates (Derbise et al., 2007). The chromosomal *dif* site and machinery of phage integration are also identical in all *Y. pestis* strains. Moreover, when phage-negative *Y. pestis* strains are infected under laboratory conditions with YpfΦ the phage genome can be found integrated into their chromosome. This confirms that these strains do have a functional integration machinery. Why the non-1.ORI natural isolates of *Y. pestis* do not carry prophage forms of YpfΦ remains an unanswered question Epigenetic differences might be involved. For instance the integration machinery could be differently expressed in the non-1.ORI strains, thus affecting YpfΦ insertion efficiency.

When *Y. pseudotuberculosis* and *E. coli* strains are transduced with YpfΦ under laboratory conditions, the phage is almost exclusively extrachromosomal, while in *Y. enterocolitica* the phage is both inserted in the chromosome and in extrachromosomal forms. Since the XerCD recombinases responsible for filamentous phage integration at the *dif* site are 99 and 100% identical between *Y. pestis* and *Y. pseudotuberculosis*, and the EndoIII sequence is 100% identical, the difference in integration efficiency may be explained either by differences in other integration host factors or by a higher excision rate of the phage genome from the bacterial chromosome.

The presence of an endogenous YpfΦ confers partial protection against a superinfection by the same phage. This is reminiscent of the immunity observed with CTXΦ which is due to a repressor of the replication encoded by the phage (Kimsey and Waldor, 1998). However when the YpfΦ superinfection occurs, the incoming phage integrates preferentially between two integrated copies of the phage genomes rather than at the 3′ extremity of the tandem repeats, as seen for CTXΦ. Since the junction between two integrated copies of YpfΦ constitutes an imperfect *dif* site (Chouikha et al., 2010), this insertion site was not predicted by classical models of phage integration. The YpfΦ insertion may also result from homologous recombination between an extrachromosomal incoming DNA and the chromosomal resident copies.

## GENETIC ORGANIZATION OF YpfΦ

The YpfΦ genome is 8.7 kb long and comprises 13 open reading frames (ORFs) organized in two opposite transcriptional orientations, with an intergenic region believed to be involved in transcription initiation (**Figure 1C**). Its genetic organization resembles those of well characterized filamentous bacteriophages such as CTXΦ of *V. cholerae* (Davis and Waldor, 2003) and

Ff (f1, fd, and M13) of *E. coli* (Model and Russel, 1988). Eight ORFs are organized in three modules involved in phage replication (YPO2274 and YPO2275), morphogenesis (YPO2276-YPO2278), and secretion (YPO2279 and YPO2280). The role of these functional modules was confirmed after disruption of genes predicted to be involved in morphogenesis (YPO2277), secretion (YPO2279), or replication (YPO2274), as each mutation abolished the production of phage particles (Chouikha et al., 2010).

Two additional ORFs (YPO2280a and YPO2281) of the YpfΦ prophage, located immediately adjacent to the *attR*, have no predictable functions. CUS-1, a very similar filamentous prophage of an *E. coli* K1 high-virulence strain is almost identical (99% nucleotide identity) over its 7.1 kb segment, covering, besides the YPO2280a and YPO2281 ORF homologs, all phage genes required for regulation, replication and assembly (**Figure 1C**; Gonzalez et al., 2002). The YPO2280a and YPO2281 homologs are absent from CTXΦ, which carries at this position two other ORFs, encoding the cholera toxin, the major virulence factor of *V. cholerae*.

The attL-adjacent segment of YpfΦ is composed of two ORFs (YPO2271 and YPO2272) that are absent from CTXΦ and that are replaced by two other unrelated ORFs (*orf1* and *orf1a*) in CUS-1 (**Figure 1C**). These two ORFs have no homologs in the databases and are therefore of unknown functions.

## REGULATION OF YpfΦ PRODUCTION

YpfΦ carries YPO2273, a gene homologous to RstR, which is a transcriptional repressor of CTXΦ. YPO2273 is located at the same position as *rstR* in the phage genome, thus suggesting that it might also regulate the bacteriophage replication. However its regulatory role awaits experimental demonstration. In addition, YpfΦ is regulated by the *Yersinia* global regulator RovA, which binds to the putative promoter regions of YPO2274. In the absence of RovA, transcription of the phage genes YPO2274 to YPO2279 is highly increased (Cathelyn et al., 2006). Whether RovA interferes with YPO2273 expression is not known.

## ROLE OF YpfΦ IN *Y. pestis* PATHOGENESIS

In *Y. pestis*, a slight increase in the $LD_{50}$ of the YpfΦ deleted strain (≈sevenfold) was observed in the mouse experimental model of bubonic plague. Furthermore, *in vivo* competitive assays showed that the presence of the phage conferred some advantages to the host bacteria, allowing a better colonization of their mammalian host. Deletion of the prophage genomes from the bacterial chromosome had no impact on *Y. pestis* capacity to grow *in vitro*, to be taken up by fleas and to multiply in their gut. Therefore, YpfΦ is not a major virulence factor of *Y. pestis*, but seems to confer a higher fitness to its bacterial host during the infection of mammals. This is similar to the effect of closely related phage CUS-1 in *E. coli* O18:K1:H7 invasive extra intestinal clones. Decreased *in vivo* fitness of an *E. coli* K1 mutant in the CUS-1 prophage containing an interrupted *puvA* gene (encoding a virion protein required for binding to the host receptors; **Figure 1C**) suggests that CUS-1 plays a role in *E. coli* virulence (Gonzalez et al., 2001). Overall, in contrast to the filamentous phage CTXΦ, that is crucial for the pathogenicity of *V. cholerae*, YpfΦ and CUS-1 have moderate impact on bacterial fitness and pathogenicity. Nevertheless, the fact that episomal YpfΦ has been maintained in the different *Y. pestis* branches despite the observed high rate of the phage loss *in vitro*, suggests that the presence of this mobile element provides an overall selective advantage to the plague bacillus.

## CONCLUSION

The YpfΦ filamentous phage has been acquired by *Y. pestis* after its divergence from *Y. pseudotuberculosis*, first as an extrachromosomal replicon, and subsequently as a stable, integrated prophage in the 1-ORI branch, the contemporary pathogen and the cause of the last plague pandemic. Whether the stabilization of the phage genome in this branch participated in its current pandemic spread is not known. Another yet unanswered question is why YpfΦ is capable of integrating itself into the bacterial chromosome in this lineage and not in the other ones, despite identical site and machinery of integration. Finally, identifying the functions of the ORFs located at each of the termini of the YpfΦ prophage genome could bring important insights into the function of the phage.

## REFERENCES


Achtman, M., Morelli, G., Zhu, P., Wirth, T., Diehl, I., Kusecek, B., et al. (2004). Microevolution and history of the plague bacillus, *Yersinia pestis*. *Proc. Natl. Acad. Sci. U.S.A.* 101, 17837–17842. doi: 10.1073/pnas.0408026101

Achtman, M., Zurth, K., Morelli, G., Torrea, G., Guiyoule, A., and Carniel, E. (1999). *Yersinia pestis*, the cause of plague, is a recently emerged clone of Yersinia pseudotuberculosis. *Proc. Natl. Acad. Sci. U.S.A.* 96, 14043–14048. doi: 10.1073/pnas.96.24.14043

Bischerour, J., Spangenberg, C., and Barre, F. X. (2012). Holliday junction affinity of the base excision repair factor Endo III contributes to cholera toxin phage integration. *EMBO J.* 31, 3757–3767. doi: 10.1038/emboj.2012.219

Cathelyn, J. S., Crosby, S. D., Lathem, W. W., Goldman, W. E., and Miller, V. L. (2006). RovA, a global regulator of *Yersinia pestis*, specifically required for bubonic plague. *Proc. Natl. Acad. Sci. U.S.A.* 103, 13514–13519. doi: 10.1073/pnas.0603456103

Chouikha, I., Charrier, L., Filali, S., Derbise, A., and Carniel, E. (2010). Insights into the infective properties of YpfPhi, the *Yersinia pestis* filamentous phage. *Virology* 407, 43–52. doi: 10.1016/j.virol.2010.07.048

Click, E. M., and Webster, R. E. (1997). Filamentous phage infection: required interactions with the TolA protein. *J. Bacteriol.* 179, 6464–6471.

Das, B., Martinez, E., Midonet, C., and Barre, F. X. (2013). Integrative mobile elements exploiting Xer recombination. *Trends Microbiol.* 21, 23–30. doi: 10.1016/j.tim.2012.10.003

Davis, B. M., and Waldor, M. K. (2003). Filamentous phages linked to virulence of *Vibrio cholerae*. *Curr. Opin. Microbiol.* 6, 35–42. doi: 10.1016/S1369-5274(02)00005-X

Derbise, A., Chenal-Francisque, V., Pouillot, F., Fayolle, C., Prevost, M. C., Medigue, C., et al. (2007). A horizontally acquired filamentous phage contributes to the pathogenicity of the plague bacillus. *Mol. Microbiol.* 63, 1145–1157. doi: 10.1111/j.1365-2958.2006.05570.x

Gonzalez, M. D., Lichtensteiger, C. A., Caughlan, R., and Vimr, E. R. (2002). Conserved filamentous prophage in *Escherichia coli* O18:K1:H7 and *Yersinia pestis* biovar orientalis. *J. Bacteriol.* 184, 6050–6055. doi: 10.1128/JB.184.21.6050-6055.2002

Gonzalez, M. D., Lichtensteiger, C. A., and Vimr, E. R. (2001). Adaptation of signature-tagged mutagenesis to *Escherichia coli* K1 and the infant-rat model of invasive disease. *FEMS Microbiol. Lett.* 198, 125–128. doi: 10.1111/j.1574-6968.2001.tb10630.x

Heilpern, A. J., and Waldor, M. K. (2000). CTXphi infection of *Vibrio cholerae* requires the tolQRA gene products. *J. Bacteriol.* 182, 1739–1747. doi: 10.1128/JB.182.6.1739-1747.2000

Huber, K. E., and Waldor, M. K. (2002). Filamentous phage integration requires the host recombinases XerC and XerD. *Nature* 417, 656–659. doi: 10.1038/nature00782

Kimsey, H. H., and Waldor, M. K. (1998). CTXphi immunity: application in the development of cholera vaccines. *Proc. Natl. Acad. Sci. U.S.A.* 95, 7035–7039. doi: 10.1073/pnas.95.12.7035

Li, Y., Dai, E., Cui, Y., Li, M., Zhang, Y., Wu, M., et al. (2008). Different region analysis for genotyping *Yersinia pestis* isolates from China. *PLoS ONE* 3:e2166. doi: 10.1371/journal.pone.0002166

Model, P., and Russel, M. (1988). "Filamentous bacteriophage," in *The Bacteriophages*, ed. R. Calendar (New York and London: Plenum press).

Russel, M., Whirlow, H., Sun, T. P., and Webster, R. E. (1988). Low-frequency infection of F- bacteria by transducing particles of filamentous bacteriophages. *J. Bacteriol.* 170, 5312–5316.

Val, M. E., Bouvier, M., Campos, J., Sherratt, D., Cornet, F., Mazel, D., et al. (2005). The single-stranded genome of phage CTX is the form used for integration into the genome of *Vibrio cholerae*. *Mol. Cell* 19, 559–566. doi: 10.1016/j.molcel.2005.07.002

**Conflict of Interest Statement:** The authors declare that the research was conducted in the absence of any commercial or financial relationships that could be construed as a potential conflict of interest.

*Received: 24 September 2014; accepted: 26 November 2014; published online: 15 December 2014.*

*Citation: Derbise A and Carniel E (2014) Ypf*Φ*: a filamentous phage acquired by Yersinia pestis. Front. Microbiol.* ***5****:701. doi: 10.3389/fmicb.2014.00701*

*This article was submitted to Virology, a section of the journal Frontiers in Microbiology.*

frontiers in
MICROBIOLOGY

REVIEW ARTICLE
published: 28 November 2014
doi: 10.3389/fmicb.2014.00650

# Mechanistic insights into filamentous phage integration in *Vibrio cholerae*

**Bhabatosh Das***

*Centre for Human Microbial Ecology, Translational Health Science and Technology Institute, Gurgaon, India*

***Edited by:***
*Jasna Rakonjac, Massey University, New Zealand*

***Reviewed by:***
*Dahlene N. Fusco, Massachusetts General Hospital, USA*
*Christophe Possoz, Centre National de la Recherche Scientifique, France*

***Correspondence:**
*Bhabatosh Das, Centre for Human Microbial Ecology, Translational Health Science and Technology Institute, 496, Phase III, Udyog Vihar, Gurgaon 122 016, Haryana, India*
*e-mail: bhabatosh@thsti.res.in*

*Vibrio cholerae*, the etiological agent of acute diarrhoeal disease cholera, harbors large numbers of lysogenic filamentous phages, contribute significantly to the host pathogenesis and provide fitness factors to the pathogen that help the bacterium to survive in natural environment. Most of the vibriophage genomes are not equipped with integrase and thus exploit two host-encoded tyrosine recombinases, XerC and XerD, for lysogenic conversion. Integration is site-specific and it occurs at dimer resolution site (*dif*) of either one or both chromosomes of *V. cholerae*. Each *dif* sequence contains two recombinase-binding sequences flanking a central region. The integration follows a sequential strand exchanges between *dif* and *attP* sites within a DNA-protein complex consisting of one pair of each recombinase and two DNA fragments. During entire process of recombination, both the DNA components and recombinases of the synaptic complex keep transiently interconnected. Within the context of synaptic complex, both of the actuated enzymes mediate cleavage of phosphodiester bonds. First cleavage generates a phosphotyrosyl-linked recombinase-DNA complex at the recombinase binding sequence and free 5′-hydroxyl end at the first base of the central region. Following the cleavage, the exposed bases with 5′-hydroxyl ends of the central region of *dif* and *attP* sites melt from their complementary strands and react with the recombinase-DNA phosphotyrosyl linkage of their recombining partner. Subsequent ligation between *dif* and *attP* strands requires complementary base pair interactions at the site of phosphodiester bond formation. Integration mechanism is mostly influenced by the compatibility of *dif* and *attP* sequences. *dif* sites are highly conserved across bacterial phyla. Different phage genomes have different *attP* sequences; therefore they rely on different mechanisms for integration. Here, I review our current understanding of integration mechanisms used by the vibriophages.

**Keywords: CTXΦ, VGJΦ, TLCΦ, XerC, XerD, *dif*, *attP***

## INTRODUCTION

Bacterial pathogens evolve continuously to adapt to the changing environment by adopting multiple mobile genetic elements into their compact, modularly organized mosaic genomes to help combat the environmental factors that are detrimental to their subsistence (Frost et al., 2005; Mercier et al., 2008; Hassan et al., 2010). *Vibrio cholerae*, the noxious enteric pathogen with extraordinary fitness competence resides in multiple niches across continents. A variety of the vibrio strains have acquired multiple genetic traits in their genomes (Heidelberg et al., 2000; Sack et al., 2004; Chun et al., 2009), with the purpose of contributing to the toxin production (Waldor and Mekalanos, 1996), intestinal colonization (Rhine and Taylor, 1994), disease development (Herrington et al., 1988), antimicrobial resistance (Mazel and Davies, 1998; Beaber et al., 2004), cell division (Hassan et al., 2010), and survival in aquatic as well as gut environments (Davies et al., 2012). In *V. cholerae*, most of the horizontally acquired genetic traits integrate site-specifically within a short region of sequence identity shared by the host chromosome and the integrative mobile genetic elements (IMGEs), using self- or host-encoded tyrosine recombinases (Huber and Waldor, 2002; Rajanna et al., 2003; Hazen et al., 2010; Das et al., 2013; Banerjee et al., 2014). Integration might be reversible or irreversible, depending upon the structures of pre- and post-integrative attachment sequences (Das et al., 2011a, 2013, 2014). Tyrosine recombinases can bind double stranded as well as folded single stranded DNA of the acquired exogenous genetic elements (Val et al., 2005; Mazel, 2006; Das et al., 2011b). Different acquired genetic traits reported in *V. cholerae* are heterogeneous, and they recognize different receptors for infection (Herrington et al., 1988; Campos et al., 2010; Das et al., 2013), follow different mechanisms to deliver DNA into the host cytoplasm (Heilpern and Waldor, 2000), have a wide range of genomic content (Heidelberg et al., 2000; Faruque and Mekalanos, 2003), and most importantly rely on catalytic activities of different recombinases for chromosomal integration (Rajanna et al., 2003; Das et al., 2010, 2011b; Midonet et al., in press). In a broader sense, these IMGEs can be classified into two different groups, depending upon the presence and absence of recombinases, the enzymes essential for their integration to the host genome. IMGEs, which encode and rely on

**Table 1 | Key components of the Xer recombination system in *V. cholerae*.**

| Gene | Gene ID in N16961 genome | Gene length (bp) | Protein | Protein length (aa) | Mol. weight (kD) |
|---|---|---|---|---|---|
| *xerC* | *VC0128* | 936 | XerC | 311 | 35.55 |
| *xerD* | *VC2419* | 909 | XerD | 302 | 34.56 |
| *ftsK* | *VC1903* | 2883 | FtsK | 960 | 105.89 |

their own recombinases for integration, are generally large in size and integrates specifically in front of tRNA or tmRNA operon (Karaolis et al., 1999; Heidelberg et al., 2000). On the other hand, IMGEs exploit host-encoded tyrosine recombinases (IMEX), are small in size and integrate at the dimer resolution sites (*dif*) of host chromosomes (Das et al., 2013, 2014).

The best-characterized IMEX, which exploits the host encoded tyrosine recombinases for its lysogenic conversion is CTXΦ, a temperate filamentous bacteriophage that encodes the cholera toxin in *V. cholerae* (Waldor and Mekalanos, 1996). The CTXΦ recognizes the toxin co-regulated pilus (TCP), a type IV pilus encoded by the vibrio pathogenic island–I (VPI-1), and subsequently introduces its $\sim 7.0 \times 10^3$ nucleotides long circular single stranded genomic DNA (+ssDNA) into the *V. cholerae* cytoplasm. Once in the bacterial cytoplasm, ssDNA may convert to dsDNA, and start the rolling circle replication, or it can be recognized by the chromosomally-encoded tyrosine recombinases, that enable CTXΦ integration into the *dif* site of host chromosome. Tandemly integrated CTXΦ can also initiate the rolling circle replication from the chromosome and produce extrachromosomal ssDNA genome that may contribute in virion production (Davis and Waldor, 2000). Compared to other episomally replicative filamentous phages, the number of phage particles produced by the CTX-prophage is very low, even upon induction, resulting in one phage particle produced per 10–100 host cells (Davis et al., 2002). The other two well-characterized IMEXs that use the same recombinases for integration at the *dif1* site of *V. cholerae* are VGJΦ and TLCΦ (Campos et al., 2003b; Hassan et al., 2010; Das et al., 2011b). Presence of single or multiple copies of VGJΦ and TLCΦ were reported in toxigenic *V. cholerae* isolates. Unlike CTXΦ, the virion production of VGJΦ, and TLCΦ mainly relies on the episomal replication. Although the genomes of the two latter elements do not encode any toxins, they are nevertheless implicated in the host fitness and play important role in acquisition of the cholera-toxin-encoding genes and CTXΦ dissemination (Hassan et al., 2010; Das et al., 2011b; Midonet et al., in press).

In this review, I will update the mechanistic insights into filamentous vibriophage integration and cooperative interactions amongst IMGEs, which support the emergence of new pathogenic strains by contributing efficient acquisition and rapid dissemination of the cholera toxin genes in closely or distantly related bacterial strains.

## XER RECOMBINATION SYSTEM IN *VIBRIO CHOLERAE*

The native function of Xer recombination system is to ensure the stable maintenance of monomeric circular replicon (Blakely et al., 1993). In *V. cholerae*, the principal components of the Xer recombination system are (i) two recombinases, XerC and XerD; (ii) a DNA motor protein, FtsK; (iii) a 28-bp DNA sequence, *dif* (Val et al., 2008) (**Table 1**). The Xer proteins are members of the tyrosine recombinase family (Esposito and Scocca, 1997). Members of this family share two conserved motifs, containing four highly conserved residues (R1-H-R2-Y), a catalytic tyrosine, which acts as the nucleophile during cleavage of phosphodiester bond, two arginines and a histidine, which have been implicated both the cleavage and rejoining of DNA strands (Esposito and Scocca, 1997). The two positively charged arginines are thought to stabilize the pentavalent phosphate transition state, whereas the histidine may act as a general base catalyst (Esposito and Scocca, 1997; Sherratt and Wigley, 1998).

During chromosome dimer resolution at the end of DNA replication, tetrameric XerC and XerD recombinase complex catalyzes successive strand exchanges between the two *dif* sites of a dimeric chromosome. The resolution is completed by a two-step transesterification reaction in which the OH- group of catalytic tyrosine residue of each recombinase is directly involved in the phosphodiester bond formation (**Figure 1**). In the first step of dimer resolution reaction, cleavage of a phosphodiester bond in DNA is introduced by the active enzyme, generating a covalently linked enzyme-DNA complex at the recombinase binding site and a free 5′-hydroxyl group at the end of the central region. Following the cleavage, the exposed sequence at the 5′-hydroxyl ends of the central region melt from their complementary strands and react with their recombinase-DNA phosphotyrosyl linked recombining partner. Subsequent joining between *dif* and *attP* strands requires complementary base pair interactions at the site of the phosphodiester bond formation (MacDonald et al., 2006; Das et al., 2010).

FtsK, a bifunctional protein essential for cell division and chromosome partitioning, induces the XerD function during chromosome dimer resolution (Recchia et al., 1999; Aussel et al., 2002; Demarre et al., 2013). The N-terminal part of FtsK forms a transmembrane domain and is directly linked to the forming septum. The cytoplasmic C-terminal domain is involved in the inter- and intracellular DNA transfer and activation of XerD recombinases (Bigot et al., 2006). Recent reports demonstrated that several IMGEs exploit the conserved Xer recombination system of bacteria to mediate their integration in the dimer resolution site of host chromosomes (Das et al., 2013). The integration mechanisms of such elements were studied in details in *V. cholerae* and revealed that the IMEXs present in the *dif* region of *V. cholerae* make use of three distinct integration mechanisms for lysogenic conversion (Das et al., 2010, 2011a,b, 2013; Midonet et al., in press).

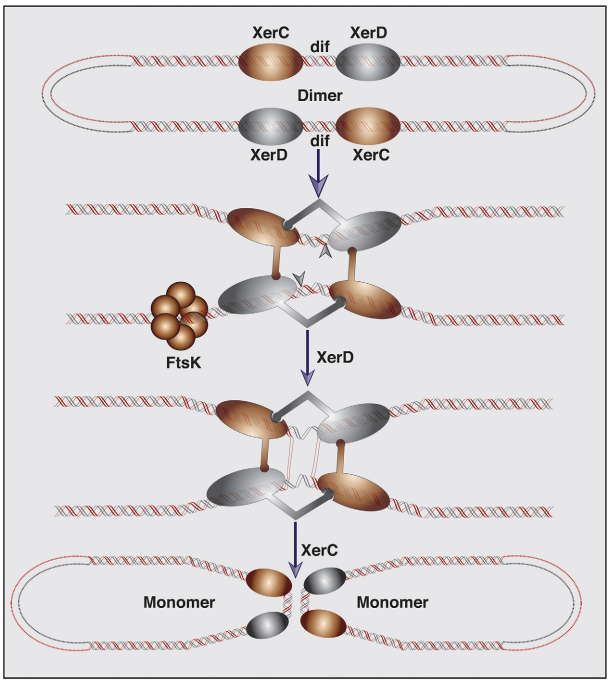


**FIGURE 1 | Schematic representation of the XerC-XerD mediated chromosome dimer resolution.** Chromosome dimers are resolved by the XerC-XerD-mediated recombination at the *dif* site. DNA motor protein FtsK brings two *dif* sites together and induces the XerD catalytic activity required for the first pair of strand exchanges. Followed isomerization, XerC mediates the second pair of strand exchanges, and completes the recombination reaction.

## LYSOGENIC FILAMENTOUS VIBRIOPHAGES EXPLOIT XER RECOMBINASES

Most of the characterized filamentous vibriophages are lysogenic and integrate at the *dif1* and/or *dif2* sites of *V. cholerae*. All reported filamentous vibriophages are equipped with an autonomously replicating genetic module, with or without toxin-encoding genes (**Figure 2**). Some of the filamentous vibriophages are directly responsible for *V. cholerae* pathogenesis, others contribute to toxin acquisition and host fitness (Waldor and Mekalanos, 1996; Hassan et al., 2010). Their genomes may or may not be equipped with genes required for virion production and can exploit the virion structural and assembly genes of other filamentous phages for genome packaging (Hassan et al., 2010). Although most of the filamentous vibriophages use host-encoded Xer machinery for their integration, their attachment sites (*attP*), and their genomic organization are fairly distinct (**Figure 2**). The best-studied CTXΦ genome is organized into two structurally and functionally distinct modules called repeat sequence 2 (RS2) and core (**Figure 2**). The RS2 module carries genetic traits essential for CTXΦ replication, maintenance of the ssDNA genome, and transcriptional regulation from phage originated $P_{RSTA}$ promoter (Waldor et al., 1997). The replicating genome of CTXΦ is detrimental to *V. cholerae* growth, but is tolerated upon integration into the *dif* sites of either one or both chromosomes (Das et al., 2010; Faruque and Mekalanos, 2012). Compared to toxigenic strains, that contain a single or multiple integrated CTXΦ genomes, *V. cholerae* cells carrying a replicative form of CTXΦ grow slowly and rapidly lose the replicative phage both under the standard laboratory growth conditions and in rabbit gastrointestinal tract animal model (Faruque et al., 2001).

VGJΦ, a filamentous (+)ssDNA lysogenic bacteriophage, infects both clinical and environmental isolates of cholera pathogen and exploits the host-encoded Xer recombinases to integrate at the *dif1* site in the large chromosome of *V. cholerae* (Campos et al., 2003b, 2010; Das et al., 2011b). In contrast to complex attachment site of CTXΦ that contains two *dif*-like *attP* sites in an inverted orientation, the 7.5-kb genome of VGJΦ harbors a single *dif*-like 29-bp attachment sequence, called $attP^{VGJ}$ and integrates specifically into the *dif1* site.

TLCΦ, a satellite temperate phage with an autonomous replication module but lacking the morphogenesis and structural virion-encoding genes, is often present in the *dif1* region of toxigenic *V. cholerae* isolates (Rubin et al., 1998). Recent reports demonstrated that, like CTXΦ, and VGJΦ, TLCΦ also relies on the host-encoded Xer machinery for establishing lysogeny (Hassan et al., 2010; Midonet et al., in press). Interestingly, although both the XerC and XerD recombinases are essential for integration of IMEXs, none of the reported IMEXs rely on FtsK for recombination.

Different vibriophages have different *attP* structures and therefore rely on to a certain extent of different mechanisms of interaction with the Xer recombinases and integration (Das et al., 2013).

### MECHANISTIC INSIGHTS INTO LYSOGENIC CONVERSION OF VIBRIOPHAGES

Most lysogenic filamentous vibriophages are IMEXs that depend on the host-encoded Xer recombinases for their lysogeny. The attachment site in the phage genome mimics the native chromosomal Xer binding sites and exploits Xer recombinases to catalyze site-specific recombination and enable phage integration. Based on the *attP* structure and integration mechanisms, vibriophages can be categorized into three classes (**Table 2**). Although the constituents of the integration reaction are very similar, integration is achieved by three distinct mechanisms, where catalytic activity of recombinases, order of strand exchanges and the resolution of reaction intermediates into end products are different (**Figures 3–5**). In this review, I will concentrate on CTXΦ, VGJΦ, and TLCΦ lysogenic conversions to describe the most updated integration mechanisms of these phages studied in *V. cholerae* and related bacterial cells.

### MECHANISTIC INSIGHTS INTO CTXΦ INTEGRATION

CTX-prophages are ubiquitously present in the chromosomes of all epidemics *V. cholerae* isolates (Mekalanos et al., 1983; Mekalanos, 1985; Vanden Broeck et al., 2007). Phage to prophage conversion is rapid and efficient process achieved through site-specific recombination between *attP*(+) of CTXΦ and *dif* sites of *V. cholerae* (Val et al., 2005) that results in a stable integration. The functional *attP*(+) structure is formed by intra-strand base pairing interactions between two inversely oriented *attP*

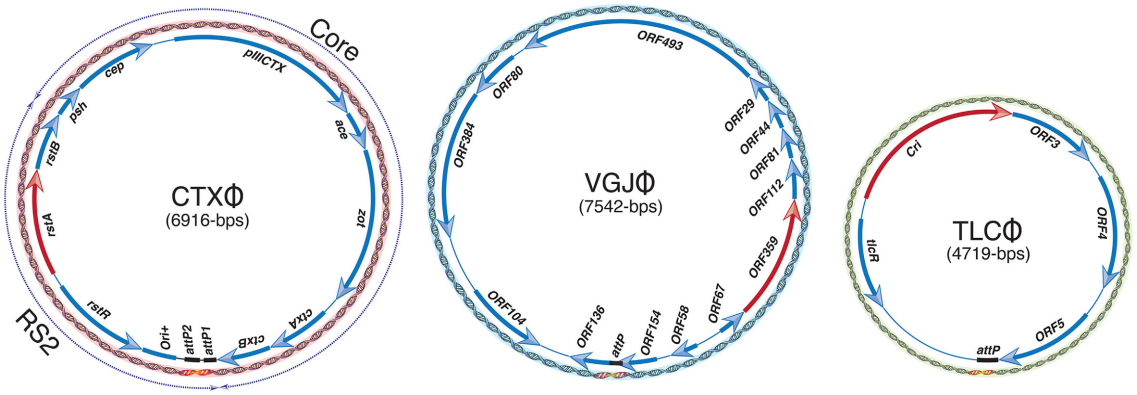


**FIGURE 2 | Genomic organization of CTXΦ, VGJΦ, and TLCΦ phages.** A red arrow depicts gene essential for replication in each genome. A solid black line denotes attachment sequence, recognized by the Xer recombinases. Replicative form (RF) of each phage genome is presented as dsDNA. Arrows indicate the direction of transcription of each ORF. A thin solid line illustrates intergenic regions. Dashed arrows above the CTXΦ genome represent the core and RS2 modules.

**Table 2 | Different components and strategies used by three different filamentous Vibriophages for their integration at *dif* sites of *V. cholerae* chromosome.**

| Class | CTXΦ | VGJΦ | TLCΦ |
|---|---|---|---|
| Integration site in chromosome | *dif1/dif2* | *dif1* | *dif1* |
| Phage attachment site | *attp(+) (~150 nt)* | $attp^{VGJ}$ *(29-bp)* | $attp^{TLC}$ *(28-bp)* |
| Integrative phage DNA | (+)ssDNA | dsDNA | dsDNA |
| Essential components for integration | XerC, XerD, *attp(+)*, *dif1/dif2* | XerC, XerD, $attp^{VGJ}$, *dif1* | XerC, XerD, $att^{TLC}$, *dif1* |
| First pair of strand exchanges is mediated by | XerC | XerC | XerD |
| Integration is completed by | Host DNA replication | Host DNA replication | XerC |
| Integration event | Irreversible | Reversible | Reversible |
| Excision initiated by | – | XerC | XerD |
| Excision completed by | – | Host DNA replication | XerC |
| Prophage to phage production depends on | Rolling circle replication | Excision | Excision |
| Related members | RS1, YpfΦ, CUS-1Φ | VEJΦ, VSKK, VSK, fs2, Vf12, VfO4K68 | ΦLf, XfΦf1, Cf1c, GGI |

sequences located between the *ctxB* and *rstR* genes in the circular CTXΦ genome (**Figure 2**). In a replicating form (RF) of the genome, *attP1* consists of XerC and XerD binding sites separated by a 12 bp central region. The *attP2* is consists of 11-bp XerC and XerD binding sites and a 5–7 bp central region. Neither *attP1* nor *attP2* are suitable for Xer-mediated integration due to extended central region or presence of incompatible bases in the central region, respectively (Das et al., 2010). The specificity and compatibility of CTXΦ integration is solely determined by the homology of bases next to the XerC-binding site between the overlapping (or corresponding) regions of *attP* and *dif* sequence (Das et al., 2010). A 90-bp DNA fragment separates the *attP1* and *attP2* of CTXΦ. The CTXΦ integration sites in *V. cholerae* chromosomes (*dif1* and *dif2*) each consist of 28 bp DNA sequence. In *dif1*, a 6 bp central region, at the border of which the strand exchange occurs, separates the 11 bp binding sites of XerC and XerD. The chromosomally-encoded Xer recombinases can recognize both the double stranded chromosomal *dif* site and folded single stranded *attP*(+) of CTXΦ and catalyze recombination to facilitate the phage ssDNA integration.

The CTXΦ ssDNA integration takes place within a DNA-protein complex, where DNA strands are cleaved and rejoined sequentially by XerC recombinase through transient nucleoprotein covalent intermediates. The catalytic tyrosine residue of Xer recombinases functions as a nucleophile and mediates the cleavage of a phosphodiester bond between the last base of the recombinase-binding site and the first base of central region. The key components within the nucleoprotein complex are XerC, XerD, *attP*(+), and *dif* sequences. Although the presence of both recombinases are essential for recombination, successful integration of the CTXΦ ssDNA needs only the catalytic activity of XerC (Val et al., 2005). At the onset of recombination reaction, XerC introduces a cut of the phosphodiester bond between the last base of XerC binding site and the first base of the central region, of *dif1/dif2*, and *attP*(+) (**Figure 3**). On one side, a XerC-DNA complex is formed through a covalent phosphotyrosyl bond. On the other side, the DNA strand with a free 5′-OH end melts away from the central region of the reaction complex, migrates to the central region of the partner strand and forms complementary base pairing interactions to stabilize the exchanged

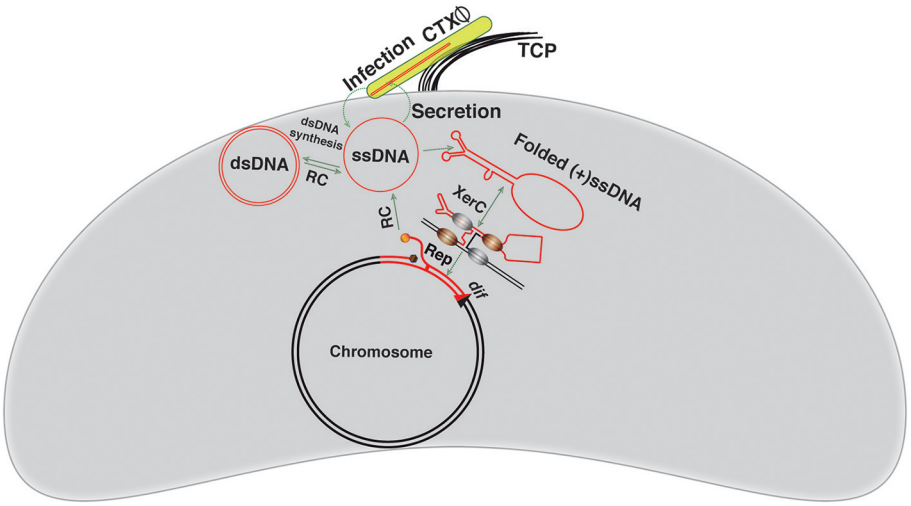


**FIGURE 3 | Visual depiction of the CTXΦ integration and replication.** The CTXΦ virion recognizes the cognate *V. cholerae* cell surface receptor TCP and delivers its ssDNA genome into the *V. cholerae* cytoplasm. The ssDNA genome of CTXΦ may be converted into dsDNA or directly integrated into a chromosomal *dif* site using the host-encoded XerC-XerD recombinases. XerC mediates first pair of strand exchanges. The host DNA replication, possibly, resolves the resulting Holiday junction. The red line depicts the phage genome, while a black line shows bacterial genome. Newly generated *dif* site is represented by a triangle.

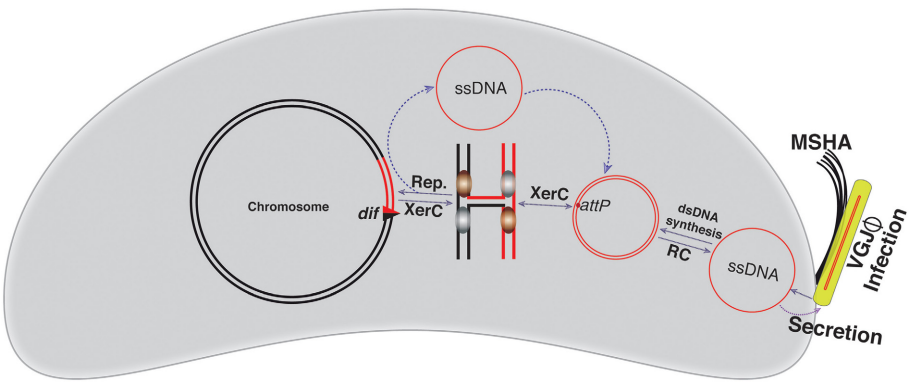


**FIGURE 4 | Schematic representation of the VGJΦ integration and replication.** VGJΦ uses mannose-sensitive hemagglutinin A (MSHA) to as a primary host receptor and delivers its ssDNA genome into the host cytoplasm. The ssDNA genome of VGJΦ is first converted into dsDNA and for this it contains a *dif* like DNA sequence, $attP^{VGJ}$. XerC mediates the first pair of strand exchanges and the host DNA replication resolves the resulting Holiday junction. The VGJΦ integration is reversible. Excision follows the same sequence of strand exchanges as described for integration. The red line depicts the phage genome while a black line depicts bacterial genome. Newly generated *dif* site is represented by a triangle.

strands and form of a phosphodiester bond between the deoxyriboses of two adjacent nucleotides. This step is the determining factor for phage integration specificity (Das et al., 2010). The resulting strand exchanges generate a Holiday Junction (HJ) intermediate. Host DNA replication, possibly, resolves the resulting, transient HJ intermediate and accomplishes the CTXΦ ssDNA integration into the *V. cholerae* chromosome (**Figure 3**). The absence of any homology between central region bases at the XerD-side of *attP*(+) and *dif1/dif2* impedes any XerD mediated strand exchange. A recent report revealed that the host-encoded DNA repair protein, endonuclease III, a product of *nth* gene with N-glycosylase and AP-lyase functions, facilitates the CTXΦ genome integration, possibly by stabilizing the transient HJ intermediate (Bischerour et al., 2012). Each individual step in the CTXΦ genome integration pathway is in principle reversible, but the prophage excision has never been detected under the standard laboratory conditions. This is due to the loss of a functional folded *attP*(+) structure in the double-stranded form of prophage (Val et al., 2005), in which the intra- strand base pairing between *attP1* and *attP2* is excluded. In the prophage genome, both *attP* sequences retained the XerC and XerD binding sites, but the central region of both sites, where the strand exchange occurs during integration, are incompatible with the Xer reaction and make the CTXΦ integration irreversible (Das et al., 2010).

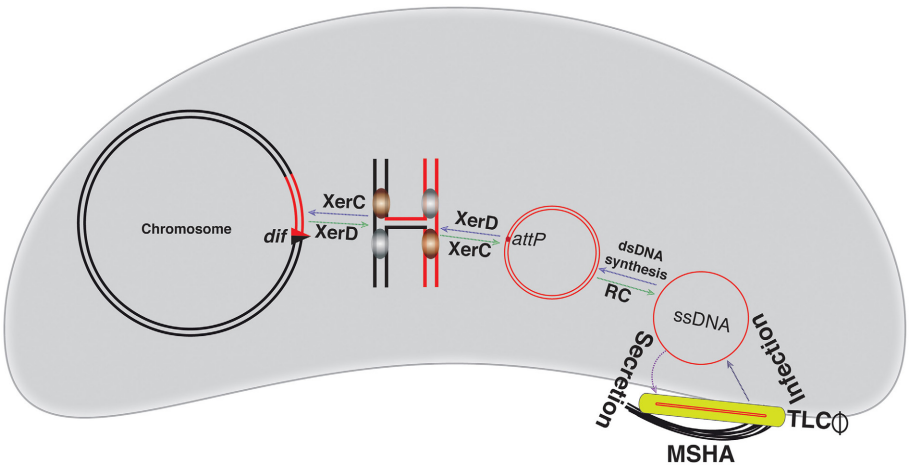


**FIGURE 5 | Illustration of the TLCΦ integration and replication.** The TLCΦ satellite prophage uses morphogenesis proteins of other filamentous phages, like fs2 for assembly. It uses the mannose-sensitive hemagglutinin A (MSHA) as the primary host receptor and delivers its ssDNA genome into host cytoplasm. The ssDNA genome of the TLCΦ is first converted into dsDNA. The $attP^{TLC}$ in the dsDNA replicative genome of TLCΦ is recognized by the XerC-XerD recombinases. XerD mediates the first pair of strand exchanges and generates a Holiday junction. After isomerization, XerC mediates second pair of strand exchanges and enables the TLCΦ integration. TLCΦ integration, which is reversible. Excision follows the same sequence of strand exchanges as described for integration. The blue and green arrows indicate integration and excision pathways, respectively. The red line depicts phage genome, while a black line represents bacterial genome. Newly generated *dif* site is symbolized by a triangle.

## MECHANISTIC INSIGHTS INTO VGJΦ INTEGRATION

VGJΦ, a filamentous (+)ssDNA lysogenic bacteriophage, infects both clinical and environmental isolates of cholera pathogen and exploits the host-encoded Xer recombinases to integrate at the *dif1*site in the large chromosome of cholera pathogen (Campos et al., 2003b; Das et al., 2011b). In contrast to CTXΦ, the 7.5 kb genome of VGJΦ harbors a single *dif* like 29-bp DNA sequence, called $attP^{VGJ}$ (**Figure 2**). Presence of the single functional *dif* like site allows integration of VGJΦ genome into the *V. cholerae* chromosome as dsDNA. Like CTXΦ, integration of VGJΦ also relies on the catalytic activity of XerC (**Figure 4**). Due to an absence of the sequence homology in the central region adjacent to the XerD-binding site between the $attP^{VGJ}$ and *dif1* site of *V. cholerae*, XerD catalytic activities are not been used either to generate HJ or to resolve the HJ during integration. The XerC generated HJ junction is resolved either by the host DNA replication or other DNA repair proteins and assist VGJΦ integration (**Figure 4**). After integration, two compatible Xer recombination sites (*attL* and *attR*) flank the VGJ-prophage. The 7.5-kb distance between the two Xer binding sites does not impede assembly of the recombination complex and excision of the VGJΦ prophage. Like integration, excision of VGJΦ also depends on the XerC-mediated strand exchanges (**Figure 4**). *In vitro* recombination reactions between synthetic $attP^{VGJ}$ and *dif1* substrates confirmed that only XerC and XerD recombinases are sufficient for DNA rearrangement (Das et al., 2011b).

## MECHANISTIC INSIGHTS INTO TLCΦ INTEGRATION

TLCΦ, a satellite temperate phage with an autonomous replication module, is mostly present in the *dif1* region of toxigenic *V. cholerae* isolates. Recent reports demonstrated that like CTXΦ, and VGJΦ, TLCΦ also relies on host encoded Xer machinery for its lysogeny (Hassan et al., 2010; Midonet et al., in press). In sharp contrast to the first two elements, the XerD binding site of TLCΦ is degenerated (Das et al., 2013; Midonet et al., in press). The XerC binding site and central region of $attP^{TLC}$ are almost identical to *dif1* of *V. cholerae*, but XerD binding sequence has very little similarity (Midonet et al., in press). Despite the absence of bona fide XerD binding site in $attP^{TLC}$, TLCΦ integration is strictly related to XerD catalytic activity (Midonet et al., in press). The integration mechanism of TLCΦ is unique compared to the integration strategy adopted by CTXΦ, and VGJΦ (**Table 2**).

Like CTXΦ and VGJΦ, TLCΦ integration also needs both XerC and XerD recombinases. During TLCΦ integration, XerC and XerD form a hetero-tetrameric complex with *dif1* and $attP^{TLC}$, within which XerD exchanges first pair of DNA strands and form the HJ. The resulting HJ proceed to DNA isomerization and is subsequently resolved by the XerC-mediated second strand exchanges (**Figure 5**). Tyrosine recombinases-mediated reactions are reversible, and therefore the TLCΦ integration is also reversible. Like integration excision is also depends on XerD catalytic activity (**Figure 5**). The action of both recombinases and the sequence of strand-exchanges stages in both integration and excision are very similar to chromosome dimer resolution, however the TLCΦ integration occurs without direct participation of DNA motor protein FtsK. Since the recombination reaction between *dif1* and $attP^{TLC}$ is not reconstituted in defined *in vitro* reactions, it is yet not clear whether only the 28-bp $attP^{TLC}$ is sufficient for Xer reaction or whether the TLCΦ needs extended $attP^{TLC}$ region and support from additional host proteins for efficient integration. Similarly, the mechanistic insights into TLCΦ excision in defined reaction conditions are yet to be explored.

## COOPERATIVE INTERACTIONS AMONG FILAMENTOUS VIBRIOPHAGES

Metagenomic studies revealed several IMEXs integrated at one or both chromosomes of cholera pathogenic strains (Chun et al.,

**Box 1 | Outstanding questions.**

- How is the CTXΦ integration efficiency modulated? Does TLCΦ modulate efficiency of CTXΦ integration into the *V. cholerae* chromosomes?
- How is the CTXΦ virion produced from toxigenic *V. cholerae* cells, in the case when it harbors only a single copy of the prophage in either chromosome?
- Does the TLCΦ contribute to the CTXΦ rolling circle replication?
- Is there any relation between the LexA regulon and the CTXΦ integration? Does ssDNA of CTXΦ induced the SOS response in the host cell?
- How does the TLCΦ genome integrate in the chromosome of classical *V. cholerae* strains, where both chromosomes contained an $attP^{TLC}$ incompatible *dif2* sequence?
- Are there any accessory proteins other than Xer recombinases that may help the TLCΦ genome integration into the *V. cholerae* chromosome?
- What are the host factors implicated in the CTXΦ, VGJΦ, and TLCΦ replication?

2009). The co-occurrence of multiple IMEXs in the genome of cholera pathogens is not simply a coincidence. Recent reports demonstrated that there are remarkable cooperative interactions between closely or distantly located IMEXs in cholera pathogen (Taylor et al., 1986; Hassan et al., 2010; Das et al., 2011b). Interactions between IMEXs happen at different levels, including the host recognition, receptor binding and DNA entry into the cytoplasm, chromosomal integration, and virion production (Waldor and Mekalanos, 1996; Hassan et al., 2010). The best example of this interaction is acquisition of cholera toxin. The first step of CTXΦ infection in *V. cholerae* is to recognize its host receptor. TCP, the cell surface receptor of *V. cholerae* for CTXΦ, is encoded by VPI-1, a ∼41-kb mobile genomic island. The same genomic island also helps cholera toxin production by providing transcriptional inducer ToxT, which specifically binds to the "TATTA" repeat, invariably present upstream of the *ctxAB* operon.

Cooperative interactions between VGJΦ and CTXΦ have been reported very recently (Campos et al., 2003a; Das et al., 2011b). CTXΦ integration is irreversible and phage production depends on the presence of tandem copies of prophages or related RS1 elements (Waldor et al., 1997; Val et al., 2005). A recent report demonstrated that VGJΦ could help CTXΦ excision and its dissemination to the *V. cholerae* strains devoid of TCP island. When the CTXΦ prophage is inserted between the attachment site of VGJΦ and the *dif1* of *V. cholerae*, a hybrid VGJΦ-CTXΦ is often detected (Das et al., 2011b). The hybrid phage genome is packed within the VGJΦ coat proteins and infects *V. cholerae* cells expressing mannose-sensitive hemagglutinin (MSHA) pilus, a type IV pilus present on the cell surface whose structural pilin subunit is encoded by the *mshA* gene. MSHA pilus is ubiquitous and constitutively expressed in all *V. cholerae* serotypes and thus, host range of the hybrid phage containing the CTXΦ genome encapsulated in the VGJΦ-encoded virion is not restricted to the cells that expressed TCP (Fullner and Mekalanos, 1999). Similarly, TLCΦ also helps the CTXΦ excision if both elements are present in tandem in the *V. cholerae* chromosome (Midonet et al., in press). Since the TLC prophage is present in most toxigenic strains where a single or multiple copies of the CTXΦ genome are integrated at the chromosomal *dif1* site, the TLCΦ is more significant for the CTXΦ excision than is the VGJΦ-prophage. Other than TLCΦ and VGJΦ elements, several other IMGEs could help CTXΦ replication as well as its interaction with the *V. cholerae* in natural environment by providing cell surface receptor. They can also help increase the amount of cholera toxin production by up-regulating *ctxAB* operon, protein required for the hybrid virion production and dissemination in the environment.

## CONCLUSIONS

In this review, several fundamental questions related to IMEXs integration have been addressed, such as contribution of these elements to continuous evolution of the cholera pathogenic strains. Although hypothesis for the adaptive advantage of lysogenic conversion of filamentous vibriophages was proposed, many important questions are still open and need to be addressed in order to improve understanding of the *V. cholerae* biology and cholera management (**Box 1**). Pangenomic studies revealed that IMEXs are not limited only to clinical isolates but are also widely distributed in the environmental *V. cholerae* isolates that are closely or distantly related to pathogenic strains. Much emphasis has been put on the biology of those IMEXs that are mostly present in the clinical isolates. Our knowledge on IMEXs present in the environmental isolates is limited. It is widely accepted that the environmental *V. cholerae* strains are ubiquitously distributed in aquatic environment and could serve as a reservoir of toxin-encoding genes as well as other fitness factors for clinical strains. Comprehensive studies of IMEXs present both in clinical and environmental isolates of *V. cholerae* and related pathogenic strains are required in order to understand the microevolution of the species pertinent to epidemiology. On the other hand, better mechanistic and structural knowledge of IMEXs will help to develop therapeutic agents and limit the emergence of the new cholera pathogenic strains and other strains that may pose a serious threat to human beings as well as animals.

## ACKNOWLEDGMENTS

I thank Dr. G.B. Nair and other members of CHME-THSTI for invaluable suggestions and help during the preparation of this review. The work is supported by the Department of Science and Technology (Grant No. SB/FT/LS-309/2012), Government of India (GOI) and the Department of Biotechnology (Grant No. BT/MB/THSTI/HMC-SFC/2011), GOI.

## REFERENCES


Aussel, L., Barre, F. X., Aroyo, M., Stasiak, A., Stasiak, A. Z., and Sherratt, D. (2002). FtsK Is a DNA motor protein that activates chromosome dimer resolution by switching the catalytic state of the XerC and XerD recombinases. *Cell* 108, 195–205. doi: 10.1016/S0092-8674(02)00624-4

Banerjee, R., Das, B., Balakrish Nair, G., and Basak, S. (2014). Dynamics in genome evolution of *Vibrio cholerae*. *Infect. Genet. Evol.* 23C, 32–41. doi: 10.1016/j.meegid.2014.01.006

Beaber, J. W., Hochhut, B., and Waldor, M. K. (2004). SOS response promotes horizontal dissemination of antibiotic resistance genes. *Nature* 427, 72–74. doi: 10.1038/nature02241

Bigot, S., Saleh, O. A., Cornet, F., Allemand, J. F., and Barre, F. X. (2006). Oriented loading of FtsK on KOPS. *Nat. Struct. Mol. Biol.* 13, 1026–1028. doi: 10.1038/nsmb1159

Bischerour, J., Spangenberg, C., and Barre, F. X. (2012). Holliday junction affinity of the base excision repair factor Endo III contributes to cholera toxin phage integration. *EMBO J.* 31, 3757–3767. doi: 10.1038/emboj.2012.219

Blakely, G., May, G., McCulloch, R., Arciszewska, L. K., Burke, M., Lovett, S. T., et al. (1993). Two related recombinases are required for site-specific recombination at dif and cer in *E. coli* K12. *Cell* 75, 351–361. doi: 10.1016/0092-8674(93)80076-Q

Campos, J., Martinez, E., Izquierdo, Y., and Fando, R. (2010). VEJ{phi}, a novel filamentous phage of *Vibrio cholerae* able to transduce the cholera toxin genes. *Microbiology* 156, 108–115. doi: 10.1099/mic.0.032235-0

Campos, J., Martinez, E., Marrero, K., Silva, Y., Rodriguez, B. L., Suzarte, E., et al. (2003a). Novel type of specialized transduction for CTX or its satellite phage RS1 mediated by filamentous phage VGJ in *Vibrio cholerae*. *J. Bacteriol.* 185, 7231–7240. doi: 10.1128/JB.185.24.7231-7240.2003

Campos, J., Martinez, E., Suzarte, E., Rodriguez, B. L., Marrero, K., Silva, Y., et al. (2003b). VGJ, a novel filamentous phage of *Vibrio cholerae*, integrates into the same chromosomal site as CTX. *J. Bacteriol.* 185, 5685–5696. doi: 10.1128/JB.185.19.5685-5696.2003

Chun, J., Grim, C. J., Hasan, N. A., Lee, J. H., Choi, S. Y., Haley, B. J., et al. (2009). Comparative genomics reveals mechanism for short-term and long-term clonal transitions in pandemic *Vibrio cholerae*. *Proc. Natl. Acad. Sci. U.S.A.* 106, 15442–15447. doi: 10.1073/pnas.0907787106

Das, B., Bischerour, J., and Barre, F. X. (2011a). Molecular mechanism of acquisition of the cholera toxin genes. *Indian J. Med. Res.* 133, 195–200.

Das, B., Bischerour, J., and Barre, F. X. (2011b). VGJphi integration and excision mechanisms contribute to the genetic diversity of *Vibrio cholerae* epidemic strains. *Proc. Natl. Acad. Sci. U.S.A.* 108, 2516–2521. doi: 10.1073/pnas.1017061108

Das, B., Bischerour, J., Val, M. E., and Barre, F. X. (2010). Molecular keys of the tropism of integration of the cholera toxin phage. *Proc. Natl. Acad. Sci. U.S.A.* 107, 4377–4382. doi: 10.1073/pnas.0910212107

Das, B., Kumari, R., Pant, A., Sen Gupta, S., Saxena, S., Mehta, O., et al. (2014). A novel broad range CTXPhi derived stable integrative expression vector for functional studies. *J. Bacteriol.* 196, 4071–4080. doi: 10.1128/JB.01966-14

Das, B., Martinez, E., Midonet, C., and Barre, F. X. (2013). Integrative mobile elements exploiting Xer recombination. *Trends Microbiol.* 21, 23–30. doi: 10.1016/j.tim.2012.10.003

Davies, B. W., Bogard, R. W., Young, T. S., and Mekalanos, J. J. (2012). Coordinated regulation of accessory genetic elements produces cyclic di-nucleotides for V. *cholerae virulence*. *Cell* 149, 358–370. doi: 10.1016/j.cell.2012.01.053

Davis, B. M., Kimsey, H. H., Kane, A. V., and Waldor, M. K. (2002). A satellite phage-encoded antirepressor induces repressor aggregation and cholera toxin gene transfer. *EMBO J.* 21, 4240–4249. doi: 10.1093/emboj/cdf427

Davis, B. M., and Waldor, M. K. (2000). CTXphi contains a hybrid genome derived from tandemly integrated elements. *Proc. Natl. Acad. Sci. U.S.A.* 97, 8572–8577. doi: 10.1073/pnas.140109997

Demarre, G., Galli, E., and Barre, F. X. (2013). The FtsK family of DNA pumps. *Adv. Exp. Med. Biol.* 767, 245–262. doi: 10.1007/978-1-4614-5037-5_12

Esposito, D., and Scocca, J. J. (1997). The integrase family of tyrosine recombinases: evolution of a conserved active site domain. *Nucleic Acids Res.* 25, 3605–3614. doi: 10.1093/nar/25.18.3605

Faruque, S. M., and Mekalanos, J. J. (2003). Pathogenicity islands and phages in *Vibrio cholerae* evolution. *Trends Microbiol.* 11, 505–510. doi: 10.1016/j.tim.2003.09.003

Faruque, S. M., and Mekalanos, J. J. (2012). Phage-bacterial interactions in the evolution of toxigenic *Vibrio cholerae*. *Virulence* 3, 556–565. doi: 10.4161/viru.22351

Faruque, S. M., Rahman, M. M., Hasan, A. K., Nair, G. B., Mekalanos, J. J., and Sack, D. A. (2001). Diminished diarrheal response to *Vibrio cholerae* strains carrying the replicative form of the CTX(Phi) genome instead of CTX(Phi) lysogens in adult rabbits. *Infect. Immun.* 69, 6084–6090. doi: 10.1128/IAI.69.10.6084-6090.2001

Frost, L. S., Leplae, R., Summers, A. O., and Toussaint, A. (2005). Mobile genetic elements: the agents of open source evolution. *Nat. Rev. Microbiol.* 3, 722–732. doi: 10.1038/nrmicro1235

Fullner, K. J., and Mekalanos, J. J. (1999). Genetic characterization of a new type IV-A pilus gene cluster found in both classical and El Tor biotypes of *Vibrio cholerae*. *Infect. Immun.* 67, 1393–1404.

Hassan, F., Kamruzzaman, M., Mekalanos, J. J., and Faruque, S. M. (2010). Satellite phage TLCphi enables toxigenic conversion by CTX phage through dif site alteration. *Nature* 467, 982–985. doi: 10.1038/nature09469

Hazen, T. H., Pan, L., Gu, J. D., and Sobecky, P. A. (2010). The contribution of mobile genetic elements to the evolution and ecology of *Vibrios*. *FEMS Microbiol. Ecol.* 74, 485–499. doi: 10.1111/j.1574-6941.2010.00937.x

Heidelberg, J. F., Eisen, J. A., Nelson, W. C., Clayton, R. A., Gwinn, M. L., Dodson, R. J., et al. (2000). DNA sequence of both chromosomes of the cholera pathogen *Vibrio cholerae*. *Nature* 406, 477–483. doi: 10.1038/35020000

Heilpern, A. J., and Waldor, M. K. (2000). CTXphi infection of *Vibrio cholerae* requires the tolQRA gene products. *J. Bacteriol.* 182, 1739–1747. doi: 10.1128/JB.182.6.1739-1747.2000

Herrington, D. A., Hall, R. H., Losonsky, G., Mekalanos, J. J., Taylor, R. K., and Levine, M. M. (1988). Toxin, toxin-coregulated pili, and the toxR regulon are essential for *Vibrio cholerae* pathogenesis in humans. *J. Exp. Med.* 168, 1487–1492. doi: 10.1084/jem.168.4.1487

Huber, K. E., and Waldor, M. K. (2002). Filamentous phage integration requires the host recombinases XerC and XerD. *Nature* 417, 656–659. doi: 10.1038/nature00782

Karaolis, D. K., Somara, S., Maneval, D. R. Jr., Johnson, J. A., and Kaper, J. B. (1999). A bacteriophage encoding a pathogenicity island, a type-IV pilus and a phage receptor in cholera bacteria. *Nature* 399, 375–379. doi: 10.1038/20715

MacDonald, D., Demarre, G., Bouvier, M., Mazel, D., and Gopaul, D. N. (2006). Structural basis for broad DNA-specificity in integron recombination. *Nature* 440, 1157–1162. doi: 10.1038/nature04643

Mazel, D. (2006). Integrons: agents of bacterial evolution. *Nat. Rev. Microbiol.* 4, 608–620. doi: 10.1038/nrmicro1462

Mazel, D., and Davies, J. (1998). Antibiotic resistance. The big picture. *Adv. Exp. Med. Biol.* 456, 1–6. doi: 10.1007/978-1-4615-4897-3_1

Mekalanos, J. J. (1985). Cholera toxin: genetic analysis, regulation, and role in pathogenesis. *Curr. Top. Microbiol. Immunol.* 118, 97–118. doi: 10.1007/978-3-642-70586-1_6

Mekalanos, J. J., Swartz, D. J., Pearson, G. D., Harford, N., Groyne, F., and de Wilde, M. (1983). Cholera toxin genes: nucleotide sequence, deletion analysis and vaccine development. *Nature* 306, 551–557. doi: 10.1038/306551a0

Mercier, R., Petit, M. A., Schbath, S., Robin, S., El Karoui, M., Boccard, F., et al. (2008). The MatP/matS site-specific system organizes the terminus region of the *E. coli* chromosome into a macrodomain. *Cell* 135, 475–485. doi: 10.1016/j.cell.2008.08.031

Midonet, C., Das, B., Paly, E., and Barre, F. X. (in press). XerD initiates the integration of TLCφ into the *Vibrio cholerae* genome independently of FtsK. *Proc. Natl. Acad. Sci. U.S.A.* doi: 10.1073/pnas.1404047111

Rajanna, C., Wang, J., Zhang, D., Xu, Z., Ali, A., Hou, Y. M., et al. (2003). The *Vibrio* pathogenicity island of epidemic *Vibrio cholerae* forms precise extra-chromosomal circular excision products. *J. Bacteriol.* 185, 6893–6901. doi: 10.1128/JB.185.23.6893-6901.2003

Recchia, G. D., Aroyo, M., Wolf, D., Blakely, G., and Sherratt, D. J. (1999). FtsK-dependent and -independent pathways of Xer site-specific recombination. *EMBO J.* 18, 5724–5734. doi: 10.1093/emboj/18.20.5724

Rhine, J. A., and Taylor, R. K. (1994). TcpA pilin sequences and colonization requirements for O1 and O139 vibrio cholerae. *Mol. Microbiol.* 13, 1013–1020. doi: 10.1111/j.1365-2958.1994.tb00492.x

Rubin, E. J., Lin, W., Mekalanos, J. J., and Waldor, M. K. (1998). Replication and integration of a *Vibrio cholerae* cryptic plasmid linked to the CTX prophage. *Mol. Microbiol.* 28, 1247–1254. doi: 10.1046/j.1365-2958.1998.00889.x

Sack, D. A., Sack, R. B., Nair, G. B., and Siddique, A. K. (2004). Cholera. *Lancet* 363, 223–233. doi: 10.1016/S0140-6736(03)15328-7

Sherratt, D. J., and Wigley, D. B. (1998). Conserved themes but novel activities in recombinases and topoisomerases. *Cell* 93, 149–152. doi: 10.1016/S0092-8674(00)81566-4

Taylor, R. K., Miller, V. L., Furlong, D. B., and Mekalanos, J. J. (1986). Identification of a pilus colonization factor that is coordinately regulated with cholera toxin. *Ann. Sclavo Collana Monogr.* 3, 51–61.

Val, M. E., Bouvier, M., Campos, J., Sherratt, D., Cornet, F., Mazel, D., et al. (2005). The single-stranded genome of phage CTX is the form used for integration into the genome of *Vibrio cholerae*. *Mol. Cell* 19, 559–566. doi: 10.1016/j.molcel.2005.07.002

Val, M. E., Kennedy, S. P., El Karoui, M., Bonne, L., Chevalier, F., and Barre, F. X. (2008). FtsK-dependent dimer resolution on multiple chromosomes in the pathogen *Vibrio cholerae*. *PLoS Genet.* 4:e1000201. doi: 10.1371/journal.pgen.1000201

Vanden Broeck, D., Horvath, C., and De Wolf, M. J. (2007). *Vibrio cholerae*: cholera toxin. *Int. J. Biochem. Cell Biol.* 39, 1771–1775. doi: 10.1016/j.biocel.2007.07.005

Waldor, M. K., and Mekalanos, J. J. (1996). Lysogenic conversion by a filamentous phage encoding cholera toxin. *Science* 272, 1910–1914. doi: 10.1126/science.272.5270.1910

Waldor, M. K., Rubin, E. J., Pearson, G. D., Kimsey, H., and Mekalanos, J. J. (1997). Regulation, replication, and integration functions of the *Vibrio cholerae* CTXphi are encoded by region RS2. *Mol. Microbiol.* 24, 917–926. doi: 10.1046/j.1365-2958.1997.3911758.x

**Conflict of Interest Statement:** The Guest Associate Editor, Jasna Rakonjac, declares that, despite having collaborated on the same research topic as author Bhabatosh Das, the review process was handled objectively and no conflict of interest exists.

*Received: 02 August 2014; accepted: 10 November 2014; published online: 28 November 2014.*

*Citation: Das B (2014) Mechanistic insights into filamentous phage integration in Vibrio cholerae. Front. Microbiol. **5**:650. doi: 10.3389/fmicb.2014.00650*

*This article was submitted to Virology, a section of the journal Frontiers in Microbiology.*

frontiers in Microbiology

REVIEW
published: 04 August 2015
doi: 10.3389/fmicb.2015.00755

# Beyond phage display: non-traditional applications of the filamentous bacteriophage as a vaccine carrier, therapeutic biologic, and bioconjugation scaffold

*Kevin A. Henry*[1]*, *Mehdi Arbabi-Ghahroudi*[1,2,3] and *Jamie K. Scott*[4,5]

[1] Human Health Therapeutics Portfolio, National Research Council Canada, Ottawa, ON, Canada, [2] School of Environmental Sciences, University of Guelph, Guelph, ON, Canada, [3] Department of Biology, Carleton University, Ottawa, ON, Canada, [4] Department of Molecular Biology and Biochemistry, Simon Fraser University, Burnaby, BC, Canada, [5] Faculty of Health Sciences, Simon Fraser University, Burnaby, BC, Canada

OPEN ACCESS

**Edited by:**
Jasna Rakonjac,
Massey University, New Zealand

**Reviewed by:**
Piergiuseppe De Berardinis,
National Research Council – Institute of Protein Biochemistry, Italy
Dragana Gagic,
AgResearch, New Zealand

***Correspondence:**
Kevin A. Henry,
Human Health Therapeutics Portfolio,
National Research Council Canada,
100 Sussex Drive, Ottawa,
ON K1A 0R6, Canada
kevin.henry@nrc-cnrc.gc.ca

**Specialty section:**
This article was submitted to Virology, a section of the journal Frontiers in Microbiology

**Received:** 21 January 2015
**Accepted:** 10 July 2015
**Published:** 04 August 2015

**Citation:**
Henry KA, Arbabi-Ghahroudi M and Scott JK (2015) Beyond phage display: non-traditional applications of the filamentous bacteriophage as a vaccine carrier, therapeutic biologic, and bioconjugation scaffold. Front. Microbiol. 6:755. doi: 10.3389/fmicb.2015.00755

For the past 25 years, phage display technology has been an invaluable tool for studies of protein–protein interactions. However, the inherent biological, biochemical, and biophysical properties of filamentous bacteriophage, as well as the ease of its genetic manipulation, also make it an attractive platform outside the traditional phage display canon. This review will focus on the unique properties of the filamentous bacteriophage and highlight its diverse applications in current research. Particular emphases are placed on: (i) the advantages of the phage as a vaccine carrier, including its high immunogenicity, relative antigenic simplicity and ability to activate a range of immune responses, (ii) the phage's potential as a prophylactic and therapeutic agent for infectious and chronic diseases, (iii) the regularity of the virion major coat protein lattice, which enables a variety of bioconjugation and surface chemistry applications, particularly in nanomaterials, and (iv) the phage's large population sizes and fast generation times, which make it an excellent model system for directed protein evolution. Despite their ubiquity in the biosphere, metagenomics work is just beginning to explore the ecology of filamentous and non-filamentous phage, and their role in the evolution of bacterial populations. Thus, the filamentous phage represents a robust, inexpensive, and versatile microorganism whose bioengineering applications continue to expand in new directions, although its limitations in some spheres impose obstacles to its widespread adoption and use.

**Keywords: filamentous phage, vaccine, therapeutic, antimicrobial, bioconjugation**

## Introduction

The filamentous bacteriophage (genera *Inovirus* and *Plectrovirus*) are non-enveloped, rod-shaped viruses of *Escherichia coli* whose long helical capsids encapsulate a single-stranded circular DNA genome. Subsequent to the independent discovery of bacteriophage by Twort (1915) and d'Hérelle (1917), the first filamentous phage, f1, was isolated in Loeb (1960) and later characterized as a member of a larger group of phage (Ff, including f1, M13, and fd phage) specific for the *E. coli*

conjugative F pilus (Hofschneider and Mueller-Jensen, 1963; Marvin and Hoffmann-Berling, 1963; Zinder et al., 1963; Salivar et al., 1964). Soon thereafter, filamentous phage were discovered that do not use F-pili for entry (If and Ike; Meynell and Lawn, 1968; Khatoon et al., 1972), and over time the list of known filamentous phage has expanded to over 60 members (Fauquet et al., 2005), including temperate and Gram-positive-tropic species. Work by multiple groups over the past 50 years has contributed to a relatively sophisticated understanding of filamentous phage structure, biology and life cycle (reviewed in Marvin, 1998; Rakonjac et al., 2011; Rakonjac, 2012).

In the mid-1980s, the principle of modifying the filamentous phage genome to display polypeptides as fusions to coat proteins on the virion surface was invented by Smith and colleagues (Smith, 1985; Parmley and Smith, 1988). Based on the ideas described in Parmley and Smith (1988), groups in California, Germany, and the UK developed phage-display platforms to create and screen libraries of peptide and folded-protein variants (Bass et al., 1990; Devlin et al., 1990; McCafferty et al., 1990; Scott and Smith, 1990; Breitling et al., 1991; Kang et al., 1991). This technology allowed, for the first time, the ability to seamlessly connect genetic information with protein function for a large number of protein variants simultaneously, and has been widely and productively exploited in studies of protein–protein interactions. Many excellent reviews are available on phage-display libraries and their applications (Kehoe and Kay, 2005; Bratkovic, 2010; Pande et al., 2010). However, the phage also has a number of unique structural and biological properties that make it highly useful in areas of research that have received far less attention.

Thus, the purpose of this review is to highlight recent and current work using filamentous phage in novel and non-traditional applications. Specifically, we refer to projects that rely on the filamentous phage as a key element, but whose primary purpose is not the generation or screening of phage-displayed libraries to obtain binding polypeptide ligands. These tend to fall into four major categories of use: (i) filamentous phage as a vaccine carrier; (ii) engineered filamentous phage as a therapeutic biologic agent in infectious and chronic diseases; (iii) filamentous phage as a scaffold for bioconjugation and surface chemistry; and (iv) filamentous phage as an engine for evolving variants of displayed proteins with novel functions. A final section is dedicated to recent developments in filamentous phage ecology and phage–host interactions. Common themes shared amongst all these applications include the unique biological, immunological, and physicochemical properties of the phage, its ability to display a variety of biomolecules in modular fashion, and its relative simplicity and ease of manipulation.

## Filamentous Phage Display Systems: An Overview

Nearly all applications of the filamentous phage depend on its ability to display polypeptides on the virion's surface as fusions to phage coat proteins (**Table 1**). The display mode determines the maximum tolerated size of the fused polypeptide, its copy number on the phage, and potentially, the structure of the displayed polypeptide. Display may be achieved by fusing DNA encoding a polypeptide of interest directly to the gene encoding a coat protein within the phage genome (type 8 display on pVIII, type 3 display on pIII, etc.), resulting in fully recombinant phage. Much more commonly, however, only one copy of the coat protein is modified in the presence of a second, wild-type copy (e.g., type 88 display if both recombinant and wild-type pVIII genes are on the phage genome, type 8+8 display if the

**TABLE 1 | Filamentous phage display modes and their associated characteristics.**

| Phage coat protein | Display mode | Helper phage required? | Polypeptide copy number | Polypeptide size limit | Reference(s) |
|---|---|---|---|---|---|
| pIII | Fully recombinant (type 3 and 3+3* systems)[1] | Type 3+3* system | ~5 | >25 kDa | Parmley and Smith (1988), McConnell et al. (1994), Rondot et al. (2001) |
| | Hybrid (type 33 and 3+3 systems) | Type 3+3 system | <1[2] | | Smith and Scott (1993), Smith and Petrenko (1997) |
| pVI | Hybrid (type 6+6 system) | Yes | <1[2] | >25 kDa | Hufton et al. (1999) |
| pVII | Fully recombinant (type 7 system) | No | ~5 | >25 kDa | Kwasnikowski et al. (2005) |
| | Hybrid (type 7+7 system) | Yes | <1[2] | | Gao et al. (1999) |
| pVIII | Fully recombinant (landscape phage; type 8 system) | No | 2700[3] | ~5–8 residues | Kishchenko et al. (1994), Petrenko et al. (1996) |
| | Hybrid (type 88 and 8+8 systems) | Type 8+8 system | ~1–300[2] | >50 kDa | Scott and Smith (1990), Greenwood et al. (1991), Smith and Fernandez (2004) |
| pIX | Fully recombinant (type 9+9* system) | Yes | ~5 | >25 kDa | Gao et al. (2002) |
| | Hybrid (type 9+9 system) | No | <1[2] | | Gao et al. (1999), Shi et al. (2010), Tornetta et al. (2010) |

[1]*Asterisks indicate non-functional copies of the coat protein are present in the genome of the helper phage used to rescue a phagemid whose coat protein has been fused to a recombinant polypeptide.*

[2]*The copy number depends on polypeptide size; typically <1 copy per phage particle but for pVIII peptide display can be up to ~15% of pVIII molecules in hybrid virions.*

[3]*The total number of pVIII molecules depends on the phage genome size; one pVIII molecule is added for every 2.3 nucleotides in the viral genome.*

recombinant gene 8 is on a plasmid with a phage origin of replication) resulting in a hybrid virion bearing two different types of a given coat protein. Multivalent display on some coat proteins can also be enforced using helper phage bearing non-functional copies of the relevant coat protein gene (e.g., type 3*+3 display). By far the most commonly used coat proteins for display are the major coat protein, pVIII, and the minor coat protein, pIII, with the major advantage of the former being higher copy number display (up to ∼15% of recombinant pVIII molecules in a hybrid virion, at least for short peptide fusions), and of the latter being the ability to display some folded proteins at an appreciable copy number (1–5 per phage particle). While pVIII display of folded proteins on hybrid phage is possible, it typically results in a copy number of much less than 1 per virion (Sidhu et al., 2000). For the purposes of this review, we use the term "phage display" to refer to a recombinant filamentous phage displaying a single polypeptide sequence on its surface (or more rarely, bispecific display achieved *via* fusion of polypeptides to two different capsid proteins), and the term "phage-displayed library" to refer to a diverse pool of recombinant filamentous phage displaying an array of polypeptide variants (e.g., antibody fragments; peptides). Such libraries are typically screened by iterative cycles of panning against an immobilized protein of interest (e.g., antigen for phage-displayed antibody libraries; antibody for phage-displayed peptide libraries) followed by amplification of the bound phage in *E. coli* cells.

## Filamentous Phage as an Immunogenic Vaccine Carrier

Early work with anti-phage antisera generated for species classification purposes demonstrated that the filamentous phage virion is highly immunogenic in the absence of adjuvants (Meynell and Lawn, 1968) and that only the major coat protein, pVIII, and the minor coat protein, pIII, are targeted by antibodies (Pratt et al., 1969; Woolford et al., 1977). Thus, the idea of using the phage as carrier to elicit antibodies against poorly immunogenic haptens or polypeptide was a natural extension of the ability to display recombinant exogenous sequences on its surface, which was first demonstrated by de la Cruz et al. (1988). The phage particle's low cost of production, high stability and potential for high valency display of foreign antigen (*via* pVIII display) also made it attractive as a vaccine carrier, especially during the early stages of development of recombinant protein technology.

### Antibody Epitope-Based Peptide Vaccines

Building upon existing peptide-carrier technology, the first filamentous phage-based vaccine immunogens displayed short amino acid sequences derived directly from proteins of interest as recombinant fusions to pVIII or pIII (de la Cruz et al., 1988). As library technology was developed and refined, phage-based antigens displaying peptide ligands of monoclonal antibodies (selected from random peptide libraries using the antibody, thus simulating with varying degrees of success the antibody's folded epitope on its cognate antigen; Geysen et al., 1986; Knittelfelder et al., 2009) were also generated for immunization purposes, with the goal of eliciting anti-peptide antibodies that also recognize the native protein. Some of the pioneering work in this area used peptides derived from infectious disease antigens (or peptide ligands of antibodies against these antigens; **Table 2**), including malaria and human immunodeficiency virus type 1 (HIV-1). When displayed on phage, peptides encoding the repeat regions of the malarial circumsporozoite protein and merozoite surface protein 1 were immunogenic in mice and rabbits (de la Cruz et al., 1988; Greenwood et al., 1991; Willis et al., 1993; Demangel et al., 1996), and antibodies raised against the latter cross-reacted with the full-length protein. Various peptide determinants (or mimics thereof) of HIV-1 gp120, gp41, gag, and reverse transcriptase were immunogenic when displayed on or conjugated to phage coat proteins (Minenkova et al., 1993; di Marzo Veronese et al., 1994; De Berardinis et al., 1999; Scala et al., 1999; Chen et al., 2001; van Houten et al., 2006, 2010), and in some cases elicited antibodies that were able to weakly neutralize lab-adapted viruses (di Marzo Veronese et al., 1994; Scala et al., 1999). The list of animal and human infections for which phage-displayed peptide immunogens have been developed as vaccine leads continues to expand and includes bacterial, fungal, viral, and parasitic pathogens (**Table 2**). While in some cases the results of these studies have been promising, antibody epitope-based peptide vaccines are no longer an area of active research for several reasons: (i) in many cases, peptides incompletely or inadequately mimic epitopes on folded proteins (Irving et al., 2010; see below); (ii) antibodies against a single epitope may be of limited utility, especially for highly variable pathogens (Van Regenmortel, 2012); and (iii) for pathogens for which protective immune responses are generated efficiently during natural infection, peptide vaccines offer few advantages over recombinant subunit and live vector vaccines, which have become easier to produce over time.

More recently, peptide-displaying phage have been used in attempts to generate therapeutic antibody responses for chronic diseases, cancer, immunotherapy, and immunocontraception. Immunization with phage displaying Alzheimer's disease β-amyloid fibril peptides elicited anti-aggregating antibodies in mice and guinea pigs (Frenkel et al., 2000, 2003; Esposito et al., 2008; Tanaka et al., 2011), possibly reduced amyloid plaque formation in mice (Frenkel et al., 2003; Solomon, 2005; Esposito et al., 2008), and may have helped maintain cognitive abilities in a transgenic mouse model of Alzheimer's disease (Lavie et al., 2004); however, it remains unclear how such antibodies are proposed to cross the blood–brain barrier. Yip et al. (2001) found that antibodies raised in mice against an ERBB2/HER2 peptide could inhibit breast-cancer cell proliferation. Phage displaying peptide ligands of an anti-IgE antibody elicited antibodies that bound purified IgE molecules (Rudolf et al., 1998), which may be useful in allergy immunotherapy. Several strategies for phage-based contraceptive vaccines have been proposed for control of animal populations. For example, immunization with phage displaying follicle-stimulating hormone peptides on pVIII elicited antibodies that impaired the fertility of mice and ewes (Abdennebi et al., 1999). Phage displaying or chemically

**TABLE 2 | Studies using filamentous phage as an immunogenic carrier for peptide B-cell epitopes.**

| Antigen | Species | Epitope type(s) | Display format(s) | Ab response against peptide | Ab response against native protein | Reference(s) |
|---|---|---|---|---|---|---|
| Alzheimer's disease β-amyloid fibrils | Mouse (BALB/c, APP transgenic), Guinea pig | Linear | pVIII hybrid, pIII fully recombinant | + | + | Frenkel et al. (2000, 2003), Lavie et al. (2004), Esposito et al. (2008), Tanaka et al. (2011) |
| *Aspergillus fumigatus* MIRB | Mouse (BALB/c) | Linear | Chemical conjugate | + | + | Raymond-Bouchard et al. (2012) |
| *Bordetella pertussis* toxin | Mouse (BALB/c) | Discontinuous | pVIII hybrid | + | – | Felici et al. (1993) |
| *Candida albicans* HSP90 | Mouse (C57/BL6, BALB/c) | Linear | pVIII hybrid | + | + | Yang et al. (2005a), Wang et al. (2006, 2014d) |
| *Chlamydia trachomatis* major outer membrane protein | Mouse (C57/BL6, BALB/c, CBA/j) | Linear | pVIII hybrid | + | + | Zhong et al. (1994) |
| *Coronavirus S* glycoprotein | Mouse (C57/BL6, BALB/c) | Linear | pVIII hybrid | + | + | Yu et al. (2000) |
| ERBB2/HER2 | Mouse (BALB/c) | Linear | pVIII hybrid, pIII fully recombinant | + | + | Yip et al. (2001) |
| *Entamoeba histolytica* proteophosphoglycan | Mouse (BALB/c) | Discontinuous | pVIII hybrid | + | + | Melzer et al. (2002) |
| Follicle-stimulating hormone | Sheep | Linear | pVIII hybrid | + | + | Abdennebi et al. (1999) |
| Foot-and-mouth disease VP1 | Guinea pig | Linear | pVIII hybrid | ND | + | Kim et al. (2004) |
| Gonadotropin-releasing hormone | Mouse (CD-1) | Linear | Chemical conjugate | ND | ND | Samoylov et al. (2012) |
| HBV surface antigen | Mouse (C57/BL6, BALB/c, B10.M) | Linear | pVIII hybrid, pIII fully recombinant | + | + | Folgori et al. (1994), Motti et al. (1994), Meola et al. (1995), Delmastro et al. (1997) |
| HCV core antigen and NS4B protein | Mouse (C57/BL6, BALB/c, MF1) | Linear | pVIII hybrid | + | ND | Prezzi et al. (1996), Delmastro et al. (1997) |
| HCV E2 protein | Mouse (BALB/c) | Linear | pVIII hybrid | + | ND | Puntoriero et al. (1998) |
| *Helicobacter pylori* Urease B | Mouse (BALB/c) | Linear | pIII fully recombinant | + | + | Li et al. (2010c) |
| HIV-1 gp120 V3 loop | Mouse (BALB/c) | Linear | pVIII hybrid | + | + | di Marzo Veronese et al. (1994) |
| HIV-1 gp120 CD4-binding site | Mouse (BALB/c) | Discontinuous | Chemical conjugate | + | – | van Houten et al. (2006) |
| HIV-1 gp120 and gp41 | Mouse (C57/BL6, BALB/c), *Rhesus macaque* | Linear, Discontinuous | pVIII hybrid, pIII hybrid, Chemical conjugate | + | ND | Scala et al. (1999), Chen et al. (2001), van Houten et al. (2010) |
| HIV-1 gag p17 | Rabbit | Linear | pVIII fully recombinant | + | + | Minenkova et al. (1993) |
| HIV-1 reverse transcriptase | Mouse (C57BL/6, HLA-A2 transgenic) | Linear | pVIII hybrid | + | ND | De Berardinis et al. (1999) |
| HPV E7 protein | Mouse (BALB/c) | Linear | pVIII hybrid | + | + | Lidqvist et al. (2008) |
| HSV-2 glycoprotein G | Mouse (BALB/c) | Linear | pVIII hybrid | + | + | Grabowska et al. (2000) |
| Immunoglobulin E | Rabbit | Discontinuous | pVIII hybrid | ND | + | Rudolf et al. (1998) |
| *Mycoplasma hyopneumoniae* unknown proteins | Mouse (BALB/cByJ) | Linear, Discontinuous | pIII fully recombinant | + | + | Yang et al. (2005b) |
| *Neisseria meningitidis* PorA protein | Mouse (BALB/c) | Linear | pVIII hybrid | + | + | Menendez et al. (2001) |

*(Continued)*

**TABLE 2 | Continued**

| Antigen | Species | Epitope type(s) | Display format(s) | Ab response against peptide | Ab response against native protein | Reference(s) |
|---|---|---|---|---|---|---|
| *Plasmodium falciparum* CSP | Mouse (BALB/c, C57/BL10, Swiss, Str/ort), rabbit | Linear | pVIII hybrid, pIII fully recombinant | + | ND | de la Cruz et al. (1988), Greenwood et al. (1991), Willis et al. (1993) |
| *Plasmodium vivax* MSP1 | Mouse (C57/BL6, BALB/c, Biozzi) | Linear, Discontinuous | pIII hybrid | ND | + | Demangel et al. (1996) |
| Rhabdovirus RABVG | Mouse (BALB/c) | Linear | pIII fully recombinant | + | + | Houimel and Dellagi (2009) |
| RSV glycoprotein G | Mouse (BALB/c) | Linear | pIII fully recombinant | + | − | Bastien et al. (1997) |
| *Schistosoma japonicum* unknown protein(s) | Mouse (Kunming) | Discontinuous | pIII fully recombinant | + | ND | |
| *Shigella flexneri* LPS | Mouse (BALB/c) | Discontinuous | pVIII hybrid, Chemical conjugate | + | − | van Houten et al. (2010), Henry et al. (2011) |
| Sperm | Mouse (CD-1), Pig | Discontinuous | pVIII fully recombinant | + | + | Samoylova et al. (2012a,b) |
| Toxic shock syndrome toxin | Mouse (BALB/c) | Linear | pIII fully recombinant | + | ND | Rubinchik and Chow (2000) |

conjugated to sperm antigen peptides or peptide mimics (Samoylova et al., 2012a,b) and gonadotropin-releasing hormone (Samoylov et al., 2012) are also in development.

For the most part, peptides displayed on phage elicit antibodies in experimental animals (**Table 2**), although this depends on characteristics of the peptide and the method of its display: pIII fusions tend toward lower immunogenicity than pVIII fusions (Greenwood et al., 1991) possibly due to copy number differences (pIII: 1–5 copies vs. pVIII: estimated at several hundred copies; Malik et al., 1996). In fact, the phage is at least as immunogenic as traditional carrier proteins such as bovine serum albumin (BSA) and keyhole limpet hemocyanin (KLH; Melzer et al., 2003; Su et al., 2007), and has comparatively few endogenous B-cell epitopes to divert the antibody response from its intended target (Henry et al., 2011). Excepting small epitopes that can be accurately represented by a contiguous short amino acid sequence, however, it has been extremely difficult to elicit antibody responses that cross-react with native protein epitopes using peptides. The overall picture is considerably bleaker than that painted by **Table 2**, since in several studies either: (i) peptide ligands selected from phage-displayed libraries were classified by the authors as mimics of discontinuous epitopes if they bore no obvious sequence homology to the native protein, which is weak evidence of non-linearity, or (ii) the evidence for cross-reactivity of antibodies elicited by immunization with phage-displayed peptides with native protein was uncompelling. Irving et al. (2010) describe at least one reason for this lack of success: it seems that peptide antigens elicit a set of topologically restricted antibodies that are largely unable to recognize discontinuous or complex epitopes on larger biomolecules. While the peptide may mimic the chemistry of a given epitope on a folded protein (allowing it to cross-react with a targeted antibody), being a smaller molecule, it cannot mimic the topology of that antibody's full epitope. Despite this, the filamentous phage remains highly useful as a carrier for peptides with relatively simple secondary structures, which may be stablilized *via* anchoring to the coat proteins (Henry et al., 2011). This may be especially true of peptides with poor inherent immunogenicity, which may be increased by high-valency display and phage-associated adjuvanticity (see Immunological Mechanisms of Vaccination with Filamentous Phage below).

## Cytotoxic T-Cell-Based Vaccines

The filamentous phage has been used to a lesser extent as a carrier for T-cell peptide epitopes, primarily as fusion proteins with pVIII (**Table 3**). Early work, showing that immunization with phage elicited T-cell help (Kölsch et al., 1971; Willis et al., 1993), was confirmed by several subsequent studies (De Berardinis et al., 1999; Ulivieri et al., 2008). From the perspective of vaccination against infectious disease, De Berardinis et al. (2000) showed that a cytotoxic T-cell (CTL) epitope from HIV-1 reverse transcriptase could elicit antigen-specific CTLs *in vitro* and *in vivo* without addition of exogenous helper T-cell epitopes, presumably since these are already present in the phage coat proteins (Mascolo et al., 2007). Similarly, efficient priming of CTLs was observed against phage-displayed T-cell epitopes from Hepatitis B virus (Wan et al., 2001) and *Candida albicans* (Yang et al., 2005a; Wang et al., 2006, 2014d), which, together with other types of immune responses, protected mice against systemic candidiasis. Vaccination with a combination of phage-displayed peptides elicited antigen-specific CTLs that proved effective in reducing porcine cysticercosis in a randomized controlled trial (Manoutcharian et al., 2004; Morales et al., 2008).

While the correlates of vaccine-induced immune protection for infectious diseases, where they are known, are almost exclusively serum or mucosal antibodies (Plotkin, 2010),

**TABLE 3 | Studies using filamentous phage as an immunogenic carrier for peptide T-cell epitopes.**

| Antigen | Species | Epitope type(s) | Display format(s) | T-cell response against peptide | Reference(s) |
|---|---|---|---|---|---|
| *Taenia crassiceps* KETc1, KETc7, and KETc12 | Pig | MHC class I | pVIII hybrid, pIII fully recombinant | + | Manoutcharian et al. (2004), Morales et al. (2008) |
| Ovalbumin | Mouse (C57BL/6) | MHC class I | pVIII hybrid | + | Mascolo et al. (2007) |
| HIV-1 reverse transcriptase | Mouse (C57BL/6, HLA-A2 transgenic) | MHC class I, MHC class II | pVIII hybrid | + | De Berardinis et al. (1999, 2000) |
| PIA tumor antigen | Mouse (DBA/2) | MHC class I | pVIII hybrid | + | Wu et al. (2002) |
| Ovalbumin (B16.OVA model) | Mouse (C57BL/6, tlr4$^{-/-}$, OT-I) | MHC class I | pVIII hybrid | + | Sartorius et al. (2011) |
| MAGE-A1, MAGE-A10, MAGE-A3 | Mouse (C57BL/6, HLA-A2 transgenic) | MHC class I | pVIII hybrid | + | Fang et al. (2005), Sartorius et al. (2008) |
| *Candida albicans* HSP90 | Mouse (C57BL6/, BALB/c) | MHC class I, MHC class II | pVIII hybrid | + | Yang et al. (2005a), Wang et al. (2006, 2014d) |
| HBV | Mouse (BALB/c) | MHC class I | pVIII hybrid | + | Wan et al. (2001) |

a primary goal of cancer vaccines is to elicit therapeutic CTL responses and/or suppress $CD4^+$ regulatory T cells against tumor antigens while avoiding triggering adverse autoimmune responses. To this end, Wu et al. (2002) showed that a phage-displayed CTL epitope derived from the P1A tumor antigen was immunogenic and that the CTLs elicited in response to immunization both prevented mastocytoma tumor establishment and prolonged survival in mice with established tumors. Similarly, melanoma tumor CTL epitopes (MAGE-A1, MAGE-A3, and MAGE-A10) elicited CTLs that slowed tumor growth in mice and prolonged their survival (Fang et al., 2005; Sartorius et al., 2008). This work was later extended by Sartorius et al. (2011), who showed using the B16-OVA tumor model that phage double-displaying an ovalbumin CTL epitope on pVIII and an scFv against DEC-205 (a dendritic cell marker) on pIII could elicit much stronger anti-B16 tumor CTL responses that further improved survival rates. Thus, despite their large size, filamentous phage particles can elicit vigorous CTL responses, which can be enhanced in some cases by direct targeting of the phage to antigen-presenting cells. Although no studies have conducted a thorough comparison of the immunogenicity of a single CTL epitope in the context of different carriers, it is possible that the filamentous phage virion may induce stronger and more durable CTL responses compared to soluble exogenous proteins because of its efficient cross-presentation into the MHC class I pathway (see Immunological Mechanisms of Vaccination with Filamentous Phage below).

## Recombinant Protein and DNA Vaccines

In certain vaccine applications, the filamentous phage has been used as a carrier for larger molecules that would be immunogenic even in isolation. Initially, the major advantages to phage display of such antigens were speed, ease of purification and low cost of production (Gram et al., 1993). *E. coli* F17a-G adhesin (Van Gerven et al., 2008), hepatitis B core antigen (Bahadir et al., 2011), and hepatitis B surface antigen (Balcioglu et al., 2014) all elicited antibody responses when displayed on pIII, although none of these studies compared the immunogenicity of the phage-displayed proteins with that of the purified protein alone. Phage displaying *Schistosoma mansoni* glutathione *S*-transferase on pIII elicited an antibody response that was both higher in titer and of different isotypes compared to immunization with the protein alone (Rao et al., 2003). Two studies of anti-idiotypic vaccines have used the phage as a carrier for antibody fragments bearing immunogenic idiotypes. Immunization with phage displaying the 1E10 idiotype scFv (mimicking a *Vibrio anguillarum* surface epitope) elicited antibodies that protected flounder fish from *Vibrio anguillarum* challenge (Xia et al., 2005). A chemically linked phage-BCL1 tumor-specific idiotype vaccine was weakly immunogenic in mice but extended survival time in a B-cell lymphoma model (Roehnisch et al., 2013), and was well-tolerated and immunogenic in patients with multiple myeloma (Roehnisch et al., 2014). One study of DNA vaccination with an anti-laminarin scFv found that DNA encoding a pIII-scFv fusion protein elicited stronger humoral and cell-mediated immune responses than DNA encoding the scFv alone (Cuesta et al., 2006), suggesting that under some circumstances, endogenous phage T-cell epitopes can enhance the immunogenicity of associated proteins. Taken together, the results of these studies show that as a particulate virus-like particle, the filamentous phage likely triggers different types of immune responses than recombinant protein antigens, and provide additional T-cell help to displayed or conjugated proteins. However, the low copy number of pIII-displayed proteins, as well as potentially unwanted phage-associated adjuvanticity, can make display of recombinant proteins by phage a suboptimal vaccine choice.

## Immunological Mechanisms of Vaccination with Filamentous Phage

Although our understanding of the immune response against the filamentous phage pales in comparison to classical model antigens such as ovalbumin, recent work has begun to shed light on the immune mechanisms activated in response to phage

vaccination (**Figure 1**). The phage particle is immunogenic without adjuvant in all species tested to date, including mice (Willis et al., 1993), rats (Dente et al., 1994), rabbits (de la Cruz et al., 1988), guinea pigs (Frenkel et al., 2000; Kim et al., 2004), fish (Coull et al., 1996; Xia et al., 2005), non-human primates (Chen et al., 2001), and humans (Roehnisch et al., 2014). Various routes of immunization have been employed, including oral administration (Delmastro et al., 1997) as well as subcutaneous (Grabowska et al., 2000), intraperitoneal (van Houten et al., 2006), intramuscular (Samoylova et al., 2012a), intravenous (Vaks and Benhar, 2011), and intradermal injection (Roehnisch et al., 2013); no published study has directly compared the effect of administration route on filamentous phage immunogenicity. Antibodies are generated against only three major sites on the virion: (i) the surface-exposed N-terminal ~12 residues of the pVIII monomer lattice (Terry et al., 1997; Kneissel et al., 1999); (ii) the N-terminal N1 and N2 domains of pIII (van Houten et al., 2010); and (iii) bacterial lipopolysaccharide (LPS) embedded in the phage coat (Henry et al., 2011). In mice, serum antibody titers against the phage typically reach $1{:}10^5$–$1{:}10^6$ after 2–3 immunizations, and are maintained for at least 1 year post-immunization (Frenkel et al., 2000). Primary antibody responses against the phage appear to be composed of a mixture of IgM and IgG2b isotypes in C57BL/6 mice, while secondary antibody responses are composed primarily of IgG1 and IgG2b isotypes, with a lesser contribution of IgG2c and IgG3 isotypes (Hashiguchi et al., 2010). Deletion of the surface-exposed N1 and N2 domains of pIII produces a truncated form of this protein that does not elicit antibodies, but also results in a non-infective phage particle with lower overall immunogenicity (van Houten et al., 2010).

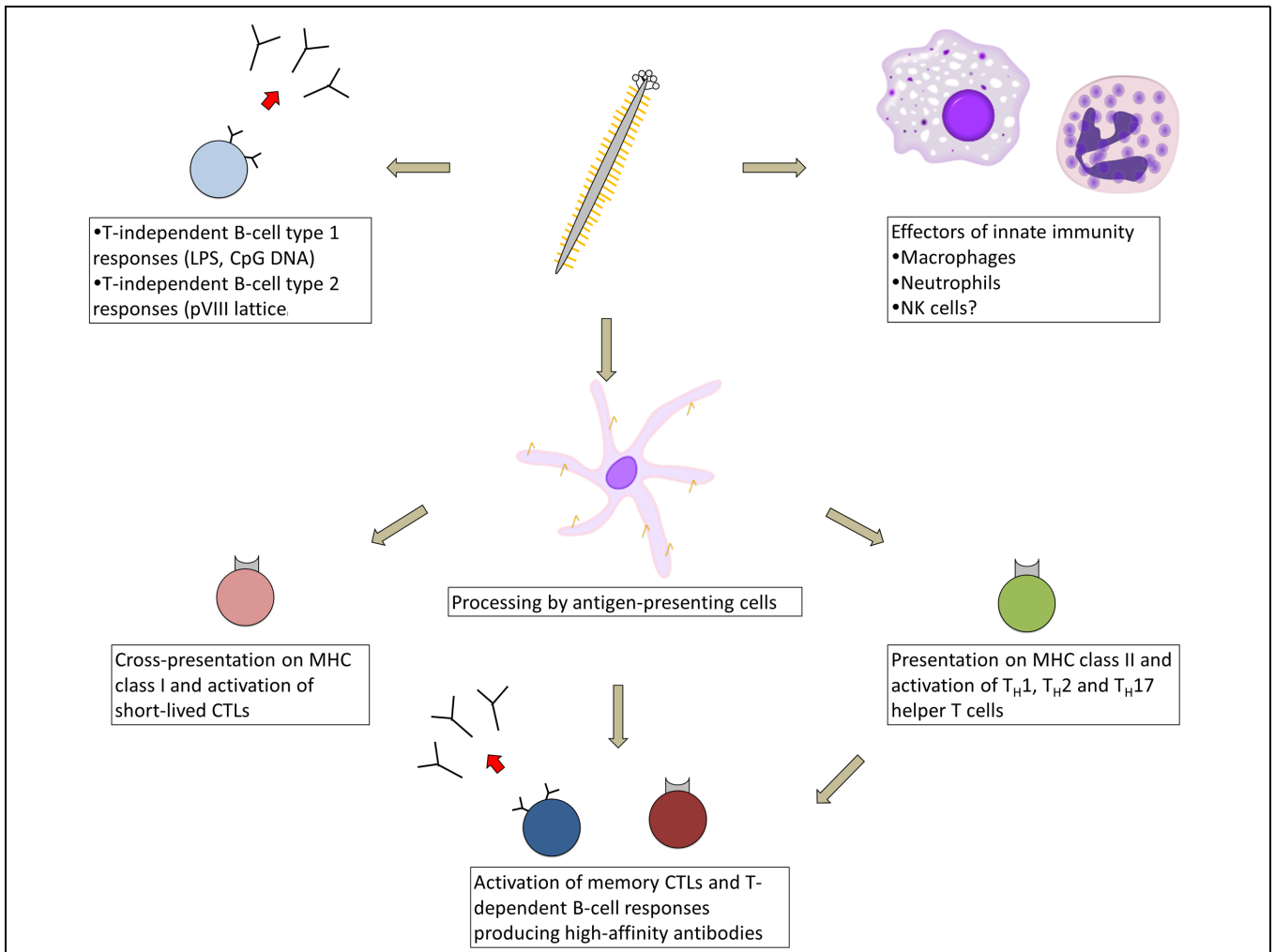


**FIGURE 1 | Types of immune responses elicited in response to immunization with filamentous bacteriophage.** As a virus-like particle, the filamentous phage engages multiple arms of the immune system, beginning with cellular effectors of innate immunity (macrophages, neutrophils, and possibly natural killer cells), which are recruited to tumor sites by phage displaying tumor-targeting moieties. The phage likely activates T-cell independent antibody responses, either via phage-associated TLR ligands or cross-linking by the pVIII lattice. After processing by antigen-presenting cells, phage-derived peptides are presented on MHC class II and cross-presented on MHC class I, resulting in activation of short-lived CTLs and an array of helper T-cell types, which help prime memory CTL and high-affinity B-cell responses.

Although serum anti-phage antibody titers appear to be at least partially T-cell dependent (Kölsch et al., 1971; Willis et al., 1993; De Berardinis et al., 1999; van Houten et al., 2010), many circulating pVIII-specific B cells in the blood are devoid of somatic mutation even after repeated biweekly immunizations, suggesting that under these conditions, the phage activates T-cell-independent B-cell responses in addition to high-affinity T-cell-dependent responses (Murira, 2014). Filamentous phage particles can be processed by antigen-presenting cells and presented on MHC class II molecules (Gaubin et al., 2003; Ulivieri et al., 2008) and can activate $T_H1$, $T_H2$, and $T_H17$ helper T cells (Yang et al., 2005a; Wang et al., 2014d). Anti-phage $T_H2$ responses were enhanced through display of CTLA-4 peptides fused to pIII (Kajihara et al., 2000). Phage proteins can also be cross-presented on MHC class I molecules (Wan et al., 2005) and can prime two waves of CTL responses, consisting first of short-lived CTLs and later of long-lived memory CTLs that require $CD4^+$ T-cell help (Del Pozzo et al., 2010). The latter CTLs mediate a delayed-type hypersensitivity reaction (Fang et al., 2005; Del Pozzo et al., 2010).

The phage particle is self-adjuvanting through multiple mechanisms. Host cell wall-derived LPS enhances the virion's immunogenicity, and its removal by polymyxin B chromatography reduces antibody titers against phage coat proteins (Grabowska et al., 2000). The phage's single-stranded DNA genome contains CpG motifs and may also have an adjuvant effect. The antibody response against the phage is entirely dependent on MyD88 signaling and is modulated by stimulation of several Toll-like receptors (Hashiguchi et al., 2010), indicating that innate immunity plays an important but largely uncharacterized role in the activation of anti-phage adaptive immune responses. Biodistribution studies of the phage after intravenous injection show that it is cleared from the blood within hours through the reticuloendothelial system (Molenaar et al., 2002), particularly of the liver and spleen, where it is retained for days (Zou et al., 2004), potentially activating marginal-zone B-cell responses. Thus, the filamentous phage is not only a highly immunogenic carrier, but by virtue of activating a range of innate and adaptive immune responses, serves as an excellent model virus-like particle antigen.

## Filamentous Phage as a Therapeutic and Prophylactic Agent in Bacterial Infection, Cancer, and Chronic Disease

Long before the identification of filamentous phage, other types of bacteriophage were already being used for antibacterial therapy in the former Soviet Union and Eastern Europe (reviewed in Sulakvelidze et al., 2001). The filamentous phage, with its non-lytic life cycle, has less obvious clinical uses, despite the fact that the host specificity of *Inovirus* and *Plectrovirus* includes many pathogens of medical importance, including *Salmonella*, *E. coli*, *Shigella*, *Pseudomonas*, *Clostridium,* and *Mycoplasma* species. In an effort to enhance their bactericidal activity, genetically modified filamentous phage have been used as a "Trojan horse" to introduce various antibacterial agents into cells. M13 and Pf3 phage engineered to express either *BglII* restriction endonuclease (Hagens and Blasi, 2003; Hagens et al., 2004), lambda phage S holin (Hagens and Blasi, 2003) or a lethal catabolite gene activator protein (Moradpour et al., 2009) effectively killed *E. coli* and *Pseudomonas aeruginosa* cells, respectively, with no concomitant release of LPS (Hagens and Blasi, 2003; Hagens et al., 2004). Unfortunately, the rapid emergence of resistant bacteria with modified F pili represents a major and possibly insurmountable obstacle to this approach. However, there are some indications that filamentous phage can exert useful but more subtle effects upon their bacterial hosts that may not result in the development of resistance to infection. Several studies have reported increased antibiotic sensitivity in bacterial populations simultaneously infected with either wild type filamentous phage (Hagens et al., 2006) or phage engineered to repress the cellular SOS response (Lu and Collins, 2009). Filamentous phage f1 infection inhibited early stage, but not mature, biofilm formation in *E. coli* (May et al., 2011). Thus, unmodified filamentous phage may be of future interest as elements of combination therapeutics against certain drug-resistant infections.

More advanced therapeutic applications of the filamentous phage emerge when it is modified to express a targeting moiety specific for pathogenic cells and/or proteins for the treatment of infectious diseases, cancer and autoimmunity (**Figure 2**). The first work in this area showed as proof-of-concept that phage encoding a GFP expression cassette and displaying a HER2-specific scFv on all copies of pIII were internalized into breast tumor cells, resulting in GFP expression (Poul and Marks, 1999). M13 or fd phage displaying either a targeting peptide or antibody fragment and tethered to chloramphenicol by a labile crosslinker were more potent inhibitors of *Staphylococcus aureus* growth than high-concentration free chloramphenicol (Yacoby et al., 2006; Vaks and Benhar, 2011). M13 phage loaded with doxorubicin and displaying a targeting peptide on pIII specifically killed prostate cancer cells *in vitro* (Ghosh et al., 2012a). Tumor-specific peptide:pVIII fusion proteins selected from "landscape" phage (Romanov et al., 2001; Abbineni et al., 2010; Fagbohun et al., 2012, 2013; Lang et al., 2014; Wang et al., 2014a) were able to target and deliver siRNA-, paclitaxel-, and doxorubicin-containing liposomes to tumor cells (Jayanna et al., 2010a; Wang et al., 2010a,b,c, 2014b,c; Bedi et al., 2011, 2013, 2014); they were non-toxic and increased tumor remission rates in mouse models (Jayanna et al., 2010b; Wang et al., 2014b,c). Using the B16-OVA tumor model, Eriksson et al. (2007) showed that phage displaying peptides and/or Fabs specific for tumor antigens delayed tumor growth and improved survival, owing in large part to activation of tumor-associated macrophages and recruitment of neutrophils to the tumor site (Eriksson et al., 2009). Phage displaying an scFv against β-amyloid fibrils showed promise as a diagnostic (Frenkel and Solomon, 2002) and therapeutic (Solomon, 2008) reagent for Alzheimer's disease and Parkinson's disease due to the unanticipated ability of the phage to penetrate into brain tissue (Ksendzovsky et al., 2012). Similarly, phage displaying an immunodominant peptide epitope

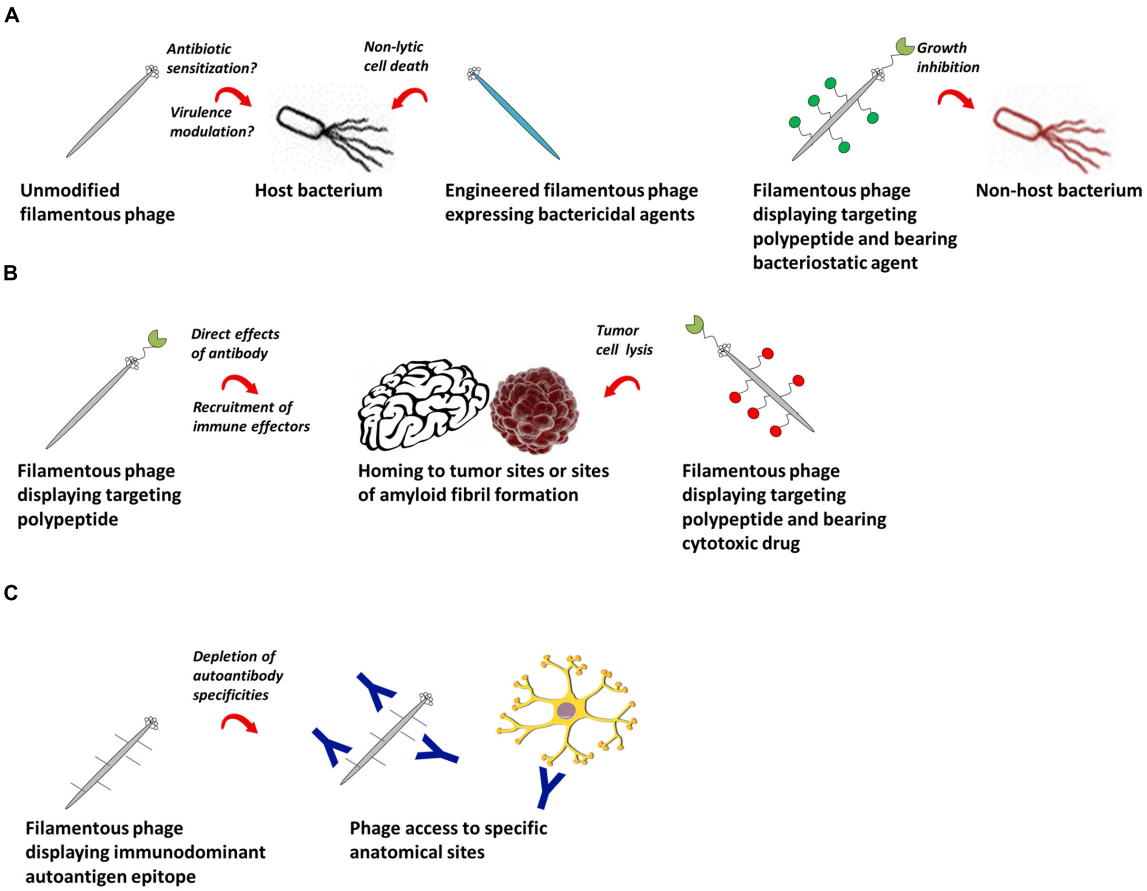


**FIGURE 2 | Potential therapeutic applications of filamentous bacteriophage. (A)** Filamentous phage as a therapeutic against bacterial infections. Left: wild-type or engineered phage bearing genes encoding antibacterial agents can be used as therapeutics against their natural bacterial hosts. Right: filamentous phage displaying antibodies or polypeptides can target bacterial cells outside their natural species tropism. **(B)** Filamentous phage as a therapeutic in cancer and chronic diseases. Phage encoding targeting peptides home specifically to tumor or amyloid fibril sites, where they can have direct effects, recruit immune effector cells, or deliver conjugated cytotoxic drugs. **(C)** Filamentous phage as a therapeutic for autoantibody-mediated autoimmune conditions. Phage displaying immunodominant autoantigen epitopes can selectively deplete autoantibodies of defined specificities.

derived from myelin oligodendrocyte glycoprotein depleted pathogenic demyelinating antibodies in brain tissue in the murine experimental autoimmune encephalomyelitis model of multiple sclerosis (Rakover et al., 2010). The advantages of the filamentous phage in this context over traditional antibody-drug or protein–peptide conjugates are (i) its ability to carry very high amounts of drug or peptide, and (ii) its ability to access anatomical compartments that cannot generally be reached by systemic administration of a protein.

Unlike most therapeutic biologics, the filamentous phage's production in bacteria complicates its use in humans in several ways. First and foremost, crude preparations of filamentous phage typically contain very high levels of contaminating LPS, in the range of $\sim 10^2$–$10^4$ endotoxin units (EU)/mL (Boratynski et al., 2004; Branston et al., 2015), which have the potential to cause severe adverse reactions. LPS is not completely removed by polyethylene glycol precipitation or cesium chloride density gradient centrifugation (Smith and Gingrich, 2005; Branston et al., 2015), but its levels can be reduced dramatically using additional purification steps such as size exclusion chromatography (Boratynski et al., 2004; Zakharova et al., 2005), polymyxin B chromatography (Grabowska et al., 2000), and treatment with detergents such as Triton X-100 or Triton X-114 (Roehnisch et al., 2014; Branston et al., 2015). These strategies routinely achieve endotoxin levels of <1 EU/mL as measured by the limulus amebocyte lysate (LAL) assay, well below the FDA limit for parenteral administration of 5 EU/kg body weight/dose, although concerns remain regarding the presence of residual virion-associated LPS which may be undetectable. A second and perhaps unavoidable consequence of the filamentous phage's bacterial production is inherent heterogeneity of particle size and the spectrum of host cell-derived virion-associated and soluble contaminants, which may be cause for safety concerns and restrict its use to high-risk groups.

Many types of bacteriophage and engineered phage variants, including filamentous phage, have been proposed for prophylactic use *ex vivo* in food safety, either in the

production pipeline (reviewed in Dalmasso et al., 2014) or for detection of foodborne pathogens post-production (reviewed in Schmelcher and Loessner, 2014). Filamentous phage displaying a tetracysteine tag on pIII were used to detect *E. coli* cells through staining with biarsenical dye (Wu et al., 2011). M13 phage functionalized with metallic silver were highly bactericidal against *E. coli* and *Staphylococcus epidermidis* (Mao et al., 2010). Biosensors based on surface plasmon resonance (Nanduri et al., 2007), piezoelectric transducers (Olsen et al., 2006), linear dichroism (Pacheco-Gomez et al., 2012), and magnetoelastic sensor technology (Lakshmanan et al., 2007; Huang et al., 2009) were devised using filamentous phage displaying scFv or conjugated to whole IgG against *E. coli*, *Listeria monocytogenes*, *Salmonella typhimurium,* and *Bacillus anthracis* with limits of detection on the order of $10^2$–$10^6$ bacterial cells/mL. Proof of concept has been demonstrated for use of such phage-based biosensors to detect bacterial contamination of live produce (Li et al., 2010b) and eggs (Chai et al., 2012).

## Filamentous Phage as a Scaffold for Bioconjugation and Surface Chemistry

The filamentous phage particle is enclosed by a rod-like protein capsid, ∼1000 nm long and 5 nm wide, made up almost entirely of overlapping pVIII monomers, each of which lies ∼27 angstroms from its nearest neighbor and exposes two amine groups as well as at least three carboxyl groups (Henry et al., 2011). The regularity of the phage pVIII lattice and its diversity of chemically addressable groups make it an ideal scaffold for bioconjugation (**Figure 3**). The most commonly used approach is functionalization of amine groups with NHS esters (van Houten et al., 2006, 2010; Yacoby et al., 2006), although this can result in unwanted acylation of pIII and any displayed biomolecules. Carboxyl groups and tyrosine residues can also be functionalized using carbodiimide coupling and diazonium coupling, respectively (Li et al., 2010a). Carrico et al. (2012) developed methods to specifically label pVIII N-termini without modification of exposed lysine residues through a two-step transamination-oxime formation reaction. Specific modification of phage coat proteins is even more easily accomplished using genetically modified phage displaying peptides (Ng et al., 2012) or enzymes (Chen et al., 2007; Hess et al., 2012), but this can be cumbersome and is less general in application.

For more than a decade, interest in the filamentous phage as a building block for nanomaterials has been growing because of its unique physicochemical properties, with emerging applications in magnetics, optics, and electronics. It has long been known that above a certain concentration threshold, phage can form ordered crystalline suspensions (Welsh et al., 1996). Lee et al. (2002) engineered M13 phage to display a ZnS-binding peptide on pIII and showed that, in the presence of ZnS nanoparticles, they self-assemble into highly ordered film biomaterials that can be aligned using magnetic fields. Taking advantage of the ability to display substrate-specific peptides at known locations on the phage filament (Huang et al., 2005; Hess et al., 2012), this pioneering

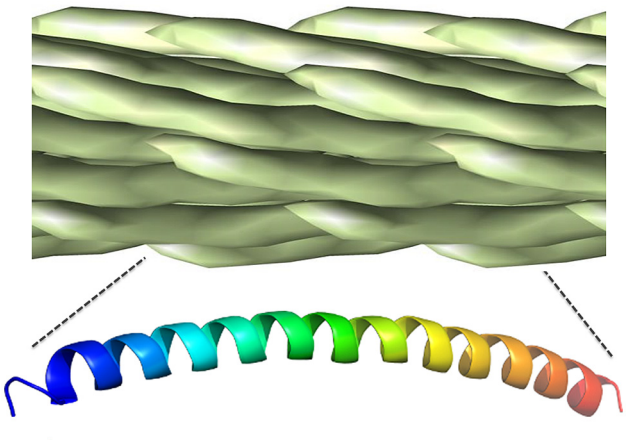


**FIGURE 3 | Chemically addressable groups of the filamentous bacteriophage major coat protein lattice.** The filamentous phage virion is made up of ∼2,500–4,000 overlapping copies of the 50-residue major coat protein, pVIII, arranged in a shingle-type lattice. Each monomer has an array of chemically addressable groups available for bioorthogonal conjugation, including two primary amine groups (shown in red), three carboxyl groups (show in blue) and two hydroxyl groups (show in green). The 12 N-terminal residues generally exposed to the immune system for antibody binding are in bold underline. Figure adapted from structural data of Marvin, 1990, freely available in PDB and SCOPe databases.

work became the basis for construction of two- and three-dimensional nanomaterials with more advanced architectures, including semiconducting nanowires (Mao et al., 2003, 2004), nanoparticles (Yoo et al., 2006), and nanocomposites (Oh et al., 2012; Chen et al., 2014). Using hybrid M13 phage displaying $Co_3O_4$- and gold-binding peptides on pVIII as a scaffold to assemble nanowires on polyelectrolyte multilayers, Nam et al. (2006) produced a thin, flexible lithium ion battery, which could be stamped onto platinum microband current collectors (Nam et al., 2008). The electrochemical properties of such batteries were further improved through pIII-display of single-walled carbon nanotube-binding peptides (Lee et al., 2009), offering an approach for sustainable production of nanostructured electrodes from poorly conductive starting materials. Phage-based nanomaterials have found applications in cancer imaging (Ghosh et al., 2012b; Yi et al., 2012), photocatalytic water splitting (Nam et al., 2010a; Neltner et al., 2010), light harvesting (Nam et al., 2010b; Chen et al., 2013), photoresponsive technologies (Murugesan et al., 2013), neural electrodes (Kim et al., 2014), and piezoelectric energy generation (Murugesan et al., 2013).

Thus, the unique physicochemical properties of the phage, in combination with modular display of peptides and proteins with known binding specificity, have spawned wholly novel materials with diverse applications. It is worth noting that the unusual biophysical properties of the filamentous phage can also be exploited in the study of structures of other macromolecules. Magnetic alignment of high-concentration filamentous phage in solution can partially order DNA, RNA, proteins, and other biomolecules for measurement of dipolar coupling interactions

(Hansen et al., 1998, 2000; Dahlke Ojennus et al., 1999) in NMR spectroscopy.

## Filamentous Phage as an Engine for Experimental Protein Evolution

Because of their large population sizes, short generation times, small genome sizes and ease of manipulation, various filamentous and non-filamentous bacteriophages have been used as models of experimental evolution (reviewed in Husimi, 1989; Wichman and Brown, 2010; Kawecki et al., 2012; Hall et al., 2013). The filamentous phage has additional practical uses in protein engineering and directed protein evolution, due to its unique tolerance of genetic modifications that allow biomolecules to be displayed on the virion surface. First and foremost among these applications is *in vitro* affinity maturation of antibody fragments displayed on pIII. Libraries of variant Fabs and single chain antibodies can be generated *via* random or site-directed mutagenesis and selected on the basis of improved or altered binding, roughly mimicking the somatic evolution strategy of the immune system (Marks et al., 1992; Bradbury et al., 2011). However, other *in vitro* display systems, such as yeast display, have important advantages over the filamentous phage for affinity maturation (although each display technology has complementary strengths; Koide and Koide, 2012), and regardless of the display method, selection of "improved" variants can be slow and cumbersome. Iterative methods have been developed to combine computationally designed mutations (Lippow et al., 2007) and circumvent the screening of combinatorial libraries, but these have had limited success to date.

Recently, Esvelt et al. (2011) developed a novel strategy for directed evolution of filamentous phage-displayed proteins, called phage-assisted continuous evolution (PACE), which allows multiple rounds of evolution per day with little experimental intervention. The authors engineered M13 phage to encode an exogenous protein (the subject for directed evolution), whose functional activity triggers gene III expression from an accessory plasmid; variants of the exogenous protein arise by random mutagenesis during phage replication, the rate of which can be increased by inducible expression of error-prone DNA polymerases. By supplying limiting amounts of receptive *E. coli* cells to the engineered phage variants, Esvelt et al. (2011) elegantly linked phage infectivity and production of offspring with the presence of a desired protein phenotype. Carlson et al. (2014) later showed that PACE selection stringency could be modulated by providing small amounts of pIII independently of protein phenotype, and undesirable protein functions negatively selected by linking them to expression of a truncated pIII variant that impairs infectivity in a dominant negative fashion. PACE is currently limited to protein functions that can be linked in some way to the expression of a gene III reporter, such as protein–protein interaction, recombination, DNA or RNA binding, and enzymatic catalysis (Meyer and Ellington, 2011). This approach represents a promising avenue for both basic research in molecular evolution (Dickinson et al., 2013) and synthetic biology, including antibody engineering.

## Filamentous Phage Ecology

Filamentous bacteriophage have been recovered from diverse environmental sources, including soil (Murugaiyan et al., 2011), coastal fresh water (Xue et al., 2012), alpine lakes (Hofer and Sommaruga, 2001) and deep sea bacteria (Jian et al., 2012), but not, perhaps surprisingly, the human gut (Kim et al., 2011). The environmental "phageome" in soil and water represent the largest source of replicating DNA on the planet, and is estimated to contain upward of $10^{30}$ viral particles (Ashelford et al., 2003; Chibani-Chennoufi et al., 2004; Suttle, 2005). The few studies attempting to investigate filamentous phage environmental ecology using classical environmental microbiology techniques (typically direct observation by electron microscopy) found that filamentous phage made up anywhere from 0 to 100% of all viral particles (Demuth et al., 1993; Pina et al., 1998; Hofer and Sommaruga, 2001). There was some evidence of seasonal fluctuation of filamentous phage populations in tandem with the relative abundance of free-living heterotrophic bacteria (Hofer and Sommaruga, 2001). Environmental metagenomics efforts are just beginning to unravel the composition of viral ecosystems. The existing data suggest that filamentous phage comprise minor constituents of viral communities in freshwater (Roux et al., 2012) and reclaimed and potable water (Rosario et al., 2009) but have much higher frequencies in wastewater and sewage (Cantalupo et al., 2011; Alhamlan et al., 2013), with the caveat that biases inherent to the methodologies for ascertaining these data (purification of viral particles, sequencing biases) have not been not well validated. There are no data describing the population dynamics of filamentous phage and their host species in the natural environment.

At the individual virus-bacterium level, it is clear that filamentous phage can modulate host phenotype, including the virulence of important human and crop pathogens. This can occur either through direct effects of phage replication on cell growth and physiology, or, more typically, by horizontal transfer of genetic material contained within episomes and/or chromosomally integrated prophage. Temperate filamentous phage may also play a role in genome evolution (reviewed in Canchaya et al., 2003). Perhaps the best-studied example of virulence modulation by filamentous phage is that of *Vibrio cholerae*, whose full virulence requires lysogenic conversion by the cholera toxin-encoding CTXϕ phage (Waldor and Mekalanos, 1996). Integration of CTXϕ phage occurs at specific sites in the genome; these sequences are introduced through the combined action of another filamentous phage, fs2ϕ, and a satellite filamentous phage, TLC-Knϕ1 (Hassan et al., 2010). Thus, filamentous phage species interact and coevolve with each other in addition to their hosts. Infection by filamentous phage has been implicated in the virulence of *Yersinia pestis* (Derbise et al., 2007), *Neisseria meningitidis* (Bille et al., 2005, 2008), *Vibrio parahaemolyticus* (Iida et al., 2001), *E. coli* 018:K1:H7 (Gonzalez et al., 2002), *Xanthomonas campestris* (Kamiunten and Wakimoto, 1982), and *P. aeruginosa* (Webb et al., 2004), although in most of these cases, the specific mechanisms modulating virulence are unclear. Phage infection can both enhance or repress virulence depending on the characteristics of the phage,

the host bacterium, and the environmental milieu, as is the case for the bacterial wilt pathogen *Ralstonia solanacearum* (Yamada, 2013). Since infection results in downregulation of the pili used for viral entry, filamentous phage treatment has been proposed as a hypothetical means of inhibiting bacterial conjugation and horizontal gene transfer, so as to prevent the spread of antibiotic resistance genes (Lin et al., 2011).

Finally, the filamentous phage may also play a future role in the preservation of biodiversity of other organisms in at-risk ecosystems. Engineered phage have been proposed for use in bioremediation, either displaying antibody fragments of desired specificity for filtration of toxins and environmental contaminants (Petrenko and Makowski, 1993), or as biodegradable polymers displaying peptides selected for their ability to aggregate pollutants, such as oil sands tailings (Curtis et al., 2011, 2013). Engineered phage displaying peptides that specifically bind inorganic materials have also been proposed for use in more advanced and less intrusive mineral separation technologies (Curtis et al., 2009).

## Conclusion and Future Perspectives

The filamentous phage represents a highly versatile organism whose uses extend far beyond traditional phage display and affinity selection of antibodies and polypeptides of desired specificity. Its high immunogenicity and ability to display a variety of surface antigens make the phage an excellent particulate vaccine carrier, although its bacterial production and preparation heterogeneity likely limits its applications in human vaccines at present, despite being apparently safe and well-tolerated in animals and people. Unanticipated characteristics of the phage particle, such as crossing of the blood–brain barrier and formation of highly ordered liquid crystalline phases, have opened up entirely new avenues of research in therapeutics for chronic disease and the design of nanomaterials. Our comparatively detailed understanding of the interactions of model filamentous phage with their bacterial hosts has allowed researchers to harness the phage life cycle to direct protein evolution in the lab. Hopefully, deeper knowledge of phage–host interactions at an ecological level may produce novel strategies to control bacterial pathogenesis. While novel applications of the filamentous phage continue to be developed, the phage is likely to retain its position as a workhorse for therapeutic antibody discovery for many years to come, even with the advent of competing technologies.

## Author Contributions

KH and JS conceived and wrote the manuscript. MA-G read the manuscript and commented on the text.

## Acknowledgments

This work was supported by funding from the National Research Council of Canada (KH, MA-G) and the Canada Research Chair Program (JS). We thank Jyothi Kumaran and Roger MacKenzie for critical appraisal of the manuscript, and Jasna Rakonjac for inviting us to contribute it. This is National Research Council Canada publication number 53282.

## References

Abbineni, G., Modali, S., Safiejko-Mroczka, B., Petrenko, V. A., and Mao, C. (2010). Evolutionary selection of new breast cancer cell-targeting peptides and phages with the cell-targeting peptides fully displayed on the major coat and their effects on actin dynamics during cell internalization. *Mol. Pharm.* 7, 1629–1642. doi: 10.1021/mp100052y

Abdennebi, L., Couture, L., Grebert, D., Pajot, E., Salesse, R., and Remy, J. J. (1999). Generating FSH antagonists and agonists through immunization against FSH receptor N-terminal decapeptides. *J. Mol. Endocrinol.* 22, 151–159. doi: 10.1677/jme.0.0220151

Alhamlan, F. S., Ederer, M. M., Brown, C. J., Coats, E. R., and Crawford, R. L. (2013). Metagenomics-based analysis of viral communities in dairy lagoon wastewater. *J. Microbiol. Methods* 92, 183–188. doi: 10.1016/j.mimet.2012.11.016

Ashelford, K. E., Day, M. J., and Fry, J. C. (2003). Elevated abundance of bacteriophage infecting bacteria in soil. *Appl. Environ. Microbiol.* 69, 285–289. doi: 10.1128/AEM.69.1.285-289.2003

Bahadir, A. O., Balcioglu, B. K., Uzyol, K. S., Hatipoglu, I., Sogut, I., Basalp, A., et al. (2011). Phage displayed HBV core antigen with immunogenic activity. *Appl. Biochem. Biotechnol.* 165, 1437–1447. doi: 10.1007/s12010-011-9365-1

Balcioglu, B. K., Ozdemir-Barahir, A., Hinc, D., Tamerler, C., and Erdag, B. (2014). Cost effective filamentous phage based immunization nanoparticles displaying a full-length hepatitis B virus surface antigen. *Adv. Biosci. Biotechnol.* 5, 7. doi: 10.4236/abb.2014.51008

Bass, S., Greene, R., and Wells, J. A. (1990). Hormone phage: an enrichment method for variant proteins with altered binding properties. *Proteins* 8, 309–314. doi: 10.1002/prot.340080405

Bastien, N., Trudel, M., and Simard, C. (1997). Protective immune responses induced by the immunization of mice with a recombinant bacteriophage displaying an epitope of the human respiratory syncytial virus. *Virology* 234, 118–122. doi: 10.1006/viro.1997.8632

Bedi, D., Gillespie, J. W., and Petrenko, V. A. (2014). Selection of pancreatic cancer cell-binding landscape phages and their use in development of anticancer nanomedicines. *Protein Eng. Des. Sel.* 27, 235–243. doi: 10.1093/protein/gzu020

Bedi, D., Gillespie, J. W., Petrenko, V. A. Jr., Ebner, A., Leitner, M., Hinterdorfer, P., et al. (2013). Targeted delivery of siRNA into breast cancer cells via phage fusion proteins. *Mol. Pharm.* 10, 551–559. doi: 10.1021/mp3006006

Bedi, D., Musacchio, T., Fagbohun, O. A., Gillespie, J. W., Deinnocentes, P., Bird, R. C., et al. (2011). Delivery of siRNA into breast cancer cells via phage fusion protein-targeted liposomes. *Nanomedicine* 7, 315–323. doi: 10.1016/j.nano.2010.10.004

Bille, E., Ure, R., Gray, S. J., Kaczmarski, E. B., Mccarthy, N. D., Nassif, X., et al. (2008). Association of a bacteriophage with meningococcal disease in young adults. *PLoS ONE* 3:e3885. doi: 10.1371/journal.pone.0003885

Bille, E., Zahar, J. R., Perrin, A., Morelle, S., Kriz, P., Jolley, K. A., et al. (2005). A chromosomally integrated bacteriophage in invasive meningococci. *J. Exp. Med.* 201, 1905–1913. doi: 10.1084/jem.20050112

Boratynski, J., Syper, D., Weber-Dabrowska, B., Lusiak-Szelachowska, M., Pozniak, G., and Gorski, A. (2004). Preparation of endotoxin-free bacteriophages. *Cell Mol. Biol. Lett.* 9, 253–259.

Bradbury, A. R., Sidhu, S., Dubel, S., and Mccafferty, J. (2011). Beyond natural antibodies: the power of in vitro display technologies. *Nat. Biotechnol.* 29, 245–254. doi: 10.1038/nbt.1791

Branston, S. D., Wright, J., and Keshavarz-Moore, E. (2015). A non-chromatographic method for the removal of endotoxins from bacteriophages. *Biotechnol. Bioeng.* 112, 1714–1719. doi: 10.1002/bit.25571

Bratkovic, T. (2010). Progress in phage display: evolution of the technique and its application. *Cell. Mol. Life Sci.* 67, 749–767. doi: 10.1007/s00018-009-0192-2

Breitling, F., Dubel, S., Seehaus, T., Klewinghaus, I., and Little, M. (1991). A surface expression vector for antibody screening. *Gene* 104, 147–153. doi: 10.1016/0378-1119(91)90244-6

Canchaya, C., Proux, C., Fournous, G., Bruttin, A., and Brussow, H. (2003). Prophage genomics. *Microbiol. Mol. Biol. Rev.* 67, 238–276. doi: 10.1128/MMBR.67.2.238-276.2003

Cantalupo, P. G., Calgua, B., Zhao, G., Hundesa, A., Wier, A. D., Katz, J. P., et al. (2011). Raw sewage harbors diverse viral populations. *MBio* 2:e00180–11. doi: 10.1128/mBio.00180-111

Carlson, J. C., Badran, A. H., Guggiana-Nilo, D. A., and Liu, D. R. (2014). Negative selection and stringency modulation in phage-assisted continuous evolution. *Nat. Chem. Biol.* 10, 216–222. doi: 10.1038/nchembio.1453

Carrico, Z. M., Farkas, M. E., Zhou, Y., Hsiao, S. C., Marks, J. D., Chokhawala, H., et al. (2012). N-Terminal labeling of filamentous phage to create cancer marker imaging agents. *ACS Nano* 6, 6675–6680. doi: 10.1021/nn301134z

Chai, Y., Li, S., Horikawa, S., Park, M. K., Vodyanoy, V., and Chin, B. A. (2012). Rapid and sensitive detection of *Salmonella* Typhimurium on eggshells by using wireless biosensors. *J. Food. Prot.* 75, 631–636. doi: 10.4315/0362-028X.JFP-11-339

Chen, I., Choi, Y. A., and Ting, A. Y. (2007). Phage display evolution of a peptide substrate for yeast biotin ligase and application to two-color quantum dot labeling of cell surface proteins. *J. Am. Chem. Soc.* 129, 6619–6625. doi: 10.1021/ja071013g

Chen, P. Y., Dang, X., Klug, M. T., Qi, J., Courchesne, N.-M. D., Burpo, F. J., et al. (2013). Versatile three-dimensional virus-based template for dye-sensitized solar cells with improved electron transport and light harvesting. *ACS Nano* 7, 6563–6574. doi: 10.1021/nn4014164

Chen, P. Y., Hyder, M. N., Mackanic, D., Courchesne, N. M., Qi, J., Klug, M. T., et al. (2014). Assembly of viral hydrogels for three-dimensional conducting nanocomposites. *Adv. Mater.* 26, 5101–5107. doi: 10.1002/adma.201400828

Chen, X., Scala, G., Quinto, I., Liu, W., Chun, T. W., Justement, J. S., et al. (2001). Protection of rhesus macaques against disease progression from pathogenic SHIV-89.6PD by vaccination with phage-displayed HIV-1 epitopes. *Nat. Med.* 7, 1225–1231. doi: 10.1038/nm1101-1225

Chibani-Chennoufi, S., Bruttin, A., Dillmann, M. L., and Brussow, H. (2004). Phage-host interaction: an ecological perspective. *J. Bacteriol.* 186, 3677–3686. doi: 10.1128/JB.186.12.3677-3686.2004

Coull, J. J., Melvin, W. T., Labus, M. B., Raynard, R. S., King, J., and Munro, A. L. (1996). Evaluation of filamentous bacteriophage as immunogens in Atlantic salmon. *Biochem. Soc. Trans.* 24, 255S.

Cuesta, A. M., Suarez, E., Larsen, M., Jensen, K. B., Sanz, L., Compte, M., et al. (2006). Enhancement of DNA vaccine potency through linkage of antigen to filamentous bacteriophage coat protein III domain I. *Immunology* 117, 502–506. doi: 10.1111/j.1365-2567.2006.02325.x

Curtis, S. B., Dunbar, W. S., and Macgillivray, R. T. (2013). Bacteriophage-induced aggregation of oil sands tailings. *Biotechnol. Bioeng.* 110, 803–811. doi: 10.1002/bit.24745

Curtis, S. B., Hewitt, J., Macgillivray, R. T., and Dunbar, W. S. (2009). Biomining with bacteriophage: selectivity of displayed peptides for naturally occurring sphalerite and chalcopyrite. *Biotechnol. Bioeng.* 102, 644–650. doi: 10.1002/bit.22073

Curtis, S. B., Macgillivray, R. T., and Dunbar, W. S. (2011). Effects of bacteriophage on the surface properties of chalcopyrite (CuFeS(2)), and phage-induced flocculation of chalcopyrite, glacial till, and oil sands tailings. *Biotechnol. Bioeng.* 108, 1579–1590. doi: 10.1002/bit.23097

Dahlke Ojennus, D., Mitton-Fry, R. M., and Wuttke, D. S. (1999). Induced alignment and measurement of dipolar couplings of an SH2 domain through direct binding with filamentous phage. *J. Biomol. NMR* 14, 175–179. doi: 10.1023/A:1008304332574

Dalmasso, M., Hill, C., and Ross, R. P. (2014). Exploiting gut bacteriophages for human health. *Trends Microbiol.* 22, 399–405. doi: 10.1016/j.tim.2014.02.010

De Berardinis, P., D'apice, L., Prisco, A., Ombra, M. N., Barba, P., Del Pozzo, G., et al. (1999). Recognition of HIV-derived B and T cell epitopes displayed on filamentous phages. *Vaccine* 17, 1434–1441. doi: 10.1016/S0264-410X(98)00377-6

De Berardinis, P., Sartorius, R., Fanutti, C., Perham, R. N., Del Pozzo, G., and Guardiola, J. (2000). Phage display of peptide epitopes from HIV-1 elicits strong cytolytic responses. *Nat. Biotechnol.* 18, 873–876. doi: 10.1038/78490

de la Cruz, V. F., Lal, A. A., and Mccutchan, T. F. (1988). Immunogenicity and epitope mapping of foreign sequences via genetically engineered filamentous phage. *J. Biol. Chem.* 263, 4318–4322.

Del Pozzo, G., Mascolo, D., Sartorius, R., Citro, A., Barba, P., D'Apice, L., et al. (2010). Triggering DTH and CTL activity by fd filamentous bacteriophages: role of CD4+ T cells in memory responses. *J. Biomed. Biotechnol.* 2010:894971. doi: 10.1155/2010/894971

Delmastro, P., Meola, A., Monaci, P., Cortese, R., and Galfre, G. (1997). Immunogenicity of filamentous phage displaying peptide mimotopes after oral administration. *Vaccine* 15, 1276–1285. doi: 10.1016/S0264-410X(97)00072-8

Demangel, C., Lafaye, P., and Mazie, J. C. (1996). Reproducing the immune response against the *Plasmodium vivax* merozoite surface protein 1 with mimotopes selected from a phage-displayed peptide library. *Mol. Immunol.* 33, 909–916. doi: 10.1016/S0161-5890(96)00058-2

Demuth, J., Neve, H., and Witzel, K. P. (1993). Direct electron microscopy study on the morphological diversity of bacteriophage populations in lake Plußsee. *Appl. Environ. Microbiol.* 59, 3378–3384.

Dente, L., Cesareni, G., Micheli, G., Felici, F., Folgori, A., Luzzago, A., et al. (1994). Monoclonal antibodies that recognise filamentous phage: tools for phage display technology. *Gene* 148, 7–13. doi: 10.1016/0378-1119(94)90227-5

Derbise, A., Chenal-Francisque, V., Pouillot, F., Fayolle, C., Prevost, M. C., Medigue, C., et al. (2007). A horizontally acquired filamentous phage contributes to the pathogenicity of the plague bacillus. *Mol. Microbiol.* 63, 1145–1157. doi: 10.1111/j.1365-2958.2006.05570.x

Devlin, J. J., Panganiban, L. C., and Devlin, P. E. (1990). Random peptide libraries: a source of specific protein binding molecules. *Science* 249, 404–406. doi: 10.1126/science.2143033

Dickinson, B. C., Leconte, A. M., Allen, B., Esvelt, K. M., and Liu, D. R. (2013). Experimental interrogation of the path dependence and stochasticity of protein evolution using phage-assisted continuous evolution. *Proc. Natl. Acad. Sci. U.S.A.* 110, 9007–9012. doi: 10.1073/pnas.1220670110

di Marzo Veronese, F., Willis, A. E., Boyer-Thompson, C., Appella, E., and Perham, R. N. (1994). Structural mimicry and enhanced immunogenicity of peptide epitopes displayed on filamentous bacteriophage. The V3 loop of HIV-1 gp120. *J. Mol. Biol.* 243, 167–172. doi: 10.1006/jmbi.1994.1643

d'Hérelle, F. (1917). Sur un microbe invisible antagoniste des bacilles dysentérique. *Acad. Sci. Paris* 165, 3.

Eriksson, F., Culp, W. D., Massey, R., Egevad, L., Garland, D., Persson, M. A., et al. (2007). Tumor specific phage particles promote tumor regression in a mouse melanoma model. *Cancer Immunol. Immunother.* 56, 677–687. doi: 10.1007/s00262-006-0227–226

Eriksson, F., Tsagozis, P., Lundberg, K., Parsa, R., Mangsbo, S. M., Persson, M. A., et al. (2009). Tumor-specific bacteriophages induce tumor destruction through activation of tumor-associated macrophages. *J. Immunol.* 182, 3105–3111. doi: 10.4049/jimmunol.0800224

Esposito, M., Luccarini, I., Cicatiello, V., De Falco, D., Fiorentini, A., Barba, P., et al. (2008). Immunogenicity and therapeutic efficacy of phage-displayed beta-amyloid epitopes. *Mol. Immunol.* 45, 1056–1062. doi: 10.1016/j.molimm.2007.07.023

Esvelt, K. M., Carlson, J. C., and Liu, D. R. (2011). A system for the continuous directed evolution of biomolecules. *Nature* 472, 499–503. doi: 10.1038/nature09929

Fagbohun, O. A., Bedi, D., Grabchenko, N. I., Deinnocentes, P. A., Bird, R. C., and Petrenko, V. A. (2012). Landscape phages and their fusion proteins targeted to breast cancer cells. *Protein Eng. Des. Sel.* 25, 271–283. doi: 10.1093/protein/gzs013

Fagbohun, O. A., Kazmierczak, R. A., Petrenko, V. A., and Eisenstark, A. (2013). Metastatic prostate cancer cell-specific phage-like particles as a targeted gene-delivery system. *J. Nanobiotechnol.* 11, 31. doi: 10.1186/1477-3155-11-31

Fang, J., Wang, G., Yang, Q., Song, J., Wang, Y., and Wang, L. (2005). The potential of phage display virions expressing malignant tumor specific antigen MAGE-A1 epitope in murine model. *Vaccine* 23, 4860–4866. doi: 10.1016/j.vaccine.2005.05.024

Fauquet, C. M., Mayo, M. A., Maniloff, J., Desselberger, U., and Ball, L. A. (ed.). (2005). *Virus Taxonomy. 8th report of the International Committee on the Taxonomy of Viruses*. London: Elsevier/Academic Press.

Felici, F., Luzzago, A., Folgori, A., and Cortese, R. (1993). Mimicking of discontinuous epitopes by phage-displayed peptides, II. Selection of clones recognized by a protective monoclonal antibody against the *Bordetella pertussis* toxin from phage peptide libraries. *Gene* 128, 21–27. doi: 10.1016/0378-1119(93)90148-V

Folgori, A., Tafi, R., Meola, A., Felici, F., Galfre, G., Cortese, R., et al. (1994). A general strategy to identify mimotopes of pathological antigens using only random peptide libraries and human sera. *EMBO J.* 13, 2236–2243.

Frenkel, D., Dewachter, I., Van Leuven, F., and Solomon, B. (2003). Reduction of β-amyloid plaques in brain of transgenic mouse model of Alzheimer's disease by EFRH-phage immunization. *Vaccine* 21, 1060–1065. doi: 10.1016/S0264-410X(02)00609-6

Frenkel, D., Katz, O., and Solomon, B. (2000). Immunization against Alzheimer's β-amyloid plaques via EFRH phage administration. *Proc. Natl. Acad. Sci. U.S.A.* 97, 11455–11459. doi: 10.1073/pnas.97.21.11455

Frenkel, D., and Solomon, B. (2002). Filamentous phage as vector-mediated antibody delivery to the brain. *Proc. Natl. Acad. Sci. U.S.A.* 99, 5675–5679. doi: 10.1073/pnas.072027199

Gao, C., Mao, S., Kaufmann, G., Wirsching, P., Lerner, R. A., and Janda, K. D. (2002). A method for the generation of combinatorial antibody libraries using pIX phage display. *Proc. Natl. Acad. Sci. U.S.A.* 99, 12612–12616. doi: 10.1073/pnas.192467999

Gao, C., Mao, S., Lo, C. H., Wirsching, P., Lerner, R. A., and Janda, K. D. (1999). Making artificial antibodies: a format for phage display of combinatorial heterodimeric arrays. *Proc. Natl. Acad. Sci. U.S.A.* 96, 6025–6030. doi: 10.1073/pnas.96.11.6025

Gaubin, M., Fanutti, C., Mishal, Z., Durrbach, A., De Berardinis, P., Sartorius, R., et al. (2003). Processing of filamentous bacteriophage virions in antigen-presenting cells targets both HLA class I and class II peptide loading compartments. *DNA Cell Biol.* 22, 11–18. doi: 10.1089/104454903321112451

Geysen, H. M., Rodda, S. J., and Mason, T. J. (1986). *A priori* delineation of a peptide which mimics a discontinuous antigenic determinant. *Mol. Immunol.* 23, 709–715. doi: 10.1016/0161-5890(86)90081-7

Ghosh, D., Kohli, A. G., Moser, F., Endy, D., and Belcher, A. M. (2012a). Refactored M13 bacteriophage as a platform for tumor cell imaging and drug delivery. *ACS Synth. Biol.* 1, 576–582. doi: 10.1021/sb300052u

Ghosh, D., Lee, Y., Thomas, S., Kohli, A. G., Yun, D. S., Belcher, A. M., et al. (2012b). M13-templated magnetic nanoparticles for targeted *in vivo* imaging of prostate cancer. *Nat. Nanotechnol.* 7, 677–682. doi: 10.1038/nnano.2012.146

Gonzalez, M. D., Lichtensteiger, C. A., Caughlan, R., and Vimr, E. R. (2002). Conserved filamentous prophage in *Escherichia coli* O18:K1:H7 and *Yersinia pestis* biovar orientalis. *J. Bacteriol.* 184, 6050–6055. doi: 10.1128/JB.184.21.6050-6055.2002

Grabowska, A. M., Jennings, R., Laing, P., Darsley, M., Jameson, C. L., Swift, L., et al. (2000). Immunisation with phage displaying peptides representing single epitopes of the glycoprotein G can give rise to partial protective immunity to HSV-2. *Virology* 269, 47–53. doi: 10.1006/viro.2000.0185

Gram, H., Strittmatter, U., Lorenz, M., Gluck, D., and Zenke, G. (1993). Phage display as a rapid gene expression system: production of bioactive cytokine-phage and generation of neutralizing monoclonal antibodies. *J. Immunol. Methods* 161, 169–176. doi: 10.1016/0022-1759(93)90292-F

Greenwood, J., Willis, A. E., and Perham, R. N. (1991). Multiple display of foreign peptides on a filamentous bacteriophage. Peptides from *Plasmodium falciparum* circumsporozoite protein as antigens. *J. Mol. Biol.* 220, 821–827. doi: 10.1016/0022-2836(91)90354-9

Hagens, S., and Blasi, U. (2003). Genetically modified filamentous phage as bactericidal agents: a pilot study. *Lett. Appl. Microbiol.* 37, 318–323. doi: 10.1046/j.1472-765X.2003.01400.x

Hagens, S., Habel, A., and Blasi, U. (2006). Augmentation of the antimicrobial efficacy of antibiotics by filamentous phage. *Microb. Drug Resist.* 12, 164–168. doi: 10.1089/mdr.2006.12.164

Hagens, S., Habel, A., Von Ahsen, U., Von Gabain, A., and Blasi, U. (2004). Therapy of experimental *Pseudomonas* infections with a nonreplicating genetically modified phage. *Antimicrob. Agents Chemother.* 48, 3817–3822. doi: 10.1128/AAC.48.10.3817-3822.2004

Hall, J. P., Harrison, E., and Brockhurst, M. A. (2013). Viral host-adaptation: insights from evolution experiments with phages. *Curr. Opin. Virol.* 3, 572–577. doi: 10.1016/j.coviro.2013.07.001

Hansen, M. R., Hanson, P., and Pardi, A. (2000). Pf1 filamentous phage as an alignment tool for generating local and global structural information in nucleic acids. *J. Biomol. Struct. Dyn.* 17(Suppl. 1), 365–369. doi: 10.1080/07391102.2000.10506642

Hansen, M. R., Mueller, L., and Pardi, A. (1998). Tunable alignment of macromolecules by filamentous phage yields dipolar coupling interactions. *Nat. Struct. Biol.* 5, 1065–1074. doi: 10.1038/4176

Hashiguchi, S., Yamaguchi, Y., Takeuchi, O., Akira, S., and Sugimura, K. (2010). Immunological basis of M13 phage vaccine: regulation under MyD88 and TLR9 signaling. *Biochem. Biophys. Res. Commun.* 402, 19–22. doi: 10.1016/j.bbrc.2010.09.094

Hassan, F., Kamruzzaman, M., Mekalanos, J. J., and Faruque, S. M. (2010). Satellite phage TLCϕ enables toxigenic conversion by CTX phage through dif site alteration. *Nature* 467, 982–985. doi: 10.1038/nature09469

Henry, K. A., Murira, A., Van Houten, N. E., and Scott, J. K. (2011). Developing strategies to enhance and focus humoral immune responses using filamentous phage as a model antigen. *Bioengineered* 2, 275–283. doi: 10.4161/bbug.2.5.16559

Hess, G. T., Cragnolini, J. J., Popp, M. W., Allen, M. A., Dougan, S. K., Spooner, E., et al. (2012). M13 bacteriophage display framework that allows sortase-mediated modification of surface-accessible phage proteins. *Bioconjug. Chem.* 23, 1478–1487. doi: 10.1021/bc300130z

Hofer, J. S., and Sommaruga, R. (2001). Seasonal dynamics of viruses in an alpine lake: importance of filamentous forms. *Aquat. Microb. Ecol.* 26, 11. doi: 10.3354/ame026001

Hofschneider, P. H., and Mueller-Jensen, K. (1963). On infectious substructures from *E. coli* bacteriophages. 3. Demonstration and properties of "Ht2" particles. *Z. Naturforsch B* 18, 922–927.

Houimel, M., and Dellagi, K. (2009). Peptide mimotopes of rabies virus glycoprotein with immunogenic activity. *Vaccine* 27, 4648–4655. doi: 10.1016/j.vaccine.2009.05.055

Huang, S., Yang, H., Lakshmanan, R. S., Johnson, M. L., Wan, J., Chen, I. H., et al. (2009). Sequential detection of *Salmonella typhimurium* and *Bacillus anthracis* spores using magnetoelastic biosensors. *Biosens. Bioelectron.* 24, 1730–1736. doi: 10.1016/j.bios.2008.09.006

Huang, Y., Chiang, C. Y., Lee, S. K., Gao, Y., Hu, E. L., De Yoreo, J., et al. (2005). Programmable assembly of nanoarchitectures using genetically engineered viruses. *Nano Lett.* 5, 1429–1434. doi: 10.1021/nl050795d

Hufton, S. E., Moerkerk, P. T., Meulemans, E. V., De Bruine, A., Arends, J. W., and Hoogenboom, H. R. (1999). Phage display of cDNA repertoires: the pVI display system and its applications for the selection of immunogenic ligands. *J. Immunol. Methods* 231, 39–51. doi: 10.1016/S0022-1759(99)00139-8

Husimi, Y. (1989). Selection and evolution of bacteriophages in cellstat. *Adv. Biophys.* 25, 1–43. doi: 10.1016/0065-227X(89)90003-8

Iida, T., Hattori, A., Tagomori, K., Nasu, H., Naim, R., and Honda, T. (2001). Filamentous phage associated with recent pandemic strains of *Vibrio parahaemolyticus*. *Emerg. Infect. Dis.* 7, 477–478. doi: 10.3201/eid0703.010325

Irving, M. B., Craig, L., Menendez, A., Gangadhar, B. P., Montero, M., van Houten, N. E., et al. (2010). Exploring peptide mimics for the production of antibodies against discontinuous protein epitopes. *Mol. Immunol.* 47, 1137–1148. doi: 10.1016/j.molimm.2009.10.015

Jayanna, P. K., Bedi, D., Deinnocentes, P., Bird, R. C., and Petrenko, V. A. (2010a). Landscape phage ligands for PC3 prostate carcinoma cells. *Protein Eng. Des. Sel.* 23, 423–430. doi: 10.1093/protein/gzq011

Jayanna, P. K., Bedi, D., Gillespie, J. W., Deinnocentes, P., Wang, T., Torchilin, V. P., et al. (2010b). Landscape phage fusion protein-mediated targeting of nanomedicines enhances their prostate tumor cell association and cytotoxic efficiency. *Nanomedicine* 6, 538–546. doi: 10.1016/j.nano.2010.01.005

Jian, H., Xu, J., Xiao, X., and Wang, F. (2012). Dynamic modulation of DNA replication and gene transcription in deep-sea filamentous phage SW1 in response to changes of host growth and temperature. *PLoS ONE* 7:e41578. doi: 10.1371/journal.pone.0041578

Kajihara, Y., Hashiguchi, S., Ito, Y., and Sugimura, K. (2000). Th2-type immune response induced by a phage clone displaying a CTLA4-binding domain mimic-motif. *Gene Ther. Mol. Biol.* 5, 6.

Kamiunten, H., and Wakimoto, S. (1982). Effect of infection with filamentous phage xf on the growth, ultrastructure and virulence of *Xanthomonas campestris* pv. *oryzae* N 5850. *Jpn. J. Phytopatholo.* 48, 642–647. doi: 10.3186/jjphytopath.48.642

Kang, A. S., Barbas, C. F., Janda, K. D., Benkovic, S. J., and Lerner, R. A. (1991). Linkage of recognition and replication functions by assembling combinatorial antibody Fab libraries along phage surfaces. *Proc. Natl. Acad. Sci. U.S.A.* 88, 4363–4366. doi: 10.1073/pnas.88.10.4363

Kawecki, T. J., Lenski, R. E., Ebert, D., Hollis, B., Olivieri, I., and Whitlock, M. C. (2012). Experimental evolution. *Trends Ecol. Evol.* 27, 547–560. doi: 10.1016/j.tree.2012.06.001

Kehoe, J. W., and Kay, B. K. (2005). Filamentous phage display in the new millennium. *Chem. Rev.* 105, 4056–4072. doi: 10.1021/cr000261r

Khatoon, H., Iyer, R. V., and Iyer, V. N. (1972). A new filamentous bacteriophage with sex-factor specificity. *Virology* 48, 145–155. doi: 10.1016/0042-6822(72)90122-5

Kim, M. S., Park, E. J., Roh, S. W., and Bae, J. W. (2011). Diversity and abundance of single-stranded DNA viruses in human feces. *Appl. Environ. Microbiol.* 77, 8062–8070. doi: 10.1128/AEM.06331-1

Kim, Y. J., Jin, Y. H., Salieb-Beugelaar, G. B., Nam, C. H., and Stieglitz, T. (2014). Genetically engineered bacteriophage delivers a tumor necrosis factor alpha antagonist coating on neural electrodes. *Biomed. Mater.* 9:015009. doi: 10.1088/1748-6041/9/1/015009

Kim, Y. J., Lebreton, F., Kaiser, C., Cruciere, C., and Remond, M. (2004). Expression of a foot-and-mouth disease virus immunodominant epitope by a filamentous bacteriophage vector. *Arch. Virol.* 149, 365–377. doi: 10.1007/s00705-003-0192-198

Kishchenko, G., Batliwala, H., and Makowski, L. (1994). Structure of a foreign peptide displayed on the surface of bacteriophage M13. *J. Mol. Biol.* 241, 208–213. doi: 10.1006/jmbi.1994.1489

Kneissel, S., Queitsch, I., Petersen, G., Behrsing, O., Micheel, B., and Dubel, S. (1999). Epitope structures recognised by antibodies against the major coat protein (g8p) of filamentous bacteriophage fd (*Inoviridae*). *J. Mol. Biol.* 288, 21–28. doi: 10.1006/jmbi.1999.2676

Knittelfelder, R., Riemer, A. B., and Jensen-Jarolim, E. (2009). Mimotope vaccination–from allergy to cancer. *Expert. Opin. Biol. Ther.* 9, 493–506. doi: 10.1517/14712590902870386

Koide, A., and Koide, S. (2012). Affinity maturation of single-domain antibodies by yeast surface display. *Methods Mol. Biol.* 911, 431–443. doi: 10.1007/978-1-61779-968-6-26

Kölsch, E., Diller, E., Weber, G., and Davies, A. J. (1971). Genetics of the immune response. I. The immune response to the phage fd in high and low responding inbred strains of mice. *Eur. J. Immunol.* 1, 201–210. doi: 10.1002/eji.1830010310

Ksendzovsky, A., Walbridge, S., Saunders, R. C., Asthagiri, A. R., Heiss, J. D., and Lonser, R. R. (2012). Convection-enhanced delivery of M13 bacteriophage to the brain. *J. Neurosurg.* 117, 197–203. doi: 10.3171/2012.4.JNS111528

Kwasnikowski, P., Kristensen, P., and Markiewicz, W. T. (2005). Multivalent display system on filamentous bacteriophage pVII minor coat protein. *J. Immunol. Methods* 307, 135–143. doi: 10.1016/j.jim.2005.10.002

Lakshmanan, R. S., Guntupalli, R., Hu, J., Kim, D. J., Petrenko, V. A., Barbaree, J. M., et al. (2007). Phage immobilized magnetoelastic sensor for the detection of *Salmonella typhimurium*. *J. Microbiol. Methods* 71, 55–60. doi: 10.1016/j.mimet.2007.07.012

Lang, Q., Wang, F., Yin, L., Liu, M., Petrenko, V. A., and Liu, A. (2014). Specific probe selection from landscape phage display library and its application in enzyme-linked immunosorbent assay of free prostate-specific antigen. *Anal. Chem.* 86, 2767–2774. doi: 10.1021/ac404189k

Lavie, V., Becker, M., Cohen-Kupiec, R., Yacoby, I., Koppel, R., Wedenig, M., et al. (2004). EFRH-phage immunization of Alzheimer's disease animal model improves behavioral performance in Morris water maze trials. *J. Mol. Neurosci.* 24, 105–113. doi: 10.1385/JMN:24:1105

Lee, S. W., Mao, C., Flynn, C. E., and Belcher, A. M. (2002). Ordering of quantum dots using genetically engineered viruses. *Science* 296, 892–895. doi: 10.1126/science.1068054

Lee, Y. J., Yi, H., Kim, W. J., Kang, K., Yun, D. S., Strano, M. S., et al. (2009). Fabricating genetically engineered high-power lithium-ion batteries using multiple virus genes. *Science* 324, 1051–1055. doi: 10.1126/science.1171541

Li, K., Chen, Y., Li, S., Nguyen, H. G., Niu, Z., You, S., et al. (2010a). Chemical modification of M13 bacteriophage and its application in cancer cell imaging. *Bioconjug. Chem.* 21, 1369–1377. doi: 10.1021/bc900405q

Li, S., Li, Y., Chen, H., Horikawa, S., Shen, W., Simonian, A., et al. (2010b). Direct detection of *Salmonella typhimurium* on fresh produce using phage-based magnetoelastic biosensors. *Biosens. Bioelectron.* 26, 1313–1319. doi: 10.1016/j.bios.2010.07.029

Li, Y., Ning, Y., Wang, Y., Peng, D., Jiang, Y., Zhang, L., et al. (2010c). Mimotopes selected with a neutralizing antibody against urease B from *Helicobacter pylori* induce enzyme inhibitory antibodies in mice upon vaccination. *BMC Biotechnol.* 10:84. doi: 10.1186/1472-6750-10-84

Lidqvist, M., Nilsson, O., Holmgren, J., Hall, C., and Fermer, C. (2008). Phage display for site-specific immunization and characterization of high-risk human papillomavirus specific E7 monoclonal antibodies. *J. Immunol. Methods* 337, 88–96. doi: 10.1016/j.jim.2008.06.002

Lin, A., Jimenez, J., Derr, J., Vera, P., Manapat, M. L., Esvelt, K. M., et al. (2011). Inhibition of bacterial conjugation by phage M13 and its protein g3p: quantitative analysis and model. *PLoS ONE* 6:e19991. doi: 10.1371/journal.pone.0019991

Lippow, S. M., Wittrup, K. D., and Tidor, B. (2007). Computational design of antibody-affinity improvement beyond *in vivo* maturation. *Nat. Biotechnol.* 25, 1171–1176. doi: 10.1038/nbt1336

Loeb, T. (1960). Isolation of a bacteriophage specific for the F plus and Hfr mating types of *Escherichia coli* K-12. *Science* 131, 932–933. doi: 10.1126/science.131.3404.932

Lu, T. K., and Collins, J. J. (2009). Engineered bacteriophage targeting gene networks as adjuvants for antibiotic therapy. *Proc. Natl. Acad. Sci. U.S.A.* 106, 4629–4634. doi: 10.1073/pnas.0800442106

Malik, P., Terry, T. D., Gowda, L. R., Langara, A., Petukhov, S. A., Symmons, M. F., et al. (1996). Role of capsid structure and membrane protein processing in determining the size and copy number of peptides displayed on the major coat protein of filamentous bacteriophage. *J. Mol. Biol.* 260, 9–21. doi: 10.1006/jmbi.1996.0378

Manoutcharian, K., Diaz-Orea, A., Gevorkian, G., Fragoso, G., Acero, G., Gonzalez, E., et al. (2004). Recombinant bacteriophage-based multiepitope vaccine against *Taenia solium* pig cysticercosis. *Vet. Immunol. Immunopathol.* 99, 11–24. doi: 10.1016/j.vetimm.2003.12.009

Mao, C., Flynn, C. E., Hayhurst, A., Sweeney, R., Qi, J., Georgiou, G., et al. (2003). Viral assembly of oriented quantum dot nanowires. *Proc. Natl. Acad. Sci. U.S.A.* 100, 6946–6951. doi: 10.1073/pnas.0832310100

Mao, C., Solis, D. J., Reiss, B. D., Kottmann, S. T., Sweeney, R. Y., Hayhurst, A., et al. (2004). Virus-based toolkit for the directed synthesis of magnetic and semiconducting nanowires. *Science* 303, 213–217. doi: 10.1126/science.1092740

Mao, J. Y., Belcher, A. M., and Van Vliet, K. J. (2010). Genetically engineered phage fibers and coatings for antibacterial applications. *Adv. Funct. Mater.* 20, 5. doi: 10.1002/adfm.200900782

Marks, J. D., Hoogenboom, H. R., Griffiths, A. D., and Winter, G. (1992). Molecular evolution of proteins on filamentous phage. Mimicking the strategy of the immune system. *J. Biol. Chem.* 267, 16007–16010.

Marvin, D. A. (1990). Model-building studies of *Inovirus*: genetic variations on a geometric theme. *Int. J. Biol. Macromol.* 12, 125–138. doi: 10.1016/0141-8130(90)90064-H

Marvin, D. A. (1998). Filamentous phage structure, infection and assembly. *Curr. Opin. Struct. Biol.* 8, 150–158. doi: 10.1016/S0959-440X(98)80032-8

Marvin, D. A., and Hoffmann-Berling, H. (1963). A fibrous DNA phage (Fd) and a spherical RNA phage (Fr) specific for male strains of *E. coli*. II. Physical characteristics. *Z. Naturforsch. B* 18, 884–893. doi: 10.1515/znb-1963-1106

Mascolo, D., Barba, P., De Berardinis, P., Di Rosa, F., and Del Pozzo, G. (2007). Phage display of a CTL epitope elicits a long-term *in vivo* cytotoxic response. *FEMS Immunol. Med. Microbiol.* 50, 59–66. doi: 10.1111/j.1574-695X.2007.00229.x

May, T., Tsuruta, K., and Okabe, S. (2011). Exposure of conjugative plasmid carrying *Escherichia coli* biofilms to male-specific bacteriophages. *ISME J.* 5, 771–775. doi: 10.1038/ismej.2010.158

McCafferty, J., Griffiths, A. D., Winter, G., and Chiswell, D. J. (1990). Phage antibodies: filamentous phage displaying antibody variable domains. *Nature* 348, 552–554. doi: 10.1038/348552a0

McConnell, S. J., Kendall, M. L., Reilly, T. M., and Hoess, R. H. (1994). Constrained peptide libraries as a tool for finding mimotopes. *Gene* 151, 115–118. doi: 10.1016/0378-1119(94)90640-8

Melzer, H., Baier, K., Felici, F., Von Specht, B. U., Wiedermann, G., Kollaritsch, H., et al. (2003). Humoral immune response against proteophosphoglycan surface antigens of *Entamoeba histolytica* elicited by immunization with synthetic mimotope peptides. *FEMS Immunol. Med. Microbiol.* 37, 179–183. doi: 10.1016/S092882440300074-9

Melzer, H., Fortugno, P., Mansouri, E., Felici, F., Marinets, A., Wiedermann, G., et al. (2002). Antigenicity and immunogenicity of phage library-selected peptide mimics of the major surface proteophosphoglycan antigens of *Entamoeba histolytica*. *Parasite Immunol.* 24, 321–328. doi: 10.1046/j.1365-3024.2002.00463.x

Menendez, T., De Haz, I., Delgado, M., Garay, H., Martin, A., and Vispo, N. S. (2001). Immunisation with phage-displayed variable region 2 from meningococcal PorA outer membrane protein induces bactericidal antibodies against *Neisseria meningitidis*. *Immunol. Lett.* 78, 143–148. doi: 10.1016/S0165-2478(01)00245-0

Meola, A., Delmastro, P., Monaci, P., Luzzago, A., Nicosia, A., Felici, F., et al. (1995). Derivation of vaccines from mimotopes. Immunologic properties of human hepatitis B virus surface antigen mimotopes displayed on filamentous phage. *J. Immunol.* 154, 3162–3172.

Meyer, A. J., and Ellington, A. D. (2011). Molecular evolution picks up the PACE. *Nat. Biotechnol.* 29, 502–503. doi: 10.1038/nbt.1884

Meynell, G. G., and Lawn, A. M. (1968). Filamentous phages specific for the I sex factor. *Nature* 217, 1184–1186. doi: 10.1038/2171184a0

Minenkova, O. O., Ilyichev, A. A., Kishchenko, G. P., and Petrenko, V. A. (1993). Design of specific immunogens using filamentous phage as the carrier. *Gene* 128, 85–88. doi: 10.1016/0378-1119(93)90157-X

Molenaar, T. J., Michon, I., De Haas, S. A., Van Berkel, T. J., Kuiper, J., and Biessen, E. A. (2002). Uptake and processing of modified bacteriophage M13 in mice: implications for phage display. *Virology* 293, 182–191. doi: 10.1006/viro.2001.1254

Moradpour, Z., Sepehrizadeh, Z., Rahbarizadeh, F., Ghasemian, A., Yazdi, M. T., and Shahverdi, A. R. (2009). Genetically engineered phage harbouring the lethal catabolite gene activator protein gene with an inducer-independent promoter for biocontrol of *Escherichia coli*. *FEMS Microbiol. Lett.* 296, 67–71. doi: 10.1111/j.1574-6968.2009.01620.x

Morales, J., Martinez, J. J., Manoutcharian, K., Hernandez, M., Fleury, A., Gevorkian, G., et al. (2008). Inexpensive anti-cysticercosis vaccine: S3Pvac expressed in heat inactivated M13 filamentous phage proves effective against naturally acquired *Taenia solium* porcine cysticercosis. *Vaccine* 26, 2899–2905. doi: 10.1016/j.vaccine.2008.03.042

Motti, C., Nuzzo, M., Meola, A., Galfre, G., Felici, F., Cortese, R., et al. (1994). Recognition by human sera and immunogenicity of HBsAg mimotopes selected from an M13 phage display library. *Gene* 146, 191–198. doi: 10.1016/0378-1119(94)90292-5

Murira, A. (2014). *Characterization of Molecular Correlates of the Chronic Humoral Immune Response: Clues towards Eliciting Broadly Neutralizing Antibodies against HIV*. Ph.D. thesis, Simon Fraser University, Burnaby, BC.

Murugaiyan, S., Bae, J. Y., Wu, J., Lee, S. D., Um, H. Y., Choi, H. K., et al. (2011). Characterization of filamentous bacteriophage PE226 infecting *Ralstonia solanacearum* strains. *J. Appl. Microbiol.* 110, 296–303. doi: 10.1111/j.1365-2672.2010.04882.x

Murugesan, M., Abbineni, G., Nimmo, S. L., Cao, B., and Mao, C. (2013). Virus-based photo-responsive nanowires formed by linking site-directed mutagenesis and chemical reaction. *Sci. Rep.* 3:1820. doi: 10.1038/srep01820

Nam, K. T., Kim, D. W., Yoo, P. J., Chiang, C. Y., Meethong, N., Hammond, P. T., et al. (2006). Virus-enabled synthesis and assembly of nanowires for lithium ion battery electrodes. *Science* 312, 885–888. doi: 10.1126/science.1122716

Nam, K. T., Wartena, R., Yoo, P. J., Liau, F. W., Lee, Y. J., Chiang, Y. M., et al. (2008). Stamped microbattery electrodes based on self-assembled M13 viruses. *Proc. Natl. Acad. Sci. U.S.A.* 105, 17227–17231. doi: 10.1073/pnas.0711620105

Nam, Y. S., Magyar, A. P., Lee, D., Kim, J. W., Yun, D. S., Park, H., et al. (2010a). Biologically templated photocatalytic nanostructures for sustained light-driven water oxidation. *Nat. Nanotechnol.* 5, 340–344. doi: 10.1038/nnano.2010.57

Nam, Y. S., Shin, T., Park, H., Magyar, A. P., Choi, K., Fantner, G., et al. (2010b). Virus-templated assembly of porphyrins into light-harvesting nanoantennae. *J. Am. Chem. Soc.* 132, 1462–1463. doi: 10.1021/ja908812b

Nanduri, V., Bhunia, A. K., Tu, S. I., Paoli, G. C., and Brewster, J. D. (2007). SPR biosensor for the detection of *L. monocytogenes* using phage-displayed antibody. *Biosens. Bioelectron.* 23, 248–252. doi: 10.1016/j.bios.2007.04.007

Neltner, B., Peddie, B., Xu, A., Doenlen, W., Durand, K., Yun, D. S., et al. (2010). Production of hydrogen using nanocrystalline protein-templated catalysts on m13 phage. *ACS Nano* 4, 3227–3235. doi: 10.1021/nn100346h

Ng, S., Jafari, M. R., Matochko, W. L., and Derda, R. (2012). Quantitative synthesis of genetically encoded glycopeptide libraries displayed on M13 phage. *ACS Chem. Biol.* 7, 1482–1487. doi: 10.1021/cb300187t

Oh, D., Dang, X., Yi, H., Allen, M. A., Xu, K., Lee, Y. J., et al. (2012). Graphene sheets stabilized on genetically engineered M13 viral templates as conducting frameworks for hybrid energy-storage materials. *Small* 8, 1006–1011. doi: 10.1002/smll.201102036

Olsen, E. V., Sorokulova, I. B., Petrenko, V. A., Chen, I. H., Barbaree, J. M., and Vodyanoy, V. J. (2006). Affinity-selected filamentous bacteriophage as a probe for acoustic wave biodetectors of *Salmonella typhimurium*. *Biosens. Bioelectron.* 21, 1434–1442. doi: 10.1016/j.bios.2005.06.004

Pacheco-Gomez, R., Kraemer, J., Stokoe, S., England, H. J., Penn, C. W., Stanley, E., et al. (2012). Detection of pathogenic bacteria using a homogeneous immunoassay based on shear alignment of virus particles and linear dichroism. *Anal. Chem.* 84, 91–97. doi: 10.1021/ac201544h

Pande, J., Szewczyk, M. M., and Grover, A. K. (2010). Phage display: concept, innovations, applications and future. *Biotechnol. Adv.* 28, 849–858. doi: 10.1016/j.biotechadv.2010.07.004

Parmley, S. F., and Smith, G. P. (1988). Antibody-selectable filamentous fd phage vectors: affinity purification of target genes. *Gene* 73, 305–318. doi: 10.1016/0378-1119(88)90495-7

Petrenko, V. A., and Makowski, L. (1993). "Potential applications of phage display to bioremediation," in *Bioremediation of Chlorinated and Polycyclic Aromatic Hydrocarbon Compounds*, eds R. E. Hinchee, L. Semprini, and S. K. Ong (Columbus, OH: Taylor and Francis Group), 266–280.

Petrenko, V. A., Smith, G. P., Gong, X., and Quinn, T. (1996). A library of organic landscapes on filamentous phage. *Protein Eng.* 9, 797–801. doi: 10.1093/protein/9.9.797

Pina, S., Creus, A., Gonzaalez, N., Gironees, R., Felip, M., and Sommaruga, R. (1998). Abundance, morphology and distribution of planktonic virus-like particles in two high-mountain lakes. *J. Plankton Res.* 20:8. doi: 10.1093/plankt/20.12.2413

Plotkin, S. A. (2010). Correlates of protection induced by vaccination. *Clin. Vacc. Immunol.* 17, 1055–1065. doi: 10.1128/CVI.00131-110

Poul, M. A., and Marks, J. D. (1999). Targeted gene delivery to mammalian cells by filamentous bacteriophage. *J. Mol. Biol.* 288, 203–211. doi: 10.1006/jmbi.1999.2678

Pratt, D., Tzagoloff, H., and Beaudoin, J. (1969). Conditional lethal mutants of the small filamentous coliphage M13. II. Two genes for coat proteins. *Virology* 39, 42–53. doi: 10.1016/0042-6822(69)90346-8

Prezzi, C., Nuzzo, M., Meola, A., Delmastro, P., Galfre, G., Cortese, R., et al. (1996). Selection of antigenic and immunogenic mimics of hepatitis C virus using sera from patients. *J. Immunol.* 156, 4504–4513.

Puntoriero, G., Meola, A., Lahm, A., Zucchelli, S., Ercole, B. B., Tafi, R., et al. (1998). Towards a solution for hepatitis C virus hypervariability: mimotopes of the hypervariable region 1 can induce antibodies cross-reacting with a large number of viral variants. *EMBO J.* 17, 3521–3533. doi: 10.1093/emboj/17.13.3521

Rakonjac, J. (2012). "Filamentous bacteriophages: biology and applications," in *eLS (the Encyclopaedia of Life Sciences)*, Chichester: John Wiley & Sons, Ltd. doi: 10.1002/9780470015902.a0000777

Rakonjac, J., Bennett, N. J., Spagnuolo, J., Gagic, D., and Russel, M. (2011). Filamentous bacteriophage: biology, phage display and nanotechnology applications. *Curr. Issues Mol. Biol.* 13, 51–76.

Rakover, I. S., Zabavnik, N., Kopel, R., Paz-Rozner, M., and Solomon, B. (2010). Antigen-specific therapy of EAE via intranasal delivery of filamentous phage

displaying a myelin immunodominant epitope. *J. Neuroimmunol.* 225, 68–76. doi: 10.1016/j.jneuroim.2010.04.014

Rao, K. V., He, Y. X., and Kalyanasundaram, R. (2003). Expression of a 28-kilodalton glutathione S-transferase antigen of *Schistosoma mansoni* on the surface of filamentous phages and evaluation of its vaccine potential. *Clin. Diagn. Lab. Immunol.* 10, 536–541. doi: 10.1128/cdli.10.4.536-541.2003

Raymond-Bouchard, I., Carroll, C. S., Nesbitt, J. R., Henry, K. A., Pinto, L. J., Moinzadeh, M., et al. (2012). Structural requirements for the activity of the MirB ferrisiderophore transporter of *Aspergillus fumigatus*. *Eukaryot. Cell* 11, 1333–1344. doi: 10.1128/EC.00159-112

Roehnisch, T., Then, C., Nagel, W., Blumenthal, C., Braciak, T., Donzeau, M., et al. (2013). Chemically linked phage idiotype vaccination in the murine B cell lymphoma 1 model. *J. Transl. Med.* 11:267. doi: 10.1186/1479-5876-11-267

Roehnisch, T., Then, C., Nagel, W., Blumenthal, C., Braciak, T., Donzeau, M., et al. (2014). Phage idiotype vaccination: first phase I/II clinical trial in patients with multiple myeloma. *J. Transl. Med.* 12, 119. doi: 10.1186/1479-5876-12-119

Romanov, V. I., Durand, D. B., and Petrenko, V. A. (2001). Phage display selection of peptides that affect prostate carcinoma cells attachment and invasion. *Prostate* 47, 239–251. doi: 10.1002/pros.1068

Rondot, S., Koch, J., Breitling, F., and Dubel, S. (2001). A helper phage to improve single-chain antibody presentation in phage display. *Nat. Biotechnol.* 19, 75–78. doi: 10.1038/83567

Rosario, K., Nilsson, C., Lim, Y. W., Ruan, Y., and Breitbart, M. (2009). Metagenomic analysis of viruses in reclaimed water. *Environ. Microbiol.* 11, 2806–2820. doi: 10.1111/j.1462-2920.2009.01964.x

Roux, S., Enault, F., Robin, A., Ravet, V., Personnic, S., Theil, S., et al. (2012). Assessing the diversity and specificity of two freshwater viral communities through metagenomics. *PLoS ONE* 7:e33641. doi: 10.1371/journal.pone.0033641

Rubinchik, E., and Chow, A. W. (2000). Recombinant expression and neutralizing activity of an MHC class II binding epitope of toxic shock syndrome toxin-1. *Vaccine* 18, 2312–2320. doi: 10.1016/S0264-410X(99)00554-X

Rudolf, M. P., Vogel, M., Kricek, F., Ruf, C., Zurcher, A. W., Reuschel, R., et al. (1998). Epitope-specific antibody response to IgE by mimotope immunization. *J. Immunol.* 160, 3315–3321.

Salivar, W. O., Tzagoloff, H., and Pratt, D. (1964). Some physical-chemical and biological properties of the rod-shaped coliphage M13. *Virology* 24, 359–371. doi: 10.1016/0042-6822(64)90173-4

Samoylov, A., Cox, N., Cochran, A., Wolfe, K., Donovan, C., Kutzler, M., et al. (2012). Generation and characterization of phage-GnRH chemical conjugates for potential use in cat and dog immunocontraception. *Reprod. Domest. Anim.* 47(Suppl. 6), 406–411. doi: 10.1111/rda.12061

Samoylova, T. I., Cochran, A. M., Samoylov, A. M., Schemera, B., Breiteneicher, A. H., Ditchkoff, S. S., et al. (2012a). Phage display allows identification of zona pellucida-binding peptides with species-specific properties: novel approach for development of contraceptive vaccines for wildlife. *J. Biotechnol.* 162, 311–318. doi: 10.1016/j.jbiotec.2012.10.006

Samoylova, T. I., Norris, M. D., Samoylov, A. M., Cochran, A. M., Wolfe, K. G., Petrenko, V. A., et al. (2012b). Infective and inactivated filamentous phage as carriers for immunogenic peptides. *J. Virol. Methods* 183, 63–68. doi: 10.1016/j.jviromet.2012.03.032

Sartorius, R., Bettua, C., D'apice, L., Caivano, A., Trovato, M., Russo, D., et al. (2011). Vaccination with filamentous bacteriophages targeting DEC-205 induces DC maturation and potent anti-tumor T-cell responses in the absence of adjuvants. *Eur. J. Immunol.* 41, 2573–2584. doi: 10.1002/eji.201141526

Sartorius, R., Pisu, P., D'apice, L., Pizzella, L., Romano, C., Cortese, G., et al. (2008). The use of filamentous bacteriophage fd to deliver MAGE-A10 or MAGE-A3 HLA-A2-restricted peptides and to induce strong antitumor CTL responses. *J. Immunol.* 180, 3719–3728. doi: 10.4049/jimmunol.180.6.3719

Scala, G., Chen, X., Liu, W., Telles, J. N., Cohen, O. J., Vaccarezza, M., et al. (1999). Selection of HIV-specific immunogenic epitopes by screening random peptide libraries with HIV-1-positive sera. *J. Immunol.* 162, 6155–6161.

Schmelcher, M., and Loessner, M. J. (2014). Application of bacteriophages for detection of foodborne pathogens. *Bacteriophage* 4:e28137. doi: 10.4161/bact.28137

Scott, J. K., and Smith, G. P. (1990). Searching for peptide ligands with an epitope library. *Science* 249, 386–390. doi: 10.1126/science.1696028

Shi, L., Wheeler, J. C., Sweet, R. W., Lu, J., Luo, J., Tornetta, M., et al. (2010). *De novo* selection of high-affinity antibodies from synthetic Fab libraries displayed on phage as pIX fusion proteins. *J. Mol. Biol.* 397, 385–396. doi: 10.1016/j.jmb.2010.01.034

Sidhu, S. S., Weiss, G. A., and Wells, J. A. (2000). High copy display of large proteins on phage for functional selections. *J. Mol. Biol.* 296, 487–495. doi: 10.1006/jmbi.1999.3465

Smith, G. P. (1985). Filamentous fusion phage: novel expression vectors that display cloned antigens on the virion surface. *Science* 228, 1315–1317. doi: 10.1126/science.4001944

Smith, G. P., and Fernandez, A. M. (2004). Effect of DNA copy number on genetic stability of phage-displayed peptides. *Biotechniques* 36, 610–614.

Smith, G. P., and Gingrich, T. R. (2005). Hydroxyapatite chromatography of phage-display virions. *BioTechniques* 39, 879–884. doi: 10.2144/000112032

Smith, G. P., and Petrenko, V. A. (1997). Phage display. *Chem. Rev.* 97, 391–410. doi: 10.1021/cr960065d

Smith, G. P., and Scott, J. K. (1993). Libraries of peptides and proteins displayed on filamentous phage. *Methods Enzymol.* 217, 228–257. doi: 10.1016/0076-6879(93)17065-D

Solomon, B. (2005). Generation of anti-β-amyloid antibodies via phage display technology towards Alzheimer's disease vaccination. *Vaccine* 23, 2327–2330. doi: 10.1016/j.vaccine.2005.01.034

Solomon, B. (2008). Filamentous bacteriophage as a novel therapeutic tool for Alzheimer's disease treatment. *J. Alzheimers Dis.* 15, 193–198.

Su, Q. P., Wen, D. Z., Yang, Q., Zhang, Y. H., Liu, C., and Wang, L. (2007). Comparison of phage pVIII and KLH as vector in inducing the production of cytokines in C57BL/6J mice. *Vaccine* 25, 970–975. doi: 10.1016/j.vaccine.2006.08.045

Sulakvelidze, A., Alavidze, Z., and Morris, J. G. Jr. (2001). Bacteriophage therapy. *Antimicrob. Agents Chemother.* 45, 649–659. doi: 10.1128/AAC.45.3.649-659.2001

Suttle, C. A. (2005). Viruses in the sea. *Nature* 437, 356–361. doi: 10.1038/nature04160

Tanaka, K., Nishimura, M., Yamaguchi, Y., Hashiguchi, S., Takiguchi, S., Yamaguchi, M., et al. (2011). A mimotope peptide of Aβ42 fibril-specific antibodies with Aβ42 fibrillation inhibitory activity induces anti-Aβ42 conformer antibody response by a displayed form on an M13 phage in mice. *J. Neuroimmunol.* 236, 27–38. doi: 10.1016/j.jneuroim.2011.04.010

Terry, T. D., Malik, P., and Perham, R. N. (1997). Accessibility of peptides displayed on filamentous bacteriophage virions: susceptibility to proteinases. *Biol. Chem.* 378, 523–530. doi: 10.1515/bchm.1997.378.6.523

Tornetta, M., Baker, S., Whitaker, B., Lu, J., Chen, Q., Pisors, E., et al. (2010). Antibody Fab display and selection through fusion to the pIX coat protein of filamentous phage. *J. Immunol. Methods* 360, 39–46. doi: 10.1016/j.jim.2010.06.001

Twort, F. W. (1915). An investigation on the nature of ultra-microscopic viruses. *Lancet* 186:3. doi: 10.1016/S0140-6736(01)20383-3

Ulivieri, C., Citro, A., Ivaldi, F., Mascolo, D., Ghittoni, R., Fanigliulo, D., et al. (2008). Antigenic properties of HCMV peptides displayed by filamentous bacteriophages vs. synthetic peptides. *Immunol. Lett.* 119, 62–70. doi: 10.1016/j.imlet.2008.04.004

Vaks, L., and Benhar, I. (2011). In vivo characteristics of targeted drug-carrying filamentous bacteriophage nanomedicines. *J. Nanobiotechnol.* 9, 58. doi: 10.1186/1477-3155-9-58

Van Gerven, N., De Greve, H., and Hernalsteens, J. P. (2008). Presentation of the functional receptor-binding domain of the bacterial adhesin F17a-G on bacteriophage M13. *Antonie Van Leeuwenhoek* 93, 219–226. doi: 10.1007/s10482-007-9195-x

van Houten, N. E., Henry, K. A., Smith, G. P., and Scott, J. K. (2010). Engineering filamentous phage carriers to improve focusing of antibody responses against peptides. *Vaccine* 28, 2174–2185. doi: 10.1016/j.vaccine.2009.12.059

van Houten, N. E., Zwick, M. B., Menendez, A., and Scott, J. K. (2006). Filamentous phage as an immunogenic carrier to elicit focused antibody responses against a synthetic peptide. *Vaccine* 24, 4188–4200. doi: 10.1016/j.vaccine.2006.01.001

Van Regenmortel, M. H. (2012). Basic research in HIV vaccinology is hampered by reductionist thinking. *Front. Immunol.* 3:194. doi: 10.3389/fimmu.2012.00194

Waldor, M. K., and Mekalanos, J. J. (1996). Lysogenic conversion by a filamentous phage encoding cholera toxin. *Science* 272, 1910–1914. doi: 10.1126/science.272.5270.1910

Wan, Y., Wu, Y., Bian, J., Wang, X. Z., Zhou, W., Jia, Z. C., et al. (2001). Induction of hepatitis B virus-specific cytotoxic T lymphocytes response *in vivo* by filamentous phage display vaccine. *Vaccine* 19, 2918–2923. doi: 10.1016/S0264-410X(00)00561-2

Wan, Y., Wu, Y., Zhou, J., Zou, L., Liang, Y., Zhao, J., et al. (2005). Cross-presentation of phage particle antigen in MHC class II and endoplasmic reticulum marker-positive compartments. *Eur. J. Immunol.* 35, 2041–2050. doi: 10.1002/eji.200425322

Wang, F., Liu, P., Sun, L., Li, C., Petrenko, V. A., and Liu, A. (2014a). Bio-mimetic nanostructure self-assembled from Au@Ag heterogeneous nanorods and phage fusion proteins for targeted tumor optical detection and photothermal therapy. *Sci. Rep.* 4:6808. doi: 10.1038/srep06808

Wang, T., Hartner, W. C., Gillespie, J. W., Praveen, K. P., Yang, S., Mei, L. A., et al. (2014b). Enhanced tumor delivery and antitumor activity in vivo of liposomal doxorubicin modified with MCF-7-specific phage fusion protein. *Nanomedicine* 10, 421–430. doi: 10.1016/j.nano.2013.08.009

Wang, T., Yang, S., Mei, L. A., Parmar, C. K., Gillespie, J. W., Praveen, K. P., et al. (2014c). Paclitaxel-loaded PEG-PE-based micellar nanopreparations targeted with tumor specific landscape phage fusion protein enhance apoptosis and efficiently reduce tumors. *Mol. Cancer Ther.* doi: 10.1158/1535-7163.MCT-14-0052

Wang, Y., Su, Q., Dong, S., Shi, H., Gao, X., and Wang, L. (2014d). Hybrid phage displaying SLAQVKYTSASSI induces protection against *Candida albicans* challenge in BALB/c mice. *Hum. Vaccin. Immunother.* 10, 1057–1063. doi: 10.4161/hv.27714

Wang, G., Sun, M., Fang, J., Yang, Q., Tong, H., and Wang, L. (2006). Protective immune responses against systemic candidiasis mediated by phage-displayed specific epitope of *Candida albicans* heat shock protein 90 in C57BL/6J mice. *Vaccine* 24, 6065–6073. doi: 10.1016/j.vaccine.2006.05.022

Wang, T., D'souza, G. G., Bedi, D., Fagbohun, O. A., Potturi, L. P., Papahadjopoulos-Sternberg, B., et al. (2010a). Enhanced binding and killing of target tumor cells by drug-loaded liposomes modified with tumor-specific phage fusion coat protein. *Nanomedicine* 5, 563–574. doi: 10.2217/nnm.10.30

Wang, T., Petrenko, V. A., and Torchilin, V. P. (2010b). Paclitaxel-loaded polymeric micelles modified with MCF-7 cell-specific phage protein: enhanced binding to target cancer cells and increased cytotoxicity. *Mol. Pharm.* 7, 1007–1014. doi: 10.1021/mp1001125

Wang, T., Yang, S., Petrenko, V. A., and Torchilin, V. P. (2010c). Cytoplasmic delivery of liposomes into MCF-7 breast cancer cells mediated by cell-specific phage fusion coat protein. *Mol. Pharm.* 7, 1149–1158. doi: 10.1021/mp1000229

Webb, J. S., Lau, M., and Kjelleberg, S. (2004). Bacteriophage and phenotypic variation in *Pseudomonas aeruginosa* biofilm development. *J. Bacteriol.* 186, 8066–8073. doi: 10.1128/JB.186.23.8066-8073.2004

Welsh, L. C., Symmons, M. F., Nave, C., Perham, R. N., Marseglia, E. A., and Marvin, D. A. (1996). Evidence for tilted smectic liquid crystalline packing of fd inovirus from X-ray fiber diffraction. *Macromolecules* 29, 8. doi: 10.1021/ma9605614

Wichman, H. A., and Brown, C. J. (2010). Experimental evolution of viruses: Microviridae as a model system. *Philos. Trans. R. Soc. Lond. B Biol. Sci.* 365, 2495–2501. doi: 10.1098/rstb.2010.0053

Willis, A. E., Perham, R. N., and Wraith, D. (1993). Immunological properties of foreign peptides in multiple display on a filamentous bacteriophage. *Gene* 128, 79–83. doi: 10.1016/0378-1119(93)90156-W

Woolford, J. L. Jr., Steinman, H. M., and Webster, R. E. (1977). Adsorption protein of bacteriophage fl: solubilization in deoxycholate and localization in the fl virion. *Biochemistry* 16, 2694–2700. doi: 10.1021/bi00631a017

Wu, L., Huang, T., Yang, L., Pan, J., Zhu, S., and Yan, X. (2011). Sensitive and selective bacterial detection using tetracysteine-tagged phages in conjunction with biarsenical dye. *Angew. Chem. Int. Ed. Engl.* 50, 5873–5877. doi: 10.1002/anie.201100334

Wu, Y., Wan, Y., Bian, J., Zhao, J., Jia, Z., Zhou, L., et al. (2002). Phage display particles expressing tumor-specific antigens induce preventive and therapeutic anti-tumor immunity in murine p815 model. *Int. J. Cancer* 98, 748–753. doi: 10.1002/ijc.10260

Xia, Y. J., Wen, W. H., Huang, W. Q., and Huang, B. C. (2005). Development of a phage displayed disulfide-stabilized Fv fragment vaccine against *Vibrio anguillarum*. *Vaccine* 23, 3174–3180. doi: 10.1016/j.vaccine.2004.12.018

Xue, H., Xu, Y., Boucher, Y., and Polz, M. F. (2012). High frequency of a novel filamentous phage, VCYϕ, within an environmental *Vibrio cholerae* population. *Appl. Environ. Microbiol.* 78, 28–33. doi: 10.1128/AEM.06297-1

Yacoby, I., Shamis, M., Bar, H., Shabat, D., and Benhar, I. (2006). Targeting antibacterial agents by using drug-carrying filamentous bacteriophages. *Antimicrob. Agents Chemother.* 50, 2087–2097. doi: 10.1128/AAC.00169-6

Yamada, T. (2013). Filamentous phages of *Ralstonia solanacearum*: double-edged swords for pathogenic bacteria. *Front. Microbiol.* 4:325. doi: 10.3389/fmicb.2013.00325

Yang, Q., Wang, L., Lu, D. N., Gao, R. J., Song, J. N., Hua, P. Y., et al. (2005a). Prophylactic vaccination with phage-displayed epitope of *C. albicans* elicits protective immune responses against systemic candidiasis in C57BL/6 mice. *Vaccine* 23, 4088–4096. doi: 10.1016/j.vaccine.2004.07.005

Yang, W. J., Lai, J. F., Peng, K. C., Chiang, H. J., Weng, C. N., and Shiuan, D. (2005b). Epitope mapping of *Mycoplasma hyopneumoniae* using phage displayed peptide libraries and the immune responses of the selected phagotopes. *J. Immunol. Methods* 304, 15–29. doi: 10.1016/j.jim.2005.05.009

Yi, H., Ghosh, D., Ham, M. H., Qi, J., Barone, P. W., Strano, M. S., et al. (2012). M13 phage-functionalized single-walled carbon nanotubes as nanoprobes for second near-infrared window fluorescence imaging of targeted tumors. *Nano Lett.* 12, 1176–1183. doi: 10.1021/nl2031663

Yip, Y. L., Smith, G., and Ward, R. L. (2001). Comparison of phage pIII, pVIII and GST as carrier proteins for peptide immunisation in Balb/c mice. *Immunol. Lett.* 79, 197–202. doi: 10.1016/S0165-2478(01)00281-4

Yoo, P. J., Nam, K. T., Qi, J., Lee, S. K., Park, J., Belcher, A. M., et al. (2006). Spontaneous assembly of viruses on multilayered polymer surfaces. *Nat. Mater.* 5, 234–240. doi: 10.1038/nmat1596

Yu, M. W., Scott, J. K., Fournier, A., and Talbot, P. J. (2000). Characterization of murine coronavirus neutralization epitopes with phage-displayed peptides. *Virology* 271, 182–196. doi: 10.1006/viro.2000.0310

Zakharova, M. Y., Kozyr, A. V., Ignatova, A. N., Vinnikov, I. A., Shemyakin, I. G., and Kolesnikov, A. V. (2005). Purification of filamentous bacteriophage for phage display using size-exclusion chromatography. *Biotechniques* 38:194. doi: 10.2144/05382BM04

Zhong, G., Smith, G. P., Berry, J., and Brunham, R. C. (1994). Conformational mimicry of a chlamydial neutralization epitope on filamentous phage. *J. Biol. Chem.* 269, 24183–24188.

Zinder, N. D., Valentine, R. C., Roger, M., and Stoeckenius, W. (1963). f1, a rod-shaped male-specific bacteriophage that contains DNA. *Virology* 20, 638–640. doi: 10.1016/0042-6822(63)90290-3

Zou, J., Dickerson, M. T., Owen, N. K., Landon, L. A., and Deutscher, S. L. (2004). Biodistribution of filamentous phage peptide libraries in mice. *Mol. Biol. Rep.* 31, 121–129. doi: 10.1023/B:MOLE.0000031459.14448.af

**Conflict of Interest Statement:** The authors declare that the research was conducted in the absence of any commercial or financial relationships that could be construed as a potential conflict of interest.

frontiers in Microbiology

REVIEW
published: 07 April 2016
doi: 10.3389/fmicb.2016.00429

# Exploring the Secretomes of Microbes and Microbial Communities Using Filamentous Phage Display

*Dragana Gagic[1,2]*, Milica Ciric[1,2], Wesley X. Wen[1], Filomena Ng[2] and Jasna Rakonjac[1]*

*[1] Institute of Fundamental Sciences, Massey University, Palmerston North, New Zealand, [2] Animal Science, Grasslands Research Centre, AgResearch Ltd, Palmerston North, New Zealand*

Microbial surface and secreted proteins (the secretome) contain a large number of proteins that interact with other microbes, host and/or environment. These proteins are exported by the coordinated activities of the protein secretion machinery present in the cell. A group of bacteriophage, called filamentous phage, have the ability to hijack bacterial protein secretion machinery in order to amplify and assemble *via* a secretion-like process. This ability has been harnessed in the use of filamentous phage of *Escherichia coli* in biotechnology applications, including screening large libraries of variants for binding to "bait" of interest, from tissues *in vivo* to pure proteins or even inorganic substrates. In this review we discuss the roles of secretome proteins in pathogenic and non-pathogenic bacteria and corresponding secretion pathways. We describe the basics of phage display technology and its variants applied to discovery of bacterial proteins that are implicated in colonization of host tissues and pathogenesis, as well as vaccine candidates through filamentous phage display library screening. Secretome selection aided by next-generation sequence analysis was successfully applied for selective display of the secretome at a microbial community scale, the latter revealing the richness of secretome functions of interest and surprising versatility in filamentous phage display of secretome proteins from large number of Gram-negative as well as Gram-positive bacteria and archaea.

**Keywords: phage display, secretome, adhesins, metagenomics, next generation sequencing, bacteriophage**

OPEN ACCESS

***Edited by:***
*Gilbert Greub,*
*University of Lausanne, Switzerland*

***Reviewed by:***
*Bradley D. Jones,*
*The University of Iowa, USA*
*Nicole Jane Moreland,*
*University of Auckland, New Zealand*

****Correspondence:***
*Dragana Gagic*
*d.gagic@massey.ac.nz*

***Specialty section:***
*This article was submitted to Virology, a section of the journal Frontiers in Microbiology*

***Received:*** *22 September 2015*
***Accepted:*** *17 March 2016*
***Published:*** *07 April 2016*

***Citation:***
*Gagic D, Ciric M, Wen WX, Ng F and Rakonjac J (2016) Exploring the Secretomes of Microbes and Microbial Communities Using Filamentous Phage Display. Front. Microbiol. 7:429. doi: 10.3389/fmicb.2016.00429*

## INTRODUCTION

Microbial secretome is a portion of the proteome comprising proteins that are targeted to the envelope of microbial cells, or are secreted into extracellular milieu. Microbial surface proteins mediate adhesion to other microbes or environmental surfaces, to facilitate colonization of an environment. They include secreted enzymes involved in breaking up various polymeric molecules to produce mono- or oligomeric foodstuffs that microbes can absorb and use as carbon and nitrogen sources for growth. Secretome harbors dominant targets of the host immune responses and are therefore of interest for vaccine development. In commensal and pathogenic bacteria these proteins are also involved in manipulating the innate and adaptive immune system's signaling pathways. Although many surface proteins that mediate these functions have been identified in individual cultivated bacteria through genetic screens, identities of proteins that bind to specific targets of interest from archaea or from yet uncultivated microbes in complex microbial

communities are largely unknown. Partial reason for this is that, with respect to primary sequence conservation, the secretome proteins are most variable group in microbial proteomes; it is rarely possible to predict the binding specificity of annotated secretome proteins using bioinformatics. In the absence of cultivation or genetic manipulation methods for a microbe, affinity screening of recombinant libraries is a suitable approach to identify proteins implicated in interactions of microbes with their hosts or environment. Phage display is a powerful combinatorial technology for affinity-selection of rare variants in vast libraries; due to the physical link between coding sequence inside the virion and protein displayed on the surface of the virion, large number of individual recombinant clones (up to $10^{12}$ per mL) can be affinity screened against complex baits of interest, such as tissues or extracellular matrix (ECM). Ff (f1, fd, or M13) phage whose virion proteins belong to the secretome and the virion itself is secreted out of *Escherichia coli*, is ideally suited for capture, correct folding and display of the secretome proteins. This article reviews the secretome and phage display technology applications in discovery of eubacterial and archaeal secretome proteins and emerging applications in functional metagenomics of the microbial communities' secretomes.

## EUBACTERIAL SECRETOME AND MECHANISMS OF SECRETION

The term 'secretome', coined by Tjalsma et al. (2000), was originally proposed to refer to both the secreted proteins and components of the protein secretion machineries in bacteria. Today, the secretome is broadly described as a subset of bacterial proteome, containing the extracellular proteome (exoproteome), released to the extracellular milieu and the surface-associated proteome, either exposed to the bacterial surface or intrinsic to the external side of plasma membrane and the cell wall, but excluding integral membrane proteins and proteins intrinsic to the internal side of the plasma membrane (Desvaux et al., 2009; Zhou et al., 2010).

Secretome proteins (e.g., receptors, transporters, adhesins, complex cell structures, secreted enzymes, toxins, and virulence factors) allow bacteria to interact with, and adapt to their environment. Bacterial secretory proteins are known to be involved in processes such as: provision of nutrients through recognition; binding, degradation, and uptake of complex extracellular molecules; communication between bacterial cells; detoxification of the environment; attachment to host cells and signal transduction; while in pathogenic bacteria they also play critical roles in virulence and immunogenicity (Walsh, 2000; Antelmann et al., 2001; Tjalsma et al., 2004; Wooldridge, 2009; Dalbey and Kuhn, 2012). Secretome proteins have been reported to occupy 10–30% of the total coding capacity of bacterial genomes (Wallin and Heijne, 1998; Kudva et al., 2013).

Secretome includes multi-protein surface appendages such as pili and flagellae, which have pivotal roles in bacterial attachment, horizontal gene transfer, and motility (Van Gerven et al., 2011). The pathways for membrane targeting are also "hijacked" by the filamentous phage or inoviruses, whose virion and assembly proteins belong to the secretome and which are secreted from bacteria without killing the host (Russel and Model, 2006; Rakonjac et al., 2011; Mai-Prochnow et al., 2015).

### Secretion Pathways of Bacteria

The cell envelope of Gram-positive bacteria consists of a single, cytoplasmic membrane and a cell wall, comprised of a thick peptidoglycan layer cross-linked with different molecules, such as capsular polysaccharides, cell wall teichoic acids, and proteins (Freudl, 2013). In contrast, Gram-negative bacteria are enveloped by inner (cytoplasmic) and outer membranes. The presence of two membranes defines an additional subcellular compartment (the periplasmic space), containing a thin meshwork of peptidoglycans. Some Gram-positive bacteria also have a distinctive thin granular layer (inner wall zone) between the membrane and the mature cell wall, equivalent to the periplasmic space in Gram-negative bacteria (Zuber et al., 2006).

In order to be anchored to the cell surface or released into the extracellular milieu, secretome proteins must be translocated across one or more biological membranes (Desvaux et al., 2006). Transport of proteins into or across biological membranes (translocation), catalyzed by membrane-bound proteinaceous transport machineries, is a universal event in the protein secretion mechanism, and it can occur several times during the course of secretion (Desvaux et al., 2009). Once a secreted protein is translocated across the outermost membrane, it can remain anchored (covalently or non-covalently associated with cell-wall components in Gram-positive bacteria or outer membrane components in Gram-negative bacteria), assemble into macromolecular structures on the cell surface (flagella, pili), be injected into host cells, or released to the extracellular milieu.

A remarkable array of systems for export of proteins have been described in Gram-positive and Gram-negative bacteria. Descriptive names are used in the nomenclature of systems involved in protein translocation across cytoplasmic membranes of both Gram-negative and Gram-positive bacteria, while an alphanumerical system has been adopted for naming protein secretion systems of Gram-negative bacteria (Desvaux et al., 2009).

Systems that are universally involved in protein translocation across the cytoplasmic membrane, and encoded in both Gram-positive and Gram-negative bacteria are: the conserved general secretion (Sec) system, YidC insertase, the twin-arginine translocation (Tat) system and hole-forming pathway *via* holins (Desvaux et al., 2009).

The Sec system is a major secretory pathway for protein insertion into the inner (cytoplasmic) membrane, and is conserved in all eubacteria. It is also ubiquitous in archaea, and the membranes of eukaryotic endoplasmic reticulum and chloroplasts (Szabo and Pohlschroder, 2012). This system also plays a key role in further transport of some proteins into the periplasmic space, outer membrane (e.g., lipoproteins and beta barrel proteins), or their assembly into the surface-associated structures (e.g., pili subunits). Furthermore, some of the components of the specialized secretion systems in Gram-negatives and their substrates (proteins transported *via* these

secretion systems) are initially transported across the inner membrane by the SecYEG translocon (Beckwith, 2013; Kudva et al., 2013).

In bacteria, the Sec system is composed of the SecYEG translocon and three major accessory systems that target the secretome proteins to the translocon: SecB/A, SRP/FtsY, and YidC. SecYEG is an evolutionarily conserved heterotrimeric protein complex, and its SecY subunit forms an hourglass-shaped aqueous protein transport channel embedded in the inner membrane (Dalbey and Kuhn, 2012; Kudva et al., 2013). The translocon transiently interacts with different proteins during the transport process (e.g., SecA, FtsY, SecDF). SecA, a post-translational pathway motor protein accepts the substrate protein delivered by the cytosolic targeting factor SecB, and pushes it through the translocon in a stepwise and ATP-dependent manner (Lycklama et al., 2012). FtsY, the SRP-receptor, occupies the ribosome binding site (RBS) of SecY until its displacement by the translating ribosome during co-translational targeting (Kudva et al., 2013). The membrane-integrated SecDF chaperone uses proton-motive force to power ATP-independent protein translocation through the SecYEG channel (Tsukazaki et al., 2011).

In addition to universal secretion systems, Gram-positive bacteria possess Wss (WXG100 secretion systems), accessory Sec systems (SecA2-only and SecA2/SecY2 export pathways), flagella export apparatus (FEA), the fimbrilin-protein exporter (FPE), ABC protein exporter and Sec-dependent sortases. In Gram-positive bacteria, secreted proteins have several different fates. They are transported across the cytoplasmic membrane and then secreted into the extracellular milieu by SecYEG, Tat, holin, or Wss, in addition to being attached (covalently or non-covalently) to the cell wall using the sortase or assembled into the cell surface appendages *via* Sec pathway (e.g., cellulosomes or pili), *via* FPE (e.g., competence pseudo-pili), or *via* FEA (e.g., flagella).

Due to the added complexity of their cell envelope, at least two additional systems for targeting proteins to the outer membrane and eight additional systems for secretion of proteins outside of the cell have been described in Gram-negative bacteria. After Sec- or Tat- dependent translocation across the inner membrane, outer membrane-specific lipoproteins and unfolded β-barrel proteins are targeted to the outer membrane *via* the Lol pathway and β-barrel assembly machinery (BAM) pathway, respectively (Dalbey and Kuhn, 2012).

Secreted proteins targeted to the extracellular milieu, or to another cell, can be exported out of the cell directly, or by a two-step secretion process *via* type 1–6 secretion systems (T1SS–T6SS). In addition, the chaperone-usher system (CU or T7SS), the extracellular nucleation-precipitation mechanism (ENP or T8SS) system, as well as type IV pilus biogenesis (T4PBS) and tight-adherence (Tad) piliation systems are dedicated to exporting different types of pili subunits across the outer membrane (Chagnot et al., 2013).

The direct (Sec pathway-independent) secretion in Gram-negatives exports proteins through a contiguous secretion machinery spanning two membranes and the periplasm (T1SS, T3SS, T4SS, and T6SS systems). The two-step secretion process involves protein export to the periplasm by the Sec or, less frequently the Tat pathway, followed by export across outer membrane *via* T2SS, T5SS, T7SS, or T8SS systems. T1SS and T5SS are relatively simple systems involving few proteins, while T2SS, T3SS, T4SS, and T6SS are complex structures composed of large number of subunits, and spanning the entire bacterial cell envelope (Chagnot et al., 2013).

The filamentous phage assembly system follows a variant of the two-step secretion process, where all virion proteins are first inserted into the inner membrane, followed by the export-coupled assembly of the phage. The assembly is initiated by minor proteins pVII and pIX that interact with a specific phage genome sequence called the packaging signal, followed by rapid elongation by addition of major coat (pVIII) subunits (Rakonjac et al., 2011; Marvin et al., 2014). The virion proteins egress from the inner membrane to form a filament by attaching to double-helical DNA genome *via* few positively charged C-terminal residues that face the cytoplasm prior to assembly. The assembly process is catalyzed by phage-encoded inner membrane ATPase and requires ATP and proton motive force (Feng et al., 1997); the filament is released from the assembly site by two minor proteins, pIII and pVI (which themselves are integral membrane proteins) when the DNA is completely covered with pVIII (Rakonjac et al., 1999). The resulting filament has no phospholipids and has high temperature (70°C) and detergent (1% Sarkosyl) resistance (Crissman and Smith, 1984; Branston et al., 2013). Whereas over 70 filamentous phage of Gram-negative bacteria have been identified, only two were found in Gram-positives (Day, 2011).

## Secretion and Membrane Targeting Signals

The first stage in the secretome protein export is sorting and targeting of proteins to the cytoplasmic membrane, followed by membrane crossing and maturation/release of the translocated protein. The sorting process, through which proteins are directed to their specific subcellular compartments, is based on localization information contained in a short amino acid sequence that acts as a protein sorting signal ('zip code') governing protein traffic, transport, and localization in the cell (Blobel and Sabatini, 1971). Discrimination between secreted and cytoplasmic proteins is based on the presence of membrane-targeting sequences, such as signal sequences and transmembrane α-helices that are recognized by distinct secretory pathway-associated molecular chaperones, and are necessary for correctly targeting secreted proteins to the translocation pathway.

Most secreted proteins contain N-terminal signal sequences that are cleavable. The function and overall structure of the signal sequence, transmembrane alpha helix targeted to the SecYEG translocon, are conserved in all domains of life; however, these peptides lack primary sequence homology even within a species (Rusch and Kendall, 2007). Several types of signal sequences have been described: type I (classic) signal sequence, type II (lipoprotein) signal sequence, Tat signal sequence, type IV (pseudopilin-like) signal sequence and bacteriocin/pheromone signal sequence. Based on hydrophobicity and charge, most signal sequences have a conserved overall tripartite organization consisting of an hydrophobic core (h-domain),

flanked by hydrophilic positively charged N-terminal region (n-domain) and a polar C-terminal region (c-domain) with cleavage/retention sites (Rusch and Kendall, 2007; Driessen and Nouwen, 2008; Zhou et al., 2008). However, the type IV and bacteriocin/pheromone signal sequences do not precisely follow such a structural layout (Zhou et al., 2008).

Signal sequences are usually removed during or shortly after their translocation across the membrane by several types of membrane-associated signal peptidases (SPases), which also have a role in quality control and regulated turnover of exported proteins (Dalbey et al., 2012). In bacteria, precursor proteins that are translocated through the Sec and Tat-pathways apart from pre-proteins (Lüke et al., 2009) are proteolytically processed by a 'general' type I signal peptidase (SPaseI) (Lüke et al., 2009; Auclair et al., 2012). Processing of the lipoprotein signal sequences is performed by type II lipoprotein signal peptidase (SPaseII). The lipoproteins are transported across the inner membrane in a Sec-dependent manner (Okuda and Tokuda, 2011). The Tat-dependent export of lipoproteins has only been demonstrated in streptomycetes (Thompson et al., 2010; Dalbey and Kuhn, 2012). The prepilin signal peptidase (SPaseIV) is responsible for processing proteins containing type IV signal sequence, such as pilins and related pseudopilins, that have mainly Sec-dependent export across the inner membrane (Peabody et al., 2003; Arts et al., 2007; Francetic et al., 2007).

Among the Ff (f1, M13, or fd) filamentous phage virion proteins, major coat protein pVIII that forms body of the filament (**Figure 1**) has a type I signal sequence and is secreted by SecYEG translocons and, YidC (Samuelson et al., 2000); it is targeted to the inner membrane by a C-terminal transmembrane helix. The length of the mature pVIII protein (after signal sequence cleavage) is 50 amino acids. Once assembled into the viral particle, it is DNA-bound and helically arranged to form the shaft of the filament (**Figure 1**). The four minor proteins are all integral membrane proteins, however, only the largest, pIII (406 aa) has a type I signal sequence and its membrane targeting is SecYEG/SecAB-dependent (Chang et al., 1978). Minor protein pVI (112aa) has three predicted transmembrane helices, but no signal sequence. The remaining two minor proteins, pVII (33 aa) and pIX (32 aa) are very small and hydrophobic, each containing a transmembrane helix, but no signal sequences.

## Methods for Study of the Secretome

Mining bacterial secretomes is important for a range of applications, including identification of novel enzymes, understanding bacterial adhesion and their interactions with the environment, investigating pathogenic mechanisms, epitope mapping and identification of new vaccine candidates. Secretomes are traditionally studied *in vitro*, using biochemical and proteomics approaches, and *in silico*, using bioinformatic tools. Surface display screening methods and reporter fusion systems (Georgiou et al., 1997; Chen and Georgiou, 2002; Åvall-Jääskeläinen et al., 2003; Lee et al., 2003; Wernérus and Ståhl, 2004; Liu et al., 2013), as well as phage-display based systems (Rosander et al., 2002, 2011; Jacobsson et al., 2003; Bjerketorp et al., 2004), described in detail in section 3, have also been used for screening, identifying, and characterizing secretome proteins.

Secretomes are studied *in vitro* using high-resolution separation (2D gel electrophoresis and/or liquid chromatography) of secreted or extracted membrane proteins, coupled with mass spectrometric methods for the identification of peptides and proteins in the sample (Yang et al., 2012). Biochemical approaches for elucidating the secretome of a microorganism allow direct functional characterization of identified proteins; however, they are very tedious and limited only to cultivable bacteria. Furthermore, construction of a proteome map of surface-associated and membrane proteins can be hindered by technical limitations of protein extraction from the membranes. In the absence of experimental data, a secretome can be deduced from a completely sequenced genome *in silico*, using bioinformatic tools for the prediction of secretome proteins based on their specific conserved features.

Computational methods for secretome protein prediction are based on weight matrices, sequence alignment or machine learning algorithms, and can be roughly grouped into global tools for subcellular protein localization prediction, and specialized tools for the prediction of signal sequences (Goudenège et al., 2010; Caccia et al., 2013). More sophisticated machine learning algorithms, based on neural networks and decision trees, support vector machines, Bayesian networks, HMMs, or their combination, are now more prominently used for discriminating secreted and non-secreted proteins (Zhou et al., 2008; Choo et al., 2009). During the training phase, typical signal and non-signal peptides are presented to the algorithm, and a classification model is subsequently built. Tools for signal sequence prediction such as SignalP (Petersen et al., 2011), LipoP (Juncker et al., 2003), TMHMM (Krogh et al., 2001), PRED-LIPO (Bagos et al., 2008), PRED-TAT (Bagos et al., 2010), SecretomeP (Bendtsen et al., 2005), and tools for subcellular protein localization prediction, such as PSORTb (Yu et al., 2010) or TargetP (Emanuelsson et al., 2000) belong to this class.

In bacteria, classically secreted proteins can be predicted based on recognition of the tripartite organization of their N-terminal, cleavable signal sequences, and conserved amino acid residues at the −3 and −1 positions relative to the cleavage sites. In addition to these, the lipobox of type II signal sequences and the Tat motif in Tat signal sequences are highly amenable to identification by bioinformatic tools, while transmembrane α-helices can be identified based on their hydrophobicity (Rahman et al., 2008; Goudenège et al., 2010). Recognition of the SPaseIV cleavage motif is not sufficient for the accurate detection of type IV signal sequences, since these have no tripartite structure like other Sec-dependent substrates. It was demonstrated that the specificity of searches for type IV pilin-like proteins may be enhanced by including additional search requirements, such as the presence of 14 sequential uncharged amino acid residues immediately after the cleavage motif or presence of a single transmembrane helix within 50 amino acid residues of the N-terminus, since true pilins contain only one transmembrane helix, typically close to the cleavage motif (Imam et al., 2011).

Cleavable N-terminal signal peptides of secreted proteins are readily distinguishable from longer hydrophobic N-terminal transmembrane helices of transmembrane proteins. In contrast, their discrimination from uncleaved N-terminal signal anchors,

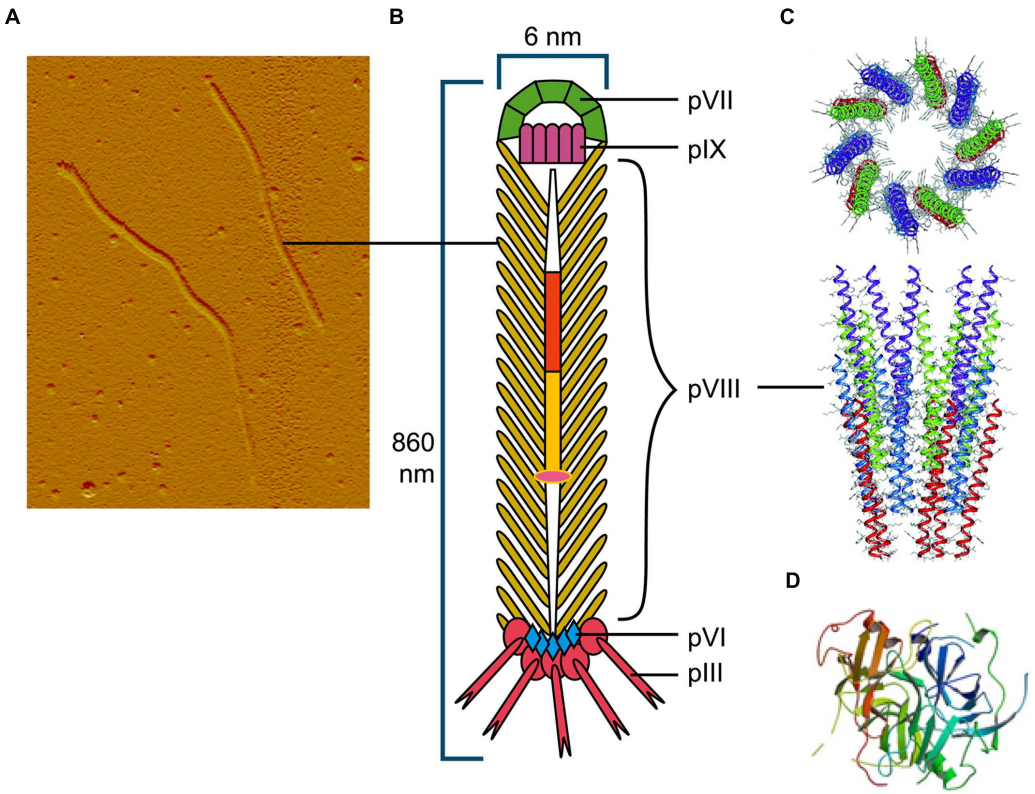


**FIGURE 1 | The Ff bacteriophage structure and virion proteins used most commonly in phage display. (A)** Ff virion visualized by atomic force microscope (M. Russel and P. Model, sample prepared by J. Rakonjac). **(B)** Schematic diagram of Ff bacteriophage. **(C)** Ribbon representations (top and side view) of the pVIII coat protein (RCSB PDB database accession number 2cOw; (Marvin et al., 2006) arranged around bacteriophage single stranded DNA (not shown). **(D)** Ribbon representation of N1 and N2 domains of pIII (RCSB PDB database accession number1g3p; Lubkowski et al., 1998).

which tether some of these Sec-exported proteins to the membrane, is often problematic (Natale et al., 2008; Zhou et al., 2008; Caccia et al., 2013). However, tools such as SignalP 4.0 are trying to overcome this challenge by combining predictions of transmembrane protein topology with signal sequence identification.

The disadvantages of *in silico* secretome analysis is that it can be only applied to organisms with sequenced genomes; its accuracy depends on prediction algorithm performance, as well as on genomic annotation accuracy. Therefore, to improve the identification of secretome proteins, genomic predictions need to be integrated with transcriptomics and proteomics data (Caccia et al., 2013). The task of predicting the metasecretomes of complex environmental microbial communities is even more challenging. This is due to current limitations in the identification of complete genes *via* sequence-based metagenomics approaches from low-coverage metagenomic assemblies derived through next-generation sequencing of complex environmental microbial communities, often containing numerous closely related microbial species (Hess et al., 2011; Luo et al., 2011).

Despite the versatility of bioinformatics approaches in predicting the targeting sequences and cellular location of proteins, these methods are not capable of predicting exact functions that are essential for understanding vital and specific functions such as interacting with partners in the microbes' surroundings. One experimental method that is well-suited for finding genes that fulfill the functions of interest is expression library screening and display of secretome proteins on the surface of bacteria or filamentous phage as recombinant fusion proteins. This method ensures that protein folding occurs under similar conditions to those where these proteins naturally fold – on cell surfaces. Bacterial cell surface display and yeast surface display are described elsewhere (Georgiou et al., 1997; Chen and Georgiou, 2002; Åvall-Jääskeläinen et al., 2003; Lee et al., 2003; Wernérus and Ståhl, 2004; Liu et al., 2013); this review focuses on filamentous phage display.

## PHAGE DISPLAY

The physical link between phenotype and genotype of a (poly) peptide displayed on the surface of the virion, the high replication capacity of bacteriophage and subsequent affinity selection are the elements that underpin phage display technology. In phage display, a very large repertoire of recombinant phage particles displaying (poly) peptides can be generated ($10^{12}$–$10^{13}$ different clones) at very low cost using simple methods

of microbiology and molecular biology. Nucleotide sequence repertoires such as cDNAs, synthetic oligonucleotides, genomic DNA fragments derived from single organisms or metagenomes, and mRNAs are cloned directly into phage display vectors. Display of peptides encoded by cloned sequences is achieved by translational fusion of a protein or a library of proteins of interest to any of the five structural virion proteins, pVIII, pIII, pVI, pVII, or pIX at N- or C-terminus, although the pIII and pVIII proteins are used most frequently (Russel et al., 2004; Kehoe and Kay, 2005). Peptides fused to the Ff virion proteins fold in the periplasm of *E. coli* (**Figure 2A**), therefore display on filamentous phage is suitable for surface and secreted proteins.

In contrast to Ff phage proteins, "tailed" bacteriophages λ, T7, T4, and P4 fold in *E. coli* cytoplasm and are therefore most commonly used for the display of cytoplasmic proteins. The distinction between cytoplasmic and extracytoplasmic environments mostly refers to oxidative state of Cys residues; which are nearly always reduced in cytoplasmic (or nuclear) proteins, whereas they are oxidized in the periplasm of Gram-negative bacteria or membranous organelles in eukaryotic cells. The readers are referred to several reviews for the latest developments in tailed phage display (Krumpe et al., 2006; Beghetto and Gargano, 2011; Gamkrelidze and Dabrowska, 2014).

Despite the enormous body of reports describing display of a variety of proteins on pIII and pVIII display platforms, there are still many proteins that are recalcitrant to functional display due to host restrictions such as codon usage, protein folding and toxicity to the *E. coli* host. To some degree folding constraints can be alleviated by introducing changes to the host periplasm environment, for example using Δ*dsbA E. coli* strains that do not form S–S bridges between Cys residues to allow folding and display of cytoplasmic proteins, or co-expressing with periplasmic chaperones such as Skp and FkpAto facilitate folding of the fusion counterpart (Hayhurst and Harris, 1999; Gunnarsen et al., 2013), or using alternative signal sequences or translocation routes *via* SRP-dependent or indirect Tat phage display systems (Steiner et al., 2008; Speck et al., 2011).

The non-specific binding to matrices where bait is immobilized can be decreased by "wrapping" the phage in desired charge that is repulsive to the matrix. For example, fusing $Lys_8$ peptide to all major coat protein subunits can be used for positively charged surfaces (Lamboy et al., 2008). To overcome limitations of using only 20 amino acids for the construction of peptide or protein libraries, phage display technology was adapted to incorporate unnatural amino acids by using host strains that express mutant tRNAs and aminoacyl-tRNA synthetases (Tian et al., 2004; Bratkovic, 2010; Bernard and Francis, 2014).

Recently, the scope of phage display extended toward the display of polypeptides containing posttranslational modifications, including phosphorylation, phosphopantetheinylation (Yen and Yin, 2007) and glycosylation (Celik et al., 2010; Dürr et al., 2010; Ng S. et al., 2015). As glycosylation is the most frequent posttranslational modification [>50% of total eukaryotic proteins and an increasing number of archaeal and bacterial proteins (Abu-Qarn et al., 2008)], modification of displayed proteins has promising future applications.

## Filamentous Phage Display Types

There are two general types of filamentous phage display based on whether the library is constructed in Ff phage vectors or in specially modified plasmids called phagemids in conjunction with helper phage. The advantage of a phage vector system is in its simplicity. The library constructed in a simple Ff phage vector results in fusion gene products being displayed by all copies of a particular virion protein. Given that some protein fusions in a library are likely to interfere with assembly and infectivity, they are reported to be counter-selected during the phage life cycle and are lost from the library (Rodi and Makowski, 1999; Derda et al., 2011). Insertion of a second copy of a particular virion protein-encoding gene is one strategy to overcome the interference (Barbas et al., 2001). For pIII fusions, the inter-domain display is solution to prevent censorship due to proteolytic degradation of peptides (Tjhung et al., 2015).

Another type of phage display system that allows more flexibility and provides independence from phage assembly in the amplification phase is based on phagemid vectors (**Figure 2**). Phagemids are plasmid vectors that contain the Ff origin of replication, packaging signal, a plasmid origin of replication, and a selective (antibiotic resistance) marker. Phage display phagemid vectors in addition contain a display cassette, allowing construction of fusion to a virion protein. The Ff origin of replication, packaging signal and the display cassette allow packaging of the phagemid genome into phage-like "phagemid particles" (PPs) and display of phagemid-encoded protein fusion on the surface of the particle (**Figure 2**). A helper phage is the obligatory source of proteins necessary for replication from Ff origin and assembly of a complete virion.

Helper phage typically have an interference-resistant Ff origin of replication and/or truncated packaging signal, or additional (plasmid) origin of replication, allowing preferential replication and packaging of the phagemid single stranded DNA so that the majority (∼90%) of secreted virions are PPs rather than the helper phage (Barbas et al., 2001). Helper phage that encode all virion proteins and contribute them to the PPs are herein referred to as a wild-type helpers. The phagemid/wild-type helper system typically results in monovalent display of recombinant protein fusions to minor virion proteins (pIII, pVII, pIX, and pVI); i.e., PPs are mosaic for recombinant and wild-type capsid proteins produced by phagemid encoding the fusion protein and by a helper, respectively (**Figure 2A**). To increase the copy number of displayed fusion proteins, helper phage containing deletion of the gene encoding the virion protein that is expressed from the phagemid can be used. In the case of most frequently used phagemid vectors that encode virion protein pIII, helper phage that carry deletion of corresponding gene (e.g., Δ*gIII*) are used. The obtained virions exhibit polyvalent display (Griffiths et al., 1993; Rakonjac et al., 1997; Joo et al., 2008). Additional refinements of some phage display phagemid vectors are peptide tags (e.g., c-myc or E-tag), followed by an *amber* stop codon between the insert and downstream pIII. These additions allow

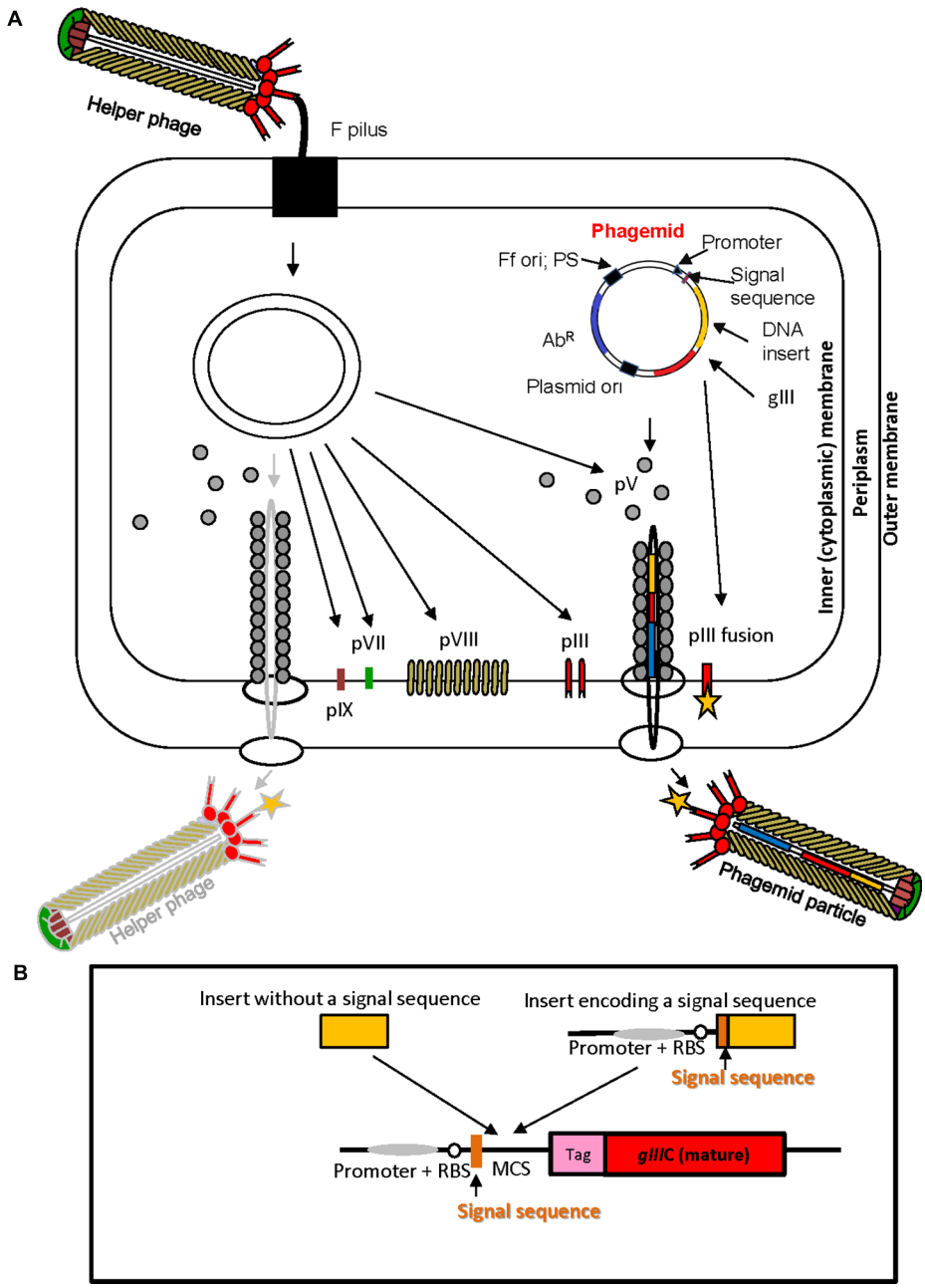


**FIGURE 2 | Ff virion protein targeting, virion assembly, phagemid display system, and display cassette in phagemid vectors. (A)** In *Escherichia coli* phagemids can be replicated as plasmids or alternatively, in the presence of a helper phage, packaged as "transducing" or "phagemid" particles (PPs). Phagemid encodes phage protein pIII as a fusion partner for display. The resulting phagemid particles may incorporate either pIII derived from the helper phage (red lollipop-like structure) or the polypeptide-pIII fusion protein (red lollipop-like structure decorated with a yellow star), encoded by the phagemid. $Ab^R$, antibiotic resistance marker, Ff ori; PS, filamentous phage origin of replication and packaging signal; Plasmid ori, plasmid origin of replication; gIII, gene III; pIII, pV, pVI, pVII, pVIII, and pIX, filamentous phage proteins. Phagemid particles are produced at a 10–100-fold excess over the helper phage (denoted by solid vs. faded lines for phagemid particle vs. helper phage. **(B)** Typical phage display cloning cassette in a phagemid vector: promoter, a ribosome binding site (RBS), signal sequence (commonly used PelB signal sequence from *Erwinia carotovora* (Lei et al., 1987); multiple cloning site (MCS), affinity tag (tag), and sequence encoding the mature portion (C-terminal domain) of pIII (*gIIIC*; required for assembly of the fusion into the virion). Two types of inserts derived from fragmented bacterial or archaeal genomic DNA are shown above the cloning site. Insert without signal sequence, in order to result in displayed peptide, has to correspond to a CDS that is in frame with the upstream signal sequence and downstream *gIII* (encoding the C-terminal domain). It is typically truncated at the 5′ and 3′ ends to avoid stop codons that terminate translation. A second type of insert, that contains signal sequence, can be displayed if the CDS is truncated at the 3′ end, and is in frame with *gIII*. The latter type of inserts typically carries its own promoter and RBS. *E. coli* host strains that contain suppressor mutations (such as *supE44*) can read through *amber* stop codons at 50% efficiency and result in display of fusions that include this codon.

a soluble version of foreign protein to be produced if phagemids are transformed into an appropriate *E. coli* strain that does not contain an amber codon suppressor (Hoogenboom et al., 1991).

## Affinity Selection of Binding Targets – Bio-Panning

When a library of fusion proteins is constructed and displayed on the phage surface, a recombinant phage clone displaying a certain binding affinity can be selected from the majority of other (non-binding) recombinant phages present in a library, by an affinity selection procedure known as bio-panning (**Figure 3**) (Parmley and Smith, 1988). Through successive rounds of binding, washing, elution, and amplification, an originally very diverse phage display library, up to $10^{12}$ variants (Schier et al., 1996) is increasingly enriched for the phage library clones with a propensity to bind to the target molecule. Ultimately, monoclonal phage populations with desired specificities can be identified using sequencing and analyzed using affinity binding assays.

Biopanning has potential to identify proteins that bind to enormous diversity of ligands, from extremely complex, including the whole animal (Arap et al., 1998), *ex vivo* tissues (Antonara et al., 2007), complex mixture of organisms (Ng F. et al., 2015) and whole cells (Fevre et al., 2014) to very simple, such as purified proteins, peptides, nucleic acids, carbohydrates (Zwick et al., 1998; Rodi and Makowski, 1999) or inorganic powders (Mao et al., 2004; Ploss et al., 2014). The outcome of biopanning, however, depends on library complexity (or primary size, equivalent to the number of different variants or recombinant inserts), functionality of displayed fusions and affinity of interaction with the bait used in the biopanning. For isolation of high-affinity binders, monovalent phage display libraries are usually used because they allow selection based on strong affinity. In contrast, multivalent display, in particular on the major coat protein (pVIII), is more suitable for selection of low-affinity binders since the avidity of the virion compensates for low affinity of individual peptides (Shallom and Shoham, 2003).

## Phage Display Applications in Functional Identification of Microbial Secretome Proteins

Microbial interactions with the environment have beneficial or detrimental effects on microorganisms involved in interactions or/and the host. In general, these interactions are mediated *via* microbial secretome proteins that interact with receptor molecules on host cells or other microbes, or with the host cell surface or proteins of the host signaling pathways involved in the immune response. Phage display has been used extensively for identification of bacterial proteins that interact with the

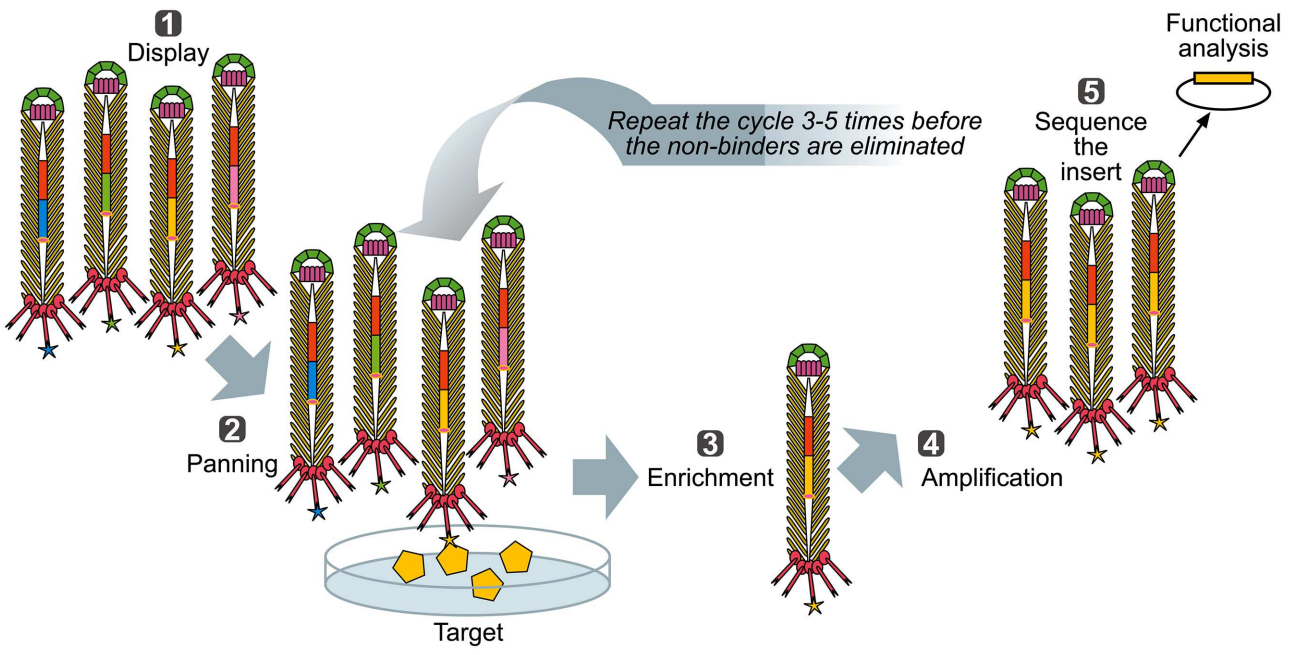


**FIGURE 3 | Biopanning – a basic selection for binding peptides.** (1) Display: Filamentous phage displaying variants of proteins/peptides/antibodies is created, cloned into phage, or phagemid vectors as fusions to a coat protein gene(s) and displayed on the surface of the virions. (2) Panning: The phage library displaying variant peptides or proteins (different-color stars) is exposed to immobilized ligand (yellow pentagon) and phage with appropriate binding specificity is captured (yellow star). (3) Enrichment: Non-binding phages are washed off and bound phage(s) is (are) eluted by conditions that disrupt the peptide-ligand interactions, leading to enrichment for a specific binder. (4) Amplification: Eluted phage is then amplified by infection of a suitable *E. coli* strain. This amplified phage population is greatly enriched in recombinant phage clones displaying peptides that bind to the target. The biopanning steps (two to four) are repeated for several (three to five) rounds, ultimately resulting in a clonal population of recombinant phages that bind to the target used for affinity panning of the library. Captured putative binder can then be identified by sequencing (5) and functionally analyzed.

host surfaces or are dominant immunogens recognized by host antibodies (Mullen et al., 2006). Bacterial and more recently archaeal phage display libraries are constructed in phagemid vectors, as fusions to pIII or pVIII. Given the lack of introns in bacterial coding sequences, fragmented genomic DNA is used for construction of libraries. These are ligated to a vector that contains a multiple cloning site (MCS) between the signal sequence and the mature portion of gene III or VIII (**Figure 2B**). If a fragment is ligated such that the coding sequence is in the same direction and frame with the vector sequence encoding both the upstream signal sequence and downstream mature portion of protein, the encoded peptide will be displayed on the surface of phage. This type of fusion can display both the cytosolic and secretome proteins. Alternatively, if a CDS segment encoding a signal sequence is inserted in frame with the mature portion of pIII or pVIII (but not the vector-encoded signal sequence), it is also displayed on Ff. This type of recombinant clone will often contain the native promoter and RBS derived from the genomic DNA. Given the higher probability of a single in-frame joint than that of double, the secretome clones are expected to be reasonably frequent in the shot-gun filamentous phage display libraries. All clones that have inserts whose translated peptide is displayed on the phage surface can be pre-selected by virtue of peptide tags engineered into the mature portion of pIII (**Figure 2B**). Both types of fusions can be selected in the shot-gun phage display library screenings (Gagic et al., 2013; Ng F. et al., 2015).

Phagemids that rely on pIII for bacterial phage display library construction contain only the coding sequence for the C-terminal domain. The reason for this is that the pIII N-terminal domain expression results in resistance of phagemid-containing cells to helper phage infection, if a promoter sequence is present in the insert (Jankovic et al., 2007).

In the past two decades, particularly in the area of infectious diseases, phage display has proven to be a powerful technology for identification of genes encoding bacterial adhesins and characterization of adhesin domains that mediate interactions with host cells and ECM components such as fibronectin, fibrinogen, collagens, vitronectin, laminin, and heparin sulfate (Mullen et al., 2006). In pathogenic bacteria, microbial adhesion precedes colonization and internalization into the host cell and increases resistance to host defenses. Global spread of antibiotic-resistant pathogenic bacteria commands increased efforts to find new antigenic epitopes for vaccine development and alternative therapies that include interference with microbial adhesion or prevention of immune manipulation by pathogenic bacteria. Shot-gun filamentous phage display (display of random fragments of bacterial genomic DNA) was first exploited by Jacobsson and Frykberg (1996) to identify *Staphylococcus aureus* proteins that interact with ECM components and host serum or plasma. Following this initial publication many genes encoding proteins involved in host-microbial interactions from a number of bacterial species have been identified using phage display [**Table 1**; (Ausmees et al., 2001; Lauterbach et al., 2003; Benedek et al., 2005; Mullen et al., 2006; Antonara et al., 2007; Posadas et al., 2012; Evangelista K. V. et al., 2014]. A shot-gun phage display library of *Borrelia burgdorferi* was used for the *in vivo* screening for potential adhesins, resulting in discovery of at least five new adhesion proteins (Antonara et al., 2007). Phage display allows not only identification of a gene of interest, but also domains that mediate binding, by identifying a consensus among the library inserts that bind to a bait. For example, this approach was used to identify and map von Willebrand factor binding protein from pathogenic *Staphylococcus aureus* (Bjerketorp et al., 2002) and novel neutrophil-binding proteins of *S. aureus* that inhibit neutrophil recruitment to the site of infection (Fevre et al., 2014). Phage display has recently been used for identification of antigenic determinants of *Salmonella enterica sv.* Typhimurium (Meyer et al., 2012).

Most bacteria in the environment, as well as commensal bacteria that colonize eukaryotic organisms, use adhesins for interactions with inorganic environment, other microbes and multicellular hosts. In comparison to the plethora of adhesins from pathogenic bacteria that we recognize today, adhesins from non-pathogenic bacteria are as numerous; however, their interacting partners are largely unknown. In one example of phage display application in symbiotic bacteria, it was used to identify and map the cell-surface-associated agglutinin (RapA) from legume root nitrogen-fixing bacterium, *Rhizobium leguminosarum* (Ausmees et al., 2001). Another large bacterial group of interest are probiotics. Although benefits of probiotic bacteria to human health are still debated, adhesion to gut mucosal surface is a mechanism by which they can persist in gut and also may preclude attachment of enteropathogenic bacteria and viruses to the host's intestinal epithelial cells, possibly leading to beneficial effect. Several proteins from probiotic *Lactobacillus casei* binding to collagen and fibronectin have been identified (Munoz-Provencio and Monedero, 2011), as well as a *Lactobacillus rhamnosus* surface protein complex have been identified by affinity-screeing of phage display libraries (Gagic et al., 2013). Surface proteins from probiotic bacteria *Lactobacillus reuteri* and *Lactobacillus rhamnosus* at genome level have also been displayed using secretome-specific phage display method to obtain clone banks of displayed surface and secreted proteins suitable for binding and functional assays (Wall et al., 2003; Jankovic et al., 2007; Gagic et al., 2013).

Microbe-microbe interactions in complex environments and secretome proteins involved in these interactions are another research area of interest in recent years. For example in fermentative forestomach (rumen) of ruminants protozoa and specific group of archaea, methanogens, can be found in association. This interaction may facilitate hydrogen transfer from protozoa (hydrogen producers) to archaea, which use hydrogen to produce methane (Ushida et al., 1997; Belanche et al., 2014). Recently Ng F. et al. (2015) used shot-gun phage display in a phagemid/helper phage platform to identify a secretome protein Mru_1499, from rumen methanogenic archaeon *Methanobrevibacte rruminantium* M1 (Leahy et al., 2010) as a binder to a broad range of rumen protozoa and rumen bacterium *Butyrivibrio proteoclasticus*, suggesting a broad adhesion spectrum for this protein. Interestingly, the library insert contained an archaeal signal sequence and the 5′ portion of the Mru_1499 gene fused to the mature portion of pIII. Display and selection of this recombinant

**TABLE 1 | Bacterial adhesins identified using phage display technology.**

| Organism | Ligand | Gene product or ORF encoding for bacterial adhesin | Reference |
|---|---|---|---|
| **Pathogenic bacteria** | | | |
| *Helicobacter pylori* | Plasminogen | PgbB | Jönsson et al., 2004 |
| *Staphylococcus aureus* | Human IgG | Sbi | Jacobsson and Frykberg, 1995 |
| | von Willebrand factor | vWBp | Bjerketorp et al., 2002 |
| | Platelets | FnBPA, FnBPB | Heilmann et al., 2002 |
| | Fibronectin | FnBPA | Ingham et al., 2004 |
| | Neutrophils | Selx | Fevre et al., 2014 |
| | Neutrophils | SSL6 | Fevre et al., 2014 |
| | Fibronectin | Embp | Williams et al., 2002a |
| *Staphylococcus epidermidis* | MC3T3-E1 osteoblast cell line and Fibronectin | FnBPA, FnBPB | Williams et al., 2002b |
| | Fibrinogen | Fbe | Nilsson et al., 1998 |
| *Staphylococcus lungdunensis* | Fibrinogen | Fb1 | Nilsson et al., 2004a |
| | von Willebrand factor | vWbl | Nilsson et al., 2004b |
| *Streptococcus agalactiae* | Fibronectin | ScpB | Beckmann et al., 2002 |
| | Fibrinogen | FgagV1, FgagV2, FgagV3 | Jacobsson et al., 2003 |
| *Streptococcus dysagalactiae* | Fibrinogen | DemA | Vasi et al., 2000 |
| *Streptococcus equi* | Fibronectin | FnBP | Lindmark and Guss, 1999 |
| *Haemophilus influenzae* | Bovine serum albumin | Hi0367 | Mullen et al., 2007 |
| *Actinobacillus pleuropneumoniae* | Bovine serum albumin | ORF16 | Mullen et al., 2007 |
| *Pasteurella multicida* | Fibronectin | Pm1665 | Mullen et al., 2007 |
| *Aggregatibacter actinomycetemcomitans* | Bovine serum albumin | ORF10 | Mullen et al., 2007 |
| *Salmonella enterica sv.* Typhimurium | Antisera from convalescent pigs | 16 antigenic peptides | Meyer et al., 2012 |
| *Leptospira interrogans* | Heparin | LigB | Ching et al., 2012 |
| | EA.hy926 endothelial cells | LIC10508 | Evangelista K. et al., 2014 |
| | EA.hy926 endothelial cells | LIC13411 | Evangelista K. et al., 2014 |
| | EA.hy926 endothelial cells and VE-cadherin | LIC12341 | Evangelista K. et al., 2014 |
| | EA.hy926 endothelial cells and VE-cadherin | LIC13411 | Evangelista K. et al., 2014 |
| *Brucella suis* | Fibronectin | BmaC | Posadas et al., 2012 |
| | Fibronectin | BRA0095 | Posadas et al., 2012 |
| | Fibronectin | BRA0175 | Posadas et al., 2012 |
| *Mycobacterium tuberculosis* | TB patient sera | LpqB | Liu et al., 2011 |
| | TB patient sera | CpsA | Liu et al., 2011 |
| | TB patient sera | PapA2 | Liu et al., 2011 |
| *Borrelia burgdorferi* | Mammalian cells | P66, OspC, VlsE, Lmp1, BmpD, OspF homolog, ErpK, ErpL, OspG | Coburn et al., 2013 and references therein |
| *Campylobacter jejuni* | Holo- and apo-lactoferin | LimC | Abruquah, 2009 |
| *Yersinia pestis* | Laminin | Pla | Benedek et al., 2005 |
| **Non-pathogenic bacteria** | | | |
| *Lactobacilllus rhamnosus* HN001 | HN001 cells | SpcA | Gagic et al., 2013 |
| | SpcA | SpcB | Gagic et al., 2013 |
| *Lactobacillus casei* BL23 | Collagen | XpkR, LCABL_01820 | Munoz-Provencio and Monedero, 2011 |
| | Fibronectin | Ps356 endolysin-homolog | Munoz-Provencio and Monedero, 2011 |
| *Rhizobium leguminosarum* bv. *trifolii* | *Rhizobium leguminosarum* bv. *trifolii R200 cells* | RapA1 | Ausmees et al., 2001 |
| *Bifidobacterium longum* VMKB44 | HT-29 epithelium cells | ABC transporter – BL0155 | Shkoporov et al., 2008 |

phagemid from the library therefore showed that archaeal signal sequences are functional in *E. coli*. Protozoa isolated from the sheep rumen were used as bait for the library panning to identify Mru_1499, and in turn the phagemid particles displaying Mru_1499 were used as bait to identify, among rumen protozoans, those that interact with this protein, by sequencing the 18S rRNAgene from the captured protozoa (Ng F. et al., 2015).

## Selective Display of Bacterial Secretome

A standard strategy for identifying targets for vaccine development in the genomics era is bioinformatic identification followed by expression of each individual bacterial secretome protein. This involves cloning and expression of up to several hundred surface proteins and testing their immunogenicity. Selective display of the secretome was proposed as an alternative to this path to allow, in one cloning step, the production of a library and/or clone bank of those recombinant phagemids that display surface-associated and secreted proteins. Secretome-selective phage display methods exploit the requirement of a signal sequence to target a fusion protein that is in frame with the mature portion of pIII to *E. coli* inner membrane (**Figure 4**). The phagemids used in these conditional display strategies contain C-terminal domain of pIII without a signal sequence. For assembly of signal sequence-encoding inserts (Rosander et al., 2002) used *gIII*-positive helper phage and for selection, biopanning based on the presence of a vector-encoded affinity tag incorporated into the fusions that were displayed on the phagemid particles thanks to a functional signal sequence. In the second method, a helper phage with *gIII* deletion was used for assembly of the particles (Jankovic et al., 2007). Here, the selection was based on removal of pIII-deficient phagemid particles which are structurally unstable and easily disassembled by detergent sarkosyl (Rakonjac and Model, 1998; Rakonjac et al., 1999). This approach was further used to identify six secretome proteins from *Mycobacterium tuberculosis* by subtractive panning between the sera of *M. tuberculosis* patients and BCG-vaccinated healthy subjects (Liu et al., 2011), three of which have not been identified prior to this study and which therefore were novel vaccine candidates. Interestingly, the breakdown of targeting sequences that were able to guide the fusion to the inner *E. coli* membrane and allow assembly of the virion included not only type I signal sequences, but also type II (lipoprotein) and type IV pre-pilin signal sequences as well as transmembrane helices. Moreover, a few "moonlighting" proteins that do not contain SecYEG-dependent signal sequences were identified among the selected fusions (Jankovic et al., 2007; Liu et al., 2011). Together with chance identification of an archaeal-signal-sequence-driven secretome protein fusion reported by Ng F. et al. (2015), the findings that signal sequences and transmembrane helices from Gram-positive bacteria, Mycobacteria and Archaea guide the pIII fusion protein to correctly insert into the inner membrane of *E. coli* and be processed to be displayed on the surface of the virion, indicate great plasticity in processing of the SecYEG-translocated pIII fusions. With respect to transmembrane helices and signal sequences other than type I, this process most likely involves periplasmic proteases other than signal peptidases, and in the case of moonlighting proteins it could involve SecYEG- and signal-sequence-independent translocons such as ABC transporters. These hypotheses remain to be experimentally verified.

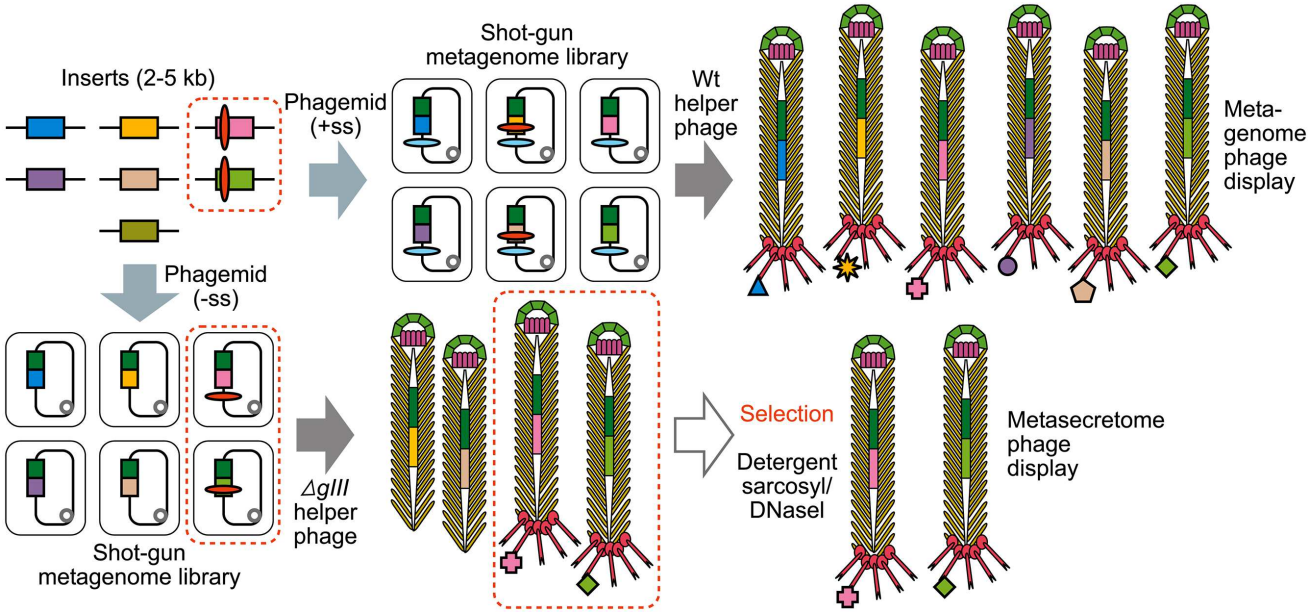


**FIGURE 4 | The construction of shotgun metagenomic and metasecretome filamentous phage display libraries.** Metagenomic DNA is randomly sheared and cloned into phagemid that contains signal sequence (+ss) or as in case for metasecretome into phagemid without signal sequence (−ss). In both cases constructed metagenomic inserts contain endogenous signal sequences, represented by red ovals. Depending on helper phage used [wild-type (wt) or *gIII*-deleted helper phage] for aid in replication and assembly of recombinant virions, the library will contain virions displaying the whole metaproteome (metagenome phage display) or it will consist of virions capped by insert-pIII fusion proteins (signal sequence-positive clones) that are resistant to sarkosyl ($Sarkosyl^R$, virions inside the dotted line) and uncapped virions (signal sequence-negative clones) that are sensitive to sarkosyl ($Sarkosyl^S$). Sarkosyl resistance is used as a basis for selection in metasecretome phage display. Single stranded DNA (ssDNA) purified from $Sarkosyl^R$ virions after the selection can be used to obtain the amplified metasecretome plasmid library for preliminary assessment of metasecretome diversity by next-generation sequencing [Taken from (Ciric et al., 2014) with permission].

Although in some cases secretome display was used for screening of libraries to identify binders to targets of interest (Fevre et al., 2014), this method is very strongly biased toward display of N-terminal portions of the secretome proteins, thereby eliminating binding domains encoded toward the C-terminal end of the large adhesins. Furthermore, with a few exceptions listed above this strategy is not expected to display important SecYEG-independent virulence factors, such as those secreted by the Type 1, 3, 4, and 6 secretion systems, which are predominant in enteric pathogens including *Yersinia*, *E. coli,* and *S. enterica* (Chagnot et al., 2013). Therefore, shot-gun phage display is more suitable than secretome display for screening to identify binding domains for novel ligands.

## Filamentous Phage Display in Functional Metagenomics

It is clear from the vast number of research reports that phage display technology has been used successfully to identify and characterize microbial proteins that interact with complex and simple targets as well as to build clone banks of secretome proteins from single organisms. Currently, the large volumes of data generated from fast improving next-generation-sequencing (NGS) technologies and metagenomics research are mainly used for cataloging and comparing the composition of microbial communities. An interesting question is whether the power of phage display and NGS could be combined to identify specific ligand-binding or representative (meta) secretome protein libraries from complex microbial communities.

Metagenomic approaches for analysis of microbial DNA recovered directly from the environment (Handelsman, 2004) have been used over the past decade to uncover extraordinary functional potential of complex microbial communities. Major strategies applied for identification of genes encoding "high-value targets" (enzymes for synthesis of novel bioactive molecules or novel biological activities) from metagenome are sequence-based bioinformatics analyses of the gene content, or function-based, by functional screening of metagenomic expression libraries (Tuffin et al., 2009; Ekkers et al., 2012; Culligan et al., 2013). Sequence-based metagenome mining aims to identify *in silico* high-value target gene or gene cluster candidates for heterologous expression, while function-based screens aim to phenotypically detect biosynthetically or enzymatically active clones (Charlop-Powers et al., 2014). Use of next generation sequencing (NGS) technologies in metagenomics enables significantly higher resolution and throughput in gene discovery from environmental microbes compared to traditional genomic approaches.

Genetic diversity of most microbial communities is tremendous. This implies an immense DNA sequencing volume is required to find, very sparse high-value target genes and gene clusters. A variety of enrichment strategies ranging from the whole-cell approach based on nutritional, chemical or physical selection, to increasing the frequency and diversity of genes likely to encode novel bioactive molecules, have been applied to increase the screening hit rate and speed up the process of gene discovery using functional metagenomic approaches (Cowan et al., 2005; Banik and Brady, 2010; Xing et al., 2012). DNA stable-isotope probing (Chen and Murrell, 2010; Mazard and Schäfer, 2014), complementation (Charlop-Powers et al., 2012), affinity capture and a number of strategies based on PCR and/or DNA hybridization, such as suppression subtractive hybridization (Galbraith et al., 2004; Meyer et al., 2007; Meiring et al., 2010), differential display, sequence tag interrogation approach (Owen et al., 2013) and metagenome arrays (He et al., 2007; Park et al., 2008; He et al., 2010) have been explored for enriching environmental DNA samples for genes of interest.

Although successful affinity screening of metagenomic Ff phage display libraries is yet to be reported, the precedents for this have been published in the form of selective metasecretome display and NGS-facilitated phage display library screening.

## Phage Display Combined with Next-Generation Sequencing

The traditional approach for screening of phage display libraries, consisting of 3–5 rounds of affinity selection (biopanning) followed by sequencing of inserts from limited number of clones (**Figure 3**), is laborious and unsuitable for screening of metagenomes of diverse microbial community or complex antibody repertoires of higher organisms. In contrast, use of NGS technologies, typically delivering $>10^6$ of sequencing reads, is well suited for high-throughput exploration of the diversity of phage binding variants enriched after one or two rounds of panning on ligand of interest. The NGS analysis after limited panning allows high sequence coverage of binding variants, thereby overcoming a problem of competition between high-affinity and low-affinity binders and reducing false positive hits that often arise as a result of binding to non-bait materials present in the selection system (e.g., plastics, BSA) and propagation advantages (Vodnik et al., 2011).

Dias-Neto et al. (2009) proposed the use of NGS in combination with real-time PCR to improve phage quantification and analysis of the library inserts encoding phage-displayed variants. The authors adapted pyrosequencing for deep-sequencing of amplicons derived from phage ssDNA, retrieved directly after two rounds of panning of combinatorial library of random heptapeptides *in vivo* from four human tissues biopsies, using primers flanking the library insert within the fusion. This approach was applied to obtain sequencing reads directly from tissue-selected and unselected phage display libraries (library before and after panning) in a single run.

Di Niro et al. (2010) screened an ORF-filtered (Zacchi et al., 2003) cDNA phage display library, obtained from mRNA derived from several human cell lines, to identify proteins interacting with tissue transglutaminase 2, an enzyme implicated in different pathological conditions. In this study the authors combined phage display and NGS, enabling at least two orders of magnitude increase in the number of affinity-selected clones compared to traditional affinity screening, with two rounds of panning, to achieve an optimal balance between high numbers of positive clones and broad diversity. This approach led to identification of a "landscape" of binding variants from the phage display library, three of

which had been previously characterized as transglutaminase 2-interacting proteins, with the remainder being novel proteins that were subsequently confirmed by functional assays. Based on the ranking of the most frequently selected ORFs within the selected phage population, detected through the high-throughput sequencing, it was estimated that at least 1000 clones would have to be picked and analyzed using traditional screening approach in order to capture the top five most frequent clones after two rounds of selection with 99% probability.

Recently, t Hoen et al. (2012) demonstrated that NGS can improve and accelerate finding of specific binders by screening of the phage display libraries, while reducing the number of false positive hits. Illumina platform was used to compare diversity of Ph.D.−7 M13 peptide phage display library before panning and phage display library retrieved after each of several rounds of panning on osteoblasts, performed to select heptapeptides that mediate binding to and uptake into osteoblasts. It was demonstrated that deep sequencing of the phage pool obtained after the first round of biopanning on osteoblasts was sufficient to identify positive hits. Selection of peptides with high binding to and uptake into osteoblasts was confirmed by confocal microscopy and live cell imaging. In addition, by sequencing the starting phage display library before screening (after one round of amplification in bacterial host), authors identified propagation advantage as an important source of false positive hits (t Hoen et al., 2012).

Due to the high diversity of antibody phage display libraries (typically between $10^7$ and $10^{11}$ variants) and observed correlation between the size of the repertoire and the antibody affinities isolated from it (Hust and Dubel, 2004), filamentous phage display coupled with NGS is routinely used for in-depth characterization of immunoglobulin antibody repertoires of different organisms and high-throughput screening of ligand-antibody interactions (Ravn et al., 2010; Reddy et al., 2010; Saggy et al., 2012). This advance in technology can be readily applied to other high complexity samples, such as metagenome shot-gun phage display libraries.

## Selective Metasecretome Phage Display

At present, published data on applications of phage display to aid metagenomic gene discovery is limited to "proof-of-principle" studies. T7 phage display and affinity capture was employed for enrichment and identification of genes encoding acyl carrier proteins and peptidyl carrier proteins from soil metagenome (Zhang et al., 2009). These proteins are essential components of biosynthetic enzymes (polyketide synthases and non-ribosomal peptide synthetases) that synthesize natural products with proposed antibiotic, immunosuppressant, and anticancer activities. After six iterative rounds of selection for enrichment of carrier proteins, a limited number (60) of phage clones were sequenced to evaluate usefulness of this approach for identification of carrier protein genes from large metagenomic DNA libraries. Display of the same soil metagenomic DNA library on the surface of filamentous phage and subsequent five rounds of panning did not yield any enrichment. Authors hypothesized that T7 phage display system is more suitable for functional selection of metagenome-encoded cytoplasmic enzymes because the T7 phage capsid protein is displayed on virions that are assembled in the cytoplasm and released by host cell lysis. In contrast, expression and display on filamentous phage depends on host secretion systems for translocation to the periplasm that is an oxidizing environment and therefore not suitable for most cytosolic enzymes which commonly contain an active site Cys residues.

Ciric et al. (2014) combined secretome-selective filamentous phage display (Jankovic et al., 2007) and NGS for the enrichment and sequence-based mining of bovine rumen plant-adherent microbial metagenome for fibrolityc enzymes (Ciric et al., 2014) (**Figure 4**). This approach enabled enrichment of metagenomic genes encoding surface, transmembrane and secreted proteins (metasecretome). Given that the selection relies on *E. coli* SecYEG translocons, this publication gave the first assessment of the selection system's promiscuity, in particular for Gram-positive vs. Gram-negative secretion signals. Whereas secretome proteins from both types of bacteria have been selected for, taxonomic assignment of the sequenced inserts showed an increased frequency of secretome proteins from Gram-negative bacteria in the phylum Bacteroidetes (**Figure 5B**) relative to those from random shotgun sequence dataset. In terms of the type of secretion signals selected for at the metasecretome scale, inserts containing recognition sites for type I signal sequences were the most prominent, similar to what was reported for the genome-scale secretome selection (**Figure 5A**).

Next-generation-sequencing analysis of the metasecretome identified an increased frequency of putative ORFs encoding catalytic and binding modules of fibrolytic enzymes, as well as large numbers of putative modules (cohesins and dockerins) that are constructing blocks of cell-surface organelles called cellulosomes (Bayer et al., 2004), specialized for recognition and degradation of plant fiber, were detected (**Figure 5C**). A high proportion and taxonomic variety of cellulosomal modules, particularly those from cohesins and dockerins has not been reported in previously published metagenomic studies of the rumen microbiome, suggesting that phage display could be a powerful method for enrichment, display and identification of these modules which subsequently can be used in building of microbial "designer" fiber-degrading hyper structures. Genes encoding putative fibrolytic enzyme modules and cellulosome modules are candidates for functional characterization *via* affinity screening of methagenomic shot-gun phage display libraries.

Despite its power, there are several shortcomings of the metasecretome phage display approach, some of which could potentially be overcome with new and upcoming technologies. As is the case with the genome-scale secretome phage display, the metasecretome library is biased toward the sequences encoding the N-terminal portion of the secretome proteins, hence representation of the C-terminal domains is low. This can in principle be overcome by constructing fosmid- or cosmid-based phage display vectors that would have a capacity for large inserts (up to 40 kb) and would therefore be able to accommodate large portions of secretome proteins fused to pIII.

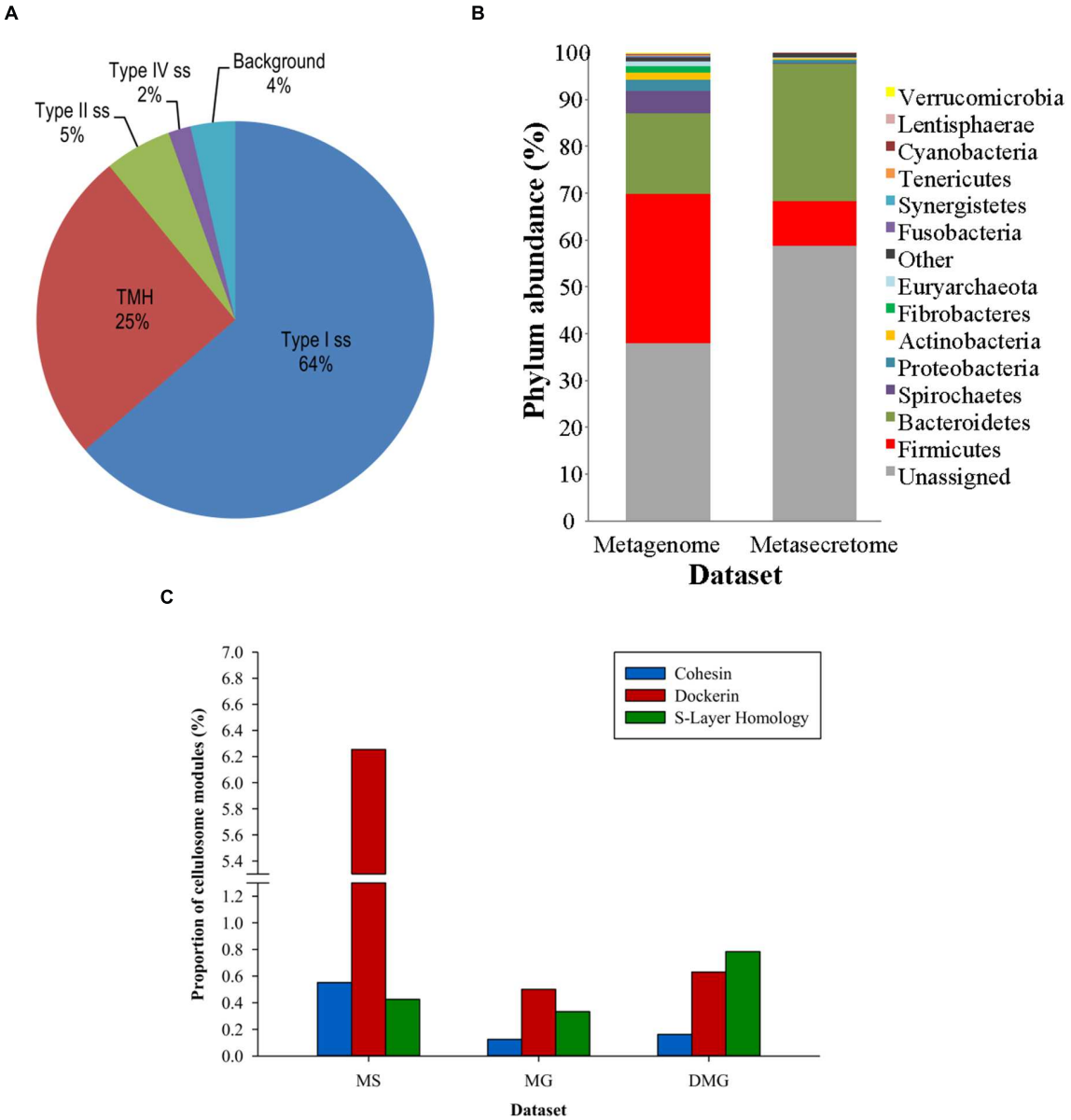


**FIGURE 5 | Taxonomic distribution, signal sequence types, and cellulosome components enrichment in metasecretome phage display of fiber-adherent rumen microbial community. (A)** Distribution of signal sequence types and transmembrane helices in selected metasecretome recombinants; Abbreviations: Type I ss, classical signal sequence; Type II ss, lipoprotein signal sequence; Type IV ss, prepilin-like signal sequence; TMH, N-terminal or internal transmembrane α- helix/helices; background, ORFs encoding putative proteins without a predicted membrane-targeting signal/non-classical secretion, or ORFs encoding putative proteins and peptides ≤24 amino acid residues. **(B)** Taxonomic distribution of the phage-display-selected metasecretome; The taxonomic assignments, at the phylum level, were based on the distribution of the best BLASTP hits at a 30% amino acid sequence identity threshold for protein-coding genes predicted in metagenome and metasecretome datasets. Each section of the stacked columns represents the percentage of total protein-coding genes assigned to the corresponding phylum. The section labeled 'Other' contains putative protein-coding genes assigned to a phylogenetic group with low abundance in the dataset (<0.1%), while the section labeled 'Unassigned' corresponds to putative protein-coding genes with best BLASTP hit below 30% identity cut-off. **(C)** Enrichment for the components of cellulosome; Frequency of three putative distinct 'signature' cellulosome modules: cohesins (blue); dockerins (red) and surface S-layer homology (SLH) domains (green) in three datasets: MS, metasecretome dataset; MG, metagenome dataset and published deep-sequenced metagenome (DMG). The latter dataset is from (Hess et al., 2011). **(A,C)** are taken from (Ciric et al., 2014) and **(B)** from (Ciric, 2014) with permission.

Next-generation sequencing using 454 or Illumina technologies is powerful in covering the totality of the meta-secretome library inserts. However, due to the short lengths of templates required for these sequencing technologies and a PCR amplification step that is necessary in order to produce the sequencing library, sequence information is disconnected

from the physical recombinant clones from which it was derived (Ciric et al., 2014), making it impossible to form a clone library without the standard Sanger sequencing. This issue, however, can be overcome by using novel sequencing technologies, like PACBio, which use long templates (Fichot and Norman, 2013; Wang et al., 2015) and could, in principle, be used in an approach that would allow tracking of a sequence to the template. This approach for sequencing could be combined with subtractive or normalization methods to enrich the library for the rare recombinant sequences (Gagic et al., 2015), and to build a balanced metasecretome clone bank that can be used as a resource for expression and purification of large number of secretome proteins from a microbial community, by virtue of their display on PPs.

A shot-gun metagenomic phage display libraries in Ff and T7 have potential to provide the widest possible coverage of SecYEG-dependent and –independent secretome proteins for affinity selection against complex or simple targets of interest to identify adhesins, secreted virulence factors or enzymes, whereas the metasecretome libraries provide a good source of data for large scale identification of immunogenic peptides. Amenability of phage display to large-scale, high-throughput screening using NGS and emerging phage display-based methods for enrichment of target genes in metagenomes, indicate that this is just a beginning of wider use of phage display to accelerate target gene discovery in metagenomics.

## CONCLUDING REMARKS

Phage display on Ff, combined with recent developments in sequencing technologies, provides a powerful approach for discovery of novel secretome proteins in variety of microorganisms and in microbial communities.

## AUTHOR CONTRIBUTIONS

DG (50%), MC (30%), WW (5%) FN (5%), and JR (10%) have written the manuscript.

## ACKNOWLEDGMENTS

This work was supported by the New Zealand Ministry for Business, Innovation and Employment grant (contract # C10X0803) and The Royal Society of New Zealand through a Marsden Fast Start grant (contract AGR1003), JR laboratory was supported by Anonymous Donor, Massey University Research Fund, Palmerston North Medical Research Foundation and Institute of Fundamental Sciences, Massey University. FN was supported by a Commonwealth Ph.D. Fellowship and WXW by an Institute of Fundamental Sciences (Massey University) Ph.D. scholarship. FN and WXW were also supported by a Completion Bursary Scholarship by Massey University.

## REFERENCES

Abruquah, H. H. (2009). *Identification of Host-pathogen Interacting Molecules of Campylobacter Jejuni Using Phage Display Technology and In silico Sequence Analysis.* Ph.D. thesis, submitted to the University of Nottingham for the degree of Doctor of Philosophy Microbiology, The University of Nottingham, Nottingham.

Abu-Qarn, M., Eichler, J., and Sharon, N. (2008). Not just for Eukarya anymore: protein glycosylation in Bacteria and Archaea. *Curr. Opin. Struct. Biol.* 18, 544–550. doi: 10.1016/j.sbi.2008.06.010

Antelmann, H., Tjalsma, H., Voigt, B., Ohlmeier, S., Bron, S., Van Dijl, J. M., et al. (2001). A proteomic view on genome-based signal peptide predictions. *Genome Res.* 11, 1484–1502. doi: 10.1101/gr.182801

Antonara, S., Chafel, R. M., Lafrance, M., and Coburn, J. (2007). Borrelia burgdorferi adhesins identified using in vivo phage display. *Mol. Microbiol.* 66, 262–276. doi: 10.1111/j.1365-2958.2007.05924.x

Arap, W., Pasqualini, R., and Ruoslahti, E. (1998). Cancer treatment by targeted drug delivery to tumor vasculature in a mouse model. *Science* 279, 377–380 doi: 10.1126/science.279.5349.377

Arts, J., Van Boxtel, R., Filloux, A., Tommassen, J., and Koster, M. (2007). Export of the pseudopilin XcpT of the *Pseudomonas aeruginosa* type II secretion system via the signal recognition particle-Sec pathway. *J. Bacteriol.* 189, 2069–2076. doi: 10.1128/JB.01236-06

Auclair, S. M., Bhanu, M. K., and Kendall, D. A. (2012). Signal peptidase I: cleaving the way to mature proteins. *Protein Sci.* 21, 13–25. doi: 10.1002/pro.757

Ausmees, N., Jacobsson, K., and Lindberg, M. (2001). A unipolarly located, cell-surface-associated agglutinin, RapA, belongs to a family of Rhizobium-adhering proteins (Rap) in *Rhizobium leguminosarum* bv. trifolii. *Microbiology* 147, 549–559.

Åvall-Jääskeläinen, S., Lindholm, A., and Palva, A. (2003). Surface display of the receptor-binding region of the *Lactobacillus brevis* S-layer protein in Lactococcus lactis provides nonadhesive lactococci with the ability to adhere to intestinal epithelial cells. *Appl. Environ. Microbiol.* 69, 2230–2236. doi: 10.1128/AEM.69.4.2230-2236.2003

Bagos, P. G., Nikolaou, E. P., Liakopoulos, T. D., and Tsirigos, K. D. (2010). Combined prediction of Tat and Sec signal peptides with Hidden Markov Models. *Bioinformatics* 26, 2811–2817. doi: 10.1093/bioinformatics/btq530

Bagos, P. G., Tsirigos, K. D., Liakopoulos, T. D., and Hamodrakas, S. J. (2008). Prediction of lipoprotein signal peptides in Gram-positive bacteria with a Hidden Markov Model. *J. Proteome Res.* 7, 5082–5093. doi: 10.1021/pr800162c.

Banik, J. J., and Brady, S. F. (2010). Recent application of metagenomic approaches toward the discovery of antimicrobials and other bioactive small molecules. *Curr. Opin. Microbiol.* 13, 603–609. doi: 10.1016/j.mib.2010.08.012

Barbas, C. F. III, Burton, D. R., Scott, J. K., and Silverman, G. J. (2001). *Phage display: a laboratory manual. Cold Spring Harbor*. New York, NY: Cold Spring Harbor Laboratory Press.

Bayer, E. A., Belaich, J. -P., Shoham, Y., and Lamed, R. (2004). The cellulosomes: multienzyme machines for degradation of plant cell wall polysaccharides. *Annu. Rev. Microbiol.* 58, 521–554. doi: 10.1146/annurev.micro.57.030502.091022

Beckmann, C., Waggoner, J. D., Harris, T. O., Tamura, G. S., and Rubens, C. E. (2002). Identification of novel adhesins from Group B streptococci by use of phage display reveals that C5a peptidase mediates fibronectin binding. *Infect. Immun.* 70, 2869–2876. doi: 10.1128/IAI.70.6.2869-2876.2002

Beckwith, J. (2013). The Sec-dependent pathway. *Res. Microbiol.* 164, 497–504. doi: 10.1016/j.resmic.2013.03.007

Beghetto, E., and Gargano, N. (2011). Lambda-display: a powerful tool for antigen discovery. *Molecules* 16, 3089–3105. doi: 10.3390/molecules16043089

Belanche, A., De La Fuente, G., and Newbold, C. J. (2014). Study of methanogen communities associated with different rumen protozoal populations. *FEMS Microbiol. Ecol.* 90, 663–677. doi: 10.1111/1574-6941.12423.

Bendtsen, J. D., Kiemer, L., Fausbøll, A., and Brunak, S. (2005). Non-classical protein secretion in bacteria. *BMC Microbiol.* 5:58. doi: 10.1186/1471-2180-5-58

Benedek, O., Khan, A. S., Schneider, G., Nagy, G., Autar, R., Pieters, R. J., et al. (2005). Identification of laminin-binding motifs of *Yersinia pestis*

plasminogen activator by phage display. *Int. J. Med. Microbiol.* 295, 87–98. doi: 10.1016/j.ijmm.2005.02.002

Bernard, J. M., and Francis, M. B. (2014). Chemical strategies for the covalent modification of filamentous phage. *Front. Microbiol.* 5:734. doi: 10.3389/fmicb.2014.00734

Bjerketorp, J., Nilsson, M., Ljungh, Å., Flock, J.-I., Jacobsson, K., and Frykberg, L. (2002). A novel von Willebrand factor binding protein expressed by *Staphylococcus aureus*. *Microbiology* 148, 2037–2044.

Bjerketorp, J., Rosander, A., Nilsson, M., Jacobsson, K., and Frykberg, L. (2004). Sorting a *Staphylococcus aureus* phage display library against ex vivo biomaterial. *J. Med. Microbiol.* 53, 945–951. doi: 10.1099/jmm.0.45638-0

Blobel, G., and Sabatini, D. D. (1971). "Ribosome-membrane interaction in eukaryotic cells," in *Biomembranes*, ed. Hanson (Berlin: Springer), 193–195.

Branston, S. D., Stanley, E. C., Ward, J. M., and Keshavarz-Moore, E. (2013). Determination of the survival of bacteriophage M13 from chemical and physical challenges to assist in its sustainable bioprocessing. *Biotechnol. Bioproc. E* 18, 560–566. doi: 10.1007/s12257-012-0776–779

Bratkovic, T. (2010). Progress in phage display: evolution of the technique and its application. *Cell Mol. Life. Sci.* 67, 749–767. doi: 10.1007/s00018-009-0192-2

Caccia, D., Dugo, M., and Callari, M. (2013). Bioinformatics tools for secretome analysis. *Biochim. Biophys. Acta* 1834, 2442–2453. doi: 10.1016/j.bbapap.2013.01.039

Celik, E., Fisher, A. C., Guarino, C., Mansell, T. J., and Delisa, M. P. (2010). A filamentous phage display system for N-linked glycoproteins. *Protein Sci.* 19, 2006–2013. doi: 10.1002/pro.472

Chagnot, C., Zorgani, M. A., Astruc, T., and Desvaux, M. (2013). Proteinaceous determinants of surface colonization in bacteria: bacterial adhesion and biofilm formation from a protein secretion perspective. *Front. Microbiol.* 4:303. doi: 10.3389/fmicb.2013.00303

Chang, C. N., Blobel, G., and Model, P. (1978). Detection of prokaryotic signal peptidase in an *Escherichia coli* membrane fraction: endoproteolytic cleavage of nascent f1 pre-coat protein. *Proc. Natl. Acad. Sci. U.S.A.* 75, 361–365. doi: 10.1073/pnas.75.1.361

Charlop-Powers, Z., Banik, J. J., Owen, J. G., Craig, J. W., and Brady, S. F. (2012). Selective enrichment of environmental DNA libraries for genes encoding nonribosomal peptides and polyketides by phosphopantetheine transferase-dependent complementation of siderophore biosynthesis. *ACS Chem. Biol.* 8, 138–143. doi: 10.1021/cb3004918

Charlop-Powers, Z., Milshteyn, A., and Brady, S. F. (2014). Metagenomic small molecule discovery methods. *Curr. Opin. Microbiol.* 19, 70–75. doi: 10.1016/j.mib.2014.05.021

Chen, W., and Georgiou, G. (2002). Cell-surface display of heterologous proteins: from high-throughput screening to environmental applications. *Biotechnol. Bioeng.* 79, 496–503. doi: 10.1002/bit.10407

Chen, Y., and Murrell, J. C. (2010). When metagenomics meets stable-isotope probing: progress and perspectives. *Trends Microbiol.* 18, 157–163. doi: 10.1016/j.tim.2010.02.002

Ching, A. T., Favaro, R. D., Lima, S. S., Chaves Ade, A., De Lima, M. A., Nader, H. B., et al. (2012). Leptospira interrogans shotgun phage display identified LigB as a heparin-binding protein. *Biochem. Biophys. Res. Commun.* 427, 774–779. doi: 10.1016/j.bbrc.2012.09.137

Choo, K. H., Tan, T. W., and Ranganathan, S. (2009). A comprehensive assessment of N-terminal signal peptides prediction methods. *BMC Bioinform.* 10:S2. doi: 10.1186/1471-2105-10-S15-S2

Ciric, M. (2014). *Metasecretome Phage Display : a New Approach for Mining Surface and Secreted Proteins from Microbial Communities,* Ph.D. thesis, Massey University, Palmerston North.

Ciric, M., Moon, C. D., Leahy, S. C., Creevey, C. J., Altermann, E., Attwood, G. T., et al. (2014). Metasecretome-selective phage display approach for mining the functional potential of a rumen microbial community. *BMC Genomics* 15:356. doi: 10.1186/1471-2164-15–356.

Coburn, J., Leong, J., and Chaconas, G. (2013). Illuminating the roles of the *Borrelia burgdorferi* adhesins. *Trends Microbiol.* 21, 372–379. doi: 10.1016/j.tim.2013.06.005

Cowan, D., Meyer, Q., Stafford, W., Muyanga, S., Cameron, R., and Wittwer, P. (2005). Metagenomic gene discovery: past, present and future. *Trends Biotechnol.* 23, 321–329. doi: 10.1016/j.tibtech.2005.04.001

Crissman, J. W., and Smith, G. P. (1984). Gene-III protein of filamentous phages: evidence for a carboxyl-terminal domain with a role in morphogenesis. *Virology* 132, 445–455. doi: 10.1016/0042-6822(84)90049-7

Culligan, E. P., Sleator, R. D., Marchesi, J. R., and Hill, C. (2013). Metagenomics and novel gene discovery: promise and potential for novel therapeutics. *Virulence* 5, 399–412. doi: 10.4161/viru.27208

Dalbey, R. E., and Kuhn, A. (2012). Protein traffic in Gram-negative bacteria: how exported and secreted proteins find their way. *FEMS Microbiol. Rev.* 36, 1023–1045. doi: 10.1111/j.1574-6976.2012.00327.x

Dalbey, R. E., Wang, P., and Van Dijl, J. M. (2012). Membrane proteases in the bacterial protein secretion and quality control pathway. *Microbiol. Mol. Biol. Rev.* 76, 311–330. doi: 10.1128/MMBR.05019-11

Day, L. A. (2011). "Family Inoviridae," in *Virus Taxonomy: Classification and Nomenclature of Viruses: Ninth Report of the International Committee on Taxonomy of Viruses*, eds A. M. Q. King, M. J. Adams, E. B. Carstens and E. J. Lefkowitz (San Diego: Elsevier Academic Press), 375–384.

Derda, R., Tang, S. K., Li, S. C., Ng, S., Matochko, W., and Jafari, M. R. (2011). Diversity of phage-displayed libraries of peptides during panning and amplification. *Molecules* 16, 1776–1803. doi: 10.3390/molecules16021776

Desvaux, M., Dumas, E., Chafsey, I., and Hebraud, M. (2006). Protein cell surface display in Gram-positive bacteria: from single protein to macromolecular protein structure. *FEMS Microbiol. Lett.* 256, 1–15. doi: 10.1111/j.1574-6968.2006.00122.x

Desvaux, M., Hébraud, M., Talon, R., and Henderson, I. R. (2009). Secretion and subcellular localizations of bacterial proteins: a semantic awareness issue. *Trends Microbiol.* 17, 139–145. doi: 10.1016/j.tim.2009.01.004

Di Niro, R., Sulic, A. M., Mignone, F., D'angelo, S., Bordoni, R., Iacono, M., et al. (2010). Rapid interactome profiling by massive sequencing. *Nucleic Acids Res.* 38:e110. doi: 10.1093/nar/gkq052

Dias-Neto, E., Nunes, D. N., Giordano, R. J., Sun, J., Botz, G. H., Yang, K., et al. (2009). Next-generation phage display: integrating and comparing available molecular tools to enable cost-effective high-throughput analysis. *PLoS ONE* 4:e8338. doi: 10.1371/journal.pone.0008338

Driessen, A. J., and Nouwen, N. (2008). Protein translocation across the bacterial cytoplasmic membrane. *Annu. Rev. Biochem.* 77, 643–667. doi: 10.1146/annurev.biochem.77.061606.160747

Dürr, C., Nothaft, H., Lizak, C., Glockshuber, R., and Aebi, M. (2010). The *Escherichia coli* glycophage display system. *Glycobiology* 20, 1366–1372. doi: 10.1093/glycob/cwq102

Ekkers, D. M., Cretoiu, M. S., Kielak, A. M., and Van Elsas, J. D. (2012). The great screen anomaly—a new frontier in product discovery through functional metagenomics. *Appl. Microbiol. Biotechnol.* 93, 1005–1020. doi: 10.1007/s00253-011-3804-3

Emanuelsson, O., Nielsen, H., Brunak, S., and Von Heijne, G. (2000). Predicting subcellular localization of proteins based on their N-terminal amino acid sequence. *J. Mol. Biol.* 300, 1005–1016. doi: 10.1006/jmbi.2000.3903

Evangelista, K., Franco, R., Schwab, A., and Coburn, J. (2014). Leptospira interrogans binds to cadherins. *PLoS Negl. Trop Dis.* 8:e2672. doi: 10.1371/journal.pntd.0002672

Evangelista, K. V., Hahn, B., Wunder, E. A. Jr., Ko, A. I., Haake, D. A., and Coburn, J. (2014). Identification of cell-binding adhesins of *Leptospira interrogans*. *PLoS Negl. Trop. Dis.* 8:e3215. doi: 10.1371/journal.pntd.0003215

Feng, J. N., Russel, M., and Model, P. (1997). A permeabilized cell system that assembles filamentous bacteriophage. *Proc. Natl. Acad. Sci. U.S.A.* 94, 4068–4073. doi: 10.1073/pnas.94.8.4068

Fevre, C., Bestebroer, J., Mebius, M. M., De Haas, C. J. C., Van Strijp, J. A. G., Fitzgerald, J. R., et al. (2014). *Staphylococcus aureus* proteins SSL6 and SElX interact with neutrophil receptors as identified using secretome phage display. *Cell Microbiol.* 16, 1646–1665. doi: 10.1111/cmi.12313

Fichot, E. B., and Norman, R. S. (2013). Microbial phylogenetic profiling with the Pacific Biosciences sequencing platform. *Microbiome* 1:10. doi: 10.1186/2049-2618-1–10

Francetic, O., Buddelmeijer, N., Lewenza, S., Kumamoto, C. A., and Pugsley, A. P. (2007). Signal recognition particle-dependent inner membrane targeting of the PulG pseudopilin component of a type II secretion system. *J. Bacteriol.* 189, 1783–1793. doi: 10.1128/JB.01230-06

Freudl, R. (2013). Leaving home ain't easy: protein export systems in Gram-positive bacteria. *Res. Microbiol.* 164, 664–674.

Gagic, D., Maclean, P. H., Li, D., Attwood, G. T., and Moon, C. D. (2015). Improving the genetic representation of rare taxa within complex microbial communities using DNA normalization methods. *Mol. Ecol. Resour.* 15, 464–476. doi: 10.1111/1755-0998.12321

Gagic, D., Wen, W., Collett, M. A., and Rakonjac, J. (2013). Unique secreted-surface protein complex of *Lactobacillus rhamnosus*, identified by phage display. *Microbiologyopen* 2, 1–17. doi: 10.1002/mbo3.53

Galbraith, E. A., Antonopoulos, D. A., and White, B. A. (2004). Suppressive subtractive hybridization as a tool for identifying genetic diversity in an environmental metagenome: the rumen as a model. *Environ. Microbiol.* 6, 928–937. doi: 10.1111/j.1462-2920.2004.00575.x

Gamkrelidze, M., and Dabrowska, K. (2014). T4 bacteriophage as a phage display platform. *Arch. Microbiol.* 196, 473–479. doi: 10.1007/s00203-014-0989–988

Georgiou, G., Stathopoulos, C., Daugherty, P. S., Nayak, A. R., Iverson, B. L., and Curtiss, R. III (1997). Display of heterologous proteins on the surface of microorganisms: from the screening of combinatorial libraries to live recombinant vaccines. *Nat. Biotechnol.* 15, 29–34. doi: 10.1038/nbt0197-29

Goudenège, D., Avner, S., Lucchetti-Miganeh, C., and Barloy-Hubler, F. (2010). CoBaltDB: complete bacterial and archaeal orfeomes subcellular localization database and associated resources. *BMC Microbiol.* 10:88. doi: 10.1186/1471-2180-10-88

Griffiths, A. D., Malmqvist, M., Marks, J. D., Bye, J. M., Embleton, M. J., Mccafferty, J., et al. (1993). Human anti-self antibodies with high specificity from phage display libraries. *EMBO J.* 12, 725–734.

Gunnarsen, K. S., Kristinsson, S. G., Justesen, S., Frigstad, T., Buus, S., Bogen, B., et al. (2013). Chaperone-assisted thermostability engineering of a soluble T cell receptor using phage display. *Sci. Rep.* 3:1162. doi: 10.1038/srep01162

Handelsman, J. (2004). Metagenomics: application of genomics to uncultured microorganisms. *Microbiol. Mol. Biol. Rev.* 68, 669–685. doi: 10.1128/MMBR.68.4.669-685.2004.

Hayhurst, A., and Harris, W. J. (1999). *Escherichia coli* skp chaperone coexpression improves solubility and phage display of single-chain antibody fragments. *Protein Expr. Purif.* 15, 336–343. doi: 10.1006/prep.1999.1035

He, Z., Deng, Y., Van Nostrand, J. D., Tu, Q., Xu, M., Hemme, C. L., et al. (2010). GeoChip 3.0 as a high-throughput tool for analyzing microbial community composition, structure and functional activity. *ISME J.* 4, 1167–1179. doi: 10.1038/ismej.2010.46

He, Z., Gentry, T. J., Schadt, C. W., Wu, L., Liebich, J., Chong, S. C., et al. (2007). GeoChip: a comprehensive microarray for investigating biogeochemical, ecological and environmental processes. *ISME J.* 1, 67–77. doi: 10.1038/ismej.2007.2

Heilmann, C., Herrmann, M., Kehrel, B. E., and Peters, G. (2002). Platelet-binding domains in 2 fibrinogen-binding proteins of *Staphylococcus aureus* identified by phage display. *J. Infect. Dis.* 186, 32–39. doi: 10.1086/341081

Hess, M., Sczyrba, A., Egan, R., Kim, T. W., Chokhawala, H., Schroth, G., et al. (2011). Metagenomic discovery of biomass-degrading genes and genomes from cow rumen. *Science* 331, 463–467. doi: 10.1126/science.1200387

Hoogenboom, H. R., Griffiths, A. D., Johnson, K. S., Chiswell, D. J., Hudson, P., and Winter, G. (1991). Multi-subunit proteins on the surface of filamentous phage: methodologies for displaying antibody (Fab) heavy and light chains. *Nucleic Acids Res.* 19, 4133–4137. doi: 10.1093/nar/19.15.4133

Hust, M., and Dubel, S. (2004). Mating antibody phage display with proteomics. *Trends Biotechnol.* 22, 8–14. doi: 10.1016/j.tibtech.2003.10.011

Imam, S., Chen, Z., Roos, D. S., and Pohlschröder, M. (2011). Identification of surprisingly diverse type IV pili, across a broad range of Gram-positive bacteria. *PLoS ONE* 6:e28919. doi: 10.1371/journal.pone.0028919

Ingham, K. C., Brew, S., Vaz, D., Sauder, D. N., and McGavin, M. J. (2004). Interaction of *Staphylococcus aureus* fibronectin-binding protein with fibronectin: affinity, stoichiometry, and modular requirements. *J. Biol. Chem.* 279, 42945–42953. doi: 10.1074/jbc.M406984200

Jacobsson, K., and Frykberg, L. (1995). Cloning of ligand-binding domains of bacterial receptors by phage display. *Biotechniques* 18, 878–885.

Jacobsson, K., and Frykberg, L. (1996). Phage display shot-gun cloning of ligand-binding domains of prokaryotic receptors approaches 100% correct clones. *Biotechniques* 20, 1080–1071.

Jacobsson, K., Rosander, A., Bjerketorp, J., and Frykberg, L. (2003). Shotgun phage display - selection for bacterial receptins or other exported proteins. *Biol. Proced.* 5, 123–135. doi: 10.1251/bpo54

Jankovic, D., Collett, M. A., Lubbers, M. W., and Rakonjac, J. (2007). Direct selection and phage display of a Gram-positive secretome. *Genome Biol.* 8:R266. doi: 10.1186/gb-2007-8-12-r266

Jönsson, K., Guo, B. P., Monstein, H. J., Mekalanos, J. J., and Kronvall, G. (2004). Molecular cloning and characterization of two *Helicobacter pylori* genes coding for plasminogen-binding proteins. *Proc. Natl. Acad. Sci. U.S.A.* 101, 1852–1857. doi: 10.1073/pnas.0307329101

Joo, H. Y., Hur, B. U., Lee, K. W., Song, S. Y., and Cha, S. H. (2008). Establishment of a reliable dual-vector system for the phage display of antibody fragments. *J. Immunol. Methods* 333, 24–37. doi: 10.1016/j.jim.2007.11.015

Juncker, A. S., Willenbrock, H., Von Heijne, G., Brunak, S., Nielsen, H., and Krogh, A. (2003). Prediction of lipoprotein signal peptides in Gram-negative bacteria. *Protein Sci.* 12, 1652–1662. doi: 10.1110/ps.0303703

Kehoe, J. W., and Kay, B. K. (2005). Filamentous phage display in the new millennium. *Chem. Rev.* 105, 4056–4072. doi: 10.1021/cr000261r

Krogh, A., Larsson, B., Von Heijne, G., and Sonnhammer, E. L. (2001). Predicting transmembrane protein topology with a hidden Markov model: application to complete genomes. *J. Mol. Biol.* 305, 567–580. doi: 10.1006/jmbi.2000.4315

Krumpe, L. R. H., Atkinson, A. J., Smythers, G. W., Kandel, A., Schumacher, K. M., Mcmahon, J. B., et al. (2006). T7 lytic phage-displayed peptide libraries exhibit less sequence bias than M13 filamentous phage-displayed peptide libraries. *Proteomics* 6, 4210–4222. doi: 10.1002/pmic.200500606

Kudva, R., Denks, K., Kuhn, P., Vogt, A., Müller, M., and Koch, H. -G. (2013). Protein translocation across the inner membrane of Gram-negative bacteria: the Sec and Tat dependent protein transport pathways. *Res. Microbiol.* 164, 505–534. doi: 10.1016/j.resmic.2013.03.016

Lamboy, J. A., Tam, P. Y., Lee, L. S., Jackson, P. J., Avrantinis, S. K., Lee, H. J., et al. (2008). Chemical and genetic wrappers for improved phage and RNA display. *Chembiochem* 9, 2846–2852. doi: 10.1002/cbic.200800366

Lauterbach, S. B., Lanzillotti, R., and Coetzer, T. L. (2003). Construction and use of *Plasmodium falciparum* phage display libraries to identify host parasite interactions. *Malar. J.* 2:47. doi: 10.1186/1475-2875-2–47.

Leahy, S. C., Kelly, W. J., Altermann, E., Ronimus, R. S., Yeoman, C. J., Pacheco, D. M., et al. (2010). The genome sequence of the rumen methanogen *Methanobrevibacter ruminantium* reveals new possibilities for controlling ruminant methane emissions. *PLoS ONE* 5:e8926. doi: 10.1371/journal.pone.0008926

Lee, S. Y., Choi, J. H., and Xu, Z. (2003). Microbial cell-surface display. *Trends Biotechnol.* 21, 45–52. doi: 10.1016/S0167-7799(02)00006-9

Lei, S. P., Lin, H. C., Wang, S. S., Callaway, J., and Wilcox, G. (1987). Characterization of the Erwinia carotovora pelB gene and its product pectate lyase. *J. Bacteriol.* 169, 4379–4383.

Lindmark, H., and Guss, B. (1999). SFS, a novel fibronectin-binding protein from *Streptococcus equi*, inhibits the binding between fibronectin and collagen. *Infect. Immun.* 67, 2383–2388.

Liu, R., Yang, C., Xu, Y., Xu, P., Jiang, H., and Qiao, C. (2013). Development of a whole-cell biocatalyst/biosensor by display of multiple heterologous proteins on the *Escherichia coli* cell surface for the detoxification and detection of organophosphates. *J. Agric. Food Chem.* 61, 7810–7816. doi: 10.1021/jf4 02999b

Liu, S., Han, W., Sun, C., Lei, L., Feng, X., Yan, S., et al. (2011). Subtractive screening with the *Mycobacterium tuberculosis* surface protein phage display library. *Tuberculosis* 91, 579–586. doi: 10.1016/j.tube.2011.07.007

Lubkowski, J., Hennecke, F., Pluckthun, A., and Wlodawer, A. (1998). The structural basis of phage display elucidated by the crystal structure of the N-terminal domains of g3p. *Nat. Struct. Biol.* 5, 140–147. doi: 10.1038/nsb0298-140

Lüke, I., Handford, J. I., Palmer, T., and Sargent, F. (2009). Proteolytic processing of *Escherichia coli* twin-arginine signal peptides by LepB. *Arch. Microbiol.* 191, 919–925. doi: 10.1007/s00203-009-0516-5

Luo, C., Tsementzi, D., Kyrpides, N. C., and Konstantinidis, K. T. (2011). Individual genome assembly from complex community short-read metagenomic datasets. *ISME J.* 6, 898–901. doi: 10.1038/ismej.2011.147

Lycklama, A., Nijeholt, J. A., and Driessen, A. J. (2012). The bacterial Sec-translocase: structure and mechanism. *Philos. Trans. R. Soc. Lond. B Biol. Sci.* 367, 1016–1028. doi: 10.1098/rstb.2011.0201

Mai-Prochnow, A., Hui, J. G., Kjelleberg, S., Rakonjac, J., Mcdougald, D., and Rice, S. A. (2015). 'Big things in small packages: the genetics of filamentous phage

and effects on fitness of their host'. *FEMS Microbiol. Rev.* 39, 465–487. doi: 10.1093/femsre/fuu007

Mao, C., Solis, D. J., Reiss, B. D., Kottmann, S. T., Sweeney, R. Y., Hayhurst, A., et al. (2004). Virus-based toolkit for the directed synthesis of magnetic and semiconducting nanowires. *Science* 303, 213–217. doi: 10.1126/science.1092740

Marvin, D. A., Symmons, M. F., and Straus, S. K. (2014). Structure and assembly of filamentous bacteriophages. *Prog. Biophys. Mol. Biol.* 114, 80–122. doi: 10.1016/j.pbiomolbio.2014.02.003

Marvin, D. A., Welsh, L. C., Symmons, M. F., Scott, W. R., and Straus, S. K. (2006). Molecular structure of fd (f1, M13) filamentous bacteriophage refined with respect to X-ray fibre diffraction and solid-state NMR data supports specific models of phage assembly at the bacterial membrane. *J. Mol. Biol.* 355, 294–309. doi: 10.1016/j.jmb.2005.10.048

Mazard, S., and Schäfer, H. (2014). Stable isotope probing to study functional components of complex microbial ecosystems. *Methods Mol. Biol.* 668, 169–180.

Meiring, T., Mulako, I., Tuffin, M. I., Meyer, Q., and Cowan, D. A. (2010). Retrieval of full-length functional genes using subtractive hybridization magnetic bead capture. *Methods Mol. Biol.* 668, 287–297.

Meyer, Q. C., Burton, S. G., and Cowan, D. A. (2007). Subtractive hybridization magnetic bead capture: a new technique for the recovery of full-length ORFs from the metagenome. *Biotechnol. J.* 2, 36–40. doi: 10.1002/biot.200600156

Meyer, T., Schirrmann, T., Frenzel, A., Miethe, S., Stratmann-Selke, J., Gerlach, G. F., et al. (2012). Identification of immunogenic proteins and generation of antibodies against *Salmonella* Typhimurium using phage display. *BMC Biotechnol.* 12:29. doi: 10.1186/1472-6750-12-29

Mullen, L. M., Nair, S. P., Ward, J. M., Rycroft, A. N., and Henderson, B. (2006). Phage display in the study of infectious diseases. *Trends Microbiol.* 14, 141–147. doi: 10.1016/j.tim.2006.01.006

Mullen, L. M., Nair, S. P., Ward, J. M., Rycroft, A. N., Williams, R. J., and Henderson, B. (2007). Comparative functional genomic analysis of Pasteurellaceae adhesins using phage display. *Vet. Microbiol.* 122, 123–134. doi: 10.1016/j.vetmic.2006.12.022

Munoz-Provencio, D., and Monedero, V. (2011). Shotgun phage display of *Lactobacillus casei* BL23 against collagen and fibronectin. *J. Microbiol. Biotechnol.* 21, 197–203. doi: 10.4014/jmb.1009.09011

Natale, P., Brüser, T., and Driessen, A. J. (2008). Sec- and Tat- mediated protein secretion across the bacterial cytoplasmic membrane-distinct translocases and mechanisms. *Biochim. Biophys. Acta* 1778, 1735–1756. doi: 10.1016/j.bbamem.2007.07.015

Nilsson, M., Frykberg, L., Flock, J. I., Pei, L., Lindberg, M., and Guss, B. (1998). A fibrinogen-binding protein of *Staphylococcus epidermidis*. *Infect. Immun.* 66, 2666–2673.

Nilsson, M., Bjerketorp, J., Guss, B., and Frykberg, L. (2004a). A fibrinogen-binding protein of *Staphylococcus lugdunensis*. *FEMS Microbiol. Lett.* 241, 87–93. doi: 10.1016/j.femsle.2004.10.008

Nilsson, M., Bjerketorp, J., Wiebensjö, A., Ljungh, A., Frykberg, L., and Guss, B. (2004b). A von Willebrand factor-binding protein from *Staphylococcus lugdunensis*. *FEMS Microbiol. Lett.* 234, 155–161. doi: 10.1111/j.1574-6968.2004.tb09527.x

Ng, F., Kittelmann, S., Patchett, M. L., Attwood, G. T., Janssen, P. H., Rakonjac, J., et al. (2015). An adhesin from hydrogen-utilizing rumen methanogen *Methanobrevibacter ruminantium* M1 binds a broad range of hydrogen-producing microorganisms. *Environ. Microbiol.* doi: 10.1111/1462-2920.13155 [Epub ahead of print].

Ng, S., Tjhung, K. F., Paschal, B. M., Noren, C. J., and Derda, R. (2015). Chemical posttranslational modification of phage-displayed peptides. *Methods Mol. Biol.* 1248, 155–172. doi: 10.1007/978-1-4939-2020-4_11

Okuda, S., and Tokuda, H. (2011). Lipoprotein sorting in bacteria. *Annu. Rev. Microbiol.* 65, 239–259. doi: 10.1146/annurev-micro-090110-102859

Owen, J. G., Reddy, B. V. B., Ternei, M. A., Charlop-Powers, Z., Calle, P. Y., Kim, J. H., et al. (2013). Mapping gene clusters within arrayed metagenomic libraries to expand the structural diversity of biomedically relevant natural products. *Proc. Natl. Acad. Sci. U.S.A.* 110, 11797–11802. doi: 10.1073/pnas.1222159110

Park, S. J., Kang, C. H., Chae, J. C., and Rhee, S. K. (2008). Metagenome microarray for screening of fosmid clones containing specific genes. *FEMS Microbiol. Lett.* 284, 28–34. doi: 10.1111/j.1574-6968.2008.01180.x

Parmley, S. F., and Smith, G. P. (1988). Antibody-selectable filamentous fd phage vectors: affinity purification of target genes. *Gene* 73, 305–318. doi: 10.1016/0378-1119(88)90495-7

Peabody, C. R., Chung, Y. J., Yen, M.-R., Vidal-Ingigliardi, D., Pugsley, A. P., and Saier, M. H. (2003). Type II protein secretion and its relationship to bacterial type IV pili and archaeal flagella. *Microbiology* 149, 3051–3072. doi: 10.1099/mic.0.26364-0

Petersen, T. N., Brunak, S., Von Heijne, G., and Nielsen, H. (2011). SignalP 4.0: discriminating signal peptides from transmembrane regions. *Nat. Methods* 8, 785–786. doi: 10.1038/nmeth.1701

Ploss, M., Facey, S. J., Bruhn, C., Zemel, L., Hofmann, K., Stark, R. W., et al. (2014). Selection of peptides binding to metallic borides by screening M13 phage display libraries. *BMC Biotechnol.* 14:12. doi: 10.1186/1472-6750-14-12

Posadas, D. M., Ruiz-Ranwez, V., Bonomi, H. R., Martin, F. A., and Zorreguieta, A. (2012). BmaC, a novel autotransporter of *Brucella suis,* is involved in bacterial adhesion to host cells. *Cell Microbiol.* 14, 965–982. doi: 10.1111/j.1462-5822.2012.01771.x

Rahman, O., Cummings, S. P., Harrington, D. J., and Sutcliffe, I. C. (2008). Methods for the bioinformatic identification of bacterial lipoproteins encoded in the genomes of Gram-positive bacteria. *World J. Microbiol. Biotechnol.* 24, 2377–2382. doi: 10.1007/s11274-008-9795-2

Rakonjac, J., Bennett, N. J., Spagnuolo, J., Gagic, D., and Russel, M. (2011). Filamentous bacteriophage: biology, phage display and nanotechnology applications. *Curr. Issues Mol. Biol.* 13, 51–76.

Rakonjac, J., Feng, J., and Model, P. (1999). Filamentous phage are released from the bacterial membrane by a two-step mechanism involving a short C-terminal fragment of pIII. *J. Mol. Biol.* 289, 1253–1265. doi: 10.1006/jmbi.1999.2851

Rakonjac, J., Jovanovic, G., and Model, P. (1997). Filamentous phage infection-mediated gene expression: construction and propagation of the gIII deletion mutant helper phage R408d3. *Gene* 198, 99–103. doi: 10.1016/S0378-1119(97)00298-9

Rakonjac, J., and Model, P. (1998). Roles of pIII in filamentous phage assembly. *J. Mol. Biol.* 282, 25–41. doi: 10.1006/jmbi.1998.2006

Ravn, U., Gueneau, F., Baerlocher, L., Osteras, M., Desmurs, M., Malinge, P., et al. (2010). By-passing in vitro screening—next generation sequencing technologies applied to antibody display and in silico candidate selection. *Nucleic Acids Res.* 38:e193. doi: 10.1093/nar/gkq789

Reddy, S. T., Ge, X., Miklos, A. E., Hughes, R. A., Kang, S. H., Hoi, K. H., et al. (2010). Monoclonal antibodies isolated without screening by analyzing the variable-gene repertoire of plasma cells. *Nat. Biotechnol.* 28, 965–969. doi: 10.1038/nbt.1673

Rodi, D. J., and Makowski, L. (1999). Phage-display technology–finding a needle in a vast molecular haystack. *Curr. Opin. Biotechnol.* 10, 87–93. doi: 10.1016/S0958-1669(99)80016-0

Rosander, A., Bjerketorp, J., Frykberg, L., and Jacobsson, K. (2002). Phage display as a novel screening method to identify extracellular proteins. *J. Microbiol. Methods* 51, 43–55. doi: 10.1016/S0167-7012(02)00052-0

Rosander, A., Guss, B., Frykberg, L., Bjorkman, C., Naslund, K., and Pringle, M. (2011). Identification of immunogenic proteins in Treponema phagedenis-like strain V1 from digital dermatitis lesions by phage display. *Vet. Microbiol.* 153, 315–322. doi: 10.1016/j.vetmic.2011.06.005

Rusch, S. L., and Kendall, D. A. (2007). Interactions that drive Sec-dependent bacterial protein transport. *Biochemistry* 46, 9665–9673. doi: 10.1021/bi7010064

Russel, M., Lowman, H. B., and Clackson, T. (2004). "Introduction to phage biology and phage display," in *Practical Approach to Phage Display*, eds T. Clackson and H. B. Lowman (New York, NY: Oxford University Press Inc), 1–26.

Russel, M., and Model, P. (2006). "Filamentous phage," in *The Bacteriophages,* 2nd Edn. ed. R. C. Calendar (New York, NY: Oxford University Press Inc), 146–160.

Saggy, I., Wine, Y., Shefet-Carasso, L., Nahary, L., Georgiou, G., and Benhar, I. (2012). Antibody isolation from immunized animals: comparison of phage display and antibody discovery via V gene repertoire mining. *Protein Eng. Des. Sel.* 25, 539–549. doi: 10.1093/protein/gzs060

Samuelson, J. C., Chen, M., Jiang, F., Moller, I., Wiedmann, M., Kuhn, A., et al. (2000). YidC mediates membrane protein insertion in bacteria. *Nature* 406, 637–641. doi: 10.1038/35020586

Schier, R., Bye, J., Apell, G., Mccall, A., Adams, G. P., Malmqvist, M., et al. (1996). Isolation of high-affinity monomeric human anti-c-erbB-2 single chain Fv using affinity-driven selection. *J. Mol. Biol.* 255, 28–43. doi: 10.1006/jmbi.1996.0004

Shallom, D., and Shoham, Y. (2003). Microbial hemicellulases. *Curr. Opin. Biotechnol.* 6, 219–228.

Shkoporov, A. N., Khokhlova, E. V., Kafarskaia, L. I., Pavlov, K. A., Smeianov, V. V., Steele, J. L., et al. (2008). Search for protein adhesin gene in *Bifidobacterium longum* genome using surface phage display technology. *Bull. Exp. Biol. Med.* 146, 782–785. doi: 10.1007/s10517-009-0423-4

Speck, J., Arndt, K. M., and Muller, K. M. (2011). Efficient phage display of intracellularly folded proteins mediated by the TAT pathway. *Protein Eng. Des. Sel.* 24, 473–484. doi: 10.1093/protein/gzr001

Steiner, D., Forrer, P., and Pluckthun, A. (2008). Efficient selection of DARPins with sub-nanomolar affinities using SRP phage display. *J. Mol. Biol.* 382, 1211–1227. doi: 10.1016/j.jmb.2008.07.085

Szabo, Z., and Pohlschroder, M. (2012). Diversity and subcellular distribution of archaeal secreted proteins. *Front. Microbiol.* 3:207. doi: 10.3389/fmicb.2012.00207

t Hoen, P. A., Jirka, S. M., Ten Broeke, B. R., Schultes, E. A., Aguilera, B., Pang, K. H., et al. (2012). Phage display screening without repetitious selection rounds. *Analyt. Biochem.* 421, 622–631. doi: 10.1016/j.ab.2011.11.005

Thompson, B. J., Widdick, D. A., Hicks, M. G., Chandra, G., Sutcliffe, I. C., Palmer, T., et al. (2010). Investigating lipoprotein biogenesis and function in the model Gram-positive bacterium *Streptomyces coelicolor*. *Mol. Microbiol.* 77, 943–957. doi: 10.1111/j.1365-2958.2010.07261.x

Tian, F., Tsao, M. L., and Schultz, P. G. (2004). A phage display system with unnatural amino acids. *J. Am. Chem. Soc.* 126, 15962–15963. doi: 10.1021/ja045673m

Tjalsma, H., Antelmann, H., Jongbloed, J. D., Braun, P. G., Darmon, E., Dorenbos, R., et al. (2004). Proteomics of protein secretion by *Bacillus subtilis*: separating the "secrets" of the secretome. *Microbiol. Mol. Biol. Rev.* 68, 207–233. doi: 10.1128/MMBR.68.2.207-233.2004

Tjalsma, H., Bolhuis, A., Jongbloed, J. D., Bron, S., and Van Dijl, J. M. (2000). Signal peptide-dependent protein transport in *Bacillus subtilis*: a genome-based survey of the secretome. *Microbiol. Mol. Biol. Rev.* 64, 515–547. doi: 10.1128/MMBR.64.3.515-547.2000

Tjhung, K. F., Deiss, F., Tran, J., Chou, Y., and Derda, R. (2015). Intra-domain phage display (ID-PhD) of peptides and protein mini-domains censored from canonical pIII phage display. *Front. Microbiol.* 6:340. doi: 10.3389/fmicb.2015.00340

Tsukazaki, T., Mori, H., Echizen, Y., Ishitani, R., Fukai, S., Tanaka, T., et al. (2011). Structure and function of a membrane component SecDF that enhances protein export. *Nature* 474, 235–238. doi: 10.1038/nature09980

Tuffin, M., Anderson, D., Heath, C., and Cowan, D. A. (2009). Metagenomic gene discovery: how far have we moved into novel sequence space? *Biotechnol. J.* 4, 1671–1683. doi: 10.1002/biot.200900235

Ushida, K., Newbold, C. J., and Jouany, J.-P. (1997). Interspecies hydrogen transfer between the rumen ciliate *Polyplastron multivesiculatum* and *Methanosarcina barkeri*. *J. Gen. Appl. Microbiol.* 43, 129–131. doi: 10.2323/jgam.43.129

Van Gerven, N., Waksman, G., and Remaut, H. (2011). Pili and flagella biology, structure, and biotechnological applications. *Prog Mol. Biol. Transl. Sci.* 103, 21–72. doi: 10.1016/B978-0-12-415906-8.00005-4

Vasi, J., Frykberg, L., Carlsson, L. E., Lindberg, M., and Guss, B. (2000). M-like proteins of *Streptococcus dysgalactiae*. *Infect. Immun.* 68, 294–302. doi: 10.1128/IAI.68.1.294-302.2000

Vodnik, M., Zager, U., Strukelj, B., and Lunder, M. (2011). Phage display: selecting straws instead of a needle from a haystack. *Molecules* 16, 790–817. doi: 10.3390/molecules16010790

Wall, T., Roos, S., Jacobsson, K., Rosander, A., and Jonsson, H. (2003). Phage display reveals 52 novel extracellular and transmembrane proteins from *Lactobacillus reuteri* DSM 20016(T). *Microbiology* 149, 3493–3505. doi: 10.1099/mic.0.26530-0

Wallin, E., and Heijne, G. V. (1998). Genome-wide analysis of integral membrane proteins from eubacterial, archaean, and eukaryotic organisms. *Protein Sci.* 7, 1029–1038. doi: 10.1002/pro.5560070420

Walsh, C. (2000). Molecular mechanisms that confer antibacterial drug resistance. *Nature* 406, 775–781. doi: 10.1038/35021219

Wang, M., Beck, C. R., English, A. C., Meng, Q., Buhay, C., Han, Y., et al. (2015). PacBio-LITS: a large-insert targeted sequencing method for characterization of human disease-associated chromosomal structural variations. *BMC Genomics* 16:214. doi: 10.1186/s12864-015-1370-2

Wernérus, H., and Ståhl, S. (2004). Biotechnological applications for surface-engineered bacteria. *Biotechnol. Appl. Biochem.* 40, 209–228. doi: 10.1042/BA20040014

Williams, R. J., Henderson, B., and Nair, S. P. (2002a). *Staphylococcus aureus* fibronectin binding proteins A and B possess a second fibronectin binding region that may have biological relevance to bone tissues. *Calcif. Tissue Int.* 70, 416–421. doi: 10.1007/s00223-001-2073-z

Williams, R. J., Henderson, B., Sharp, L. J., and Nair, S. P. (2002b). Identification of a fibronectin-binding protein from *Staphylococcus epidermidis*. *Infect. Immun.* 70, 6805–6810. doi: 10.1128/IAI.70.12.6805-6810.2002

Wooldridge, K. (ed.). (2009). *Bacterial Secreted Proteins: Secretory Mechanisms and Role in Pathogenesis*. Norfolk: Caister Academic Press.

Xing, M. N., Zhang, X. Z., and Huang, H. (2012). Application of metagenomic techniques in mining enzymes from microbial communities for biofuel synthesis. *Biotechnol. Adv.* 30, 920–929. doi: 10.1016/j.biotechadv.2012.01.021

Yang, X.-Y., Lu, J., Sun, X., and He, Q.-Y. (2012). Application of subproteomics in the characterization of Gram-positive bacteria. *J. Proteomics* 75, ch2803–ch2810. doi: 10.1016/j.jprot.2011.12.027

Yen, M., and Yin, J. (2007). High-throughput profiling of posttranslational modification enzymes by phage display. *Biotechniques* 43, 31–33. doi: 10.2144/000112502

Yu, N. Y., Wagner, J. R., Laird, M. R., Melli, G., Rey, S., Lo, R., et al. (2010). PSORTb 3.0: improved protein subcellular localization prediction with refined localization subcategories and predictive capabilities for all prokaryotes. *Bioinformatics* 26, 1608–1615. doi: 10.1093/bioinformatics/btq249

Zacchi, P., Sblattero, D., Florian, F., Marzari, R., and Bradbury, A. R. (2003). Selecting open reading frames from DNA. *Genome Res.* 13, 980–990. doi: 10.1101/gr.861503

Zhang, K., He, J., Yang, M., Yen, M., and Yin, J. (2009). Identifying natural product biosynthetic genes from a soil metagenome by using T7 phage selection. *Chembiochem* 10, 2599–2606. doi: 10.1002/cbic.200900297

Zhou, M., Boekhorst, J., Francke, C., and Siezen, R. J. (2008). LocateP: genome-scale subcellular-location predictor for bacterial proteins. *BMC Bioinform.* 9:173. doi: 10.1186/1471-2105-9-173

Zhou, M., Theunissen, D., Wels, M., and Siezen, R. (2010). LAB-Secretome: a genome-scale comparative analysis of the predicted extracellular and surface-associated proteins of Lactic Acid Bacteria. *BMC Genomics* 11:651. doi: 10.1186/1471-2164-11-651

Zuber, B., Haenni, M., Ribeiro, T., Minnig, K., Lopes, F., Moreillon, P., et al. (2006). Granular layer in the periplasmic space of gram-positive bacteria and fine structures of *Enterococcus gallinarum* and *Streptococcus gordonii* septa revealed by cryo-electron microscopy of vitreous sections. *J. Bacteriol.* 188, 6652–6660. doi: 10.1128/JB.00391-06

Zwick, M. B., Shen, J., and Scott, J. K. (1998). Phage-displayed peptide libraries. *Curr. Opin. Biotechnol.* 9, 427–436. doi: 10.1016/S0958-1669(98)80017-7

**Conflict of Interest Statement:** The authors declare that the research was conducted in the absence of any commercial or financial relationships that could be construed as a potential conflict of interest.

frontiers in Microbiology

TECHNOLOGY REPORT
published: 28 April 2015
doi: 10.3389/fmicb.2015.00340

# Intra-domain phage display (ID-PhD) of peptides and protein mini-domains censored from canonical pIII phage display

*Katrina F. Tjhung, Frédérique Deiss, Jessica Tran, Ying Chou and Ratmir Derda* *

*Department of Chemistry, Alberta Glycomics Centre, University of Alberta, Edmonton, AB, Canada*

In this paper, we describe multivalent display of peptide and protein sequences typically censored from traditional N-terminal display on protein pIII of filamentous bacteriophage M13. Using site-directed mutagenesis of commercially available M13KE phage cloning vector, we introduced sites that permit efficient cloning using restriction enzymes between domains N1 and N2 of the pIII protein. As infectivity of phage is directly linked to the integrity of the connection between N1 and N2 domains, intra-domain phage display (ID-PhD) allows for simple quality control of the display and the natural variations in the displayed sequences. Additionally, direct linkage to phage propagation allows efficient monitoring of sequence cleavage, providing a convenient system for selection and evolution of protease-susceptible or protease-resistant sequences. As an example of the benefits of such an ID-PhD system, we displayed a negatively charged FLAG sequence, which is known to be post-translationally excised from pIII when displayed on the N-terminus, as well as positively charged sequences which suppress production of phage when displayed on the N-terminus. ID-PhD of FLAG exhibited sub-nanomolar apparent $K_d$ suggesting multivalent nature of the display. A TEV-protease recognition sequence (TEVrs) co-expressed in tandem with FLAG, allowed us to demonstrate that 99.9997% of the phage displayed the FLAG-TEVrs tandem and can be recognized and cleaved by TEV-protease. The residual 0.0003% consisted of phage clones that have excised the insert from their genome. ID-PhD is also amenable to display of protein mini-domains, such as the 33-residue minimized Z-domain of protein A. We show that it is thus possible to use ID-PhD for multivalent display and selection of mini-domain proteins (Affibodies, scFv, etc.).

**Keywords: M13 bacteriophage, phage display, protein engineering, *in vitro* selection, excised peptide**

OPEN ACCESS

***Edited by:***
*Jasna Rakonjac,*
*Massey University, New Zealand*

***Reviewed by:***
*Yoshitaka Sato,*
*Nagoya University Graduate School of Medicine, Japan*
*Brian K. Kay,*
*University of Illinois at Chicago, USA*

***Correspondence:**
*Ratmir Derda,*
*Department of Chemistry, University of Alberta, 1127 Saskatchewan Drive, Edmonton AB T6G 2G2, Canada*
*ratmir.derda@ualberta.ca*

***Specialty section:***
*This article was submitted to Virology, a section of the journal Frontiers in Microbiology*

***Received:*** *19 December 2014*
***Accepted:*** *06 April 2015*
***Published:*** *28 April 2015*

***Citation:***
*Tjhung KF, Deiss F, Tran J, Chou Y and Derda R (2015) Intra-domain phage display (ID-PhD) of peptides and protein mini-domains censored from canonical pIII phage display. Front. Microbiol. 6:340. doi: 10.3389/fmicb.2015.00340*

## Introduction

Phage display (PhD) is a powerful method for selection of peptide ligands from a diverse, random population (McCafferty et al., 1990, 1991; Scott and Smith, 1990). The diversity and uniformity of the phage-libraries are important for selection and can impact the quality of the selection process (reviewed in Derda et al., 2011). For example, it is impossible to select a sequence from a peptide library if the sequence is not present in the original library. Censorship of specific peptide sequences from phage display was recognized just a few years after PhD technology was developed.

A seminal report by Dower and co-workers described the loss of propagation efficiency of phage as the number of displayed R/K residues increases (Peters et al., 1994). Total titer decreases by over an order of magnitude for each positive charge introduced in the displayed sequence. Additional censorship studies from Makowski and co-workers identified other impeding factors such as the presence of alpha-helical motifs. Peptides that display high alpha-helical propensity are delayed in periplasmic export, leading to lower titer of phage that display such sequences (Rodi et al., 2002). Hall, Noren and co-workers (Brammer et al., 2008; Nguyen et al., 2014) identified a large number of sequences with random mutations in un-translated regions (UTR) of gene *pII*; these mutations equip clones with increased growth rate. Enrichment of these fast growing "parasite" sequences is one of the mechanisms for sequence-independent censorship/loss of diversity. We have previously shown that the censorship in phage libraries can arise even due to small differences in growth rates. For two phages with a mere 20% difference in growth rates, the ratio of phages can vary by 1000-fold after a typical round of amplification (i.e., allowing phage to propagate from $10^6$ to $10^{12}$ PFU) (Derda et al., 2011).

There are several genetic strategies to solve the censorship problem. For example, the introduction of suppressor mutations in the SecY component of the protein export complex in *Escherichia coli* enables export of charged sequences (Peters et al., 1994). To overcome problems with censorship in the SecY pathway, Plückthun and co-workers used the conjugation of an additional signal sequence to direct protein export through the signal recognition particle (SRP) co-translation pathway rather than the post-translational SecY pathway (Steiner et al., 2006). The combination of phagemid and helper phage is the most commonly used strategy toward production of mosaic phage that carries only one copy of protein fused to pIII. Censorship in mosaic libraries is reduced but not eliminated entirely (Dev Sidhu, personal communication); to our knowledge, no side-by-side comparison of censorships in phage and phagemid systems has been reported to date. Makowski and co-workers were among the first to show that the censorship can also be avoided by using a lytic T4 system instead of non-lytic M13 phage (Krumpe et al., 2006). The most popular non-genetic solution to censorship is to compartmentalize the amplification of libraries. Early publications from the groups of Smith (Scott and Smith, 1990) and Winter (Hoogenboom and Winter, 1992) amplified phage libraries as lawns of isolated colonies on agar, although later reports questioned the efficiency of such a method (McConnell et al., 1995). Recently, we demonstrated that amplification of libraries in monodisperse emulsion can also be used to avoid the competition between fast and slow-growing phage (Derda et al., 2010b; Matochko et al., 2012b) and avoid the undesired enrichment of fast-growing "parasite" clones in phage libraries (Matochko et al., 2014).

One of the least characterized censorship mechanisms is the excision of peptides due to post-translational proteolysis. It is difficult to characterize the excision of displayed sequences from pIII because it cannot be detected on the genetic level. Phage with cleaved peptide sequences might appear to be produced at good titer and with a rate comparable to the production rate of other clones, but in fact, they do not express the desired insert. Theoretically, many types of sequences may be censored, as described in a review by Wilson and Finlay (1998), but the only well-documented case to date is the excision of FLAG sequence from 95% of phage, as detected by Enzyme-Linked Immuno-Sorbent Assay (ELISA) (Grihalde et al., 1995). Indirect evidence for post-translational cleavage has been presented by Noppe et al. (2011) who used affinity chromatography to separate the monoclonal phage populations that display a ligand for human lactoferrin (HuLF) into phage populations that have distinct affinities for the target (Noppe et al., 2011). A Heterogeneous population of phage can be separated into homogeneous HuLF-binding populations, which differ by the copy number of HuLF-peptides displayed on phage. Re-amplification of the separated homogeneous populations yields heterogeneous populations; phage that evade affinity capture on HuLF regain the ability to be captured (i.e., re-express HuLf-binding peptide) after re-amplification. We observed similar evidence for post-translational cleavage in chemical biotinylation of phage-displayed peptides. For example, in a library of Cys-containing phage, up to 30% of phage cannot be alkylated by biotin-iodoacetamide even under optimized reaction conditions (Jafari et al., 2014). The "non-reactive" clones contain the genetic sequence $CX_7C$, but the peptide sequence in these phage particles is most likely cleaved during phage production.

To solve the above problems, we turned our attention to early reports of Smith (1985) and de la Cruz et al. (1988) who displayed foreign sequences between the C-terminal and N-terminal domains of pIII rather than on the N-terminus of the pIII (NT format) as it is done in modern fusion vectors. Display in between the domains was also the basis of selectively-infective phage (SIP) technology developed by Plückthun group (Krebber et al., 1997), and SAP-technology (Selection and Amplification of Phage) pioneered by Borrebaeck group (Duenas and Borrebaeck, 1994; Nilsson et al., 2002). All reports rest on the fundamental observation that M13 phage can tolerate the integration of large foreign sequences in between the domains of the pIII protein. For example, introduction of the β-lactamase protein (approximately 30 kDa) can yield infective phage, albeit the efficiency of the production of phage dropped by a factor of ten thousand from $10^{11}$ PFU/mL to $10^7$ PFU/mL (Krebber et al., 1997). Other insertions, such as RNAseT1 can also be tolerated (Sieber et al., 1998b). Inserted sequences are accessible to protein binding and can generate immune responses when phage are injected into mice (de la Cruz et al., 1988).

In this report we assess whether the insertion of short to medium-size peptide sequences between the domains of pIII in mature phage can help mitigate the problems listed above: (i) permit display of charged peptides and sequences with alpha-helical propensity; (ii) prevent loss of sequences due to post-translational proteolysis; (iii) allow direct quantification of sequences that retain the displayed sequence during production. The latter requirement is possible because the loss of displayed sequence is manifested as a loss of infectivity (Sieber et al., 1998a). Investigation of insertion of fragments of larger size is another important question; however, we focus our current report on peptide sequences of 4–40 amino acids in length. To develop a platform complementary to the fd-tet-based platform used by the Plückthun group in the 1990's (Krebber

et al., 1997), we built the intra-domain phage-display (ID-PhD) on the well-established and commercially available M13KE platform (Noren and Noren, 2001), which is one of the most utilized phage-display platforms: it was used to identify over 2000 ligands to-date according to the MimoDB 2.0 and 3.0 databases (http://i.uestc.edu.cn/mimodb/index.html) (Huang et al., 2012). As described in the results, the ID-PhD phage can be propagated, enumerated and tested in conditions analogous to those developed for M13KE phage. Here, we describe successful insertion and expression of seven functional peptide sequences that are typically censored from traditional phage display: (i) the highly-charged FLAG peptide sequence DYKDDDDK; (ii) a miniaturized triple-helical Z-domain of the IgG-binding protein A (mZ) composed of 33 residues (Braisted and Wells, 1996), and (iii–vi) four positively charged arginine-containing sequences, termed "RAE"-sequences, previously shown to impede phage amplification (Peters et al., 1994). Additionally, we cloned a library of random tetrapeptides into the ID-vector for future studies of censorship in ID vs. NT format.

## Materials and Methods

### Bacterial Strains, Culture Conditions, and Plasmids

ID1-PhD and ID2-PhD vectors were engineered from a phage clone displaying the sequence $H_2N$-SVEKNDQKTYHA originating from a Ph.D.-12 phage display library based on the filamentous bacteriophage vector M13KE (New England BioLabs, Ipswtich, MA, USA). The propagation host *E. coli* K12 ER2738 was maintained on LB agar plates with 20 μg/mL tetracycline. The double-stranded replicative form DNA phage plasmids were collected from log-phase cultures of *E. coli* grown in the presence of phage for up to 6 h in LB medium at 37°C with shaking. Cultures were processed using the GeneJET Plasmid Miniprep kit (Thermo Fisher Scientific, Waltham, MA, USA).

### Engineering and Construction of ID1-PhD and ID2-PhD

Exogenous restriction enzyme sites for SacI and SpeI were inserted into the M13KE plasmid by site-directed mutagenesis, according to manufacturer guidelines (QuikChange II kit, Agilent Technologies, Santa Clara, CA, USA). Briefly, mutagenesis primers containing both restriction enzyme sites separated by six arbitrary nucleotides and two flanking complementary regions of 13 bases in length were used to insert SacI and SpeI sites into the M13KE replicative form (RF) double-stranded DNA template by PCR (see Supplementary Materials for primer sequences). Following degradation of the template with DpnI, mutagenized plasmids were transfected into XL1-Blue supercompetent cells and screened on LB-agar plates supplemented with isopropyl-1-thio-β-D-galactopyranoside (IPTG) and 5-bromo-4-chloro-3-indolyl-β-D-galactopyranoside (X-gal). Blue colonies were selected for sequencing. Note: We used commercial Quickchange II kit with XL1-Blue Supercompetent cells (pilus-negative); although these cells cannot propagate the M13KE phage continuously, they contain a lacZΔM15 allele that allows identification of the transformants by complementing the β-galactosidase gene with the LacZα supplied by M13KE vector. We did not supplement our agar plates with kanamycin or ampicillin because M13KE does not confer antibiotic resistance; therefore, in a typical experiment the vast majority of the colonies were non-transformed (white) and rare transformed variants were identified as blue-specks in a "carpet of bacteria." If necessary, the selected colonies were resuspended in LB and immediately re-streaked on non-selective agar plates to dilute the colonies and isolate a pure monoclonal LacZ(+) population for sequencing. Alternatively to streaking on non-selective plates, we mixed the transformed XL1-Blue cells with F(+) *E. coli* K12 ER2738 an hour after heat shock transformation and plated in an agar overlay to select the M13KE-transformants as blue plaques. Sequencing data showed two independent products that contained SacI and SpeI recognition sequences (see **Figure 1** and sequencing data in Supplementary Materials). Successful insertion was also confirmed by SacI/SpeI digestion of the dsDNA.

### Cloning of FLAG, mZ, RAE-sequences, and TEV-Recognition Sequences (TEVrs) into ID-PhD Vectors

Synthetic single-stranded DNA (ssDNA) containing FLAG-TEVrs, "RAE" sequences, and mZ-TEVrs inserts were purchased from Integrated DNA Technologies (Coralville, IA, USA); sequences were designed with flanking SacI and SpeI recognition sequences complementary to the mutagenized phage vector to enable restriction enzyme cloning (see Supplementary Materials for sequences). Inserts were converted from ssDNA to dsDNA by PCR amplification of the synthetic DNA forward strand. After ethanol precipitation, restriction enzyme digestion of the mutagenized phage plasmid (1 μg per reaction) and the insert duplex (0.2 μg per reaction) was performed using 1 U each of SacI and SpeI enzymes in the provided Green Buffer at 37°C for 30 min (FastDigest Restriction Enzymes, Thermo Fisher Scientific, Waltham, MA, USA). Digested vector was purified by agarose gel purification followed by gel extraction by GeneJET Gel Extraction Kit (Thermo Fisher Scientific, Waltham, MA, USA), or DNE elution from agarose using Elutrap® Electroelution System (GE Healthcare/Whatman) run at 100 V for 3–9 h, followed by ethanol precipitation. Digested insert was purified using E-Gel® SizeSelect™ Agarose Gel, 2% (Life Technologies, Carlsbad, CA, USA) according to the instructions of the manufacturer. Test ligation reactions with plasmid-to-insert ratios of 1:1, 1:3, or 1:10 and T4 DNA Ligase were incubated overnight at 16°C (New England BioLabs, Ipswitch, MA, USA). Approximately 5 ng of ligated product was transformed into 50 μL of chemically competent *E. coli* K12 (produced in-house by $RbCl_2$ method). This low efficiency method is suitable for production of individual clones with ID1/ID2-inserts. A 10 μL sample of the transformed culture was immediately spread on LB-agar plates either undiluted or at a 100-fold dilution (*see note about spreading in* Section Engineering and Construction of ID1-PhD and ID2-PhD); alternatively, it was plated in an agar overlay supplemented with F(+) *E. coli* K12 ER2738 to select the transformants as blue plaques. For more efficient transformation and cloning of

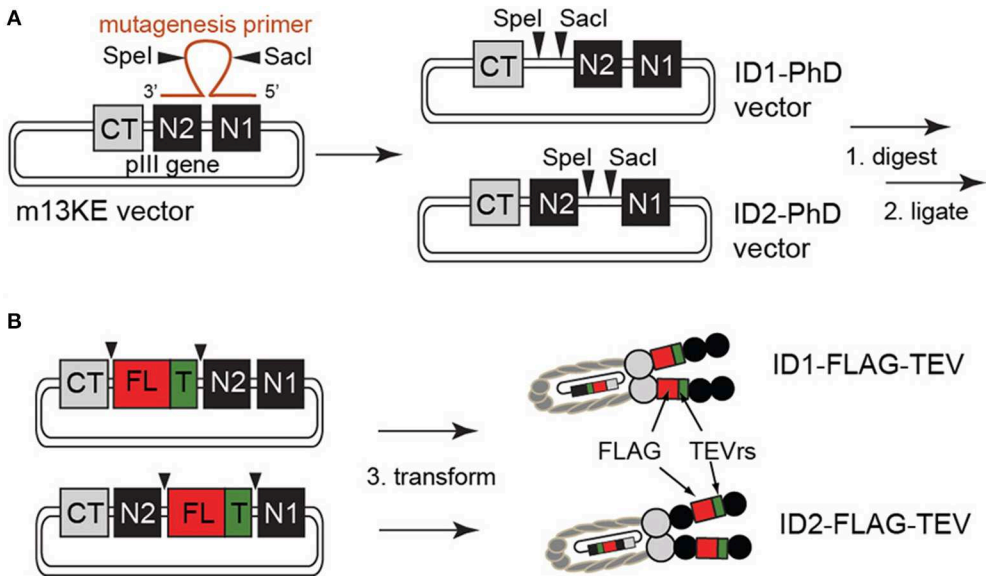


**FIGURE 1 | (A)** Construction of ID1- and ID2-cloning vectors by site-directed mutagenesis. Due to the high degree of homology of the glycine-rich linker between CT–N2 and N2–N1 domains, phage clones containing SacI and SpeI sites at both locations arise from a single round of mutagenesis. **(B)** Insertion of the FLAG peptide and TEV-protease recognition site was achieved by restriction enzyme digest and subsequent ligation of a synthetic TEVrs-FLAG DNA fragment. All constructs were validated by sequencing (see Supplementary Materials).

libraries of peptides in ID-format, we electroporated the ligated constructs using the Gene Pulser Xcell™ Electroporation System and 2 mm GenePulser/MicroPulser Electroporation Cuvettes (all from BioRad) with the settings 2500 V/400 Ohm/46 μF using commercially available F(+) TG1 electrocompetent cells and recovery media (Lucigen, Middleton, WI, USA). Where necessary, we quantified the number of transformants by mixing the cells exactly 30 min after transformation (i.e., before generation of the first progeny) with F(+) *E. coli* K12 ER2738 and plating the mix immediately in the agar overlay on X-gal/IPTG plates. We found the best plasmid-to-insert ratio to be 1:10. Individual colonies or plaques ($n = 8$) were picked and amplified in LB medium supplemented with 1:100 dilution of log-phase culture of *E. coli* K12 ER2738 for plasmid DNA isolation. Sanger DNA sequencing confirmed the incorporation of the insert (Supplementary Materials). While in this report we used restriction ligation, sequences can be cloned into the ID-vector using other techniques, such as Kunkel mutagenesis (Scholle et al., 2005).

As a control, we cloned a FLAG-TEVrs sequence (see Supplementary Materials) into the N-terminus of the pIII protein in the M13KE vector (NT-FLAG) using KpnI and EagI restriction sites and a standard protocol adapted from Ph.D.™-12 Phage Display Peptide Library Kit (New England Biolabs, Ipswitch, MA, USA) and using electroporation and TG1 electrocompetent cells as described above. All constructs were validated by Sanger sequencing (Supplementary Materials).

## Functional Validation of ID1-FLAG and ID1-mZ

To confirm complete expression of FLAG-TEVrs and mZ-TEVrs amino acid sequences, we performed enzyme-digestion and ELISA-based assays. To validate the expression of the TEVrs sequence ENLYFQS, ID1-FLAG, ID2-FLAG, and ID1-mZ phage were treated with TEV protease, according to manufacturer instructions (ProTEV Plus, Promega, Madison, WI, USA). Briefly, approximately $10^{11}$ PFU/mL of phage was added to 1x of the provided reaction buffer (100 μL) supplemented with 1 mM dithiothreitol (DTT). The mixture was incubated at room temperature (r.t.) with shaking or gentle rocking for 1–3 h (**Figure 2**). Input and output phage were titered using a standard agar overlay method with *E. coli* K12 ER2738.

We used immunoassays to validate complete expression of FLAG peptide sequence DYKDDDDK and the miniaturized Z-domain of protein A by ID2-FLAG, NT-FLAG and ID1-mZ phage, respectively. In the case of ID2-FLAG and NT-FLAG (**Figure 3A**), we coated the wells of a 96-well flat-bottomed plate (Corning Life Sciences, Tewksbury, MA, USA) with 100 μL of a 1 μg/mL solution of anti-FLAG mouse IgG (GenScript Piscataway, NJ, USA) in PBS overnight at 4°C. In the case of ID1-mZ (**Figure 4**), the coating antibody was mouse anti-human CD4 IgG (BD Biosciences, San Jose, CA, USA) at a concentration of 4 μg/mL. Following a 1 h blocking step with 3% w/v BSA in PBS, solutions of ID1-mZ phage ($3 \times 10^8$ to $1 \times 10^{10}$ PFU/mL), ID2-FLAG-TEV phage or TEV protease-digested ID2-FLAG phage ($3 \times 10^8$ to $3 \times 10^{11}$ PFU/mL) in binding buffer (0.1% w/v Tween and 0.1% w/v BSA in PBS) were added and incubated for 1 h at r.t. Following a wash step (washing buffer: 0.1% w/v Tween in PBS, 200 μL × 4 washes), 100 μL of 1:5000 dilution of HRP-conjugated anti-M13 phage antibody (GE Healthcare, Pittsburg, PA, USA) was added and incubated for 1 h at r.t. After another wash step, 100 μL of 1-Step Ultra TMB ELISA Substrate was added for 30 min, followed by a quenching step

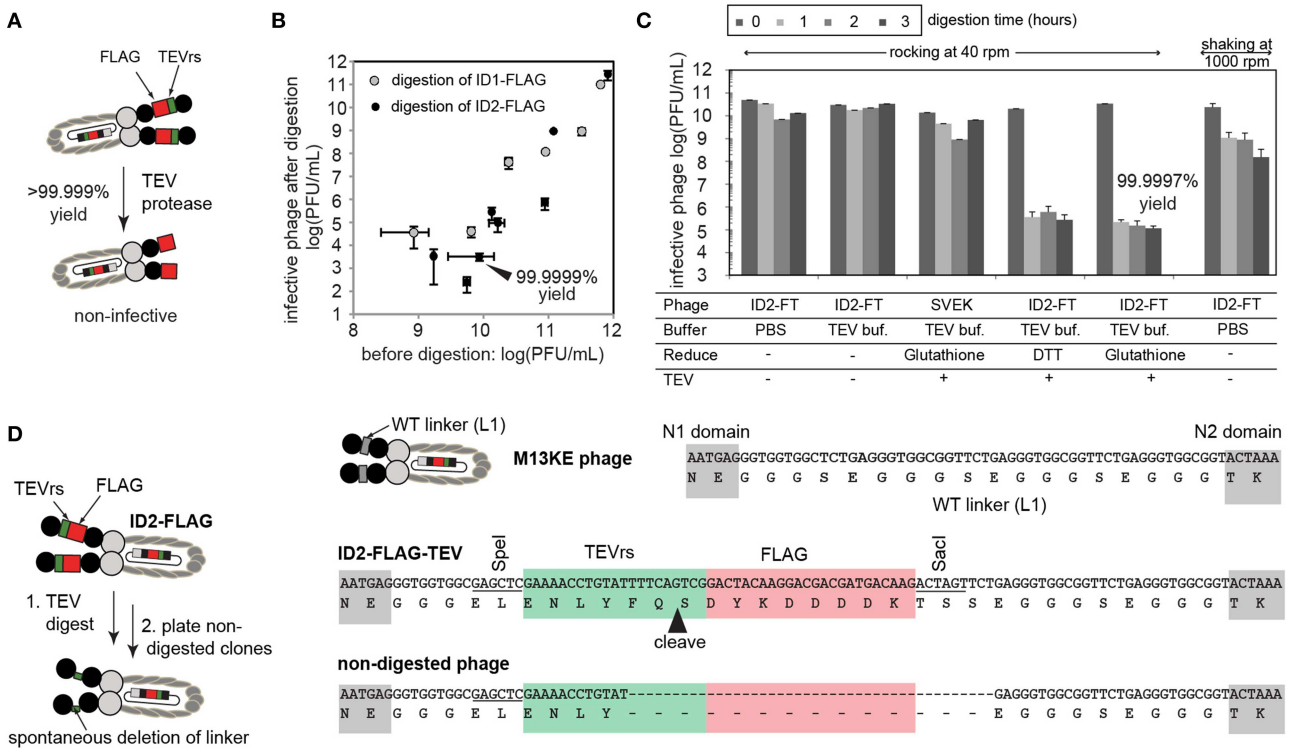


**FIGURE 2 | (A)** The presence of inserted TEV sequence can be validated by enzymatic digestion of the phage and by measuring the number of infective particles before and after digestion by TEV-protease. **(B)** Under optimized conditions (dilute concentration of phage), digestion efficiency can reach an apparent 99.9999%, indicating that the majority of phage display the insert. Each point describes a separate digestion experiment. Error bars describe standard deviation of titering. **(C)** Optimization of buffer, reducing agents, and mixing conditions used for digestion. Interestingly, simple vigorous shaking at 1000 rpm leads to drastic loss of infective particles. With gentle rocking, we observed a minor decrease in the number of infective particles due to mild toxicity of the reducing agent. Under conditions that minimize non-specific toxicity, phage is digested by TEV in <1 h. Prolonged incubation does not improve digestion beyond 99.9997% yield. Error bars represent standard deviation between three independent experiments. **(D)** Clonal culture and sequencing of the residual 0.0003% phage revealed that non-digested phage lost the insert due to genetic deletion. Note that these phage are not the result of contamination (e.g., they are clearly different from "environmental" M13 phage) as they retain fragments of TEVrs and SacI/SpeI recognition sequences.

with 100 μL of 2 M sulfuric acid. Absorbance at 450 nm was then recorded.

Oriented display of anti-FLAG antibody (**Figures 3B**, **5**) was achieved by first coating wells with 100 μL of 0.32 μg/mL (10 nM in PBS) of a fusion protein that contains IgG-binding mZ domain. The wells were then blocked for 1 h with 200 μL of 2% w/v BSA in PBS and washed using a plate washer (BioTek Plate Washer 405 TS) which repeated the following program 10 times: (i) add 200 μL/well of washing buffer; (ii) shake for 10 s; (iii) soak for 15 s; (iv) aspirate each well. After adding 50 μL of antibodies in binding buffer at a concentration of 4 μg/mL for anti-FLAG and anti-CD4 antibodies, and 2 μg/mL for anti-p32 (EMD Millipore, Temecula, CA, USA), the plate was incubated for 30 min at r.t. After another washing step with the plate washer, 50 μL of ID2-FLAG-TEV phage, ID2-FLAG phage and M13KE phage in binding buffer were added and incubated for 30 min. The unbound phages were washed away using the plate-washer procedure and each well was then incubated for 30 min at r.t. with 100 μL of HRP-conjugated anti-M13 antibody supplemented with protein A at a concentration of 100 μg/mL (**Figure 3B**) or 30 μg/mL (**Figure 5**). The addition of protein A to the solution of anti-M13 antibody was necessary to prevent non-specific binding of anti-M13 antibody to the surface of the plate. Following a final washing step with the plate washer, 50 μL of 1-Step Ultra TMB ELISA Substrate was added and quenched after 15 min with 50 μL of 2 M sulfuric acid. In all ELISA experiments, three technical replicates were used unless specified otherwise.

## Panning of ID2-FLAG and NT-FLAG on anti-FLAG

We coated a 96-well high binding Costar® Assay Plate overnight at 4°C with 100 μL of protein A (Sino Biological Inc, Beijing, China) at 10 μg/ml in PBS. To test binding of ID2-FLAG and NT-FLAG on anti-FLAG, wells were coated with anti-FLAG at $1.5 \times 10^{-3}$ mg/mL, while wells for control experiments were coated with $1.5 \times 10^{-3}$ mg/mL anti-human CD8 (BD Pharmingen™, San Jose, CA, USA) for 1 h at r.t. Wells were washed 10 times using a plate washer, programmed as follows: (i) dispense 300 μL/well of washing buffer (50 mM MOPS, 150 mM NaCl, 2 mM $CaCl_2$, 0.1% w/v Tween, pH 7.4); (ii) shake for 5 s; (iii) soak for 30 s; (iv) aspirate each well. Next, two libraries were prepared in binding

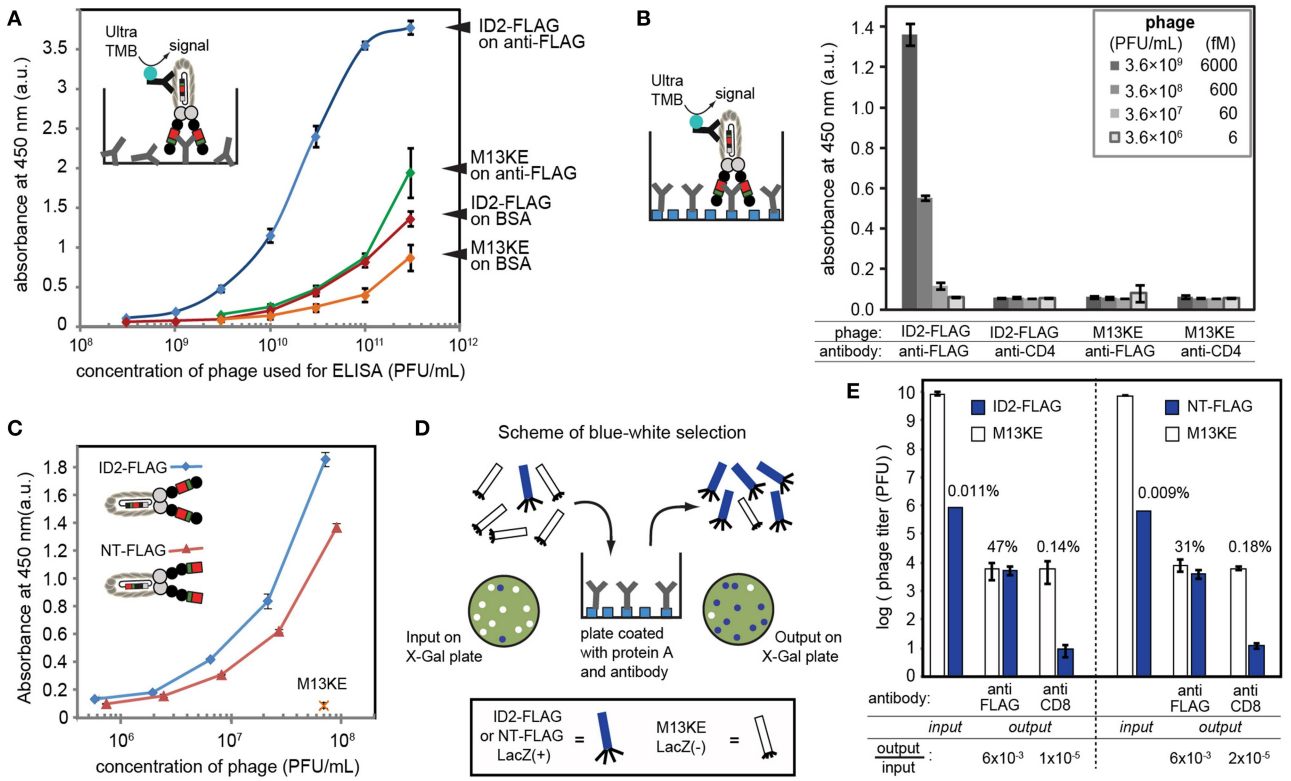


**FIGURE 3 | (A)** The presence of inserted FLAG sequence can be validated by ELISA on wells coated by anti-FLAG antibody. Phage was detected using HRP-conjugated anti-M13 antibody and Ultra-TMB substrate for horseradish peroxidase (HRP). In control experiments, we coated wells with BSA or used M13KE phage without a FLAG insert. **(B)** ELISA signal in optimal conditions with oriented immobilization of anti-FLAG IgG on protein A-coated wells yielded signal detectible at 600 femtomolar concentration of phage ($3.6 \times 10^8$ PFU/mL). In this experiment, we used wells coated by non-specific IgG (anti-CD4) as negative control. **(C)** Comparison of phage displaying FLAG at the N-terminus (NT) and in intra-domain (ID) fashion using setup analogous to **(B)**. ID-display provides statistically significantly higher signal at equivalent titers. **(D)** Scheme of selection of ID-FLAG or NT-FLAG from a 1:10,000 mixture with insert-free phage. Enrichment is monitored as increase of blue (LacZ+) plaques on agar overlay containing X-gal. **(E)** Results of selection of ID-FLAG or NT-FLAG on wells presenting anti-FLAG or anti-CD8 (negative control). ID-display provides minor yet detectable advantage. Input to output ratios for insert-containing clones are displayed below the plot. In all experiments, data represents average from three to four independent wells; error bar is one standard deviation.

buffer (50 mM MOPS, 150 mM NaCl, 2 mM $CaCl_2$) for panning: (1) ID2-FLAG mixed with LacZα(-) M13KE ("WT") (Derda et al., 2010a) at a ratio of ~1:10,000 ($9 \times 10^6$: $9 \times 10^{10}$ PFU/ml); and (2) NT-FLAG mixed with "WT" at a ratio of ~1:10,000 ($6 \times 10^6$: $8 \times 10^{10}$ PFU/mL). Libraries (100 μL) were distributed each into a separate well, resulting in four replicates of each library in wells coated with anti-FLAG, and three replicates of each library in wells coated with anti-human CD8 (control). Following 1 h incubation at r.t. and another washing step (10 cycles as described above), each well was eluted with 200 μL of elution buffer (0.2 M glycine-HCl, 0.1% w/v BSA, pH 2.2) for 9 min, neutralized with 25 μL neutralization buffer (1 M Tris-HCl, pH 9.1) and titered using an agar overlay on LB X-Gal/IPTG plates.

## Results

### ID1-PhD and ID2-PhD Cloning Vectors

**Figure 1** summarizes the structure of the pIII protein of M13 phage as C-terminal (CT) and two N-terminal (N1 and N2) domains separated by two linkers. The vectors constructed from this phage were termed ID1 if they contained the cloning sites in the first intra-domain region L1 (between CT and N2) or ID2 if the sites were in the second intra-domain region L2 (between N2 and N1). We used site-directed mutagenesis to introduce exogenous SacI and SpeI restriction enzyme sites between CT and N1 domains of a phage clone displaying $H_2N$-SVEKNDQKTYHA on the terminus of the N2 domain (hereafter referred to as M13KE phage) (Ng et al., 2012). This clone originated from the commercially available Ph.D.-12 phage display library (New England BioLabs, Ipswitch, MA, USA). While our mutagenesis primers were designed to anneal to the L1 linker, due to high redundancy between L1 and L2, we also isolated mutants that incorporated the SacI-SpeI insert in L2. These two mutants are the basis of ID1-PhD and ID2-PhD cloning vectors. Insertion of the desired displaying sequences into these vectors is accomplished by straightforward one-pot restriction digestion of vector and synthetic insert by SacI/SpeI mixture and "sticky-end ligation" of the SacI and SpeI complementary ends.

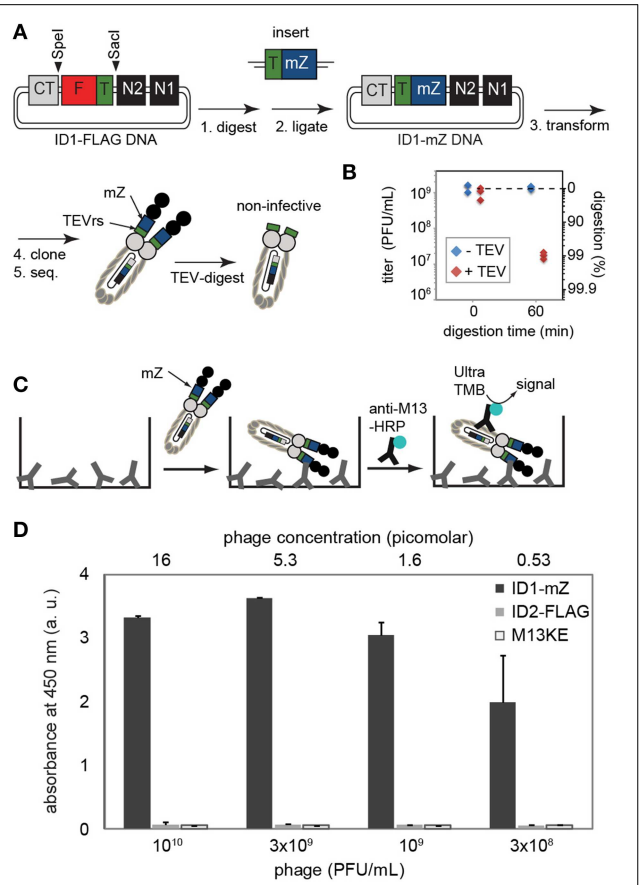


**FIGURE 4 | (A)** Steps toward displaying mZ protein and TEV recognition sequence. The complete sequence of the cloned construct is provided in Supplementary Materials. **(B)** Digestion by TEV-protease validates that at least 99% of phage contained the insert and lost infectivity in the presence of this protease. Phage do not lose infectivity in a solution that has all components (reducing agents, buffers, salts) but no TEV-protease. **(C,D)** The presence of inserted FLAG sequence can be validated by ELISA on wells coated by IgG antibody that binds to the mZ domain. Phage were detected using HRP-conjugated anti-M13 antibody and Ultra-TMB substrate for HRP. ID2-PhD phage that displayed FLAG sequence or original M13KE phage that displayed no sequence exhibited no binding to IgG-coated wells. Data represents average from three independent wells; error bar is one standard deviation.

## Construction and Validation of ID2-TEV-FLAG

As an initial test, we cloned an insert that contained both the FLAG peptide sequence DYKDDDDK and TEV-protease recognition (TEVrs) sequence ENLYFQS into cloning vectors ID1-PhD and ID2-PhD. Presence of 15 foreign amino acids with eight charged residues did not influence the growth of phage or the titer of the phage. The original M13KE, the phage expressed from cloning vectors ID1-PhD or ID2-PhD and the resulting ID1-FLAG or ID2-FLAG phage were able to reach a similar titer ($10^{12}$ PFU/mL after overnight culture in *E. coli* K12). We note that ID(1/2)-FLAG phages are formally a double-display platform because they contain a 15-mer intra-domain (FLAG-TEVrs) and 12-mer N-terminal display (SVEKNDQKTYHA) simultaneously.

## Quantification of Displayed Sequence Expression using TEV-Protease

We used enzymatic digestion by TEV-protease for detection of the insert in ID-PhD vectors. Conveniently, enzymatic digestion of TEVrs removes the N-terminal domain of phage and renders the phage non-infective (**Figure 2A**). Measuring the infectivity of phage before and after treatment of phage with TEV-protease is a rapid way to measure the digestion efficiency. For reasons we could not understand, digestion of phage was only 90% complete at high concentration of phage ($>10^{12}$ PFU/mL), possibly due to inhibition of TEV-protease by the by-products of phage preparation. At lower concentrations of phage, digestion efficiency increased exponentially, reaching over 99.9999% yield at $10^{10}$ PFU/mL. For example, after a brief treatment of $10^{10}$ PFU/mL of ID2-FLAG phage with TEV protease, only $\sim 10^{3}$ PFU/mL, or one in 10 million phage particles remained undigested (**Figure 2B**). In the same conditions, ID1-FLAG phage exhibited ~10 fold lower digestion efficiency (**Figure 2B**). It is important to note that even the mixing technique could result in significant non-specific decrease in the infectivity: for example, prolonged mixing of phage at 1000 rpm caused considerable loss in infectivity, while gentle rocking exhibited none (**Figure 2C**). To validate that this loss of infectivity is not caused by non-specific toxicity of the TEV-digestions conditions, we tested and optimized every factor in this condition to improve mixing, pH, and reducing agent. Under optimized conditions, we reproducibly observed a digestion yield of ID2-FLAG phage to be 99.9997% after 1 h, while a decrease in infectivity for all controls (TEV-free, or insert-free) was minimal (**Figure 2C**).

ID-PhD of protease recognition sequences provide the unique ability to measure the kinetics of enzymatic digestion of proteins present in solution at pico-, femto-, and theoretically even single-molecule concentrations. As ID-display of TEVrs links digestion to infectivity directly, it can complement existing methods that require affinity-capture of digested phage (McCarter et al., 2004; Scholle et al., 2006). We also investigated the origin of the one in 1,000,000 phage particles that appeared to be resistant to digestion. Specifically, during digestion of ID2-FLAG phage, concentration of TEVrs peptides decreased from ~60 picomolar to ~60 attomolar (10,000 non-digested particles) after 1 h. Prolonged incubation (**Figure 2C**) or addition of fresh TEV (not shown) could not digest the remaining 10,000 molecules. Upon inspection, we found that particles resistant to digestion were phage clones that underwent spontaneous genetic deletion of FLAG-TEVrs insert during culture. **Figure 2D** describes one sequence in which the rudiments of the TEVrs sequence can be recognized. Spontaneous deletions are known to occur in vectors based on filamentous phage.

The display of the tandem FLAG-TEVrs sequence system allowed us not only to confirm the presence of FLAG motif but also to measure that the rate of genetic deletions of the insert was one in 1,000,000. Out-of frame deletions can happen as well; however, these mutations are disruptive to the full translation of the pIII protein and result in the failure to terminate assembly and release the phage into the

medium (Rakonjac and Model, 1998). Measurement of residual infectivity in the ID-PhD system, thus, can be used to trace the stability of the insert and its propensity toward specific deletion.

## Specificity of ID2-FLAG

We tested for the presence of the FLAG sequence using ELISA, in which we tested the binding of ID2-FLAG phage and control M13KE phage to plates coated with anti-FLAG antibody or bovine-serum albumin (BSA) (**Figure 3A**). ID2-FLAG exhibited significantly stronger dose-dependent binding to anti-FLAG than any of the control combinations. While ELISA provided only an indirect estimate of binding affinity, the mid-point ($EC_{50}$) of binding of ID2-FLAG to surface-immobilized anti-FLAG can be estimated to be in the (1–3) × $10^{10}$ PFU/mL range or 10–60 picomolar. The reported affinity between monovalent FLAG peptide and anti-FLAG antibody immobilized on the surface is 300–400 nM as measured by surface plasmon resonance (Einhauer and Jungbauer, 2001). The apparent increase in affinity is a manifestation of the multivalent interaction between polyvalent display of FLAG and divalent anti-FLAG antibody on the surface. We note that direct comparison of affinity is impossible because techniques used to measure monovalent and multivalent binding are drastically different (SPR vs. ELISA). Nevertheless, we believe that it is the multivalent presentation of the relatively weak FLAG epitope on phage under optimal conditions that allowed us to detect specific binding of phage to oriented display of anti-FLAG antibody at concentration as low as $10^8$ PFU/mL or ∼100 femtomolar (**Figure 3B**). None of the mis-matched controls (non-FLAG phage, non-FLAG antibody) exhibited any detectable binding at this concentration.

By design, the efficiency of display of FLAG sequence is higher in ID vs. NT-display and this factor could make ID-display more efficient in selection procedures. In the ID-PhD vector, >99.99% of **infective** particles contain FLAG because the presence of FLAG peptide is linked to infectivity. The only mechanism for removal of the ID-displayed FLAG from an infective particle is an in-frame deletion of its coding sequence; however, such excision is rare (<0.01%) based on TEV-digestion studies (**Figures 2C,D**). In contrast, in NT display the FLAG sequence is known to be trimmed from 90 to 95% without compromising infectivity of the particles (Grihalde et al., 1995). We tested the extent of the FLAG tag removal by direct comparison of ID-FLAG and NT-FLAG binding to immobilized FLAG-specific antibody using ELISA (**Figure 3C**).When FLAG peptide is presented at the N-terminus, the efficiency of such display is lower in ELISA. We also compared the efficiency of both displays in a model selection of FLAG-containing phage from a mixture with FLAG-free phage in a 1:10,000 ratio (**Figures 3D,E**). Conveniently, FLAG-free phage has a defective LacZα sequence and produces colorless plaques. Efficiency of selection can be assessed directly by counting blue and white plaques in an agar overlay containing X-Gal/IPTG (Derda et al., 2010a). ID-display provided minor yet detectable advantage when compared to NT-display.

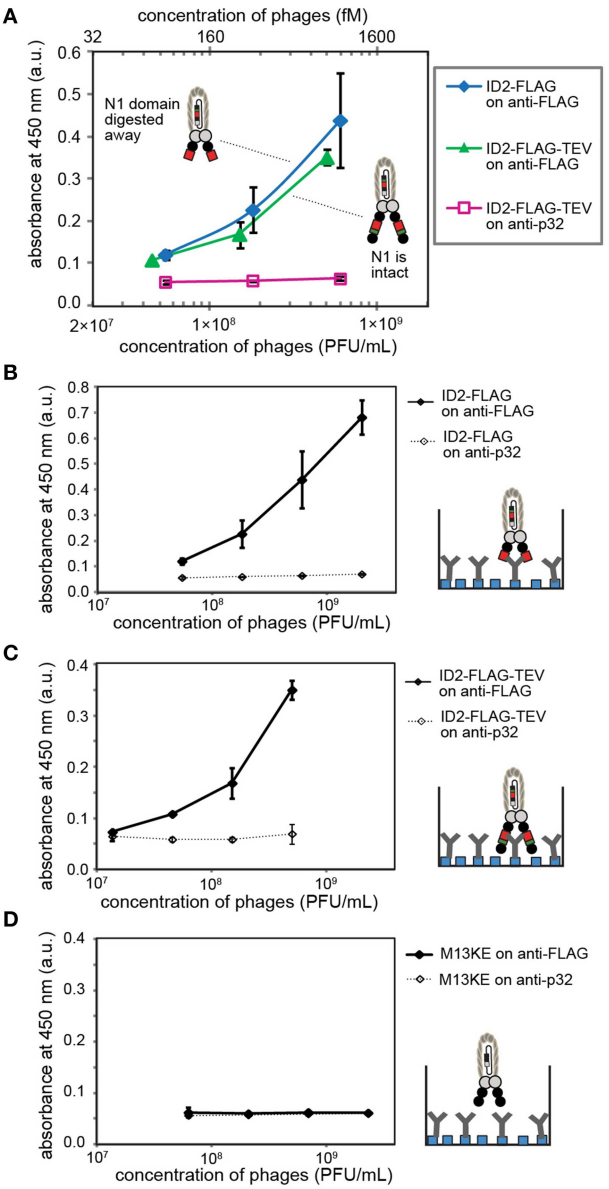


**FIGURE 5 | (A)** ELISA detects inserted FLAG sequences before and after digestion of ID2-FLAG-TEVrs phage by TEV protease. When tested side-by-side, digested and non-digested phage exhibit similar binding response. This observation suggests that the N2 domain does not interfere with binding of anti-FLAG antibody. **(B–D)** Control experiments in which we compared **(B)** binding of digested phage to matched (anti-FLAG) and mismatched (anti-p32) antibody; **(C)** binding of undigested phage to matched/mismatched antibody; **(D)** binding of insert-free phage to matched/mismatched antibody. Antibodies were immobilized on protein-A coated wells. Data represents average from three independent wells; error bar is one standard deviation.

## Characterization of ID1-mZ

To show that the ID-PhD system can be used to display larger poly-peptide sequences and therapeutically relevant mini-domain proteins, we expressed a minimized Z domain (mZ) of protein A. The three-helix bundle mZ domain is used as a

scaffold for the popular Affibody™ technology (Nord et al., 1997). Introduction of tandem mZ and TEVrs sequences, 40 amino acids in total, into the ID1-PhD vector (**Figure 4A**) had a minor effect on the phage titers. Overnight culture of ID1-mZ yielded $10^{11}$ PFU/mL; ∼10x lower than ID2-PhD phage. TEV-protease digestion confirmed presence of mZ-TEVrs insert in ∼99% of phage (**Figure 4B**). A residual fraction of non-digested phage in a clonal population of ID1-mZ (1%) was significantly higher than non-digested phage in ID1-FLAG population (∼0.001%, **Figure 2B**). This observation suggested that the frequency of spontaneous deletions of a 40 amino acid sequence (1 in 100) is more frequent than deletion of a 14 amino acid sequence (1 in $10^6$, **Figure 2**). This spontaneous deletion is likely to be the limiting factor of ID-PhD technology for display of large proteins. TEV-protease digestion of TEVrs in tandem with a peptide of interest can be used to assess display efficiency and retention of any peptide of interest in ID-format. To date, the only way to measure such efficiency was Western Blot of pIII protein with an antibody reactive to the specific sequence of interest. TEV digestion can be performed on any sequence and is conceptually simple because it requires only measurement of titer before and after addition of TEV protease.

Phage that displayed mZ protein bound specifically to the plates coated with IgG antibodies but failed to bind to the surfaces coated by control proteins (BSA) (**Figure 4D**). Similarly to ID2-FLAG, ID1-mZ exhibited exceptionally strong concentration-dependent binding to its receptor. We estimated the mid-point of binding ($EC_{50}$) of ID1-mZ to surface-immobilized IgG to be in the $3 \times 10^8$ PFU/mL or 600 femtomolar range of concentration of phage. The reported affinity between monovalent mZ domain and IgG antibody is 43 nM as measured by SPR (Braisted and Wells, 1996). Just as above, we caution that comparison based on $EC_{50}$ and $K_d$ measured by two independent methods might not be entirely accurate; nevertheless a large, apparent 50,000-fold difference between these values can be considered as strong indication for the multivalency of the ID1-mZ display.

## Prospect of ID-PhD Platform for SIP Technology

We tested whether deletion of the N1 domain by proteolysis of ID2-FLAG phage yields phage particles in which FLAG sequence can be recognized by the antibody. This recognition can be subsequently used in selectively-infective phage (SIP) technology for screening of peptide sequences that can restore infectivity of phage by recruiting a fusion of N1 and the protein of interest (Krebber et al., 1997). Side by side testing of digested and non-digested phage yielded indistinguishable concentration-dependent binding of phage to wells coated with anti-FLAG antibody (**Figure 5A**). Every control tested in this system (e.g., mismatched antibody, control phage) yielded no significant signal above background, indicating the specificity of the response (**Figures 5B–D**). In this experiment, TEV digestion conveniently converts ID-display to NT-like-display by removing the N1 domain. The observation that the epitope exhibits a similar binding affinity in digested and undigested phage suggests that intra-domain format does not interfere with the recognition of FLAG epitope by anti-FLAG antibody.

## Expression of Positively Charged Sequences and Library of Peptides in ID Format

Positively charged peptides such as AREARRAERE, RREAAAERAR, AAARRRAERA, when displayed at the N-terminus (NT) of phage, were reported by Dower and co-workers (Peters et al., 1994) to suppress formation of phage by as much as 6 orders of magnitude. Data previously collected by Peters et al. (1994), is described in columns labeled "NT-insert" (**Figure 6A**). We cloned the same sequences into the ID2-PhD vector (see Supplementary material for cloning and validation by sequencing); we then determined the titer after amplification of phage bearing these sequences. We observed that the production of phage with insert that contained Arg-rich sequences remained at levels compatible to the titer of the clone without the ID2-insert (**Figure 6A**). Specifically, the determination of the titers was conducted by mixing 3000–10,000 PFU of phage with a 1:100 dilution of log-phase culture of *E. coli* in 1 mL of LB. After overnight culture, we removed the bacteria by centrifugation and measured the number of newly produced phage in the supernatant using plaque-forming assay. For phage that displayed three Arg-residues, the titer in ID-display was several orders of magnitude higher than display

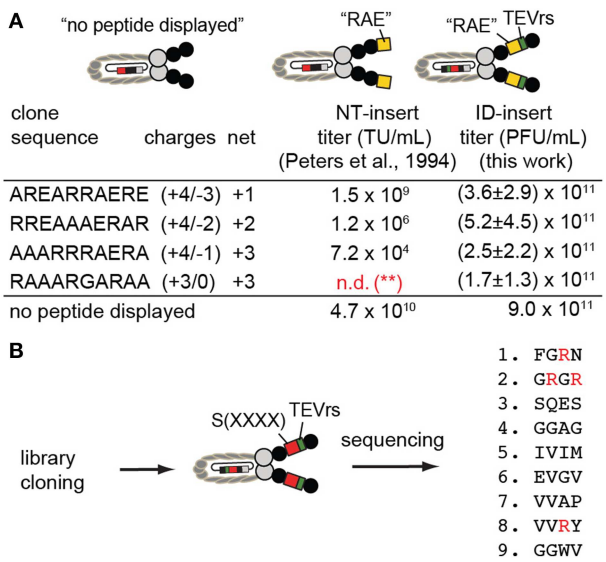


**FIGURE 6 | (A)** ID-PhD enhances the expression of positively charged peptide sequences. The data in "NT-insert"-column has been acquired by Dower and co-workers (Peters et al., 1994); it shows that Arg-rich "RAE"-sequences, when expressed at the N-terminus (NT) of pIII, impede phage titer by 2–6 orders of magnitude (TU = transducing units). We demonstrated that phage clones that display these sequences in the ID-format do not exhibit diminished titers; they are similar to the titer exhibited by phage without an insert (control phage labeled as "no peptide displayed"). Note that in experiments by Peters et al. (1994), control phage is FdTet phage displaying no N-terminal sequence. In our experiments, control phage is M13KE phage without ID-insert. The data is average and standard deviation from titer in three independent experiments. (**): n.d., not determined; **(B)** We expressed the library of random tetrapeptides in ID-PhD format and, in preliminary low-throughput sequencing, observed a significant fraction of peptides with Arg. Abundance of Arg can be further validated in this library using next-generation sequencing.

at the N-terminus suggesting that presence of Arg-rich peptides is tolerated in ID-display.

We then cloned a library of sequences in ID-PhD format and analyzed a small number (9) of clones by Sanger sequencing (**Figure 6B**). We focused our attention on Arg residues because the abundance of Arg in NT-libraries is significantly lower than expected from the codon frequencies for this amino acid (3 codons out of 32 NNK-codons encode Arg) (Rodi et al., 2002; Matochko et al., 2012a). In X4-ID-PhD library, we observed four Arg residues in nine tetra-peptides (4 out of 36 amino acids) (**Figure 6B**). These preliminary observations suggest that censorship of Arg peptides might be lower in the ID-format. In the future, it will be interesting to characterize the X4-ID-library or other libraries by Illumia sequencing to confirm this observation.

## Discussion

We demonstrated that the ID-PhD system can be used to display short charged peptides and protein mini-domains of up to 40 residues. Quality control of display and its long-term stability upon serial re-growth is important in phage display, and the ID-PhD system offers robust built-in quality control based on linkage of display and phage infectivity. For example, TEV protease-digested and residual non-digested phage can be used to measure the exact fraction of phage that display the desired sequences. The digestion process itself can be followed with single-molecule resolution, offering an intriguing opportunity to measure single-molecule enzyme kinetics. The digestion process is also a route to production of non-infective phage particles in which infectivity can be restored by SIP-technology. The aforementioned applications, however, extend beyond the scope of this report and will be described in subsequent reports.

Increased efficiency of ID-display when compared to NT-display can be understood by reviewing the mechanisms by which pIII protein is incorporated into the phage. The role of the pIII protein is termination of phage assembly (Rakonjac and Model, 1998; Rakonjac et al., 1999); the first step in this process is inner-membrane docking and translocation of pIII via the Sec pathway (Rapoza and Webster, 1993). At least two factors can lead to defective processing of pIII: (i) presence of negatively-charged residues or specific residues in specific positions (e.g., Pro in position 2) can inhibit leader peptidase processing (reviewed in Wilson and Finlay, 1998); (ii) the early formation of the loop structure in the membrane in the Sec-pathway follows "positive-inside rule" (von Heijne, 1989) and it is sensitive to the presence of positivelly charged residues in the first 20 amino acids downstream of the signal peptide (von Heijne, 1994). It is known that the transition from low to normal Arg+Lys content occurs in loops made of >60 amino acids (von Heijne, 1994). ID-PhD places the insert over 70 amino acid residues away. Display of Arg-rich sequences is effective in ID-format because the "positive-inside rule" does not apply when charged inserts are remote from the signal sequence. Similarly, display of FLAG sequence is effective because placing the insert in between the domains alleviates problems associated with peptidase processing.

In this study we confirmed ID-insertion of 15 peptide sequences and characterized the amplification for six of these sequences and recognition properties for two sequences. Investigation of a broader class of displayed peptides will be necessary to conclusively describe the behavior of this platform. To this end, cloning and deep-sequencing of several types of peptide libraries in ID-PhD format will be a fruitful direction. We validated the performance of the ID-PhD platform in selection using only a model "library" composed of two clones. Further studies with selection of ligands from a diverse library of peptides in ID-PhD format should be conducted to validate the performance of this platform. The focus of this manuscript is censorship within short peptide libraries and only briefly on protein mini-domains. Censorship in display of larger proteins involves other factors not present in short motifs (e.g., folding). Study of protein display in this system would require a separate investigation.

## Acknowledgments

The authors thank J. Maxwell Douglas for assistance with sequencing validation of ID-PhD constructs. This research was supported by the Alberta Glycomics Centre and SENTINEL Bioactive Paper Network. KT thanks Alberta Innovates – Health Solution (AIHS) and the National Science and Engineering Council of Canada (NSERC) for summer fellowship support.

## Supplementary Material

The Supplementary Material for this article can be found online at: http://journal.frontiersin.org/article/10.3389/fmicb.2015.00340/abstract

## References

Braisted, A. C., and Wells, J. A. (1996). Minimizing a binding domain from protein A. *Proc. Natl. Acad. Sci. U.S.A.* 93, 5688–5692. doi: 10.1073/pnas.93.12.5688

Brammer, L. A., Bolduc, B., Kass, J. L., Felice, K. M., Noren, C. J., and Hall, M. F. (2008). A target-unrelated peptide in an M13 phage display library traced to an advantageous mutation in the gene II ribosome-binding site. *Anal. Biochem.* 373, 88–98. doi: 10.1016/j.ab.2007.10.015

de la Cruz, V. F., Lal, A. A., and McCutchan, T. F. (1988). Immunogenicity and epitope mapping of foreign sequences via genetically engineered filamentous phage. *J. Biol. Chem.* 263, 4318–4322.

Derda, R., Musah, S., Orner, B. P., Klim, J. R., Li, L. Y., and Kiessling, L. L. (2010a). High-throughput discovery of synthetic surfaces that support proliferation of pluripotent cells. *J. Am. Chem. Soc.* 132, 1289–1295. doi: 10.1021/ja906089g

Derda, R., Tang, S. K., Li, S. C., Ng, S., Matochko, W., and Jafari, M. R. (2011). Diversity of phage-displayed libraries of peptides during panning and amplification. *Molecules* 16, 1776–1803. doi: 10.3390/molecules16021776

Derda, R., Tang, S. K., and Whitesides, G. M. (2010b). Uniform amplification of phage with different growth characteristics in individual compartments consisting of monodisperse droplets. *Angew Chem. Int. Ed Engl.* 49, 5301–5304. doi: 10.1002/anie.201001143

Duenas, M., and Borrebaeck, C. A. (1994). Clonal selection and amplification of phage displayed antibodies by linking antigen recognition and phage replication. *Biotechnology* 12, 999–1002. doi: 10.1038/nbt1094-999

Einhauer, A., and Jungbauer, A. (2001). Affinity of the monoclonal antibody M1 directed against the FLAG peptide. *J. Chromatogr. A* 921, 25–30. doi: 10.1016/S0021-9673(01)00831-7

Grihalde, N. D., Chen, Y. C., Golden, A., Gubbins, E., and Mandecki, W. (1995). Epitope mapping of anti-HIV and anti-HCV monoclonal antibodies and characterization of epitope mimics using a filamentous phage peptide library. *Gene* 166, 187–195. doi: 10.1016/0378-1119(95)00658-3

Hoogenboom, H. R., and Winter, G. (1992). By-passing immunization - human-antibodies from synthetic repertoires of germline Vh gene segments rearranged *in vitro*. *J. Mol. Biol.* 227, 381–388. doi: 10.1016/0022-2836(92)90894-P

Huang, J., Ru, B., Zhu, P., Nie, F., Yang, J., Wang, X., et al. (2012). MimoDB 2.0: a mimotope database and beyond. *Nucleic Acids Res.* 40, D271–D277. doi: 10.1093/nar/gkr922

Jafari, M. R., Deng, L., Kitov, P. I., Ng, S., Matochko, W. L., Tjhung, K. F., et al. (2014). Discovery of light-responsive ligands through screening of a light-responsive genetically encoded library. *ACS Chem. Biol.* 9, 443–450. doi: 10.1021/cb4006722

Krebber, C., Spada, S., Desplancq, D., Krebber, A., Ge, L. M., and Pluckthun, A. (1997). Selectively-infective phage (SIP): a mechanistic dissection of a novel *in vivo* selection for protein-ligand interactions. *J. Mol. Biol.* 268, 607–618. doi: 10.1006/jmbi.1997.0981

Krumpe, L. R. H., Atkinson, A. J., Smythers, G. W., Kandel, A., Schumacher, K. M., McMahon, J. B., et al. (2006). T7 lytic phage-displayed peptide libraries exhibit less sequence bias than M13 filamentous phage-displayed peptide libraries. *Proteomics* 6, 4210–4222. doi: 10.1002/pmic.200500606

Matochko, W. L., Chu, K., Jin, B., Lee, S. W., Whitesides, G. M., and Derda, R. (2012a). Deep sequencing analysis of phage libraries using Illumina platform. *Methods* 58, 47–55. doi: 10.1016/j.ymeth.2012.07.006

Matochko, W. L., Li, S. C., Tang, S. K., and Derda, R. (2014). Prospective identification of parasitic sequences in phage display screens. *Nucleic Acids Res.* 42, 1784–1798. doi: 10.1093/nar/gkt1104

Matochko, W. L., Ng, S., Jafari, M. R., Romaniuk, J., Tang, S. K., and Derda, R. (2012b). Uniform amplification of phage display libraries in monodisperse emulsions. *Methods* 58, 18–27. doi: 10.1016/j.ymeth.2012.07.012

McCafferty, J., Griffiths, A. D., Winter, G., and Chiswell, D. J. (1990). Phage antibodies - filamentous phage displaying antibody variable domains. *Nature* 348, 552–554. doi: 10.1038/348552a0

McCafferty, J., Jackson, R. H., and Chiswell, D. J. (1991). Phage-enzymes - expression and affinity-chromatography of functional alkaline-phosphatase on the surface of bacteriophage. *Protein Eng.* 4, 955–961. doi: 10.1093/protein/4.8.955

McCarter, J. D., Stephens, D., Shoemaker, K., Rosenberg, S., Kirsch, J. F., and Georgiou, G. (2004). Substrate specificity of the *Escherichia coli* outer membrane protease OmpT. *J. Bacteriol.* 186, 5919–5925. doi: 10.1128/JB.186.17.5919-5925.2004

McConnell, S. J., Uveges, A. J., and Spinella, D. G. (1995). Comparison of plate versus liquid amplification of M13 phage display libraries. *Biotechniques* 18, 803.

Ng, S., Jafari, M. R., Matochko, W. L., and Derda, R. (2012). Quantitative synthesis of genetically encoded glycopeptide libraries displayed on M13 phage. *ACS Chem. Biol.* 7, 1482–1487. doi: 10.1021/cb300187t

Nguyen, K. T., Adamkiewicz, M. A., Hebert, L. E., Zygiel, E. M., Boyle, H. R., Martone, C. M., et al. (2014). Identification and characterization of mutant clones with enhanced propagation rates from phage-displayed peptide libraries. *Anal. Biochem.* 462, 35–43. doi: 10.1016/j.ab.2014.06.007

Nilsson, N., Karlsson, F., Rakonjac, J., and Borrebaeck, C. A. (2002). Selective infection of *E-coli* as a function of a specific molecular interaction. *J. Mol. Recognit.* 15, 27–32. doi: 10.1002/jmr.557

Noppe, W., Galaev, I. Y., Mattiasson, B., and Deckmyn, H. (2011). Apparent heterogeneity in the pIII-peptide fusion protein in single-phage clones isolated from peptide libraries. *Protein Eng. Des. Sel.* 24, 721–726. doi: 10.1093/protein/gzr033

Nord, K., Gunneriusson, E., Ringdahl, J., Stahl, S., Uhlen, M., and Nygren, P. A. (1997). Binding proteins selected from combinatorial libraries of an alpha-helical bacterial receptor domain. *Nat. Biotechnol.* 15, 772–777. doi: 10.1038/nbt0897-772

Noren, K. A., and Noren, C. J. (2001). Construction of high-complexity combinatorial phage display peptide libraries. *Methods* 23, 169–178. doi: 10.1006/meth.2000.1118

Peters, E. A., Schatz, P. J., Johnson, S. S., and Dower, W. J. (1994). Membrane insertion defects caused by positive charges in the early mature region of protein pIII of filamentous phage fd can be corrected by prlA suppressors. *J. Bacteriol.* 176, 4296–4305.

Rakonjac, J., Feng, J. N., and Model, P. (1999). Filamentous phage are released from the bacterial membrane by a two-step mechanism involving a short C-terminal fragment of pIII. *J. Mol. Biol.* 289, 1253–1265. doi: 10.1006/jmbi.1999.2851

Rakonjac, J., and Model, P. (1998). Roles of pIII in filamentous phage assembly. *J. Mol. Biol.* 282, 25–41. doi: 10.1006/jmbi.1998.2006

Rapoza, M. P., and Webster, R. E. (1993). The filamentous bacteriophage assembly proteins require the bacterial seca protein for correct localization to the membrane. *J. Bacteriol.* 175, 1856–1859.

Rodi, D. J., Soares, A. S., and Makowski, L. (2002). Quantitative assessment of peptide sequence diversity in M13 combinatorial peptide phage display libraries. *J. Mol. Biol.* 322, 1039–1052. doi: 10.1016/S0022-2836(02)00844-6

Scholle, M. D., Kehoe, J. W., and Kay, B. K. (2005). Efficient construction of a large collection of phage-displayed combinatorial peptide libraries. *Comb. Chem. High Throughput Screen* 8, 545–551. doi: 10.2174/1386207054867337

Scholle, M. D., Kriplani, U., Pabon, A., Sishtla, K., Glucksman, M. J., and Kay, B. K. (2006). Mapping protease substrates by using a biotinylated phage substrate library. *Chembiochem* 7, 834–838. doi: 10.1002/cbic.200500427

Scott, J. K., and Smith, G. P. (1990). Searching for peptide ligands with an epitope library. *Science* 249, 386–390. doi: 10.1126/science.1696028

Sieber, V., Pluckthun, A., and Schmid, F. X. (1998a). Selecting proteins with improved stability by a phage-based method. *Nat. Biotechnol.* 16, 955–960. doi: 10.1038/nbt1098-955

Sieber, V., Pluckthun, A., and Schmid, F. X. (1998b). Selecting proteins with improved stability by a phage-based method. *Nat. Biotechnol.* 16, 955–960. doi: 10.1038/nbt1098-955

Smith, G. P. (1985). Filamentous fusion phage: novel expression vectors that display cloned antigens on the virion surface. *Science* 228, 1315–1317. doi: 10.1126/science.4001944

Steiner, D., Forrer, P., Stumpp, M. T., and Pluckthun, A. (2006). Signal sequences directing cotranslational translocation expand the range of proteins amenable to phage display. *Nat. Biotechnol.* 24, 823–831. doi: 10.1038/nbt1218

von Heijne, G. (1989). Control of topology and mode of assembly of a polytopic membrane-protein by positively charged residues. *Nature* 341, 456–458. doi: 10.1038/341456a0

von Heijne, G. (1994). Membrane-proteins - from sequence to structure. *Annu. Rev. Biophys. Biomol. Struct.* 23, 167–192. doi: 10.1146/annurev.bb.23.060194.001123

Wilson, D. R., and Finlay, B. B. (1998). Phage display: applications, innovations, and issues in phage and host biology. *Can. J. Microbiol.* 44, 313–329. doi: 10.1139/w98-015

**Conflict of Interest Statement:** The authors declare that the research was conducted in the absence of any commercial or financial relationships that could be construed as a potential conflict of interest.

frontiers in Microbiology

ORIGINAL RESEARCH
published: 23 June 2015
doi: 10.3389/fmicb.2015.00628

# Combinatorial synthesis and screening of cancer cell-specific nanomedicines targeted via phage fusion proteins

*James W. Gillespie, Amanda L. Gross, Anatoliy T. Puzyrev, Deepa Bedi and Valery A. Petrenko **

*Department of Pathobiology, College of Veterinary Medicine, Auburn University, Auburn, AL, USA*

OPEN ACCESS

***Edited by:***
*Jasna Rakonjac, Massey University, New Zealand*

***Reviewed by:***
*Kevin Henry, National Research Council Canada, Canada*
*Itai Benhar, Tel Aviv University, Israel*

****Correspondence:***
*Valery A. Petrenko, Department of Pathobiology, College of Veterinary Medicine, Auburn University, 253 Greene Hall, Auburn, AL 36849, USA*
*petreva@auburn.edu*

***Specialty section:***
*This article was submitted to Virology, a section of the journal Frontiers in Microbiology*

***Received:*** *20 May 2015*
***Accepted:*** *08 June 2015*
***Published:*** *23 June 2015*

***Citation:***
*Gillespie JW, Gross AL, Puzyrev AT, Bedi D and Petrenko VA (2015) Combinatorial synthesis and screening of cancer cell-specific nanomedicines targeted via phage fusion proteins. Front. Microbiol. 6:628. doi: 10.3389/fmicb.2015.00628*

Active tumor targeting of nanomedicines has recently shown significant improvements in the therapeutic activity of currently existing drug delivery systems, such as liposomal doxorubicin (Doxil/Caelyx/Lipodox). Previously, we have shown that isolated pVIII major coat proteins of the fd-tet filamentous phage vector, containing cancer cell-specific peptide fusions at their N-terminus, can be used as active targeting ligands in a liposomal doxorubicin delivery system *in vitro* and *in vivo*. Here, we show a novel major coat protein isolation procedure in 2-propanol that allows spontaneous incorporation of the hydrophobic protein core into preformed liposomal doxorubicin with minimal damage or drug loss while still retaining the targeting ligand exposed for cell-specific targeting. Using a panel of 12 structurally unique ligands with specificity toward breast, lung, and/or pancreatic cancer, we showed the feasibility of pVIII major coat proteins to significantly increase the throughput of targeting ligand screening in a common nanomedicine core. Phage protein-modified Lipodox samples showed an average doxorubicin recovery of 82.8% across all samples with 100% of protein incorporation in the correct orientation (N-terminus exposed). Following cytotoxicity screening in a doxorubicin-sensitive breast cancer line (MCF-7), three major groups of ligands were identified. Ligands showing the most improved cytotoxicity included: DMPGTVLP, ANGRPSMT, VNGRAEAP, and ANDVYLD showing a 25-fold improvement ($p < 0.05$) in toxicity. Similarly DGQYLGSQ, ETYNQPYL, and GSSEQLYL ligands with specificity toward a doxorubicin-insensitive pancreatic cancer line (PANC-1) showed significant increases in toxicity (2-fold; $p < 0.05$). Thus, we demonstrated proof-of-concept that pVIII major coat proteins can be screened in significantly higher throughput to identify novel ligands displaying improved therapeutic activity in a desired cancer phenotype.

**Keywords: phage display, targeted nanomedicines, breast cancer, pancreatic cancer, liposomal drug delivery, doxorubicin**

## Introduction

Cancer remains the second leading cause of death in the United States across all age groups for both genders and continues to produce a significant burden on the healthcare system for improved patient outcomes with an improved quality of life in cancer survivors (Siegel et al., 2015). Treatment options include surgery, chemotherapy, radiation therapy or a combination of the three and are dependent on the tumor stage at initial diagnosis and the overall health/age of the patient. For example, breast cancer is commonly treated with surgery and radiation therapy (60%) in early stages (I or II) with the addition of chemotherapy in some cases (39%). However, in later stages (III or IV), chemotherapy is used significantly more often (74%) in a patient's treatment strategy (DeSantis et al., 2014). Tumor management with chemotherapy has shown to prevent tumor recurrence and prolong a patient's overall survival, but can also decrease the quality of life due to non-specific side effects associated with the high toxicity profile of many chemotherapy treatments (Early Breast Cancer Trialists' Collaborative Group, 2005; Riihimäki et al., 2012).

Pegylated liposomal doxorubicin (Doxil, Caelyx, or Lipodox) was introduced as the first FDA-approved nanomedicine composed of the commonly used anticancer drug doxorubicin encapsulated within the core of liposomes. Liposomal doxorubicin is the first nanomedicine approved for use in the clinic for a variety of cancer types. It showed significant improvements in circulation and bioavailability, and leads to overall reduction of tumor volume while significantly increasing the long-term survival of patients (Gabizon et al., 2003). Nanomedicines provide an increase in therapeutic activity by passively targeting their therapeutic payloads and using the leaky vasculature commonly associated with many tumors, a pathophysiological phenotype known as the enhanced permeability and retention (EPR) effect (Fang et al., 2011). It has been suggested extensively from pre-clinical models that active targeting of nanomedicines can provide an additional improvement in the therapeutic activity compared to solely relying on the EPR effect and other passive targeting strategies. Active targeting commonly involves attachment of a homing molecule onto either the therapeutic drug molecule, such as a doxorubicin-conjugate (Florent and Monneret, 2008) or onto a drug delivery system, such as doxorubicin-loaded liposomes (Shroff and Kokkoli, 2012; Petrenko and Jayanna, 2014). The homing molecule would then provide cell-specific accumulation of the therapeutic molecule specifically to the desired cells, thereby reducing major side effects and also reducing dose-limiting toxicities commonly seen with highly active molecules like doxorubicin.

Two broad mechanisms are commonly used to conjugate a targeting ligand into a liposomal drug delivery system: "pre-insertion" modifications and post-insertion modifications. "Pre-insertion" modifications consist of a covalent conjugation of the targeting ligand to one of the subcomponents of the drug delivery system before assembly of the nanoparticle. Attachment of a peptide/protein is commonly achieved by covalent modification of an activated lipid or polyethylene glycol (PEG)-lipid through either an amide conjugation or a disulfide/thioether conjugation (Wang et al., 2012). Following conjugation, the protein-lipid conjugates can then be used as one of the many assembly blocks used in a self-assembly mechanism to produce larger drug delivery systems, such as observed with liposomes (Lee et al., 2014). There are several advantages of attaching a ligand prior to nanoparticle assembly including: (1) highly controlled reaction conditions of ligand to a specific lipid, (2) more commonly available characterization methods available for quality control, and (3) a highly stable conjugation of the ligand to the lipid molecule. However, "pre-insertion" modifications often require a trained chemist to optimize reaction conditions/analyze products, result in moderate yields of the desired final product which then require purification, and can also degrade the functional activity of the targeting molecule depending on reaction conditions. Alternatively, post-insertion methods of nanomedicine modification involve attachment of a targeting ligand after assembly and drug loading. It has been reported that some liposomal nanomedicines are stable enough to perform an amide conjugation to an activated lipid exposed from the nanomedicine surface, however this still requires purification of final product before testing (Kung and Redemann, 1986). Another common method of post-insertion modification includes the use of a biotinylated lipid embedded in a lipid bilayer, which will then react almost irreversibly with a streptavidin-peptide conjugate or streptavidin-biotin-peptide conjugate (Loughrey et al., 1987). Another method of post-insertion modification includes the use of pVIII major coat proteins isolated from filamentous bacteriophage, such as M13 or fd, that display a targeting motif fused at the N-terminus of the protein (Petrenko and Jayanna, 2014). Post-insertion methods offer several advantages including rapid/simple modification reactions, milder reaction conditions that keep nanomedicines and ligands functionally intact, and stable non-covalent interactions between nanomedicines and the attached ligands. However, post-insertion methods can also cause nanomedicine instability or drug loss during modification that requires the optimization of reaction conditions to prevent undesired effects.

Filamentous bacteriophage of class Ff, including phage vectors such as M13, fd, and f1, are long cylindrical virions ($\sim$1 $\mu$m $\times$ 6.5 nm) structurally composed of a single-stranded DNA genome ($<$10 kbp) and 5 structural proteins (pIII, pVI, pVII, pVIII, and pIX) (Marvin et al., 2014). Each of the wild-type phage particles consist of 2700 copies of the pVIII major coat protein, which accounts for $\sim$90% of the mass of each virion. The remaining 10% is derived from the phage's DNA genome and also a minor contribution from the four remaining structural proteins ($<$1%). Landscape phage display libraries of type f8, introduce a random peptide fusion into each of $\sim$4000 domains of the pVIII major coat protein of the fd-tet vector to create a unique landscape across the surface of each phage clone (Smith, 1993; Petrenko et al., 1996; Kuzmicheva et al., 2009). Landscape phage libraries have been used extensively to generate ligands with specificity toward various cancer phenotypes (Jayanna et al., 2010a; Fagbohun et al., 2012; Bedi et al., 2014). The pVIII major coat proteins produced from these phage vectors have an 8- or

9-mer peptide fusion at the N-terminus and also contain an intrinsic membrane-spanning domain between residues 21–39 of the wild-type vector. This highly hydrophobic core serves to accumulate the pre-coat protein in the bacterial membrane during phage morphogenesis and also participates in formation of a highly stable phage particle to protect the genome from degradation. Filamentous phage particles and their isolated proteins show superior thermal stability while also maintaining the desired binding capacity compared to antibodies and also retain functional activity after exposure to harsh environments including relatively high temperatures (Brigati and Petrenko, 2005) acidic or alkaline solutions, moderate percentages of organic solvents (Olofsson et al., 1998) and protealytic enzyme treatment (Schwind et al., 1992) making filamentous phage and their pVIII major coat proteins ideal candidates for substitute antibodies in the targeted drug development (Petrenko and Smith, 2000; Petrenko, 2008). The intrinsic membrane domain of the pVIII major coat protein has provided an ideal platform to develop targeted nanomedicines by isolating the major coat protein and introducing the solubilized proteins into preformed, drug-loaded liposomes through spontaneous interactions of the hydrophobic core with the liposome bilayer (Jayanna et al., 2010b; Wang et al., 2010a; Petrenko and Jayanna, 2014). Several methods for solubilization and isolation of phage major coat protein have been studied including phenol extraction, several classes of detergents and a number of organic solvents. However, two critical factors that significantly effect the functional activity of the isolated protein include: (1) rapid aggregation rates of the protein due to the highly hydrophobic nature of the protein, and (2) an irreversible conformation change in secondary structure from α-helical to a β-sheet (Spruijt et al., 1989; Li et al., 2007; Siegel et al., 2015). Identification of a solvation procedure that allows high recovery of phage major coat protein in an α-helical conformation that would also limit damage to the membrane of pre-formed liposomes is ideal.

One of the major limitations in ligand screening of targeted nanomedicines is due to highly complex reactions and optimizations required to prepare and purify a single targeted nanomedicine. In this study, we have developed a rapid protein isolation method to solubilize the pVIII major coat protein in high concentration, yield, and purity that also retains the desired functional activity. We show this isolated protein is then suitable to prepare targeted nanomedicines following a post-insertion modification strategy of preformed, drug-loaded liposomes (**Figure 1**). We hypothesized that optimization of ligand solubilization and insertion strategies would allow identification of cancer cell-specific ligands that increase the desired specific cytotoxic effect of liposomal nanomedicines in much higher throughput. We demonstrate the application of this technique for identifying ligands in a single combinatorial experiment combining novel cancer cell-specific ligands with a preformed liposomal doxorubicin core to generating 12 nanomedicines targeted with structurally unique ligands and subsequently screening for their anticancer activity *in vitro*. From this screening experiment, we were able to identify 8 novel targeting ligands able to significantly increase the therapeutic response of untargeted liposomal doxorubicin across two different cancer types.

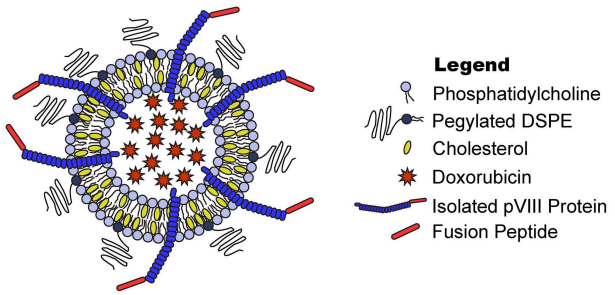


**FIGURE 1 | Phage fusion protein-targeted nanoparticles.** Target-specific phage fusion protein selected from phage libraries can be introduced into drug-loaded PEGylated liposomes exploiting their intrinsic properties to spontaneously integrate into lipid bilayers.

## Materials and Methods

### Reagents

Reagent grade or higher calcium chloride, chloroform, hydrochloric acid (HCl), 3-(4,5-dimethylthiazol-2-yl)-2,5-diphenyltetrazolium bromide (MTT), phenylmethylsulfonyl fluoride (PMSF), 2-propanol, proteinase K, and sodium dodecyl sulfate (SDS) were obtained from Sigma Aldrich (St. Louis, MO). Lipodox (PEGylated liposomal doxorubicin, composed of 1,2-distearoyl-sn-glycero-3-phosphocholine, cholesterol, 1,2-distearoyl-sn-glycero-3-phosphoethanolamine-N-[amino(polyethylene glycol)-2000] (ammonium salt) (DSPE-PEG2000) in molar ratio 56: 39: 5 containing ∼2 mg/mL encapsulated doxorubicin) was obtained from SUN Pharmaceutical Ind. Ltd. (Gujaat, India).

### Cell Culture

An established breast adenocarcinoma cell line, MCF-7 (ATCC, HTB-22™), and an established pancreatic adenocarcinoma cells line, PANC-1 (ATCC, CRL-1469™), were used throughout this study. All cell lines were purchased from the American Type Culture Collection (ATCC, Manassas, VA) as a frozen vial and maintained as described in the technical bulletins in a 37°C cell culture incubator with 5% $CO_2$. Cells were maintained in the recommended basal medium supplemented with 10% defined fetal bovine serum (FBS) and 1% v/v 100X antibiotics/antimycotics (Ab/Am). Cells were tested for mycoplasma contamination using a commercial mycoplasma PCR detection kit (ATCC) and confirmed to be free of mycoplasma contamination following all experimental procedures. Eagle's Minimum Essential Medium (EMEM) and Dulbecco's Modified Eagle's Medium (DMEM) were obtained from ATCC. Hyclone defined FBS and Gibco 100X Ab/Am, a cocktail of 10,000 U/mL penicillin, 10,000 μg/mL streptomycin, and 25 μg/mL amphotericin B, were obtained from Thermo Fisher Scientific (Waltham, MA).

## Phage Propagation and Protein Isolation in 2-propanol

All general phage handling, propagation, purification, titering, and DNA sequencing procedures have been described previously (Brigati et al., 2008; DeSantis et al., 2014). Phage clones isolated from landscape phage display libraries f8/8 and f8/9 were designated by the sequences of the foreign fusion peptides. Phage clones DMPGTVLP or VPTDTDYS were isolated from an *in vitro* biopanning of the f8/8 library over MCF-7 breast cancer cells; similarly, the phage clone VEEGGYIAA was isolated from an *in vitro* biopanning of the f8/9 library over MCF-7 breast cancer cells as described previously (Early Breast Cancer Trialists' Collaborative Group, 2005; Fagbohun et al., 2012; Riihimäki et al., 2012). Phage clones ANDVYLD, ANGRPSMT, GLNGRGDPD, or VNGRAEAP were isolated from the f8/8 library through *in vitro* biopanning with Calu-3 non-small cell lung cancer (NSCLC) cells, and phages DGQYLGSQ, DVRGDGLQ, EPSQSWSM, ETYNQPYL, or GSSEQLYL were isolated from the f8/8 library by *in vitro* biopanning with the PANC-1 pancreatic cancer cells, as described previously (Gabizon et al., 2003; Bedi et al., 2014).

Approximately $3 \times 10^{13}$ phage particles dissolved in 1X TBS were transferred to a sterile 1.7 mL microcentrifuge tube followed by addition of 3 volumes of 100% 2-propanol and 30 μL of chloroform. Phage samples were vortexed vigorously to mix and shear intact phage particles into its primary components. Phage DNA was removed from the mixture by centrifuging at 13,000 × g for 5 min at room temperature. The upper phase containing phage protein was transferred to a new sterile 1.7 mL microcentrifuge tube and stored at 4°C. Phage protein concentration was determined by measuring the UV/Vis absorbance of the solution at 280 nm with a NanoDrop. Absorbance values were converted to protein concentration, in mg/mL, using the appropriate 1 A(280) conversion factor as listed in **Table 1**.

## Characterization of Isolated Phage Protein by SDS-PAGE

Two-fold serial dilutions of isolated phage protein in 1X Laemmli sample buffer were heated at 95°C for 1 h. A 10-fold dilution of the Precision Plus Protein WesternC Standards (Bio-Rad, Hercules, CA) was diluted in 1X Laemmli sample buffer and heated at 95°C for 10 min. Prepared samples were separated on a 4–20% Mini-PROTEAN TGX polyacrylamide gel (Bio-Rad, Hercules, CA) at a constant voltage of 100 V for 45 min. Following separation, the gel was fixed for 10 min in a methanol/acetic acid/water (v/v/v 50:10:40) fixing solution. Protein bands were labeled with a Colloidal Blue Staining Kit (Thermo Fisher Scientific, Waltham, MA) as described in the manufacturer's instructions. Briefly, the fixed gel was incubated in the prepared staining solution (stainer A/stainer B/methanol/water v/v/v/v 20:5:20:55) for 3 h at room temperature with gentle shaking. The staining solution was replaced with distilled water and destained for 11 h at room temperature with gentle shaking. Following destaining, bands were visualized using an EDAS Imaging Station (Eastman Kodak Co., Rochester, NY) equipped with a DC290 digital camera and a white light box. Images were captured and analyzed using Molecular Imaging Software (v. 4.0.3; Eastman Kodak Co., Rochester, NY).

**TABLE 1 | Phage major coat protein (pVIII) properties.**

| Phage | MW (g/mol) | 1 A(280) = X mg/mL |
|---|---|---|
| ANDVYLD | 5612.49 | 0.59 |
| ANGRPSMT | 5751.67 | 0.70 |
| DGQYLGSQ | 5786.62 | 0.58 |
| DMPGTVLP | 5747.72 | 0.70 |
| DVRGDGLQ | 5777.65 | 0.70 |
| EPSQSWSM | 5869.76 | 0.42 |
| ETYNQPYL | 5946.84 | 0.52 |
| GLNGRGDPD | 5703.57 | 0.69 |
| GSSEQLYL | 5815.70 | 0.58 |
| VEEGGYIAA | 5711.63 | 0.60 |
| VNGRAEAP | 5731.62 | 0.69 |
| VPTDTDYS | 5815.64 | 0.61 |

*Phage major coat protein (pVIII) properties were calculated following sequence analysis of the full length (55 amino acid) pVIII protein sequence using DNAStar Protean version 10.0.1. Phage are identified by their 8- or 9-mer fusion peptide sequence within the full length protein sequence of $NH_2$-AXXXXXXXX[D/X]PAKAAFDSLQASATEYIGYAWAMVVVIVGATIGIKLFKKFTSKAS-COOH, where X can be any amino acid. Proteins with an 8-mer peptide fusion will contain a D in the 10th position of the pVIII fusion protein, while proteins with a 9-mer peptide fusion will have a random amino acid.*

## Preparation and Characterization of Phage Protein-modified Liposomal Doxorubicin

### Insertion of Phage Protein into Liposomal Doxorubicin (Lipodox)

Phage protein-modified Lipodox was prepared at room temperature (20°C) by rapidly introducing isolated DMPGTVLP major coat protein into a preparation of Lipodox at a protein-to-lipid weight ratio of 1:200 as described previously (Fang et al., 2011; Wang et al., 2011). Briefly, isolated phage protein (2 μL) was added to 45 μL aliquots of Lipodox (90 μg doxorubicin) and mixed vigorously before addition of 1 volume of 1X TBS, pH 7.4 to the sample. Samples were incubated at 37°C overnight with gentle rotation. For screening assays, buffer was exchanged to dilute any residual 2-propanol by washing the liposomes in a 100 K NanoSep centrifugal filter device (Pall Co., Port Washington, NY) with 5 volumes of 1X PBS, pH 7.2 for 5 min. Samples were centrifuged at 14,000 × g for 10 min and the flow through was removed. Liposomes were recovered from the retentate and analyzed as below.

### Theoretical Calculation of Ligands per Liposome

The number of lipids per liposomes was calculated based on the surface area of a unilamellar liposome with a bilayer thickness, h, of 5 nm; an average diameter, d, of 83 nm; and an average lipid headgroup area, a, of 0.5775 $nm^2$ for the mixed lipid population according to previous reports (Pidgeon and Hunt, 1981) as

discussed briefly below:

$$N_{Lipids} = \frac{4\pi}{a}\left[\left(\frac{d}{2}\right)^2 + \left(\frac{d}{2} - h\right)^2\right]$$

The concentration of liposomes was subsequently calculated as follows, where the molar concentration of lipid in Lipodox, M, was 0.0216 M; and $N_A$ is Avagadro's Number:

$$C_{Lipos}\left(Liposomes/mL\right) = \frac{M \times N_A}{N_{Lipids} \times 1000}$$

The number of ligands per liposome was calculated as follows, where $N_{ligand}$ is the number of phage proteins calculated from the molar mass:

$$N_{Ligands/Liposome} = \frac{N_{Ligands}}{N_{Liposomes}}.$$

### Purification of Phage Protein-modified Lipodox by Size Exclusion Chromatography

Protein modified Lipodox was purified by size exclusion chromatography (SEC) on a column (30 × 1 cm) packed with Superose 6 prep grade resin (GE Healthcare, Little Chalfont, UK) as described previously (Florent and Monneret, 2008; Jayanna et al., 2009). Liposomes were eluted with 10 mM Tris-HCl, pH 8.0 containing 0.2 mM EDTA at a flow rate of 0.25 mL/min. The elution profile was monitored by an Econo UV monitor (Bio-Rad, Hercules, CA) at an AUFS of 0.5 with fractions collected every 10 min (2.5 mL fractions). Fractions were stored at 4°C until further analysis.

### Quantification of Doxorubicin

Encapsulated doxorubicin was quantified by monitoring the absorbance at 492 nm following incubation with Triton X-100 (1% v/v final concentration) and comparing to a standard curve with known doxorubicin concentrations as described previously (Jayanna et al., 2010b; Shroff and Kokkoli, 2012; Petrenko and Jayanna, 2014).

### Size Distribution and Zeta Potential of Liposomes

Liposome size distribution was determined using dynamic light scattering. Briefly, samples were diluted 100-fold with 1X PBS, pH 7.4 in a plastic sizing cuvette and analyzed on a ZetaSizer Nano ZS90 (Malvern Instruments Inc., Worcestershire, UK) maintained at 25°C with a scattering angle of 90° in triplicate. All liposome samples were found to be unimodal distributions, however samples were reanalyzed if multiple populations were identified. Size distributions are presented as the mean of triplicate Z-averages (nm) ± sample standard deviation.

Liposome zeta potential was determined by particle electrophoretic mobility as measured using laser Doppler electrophoresis and phase analysis light scattering. Briefly, samples were diluted 100-fold in 10 mM Tris-HCl, pH 8.0 with 0.2 mM EDTA in a plastic sizing cuvette and analyzed on a ZetaSizer Nano ZS90 with a Zeta Dip cell (Malvern Instruments Inc., Worcestershire, UK). Samples were maintained at 25°C during measurement and performed in triplicate. All recorded samples were equal in conductivity (± 0.01 of mean). Zeta potentials are presented as the mean of triplicate zeta potentials (mV) ± sample standard deviation.

### SDS-PAGE and Western Blot of Modified Liposomes

Aliquots of each fraction following SEC were diluted with an equal volume of 2X Laemmli sample buffer and heated at 95°C for 1 h. Prepared samples were analyzed using a 4–20% Mini-PROTEAN TGX polyacrylamide gel at a constant voltage of 100 V for 45 min. Proteins separated by the SDS-PAGE were then transferred to a polyvinylidene fluoride (PVDF) membrane and blocked overnight with 1X protein-free PBS/0.05% Tween 20 blocking buffer. Membranes were probed with a rabbit polyclonal anti-fd IgG (1:5500 dilution, ∼9 μg IgG) described previously (Smith et al., 1998; Wang et al., 2012) incubated with a biotin-SP-conjugated Affinipure goat anti-rabbit secondary IgG (1:30,000 dilution, ∼1.3 μg IgG; Jackson ImmunoResearch Laboratories, Inc., West Grove, PA Cat # 111-065-003 RRID: AB_2337959) and with NeutraAvadin-Horseradish Peroxidase (HRP) (1:30,000 dilution) and visualized with West Pico substrate solution (Pierce, Rockford, IL). Membranes were imaged on a C-DiGit blot scanner (LI-COR, Inc., Lincoln, NE) and analyzed by densitometry with Image Studio Lite (v. 4.0; LI-COR, Inc.).

To ensure the N-terminus was exposed to the exterior environment of the liposome following phage protein modification, a proteinase K digestion assay was performed on modified Lipodox as described previously (Jayanna et al., 2010b; Lee et al., 2014). Briefly, an aliquot of protein-modified liposomes were treated with 1.25 μg of proteinase K containing 0.25 mM $CaCl_2$ for 1 h at room temperature. The reaction was inhibited by the addition of PMSF to a final concentration 5 mM followed by incubation at room temperature for 5 min. Samples were analyzed by SDS-PAGE and Western blot as described above.

### Phage Protein Orientation Assay of Modified Liposomes by Dot Blot Analysis

Samples were prepared as described above, except proteinase K reactions were performed overnight with gentle rotation at 37°C. Samples were then diluted 2-fold with distilled water and 1.0 μL of each sample were dotted onto a 0.2 μm nitrocellulose membrane (Bio-Rad Laboratories, Hercules, CA). Dots were allowed to dry overnight at room temperature. The resulting dots were probed with rabbit anti-Fd IgGs with specificity toward either the pVIII N-terminus (1:5000 dilution, ∼9.24 μg rabbit anti-Fd IgG) or C-terminus (1:100 dilution, ∼126 μg rabbit anti-Fd C-terminus IgG affinity purified). Membranes were then treated as above with a biotinylated-SP-conjugated goat anti-rabbit secondary IgG, NeutraAvadin-HRP and West Pico substrate before imaging with a C-DiGit blot scanner and quantified using Image Studio Lite.

### Concentration of Modified Liposomes

Liposomes were concentrated by Amicon 100 k Molecular Weight Cut Off (MWCO) centrifugal concentration devices (EMD Millipore, Billerica, MA) as follows. Briefly, a 100 k

MWCO concentrator was washed with 2 mL of 10 mM Tris-HCl, pH 8.0/0.2 mM EDTA running buffer. Samples were applied and centrifuged at 5000 × g in 15 min increments at 4°C until all samples were concentrated to a final volume of 0.5 mL. Doxorubicin liposomes found in the retentate were recovered and analyzed as above.

### Characterization of Liposome Modification by Flow Cytometry

Phage displaying the fusion peptide DMPGTVLP was propagated as above, however phage was dissolved in 1X PBS, pH 7.2 at the final recovery step. Phage proteins were labeled with an Alexa 488 Protein Labeling kit (Invitrogen, Waltham, MA) as described previously (Kung and Redemann, 1986; Fagbohun et al., 2012) and according to the manufacturer's instructions. Briefly, phage were added to a vial of reactive dye at room temperature and mixed for 1 h at room temperature. Unreacted dye was inactivated by addition of 1X TBS, 7.4 and removed by an overnight PEG precipitation of phage and solubilization in 1X TBS, pH 7.4. Phage protein was isolated in 2-propanol as described above and the degree of protein labeling was determined according to the manufacturer's instructions. Lipodox was modified with labeled protein as described above. Liposomes were analyzed on an Accuri C6 flow cytometer (BD Biosciences, Franklin Lakes, NJ) with an excitation wavelength of 488 nm and emission collected on three different channels (533/30, 585/40, and 670LP). The collection threshold was set to collect events greater than 10,000 on the forward scatter height (FSC-H) channel. After collection, a threshold to collect events greater than 1000 RFU on the 670LP height (FL3-H) channel was applied to reduce the background noise. A minimum of 100,000 events was collected per sample for analysis. Channels were compensated for channel spillover using single labeled controls. Labeled phage protein was monitored with the 533 nm emission filter channel and Lipodox was monitored on both 585 and 670 nm emission filter channels. Flow cytometry data were captured and analyzed using the Accuri C6 Software (ver. 1.0.264.21; BD Biosciences). All flow cytometry data files were annotated and deposited into the publically available flow cytometry data repository FlowRepository (Repository ID: FR-FCM-ZZJY) (Loughrey et al., 1987; Spidlen et al., 2012).

### Cell Viability of Cancer Cells Treated with Phage Protein-modified Liposomes

Cell viability was determined by MTT assay as described previously (Bedi et al., 2014; Petrenko and Jayanna, 2014). Briefly, MCF-7 breast cancer cells were seeded at an initial density of $5 \times 10^5$ cells per well in a 96-well cell culture-treated array plate and incubated at 37°C for 24 h. Lipodox samples (modified and unmodified) were diluted in EMEM containing 10% FBS and added to the cells for 24 h. For the screening assay, medium containing Lipodox was removed from the cells and replaced with an equal volume of fresh culture medium containing 10% FBS and incubated at 37°C for an additional 48 h before measuring viability. Following treatment, the medium was replaced with phenol red-free MEM containing 0.45 mg/mL MTT and incubated for 4 h at 37°C. After 4 h, 100 μL of 10% SDS in 0.01 N HCl was added to each of the wells and incubated at 37°C for an additional 4 h. The absorbance of the wells was measured at 570 nm using a Synergy H1 plate reader (BioTek, Winooski, VT). Blank wells containing only culture medium and MTT were subtracted from each sample. The percent viability was expressed as a ratio between the absorbance of treated cells by the average absorbance for a set of untreated cells.

### Quantification of Cell-associated Doxorubicin

Cell-associated doxorubicin was quantified as previously described (Bedi et al., 2014; Marvin et al., 2014) with minor modifications. Briefly, cells were plated at 5000 cells per well in a 96-well culture plate and incubated overnight in a 5% $CO_2$ cell culture incubator at 37°C. Cells were then treated with 2 μg of doxorubicin of either (1) unmodified Lipodox or (2) DMPGTVLP-Lipodox for 4 different time periods (4, 8, 12, and 24 h). Cells were washed twice with 1X PBS, pH 7.2 before extracting cell-associated doxorubicin with 0.075 N HCl in 90% 2-propanol and incubating at 4°C overnight. Doxorubicin was determined by measuring the fluorescence (470 ex/590 em) with a Synergy H1 plate reader (BioTek, Winooski, VT) using untreated cells as a blank.

### Statistics

Data from all experiments are expressed as the mean ± sample standard deviation (SD). Differences between samples were determined using the Student's independent *t*-test or and alternative appropriately identified test listed in the text with a $P < 0.05$ as being statistically significant.

## Results

### Isolation of pVIII Major Coat Protein in 2-propanol

To prepare solubilized phage major coat protein in 2-propanol, we added 3 volumes of 2-propanol to ~ $2.3 \times 10^{13}$ virions of intact DMPGTVLP phage particles, which displays the full length, 55 amino acid pVIII major coat protein sequence of $NH_2$-A**DMPGTVLP**DPAKAAFDSLQASATEYIGYAWAMVVVIVG ATIGIKLFKKFTSKAS-COOH (designated shortly by the sequence of peptide fusion at the N-terminus; DMPGTVLP) and a small volume of chloroform to perturb the hydrophobic interactions between neighboring pVIII monomers (Manning et al., 1981; Smith, 1993; Petrenko et al., 1996; Kuzmicheva et al., 2009). After exposing intact phage to increased shear force by vortexing, phage ssDNA was released from the phage particles and precipitated in 75% 2-propanol. UV/Vis spectroscopy of the phage protein supernatant (**Figure 2A**) revealed a spectrum commonly observed for a pure protein sample with a corresponding 260/280 ratio of 0.559, which is close to the theoretical 260/280 ratio of 0.5 expected for pure pVIII major coat protein. Conversion of A280 into a corresponding mass revealed a quantitative recovery of the protein mass (~1 mg).

To test the purity of isolated phage major coat protein, serially diluted samples of phage protein were separated on a 4–20% polyacrylamide gel and stained with a colloidal Coomassie blue staining solution. The stained protein gel (**Figure 2B**)

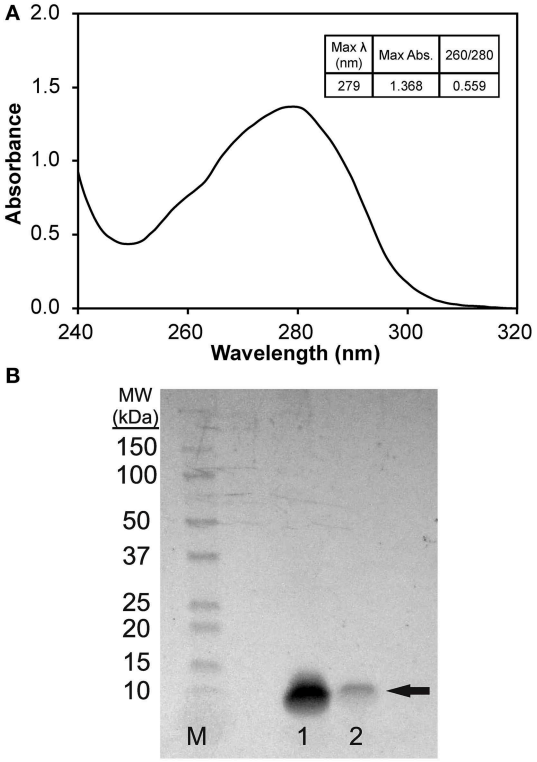


**FIGURE 2 | (A)** UV/Vis spectrum (1 nm scan) of pVIII major coat protein solubilized in 75% v/v 2-propanol/1X TBS, pH 7.4 blanked with solution of 75% v/v 2-propanol/1X TBS, pH 7.4. **(B)** SDS-PAGE of pVIII major coat protein solubilized in 75% 2-propanol/1X TBS, pH 7.4 separated on a 4–20% polyacrylamide gel. Bands were identified by staining with a colloidal blue staining kit (Invitrogen) to reveal a single, low molecular weight band of ∼7.5 kDa (as noted by the arrow) in samples 1 and 2. M (Marker)—1:10 dilution of Precision Plus Protein WesternC Standards (Bio-Rad), Sample 1–1.36 μg DMPGTVLP phage protein, Sample 2–0.27 μg DMPGTVLP phage protein.

reveals a single, low molecular weight protein band at an apparent molecular weight of ∼7.5 kDa, which corresponds to the monomeric-form of phage major coat protein (calculated molecular weight of 5.75 kDa, DNAStar Protean v. 10.0.1). Major coat protein, pVIII, was detectible down to ∼200 ng of protein under these conditions with colloidal blue staining.

## Preparation and Physicochemical Characterization of Phage Protein-modified Liposomal Doxorubicin

To prepare targeted Lipodox (pegylated liposomal doxorubicin, 2 mg/mL doxorubicin) preparations, 23.6 μg of isolated DMPGTVLP phage major coat protein was rapidly added to liposomes, composed of 4.73 mg of lipid and 0.9 mg of doxorubicin, in small aliquots to prevent dissolution of the liposomes. The residual 2-propanol and chloroform were diluted to a final concentration of 2.0 and 0.076% respectively, was shown previously to not cause an increased dissolution of liposomes (data not shown). Following incubation at 37°C overnight, samples were eluted through a size exclusion chromatography column packed with Superose 6 and the elution profile was monitored by relative absorbance with a UV/Vis monitor. The elution profile for DMPGTVLP-modified Lipodox (**Figure 3**) showed a single broad peak with 2 minor peaks at either side of the main peak (fractions 4 and 9). The broad peaks observed were also present in unmodified liposomes and is hypothesized to be due to the heterogeneous composition of the liposomes, however both minor peaks were excluded from further analysis.

To ensure phage protein was associated with the liposomes, a Western blot of each fraction (fractions 5–11) was performed with an anti-fd phage IgG that demonstrates specificity toward the N-terminus of the major coat protein. The blot revealed a single ∼5.7 kDa molecular weight band with most of the phage protein associated with the liposomes found in fractions 6 and 7, however phage protein was also recovered in fractions 5–10 (**Figure 3**). Phage protein was not observed as free protein in the absence of liposomes. Fractions 5 through 8 were further characterized for recovery of doxorubicin and physical properties (size distribution and zeta potential) of the recovered liposomes. As shown in the summary table (**Figure 3**), 862 μg of doxorubicin (95.79% yield, 900 μg doxorubicin input) was recovered in the 4 fractions, which was significantly higher than previous post-insertion methods using cholate, which commonly resulted in 50–80% doxorubicin recovery. The size distribution of the resulting fractions showed a mean diameter of 81.25 ± 3.36 nm with an average PDI of 0.127 ± 0.029, which corresponds to a monodisperse population of liposomes with a low tendency for particle aggregation. The zeta potential of the fractions showed a mean zeta potential of −30.25 ± 10.0 mV with a mean conductivity of 0.020 ± 0.005 mS/cm, which suggests a generally negative surface charge of the liposomes in a solution of constant ionic strength and composition.

Since fractions 5 through 8 displayed similar composition and physical properties, they were concentrated with 100 K MWCO centrifugal concentration devices and analyzed again for final characterization properties. After concentration, 589 μg of doxorubicin (68.4% recovery, 862 μg doxorubicin input) was recovered; suggesting a large portion of doxorubicin was lost during concentration most likely due to doxorubicin sticking or passing through the membrane. Following concentration, DMPGTVLP-modified liposomes showed a mean diameter of 80.27 ± 1.30 with an average PDI of 0.104 ± 0.015, which shows no statistically significant change in size or aggregation due to concentration effects (two-tailed $t$-test, $P = 0.605$ and $P = 0.196$ respectively). DMPGTVLP-modified liposomes showed a significant 11.3% increase in size compared to unmodified Lipodox (72.07 nm; two-tailed $t$-test, $P = 8.06 \times 10^{-3}$), however this increase is negligible in the biological systems to be tested and is hypothesized to be due to swelling associated with major coat protein incorporation. After concentration, DMPGTVLP-modified liposomes showed a mean zeta potential of −19.87 ± 0.50, which again shows no statistically significant difference in zeta potential due to concentration effects (two-tailed $t$-test, $P = 0.08$). Modified liposomes showed a significant 11.4% decrease in zeta potential compared to unmodified Lipodox (−17.83 mV; two-tailed $t$-test, $P = 4.2 \times 10^{-2}$). We hypothesize that observed decrease might be due to the introduction of the fusion pVIII major coat protein, which contains a negatively

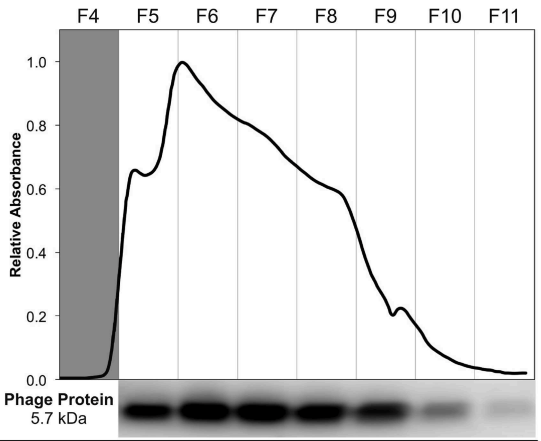


| | | | | | | | |
|---|---|---|---|---|---|---|---|
| Size (d.nm) | 81.2 | 78.6 | 79.2 | 86.0 | 88.5 | NM | NM |
| Zeta Potential (mV) | -23.7 | -25.9 | -26.2 | -45.2 | -50.9 | NM | NM |
| Doxorubicin (μg) | 161 | 435 | 665 | 862 | ND | ND | ND |
| Yield (%) | 17.9 | 30.4 | 25.6 | 21.9 | ND | ND | ND |

**FIGURE 3 | Purification and characterization of DMPGTVLP-modified Lipodox.** Size exclusion chromatography of modified Lipodox on a Superose 6 column (30 × 1 cm), 2.5 mL/fractions 4–11 of the elution profile are shown. Western blot of recovered fractions probed with a polyclonal anti-fd rabbit primary IgG, followed by a biotinylated goat anti-rabbit secondary IgG and detected with NeutrAvadin-HRP and Pico West luminol substrate. Physicochemical characterization of recovered fractions for size distribution (d.nm), zeta potential (mV), doxorubicin recovery (μg), and percent doxorubicin recovery (%).

charged N-terminus that is exposed to the environment following liposome modification and can influence the observed charge at the liposome surface.

We next sought to determine if the N-terminus of the fusion protein, which contains the cancer cell-specific targeting domain, was exposed outside of the liposomal environment following concentration as previously shown (Jayanna et al., 2010a,b; Fagbohun et al., 2012; Bedi et al., 2014). As illustrated in **Figure 4A**, treatment of modified liposomes with proteinase K causes protein not protected by the liposome membrane to be hydrolyzed. To show that the N-terminus is exposed, a portion of modified liposomes was treated with proteinase K followed by SDS-PAGE and detection of the N-terminus of major coat protein with an anti-fd antibody. The resulting blot and densitometry of bands shows that isolated major coat protein can be detected as a single 5.7 kDa molecular weight band at the same protein mass used in a matched liposome modification (∼500 ng of protein analyzed) and subsequently degraded to completion when treated with proteinase K under these conditions as expected (**Figure 4B**, lanes 1 and 2 respectively). After insertion into Lipodox, phage protein is detected in untreated samples and is absent following treatment with proteinase K (**Figure 4B**, lanes 3 and 4 respectively), suggesting that the N-terminus is exposed following modification and liposome concentration as expected.

As previously suggested, we hypothesized that the C-terminus of the phage major coat protein would be embedded in the hydrophobic membrane and protected from degradation by proteases. We therefore sought to determine the orientation of the C-terminus by a semi-quantitative dot blot assay. It was shown previously that degradation of the N-terminus produces a highly hydrophobic protein fragment that results in irreversible aggregation of monomers, causing visible smearing of bands in Western blots probed with a C-terminus specific antibody. To overcome this limitation and produce semi-quantitative estimates of the amount of each terminus following degradation, we optimized a dot blot assay and probed the resulting membranes with anti-fd IgGs with specificity to either the N- or C-terminus of the major coat protein (**Figure 4C**). Treatment of a 1X phage protein sample (∼375 ng) with proteinase K resulted in complete degradation of the protein and was undetectable with both N- and C-terminal antibodies. To ensure reaction conditions were optimal for excess phage protein, a 2X phage protein sample (∼750 ng) was digested under the same reaction conditions to again reveal complete degradation of the both N-terminus and C-terminus of the phage protein. Modified Lipodox (containing 375 ng phage protein) was digested with proteinase K using the same reaction conditions and probed with N-terminal and C-terminal specific antibodies. Probing the proteinase K treated Lipodox sample with the N-terminal antibody revealed complete degradation, confirming previously observed results obtained by Western blot (**Figure 4B**). Similarly, probing the same proteinase K treated Lipodox sample with a C-terminal specific antibody revealed no degradation of protein.

## Estimation of the Degree of Protein Modification by Flow Cytometry

We further sought to determine an approximate degree of liposome modification by monitoring individual liposomes with flow cytometry. To estimate the modification efficiency of modified liposome, we fluorescently labeled intact phage particles with Alexa Fluor-488 and isolated the labeled protein as above. We have shown previously that intact phage can be modified with an amine-reactive Alexa Fluor-488 *N*-hydroxysuccinimide (NHS)-ester that reacts with the N-terminal amine and the exposed ε-amine of Lys-13 on pVIII major coat protein (Brigati and Petrenko, 2005; Fagbohun et al., 2012). The resulting degree of fluorescence labeling was calculated to be ∼10% of the total phage protein mass, which is routinely achieved for phage after amine modification. Following isolation of pVIII protein, 25 μL of Lipodox (50 μg of doxorubicin) was modified with 14.4 μg of protein in which 10% of protein (1.4 μg) was labeled with Alexa Fluor-488.

We hypothesized that these particles could then be quantified by flow cytometry with individual particles containing doxorubicin being identified by a relative fluorescence threshold of 1000 RFU set on the 670LP emission filter to reduce background noise. Unmodified Lipodox liposomes were analyzed across two channels (Em 585/40 and 670LP filters) to accurately identify liposomes from random background events. The Lipodox positive gates were identified on each channel from the samples displaying a linear correlation across both channels, identifying 95.6% of the sample population. Due to the broad emission spectrum of doxorubicin, the fluorescently labeled

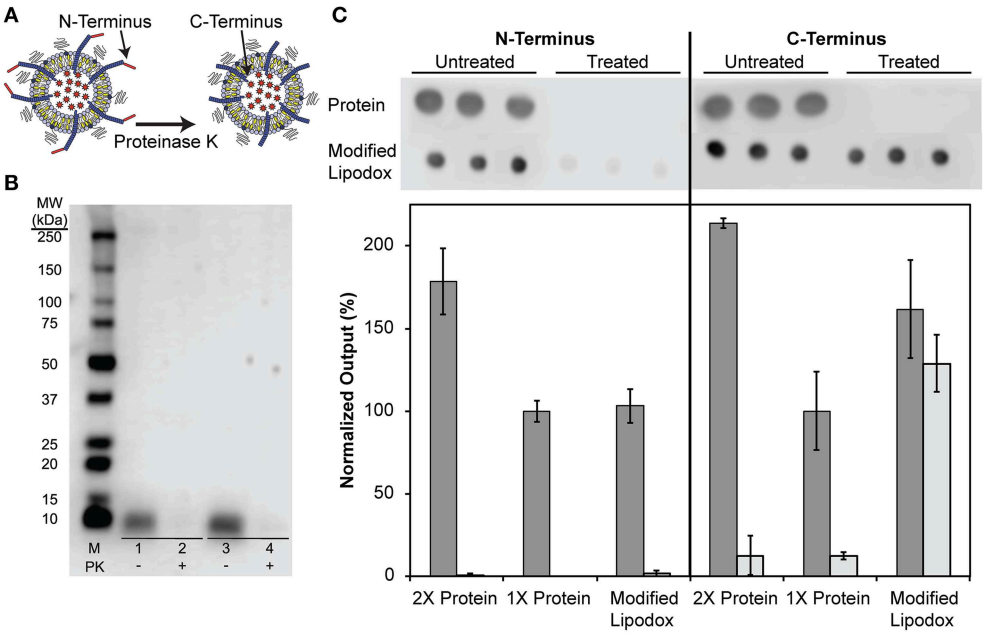


**FIGURE 4 | (A)** Schematic of phage protein orientation assay, where it is expected that the N-terminus of the protein is exposed to proteinase K degradation while the C-terminus of the protein is protected from degradation by the lipid bilayer. **(B)** N-terminal orientation assay in DMPGTVLP-modified Lipodox. SDS-PAGE of concentrated DMPGTVLP-modified Lipodox followed by assay by Western Blot. M (Marker)—1:10 dilution of Precision Plus WesternC Standards, Samples 1 and 2–500 ng DMPGTVLP isolated protein, Samples 3 and 4—DMPGTVLP-modified Lipodox (~500 ng DMPGTVLP protein). Samples 1 and 3—untreated controls, Samples 2 and 4—Proteinase K (PK) treated samples. **(C)** Phage protein orientation assay by dot blot analysis with data quantified by densitometry and presented as the mean ± standard deviation of output signal normalized to 1X untreated protein (~375 ng protein). Untreated samples (dark bars) are compared to proteinase K treated samples (light bars) $N = 3$.

protein positive gate was identified at the maximum emission fluorescence of unmodified Lipodox using a 533/30-emission filter. The resulting gate also identified free-protein aggregates displaying high particle fluorescence. Analysis of unmodified Lipodox shows that 96.5% of the total population is found in the doxorubicin positive/protein negative quadrant (lower-right) with a minimal percentage in the doxorubicin/protein positive quadrant (upper-right) (**Figure 5A**). After liposome modification, there was a significant increase to 6.5% of the total population found in the doxorubicin/protein positive quadrant (upper-right) and a significant increase to 4.5% of the total population found in the doxorubicin negative/protein positive quadrant (upper-left) (**Figure 5B**). Since free protein was found to have high channel fluorescence, we suggest that the observed increase in the doxorubicin negative/protein positive quadrant (upper-left) is due to minor loss of encapsulated doxorubicin in modified liposomes below our doxorubicin positive gate. We therefore show a total detectible protein positive population of 11%.

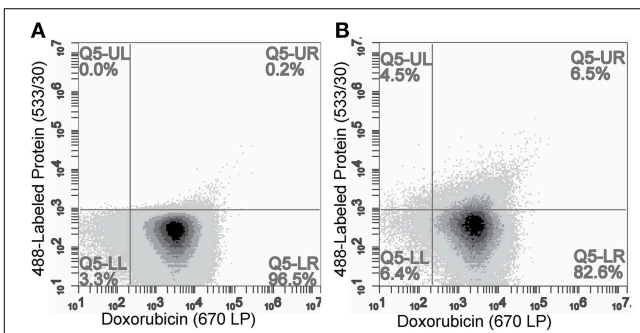


**FIGURE 5 | Flow cytometry analysis of (A) unmodified Lipodox and (B) 488-labeled-DMPGTVLP-modified Lipodox.** Doxorubicin quantified on 670LP emission channel and 488-labeled phage protein quantified on 533/30 emission channel. Samples were excited using a 488 nm laser.

## Cytotoxicity and Uptake of DMPGTVLP-modified Lipodox in Breast Cancer Cells

It was shown previously that DMPGTVLP-modified Lipodox, with modification by cholate solubilized phage protein, would significantly increase the toxicity in MCF-7 breast cancer cells *in vitro* and also *in vivo* (Olofsson et al., 1998; Wang et al., 2010a,b, 2014). We therefore sought to determine if liposome modification by phage protein solubilized in 2-propanol would produce similar results. MCF-7 cells were incubated with DMPGTVLP-modified Lipodox or unmodified Lipodox dilutions for 24 h before quantification of viable cells by MTT assay. DMPGTVLP-modified Lipodox produced a significant decrease in the number of viable cells compared to unmodified Lipodox samples under the same conditions in a dose dependent manner at higher doxorubicin concentrations of 30 μg/mL (62.7 ± 2.5 vs. 80.6 ± 3.7% viable; two tailed

*t*-test, $P = 8.11 \times 10^{-4}$) and 60 μg/mL (32.3 ± 1.3 vs. 50.8 ± 2.5% viable; two tailed *t*-test, $P = 4.97 \times 10^{-3}$) as expected (**Figure 6**).

As shown previously, the increased cytotoxicity observed with DMPGTVLP-modified Lipodox is due to an increased uptake of targeted Lipodox in target cells compared to untargeted Lipodox. We therefore hypothesized that there would be a significant increase in intracellular doxorubicin over time in DMPGTVLP-modified Lipodox compared to unmodified Lipodox. We show over a 24-h time period, there is a significant increase in cell-associated doxorubicin in DMPGTVLP-modified Lipodox compared to the unmodified control Lipodox (**Figure 7**). After 12 h of incubation, there is a significant increase in fluorescence of ∼710 RFU (two-tailed *t*-test, $P = 1.82 \times 10^{-4}$) corresponding to an increase of ∼1.6 μg of total doxorubicin compared to unmodified (328.8 pg of increased doxorubicin/cell). Similarly, after 24 h of incubation, there is a significant increase in fluorescence of ∼640 RFU (two-tailed *t*-test, $P = 3.99 \times 10^{-3}$) corresponding to an increase of ∼1.5 μg of total doxorubicin compared to unmodified (294.9 pg of increased doxorubicin/cell). We therefore can confirm that modification of Lipodox by phage major coat protein in 2-propanol retains the previously observed increased cytotoxicity of targeted Lipodox via an increased delivery of doxorubicin to breast cancer cells.

## Screening of Phage Protein-modified Lipodox

We next sought to screen a number of cancer cell-specific phage proteins isolated in 2-propanol to identify a panel of phage proteins that may enhance the specific toxicity of Lipodox toward cancer cells. We hypothesized that screening ligands in this manner would significantly increase the throughput of ligand identification for targeted drug delivery using a common Lipodox platform and varying the targeting ligand while retaining a common incorporation method. We initially screened 9 different ligands in MCF-7 breast cancer cells, which are commonly sensitive to doxorubicin. Next we screened an additional 5 ligands in PANC-1 pancreatic cancer cells, which are commonly reported to express a multiple drug resistance (MDR) phenotype and become resistant to doxorubicin treatment. Phage protein-modified Lipodox samples were prepared and characterized as above and summarized in **Table 2** to identify preparation parameters for potential bias in the observed toxicity. As shown previously, all modified samples demonstrated a significant increase in mean size distribution (two-tailed *t*-test, $P < 0.05$). Five of the prepared samples (ANDVYLD, EPQSQWSM, VEEGGYIAA, DGQYLGSQ, and DVRGDGLQ) demonstrated a statistically significant change in zeta potential (two-tailed *t*-test, $P < 0.05$), however they were all within a biologically acceptable range. On average, most insertions produced high doxorubicin recovery rates (mean recovery 82.8 ± 20.4%) with no significant loss of doxorubicin following modification (mean loss 3.34 ± 2.02%). Modification with the protein ligand ANDVYLD caused significant loss of recovered doxorubicin (33.8%), however there was still sufficient material to complete the assay and all other parameters were similar to the other preparations.

Following Lipodox modification and characterization, we hypothesized that targeting ligands specific for a certain cell type would increase the toxicity of Lipodox as suggested previously. MCF-7 breast cancer cells were treated with the 9 different phage protein-modified Lipodox and cell viability was measured 72 h after initial treatment. As shown in **Figure 8A** and from the calculated $IC_{50}$ values in **Table 2**, there were a number of protein-modified Lipodox samples that significantly increased the toxicity profile of unmodified Lipodox, including DMPGTVLP as shown previously. The ligands screened stratified into three different groups covering a 100-fold change in $IC_{50}$: (1) ligands showing no improvement from unmodified

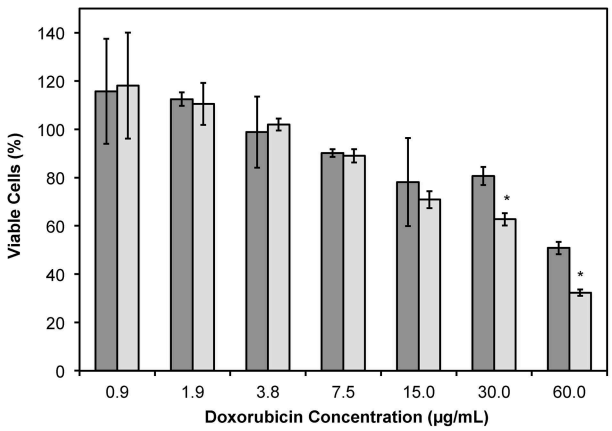


**FIGURE 6 | MTT viability assay of MCF-7 cells treated with dilutions of Lipodox (dark bars) or DMPGTVLP-modified Lipodox (light bars) after 24 h of incubation.** Data are presented as the mean ± sample standard deviation of the percent viable fraction compared to untreated control cells, which were taken as 100% viable. $N = 3$; *$P < 0.05$, paired, two-tailed Student's *t*-test vs. unmodified Lipodox.

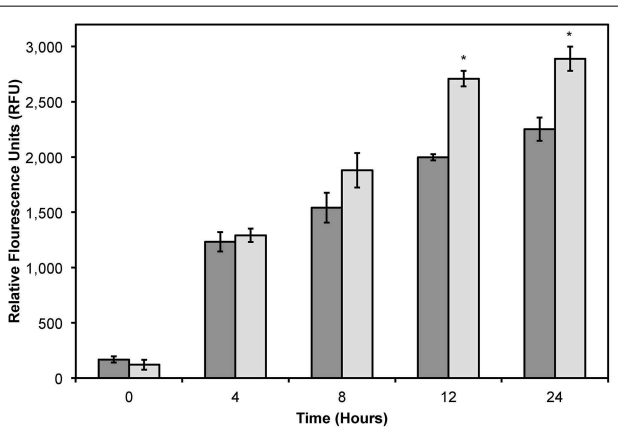


**FIGURE 7 | Doxorubicin uptake assay in MCF-7 cells treated with 2 μg of Lipodox (dark bars) or 2 μg DMPGTVLP-modified Lipodox (light bars) over 24 h.** Data are presented as the mean ± sample standard deviation of the relative fluorescence of doxorubicin at an excitation wavelength of 470 nm and emission wavelength of 590 nm. $N = 3$; *$P < 0.05$, paired, two-tailed Student's *t*-test vs. unmodified Lipodox.

**TABLE 2 | Phage protein-modified Lipodox characterization.**

| Phage | Protein added (μg) | Recovered doxorubicin (%) | Free doxorubicin (%) | Size distribution (d.nm) | Zeta potential (mV) | $IC_{50}$(μg/mL) |
|---|---|---|---|---|---|---|
| **ROUND 1—MCF-7 BREAST CANCER CELLS** | | | | | | |
| ANDVYLD | 0.41 | 33.84 | 1.61 | 81.75 ± 0.31* | −19.9 ± 0.1* | 0.6 |
| ANGRPSMT | 0.86 | 109.02 | 1.72 | 80.53 ± 0.62* | −18.4 ± 1.4 | 0.5 |
| DMPGTVLP | 0.60 | 105.38 | 6.59 | 79.50 ± 1.44* | −18.3 ± 0.7 | 1.3 |
| DVRGDGLQ | 1.49 | 85.19 | 1.62 | 82.00 ± 0.66* | −19.0 ± 0.7 | 30.0 |
| EPSQSWSM | 1.24 | 104.46 | 2.83 | 80.47 ± 0.54* | −19.7 ± 0.3* | 2.8 |
| GLNGRGDPD | 0.53 | 110.92 | 2.71 | 80.39 ± 1.40* | −18.7 ± 0.6 | 3.2 |
| VEEGGYIAA | 0.53 | 73.91 | 1.72 | 81.36 ± 1.28* | −21.3 ± 0.7* | 2.6 |
| VNGRAEAP | 0.97 | 59.18 | 1.42 | 80.80 ± 1.49* | −18.4 ± 1.3 | 0.6 |
| VPTDTDYS | 1.38 | 77.99 | 1.61 | 80.74 ± 1.30* | −18.5 ± 0.4 | 3.3 |
| No Protein | N/A | 98.51 | 1.18 | 73.46 ± 0.49 | −18.6 ± 0.4 | 13.5 |
| **ROUND 2—PANC-1 PANCREATIC CANCER CELLS** | | | | | | |
| DGQYLGSQ | 1.58 | 75.75 | 4.88 | 89.11 ± 1.70* | −16.7 ± 0.5* | NC[a] |
| DVRGDGLQ | 2.48 | 81.20 | 5.91 | 88.98 ± 0.50* | −16.7 ± 0.5* | NC[a] |
| EPSQSWSM | 0.93 | 82.34 | 5.10 | 89.06 ± 0.91* | −17.7 ± 0.5 | NC[a] |
| ETYNQPYL | 0.50 | 80.37 | 6.37 | 90.72 ± 1.21* | −19.7 ± 0.8 | NC[a] |
| GSSEQLYL | 1.22 | 79.71 | 4.80 | 89.66 ± 1.07* | −17.4 ± 0.5 | NC[a] |

[a]*NC, Not calculated; *$p < 0.05$, paired two-tailed Student's t-test vs. unmodified Lipodox (control).*

Lipodox (**Figure 8A**, squares), (2) ligands showing moderate improvement (**Figure 8A**, diamonds), and (3) ligands showing large improvements (**Figure 8A**, circles). As expected ligands with similar structural motifs grouped together, such as ANGRPSMT and VNGRAEAP, and produced similar $IC_{50}$ values. Correlations between all factors in **Table 2** compared to the $IC_{50}$ were performed to identify parameters that might have influenced the toxicity profile apart from the targeting ligand and all parameters had a low to weak Pearson's R correlation ($R < 0.3$) suggesting the observed increase in toxicity were due to the cell-specific targeting ligands.

PANC-1 pancreatic cancer cells are shown to be resistant to doxorubicin by a MDR phenotype caused by overexpression of P-glycoprotein (Pgp) efflux pumps that prevent doxorubicin from accumulating within the cancer cells (**Figure 8B**, black square). However, we hypothesized that introduction of a cell-specific targeting ligand into Lipodox would be able to overcome the observed drug resistance. We showed previously that drug resistance could be overcome by addition of the ligand EPSQSWSM to Lipodox (Schwind et al., 1992; Bedi et al., 2014). We therefore sought to identify other ligands with specificity toward pancreatic cancer that would also significantly increase the toxicity of unmodified Lipodox in PANC-1 pancreatic cancer cells. Five ligands with specificity toward PANC-1 pancreatic cancer cells were inserted and screened as above with liposome characterization parameters identified in **Table 2**. As shown in **Figure 8B**, all ligands significantly increased the toxicity of unmodified Lipodox at high concentrations (two-tailed *t*-test, $P < 0.001$) and a subset of ligands [DGQYLGSQ, ETYNQPYL, and GSSEQLYL] showed a statistically significant increase in toxicity at doxorubicin concentrations of 12 and 24 μg/mL as well (two-tailed *t*-test, $P < 0.05$).

## Discussion

Although targeted nanomedicine delivery has demonstrated its efficiency in systemic cancer treatment in animal models and recently shown success in an ongoing Phase II clinical trial (Petrenko and Smith, 2000; Petrenko, 2008; Hrkach et al., 2012) identification of ideal targeting ligands for active tumor targeting remains a significant challenge. Many methods require multiple conjugation or purification steps before testing the functional activity of a ligand in a given nanomedicine scaffold. A number of these strategies are expensive, time consuming, require large batch volumes due to reactions that produce products with a low overall yield, or require modification of an identified ligand before conjugation. These limitations effectively reduce the ability to screen large numbers of ligands even within the same nanomedicine scaffold. Phage display has been commonly used as a source of novel ligands for various cancer related diagnostic or therapeutic markers. The most commonly used phage display libraries are performed with Ff class of filamentous bacteriophage vectors (including M13, fd, and f1) that displays a random peptide on the pIII minor coat protein, which supports a peptide insert of many different sizes (Smith and Petrenko, 1997; Jayanna et al., 2010b; Wang et al., 2010a; Petrenko and Jayanna, 2014). However, the pIII minor coat protein is only expressed in 5 copies at the infectious head of each phage particle, making it necessary to synthesize the identified cell-specific ligands separately from the phage and conjugate it to the nanoparticle carrier that may compromise the specific binding properties of the selected peptides. Previously, we have generated another type of display system—landscape phage in which the N-terminus of every copy of the pVIII major coat protein is modified with a randomized peptide fusion of 8 or 9 amino acids and have been

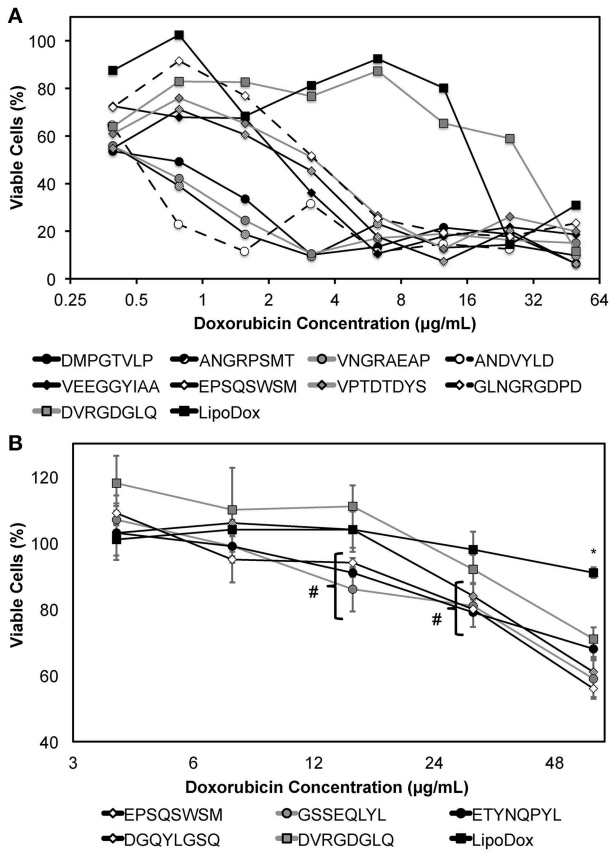


**FIGURE 8 | MTT viability assay of (A) MCF-7 or (B) PANC-1 cells treated with dilutions of phage protein-modified Lipodox after 24 h of drug incubation followed by 48 h of drug washout.** Modified samples are identified by their displayed 8- or 9-mer fusion peptide sequence in the legend above. Data are presented as the mean ± sample standard deviation of the percent viable fraction compared to untreated control cells, which were taken as 100% viable. $N = 3$; $^{*}P < 0.001$, paired, two-tailed Student's *t*-test vs. unmodified Lipodox; $^{\#}P < 0.05$, paired, two-tailed Student's *t*-test vs. unmodified Lipodox.

used extensively to identify a number of cancer-specific ligands targeting a number of different cancer phenotypes (Romanov et al., 2001; Samoylova et al., 2003; Jayanna et al., 2010a; Fagbohun et al., 2012; Bedi et al., 2014). Since the pVIII major coat protein is expressed in 4000 copies per phage in these fd-tet-type vectors (Zacher et al., 1980) scaling of phage propagations up to 1 L scale can routinely produce protein yields up to 20 mg that can subsequently be purified from the bacteriophage genomic DNA using a number of standard techniques. Unlike the pIII minor coat protein, the recovered pVIII major coat protein can then be used directly in a number of drug delivery systems via a post-insertion modification of the nanomedicine scaffold using the inherent peptide domains designed naturally into the full-length coat protein as shown previously (Petrenko and Jayanna, 2014). Here we show a novel combinatorial extension of the phage display technology that allows testing for specific tumor cytotoxicity in a common nanomedicine core modified with different phage protein ligands in much higher screening throughput than traditional technologies to identify candidate ligands for further optimization.

In this study, we showed that the pVIII major coat protein could be isolated in 2-propanol to yield highly pure protein that was free from phage DNA. We hypothesize that the protein retains the α-helical secondary structure as suggested by the interaction of protein with liposomes and the solubility of the isolated protein. Under certain conditions and long storage conditions, the phage pVIII protein commonly adopts an irreversible β-sheet conformation, which causes the solubility of the isolated protein to decrease due to aggregation of large protein multimers (Spruijt et al., 1989). We do notice that extended storage of isolated phage protein in 2-propanol at room temperature will result in precipitated protein aggregates that remain insoluble in agreement with previous studies showing freshly prepared samples lose α-helical structure with time. Thus, freshly prepared phage proteins are recommended for all applications requiring α-helical protein structure, including modification of liposomes. The ability to retain the desired α-helical secondary structure following insertion into drug-loaded liposomes remains to be studied, however modified liposomes have been reported to maintain their targeting ability at least a month after preparation (Wang et al., 2014).

Following a similar insertion scheme as described previously using sodium cholate to solubilize pVIII proteins, we prepared a model drug delivery system consisting of isolated DMPGTVLP protein in 2-propanol inserted into preformed Lipodox liposomes. We then showed that liposomes were successfully modified with protein with significantly less loss of doxorubicin during modification while still retaining functional activity. As shown from a mock insertion of isolated DMPGTVLP phage protein into buffer, the complete loss of phage protein can be suggested to be due to the highly hydrophobic nature of the pVIII major coat protein causing any free protein to precipitate or adsorb to other hydrophobic materials. Similarly, as suggested by the partition coefficient of major coat protein for POPC (1-palmitoyl-2-oleoyl-sn-glycero-e-phosphocholine) lipid membranes reported to be $1.0 \times 10^5$ $M^{-1}$, it is hypothesized that 100% of the isolated protein will partition into the lipid bilayer primarily by hydrophobic interactions (Soekarjo et al., 1996).

In an attempt to identify the degree of protein labeling per liposome, we used semi-quantitative dot blotting and flow cytometry of intact liposomes to characterize protein-loading properties following Lipodox modification. From theoretical calculations based on mass of lipid/liposome and calculated molecular weights of phage proteins, it is estimated that there are ∼50–100 ligands per liposome depending on the diameter of the liposomes used for modification. The data we obtained from dot blotting suggests there is no free protein in solution after liposome modification and we maintain a correct orientation of targeting protein with N-terminus exposed from the liposome and the C-terminus protected within the liposome core. Following degradation of phage protein-modified liposomes with Proteinase K, there was complete degradation of the N-terminus and no degradation of C-terminus. These data suggest that Proteinase K is sufficient to degrade all exposed proteins and 100% of the N-terminus is exposed from the

liposome surface. We also estimate that 100% of the C-terminus is protected from degradation suggesting that the insertion of protein was complete and that no free phage protein is found in solution. We therefore show that the C-terminus of the pVIII major coat protein was able to translocate through the liposome membrane with high orientation specificity. We also show that following insertion of Alexa 488-labeled DMPGTVLP major coat protein into Lipodox, there was a significant shift of the liposome population toward the Alexa 488-positive gate. Only 11% of the liposome population showed a detectible increase in Alexa 488-positive labeling. Due to the low labeling efficiency (∼10%) of the phage protein prior to insertion, we are unable to detect all ligand incorporations into the liposomes and can only resolve the most fluorescently intense liposomes receiving large numbers of Alexa 488-labeled phage proteins. Based on an estimate of 50 ligands/liposome, it can be expected that insertion of labeled proteins will follow a normal distribution with a mean of 5 labeled ligands/liposome. However, because of the poor resolution between the two populations, we can only observe the (11%) upper-tail of the normally distributed population which are the most bright. Optimization of fluorophore conjugation to the phage ligands or changing to a brighter fluorophore can increase the efficiency of this assay. It was also noted that there was a slight decrease in the doxorubicin mean channel fluorescence following modification (unmodified = 7929 RFU vs. modified = 5679 RFU in 670 LP-H channel) consistent with a slight loss in encapsulated doxorubicin. Free DMPGTVLP labeled protein appeared to aggregate heavily and form very bright particles, however in phage protein-modified Lipodox we observed only moderate increases in fluorescence. As we only see moderate increases in fluorescence, this suggests that there is no detectible free protein in solution with the modified Lipodox. This data is in agreement with previous reports on the completeness of insertion using different concentrations of isolate phage protein while maintaining a constant lipid mass up to a protein/lipid ratio of 1:200 (Soekarjo et al., 1996; Wang et al., 2011). We note that a significant limitation of this assay is the requirement for gating on a fluorescent population of liposomes. Since we are near the detection limits of the equipment, we found that empty liposomes, when performed with the same parameters, produce unreliable results as there is no precise method to identify liposomes from background noise during the measurement. We have seen that translocation through preformed lipid membranes is spontaneous (not requiring any host proteins), pH and temperature dependent. We propose that insertion of pVIII major coat protein is a two-stage process: (1) attachment of protein to the liposome surface, and (2) translocation of the C-terminus (**Figure 9**). The association of isolated pVIII major coat protein has been studied in detail previously, however the mechanism of C-terminal translocation has not been fully elucidated. We have previously proposed a mechanism in which the positively charged C-terminus is able to penetrate through a lipid bilayer (Petrenko and Jayanna, 2014) however detailed studies on the mechanism of translocation remain to be completed.

It remains to be seen whether there is a direct correlation between the strength of phage ligand binding to a target cell line and a subsequent increase in functional cytotoxicity activity *in vitro*. From our preliminary data, we find that sometimes weak binding phage clones perform better as targeting ligands in liposomal nanomedicines than strong binding phages. It has been suggested that low affinity ligands may be ideal for improved tumor penetration, as actively targeted drug delivery systems targeted by high affinity ligands are suggested to remain on the tumor periphery (Gray et al., 2013). For this reason, we used a functional screening assay of the final targeted nanomedicine in which new candidate ligands can be identified based on the desired increase in cytotoxicity rather than building an ideal drug delivery system based on optimization of individual components. For the functional screening assays, the drug exposure time was maintained at 24 h for all viability experiments to prevent excess drug leakage due to liposome degradation over the total

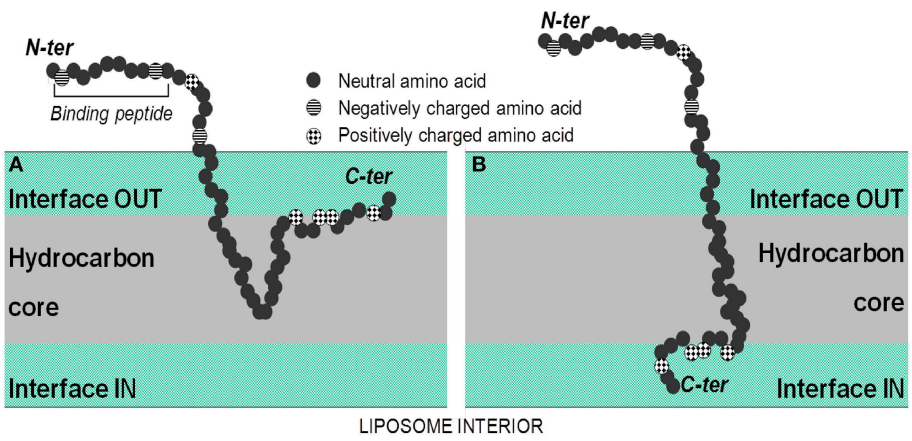


**FIGURE 9 | Spontaneous insertion of the major coat protein into lipid membranes. (A)** In the first step, the isolated coat protein binds to the lipid membrane using electrostatic interactions of the C-terminus with negatively charged phosphate headgroups of lipids, followed by the insertion of the hydrophobic region of the protein into the hydrocarbon core of the lipid bilayer. **(B)** In the second step, the hydrophilic tail is released into the *trans* side of lipid bilayer through a process similar to cell-penetrating peptides. From Petrenko and Jayanna (2014).

measurement time. We have seen minimal doxorubicin leakage of phage protein-modified doxorubicin liposomes at 37°C in the presence of serum over the total test period (data not shown), however we sought to optimize screening conditions with alternative encapsulated drugs in mind displaying less carrier stability. We also increased the total incubation time of viability assays to a total of 72 h consisting of 24 h with phage protein-modified Lipodox samples plus an additional 48 h washout period in complete culture medium. The extended assay conditions allowed all cells, irrespective of origin, sufficient time to complete a normal cell cycle and thereby produce an increased toxicity profile in doxorubicin treated cells due to the inability of genomic DNA to replicate, resulting in a stalled cell cycle phenotype in the $G_0/G_1$ phase commonly observed with doxorubicin toxicity (Lukyanova et al., 2009). Given the broadly defined parameters, this screening assay can therefore be extended to a variety of cell types and also a number of drug classes employing different mechanisms of action. A limitation of this screening assay is the inherent nature of the MTT assay as a measure of mitochondrial succinate dehydrogenase activity in metabolically active cells rather than a cytotoxic event. However, as shown in previous work by us and other authors, doxorubicin will cause cell death by activation of caspase cascades leading to apoptosis (Wang et al., 2004). As we have not changed the properties of the cytotoxic drug and we have shown that phage proteins are non-toxic (Bedi et al., 2014) we don't expect significant changes in the primary mechanism of cell death, only an increase in intracellular delivery of cytotoxic drug. Since we have shown previously that the MTT assay is a good indicator of cell death in this system and death can be confirmed by visual observations, the reduction in cell viability as determined by the MTT assay would be sufficient for identification of ligands in a screening assay.

From our screening experiment in MCF-7 cells, we were able to identify a previously validated breast cancer cell-specific protein DMPGTVLP that interacts with cell surface expressed nucleolin and increases the therapeutic effect of liposomal doxorubicin *in vitro* and in *vivo* by increasing the specific delivery of doxorubicin to MCF-7 cell nuclei (Wang et al., 2010a, 2014; Fagbohun et al., 2012). Liposomes modified with a phage fusion protein displaying the peptide ANDVYLD showed the greatest increase in toxicity with a calculated $IC_{50}$ of 0.6 μg/mL in MCF-7 cells. We also identified two peptides containing a positionally constrained **NGR** motif (A**NGR**PSMT and V**NGR**AEAP) that showed similar toxicity profiles (average $IC_{50}$ =0.55 μg/mL) as expected. Surprisingly, phage VNGRAEAP did not show binding to MCF-7 cells in our previous binding assays, however this limitation may be due to a short binding assay duration (1 h) compared to the duration of the cytotoxicity assay (24 h) or due to a difference in primary uptake mechanism between the two phage as shown previously (Gillespie et al. Submitted). A similar motif containing a positionally different **NGR** motif (GL**NGR**GDPD) showed improvement in toxicity to 3.2 μg/mL, however it was unable to reach the same toxicity of the other motifs. This may be due to a difference in the NGR motif availability to the receptor or an effect of peptide affinity. Inclusion of a pancreatic cancer-specific ligand (DVRGDLQ) resulted in no significant increase in toxicity suggesting the specificity of ligands to increase doxorubicin delivery specifically to the target cells and is not a result of modification. Screening the DVRGDLQ peptide in pancreatic cancer cells produced an increase in cytotoxicity compared to unmodified Lipodox. Interestingly, a subset of ligands with similar motifs (DGQYLGSQ, ETYNQPYL, and GSSEQLYL) grouped together to produce similar cytotoxicity profiles. Comparison of a shared **D**XXXX**G**X**D** motif showed that there was a significant difference between DVRGDGLQ and GQYLGSQ ligands at higher concentrations (two-tailed *t*-test, $P < 0.01$) with the DGQYLGSQ ligand producing greater toxicity suggesting minimal involvement of the **D**XXXX**G**X**D** motif. Comparison of the **YL** motif found in different positions of the three ligands showed no statistical differences between the three ligands (two-tailed *t*-test, $P > 0.05$), however all three showed significant differences compared to unmodified. These data therefore suggest the **YL** motif, irrespective of position, will cause an increase in toxicity. No putative receptor has been suggested for any of the three ligands at this time, however it is interesting to note the number of essential amino acids (Y, L, W, and V) present in the identified ligands that are typically underrepresented in our phage display library (Kuzmicheva et al., 2009). The presented data demonstrate the use of phage display technology along with a combinatorial screening strategy to significantly enhance the screening throughput of targeted nanomedicines that may considerably accelerate progress in actively targeted drug development.

## Author Contributions

JG, DB, AG, and AP designed and performed experiments, contributed to the interpretation of results, wrote the manuscript and approved the final version for publication; VP designed the research strategy and experiments, contributed to the interpretation of results, wrote the manuscript and approved the final version for publication.

## Acknowledgments

We would like to thank Dr. R Curtis Bird and Allison Church Bird (Flow Cytometry Facility at Auburn University) for their assistance with collection and interpretation of flow cytometry data. This study was supported by the National Cancer Institute at the National Institutes of Health [U54CA151881 to VAP] and funding support from the Auburn University Research Initiative in Cancer (AURIC) to VAP. The content is solely the responsibility of the authors and does not necessarily represent the official views of the National Institutes of Health.

## References


Bedi, D., Gillespie, J. W., and Petrenko, V. A. (2014). Selection of pancreatic cancer cell-binding landscape phages and their use in development of anticancer nanomedicines. *Protein Eng. Des. Sel.* 27, 235–243. doi: 10.1093/protein/gzu020

Brigati, J. R., and Petrenko, V. A. (2005). Thermostability of landscape phage probes. *Anal. Bioanal. Chem.* 382, 1346–1350. doi: 10.1007/s00216-005-3289-y

Brigati, J. R., Samoylova, T. I., Jayanna, P. K., and Petrenko, V. A. (2008). "Phage display for generating peptide reagents," in *Current Protocols in Protein Science,* eds J. E. Coligan, B. M. Dunn, D. W. Speicher, and P. T. Wingfield (New Jersey, NJ: John Wiley & Sons, Inc), 1–27.

DeSantis, C. E., Lin, C. C., Mariotto, A. B., Siegel, R. L., Stein, K. D., Kramer, J. L., et al. (2014). Cancer treatment and survivorship statistics. *CA Cancer J. Clin.* 4, 252–271. doi: 10.3322/caac.21235

Early Breast Cancer Trialists' Collaborative Group (EBCTCG). (2005). Effects of chemotherapy and hormonal therapy for early breast cancer on recurrence and 15-year survival: an overview of the randomised trials. *Lancet* 365, 1687–1717. doi: 10.1016/S0140-6736(05)66544-0

Fagbohun, O. A., Bedi, D., Grabchenko, N. I., DeInnocentes, P. A., Bird, R. C., and Petrenko, V. A. (2012). Landscape phages and their fusion proteins targeted to breast cancer cells. *Protein Eng. Des. Sel.* 25, 271–283. doi: 10.1093/protein/gzs013

Fang, J., Nakamura, H., and Maeda, H. (2011). The EPR effect: unique features of tumor blood vessels for drug delivery, factors involved, and limitations and augmentation of the effect. *Adv. Drug Deliv. Rev.* 63, 136–151. doi: 10.1016/j.addr.2010.04.009

Florent, J.-C., and Monneret, C. (2008). "Doxorubicin conjugates for selective delivery to tumors," in *Topics in Current Chemistry,* ed K. Krohn (Berlin: Springer), 99–140.

Gabizon, A., Shmeeda, H., and Barenholz, Y. (2003). Pharmacokinetics of pegylated liposomal Doxorubicin: review of animal and human studies. *Clin. Pharmacokinet.* 42, 419–436. doi: 10.2165/00003088-200342050-00002

Gray, B. P., McGuire, M. J., and Brown, K. C. (2013). A liposomal drug platform overrides Peptide ligand targeting to a cancer biomarker, irrespective of ligand affinity or density. *PLoS ONE* 8:e72938. doi: 10.1371/journal.pone.0072938

Hrkach, J., Hoff Von, D., Mukkaram Ali, M., Andrianova, E., Auer, J., Campbell, T., et al. (2012). Preclinical development and clinical translation of a PSMA-targeted docetaxel nanoparticle with a differentiated pharmacological profile. *Sci. Transl. Med.* 4, 128ra39. doi: 10.1126/scitranslmed.3003651

Jayanna, P. K., Bedi, D., DeInnocentes, P. A., Bird, R. C., and Petrenko, V. A. (2010a). Landscape phage ligands for PC3 prostate carcinoma cells. *Protein Eng. Des. Sel.* 23, 423–430. doi: 10.1093/protein/gzq011

Jayanna, P. K., Bedi, D., Gillespie, J. W., DeInnocentes, P. A., Wang, T., Torchilin, V. P., et al. (2010b). Landscape phage fusion protein-mediated targeting of nanomedicines enhances their prostate tumor cell association and cytotoxic efficiency. *Nanomedicine* 6, 538–546. doi: 10.1016/j.nano.2010.01.005

Jayanna, P. K., Torchilin, V. P., and Petrenko, V. A. (2009). Liposomes targeted by fusion phage proteins. *Nanomedicine* 5, 83–89. doi: 10.1016/j.nano.2008.07.006

Kung, V. T., and Redemann, C. T. (1986). Synthesis of carboxyacyl derivatives of phosphatidylethanolamine and use as an efficient method for conjugation of protein to liposomes. *Biochim. Biophys. Acta* 862, 435–439. doi: 10.1016/0005-2736(86)90247-6

Kuzmicheva, G. A., Jayanna, P. K., Sorokulova, I. B., and Petrenko, V. A. (2009). Diversity and censoring of landscape phage libraries. *Protein Eng. Des. Sel.* 22, 9–18. doi: 10.1093/protein/gzn060

Lee, D.-H., Rötger, C., Appeldoorn, C. C. M., Reijerkerk, A., Gladdines, W., Gaillard, P. J., et al. (2014). Glutathione PEGylated liposomal methylprednisolone (2B3-201) attenuates CNS inflammation and degeneration in murine myelin oligodendrocyte glycoprotein induced experimental autoimmune encephalomyelitis. *J. Neuroimmunol.* 274, 96–101. doi: 10.1016/j.jneuroim.2014.06.025

Li, W., Suez, I., and Szoka, F. C. (2007). Reconstitution of the M13 major coat protein and its transmembrane peptide segment on a DNA template. *Biochemistry* 46, 8579–8591. doi: 10.1021/bi700165m

Loughrey, H., Bally, M. B., and Cullis, P. R. (1987). A non-covalent method of attaching antibodies to liposomes. *Biochim. Biophys. Acta* 901, 157–160. doi: 10.1016/0005-2736(87)90267-7

Lukyanova, N. Y., Rusetskya, N. V., Tregubova, N. A., and Chekhun, V. F. (2009). Molecular profile and cell cycle in MCF-7 cells resistant to cisplatin and doxorubicin. *Exp. Oncol.* 31, 87–91.

Manning, M., Chrysogelos, S., and Griffith, J. (1981). Mechanism of coliphage M13 contraction: intermediate structures trapped at low temperatures. *J. Virol.* 40, 912–919. doi: 10.1016/0042-6822(70)90137-6

Marvin, D. A., Symmons, M. F., and Straus, S. K. (2014). Structure and assembly of filamentous bacteriophages. *Prog. Biophys. Mol. Biol.* 114, 80–122. doi: 10.1016/j.pbiomolbio.2014.02.003

Olofsson, L., Ankarloo, J., and Nicholls, I. A. (1998). Phage viability in organic media: insights into phage stability. *J. Mol. Recogn.* 11, 91–93.

Petrenko, V. A. (2008). Landscape phage as a molecular recognition interface for detection devices. *Microelectronics J.* 39, 202–207. doi: 10.1016/j.mejo.2006.11.007

Petrenko, V. A., and Jayanna, P. K. (2014). Phage protein-targeted cancer nanomedicines. *FEBS Lett.* 588, 341–349. doi: 10.1016/j.febslet.2013.11.011

Petrenko, V. A., and Smith, G. P. (2000). Phages from landscape libraries as substitute antibodies. *Protein Eng.* 13, 589–592. doi: 10.1093/protein/13.8.589

Petrenko, V. A., Smith, G. P., Gong, X., and Quinn, T. (1996). A library of organic landscapes on filamentous phage. *Protein Eng.* 9, 797–801. doi: 10.1093/protein/9.9.797

Pidgeon, C., and Hunt, C. A. (1981). Calculating number and surface area of liposomes in any suspension. *J. Pharm. Sci.* 70, 173–176. doi: 10.1002/jps.2600700215

Riihimäki, M., Thomsen, H., Brandt, A., Sundquist, J., and Hemminki, K. (2012). Death causes in breast cancer patients. *Ann. Oncol.* 23, 604–610. doi: 10.1093/annonc/mdr160

Romanov, V. I., Durand, D. B., and Petrenko, V. A. (2001). Phage display selection of peptides that affect prostate carcinoma cells attachment and invasion. *Prostate* 47, 239–251. doi: 10.1002/pros.1068

Samoylova, T. I., Petrenko, V. A., Morrison, N. E., Globa, L. P., Baker, H. J., and Cox, N. R. (2003). Phage probes for malignant glial cells. *Mol. Cancer Ther.* 2, 1129–1137.

Schwind, P., Kramer, H., Kremser, A., Ramsberger, U., and Rasched, I. (1992). Subtilisin removes the surface layer of the phage fd coat. *Eur. J. Biochem.* 210, 431–436. doi: 10.1111/j.1432-1033.1992.tb17438.x

Shroff, K., and Kokkoli, E. (2012). PEGylated liposomal doxorubicin targeted to α5β1-expressing MDA-MB-231 breast cancer cells. *Langmuir* 28, 4729–4736. doi: 10.1021/la204466g

Siegel, R. L., Miller, K. D., and Jemal, A. (2015). Cancer statistics. *CA Cancer J. Clin.* 65, 5–29. doi: 10.3322/caac.21254

Smith, G. P. (1993). Surface display and peptide libraries. *Gene* 128, 1–2. doi: 10.1016/0378-1119(93)90145-S

Smith, G. P., and Petrenko, V. A. (1997). Phage Display. *Chem. Rev.* 97, 391–410. doi: 10.1021/cr960065d

Smith, G. P., Petrenko, V. A., and Matthews, L. J. (1998). Cross-linked filamentous phage as an affinity matrix. *J. Immunol. Methods* 215, 151–161. doi: 10.1016/S0022-1759(98)00087-8

Soekarjo, M., Eisenhawer, M., Kuhn, A., and Vogel, H. (1996). Thermodynamics of the membrane insertion process of the M13 procoat protein, a lipid bilayer traversing protein containing a leader sequence. *Biochemistry* 35, 1232–1241. doi: 10.1021/bi951087h

Spidlen, J., Breuer, K., Rosenberg, C., Kotecha, N., and Brinkman, R. R. (2012). FlowRepository: a resource of annotated flow cytometry datasets associated with peer-reviewed publications. *Cytometry A* 81, 727–731. doi: 10.1002/cyto.a.22106

Spruijt, R. B., Wolfs, C. J., and Hemminga, M. A. (1989). Aggregation-related conformational change of the membrane-associated coat protein of bacteriophage M13. *Biochemistry* 28, 9158–9165. doi: 10.1021/bi00449a030

Wang, R., Xiao, R., Zeng, Z., Xu, L., and Wang, J. (2012). Application of poly(ethylene glycol)-distearoylphosphatidylethanolamine (PEG-DSPE) block copolymers and their derivatives as nanomaterials in drug delivery. *Int. J. Nanomedicine* 7, 4185–4198. doi: 10.2147/IJN.S34489

Wang, S., Konorev, E. A., Kotamraju, S., Joseph, J., Kalivendi, S., and Kalyanaraman, B. (2004). Doxorubicin induces apoptosis in normal and tumor cells via distinctly different mechanisms. intermediacy of H(2)O(2)- and p53-dependent pathways. *J. Biol. Chem.* 279, 25535–43. doi: 10.1074/jbc.M400944200

Wang, T., D'Souza, G. G. M., Bedi, D., Fagbohun, O. A., Potturi, L. P., Papahadjopoulos-Sternberg, B., et al. (2010a). Enhanced binding and killing of target tumor cells by drug-loaded liposomes modified with tumor-specific phage fusion coat protein. *Nanomedicine* 5, 563–574. doi: 10.2217/nnm.10.30

Wang, T., Hartner, W. C., Gillespie, J. W., Praveen, K. P., Yang, S., Mei, L. A., et al. (2014). Enhanced tumor delivery and antitumor activity *in vivo* of liposomal doxorubicin modified with MCF-7-specific phage fusion protein. *Nanomedicine* 10, 421–430. doi: 10.1016/j.nano.2013.08.009

Wang, T., Kulkarni, N., Bedi, D., D'Souza, G. G. M., Papahadjopoulos-Sternberg, B., Petrenko, V. A., et al. (2011). *In vitro* optimization of liposomal nanocarriers prepared from breast tumor cell specific phage fusion protein. *J. Drug Target.* 19, 597–605. doi: 10.3109/1061186X.2010.550920

Wang, T., Yang, S., Petrenko, V. A., and Torchilin, V. P. (2010b). Cytoplasmic delivery of liposomes into MCF-7 breast cancer cells mediated bycell-specific phage fusion coat protein. *Mol. Pharm.* 7, 1149–1158. doi: 10.1021/mp1000229

Zacher, A. N., Stock, C. A., Golden, J. W., and Smith, G. P. (1980). A new filamentous phage cloning vector: fd-tet. *Gene* 9, 127–140. doi: 10.1016/0378-1119(80)90171-7

**Conflict of Interest Statement:** The authors declare that the research was conducted in the absence of any commercial or financial relationships that could be construed as a potential conflict of interest.

frontiers in Microbiology

ORIGINAL RESEARCH
published: 27 May 2015
doi: 10.3389/fmicb.2015.00530

# Targeting glioblastoma via intranasal administration of Ff bacteriophages

*Eyal Dor-On and Beka Solomon**

*Department of Molecular Microbiology and Biotechnology, George S. Wise Faculty of Life Sciences, Tel-Aviv University, Tel-Aviv, Israel*

Bacteriophages (phages) are ubiquitous viruses that control the growth and diversity of bacteria. Although they have no tropism to mammalian cells, accumulated evidence suggests that phages are not neutral to the mammalian macro-host and can promote immunomodulatory and anti-tumorigenic activities. Here we demonstrate that Ff phages that do not display any proteins or peptides could inhibit the growth of subcutaneous glioblastoma tumors in mice and that this activity is mediated in part by lipopolysaccharide molecules attached to their virion. Using the intranasal route, a non-invasive approach to deliver therapeutics directly to the CNS, we further show that phages rapidly accumulate in the brains of mice and could attenuate progression of orthotopic glioblastoma. Taken together, this study provides new insight into phages non-bacterial activities and demonstrates the feasibility of delivering Ff phages intranasally to treat brain malignancies.

**Keywords: Ff bacteriophages, lipopolysaccharides, glioblastoma, intranasal delivery**

OPEN ACCESS

***Edited by:***
*Jasna Rakonjac, Massey University, New Zealand*

***Reviewed by:***
*Dahlene N. Fusco, Massachusetts General Hospital, USA*
*Dragana Gagic, AgResearch, New Zealand*

****Correspondence:***
*Beka Solomon, Department of Molecular Microbiology and Biotechnology, George S. Wise Faculty of Life Sciences, Tel-Aviv University, Tel-Aviv 69978, Israel*
*beka@post.tau.ac.il*

***Specialty section:***
*This article was submitted to Virology, a section of the journal Frontiers in Microbiology*

***Received:*** *19 November 2014*
***Accepted:*** *14 May 2015*
***Published:*** *27 May 2015*

***Citation:***
*Dor-On E and Solomon B (2015) Targeting glioblastoma via intranasal administration of Ff bacteriophages. Front. Microbiol. 6:530. doi: 10.3389/fmicb.2015.00530*

## Introduction

The family of Ff filamentous bacteriophages (phages) consists of three members (f1, M13, and fd) that share 98.5% homology in their DNA and a similar morphology; a flexible filament, about 900 nm long and 6–10 nm in diameter. They infect *Escherichia coli* carrying the F-episome and propagate without causing cell lysis (Rakonjac et al., 2011).

Since the introduction of phage display technique by Smith (1985), Ff phages have been extensively utilized in various biotechnology applications, both *in vitro* and *in vivo*, including in human patients (Pasqualini and Ruoslahti, 1996; Arap et al., 1998; Frenkel and Solomon, 2002; Larocca et al., 2002; Krag et al., 2006; Yacoby et al., 2006; Rakover et al., 2010; Rakonjac et al., 2011; Roehnisch et al., 2014). However, although the interaction between Ff phages and bacteria has been well studied, knowledge of their impact on the mammalian macro-host is rather sparse.

The need to study such potential interactions is underscored by the fact that phages populate different niche in the mammalian macro-host (Kutter, 2005; Letarov and Kulikov, 2009) as well as a growing body of evidence suggesting that some phages, including Ff phages, have the capacity to promote non-bacterial activities, even though they have no tropism to mammalian cells. For example, Ff phages can elicit intense humoral and cellular immune responses and thus, are utilized in vaccination as carriers of foreign motifs as well as adjuvants (Minenkova et al., 1993; Willis et al., 1993; De Berardinis et al., 1999, 2000; Frenkel et al., 2000; Wan et al., 2001; Wu et al., 2002; Prisco and De Berardinis, 2012). In addition, Ff phages have been reported to possess anti-tumorigenic properties; Stimulation of cultured tumor associated macrophages (TAM's) with lipopolysaccharide (LPS) free, wild-type M13 phages skewed their polarization toward the anti-tumorigenic M1 phenotype and promoted migration of cytotoxic neutrophils in

response to factors secreted by stimulated TAM's (Eriksson et al., 2009). Accordingly, treatment of mice bearing subcutaneous melanoma tumors with tumor specific phages (displaying B16-F10 mouse melanoma specific peptide or HLA-A2 specific Fab) led to an intense anti-tumorigenic response associated with neutrophil infiltration into the tumor microenvironment and prolonged survival (Eriksson et al., 2007).

Intranasal administration is a non-invasive approach which facilitates to bypass the blood–brain barrier and deliver therapeutics directly to the CNS. Drugs administered via the intranasal route avoid hepatic first pass metabolism and have limited effect on periphery organs compared with systematically administered drugs (Thorne et al., 2004; da Fonseca et al., 2011; Henkin, 2011; Lochhead and Thorne, 2012). Surprisingly, Ff phages (MW = $12 \times 10^6$ Da) were previously reported to gain access to the CNS of mice when given intranasally. This was demonstrated to depend on their filament structure and was further utilized to deliver anti-β amyloid antibody fragment into brains of APP transgenic mice to facilitate *in vivo* targeting of β amyloid plaques (Frenkel and Solomon, 2002).

Here, we aimed to evaluate the feasibility of treating brain malignancies via intranasal administration of Ff phages using an aggressive murine model of glioblastoma. Glioblastoma and malignant gliomas account for the majority of the malignant primary brain tumors in humans. Current treatment of glioblastoma is based on tumor resection to the extent feasible followed by radiotherapy and temozolomide chemotherapy, yet, tumor recurrence occurs in virtually all cases and the prognosis of glioblastoma patients remains dismal having a median survival of 15 months from day of diagnosis (Omuro and DeAngelis, 2013).

In our attempt to remove bacterial debris from our phage preparations prior to their administration to mice we observed that LPS, a major byproduct of coliphages preparations, could not be completely eliminated. LPS is released to the media upon lysis of Gram-negative bacteria and acts as a powerful activator of innate immune responses (Bryant et al., 2010). In fact, LPS can affect a wide range of biological processes including angiogenesis, tumorigenesis, and metastasis (Mattsby-Baltzer et al., 1994; Harmey et al., 2002; Reisser et al., 2002; Pollet et al., 2003). Picogram concentrations of LPS are sufficient to promote cell activation while high enough concentrations can lead to sepsis and septic shock accompanied by disseminated intravascular coagulation (DIC) and multiple organ failure (Gioannini et al., 2004; Angus and van der Poll, 2013). As such, the removal of LPS from phage preparations has been addressed by several studies (Kutter and Sulakvelidze, 2004; Zakharova et al., 2005; Eriksson et al., 2007; Oslizlo et al., 2011). The conventional technique applied to eliminate LPS from recombinant proteins and phages, follows the phase separation protocol using Triton X-114 (Aida and Pabst, 1990).

In this study, phage purification with Triton X-114 alone or in combination with caesium chloride yielded 1,000–10,000 fold decrease in LPS concentration compared to non-purified (NP) phages [Limulus amebocyte lysate (LAL) assay, results are not shown] but failed to result in LPS-free preparations. We show that Ff phages associate with LPS and that LPS contributes to their anti-tumorigenic activity. Using the intranasal route, we further demonstrate that Ff phages can affect progression of orthotopic glioblastoma.

## Results

### Ff Phages are Carriers of LPS

To investigate whether LPS interacts with Ff phages, NP phages were immobilized to microtiter plates by capture antibodies and exposed to anti-LPS antibodies. LPS was detected on the surface of phages in a dose dependent manner (**Figure 1A**). This was also supported by direct and sandwich ELISA based immunogold transmission electron microscopy (TEM) showing co-localization of LPS with phages (Supplementary Material, **Figure 1C**). Similar to the coat proteins of phages, LPS was mostly detected adjacent to the virion rather than in phage-clear regions (Supplementary Material). As expected, purification of phages with caesium chloride alone or in combination with Triton reduced signal intensity (**Figure 1B**). Yet, even when both techniques were applied, antibodies still detected LPS on immobilized phages. Furthermore, when denatured phages (boiled phages) were used in the same ELISA, detection of LPS was highly increased (**Figure 1D**) plausibly owing to exposure of new phages and LPS epitopes. Interestingly, NP phages or purified phages failed to react with supernatant containing LPS of stationary-phase uninfected bacteria in direct ELISA (data is not shown). Collectively these observations imply that LPS molecules associate with the virion, some in sites that are not surface exposed, yet Ff phages show no affinity to LPS in these experimental conditions.

Whether LPS carried by phages is biologically active depends on its chemical and biophysical structure (Mueller et al., 2004). Using the chromogenic LAL assay we demonstrate that LPS derived from immunopurified phages could exert biological activity (**Figure 1E**). This may also indicate that Ff phages carry LPS aggregates on their surface (Mueller et al., 2004). Furthermore, phages could interact with LPS binding protein (LBP; **Figure 1F**) which binds to LPS aggregates and catalyzes their transfer to CD14 (Hailman et al., 1994; Gioannini et al., 2004; Park and Lee, 2013).

### Ff Phages and Purified LPS Inhibit Subcutaneous Tumor Growth

We then assessed whether LPS contributes to the activity of phages *in vivo* using an immunocompetent mouse model of glioblastoma (Szatmári et al., 2006). Repeated administration of 1.7E+12 phages from preparations containing different endotoxin concentration to mice bearing subcutaneous GL261 tumors shows that phages could suppress tumor growth, yet the intensity of their anti-tumorigenic activity was positively correlated with the concentration of endotoxin found in the preparation (**Figure 2A**). To better evaluate the involvement of LPS in this activity, mice bearing subcutaneous GL261 stably expressing green fluorescent protein (GFP) were injected peritumorally with phages or purified LPS extracted from naive

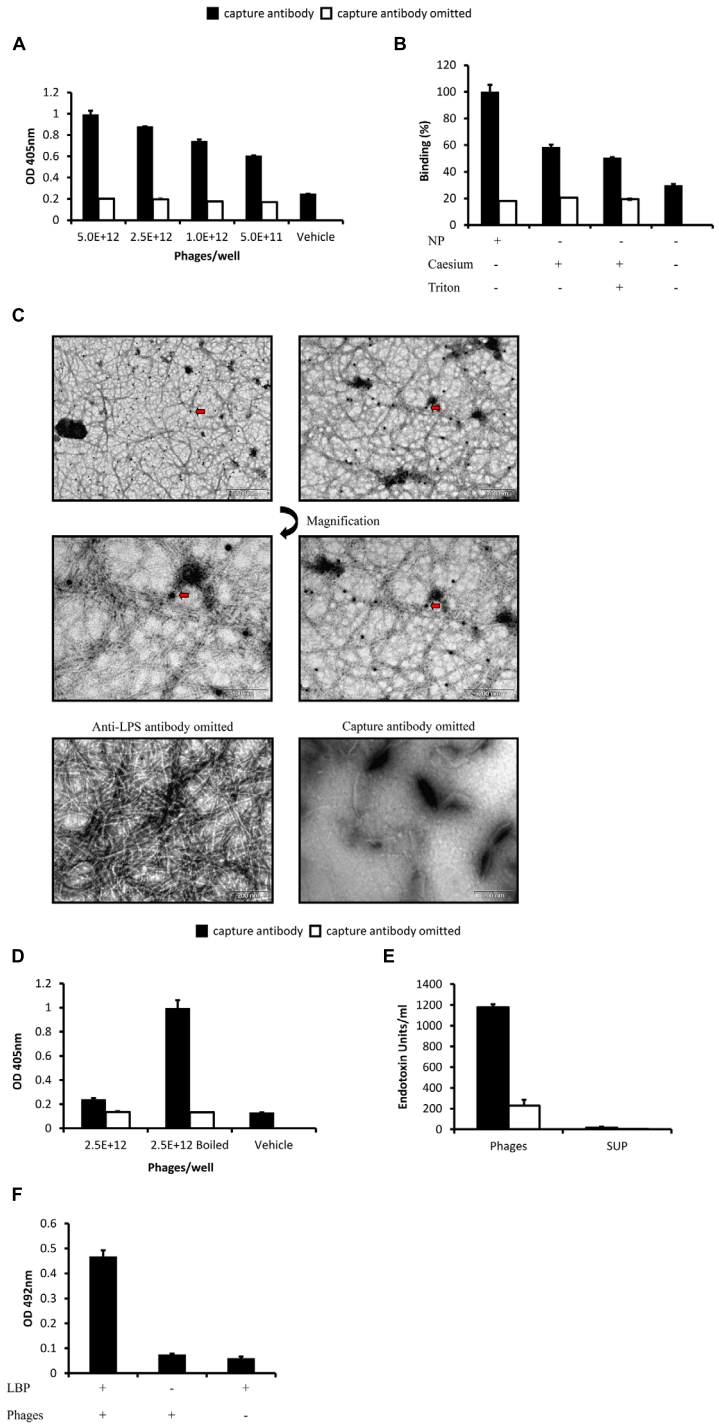


**FIGURE 1 | Detection of lipopolysaccharide (LPS) on the surface of Ff phages. (A)** ELISA plate was coated with anti-p3 antibodies (capture antibody) in coating buffer or coating buffer alone. Different concentrations of non-purified (NP) phages were applied to the plate and LPS was detected by anti-LPS antibodies followed by alkaline phosphatase (AP) conjugated antibodies. **(B)** Sandwich ELISA was performed as in **(A)**, equal concentrations of NP phages (following PEG precipitation), caesium purified phages or caesium, and Triton purified phages were applied to the plate. **(C)** NP phages were immobilized to a nickel grid by anti-p8 capture antibodies, LPS was detected by anti-LPS antibodies followed by gold conjugated antibodies (arrow). Phages were visualized by negative staining. **(D)** Sandwich ELISA was performed as in **(A)**, wells were supplemented with NP phages or equal concentration of NP phages after 3 min incubation at 95°C. The plate was read following short exposure to AP substrate. **(E)** ELISA plate was coated with anti-p3 antibodies, NP phages or bacteria supernatant were applied to the plate and the complex was detached by incubation with NaOH. Endotoxin concentration in the samples was quantified using the limulus amebocyte lysate (LAL) assay. **(F)** ELISA plate was coated with rhLBP then E+13/well NP phages were applied to the plate and were detected by anti-p8 HRP conjugated antibodies. Results are depicted as mean ± SEM.

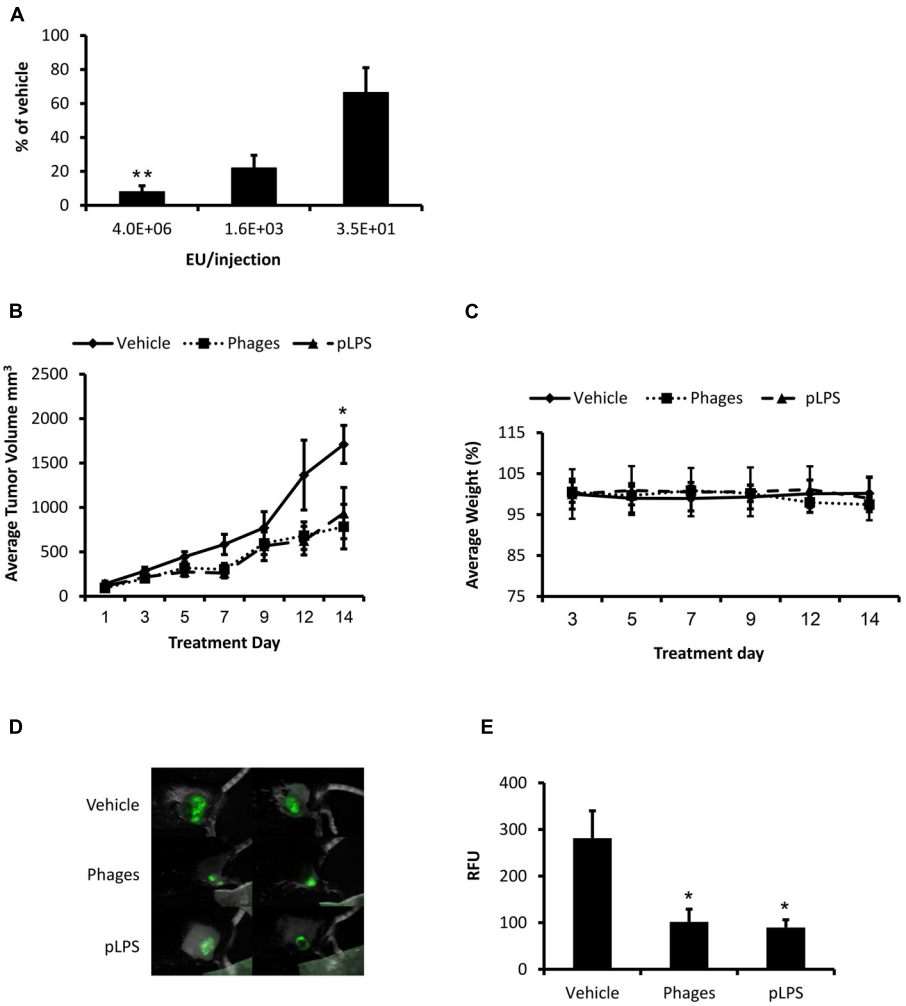


**FIGURE 2 | Ff phages and purified LPS (pLPS) inhibit tumor growth.** **(A)** C57BL/6 mice ($n = 5$) inoculated subcutaneously with GL261 cells were peritumorally administered with 1.7E+12 phages from preparations containing different endotoxin concentration every second day for approximately 10 days. Tumor dimensions were measured by a caliper and tumor volume was calculated as follows: width2*length/2 (**$P < 0.01$ as compared to 3.5E+1 EU/injection, Kruskal–Wallis test followed by Dunn–Bonferroni's *post hoc* analysis). Results were normalized to the vehicle group. **(B)** C57BL/6 mice ($n = 5$–6) were inoculated subcutaneously with 2E+6 GL261 glioblastoma cells stably expressing green fluorescent protein (GFP). Mice received peritumoral injections every second day of vehicle (PBS), 1.7E+12 Triton purified phages (430 EU/injection), or pLPS (430 EU/injection). Tumor dimensions were measured as in **(A)** (*$P < 0.05$ phages compared to vehicle, unpaired two-tail Student's *t*-test). **(C)** Change in body weight of mice during the experiment. **(D)** Intravital fluorescence imaging performed 9 days following treatment initiation, presented are representative images. **(E)** GFP intensity (total GFP signal scaled counts/s) is depicted as relative fluorescence units (RFU; *$P < 0.05$ phages and pLPS compared to vehicle, one-way ANOVA followed by Tukey's *post hoc* analysis). Results are depicted as mean ± SEM.

bacteria (pLPS). Administration of phages or pLPS containing equal endotoxin concentration (430 EU/injection) inhibited tumor growth to a similar extent (54 and 45%, respectively, vs. vehicle at day 14; **Figure 2B**) with no apparent systemic toxicity or reduction in body weight (**Figure 2C**). Consistent with these results, intravital fluorescence imaging performed after 9 days of treatment revealed reduction of 63.7% in total signal from tumors treated with phages compared to administration of vehicle alone ($P = 0.015$; **Figures 2D,E**), which was similar to the effect of treatment with pLPS (68% vs. vehicle $P = 0.01$). This trend was also supported by *ex vivo* fluorescence imaging of tumors at the end of the experiment (data is not shown). Taken together, these findings suggest that the activity of phages in this model was promoted predominantly by the presence of LPS in the preparation.

## Ff Phages Administered Intranasally Accumulate in the Brains of Mice and Inhibit Brain Tumor Progression

We previously reported that Ff phages administered via the intranasal route could be detected in sections of the olfactory bulb and hippocampus regions of mice using immunohistochemistry staining (Frenkel and Solomon, 2002). Consistent with these

results, here we demonstrate that infective phages could be isolated from both rostral and caudal regions of the brain minutes following intranasal administration (**Figure 3A**), and that phages predominantly accumulate in the olfactory bulb (**Figure 3B**). These observations indicate that phages plausibly utilize the olfactory system to penetrate the brain and that phages remain intact following intranasal delivery.

We then investigated the effect of phages and pLPS given intranasally to mice bearing orthotopic GL261 tumors. Administration of purified phages extended median survival of mice by 33% compared to mice treated with vehicle alone albeit not statistically significant (median survival of mice treated with phages was 16 vs. 12 days of mice treated with vehicle alone $P = 0.456$; **Figure 3C**). Intranasal administration of pLPS containing equal concentration of endotoxin units had virtually no effect on the survival of mice. Computed tomography (CT) scan performed on day 14 shows that mice treated with purified phages had significantly smaller tumors compared to mice treated with vehicle alone (73%, $P = 0.006$) or pLPS (65% $P = 0.016$, **Figures 3D,E**). In contrast, pLPS had only minor, non-significant effect on tumor progression (22%, vs. vehicle, $P = 1$).

Interestingly, treatment of mice with NP phages inhibited intracranial tumors by 75% (**Figures 3D,E**), however, these mice had significantly lower survival rate compared to mice treated with purified phages ($P = 0.017$) and tended to die earlier then mice treated with vehicle alone (**Figure 3C**). These observations suggest that LPS derived from DH12S cells or other factors found in the preparation are toxic in high doses. In support of this, treatment of mice bearing subcutaneous tumors with NP phage preparations produced in DH12S cells was also associated with toxicity and fatalities (data is not shown). This toxicity was diminished following phage purification.

Collectively, these results show that phages exerted an intense anti-tumorigenic activity in the CNS of mice following intranasal administration and mediated superior effect over treatment with pLPS.

## Discussion

In this study, Ff phage processing with Triton X-114 highly reduced LPS contamination but failed to result in LPS free preparations. Similar results were obtained following phage purification with caesium chloride. These observations, supported by TEM and ELISA analysis demonstrating localization of LPS molecules on the surface of NP as well as purified phages, suggest that Ff phages naturally carry LPS on their surface and at least some of these LPS molecules form a stable complex with the virion that cannot be easily dissociated. Of note, LPS was still detected on the virion even when phages immobilized to ELISA plate were repetitively washed with PBS containing tween detergent or when phages were heated to 95°C. Yet, as others have previously reported to obtain LPS free Ff phages (Paschen et al., 2005; Sartorius et al., 2011; Roehnisch et al., 2013), it is possible that optimization of the purification technique used in this study (Mantile et al., 2011; Roehnisch et al., 2014; Branston et al., 2015) could have resulted in further depletion of LPS from our preparations.

Although some coliphages such as T4 and T5 can interact with LPS (Rakhuba et al., 2010), to our knowledge, no such interactions have been reported for Ff phages. Accordingly, we were unable to show phage binding to purified (extracted from the host) or NP LPS (sup containing endotoxin) *in vitro*. As such, Ff phages might complex with LPS non-directly, for example, via outer membrane proteins localized at LPS sites that can link between phages and LPS. Such interactions were previously proposed for the TuII* and TuIB coliphages with LPS complexes of OmpA and OmpC, respectively (Datta et al., 1977; Yu et al., 1981). Interestingly, TolA which interacts with the N1 domain of p3 during infection has been implicated in the processing of the O antigen and its function is required for surface expression of O-specific LPS and to a lesser extent for the LPS core in *E. coli* (Lubkowski et al., 1999; Gaspar et al., 2000; Vines et al., 2005). However, to our knowledge, direct interaction between TolA and LPS was not reported. Nonetheless, TolA can form complexes with porin trimmers associated to LPS (Derouiche et al., 1996).

The capacity of phages to interact with LBP and the results obtained in the LAL assay further support LPS localization on the surface of phages. These findings also suggest that LPS molecules attached to the virion may participate in immune response *in vivo* and raise the possibility that they might contribute to the immunogenicity attributed to Ff phages. Of note, picomolar concentration of endotoxin (from *Neisseria meningitidis* or *E. coli*) was sufficient to promote secretion of IL-8, a neutrophil chemoattractant, from cultured human embryonic kidney 293 (HEK293) stably transfected with TLR4 (Gioannini et al., 2004; Lin et al., 2004). Therefore, minute amount of LPS localized on the virion can potentially promote immune responses and induce non-bacterial activities in the macro-host. In support of this, here we demonstrate that treatment of subcutaneous GL261-GFP tumors with pLPS or phages containing the same amount of endotoxin suppressed tumor progression to a similar extent. Thus, we propose that in this model the activity of phages was largely driven by LPS. This conclusion is further strengthen by the observation that phage preparations depleted of LPS exhibited diminished anti-tumorigenic activity in the subcutaneous tumor model. Our data extend previous work performed with tumor specific phages (Eriksson et al., 2007, 2009), suggesting that *in vivo*, wild-type Ff phages carrying an effective amount of LPS may also promote significant anti-tumorigenic activity. Indeed, LPS has been reported to induce intense anti-tumorigenic activities in both animal and human studies (Chicoine et al., 2007; Lundin and Checkoway, 2009). Similar to the activities attributed to LPS free Ff phages (Eriksson et al., 2009), LPS was reported to tilt macrophages polarization toward the M1 phenotype (Mantovani et al., 2002; Rey-Giraud et al., 2012) and induce a potent anti-tumorigenic activity associated with neutrophil infiltration into the tumor milieu (Chicoine et al., 2007). Interestingly, both LPS and LPS free Ff phages were demonstrated to mediate their anti-tumorigenic activity, at least in part, via TLR4 (Chicoine et al., 2007; Eriksson et al., 2009) which might explain the similarities in their tumor inhibition mechanism.

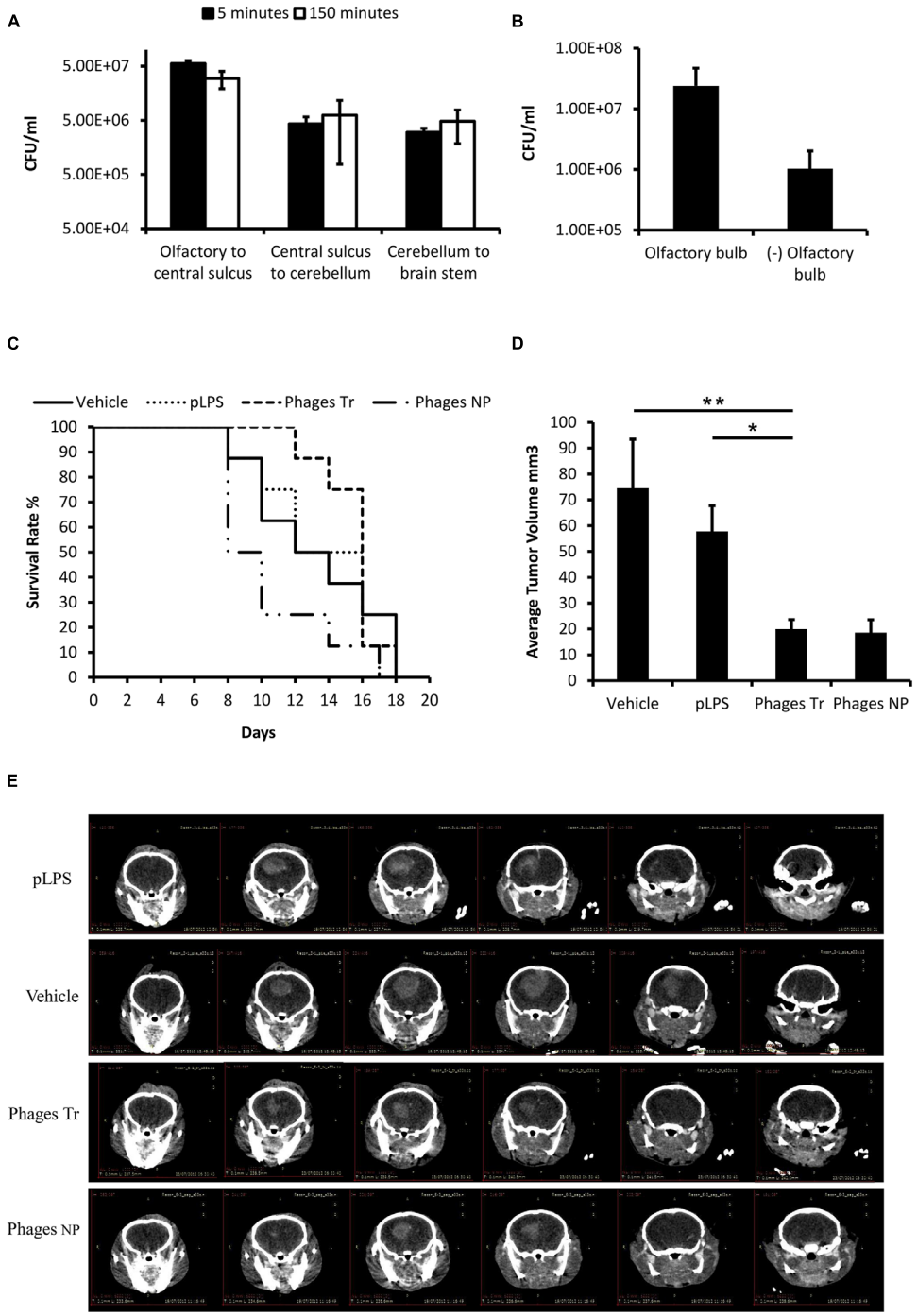


**FIGURE 3 | Ff phages delivered intranasally accumulate in the CNS of mice and suppress progression of orthotopic glioblastoma. (A,B)** Mice were intranasally administered with 2E+12 phages and perfused at the indicated time points. Phage concentration in brain homogenates was evaluated by live counting. Data is presented as colony forming units (CFU) per ml, normalized to tissue weight. **(A)** Phage concentration in different brain regions 5 and 150 min following intranasal administration ($n = 3$). **(B)** Phage concentration in the olfactory bulb and the rest of the brain 1 hour following intranasal administration ($n = 3$). **(C–E)** C57BL/6 male mice bearing orthotopic GL261 GFP tumors were intranasally administered with vehicle alone (PBS), 1.9E+12 Triton purified phages (975 EU/administration), pLPS (975 EU/administration) or 1.9E+12 NP phages (110,500 EU/administration). Treatment started three days following cell inoculation. **(C)** Kaplan–Meier analysis of survival followed by a log-rank test. Decrease of 10% in mice body weight from day of cell inoculation was set as an endpoint, $n = 8$. **(D,E)** CT imaging was performed 2 weeks following cell implantation. Depicted are axonal sections (one representative mouse per group) displayed in 1 mm intervals from frontal (left) to rostral (right). Tumor volume was extrapolated from CT images as described in material and methods. ($^*P < 0.05$, $^{**}P < 0.01$, one-way ANOVA was applied on logarithmic transformed data followed by Bonferroni's *post hoc* analysis), $n = 5$. Results are expressed as untransformed mean values ± SEM.

Although treatment of mice bearing subcutaneous glioblastoma tumors with phages or pLPS led to similar results, phages suppressed orthotopic glioblastoma significantly better than pLPS. This discrepancy may suggest that following intranasal administration, phages translocate to the brain more efficiently than pLPS and thus, facilitate pLPS accumulation in the brain. In support of this idea, soluble LPS tends to aggregate in aqueous solutions and form micelles and vesicles having diameters in sizes that possibly limit its transport through perineural spaces in the fila olfactoria (10–15 nm; Bergstrand et al., 2006; Mistry et al., 2009). Accordingly, Ff phages that acquired a spheroid morphology (having a diameter of 30–70 nm) were restricted from the brain when delivered intranasally (Frenkel and Solomon, 2002).

As previously described, phages can be genetically modified to display tumor homing motifs and chemically conjugated to cytotoxic drugs (Wu et al., 2002; Eriksson et al., 2007; Bar et al., 2008; McGuire et al., 2014). Such phages when administered non-invasively via the intranasal route, might exhibit superior anti-tumorigenic activities to the wild-type phage. Considering that Ff phages are also easily and inexpensively produced and that phages are natural habitants of the mammalian microflora and thus are relatively safe, utilizing them intranasally might be useful in treating brain malignancies.

## Materials and Methods

### Phage Production

Overnight culture of *E. coli* DH12S (kindly provided by Dr. M. Mevarech, Tel-Aviv University, Israel) transformed with M13KO7 Helper phage (NEB), was diluted 1:100 in fresh 2YT media containing 50 μg/ml Kanamycin and incubated for two nights at 37°C while shaking at 250 RPM. The preparation was centrifuged at 7000 RPM for 20 min and supernatant was supplemented with polyethylene glycol NaCl 1:5 (v/v) to facilitate phage precipitation. Following two nights incubation at 4°C, phages were centrifuged at 9000 RPM for 1 h at 4°C, resuspended in PBS and a second PEG precipitation was performed as described. Phages were filtered through a 0.45 μm filter and titer was measured spectrophotometrically according to the formula: phage particles/ml = $(O.D_{0{\cdot}269nm} - O.D_{0{\cdot}320nm})*6*10^{16}$/vector size (bp).

### Phages Purification with Caesium Chloride

Phages were mixed with 2.4 M caesium chloride solution (in PBS) and ultracentrifuged at 37,000 RPM for 65 h at 4°C to obtain a stable gradient. The fraction containing phages was drawn and caesium traces were eliminated by ultracentrifugation at 50,000 RPM for 4 h at 4°C twice. Phages were resuspended in PBS and filtered.

### Phages Purification with Triton

Non-purified or caesium purified phages supplemented with 1% Triton X-114 in PBS (1 ml) were vortexed for 1 min followed by 5 min incubation in ice. Phages were vortexed again, incubated for 10 min at 56°C and centrifuged at 22,500*g* for 10 min at 37°C. Supernatant was collected and the procedure was repeated (×3). Triton traces were eliminated by gel filtration using a sephacryl S-300 column equilibrated with PBS and connected to an Akta chromatography system. Fractions containing phages were concentrated with a 3 kDa cut-off centricon and filtered. Endotoxin concentrations were measured by the LAL assay (Loanza) according to the manufacturer's instructions and were in the range of 0.1 to 1 EU per 1E+9 phages following triton purification.

### LPS Extraction

Lipopolysaccharide was purified from DH12S bacteria using the LPS extraction kit (Intron) according to the manufacturer's instructions with the following modification: washing step with 70% ethanol was performed three times to eliminate impurities.

### Detection of LPS on Phages Surface by Sandwich ELISA

Microtiter plates were coated with anti-p3 antibodies (Exalpha) 1:50 in coating buffer (0.1 M $NaHCO_3$, pH 9.6) or coating buffer alone overnight at 4°C. Plates were washed three times with PBST (0.05% Tween) followed by three washes with PBS, blocked overnight and supplemented with phages in PBS 1% milk for 1 h at 37°C (in triplicates). Plates were washed as described and incubated with sheep anti-LPS antibodies (Pierce) 1:200 for 1 h at 37°C followed by incubation with rabbit anti-sheep alkaline phosphatase (AP) conjugated antibodies (Zymax) 1:1000 for 1 h at 37°C. Plates were developed with 4-nitrophenyl phosphate (Sigma) and signal intensity was quantified using an ELISA reader at OD 405 nm.

### Detection of LPS on Phages Surface by Direct and Sandwich ELISA Based Immunogold TEM

Nickel grid was coated with mouse anti-p8 antibodies (GE) 1:50 in PBS overnight at 4°C. The grid was rinsed 5 min in PBS (×3), blocked with 3% skim milk for 1 h at RT and incubated with 2E+13 phages/ml in PBS 1% milk (blocking buffer) for 1 h at RT followed by PBS wash as described.

For detection of LPS, the grid was incubated with sheep anti-LPS antibodies 1:50 followed by incubation with rabbit anti-sheep antibodies 1:50 and then goat anti-rabbit 1:20 gold conjugated (12 nm, Jackson Immunoresearch Laboratories). For direct ELISA immunogold TEM, the grid was coated with 2E+13 phages/ml in PBS overnight at 4°C, then LPS was detected as described. For detection of coat proteins, grids coated with phages were exposed to serum from rabbits immunized with NP phages (our laboratory preparation) followed by incubation with goat anti-rabbit gold conjugated. All antibodies were diluted in blocking buffer and incubation was performed at RT for 1 h. For negative staining the grid was incubated for 30 s with 2% uranyl acetate solution at RT. Analysis was performed using the Jeol JEM 1200EX transmission electron microscope.

### Phages Binding to LBP

Microtiter plates were coated with 4 μg/ml of recombinant human LBP (R&D) in coating buffer or coating buffer alone

overnight at 4°C. Plates were washed three times with PBST (0.05% Tween) followed by three washes with PBS, blocked with 3% skim milk and supplemented with phages in PBS 1% milk (w/v) for 1 h at 25°C (in triplicates). Plates were washed as described, incubated with mouse anti-phage (p8) HRP conjugated antibodies (GE) 1:5000 for 1 h at 37°C and developed with o-phenylenediamine (OPD, Sigma). The reaction was terminated with 4N $H_2O_2$ and signal intensity was quantified using an ELISA reader at OD 495 nm.

## Reactivity of Immunopurified Phages in the LAL Assay

Microtiter plates were coated with anti-p8 antibodies (GE) 1:50 in coating buffer or coating buffer alone overnight at 4°C. The plate was washed three times with PBST (0.05% Tween) followed by three washes with PBS, blocked with 3% skim milk overnight and supplemented with phages (2E+12/well) or bacteria supernatant (from an overnight culture of naïve cells, filtered through a 0.45 μm filter) in blocking buffer. The plate was incubated for 1 h at 37°C and rinsed thoroughly as described. To detach immobilized phages, the plate was incubated with 50 mM NaOH for 24 h. Samples containing NaOH were serially diluted in endotoxin free water (Biological Industries) and tested in the LAL assay.

## Cell Culture

GL261 cell line (kindly provided by Dr. G. Safrany department of molecular and tumor radiobiology, Frederic Joliot-Curie Institute, Hungary) was grown in Dulbecco's modified Eagle's medium (DMEM, Biological Industries) containing 10% fetal calf serum, 0.3 mg/ml L-glutamine, 100 units/ml penicillin and 0.1 mg/ml streptomycin. GL261-GFP cells were cultured in the same medium supplemented with 0.5 mg/ml hygromycin (Sigma). Cells were grown at 37°C in 5% $CO_2$.

## Construction of GL261-GFP Stable Line

Supernatant of 293T cells containing MLV viruses carrying the GFP gene was kindly provided to us by Dr. E. Bachrach (department of cells research and immunology, Tel-Aviv University, Israel). The supernatant was diluted 1:2 in DMEM medium supplemented with Polybrene at a final concentration of 8 μg/ml. The medium was added to GL261 cells at 60% confluence in 24-well plates and infection was carried out for 2 h at 37°C. The medium was replaced with fresh growing medium and following 48–72 h the culture was supplemented with 1 mg/ml hygromycin. Three days later, cells were diluted and reseeded to obtain single cell colonies. GFP positive colonies were isolated and a single clone was chosen for the rest of the work.

## GL261 Tumor Model

All animal studies were approved by the Institutional Animal Care and Use Committee (approval number: L-10-029).

C57BL/6 (3 months old) female mice were subcutaneously inoculated in their flank with 2E+6 GL261 or GL261-GFP glioblastoma cells suspended in PBS. When tumors were palpable mice were divided into treatment groups with an average tumor volume of 100 $mm^3$. Mice received peritumoral injections of phages, pLPS or vehicle alone in a total volume of 0.1 ml every second day. Tumor dimensions were measured by a caliper and tumor volume was calculated as follows: width2*length/2. For measurement of fluorescence signal, mice were anesthetized by intraperitoneal injection of Ketamine/Xylazine (100 mg/kg and 20 mg/kg body weight, respectively), treated with a depilatory cream (Veet) and imaged using the Maestro *in vivo* Imaging System (CRi, Inc.). A band-pass filter from 445 to 490 nm and a long-pass filter over 515 nm were used for emission and excitation light, respectively. The tunable filter was automatically stepped in 10-nm increments from 500 to 800 nm whereas the camera captured images at each wavelength interval with constant exposure. Skin autofluorescence and undesired background signals were eliminated by spectral analysis and linear unmixing algorithm. Mice were weighted every treatment day.

## Biodistribution of Phages in Mice Following Intranasal Administration

C57BL/6 mice were intranasally administered with NP 1E+12 phages suspended in 10 μl PBS through each nostril. Immediately before the indicated time points, mice were overdosed with intraperitoneal injection of Ketamine/Xylazine and perfused through the heart with saline. Organs were excised (surgical tools were cleaned with soap, distilled water and ethanol between dissections), supplemented with ice cold PBS (1 ml per 5 g) containing protease inhibitors (Roche) and homogenized using a mechanical homogenizer. Phages concentration was evaluated by live counting as follows: *E. coli* TG1 cells at late log were incubated with homogenate samples for 1 h at 37°C. The inoculum was serially diluted and samples were seeded on petri dishes containing 50 μg/ml Kanamycin. Following overnight incubation, number of colonies was manually counted.

## Orthotopic Glioblastoma Model

Mice were anesthetized with intraperitoneal injection of Ketamine/Xylazine and placed in a Kopf Stereotaxic Alignment System. An approximately 1 cm-long cut was made in the scalp, to expose the skull and a total of $10^5$ GL261-GFP cells in 3 μL PBS were injected 1 mm posterior and 1.5 mm lateral from the bregma at a 3 mm depth from the skull surface. Cells were injected using a Hamilton syringe at a rate of 1 μl/min. In order to avoid backflow, the needle was left for an additional 1 min before being gradually removed. The scalp tissue was glued and the mice were allowed to recover in their cages. Intranasal treatment was given every second day without anesthesia, in a total volume of 10 μl in each nostril, starting 3 days following cell injection. Mice that lost 15% of their initial body weight or demonstrated severe clinical symptoms (epileptic seizures or inability to move) were sacrificed by $CO_2$ inhalation.

## Survival Analysis

Following intracranial inoculation, mice were monitored and weighted daily. Survival endpoint was set to 10% loss of body weight from day of cell inoculation or when mice demonstrated severe clinical symptoms as described.

### Computed Tomography (CT) Scan and Brain Tumor Volume Analysis

Mice were anesthetized with an intraperitoneal injection of Ketamine/Xylazine and CT images were acquired with a high-resolution, low-dose x-ray scanner by a skilled technician. Tumor volume was calculated as follows: in a particular section x, the minor axis and the major axis of the tumor were measured using the Radiant DICOM software and the area (AE) was calculated as follows: AEx = π(major axisx) (minor axisx)/4. Next, tumor volume was calculated using the formula: V = I(AE1 + AE2 +... AEn), where I = section increment (0.8 mm) and n = the number of sections containing tumor (length of *z* axis = I n). Additional details of the volume calculation method have been previously published (Winer-Muram et al., 2002).

### Statistics

The SPSS statistics software (version 21) was used for statistical analysis. Normality distribution and homogeneity of variances were assessed by the ShapiroWilk's test and Levene's test, respectively. Significance was evaluated by an unpaired, two-tail Student's *t*-test. For multiple comparisons, one-way analysis of variance (ANOVA) was performed followed by Tukey's or Dunn–Bonferroni's *post hoc* analysis. Alternatively, the non-parametric, Kruskal–Wallis test was performed, followed by Dunn–Bonferroni's *post hoc* analysis. Survival experiments were analyzed by the Kaplan–Meier's method followed by a log-rank test. Results were considered significance at $P < 0.05$.

## Acknowledgments

This study was supported by grants from the Israel Cancer Association (ICA) under award numbers 20120103 and 20132022 (BS).

We thank Dr. Maria Becker and Beki Barbiro for technical support.

## Supplementary Material

The Supplementary Material for this article can be found online at: http://journal.frontiersin.org/article/10.3389/fmicb.2015.00530/abstract

## References

Aida, Y., and Pabst, M. J. (1990). Removal of endotoxin from protein solutions by phase separation using Triton X-114. *J. Immunol. Methods* 132, 191–195. doi: 10.1016/0022-1759(90)90029-U

Angus, D. C., and van der Poll, T. (2013). Severe sepsis and septic shock. *N. Engl. J. Med.* 369, 840–851. doi: 10.1056/NEJMra1208623

Arap, W., Pasqualini, R., and Ruoslahti, E. (1998). Cancer treatment by targeted drug delivery to tumor vasculature in a mouse model. *Science* 279, 377–380. doi: 10.1126/science.279.5349.377

Bar, H., Yacoby, I., and Benhar, I. (2008). Killing cancer cells by targeted drug-carrying phage nanomedicines. *BMC Biotechnol.* 8:37. doi: 10.1186/1472-6750-8-37

Bergstrand, A., Svanberg, C., Langton, M., and Nydén, M. (2006). Aggregation behavior and size of lipopolysaccharide from *Escherichia coli* O55:B5. *Colloids Surf. B Biointerfaces* 53, 9–14. doi: 10.1016/j.colsurfb.2006.06.007

Branston, S. D., Wright, J., and Keshavarz-Moore, E. (2015). A non-chromatographic method for the removal of endotoxins from bacteriophages. *Biotechnol. Bioeng.* doi: 10.1002/bit.25571 [Epub ahead of print].

Bryant, C. E., Spring, D. R., Gangloff, M., and Gay, N. J. (2010). The molecular basis of the host response to lipopolysaccharide. *Nat. Rev. Microbiol.* 8, 8–14. doi: 10.1038/nrmicro2266

Chicoine, M. R., Zahner, M., Won, E. K., Kalra, R. R., Kitamura, T., Perry, A., et al. (2007). The in vivo antitumoral effects of lipopolysaccharide against glioblastoma multiforme are mediated in part by Toll-like receptor 4. *Neurosurgery* 60, 372–380; discussion 381. doi: 10.1227/01.neu.0000249280.61761.2e

da Fonseca, C. O., Simão, M., Lins, I. R., Caetano, R. O., Futuro, D., and Quirico-Santos, T. (2011). Efficacy of monoterpene perillyl alcohol upon survival rate of patients with recurrent glioblastoma. *J. Cancer Res. Clin. Oncol.* 137, 287–293. doi: 10.1007/s00432-010-0873-0

Datta, D. B., Arden, B., and Henning, U. (1977). Major proteins of the *Escherichia coli* outer cell envelope membrane as bacteriophage receptors. *J. Bacteriol.* 131, 821–829.

De Berardinis, P., D'Apice, L., Prisco, A., Ombra, M. N., Barba, P., Del Pozzo, G., et al. (1999). Recognition of HIV-derived B and T cell epitopes displayed on filamentous phages. *Vaccine* 17, 1434–1441. doi: 10.1016/S0264-410X(98)00377-6

De Berardinis, P., Sartorius, R., Fanutti, C., Perham, R. N., Del Pozzo, G., and Guardiola, J. (2000). Phage display of peptide epitopes from HIV-1 elicits strong cytolytic responses. *Nat. Biotechnol.* 18, 873–876. doi: 10.1038/78490

Derouiche, R., Gavioli, M., Bénédetti, H., Prilipov, A., Lazdunski, C., and Lloubès, R. (1996). TolA central domain interacts with *Escherichia coli* porins. *EMBO J.* 15, 6408–6815.

Eriksson, F., Culp, W. D., Massey, R., Egevad, L., Garland, D., Persson, M. A. A., et al. (2007). Tumor specific phage particles promote tumor regression in a mouse melanoma model. *Cancer Immunol. Immunother.* 56, 677–687. doi: 10.1007/s00262-006-0227-6

Eriksson, F., Tsagozis, P., Lundberg, K., Parsa, R., Mangsbo, S. M., Persson, M. A., et al. (2009). Tumor-specific bacteriophages induce tumor destruction through activation of tumor-associated macrophages. *J. Immunol.* 182, 3105–3111. doi: 10.4049/jimmunol.0800224

Frenkel, D., Katz, O., and Solomon, B. (2000). Immunization against Alzheimer's beta -amyloid plaques via EFRH phage administration. *Proc. Natl. Acad. Sci. U.S.A.* 97, 11455–11459. doi: 10.1073/pnas.97.21.11455

Frenkel, D., and Solomon, B. (2002). Filamentous phage as vector-mediated antibody delivery to the brain. *Proc. Natl. Acad. Sci. U.S.A.* 99, 5675–5679. doi: 10.1073/pnas.072027199

Gaspar, J. A., Thomas, J. A., Marolda, C. L., and Valvano, M. A. (2000). Surface expression of O-specific lipopolysaccharide in *Escherichia coli* requires the function of the TolA protein. *Mol. Microbiol.* 38, 262–275. doi: 10.1046/j.1365-2958.2000.02094.x

Gioannini, T. L., Teghanemt, A., Zhang, D., Coussens, N. P., Dockstader, W., Ramaswamy, S., et al. (2004). Isolation of an endotoxin-MD-2 complex that produces Toll-like receptor 4-dependent cell activation at picomolar concentrations. *Proc. Natl. Acad. Sci. U.S.A.* 101, 4186–4191. doi: 10.1073/pnas.0306906101

Hailman, E., Lichenstein, H. S., Wurfel, M. M., Miller, D. S., Johnson, D. A., Kelley, M., et al. (1994). Lipopolysaccharide (LPS)-binding protein accelerates the binding of LPS to CD14. *J. Exp. Med.* 179, 269–277. doi: 10.1084/jem.179.1.269

Harmey, J. H., Bucana, C. D., Lu, W., Byrne, A. M., McDonnell, S., Lynch, C., et al. (2002). Lipopolysaccharide-induced metastatic growth is associated with increased angiogenesis, vascular permeability and tumor cell invasion. *Int. J. Cancer* 101, 415–422. doi: 10.1002/ijc.10632

Henkin, R. I. (2011). Intranasal delivery to the brain. *Nat. Biotechnol.* 29:480. doi: 10.1038/nbt.1866

Krag, D. N., Shukla, G. S., Shen, G. P., Pero, S., Ashikaga, T., Fuller, S., et al. (2006). Selection of tumor-binding ligands in cancer patients with phage display libraries. *Cancer Res.* 66, 7724–7733. doi: 10.1158/0008-5472.can-05-4441

Kutter, E. (2005). "Phage therapy: bacteriophages as natural, self-limiting antibiotics," in *Textbook of Natural Medicine*, eds J. E. Pizzorno and M. T. Murray (Philadelphia, PA: Churchill Livingstone), 945–956.

Kutter, E., and Sulakvelidze, A. (2004). *Bacteriophages: Biology and Applications*. London: CRC Press. doi: 10.1201/9780203491751

Larocca, D., Burg, M. A., Jensen-Pergakes, K., Ravey, E. P., Gonzalez, A. M., and Baird, A. (2002). Evolving phage vectors for cell targeted gene delivery. *Curr. Pharm. Biotechnol* 3, 45–57. doi: 10.2174/1389201023378490

Letarov, A., and Kulikov, E. (2009). The bacteriophages in human- and animal body-associated microbial communities. 107, 1–13. doi: 10.1111/j.1365-2672.2009.04143.x

Lin, F., Nguyen, C. M.-C., Wang, S.-J., Saadi, W., Gross, S. P., and Jeon, N. L. (2004). Effective neutrophil chemotaxis is strongly influenced by mean IL-8 concentration. *Biochem. Biophys. Res. Commun.* 319, 576–581. doi: 10.1016/j.bbrc.2004.05.029

Lochhead, J. J., and Thorne, R. G. (2012). Intranasal delivery of biologics to the central nervous system. *Adv. Drug Deliv. Rev.* 64, 614–628. doi: 10.1016/j.addr.2011.11.002

Lubkowski, J., Hennecke, F., Pluckthun, A., and Wlodawer, A. (1999). Filamentous phage infection: crystal structure of g3p in complex with its coreceptor, the C-terminal domain of TolA. *Structure* 7, 711–722. doi: 10.1016/S0969-2126(99)80092-6

Lundin, J. I., and Checkoway, H. (2009). Endotoxin and cancer. *Env. Heal. Perspect* 117, 1344–1350. doi: 10.1289/ehp.0800439

Mantile, F., Basile, C., Cicatiello, V., De Falco, D., Caivano, A., De Berardinis, P., et al. (2011). A multimeric immunogen for the induction of immune memory to beta-amyloid. *Immunol. Cell Biol.* 89, 604–609. doi: 10.1038/icb.2010.134

Mantovani, A., Sozzani, S., Locati, M., Allavena, P., and Sica, A. (2002). Macrophage polarization: tumor-associated macrophages as a paradigm for polarized M2 mononuclear phagocytes. *Trends Immunol* 23, 549–555. doi: 10.1016/S1471-4906(02)02302-5

Mattsby-Baltzer, I., Jakobsson, A., Sörbo, J., and Norrby, K. (1994). Endotoxin is angiogenic. *Int. J. Exp. Pathol.* 75, 191–196.

McGuire, M. J., Gray, B. P., Li, S., Cupka, D., Byers, L. A., Wu, L., et al. (2014). Identification and characterization of a suite of tumor targeting peptides for non-small cell lung cancer. *Sci. Rep.* 4:4480. doi: 10.1038/srep04480

Minenkova, O. O., Ilyichev, A. A., Kishchenko, G. P., and Petrenko, V. A. (1993). Design of specific immunogens using filamentous phage as the carrier. *Gene* 128, 85–88. doi: 10.1016/0378-1119(93)90157-X

Mistry, A., Stolnik, S., and Illum, L. (2009). Nanoparticles for direct nose-to-brain delivery of drugs. *Int. J. Pharm.* 379, 146–157. doi: 10.1016/j.ijpharm.2009.06.019

Mueller, M., Lindner, B., Kusumoto, S., Fukase, K., Schromm, A. B., and Seydel, U. (2004). Aggregates are the biologically active units of endotoxin. *J. Biol. Chem.* 279, 26307–26313. doi: 10.1074/jbc.M401231200

Omuro, A., and DeAngelis, L. M. (2013). Glioblastoma and other malignant gliomas: a clinical review. *JAMA* 310, 1842–1850. doi: 10.1001/jama.2013.280319

Oslizlo, A., Miernikiewicz, P., Piotrowicz, A., Owczarek, B., Kopciuch, A., Figura, G., et al. (2011). Purification of phage display-modified bacteriophage T4 by affinity chromatography. *BMC Biotechnol.* 11:59. doi: 10.1186/1472-6750-11-59

Park, B. S., and Lee, J.-O. (2013). Recognition of lipopolysaccharide pattern by TLR4 complexes. *Exp. Mol. Med.* 45:e66. doi: 10.1038/emm.2013.97

Paschen, A., Song, M., Osen, W., Nguyen, X. D., Mueller-Berghaus, J., Fink, D., et al. (2005). Detection of spontaneous CD4+ T-cell responses in melanoma patients against a tyrosinase-related protein-2-derived epitope identified in HLA-DRB1*0301 transgenic mice. *Clin. Cancer Res.* 11, 5241–5247. doi: 10.1158/1078-0432.CCR-05-0170

Pasqualini, R., and Ruoslahti, E. (1996). Organ targeting in vivo using phage display peptide libraries. *Nature* 380, 364–366. doi: 10.1038/380364a0

Pollet, I., Opina, C. J., Zimmerman, C., Leong, K. G., Wong, F., and Karsan, A. (2003). Brief report bacterial lipopolysaccharide directly induces angiogenesis through TRAF6-mediated activation of NF- B and c-Jun N-terminal kinase. 102, 1740–1742. doi: 10.1182/blood-2003-01-0288

Prisco, A., and De Berardinis, P. (2012). Filamentous bacteriophage fd as an antigen delivery system in vaccination. *Int. J. Mol. Sci.* 13, 5179–5194. doi: 10.3390/ijms13045179

Rakhuba, D. V., Kolomiets, E. I., Dey, E. S., and Novik, G. I. (2010). Bacteriophage receptors, mechanisms of phage adsorption and penetration into host cell. *Pol. J. Microbiol.* 59, 145–155. doi: 10.1016/j.proenv.2014.03.091

Rakonjac, J., Bennett, N. J., Spagnuolo, J., Gagic, D., and Russel, M. (2011). Filamentous bacteriophage: biology, phage display and nanotechnology applications. *Curr. Issues Mol. Biol.* 13, 51–76.

Rakover, I. S., Zabavnik, N., Kopel, R., Paz-Rozner, M., and Solomon, B. (2010). Antigen-specific therapy of EAE via intranasal delivery of filamentous phage displaying a myelin immunodominant epitope. *J. Neuroimmunol.* 225, 68–76. doi: 10.1016/j.jneuroim.2010.04.014

Reisser, Á., Pance, A., and Jeannin, Ë. (2002). Mechanisms of the antitumoral effect of lipid A. *Bioessays* 24, 284–289. doi: 10.1002/bies.10053

Rey-Giraud, F., Hafner, M., and Ries, C. H. (2012). In vitro generation of monocyte-derived macrophages under serum-free conditions improves their tumor promoting functions. *PLoS ONE* 7:e42656. doi: 10.1371/journal.pone.0042656

Roehnisch, T., Then, C., Nagel, W., Blumenthal, C., Braciak, T., Donzeau, M., et al. (2013). Chemically linked phage idiotype vaccination in the murine B cell lymphoma 1 model. *J. Transl. Med.* 11:267. doi: 10.1186/1479-5876-11-267

Roehnisch, T., Then, C., Nagel, W., Blumenthal, C., Braciak, T., Donzeau, M., et al. (2014). Phage idiotype vaccination: first phase I/II clinical trial in patients with multiple myeloma. *J. Transl. Med.* 12:119. doi: 10.1186/1479-5876-12-119

Sartorius, R., Bettua, C., D'Apice, L., Caivano, A., Trovato, M., Russo, D., et al. (2011). Vaccination with filamentous bacteriophages targeting DEC-205 induces DC maturation and potent anti-tumor T-cell responses in the absence of adjuvants. *Eur. J. Immunol.* 41, 2573–2584. doi: 10.1002/eji.201141526

Smith, G. P. (1985). Filamentous fusion phage: novel expression vectors that display cloned antigens on the virion surface. *Science* 228, 1315–1317. doi: 10.1126/science.4001944

Szatmári, T., Lumniczky, K., Désaknai, S., Trajcevski, S., Hídvégi, E. J., Hamada, H., et al. (2006). Detailed characterization of the mouse glioma 261 tumor model for experimental glioblastoma therapy. *Cancer Sci.* 97, 546–553. doi: 10.1111/j.1349-7006.2006.00208.x

Thorne, R. G., Pronk, G. J., Padmanabhan, V., and Frey, W. H. (2004). Delivery of insulin-like growth factor-I to the rat brain and spinal cord along olfactory and trigeminal pathways following intranasal administration. *Neuroscience* 127, 481–496. doi: 10.1016/j.neuroscience.2004.05.029

Vines, E. D., Marolda, C. L., Balachandran, A., and Valvano, M. A. (2005). Defective O-antigen polymerization in tolA and pal mutants of *Escherichia coli* in response to extracytoplasmic stress. *J. Bacteriol.* 187, 3359–3368. doi: 10.1128/jb.187.10.3359-3368.2005

Wan, Y., Wu, Y., Bian, J., Wang, X. Z., Zhou, W., Jia, Z. C., et al. (2001). Induction of hepatitis B virus-specific cytotoxic T lymphocytes response in vivo by filamentous phage display vaccine. *Vaccine* 19, 2918–2923. doi: 10.1016/S0264-410X(00)00561-2

Willis, A. E., Perham, R. N., and Wraith, D. (1993). Immunological properties of foreign peptides in multiple display on a filamentous bacteriophage. *Gene* 128, 79–83. doi: 10.1016/0378-1119(93)90156-W

Winer-Muram, H. T., Jennings, S. G., Tarver, R. D., Aisen, A. M., Tann, M., Conces, D. J., et al. (2002). Volumetric growth rate of stage I lung cancer prior to treatment: serial CT scanning. *Radiology* 223, 798–805. doi: 10.1148/radiol.2233011026

Wu, Y., Wan, Y., Bian, J., Zhao, J., Jia, Z., Zhou, L., et al. (2002). Phage display particles expressing tumor-specific antigens induce preventive and therapeutic anti-tumor immunity in murine p815 model. *Int. J. Cancer* 98, 748–753. doi: 10.1002/ijc.10260

Yacoby, I., Shamis, M., Bar, H., Shabat, D., and Benhar, I. (2006). Targeting antibacterial agents by using drug-carrying filamentous bacteriophages. *Antimicrob. Agents Chemother.* 50, 2087–2097. doi: 10.1128/aac.00169-06

Yu, F., Yamada, H., and Mizushima, S. (1981). Role of lipopolysaccharide in the receptor function for bacteriophage TuIb in *Escherichia coli*. *J. Bacteriol.* 148, 712–715.

Zakharova, M. Y., Kozyr, A. V., Ignatova, A. N., Vinnikov, I. A., Shemyakin, I. G., and Kolesnikov, A. V. (2005). Purification of filamentous bacteriophage for phage display using size-exclusion chromatography. *Biotechniques* 38, 194–198. doi: 10.2144/05382BM04

**Conflict of Interest Statement:** The authors declare that the research was conducted in the absence of any commercial or financial relationships that could be construed as a potential conflict of interest.

frontiers in Microbiology

METHODS
published: 20 April 2015
doi: 10.3389/fmicb.2015.00316

# Ff-nano, short functionalized nanorods derived from Ff (f1, fd, or M13) filamentous bacteriophage

*Sadia Sattar[1†], Nicholas J. Bennett[1†], Wesley X. Wen[1], Jenness M. Guthrie[1,2], Len F. Blackwell[1,2], James F. Conway[3] and Jasna Rakonjac[1]**

[1] Institute of Fundamental Sciences, Massey University, Palmerston North, New Zealand, [2] Science Haven Limited, Palmerston North, New Zealand, [3] University of Pittsburgh School of Medicine, Pittsburgh, PA, USA

OPEN ACCESS

**Edited by:**
*William Michael McShan, University of Oklahoma Health Sciences Center, USA*

**Reviewed by:**
*Eric Altermann, AgResearch Ltd., New Zealand*
*Nicole Jane Moreland, University of Auckland, New Zealand*
*John Maxim Ward, University College London, UK*

***Correspondence:**
*Jasna Rakonjac, Institute of Fundamental Sciences, Massey University, Private Bag 11-222, Palmerston North 4442, New Zealand*
*j.rakonjac@massey.ac.nz*

**†Present address:**
*Sadia Sattar, Department of Biosciences, COMSATS Institute of Information Technology, Park Road, Islamabad, Pakistan;*
*Nicholas J. Bennett, Department of Medical Microbiology and Immunology, University of Alberta, Edmonton, AB, Canada*

**Specialty section:**
*This article was submitted to Virology, a section of the journal Frontiers in Microbiology*

**Received:** *28 January 2015*
**Paper pending published:** *08 March 2015*
**Accepted:** *30 March 2015*
**Published:** *20 April 2015*

**Citation:**
*Sattar S, Bennett NJ, Wen WX, Guthrie JM, Blackwell LF, Conway JF and Rakonjac J (2015) Ff-nano, short functionalized nanorods derived from Ff (f1, fd, or M13) filamentous bacteriophage. Front. Microbiol. 6:316. doi: 10.3389/fmicb.2015.00316*

F-specific filamentous phage of *Escherichia coli* (Ff: f1, M13, or fd) are long thin filaments (860 nm × 6 nm). They have been a major workhorse in display technologies and bionanotechnology; however, some applications are limited by the high length-to-diameter ratio of Ff. Furthermore, use of functionalized Ff outside of laboratory containment is in part hampered by the fact that they are genetically modified viruses. We have now developed a system for production and purification of very short functionalized Ff-phage-derived nanorods, named Ff-nano, that are only 50 nm in length. In contrast to standard Ff-derived vectors that replicate in *E. coli* and contain antibiotic-resistance genes, Ff-nano are protein-DNA complexes that cannot replicate on their own and do not contain any coding sequences. These nanorods show an increased resistance to heating at 70°C in 1% SDS in comparison to the full-length Ff phage of the same coat composition. We demonstrate that functionalized Ff-nano particles are suitable for application as detection particles in sensitive and quantitative "dipstick" lateral flow diagnostic assay for human plasma fibronectin.

**Keywords: phage display, filamentous phage, M13 phage, fd phage, f1 phage, lateral flow, nanorod, fibronectin-binding protein**

## Introduction

Filamentous bacteriophages are filament-like bacterial viruses (Day, 2011; Rakonjac et al., 2011). The F-pilus-specific filamentous phage of *Escherichia coli*, Ff (f1, M13, and fd), are resistant to heat, wide range of pH and ionic detergents, to which the tailed phage, such as $\lambda$, are sensitive (Branston et al., 2013). The Ff phage virions are 860 nm in length and 6 nm in diameter; they contain circular single-stranded DNA of ~6400 nt (Day et al., 1988; Marvin et al., 2014). The virion is composed of five proteins. The major coat protein pVIII, that forms the shaft of the filament, is present in the virion in a few thousand copies. Two pairs of minor coat proteins, pIII/pVI and pVII/pIX, form two asymmetric ends of the filament. They are each present in the virion in up to five copies. Infection with filamentous phage is mediated by binding of a minor protein, pIII, to the primary and secondary receptors, the tip of the F-pilus and the TolQRA protein complex spanning the periplasm and the inner membrane, respectively. The primary receptor, however, is not essential for infection; in the presence of $Ca^{2+}$ ions as many as 1% of *E. coli* cells in the culture can be infected with Ff (Russel et al., 1988). TolQRA, a conserved protein complex in Gram-negative bacteria, appears to be both an essential and universally required protein for filamentous phage infection, allowing what appears to be a low-efficiency broad-spectrum infection of Gram-negative bacteria by this group of phage (Heilpern and Waldor, 2000).

After entry into the host cytoplasm, the circular ssDNA genome [the positive (+) strand] of Ff replicates as an episome via a rolling-circle mechanism, one strand at a time. Replication of each strand requires specific sequences called negative (−) strand origin and positive (+) strand origin [(−) and (+) *ori*] and host proteins (Model and Russel, 1988; Rakonjac et al., 2011). In addition, replication from (+) origin requires phage-encoded protein pII (Asano et al., 1999). In addition to origin of replication, a *cis* sequence called packaging signal (PS) is required for targeting the (+) strand ssDNA to assembly machinery and assembly of the virions (Russel and Model, 1989). The (−) and (+) strand origins of replication, as well as the packaging signal, are together often referred to as the f1 origin of replication and are located within a ∼400 nt long intergenic sequence (IG; Supplementary Figure S1A). When inserted into plasmids, the IG (f1 *ori*) allows rolling circle replication in the presence of a helper phage, followed by packaging of the resulting ssDNA into Ff-derived particles; such vectors are known as phagemids. Some phagemid vectors are designed to express translational fusions with the Ff virion proteins and are used in phage display technology (Vieira and Messing, 1987; Barbas et al., 1991).

The virion proteins are all integrated into the inner membrane prior to assembly. The Ff virions are assembled by transfer of proteins from the inner membrane onto the ssDNA genome through a mechanistically and structurally poorly understood secretion-like process, mediated by phage-encoded trans-envelope secretion-assembly machinery (Russel and Model, 2006; Rakonjac et al., 2011). Whereas the diameter of the wild-type Ff virion is constant, the length depends on the length of packaged ssDNA. The shortest Ff-derived particles reported were 50 nm in length, containing circular ssDNA of 221 nt (Specthrie et al., 1992). They were produced by helper-phage-assisted replication from a specially constructed origin of replication, 303 nt in length (Supplementary Figure S1B), inserted into a plasmid. This 303-nt sequence comprises two (+) origins of replication, *ori1* and *ori2*, flanking a packaging signal. The *ori1* corresponds to the core (I) region of the (+) *ori* and serves as an initiator of replication. The extended (II) region of the (+) *ori* was not included in the *ori1*, in order to minimize the replicon size and therefore the particle length. Replication in the absence of region II of the (+) *ori* requires a helper phage containing $gII^{IRI}$ mutant (Dotto et al., 1984). The *ori2* is further shortened; it does not bind $pII^{IRI}$ and cannot serve as an initiator; its role is to terminate replication of the (+) strand. In the presence of $pII^{IRI}$, a segment between the two pII cut sites (TTCTTT↓AATA) in the two (+) origins is replicated and the resulting 221 nt ssDNA is ligated to form a circular ssDNA molecule. A PS inserted in between the two (+) origins allows assembly of this short circular ssDNA into 50 nm-long Ff-like particles (Specthrie et al., 1992).

The physical properties of Ff phage, coupled with their amenability to genetic engineering using recombinant DNA technology, have enabled their extensive use in modern biotechnology and nanotechnology. Ff is central to phage display, a combinatorial technology in which libraries of peptides, antibodies, or proteins are displayed on the virion surface, whilst the corresponding coding sequences are encapsulated inside the virions. This physical link between the displayed protein and its coding sequence allows affinity screening and enrichment of rare variants that bind to a ligand or a bait, from vast libraries of variants (Smith, 1991; Rebar and Pabo, 1994; Zwick et al., 1998; Bradbury and Marks, 2004). The Ff phage have more recently been used as nanoparticle-templates to display arrays of organic and inorganic molecules (Bernard and Francis, 2014) for applications ranging from tissue targeting (Souza et al., 2010) and drug delivery (Bar et al., 2008) to nanoelectrodes (Lee et al., 2009), light-harvesting (Dang et al., 2013) and diagnostic devices (Petrenko, 2008). Furthermore, the liquid crystalline properties of Ff have been exploited to assemble colloidal membranes and other structures (Gibaud et al., 2012) and for applications in tissue engineering (Chung et al., 2011) and colorimetric sensors (Oh et al., 2014).

The current applications of Ff phage could be expanded by manipulating the length of the particles, potentially resulting in nanomaterials of novel properties. Short rods may be preferred over the long filaments in some applications, such as diagnostic methods that use diffusion (lateral flow) of diagnostic particles through complex matrices. Furthermore, short particles lacking viral or antibiotic-resistance genes would lower regulatory hurdles and consumer concerns, allowing wider application outside of laboratory containment.

To expand the versatility and decrease the risks Ff-derived nanoparticle use, we have developed a system for high-efficiency production of short functionalized Ff-derived particles (50 nm × 6 nm) that we named "Ff-nano." These particles do not carry any genes and cannot replicate inside a bacterial cell nor can they integrate into bacterial chromosome. We show that these short particles are more resistant to heating in the presence of ionic detergent SDS compared to the full-length phage. Furthermore we demonstrate that functionalized Ff-nano can be used as detector particles for a high-sensitivity dipstick assay detecting a test analyte, fibronectin, at a concentration of 0.35 femtomoles/μL ($2 \times 10^8$ molecules/μL).

## Materials and Methods

### Bacteria, Phage, and Growth Conditions

All *E. coli* strains used in this study are derivatives of laboratory strain K12. They are listed in **Table 1**. Strain K561 was used for growth of the helper phage R408 [f1 Δ*PS gIX(T30A)*

**TABLE 1 | Bacterial strains.**

| Strains[a] | Genotype | Reference |
|---|---|---|
| TG1 | *supE44* Δ*(hsdM-mcrB)5* ($rk^-$ $mk^-$ $McrB^-$) *thi* Δ*(lac-proAB)* F' [*traD36 lacI*$^q$ Δ*(lacZ)M15 proA*$^+$*B*$^+$] | Carter et al. (1985) |
| K561 | *HfrC* $\lambda^+$ *relA1 spoT1* $T2^R$ *(ompF627 fadL701)* Δ*lacZ lac1*$^q$ | The Rockefeller University collection |
| K1030 | *HfrC* $\lambda^-$ *relA1 spoT1* $T2^R$ *(ompF627 fadL701) supD zed508::Tn10* | The Rockefeller University collection |
| K2092 | *TG1 supD zed508::Tn10* | This work |

[a]*All strains are derivatives of* Escherichia coli *K12.*

*gII*$^{IRI}$*(C143T) gtrxA2*; Russel et al., 1986]. Strains containing a *supD* mutation, K1030, and K2092 were used for growth of *gVIII*$^{amber}$ mutant phage R777 (R408, *gVIII*$^{am25}$) or Rnano3 (R777, MCS in *gIII*) or R408-3 (R408, MCS in *gIII*). K2092 was obtained by co-transducing the *supD* mutation with the *zed508*::Tn10 (Tet$^r$ marker) from strain K1030 into strain TG1 (Carter et al., 1985) using generalized transduction with P1 (Cm$^r$ Clr-100; Sternberg and Maurer, 1991). The *zed508::Tn10* (Tet$^r$) transductants were tested for plaque formation by phage R777 (*supD* is co-transduced with *zed508::Tn10* at a frequency of 80%). Strain K1030 containing pIV-expressing plasmid pPMR132 (Linderoth et al., 1997) was used for growth of phage R676 (f1, Δ*gIV, gVIII*$^{am25}$; Feng et al., 1999).

The cultures were propagated in Difco$^{TM}$ 2xYT (Yeast Extract Tryptone) liquid medium [Becton-Dickinson (BD) and Company, USA] at 37°C with continuous shaking (200 rpm), or on 2xYT agar plates (1.2% Bacto-Agar, BD) at 37°C unless otherwise stated. The medium was supplemented with suitable antibiotics where required, sourced from Sigma–Aldrich and Goldbio (USA). Antibiotics were used at the following concentrations: Ampicillin (Amp) 100 μg/mL, Kanamycin (Km) 30 μg/mL, Chloramphenicol (Cm) 25 μg/mL, and Tetracycline (Tet) 15 μg/mL unless otherwise indicated.

## Construction of Phage and Plasmids

General molecular biology techniques for cloning, PCR amplifications and sequencing were carried out as described in (Sambrook and Russell, 2001). Molecular biology reagents were sourced from New England Biolabs Inc. (USA), Roche Molecular Biochemicals (Germany), Life Technologies Inc. (USA), and Takara (Japan). Oligonucleotides used in cloning, sequencing and PCR reactions were manufactured by Life Technologies Inc. and Integrated DNA Technologies Inc. (USA). DNA sequencing was carried out at the Massey University Genome Services, Institute of Fundamental Sciences, Palmerston North, New Zealand. The small and large scale plasmid and phage closed-circular double-stranded (RF) DNA was prepared using High Pure Plasmid Isolation Mini and Midiprep kits (Life Technologies; Roche Molecular Biochemicals) according to the manufacturers' instructions.

Construction of the recombinant phage and the plasmid pNJB7 is described in Supplementary Methods and Supplementary Figure S2. Briefly, helper phage R777 was constructed from phage R408 and R676 (Feng et al., 1999), by combining the R408 origin of replication and *gII*$^{IRI}$ with *gVIII*$^{am25}$ of R676.

The helper/vector phage Rnano3 was constructed by combining the *gVIII*$^{am25}$ mutation with a 45-nt multiple cloning site (MCS) identical to that of the phage display vector pHEN2 (Marks et al., 1991) in the R408 background. Another helper/vector, containing the identical MCS, but wild-type *gVIII*, named R408-3, was constructed in parallel.

Recombinant helper/vector Rnano3FnB was constructed by inserting coding sequence of fibronectin binding (FnB) domain from *Streptococcus pyogenes* (Rakonjac et al., 1995) into the MCS of Rnano3.

The Ff-nano-producing plasmid pNJB7 was constructed by inserting the Ff-nano origin of replication amplified from plasmid pLS7 (Specthrie et al., 1992) into the high-copy-number vector pCR4-TOPO (Life Technologies).

## Phage Growth

All helper-vector phage stocks were prepared initially from a single plaque using a plate method. Briefly, phage were extracted from a plaque into 1 mL of 2xYT by slow rotation at room temperature for 1 h, filtered through a 0.45 μm-pore filter to remove the *E. coli* cells and titrated on an appropriate strain. To make a plate stock, $10^5$-$10^7$ phage from the dissolved plaque were mixed with a culture of an appropriate host in 2xYT soft agar, plated, and incubated overnight. The phage were extracted into 5 mL of 2xYT overlaid onto the surface of the lawn, followed by slow shaking for 1 h at room temperature. The 2xYT containing extracted phage was collected and filtered to remove *E. coli*. Titers of the plate stocks were typically $\sim 10^{11}$ per mL. These plate stocks were then used for preparation of larger-volume stocks using a standard single-round infection of exponentially growing liquid cultures at a multiplicity of infection (m.o.i.) of 50 phage per bacterium.

## Purification of the Ff-nano Particles

An exponentially growing culture (2–8 L) of K1030 carrying pNJB7 (Ff-nano-producing plasmid) was infected with appropriate helper phage (R777, Rnano3, or Rnano3FnB) at an m.o.i. of 50 and incubated at 37°C without shaking for 20 min, to allow infection. Incubation was continued overnight at 37°C with shaking at 200 rpm. The subsequent day, cells were pelleted (7000 × *g* for 20 min at 4°C) and the supernatant containing the Ff-nano and full-length helper phage was subjected to differential two-step polyethylene glycol (PEG) precipitation, to separate the two types of particles from each other, as described (Specthrie et al., 1992). Briefly, in the first precipitation, culture supernatant was subjected to 2.5% w/v PEG8000/0.5 M NaCl and incubated overnight at 4°C to precipitate the full-length helper phage. Precipitated full-length helper phage were collected by centrifugation at 16,500 × *g* for 45 min at 4°C. Supernatant containing the Ff-nano particles was transferred to sterile containers, whereas the full-length phage pellet was suspended in TBS (50 mM Tris, 150 mM NaCl, pH 7.0). In the second precipitation, solid PEG8000 was added to the supernatant, to a final concentration of 15%, and incubated overnight at 4°C. The following day the Ff-nano-enriched precipitate was collected by centrifugation (at 16,500 × *g* for 45 min at 4°C) and the pellet was resuspended in TBS. The full-length phage and Ff-nano fractions (resuspended pellets from 2.5 and 15% PEG, respectively) were further subjected to successive detergent treatments and precipitations to decrease contamination with fragments of inner and outer membranes [Sarkosyl (1% w/v) and Triton X-100 (0.1% v/v)]. Full length helper phage were recovered after each detergent treatment by precipitation with 2.5% PEG and Ff-nano with 15% PEG as described above, except that precipitations were carried out at room temperature to decrease co-precipitation of detergents with the particles.

Ff-nano particles were further purified away from the remaining full-length helper phage based on the large difference in size. Native agarose gel electrophoresis was carried out as described (Nelson et al., 1981; Rakonjac and Model, 1998). Preparative native agarose gel electrophoresis was carried out on 0.8% agarose gels. Upon completion of electrophoresis, the agarose gel slabs containing the bands corresponding to full-length or Ff-nano particles were separately cut out and transferred to dialysis tubes (Novagen, D-tube dialyzer Maxi, MWCO 12–14 kDa) containing 500 μL of sterile 1 × TAE buffer (40 mM Tris-acetate buffer, pH 8.3, 1 mM EDTA). These tubes were then placed into an electrophoresis chamber in sterile 1 × TAE buffer and electrophoresed overnight at 0.5 V/cm at 4°C. After removing the gel slices from tubes, the phage particles (full-length or Ff-nano) were precipitated overnight at 4°C using 2.5 or 15% PEG, respectively, in 0.5 M NaCl. The precipitate was dissolved in an appropriate amount of 1 × PBS (137 mM NaCl, 2.7 mm KCl, 10 mM $Na_2HPO_4$, 1.8 mM $KH_2PO_4$, and stored at −80°C until further use.

## Quantification of Ff-derived Particles

Phage R777, Rnano3, and Rnano3FnB (containing *gVIII*$^{am25}$ mutation) were titrated on *E. coli supD* strains K1030 or K2092 to determine the number of plaque-forming units per milliliter, using standard phage plating, and titration methods. To quantify non-infectious Ff-nano, the particles were disassembled in SDS-containing buffer (1% SDS, 1 × TAE, 5% glycerol, 0.25% bromophenol blue) at 100°C for 5 min and subjected to electrophoresis in 1.2% agarose gel in 1 × TAE buffer. After electrophoresis, the ssDNA released from disassembled Ff-derived particles was stained with ethidium bromide (Supplementary Figure S3) and quantified by densitometry (Rakonjac and Model, 1998). The amount of ssDNA in any band is not linearly proportional to the intensity of fluorescence, therefore each gel contained a set of twofold dilutions of purified full length f1 ssDNA that were used for calibration (Supplementary Figure S3). Gels were photographed by a CCD camera (Biorad, USA). Image Gage V4.0 and Microsoft Excel were used for densitometry and calculations, respectively. A second-order polynomial function was used to fit the standard curve. Amounts of ssDNA were converted to the genome equivalents based on the molecular weight of the ssDNA genome. The molecular weight of the Ff-nano ssDNA genome was in turn calculated from its length (221 nt) and nucleotide composition (derived from the DNA sequence).

Native agarose gel electrophoresis was used to separate the intact full-length (helper) phage from Ff-nano particles, for analysis and purification. The bands containing intact particles were detected in agarose gels after the *in situ* stripping the virion proteins off the ssDNA by soaking the gel in 0.2 M NaOH for 1 h, followed by neutralization with 0.45 M Tris pH 7.0 and staining with ethidium bromide (Supplementary Figure S4).

## Microscopy

The phage samples for non-cryo TEM analysis were adsorbed onto glow-discharged carbon-coated grids, negatively stained with a 1% uranyl acetate solution, and examined on a Phillips CM-10 microscope at the Manawatu Microscopy and Imaging Centre (MMIC, Institute of Fundamental Sciences, Massey University).

Cryo-negative staining was performed at the University of Pittsburgh, Pittsburgh, PA, USA, on an FEI (Hillsboro, OR) Tecnai F20 microscope equipped with a Gatan (Pleasanton, CA, USA) 626 cryoholder and operated at 200 kV and nominal magnification of 50,000×. Briefly, 3 μL of sample were pipetted onto a holey carbon/copper grid that had been briefly glow-discharged. The grid was then placed sample-down onto a 100 μL droplet of 16% ammonium molybdate (in the pH range 7.0–8.0) and floated for 60 s, following the cryo-negative staining procedure (Adrian et al., 1998). The grid was then removed, blotted and plunge-frozen into liquid ethane using an FEI Vitrobot Mk III. Images were collected using standard low-dose techniques on a Gatan Ultrascan 4000 CCD camera with post-column magnification of 1.33×, yielding a pixel size at the sample of 2.3 Å.

## Phage ELISA Assay

Phage Enzyme Linked Immunosorbent Assay (ELISA Harlow and Lane, 1999) was carried out in the 96-well plates (Nunc-Immuno MaxySorpTM, Denmark). The wells were coated overnight at 4°C with 100 μL of human plasma fibronectin (Sigma–Aldrich, USA) at 20 μg/mL in 100 mM sodium bicarbonate buffer, pH 9.5. All subsequent steps were carried out at room temperature. The wells were washed once with 300 μL of PBS containing 0.05% Tween 20 (PBST) and blocked with 250 μL of 2% (w/v) Bovine Serum Albumin (BSA) in PBS for 2 h. After washing wells three times with 300 μL of PBST, Rnano3FnB full-length phage or Ff-nano particles ($1 \times 10^8$) in 100 μL of PBS were added to the wells. Negative controls (buffer and protein) were PBS and 2% BSA in PBS, respectively, whereas negative phage controls were the full-length phage and the Ff-nano particles derived from "empty" vector/helper Rnano3 (and therefore not displaying FnB). The plates were then incubated for 2 h. The unbound particles were removed by extensive washing with PBST (300 μL, seven times). To detect phage particles bound to fibronectin in the wells, 100 μL of rabbit anti-pVIII (polyclonal antibody to M13, fd, and f1, Progen Biotechnik; Germany) was added at the concentration of 0.1 μg/mL in 1× PBS and incubated for 1 h. The wells were then washed five times with 300 μL PBST buffer. Next, 100 μL of secondary HRP-conjugated anti rabbit antibody was added to all wells at a dilution of 1:2000 and then washed with 300 μL PBST seven times. The HRP bound to the plate was detected with 1-StepTM Turbo TMB-ELISA reagent (Thermo Scientific). The enzyme reaction was stopped by adding 25 μL of 0.5 M $H_2SO_4$. The signal was quantified by measuring absorbance at 450 nm.

## Labeling of Ff-derived Particles Using Fluorescein Isothiocyanate

Fresh Fluorescein IsoThioCyanate (FITC) solution (1 mg/mL) was prepared in 1 M $NaCO_3/NaHCO_3$ (pH 9.0) buffer. Ff-nano

($0.5 \times 10^{13}$ in 500 μL) was precipitated using 15% PEG/0.5 M NaCl and the same amount of the full-length phage with 2.5% PEG/0.5 M NaCl. The precipitate was dissolved in 200 μL of 1 M $NaCO_3/NaHCO_3$ (pH 9.0) buffer. The FITC solution (50 μL) was added to the suspension of precipitated Ff-nano or full-length phage and the reaction mixture was rotated in the dark for 1 h at room temperature. The reaction was stopped by adding 10 μL of the $NH_4Cl$ and the particles were purified by a series of two PEG8000 precipitations using the concentrations appropriate for Ff-nano (15%) and full-length phage (2.5%). The pellet obtained after the second PEG8000 precipitation was suspended in 100 μL of 1× PBS and stored at 4°C in the dark until further use.

### Dipstick Assays

Hi-Flow Plus membrane cards were used to make the dipsticks (Millipore Corporation). These cards contain nitrocellulose membranes cast on a 2 mil (0.001 inch; USA) polyester film backing. The reagents for the test and control lines were applied to the membrane using a mechanical dispenser. Collagen I (Sigma; 1 μg/μL in 0.25% acetic acid;) was dispensed at the test line, whereas undiluted mouse anti-pVIII antibody or anti-FITC antibody (0.5 to 1 μg/μL) was dispensed at the control line. The protein-loaded cards were allowed to dry at 37°C for 1 h and were subsequently cut into 0.5 cm × 2.5 cm size dipsticks using an automatic card-cutting tool (BIODOT membrane cutter; SM5000; sheet slitter). The dipsticks were stored in zip-lock sealed bags at room temperature in a dark place until use. The membrane has a flow rate of 46 s/2.5 cm (total length of the dipstick).

The distal end of protein-loaded dipstick was dipped into the 50 μL mixture of analyte (fibronectin, 5 μg/50 μL for initial detection and serial twofold dilutions starting from 0.5 μg/50 μL for quantitative detection) and the detection particles that was pre-incubated for 30 min. Full-length phage were used at $1 \times 10^{10}$ per assay, and Ff-nano (or Ff-nanoFnB) particles at $1 \times 10^{11}$ per assay. Dipsticks were allowed to stand in solution for 30 min and dried for 1 h at 37°C. The FITC-labeled particles on the dipsticks were detected using a phosphoimager (Fuji, Japan). Unlabeled particles were visualized by immune-blotting using rabbit pVIII-specific antibody (0.66 μg/mL; Progen Biotech) for 1 h at room temperature, followed by five washes of 5 min each with PBST. Rabbit IgG-specific antibody conjugated to alkaline phosphatase (Sigma, USA) was used as the secondary antibody. The dipsticks were washed again five times with PBST, and developed using Nitro Blue Tetrazolium (NBT) and 5-Bromo-4-Chloro-3-Indolyl Phosphatase (BCIP) in alkaline buffer (Blake et al., 1984). Densitometric analysis of the signal at the control and test lines in quantitative assays was performed using ImageJ software (Schneider et al., 2012).

## Results

### The Ff-nano Production and Purification System

In this work we have constructed an Ff-derived phage display system for production of functionalized nanorods (50 nm × 6 nm) we named Ff-nano (**Figure 1**). In the first stage, we modified a setup for production of short phage originally published by Specthrie et al. (1992) to increase the amount (per cell) of the 221-nt circular ssDNA available as a template for assembly of the short particles. This was achieved by inserting the 303-nt short-phage (microphage or Ff-nano) origin of replication (Supplementary Figure S1) into the high-copy-number plasmid pCR4-TOPO (in contrast to the low-copy-number plasmid pBR322 used in the original system), to obtain plasmid pNJB7. Furthermore, a new helper phage, named Rnano3, was constructed. The helper phage Rnano3, in contrast to the original helper phage R474 used for short phage production (Specthrie et al., 1992), is not only a helper but also a phage display vector. Rnano3 was designed for display of proteins as fusions with phage protein pIII that is present in up to five copies at one end of the Ff-derived particles. Infection of cells containing plasmid pNJB7 with the helper phage/vector Rnano3 resulted in production of the 50 nm × 6 nm particles (Ff-nano or microphage; **Figure 2**) and full-length phage.

The 50-nm-particle production was originally reported to be improved in the presence of helper phage that produces decreased amount of the major coat protein pVIII. Decreased amount of pVIII presumably favors initiation and termination of assembly over elongation of particles, thereby decreasing the co-packaging of short 221 nt ssDNA with the helper phage DNA into the full-length particles and increasing production of short particles (Specthrie et al., 1992). In contrast to R474 helper used previously for the short phage production, which has a mutation lowering transcription of not only *gVIII* but also in *gIX* (Russel and Model, 1989; Specthrie et al., 1992), the Rnano3 helper phage/vector that we constructed produces decreased amount of pVIII without affecting *gIX* expression. This specific effect on pVIII is achieved by using a suppressed $gVIII^{am25}$ mutation, which contains a TAG stop codon in the *gVIII* sequence at codon 25 (replacing the GAG codon for Glu). When the Rnano3 phage infects a *supD* strain, the TAG codon is translated into Glu or Ser (Rogers and Soll, 1988). The efficiency of the $gVIII^{am25}$ mutant translation in the *supD* strains (K1030 and K2092) is <50% that of the wild-type, resulting in a lower number of pVIII copies produced per cell than in an infection with phage containing a wild-type *gVIII*. Besides the helper/vector with decreased amount of pVIII, we also constructed and examined helper/vector R408-3 that is identical to Rnano3 apart from having a wild-type *gVIII*. Rnano3 and R408-3 were both found to support production of the Ff-nano particles (Supplementary Figure S5). As predicted, co-packaging of the 221-nt ssDNA derived from the Ff-nano origin of replication with the full-length phage genome appeared to be increased in the R408-3 full-length phage fraction after differential PEG precipitation, relative to that of Rnano3 ($gVIII^{am25}$ mutant), however, the production of Ff-nano particles was also increased (Supplementary Figure S5).

Ff-nano particles were partially purified away from the full-length helper phage by differential PEG precipitation (see Materials and Methods). The full-length helper phage was first precipitated out of the culture supernatant in 2.5% PEG8000, 0.5 M NaCl, followed by increase in PEG8000 to 15% to

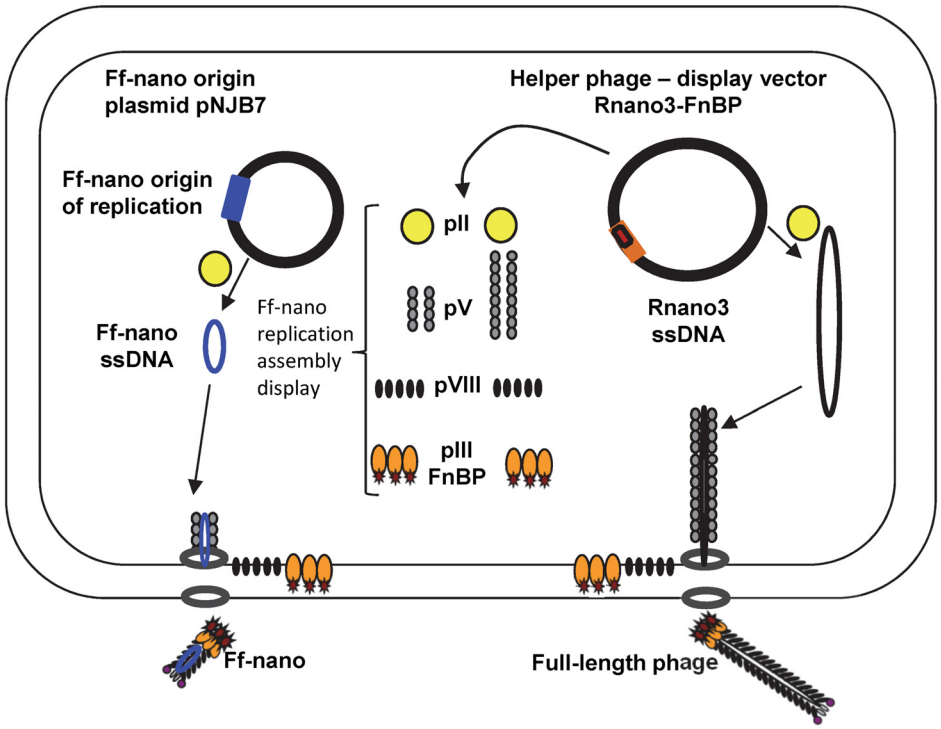


**FIGURE 1 | The system for production of functionalized Ff-nano.** *Escherichia coli* cells containing the Ff-nano production plasmid pNJB7 were infected with the helper phage Rnano3FnB containing the coding sequence of a "probe" or "detector" protein fused to pIII. Upon infection, pII from the helper phage induces positive strand replication from the pNJB7 Ff-nano origin of replication and also provides all other phage proteins and assembly machinery for production of the Ff-nano particles. All five copies of pIII are fusions to the probe (only three copies of pIII fusions are shown).

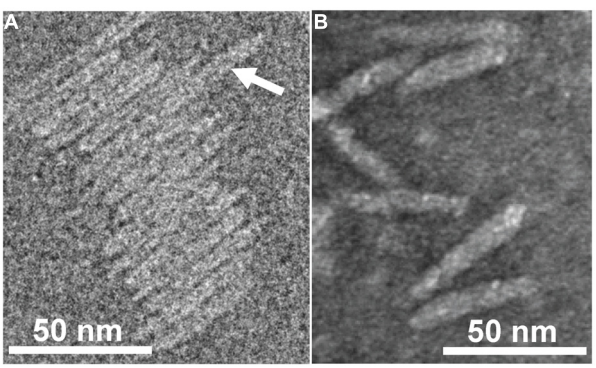


**FIGURE 2 | Transmission electron micrographs (TEM) of Ff-nano particles. (A)** Cryo-negative TEM of particles obtained using the R777 helper phage. **(B)** Negative-stain TEM of particles obtained using the Rnano3 helper/vector. Arrow in **(A)** points to a double-length particle. Samples were prepared as described in Section "Materials and Methods."

precipitate Ff-nano (Specthrie et al., 1992). However, this method resulted in 0.7% full-length phage still remaining in the Ff-nano fraction (**Table 2**). We used native agarose gel electrophoresis to separate the short particles from the full-length phage following the differential PEG precipitation (Supplementary Figure S4). Preparative agarose gel electrophoresis is simple, fast, effective, and less expensive than the size fractionation by Sepharose CL2B columns used by Specthrie et al. (1992). The band containing Ff-nano was excised and the particles were extracted by electroelution (see Materials and Methods for details of purification). The native preparative agarose gel electrophoresis purification step decreased the full-length helper phage frequency in the final purified sample by a factor of 1400, down to $5.0 \times 10^{-6}$ relative to Ff-nano (**Table 2**). This method was also relatively efficient in recovery of the Ff-nano (31% of the input; **Table 2**).

## Physical Properties of the Ff-nano

### Morphology

Purified Ff-nano were negatively stained and visualized by cryo-electron and transmission electron microscopy (**Figure 2**). Dimensions of the Ff-nano are 50 nm by 6 nm, matching those reported in Specthrie et al. (1992). The Ff-nano particle termini appear asymmetric, one pointy, and one blunt, as reported for the Ff phage (Gray et al., 1979). In the cryo-negative micrographs Ff-nano formed sheets composed of individual Ff-nano aligned in alternating orientations. In addition, in a larger field, about 3.5% (6 out of 172) double-length Ff-nano particles could be observed (Supplementary Figure S6). This is consistent with observations of full-length filamentous phage, which, depending on the genotype, contain some proportion of particles that are longer than the majority by a factor of two or multiple lengths of the virion, and containing two or more sequentially

**TABLE 2 | Purification of the Ff-nano by native agarose gel electrophoresis and electroelution.**

| | Ff-nano (total number[c]) | Recovery of the Ff-nano[d] | Helper phage (total number[e]) | Helper: Ff-nano ratio[f] | Fold decrease of helper: Ff nano ratio[g] |
|---|---|---|---|---|---|
| Input[a] | $6.4 \times 10^{14}$ | N/A (input) | $4.5 \times 10^{12}$ | $7.0 \times 10^{-3}$ | N/A (input) |
| Electro-purified Ff-nano[b] | $2.0 \times 10^{14}$ | 31% | $9.9 \times 10^{8}$ | $5.0 \times 10^{-6}$ | 1400 |

[a]*Starting material loaded onto the preparative gel corresponds to the Ff-nano-enriched lysate obtained by differential PEG precipitation.*
[b]*Ff-nano-band was excised from the agarose gel, extracted by electroelution, purified and concentrated (see Materials and Methods).*
[c]*Determined by densitometry (see Materials and Methods).*
[d]*Ratio of the Ff-nano number in the electro-purified sample to the amount in the input.*
[e]*Determined by titration.*
[f]*Determined by dividing the total number of full-length helper phage with the total number of the Ff-nano particles.*
[g]*Fold decrease of the helper to Ff-nano ratio ("helper: Ff-nano ratio") was calculated by dividing the "helper: Ff-nano ratio" in the input with the "helper: Ff-nano ratio" in the electro-purified sample (data column four; row one divided by the row two value).*

packaged genomes (Rakonjac and Model, 1998). We note that the Ff-nano particles visualized in the electron micrographs do not have any signs of the extra balls of density that are sometimes observed attached to the pIII end of the filament and correspond to free-moving N1N2 domains of pIII (Gray et al., 1979).

## Stability to Heating in the Presence of Sodium Dodecyl Sulfate

In the course of Ff-nano analyses, we observed that the standard protocol for Ff phage *in vitro* disassembly, heating in a buffer containing 1% (34 mM) ionic detergent sodium dodecyl sulfate (SDS) for 5 min at 70°C, was not efficient in releasing ssDNA from the Ff-nano particles (data not shown). This indicated that the Ff-nano particles could be more stable to heat/SDS treatment than the full length helper phage, even though both are assembled within the same *E. coli* cell. To test this hypothesis, a time-course experiment of heat exposure was used to monitor disassembly of full-length helper phage and Ff-nano isolated from the same culture using differential PEG precipitation and preparative agarose electrophoresis, as described in the previous section. Approximately $2 \times 10^{12}$ Ff-nano or $1 \times 10^{11}$ full-length phage were heated at 70°C in the presence of 1% SDS for a period from 5 to 20 min; one sample was also incubated at 100°C for 5 min. Disassembly of the helper (full-length) phage and Ff-nano particles was monitored by agarose gel electrophoresis (**Figure 3**). Released ssDNA was directly visualized by staining with ethidium bromide (**Figure 3B**), while the ssDNA that remained encapsidated inside the intact Ff-derived particles (resistant to heat/SDS treatment) was not detectable by direct staining. In order to visualize the SDS-resistant intact particle bands after electrophoresis, the coat proteins were dissociated from ssDNA *in situ* by soaking the gel in an alkaline buffer (0.4 M NaOH), followed by neutralization and re-staining of the gel by ethidium bromide (**Figure 3A**).

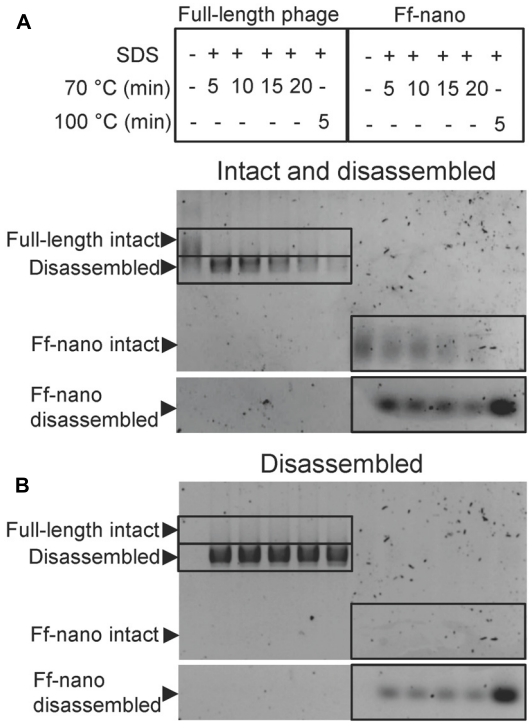


**FIGURE 3 | Ff-nano resistance to heating in SDS. (A)** Intact (undamaged) particles and free ssDNA released from particles by the heat/SDS-treatment. Free ssDNA was visualized by staining the gel with ethidium bromide. Bands corresponding to the intact particles were visualized after soaking the gel in 0.4 M NaOH (see Materials and Methods for details). Gel sections containing the bands corresponding to the free ssDNA and intact full-length and Ff-nano particles are boxed. **(B)** Free ssDNA only, released by the heat/SDS treatment (visualized by direct ethidium bromide staining of the gel prior to NaOH treatment).

When the full-length (helper) phage virions were analyzed, the untreated samples (without SDS or heating) did not contain any free ssDNA. All full-length phage were therefore intact (all ssDNA was contained within the virion; **Figure 3**; compare the corresponding untreated sample lanes in gels A and B). In the presence of 1% SDS, at the first time-point (5 min) of incubation at 70°C, however, all ssDNA was in the free form and none in the intact phage particles, hence the vast majority of the full-length phage particles were sensitive to these conditions (**Figure 3A**). In contrast, when the Ff-nano particles were subjected to the same treatment (1% SDS at 70°C), a large proportion of the intact Ff-nano particles were detected, with some free ssDNA observed at all time-points (**Figure 3**, compare the 70°C-treated sample lanes in A vs. B). The amount of intact Ff-nano particles decreased gradually at 70°C between the 5 and 20 min time points, but nearly half stayed intact throughout the

incubation. The intact Ff-nano were completely eliminated only after incubation at 100°C, confirming that only at this higher temperature is SDS able to disassemble all Ff-nano particles in the sample (**Figure 3**, compare lane 12 in A vs. B). This experiment demonstrates that the Ff-nano particles have superior resistance to heating in the presence of ionic detergent SDS in comparison to the full-length phage, requiring higher temperature (100 vs. 70°C) for dissociation of most particles.

## Functionalization of the Ff-nano

To test the potential of the Ff-nano-production system to assemble functionalized particles that can be used for display of foreign proteins, a fusion to pIII was constructed in the helper/vector Rnano3. The displayed peptide was the FnB domain from serum opacity factor (Sof), a surface protein of *S. pyogenes* (Rakonjac et al., 1995). The Sof FnB domain is composed of three repeats of a bacterial FnB motif (PF02986) that each binds to the N-terminal domain of Fibronectin (Fn) with a low nanomolar dissociation constant (Rakonjac et al., 1995; Schwarz-Linek et al., 2006). The high affinity of FnB for the Fn makes it a good candidate as a detector molecule and FnB-Fn combination is a good detector-analyte pair to investigate the use of Ff-nano as a display particle and for its applicability to lateral flow dipstick diagnostic devices.

The functionalized helper/vector encoding the FnB-gIII fusion was named Rnano3FnB. When *E. coli* containing the Ff-nano-origin plasmid (pNJB7) was infected with Rnano3FnB, the Ff-nano particles displaying FnB (named Ff-nanoFnB) were produced together with the full-length helper phage (**Figure 1**). The helper (full-length) Rnano3FnB phage and the Ff-nanoFnB particles obtained using this helper were separated by differential PEG precipitation and each of the long and the short phage were further purified using native agarose gel electrophoresis followed by electroelution, as described in the previous section. Phage ELISA was performed to confirm that the FnB domain was displayed (schematically represented in **Figure 4A**). Rnano3FnB full-length and Ff-nanoFnB particles exhibited binding to immobilized fibronectin as indicated by strong ELISA signal detected for fibronectin-coated wells incubated with these phage particles ($OD_{450}$ = 1.2 with $10^8$ particles per well in the presence of 40 ng/μL of Fn). No signal over background levels ($OD_{450}$ = 0.1; intrinsic to the phage ELISA) was detected in control wells incubated with Ff-nano particles that did not display FnB, derived from the infection with vector Rnano3 (without the FnB domain) nor in the wells coated with BSA only (from which fibronectin was omitted; **Figure 4B**), apart from the full-length Rnano3 particles (not displaying FnB) which gave a low signal $OD_{450}$ = 0.3 in the presence of Fn. In conclusion, Ff-nanoFnB particles detected Fn and were hence displaying FnB. All Ff-nano and Ff-nanoFnB samples used in the assays were imaged by TEM to confirm the purity and morphology of the particles (data not shown).

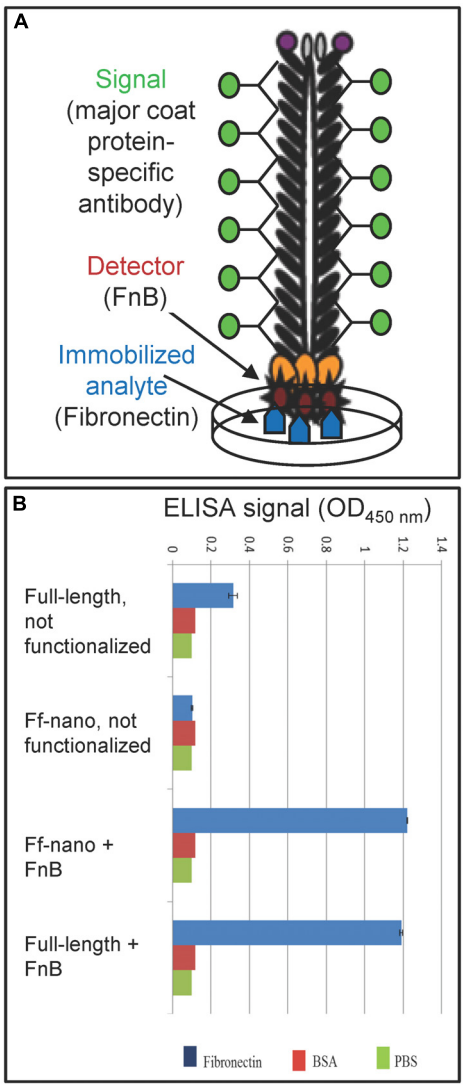


**FIGURE 4 | Confirmation of Ff-nano-FnB display by phage ELISA assay. (A)** Schematic representation of the fibronectin-binding phage ELISA assay. **(B)** Assay result. Fibronectin was immobilized on a microtiter plate at a saturating concentration of 40 ng/μL (2 μg per well of a 96-well plate), whereas control wells for each assay were coated with PBS alone or BSA (1%) in PBS. The wells were exposed to ($1 \times 10^8$) Ff-nanoFnB or full-length phage Rnano3FnB that both displayed FnB as a pIII fusion, or control particles Ff-nano and Rnano3 that did not display FnB. After washing of the wells, bound Ff-nano or full-length phage were detected using a primary antibody to the major coat protein, then the secondary HRP-conjugated antibody, followed by detection of HRP through an enzymatic reaction according to the standard ELISA protocols. Data are presented as an average of three measurements. Error bars show standard deviation.

## Development of a Lateral Flow Assay for Fibronectin Using Ff-nano

### Dipstick Assays Using Ff-nano

To investigate the detection of fibronectin (the analyte) in solution using the Ff-nano displaying FnB domains as the detector (probe) in lateral flow devices, a simple dipstick assay was designed and tested (see **Figure 5A** for a schematic representation of the Fn-detection dipstick assay). The dipsticks used in this assay contained human type I collagen at the test line. Collagen binds fibronectin with high affinity (Engvall et al., 1981).

The assays were carried out using particles that were either unlabeled (**Figure 5B**), or FITC-conjugated (**Figure 5C**). The unlabeled particles were captured on the control line using mouse

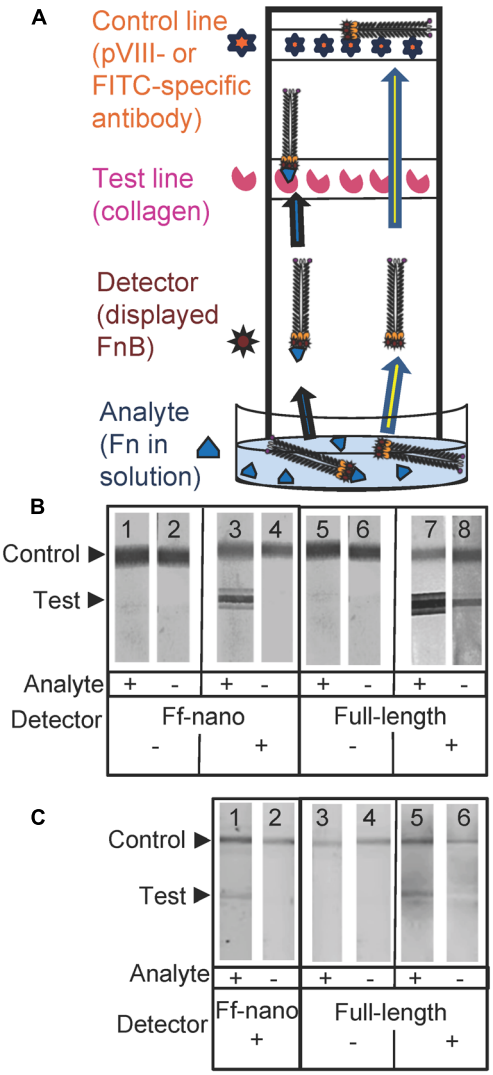


**FIGURE 5 | Fibronectin dipstick assay using Ff-nanoFnB. (A)** Schematic representation of a lateral-flow dipstick assay; Fn-detection dipstick assay using: **(B)** unlabeled; **(C)** FITC-labeled particles. Each assay (50 μL) contained $1 \times 10^{10}$ full-length Rnano3 (Rnano3FnB) or $1 \times 10^{11}$ Ff-nano (or Ff-nanoFnB) particles and 1 μg of Fn. The assay was performed and the unlabeled or FITC-labeled particles were detected as described in Section "Materials and Methods." The test line, printed with collagen solution, appears as a triple band when the signal is high. This is due to secondary lines flanking the main line that form during printing of collagen on the card. The triple banding during printing is caused by the acidity of the solution, necessary to keep the collagen soluble (0.25% acetic acid).

pVIII-specific antibodies and detected on the dipstick, after the assay was completed, using rabbit pVIII-specific antibody. The FITC-labeled phage were captured on the control line using FITC-specific antibodies and detected on the dipstick using a phosphoimager.

As expected, the Ff-nanoFnB particles and full-length phage displaying FnB (Rnano3FnB) showed binding to collagen at the test line in the presence of fibronectin [**Figure 5B** (sticks 3 and 7); **Figure 5C** (sticks 1 and 5)]. The Ff-nanoFnB particles gave no background in the absence of Fn (analyte), whereas the full-length FnB-displaying phage showed some unspecific binding to the collagen test line (**Figure 5B**, dipstick 8 and **Figure 5C**, dipstick 6) in the absence of Fn. The Ff-nano and full-length particles that did not display FnB did not bind to the test line, indicating the lack of unspecific binding of phage to collagen [**Figure 5B** (sticks 1, 2, 5, and 6); **Figure 5C** (sticks 3, 4)].

### Quantification of Fibronectin Using Dipstick Assay

To estimate the lower limit of detection using the Ff-nano dipstick assay and the range within which the signal depended on the amount of analyte, serial twofold dilutions of analyte (fibronectin) were assayed using this format. Since the dipstick assay signal was stronger in the unlabeled particle assay (**Figure 5B**) in comparison to the assay with FITC-labeled particles (**Figure 5C**), the former were used in this experiment.

The lowest concentration of fibronectin at which a signal could be detected at the test line was 0.08 ng/μL, equivalent to 0.35 femtomoles/μL or $2 \times 10^8$ molecules/μL, hence this is the sensitivity limit of the Ff-nanoFnB-based fibronectin detection dipstick assay (**Figure 6A**). The number of Ff-nano particles used in this assay was $2 \times 10^{11}$, the highest number that did not show unspecific binding to nitrocellulose (data not shown).

Densitometric analysis of the signal showed that the ratio between the test and control lines was proportional to the log of Fn (analyte) concentration (**Figures 6B,C**) over a range of concentrations between 0.625 and 10 ng/μL, consistent with simple visual comparison of control band density. These are much lower concentrations of Fn than those measured in the serum of healthy individuals (259–400 ng/μL; Allard et al., 1986). A suitable serum dilution would therefore adjust the concentration to the quantitative detection range of the assay. Furthermore, variations of Fn concentration in disease fall within one order of magnitude relative to those of healthy individuals (Choate and Mosher, 1983; Cembrowski and Mosher, 1984; Weller et al., 1988; Honest et al., 2002; Mosher, 2006; Eissa et al., 2010).

## Discussion

### Ff-nano Production and Purification

Ff-derived functionalized nanoparticles reported to date are based on the long and thin filamentous template, whose hydrodynamic properties are not favorable for diffusion-based applications. From ethical and regulatory perspectives, the use of Ff-phage outside of the laboratory containment, in particular in home-use diagnostic devices or as carriers for tissue targeting of drugs, antigens, or diagnostic markers, is potentially controversial because they are recombinant viruses. Due to the propensity of Ff to infect Gram-negative bacteria via the ubiquitous TolQRA complex in the absence of their primary receptor, the F-pilus of *E. coli* (Russel et al., 1988; Heilpern and Waldor, 2000), they could potentially infect a wide range of Gram-negative bacteria. This includes a possibility of mobilization and horizontal gene transfer of antibiotic-resistance-encoding genes, present in most

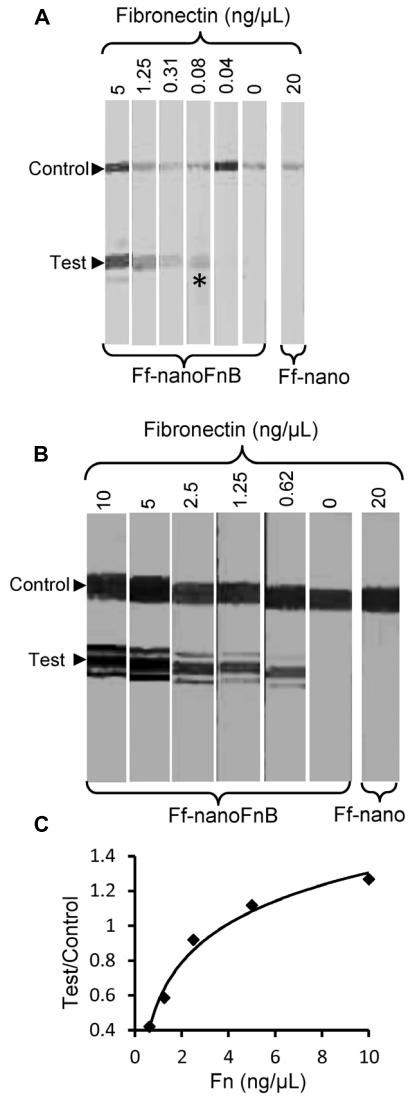


**FIGURE 6 | Detection range of Fibronectin using Ff-nanoFnB.** Series of Fn (analyte) dilutions analyzed using Ff-nanoFnB-based dipsticks were used for determination of lower detection limit **(A)** and quantitative range **(B,C)**. Asterisk in **(A)** denotes the lowest Fn concentration at which the signal was detected on the test line. The graph in **(C)** corresponds to the Test/Control signal ratio vs. Fn concentration. Each assay contained Ff-nanoFnB particles ($2 \times 10^{11}$) mixed with Fn at the indicated final concentrations in a total volume of 50 μL. The assay was performed and the signal quantified as described in the Section "Materials and Methods."

of the phage display vectors, among the gut or environmental bacteria. The Ff-derived particles (virions) containing phage display vectors have been shown to be taken up by mammalian cells in culture (Burg et al., 2002), hence there is a possibility that the encapsidated DNA permanently inserts into patient genomes.

To convert functionalized filamentous phage particles into non-replicating protein-DNA complexes, we have assembled functionalized short Ff-derived particles that contain 221-nt single-stranded DNA devoid of protein-coding sequences. Like Ff phage (f1, M13, and fd), genomes, the 221-nt ssDNA of the Ff-nano cannot integrate into *E. coli* chromosome as it lacks the necessary *cis* elements, such as genes for tRNA and/or sequences recognized by specific recombinases, that are used by some integrative filamentous phage to insert into bacterial chromosomes using the host recombinases (Rakonjac et al., 2011). Furthermore, given that it does not contain a negative (−) origin of replication, Ff-nano ssDNA cannot commence replication even if the specialized helper phage (containing *IRI* mutation in *gII*) coinfects the same cell. Therefore, Ff-nano improves the prospect of Ff filamentous phage applications outside of the laboratory. Given that these particles cannot replicate in any organism without extensive human intervention, they are considered not to be organsims in most legislatures regulating biological products, including the very strict New Zealand Hazardous Substances and New Organisms Act.

Furthermore, the length-to-diameter ratio of these particles is 15–20-fold smaller than that of the Ff particles derived from standard phagemid and phage vectors, improving the diffusion rate of the particles.

We have developed a production and purification pipeline for 50 nm particles by converting an Ff phage short-particle production system (Specthrie et al., 1992) into a high-efficiency system for producing functionalizable nanoparticles that we named Ff-nano. The increase in efficiency was achieved by using a high-copy-number plasmid containing the Ff-nano origin of replication and construction of helper phage Rnano3 and R408-3 that are also phage display vectors, containing cloning sites for construction of protein fusions to pIII.

In the Ff-nano purification, we introduced size-separation from the full-length helper phage by preparative agarose electrophoresis and electroelution. This strategy achieved excellent resolution, leading to a high enrichment of the Ff-nano particles over the full-length helper phage at a low cost and high recovery of the Ff-nano particles (31%). Overall, this production and purification system yields around $10^{14}$–$10^{15}$ Ff-nano particles from 2 to 8 L of *E. coli* culture. The Ff-nano samples obtained, however, still contain full-length phage at an approximate frequency of 1 in 200,000 ($5 \times 10^{-6}$). Although the helper phage that we use do not contain antibiotic resistance genes, they still represent an undesired population that needs to be eliminated in order to obtain fully virus-free Ff-nano samples. Helper plasmids are expected to overcome this residual phage contamination in the Ff-nano preparations, as they do not contain a Ff origin of replication (Chasteen et al., 2006). A helper plasmid derived from helper phage VCSM13 (containing $Km^r$ marker and p15A plasmid origin of replication, but not the $gII^{IRI}$ mutation) was constructed by deletion of the IG and tested for the Ff-nano production, however, it did not support the Ff-nano production to a detectable level, despite being efficient in supporting replication of standard phagemids that contain complete f1 origin of replication (Sattar, 2013). We have subsequently constructed a helper plasmid derived from Rnano3, which in preliminary analyses supported Ff-nano production (Jasna Rakonjac, unpublished). This helper plasmids is the next step toward the phage-free production of Ff-nano particles.

### Ff-nano Particle Stability

The Ff-nano were more resistant to heating in 1% (34 mM) ionic detergent SDS in comparison to the full-length phage. This property is solely due to the difference in phage length, as the assayed populations of full-length and Ff-nano particles were purified from the same *E. coli* culture and therefore had identical protein composition. Ff filamentous phage dissociation in the presence of SDS was investigated in detail by Stopar et al. (1998, 2002, 2003) using Electron Spin Resonance (ESR), circular dichroism and NMR. Solubilization of the major coat protein with detergent occurs when SDS displaces a pVIII subunit in the virion, replacing pVIII–pVIII interactions by pVIII-detergent interactions (Stopar et al., 1998). When a critical ratio of detergent to phage is reached, even a single pVIII subunit displacement across the filament triggers a cooperative dissociation of the virion (Ikehara et al., 1975; Stopar et al., 2002). In our experiment, the full-length virions were rapidly and completely disassembled after incubation in 1% SDS at 70°C for 5 min, which is the time point when over half of the Ff-nano particles in the sample remain intact (**Figure 3**). This length-dependent difference can be reconciled by the Ff-nano presenting a 17-fold smaller surface area for detergent interaction in comparison to the full-length phage, thereby decreasing the odds of steric imbalance caused by SDS–pVIII interactions per virion and resulting in much larger numbers of resistant particles under the same conditions. In addition, due to the short length of Ff-nano, the potential imperfections of pVIII packing that could occur in each particle due to mechanical bending and twisting of the filament are greatly reduced. Bending can be observed in the electron microscopic images of full-length phage (Gray et al., 1979; Rakonjac and Model, 1998), but not Ff-nano (**Figure 2A**; Supplementary Figure S5). The short length, preventing the bending of the filament may therefore confer additional stability to Ff-nano in comparison to full-length virions.

From the technological standpoint, the increased stability of Ff-nano particles may be beneficial in applications that involve high temperature in detergent-containing environment, or other harsh conditions. Given the higher resistance of Ff-nano to heating in 1% SDS at 70°C in comparison to complete sensitivity of the full-length phage, it is possible to develop conditions that will completely degrade the full-length phage in the purified Ff-nano preparation, while completely preserving the Ff-nano particles, thereby eliminating the full-length phage from the Ff-nano preparations. This approach will be possible for applications where the residue of SDS in the sample is not an issue, and where the Ff-nano particles display peptides that are resistant to denaturation by SDS.

### Ff-nano Functionalization and Use as a Detection Particle

To allow exploration of Ff-nano in biotechnological applications, we have converted the Ff-nano production system into a display system through insertion of MCS into *gIII* of the helper phage/vector, between the signal sequence and the mature portion of the protein. This system was then used to develop a dipstick fibronectin detection assay using Ff-nano displaying the fibronectin-binding domain from *S. pyogenes* (Ff-nanoFnB). No unspecific binding to the analyte was detected using the Ff-nanoFnB detection particles, in contrast to residual non-specific signal observed using the full-length phage Rnano3FnB. The quantitative range of assay using Ff-nanoFnB detection particles was found to be between 0.625 and 10 ng/μL, with the logarithmic dependence between the Fn concentration of Fn and the ratio of the signal intensity between the test and control lines. This range appropriate for measuring the Fn concentration in human serum after a suitable dilution. Variations of Fn concentration can be used as indicators of several diseases, such as bladder cancer, liver damage, defibrination syndrome, arterial thrombosis, preterm birth, or ocular damage (Choate and Mosher, 1983; Cembrowski and Mosher, 1984; Weller et al., 1988; Honest et al., 2002; Mosher, 2006; Eissa et al., 2010). These variations fall within one order of magnitude, corresponding to the quantitative range of the Ff-nanoFnB-based dipstick assay. The Ff-nanoFnB can therefore be the basis for development of quantitative fibronectin assay.

In conclusion, this work describes a novel display system that functionalizes short Ff phage-derived nanorods. It further demonstrates one application for use in dipstick assays. Given a large range of publications describing applications where Ff virions are used, including the templates for assembly of inorganic structures, diagnostics, tissue templating, imaging, and drug targeting (Bar et al., 2008; Petrenko, 2008; Lee et al., 2009; Souza et al., 2010; Chung et al., 2011; Dang et al., 2013; Bernard and Francis, 2014; Oh et al., 2014), Ff-nano as short non-viral functionalized particles will likely find many diverse applications.

## Acknowledgments

We are grateful to Marjorie Russel for comments on the manuscript. Marjorie Russel and Peter Model are acknowledged for generously providing the Ff and P1 phage, plasmids pLS7 and pPMR132 and *E. coli* strains. We also thank Dr. Dalaver Anjum for his expert technical assistance with the cryo-EM work (Pittsburgh University) and Doug Hopcroft for the TEM work at Manawatu Imaging and Microscopy Centre (Massey University). Funding for this project by a Marsden Fund Grant (contract number 02-MAU-210), Massey University Research Fund, Anonymous Donor, Palmerston North Medical Research Foundation, Massey University Institute of Fundamental Sciences Postgraduate Research Fund and the New Zealand Foundation for Research, and Technology contract C03X0701, is gratefully acknowledged. SS was supported by a Pakistani High Education Commission Doctoral Scholarship and NB by a Massey University Ph.D. scholarship.

## Supplementary Material

The Supplementary Material for this article can be found online at: http://www.frontiersin.org/journal/10.3389/fmicb.2015.00316/abstract

## References


Adrian, M., Dubochet, J., Fuller, S. D., and Harris, J. R. (1998). Cryo-negative staining. *Micron* 29, 145–160. doi: 10.1016/S0968-4328(97)00068-1

Allard, D., Rapin, J., Jacqueson, A., Freund, M., Coulaud, J. M., and Labrousse, J. (1986). Plasma fibronectin levels in normal subjects. *Thromb. Res.* 43, 375–378. doi: 10.1016/0049-3848(86)90158-1

Asano, S., Higashitani, A., and Horiuchi, K. (1999). Filamentous phage replication initiator protein gpII forms a covalent complex with the 5′ end of the nick it introduced. *Nucleic Acids Res.* 27, 1882–1889. doi: 10.1093/nar/27.8.1882

Bar, H., Yacoby, I., and Benhar, I. (2008). Killing cancer cells by targeted drug-carrying phage nanomedicines. *BMC Biotechnol.* 8:37. doi: 10.1186/1472-6750-8-37

Barbas, C. F. III, Kang, A. S., Lerner, R. A., and Benkovic, S. J. (1991). Assembly of combinatorial antibody libraries on phage surfaces: the gene III site. *Proc. Natl. Acad. Sci. U.S.A.* 88, 7978–7982. doi: 10.1073/pnas.88.18.7978

Bernard, J. M., and Francis, M. B. (2014). Chemical strategies for the covalent modification of filamentous phage. *Front. Microbiol.* 5:734. doi: 10.3389/fmicb.2014.00734

Blake, M. S., Johnston, K. H., Russell-Jones, G. J., and Gotschlich, E. C. (1984). A rapid, sensitive method for detection of alkaline phosphatase-conjugated anti-antibody on Western blots. *Anal. Biochem.* 136, 175–179. doi: 10.1016/0003-2697(84)90320-8

Bradbury, A. R., and Marks, J. D. (2004). Antibodies from phage antibody libraries. *J. Immunol. Methods* 290, 29–49. doi: 10.1016/j.jim.2004.04.007

Branston, S. D., Stanley, E. C., Ward, J. M., and Keshavarz-Moore, E. (2013). Determination of the survival of bacteriophage M13 from chemical and physical challenges to assist in its sustainable bioprocessing. *Biotechnol. Bioprocess. Eng.* 18, 560–566. doi: 10.1007/s12257-012-0776-9

Burg, M. A., Jensen-Pergakes, K., Gonzalez, A. M., Ravey, P., Baird, A., and Larocca, D. (2002). Enhanced phagemid particle gene transfer in camptothecin-treated carcinoma cells. *Cancer Res.* 62, 977–981.

Carter, P., Bedouelle, H., and Winter, G. (1985). Improved oligonucleotide site-directed mutagenesis using M13 vectors. *Nucleic Acids Res.* 13, 4431–4443. doi: 10.1093/nar/13.12.4431

Cembrowski, G. S., and Mosher, D. F. (1984). Plasma fibronectin concentration in patients with acquired consumptive coagulopathies. *Thromb. Res.* 36, 437–445. doi: 10.1016/0049-3848(84)90300-1

Chasteen, L., Ayriss, J., Pavlik, P., and Bradbury, A. R. (2006). Eliminating helper phage from phage display. *Nucleic Acids Res.* 34:e145. doi: 10.1093/nar/gkl772

Choate, J. J., and Mosher, D. F. (1983). Fibronectin concentration in plasma of patients with breast cancer, colon cancer, and acute leukemia. *Cancer* 51, 1142–1147. doi: 10.1002/1097-0142(19830315)51:6<1142::AID-CNCR2820510628>3.0.CO;2-S

Chung, W. J., Oh, J. W., Kwak, K., Lee, B. Y., Meyer, J., Wang, E., et al. (2011). Biomimetic self-templating supramolecular structures. *Nature* 478, 364–368. doi: 10.1038/nature10513

Dang, X., Qi, J., Klug, M. T., Chen, P. Y., Yun, D. S., Fang, N. X., et al. (2013). Tunable localized surface plasmon-enabled broadband light-harvesting enhancement for high-efficiency panchromatic dye-sensitized solar cells. *Nano Lett.* 13, 637–642. doi: 10.1021/nl3043823

Day, L. A. (2011). "Family Inoviridae," in *Virus Taxonomy: Classification and Nomenclature of Viruses: Ninth Report of the International Committee on Taxonomy of Viruses*, eds A. M. Q. King, M. J. Adams, E. B. Carstens, and E. J. Lefkowitz (San Diego, CA: Elsevier Academic Press), 375–384.

Day, L. A., Marzec, C. J., Reisberg, S. A., and Casadevall, A. (1988). DNA packing in filamentous bacteriophages. *Ann. Rev. Biophys. Biophys. Chem.* 17, 509–539. doi: 10.1146/annurev.bb.17.060188.002453

Dotto, G. P., Horiuchi, K., and Zinder, N. D. (1984). The origin of DNA replication of bacteriophage f1 and its interaction with the phage gene II protein. *Adv. Exp. Med. Biol.* 179, 185–191. doi: 10.1007/978-1-4684-8730-5_18

Eissa, S., Zohny, S. F., Zekri, A. R., El-Zayat, T. M., and Maher, A. M. (2010). Diagnostic value of fibronectin and mutant p53 in the urine of patients with bladder cancer: impact on clinicopathological features and disease recurrence. *Med. Oncol.* 27, 1286–1294. doi: 10.1007/s12032-009-9375-9

Engvall, E., Bell, M. L., and Ruoslahti, E. (1981). Affinity chromatography of collagen on collagen-binding fragments of fibronectin. *Coll. Relat. Res.* 1, 505–516. doi: 10.1016/S0174-173X(81)80032-5

Feng, J. N., Model, P., and Russel, M. (1999). A trans-envelope protein complex needed for filamentous phage assembly and export. *Mol. Microbiol.* 34, 745–755. doi: 10.1046/j.1365-2958.1999.01636.x

Gibaud, T., Barry, E., Zakhary, M. J., Henglin, M., Ward, A., Yang, Y., et al. (2012). Reconfigurable self-assembly through chiral control of interfacial tension. *Nature* 481, 348–351. doi: 10.1038/nature10769

Gray, C. W., Brown, R. S., and Marvin, D. A. (1979). Direct visualization of adsorption protein of fd phage. *J. Supramol. Str.* 1979, 91–91.

Harlow, E., and Lane, D. (1999). *Using Antibodies: A Laboratory Manual*. Cold Spring Harbor, NY: Cold Spring Harbor Laboratory Press.

Heilpern, A. J., and Waldor, M. K. (2000). CTXf infection of *Vibrio cholerae* requires the tolQRA gene products. *J. Bacteriol.* 182, 1739–1747. doi: 10.1128/JB.182.6.1739-1747.2000

Honest, H., Bachmann, L. M., Gupta, J. K., Kleijnen, J., and Khan, K. S. (2002). Accuracy of cervicovaginal fetal fibronectin test in predicting risk of spontaneous preterm birth: systematic review. *BMJ* 325:301. doi: 10.1136/bmj.325.7359.301

Ikehara, K., Utiyama, H., and Kurata, M. (1975). Studies on the structure of filamentous bacteriophage fd. II. All-or-none disassembly in guanidine-HCl and sodium dodecyl sulfate. *Virology* 66, 306–315. doi: 10.1016/0042-6822(75)90200-7

Lee, Y. J., Yi, H., Kim, W. J., Kang, K., Yun, D. S., Strano, M. S., et al. (2009). Fabricating genetically engineered high-power lithium-ion batteries using multiple virus genes. *Science* 324, 1051–1055. doi: 10.1126/science.1171541

Linderoth, N. A., Simon, M. N., and Russel, M. (1997). The filamentous phage pIV multimer visualized by scanning transmission electron microscopy. *Science* 278, 1635–1638. doi: 10.1126/science.278.5343.1635

Marks, J. D., Hoogenboom, H. R., Bonnert, T. P., Mccafferty, J., Griffiths, A. D., and Winter, G. (1991). By-passing immunization. Human antibodies from V-gene libraries displayed on phage. *J. Mol. Biol.* 222, 581–597. doi: 10.1016/0022-2836(91)90498-U

Marvin, D. A., Symmons, M. F., and Straus, S. K. (2014). Structure and assembly of filamentous bacteriophages. *Prog. Biophys. Mol. Biol.* 114, 80–122. doi: 10.1016/j.pbiomolbio.2014.02.003

Model, P., and Russel, M. (1988). "Filamentous bacteriophage," in *The Bacteriophages*, ed. R. Calendar (New York, NY: Plenum Publishing), 375–456.

Mosher, D. F. (2006). Plasma fibronectin concentration: a risk factor for arterial thrombosis? *Arterioscler. Thromb. Vasc. Biol.* 26, 1193–1195. doi: 10.1161/01.ATV.0000223342.15969.7a

Nelson, F. K., Friedman, S. M., and Smith, G. P. (1981). *Filamentous phage* DNA cloning vectors: a noninfective mutant with a nonpolar deletion in gene III. *Virology* 108, 338–350. doi: 10.1016/0042-6822(81)90442-6

Oh, J. W., Chung, W. J., Heo, K., Jin, H. E., Lee, B. Y., Wang, E., et al. (2014). Biomimetic virus-based colourimetric sensors. *Nat. Commun.* 5:3043. doi: 10.1038/ncomms4043

Petrenko, V. (2008). Evolution of phage display: from bioactive peptides to bioselective nanomaterials. *Expert Opin. Drug Deliv.* 5, 825–836. doi: 10.1517/17425247.5.8.825

Rakonjac, J., Bennett, N. J., Spagnuolo, J., Gagic, D., and Russel, M. (2011). Filamentous bacteriophage: biology, phage display and nanotechnology applications. *Curr. Issues Mol. Biol.* 13, 51–76.

Rakonjac, J., and Model, P. (1998). Roles of pIII in filamentous phage assembly. *J. Mol. Biol.* 282, 25–41. doi: 10.1006/jmbi.1998.2006

Rakonjac, J. V., Robbins, J. C., and Fischetti, V. A. (1995). DNA sequence of the serum opacity factor of group A streptococci: identification of a fibronectin-binding repeat domain. *Infect. Immun.* 63, 622–631.

Rebar, E. J., and Pabo, C. O. (1994). Zinc finger phage: affinity selection of fingers with new DNA-binding specificities. *Science* 263, 671–673. doi: 10.1126/science.8303274

Rogers, M. J., and Soll, D. (1988). Discrimination between glutaminyl-tRNA synthetase and seryl-tRNA synthetase involves nucleotides in the acceptor helix of tRNA. *Proc. Natl. Acad. Sci. U.S.A.* 85, 6627–6631. doi: 10.1073/pnas.85.18.6627

Russel, M., Kidd, S., and Kelley, M. R. (1986). An improved filamentous helper phage for generating single-stranded plasmid DNA. *Gene* 45, 333–338. doi: 10.1016/0378-1119(86)90032-6

Russel, M., and Model, P. (1989). Genetic analysis of the *Filamentous bacteriophage* packaging signal and of the proteins that interact with it. *J. Virol.* 63, 3284–3295.

Russel, M., and Model, P. (2006). "Filamentous phage," in *The Bacteriophages*, 2nd Edn, ed. R. C. Calendar (New York, NY: Oxford University Press, Inc.), 146–160.

Russel, M., Whirlow, H., Sun, T. P., and Webster, R. E. (1988). Low-frequency infection of F- bacteria by transducing particles of filamentous bacteriophages. *J. Bacteriol.* 170, 5312–5316.

Sambrook, J., and Russell, D. W. (2001). *Molecular Cloning: A Laboratory Manual*, 3rd Edn. Cold Spring Harbor, NY: Cold Spring Harbor.

Sattar, S. (2013). *Filamentous Phage-Derived Nano-Rods for Applications in Diagnostics and Vaccines*. Ph.D. thesis, Massey University, Palmerston North.

Schneider, C. A., Rasband, W. S., and Eliceiri, K. W. (2012). NIH Image to ImageJ: 25 years of image analysis. *Nat. Methods* 9, 671–675. doi: 10.1038/nmeth.2089

Schwarz-Linek, U., Hook, M., and Potts, J. R. (2006). Fibronectin-binding proteins of Gram-positive cocci. *Microbes Infect.* 8, 2291–2298. doi: 10.1016/j.micinf.2006.03.011

Smith, G. P. (1991). Surface presentation of protein epitopes using bacteriophage expression systems. *Curr. Opin. Biotechnol.* 2, 668–673. doi: 10.1016/0958-1669(91)90032-Z

Souza, G. R., Molina, J. R., Raphael, R. M., Ozawa, M. G., Stark, D. J., Levin, C. S., et al. (2010). Three-dimensional tissue culture based on magnetic cell levitation. *Nat. Nanotechnol.* 5, 291–296. doi: 10.1038/nnano.2010.23

Specthrie, L., Bullitt, E., Horiuchi, K., Model, P., Russel, M., and Makowski, L. (1992). Construction of a microphage variant of filamentous bacteriophage. *J. Mol. Biol.* 228, 720–724. doi: 10.1016/0022-2836(92)90858-H

Sternberg, N. L., and Maurer, R. (1991). Bacteriophage-mediated generalized transduction in *Escherichia coli* and *Salmonella typhimurium*. *Methods Enzymol.* 204, 18–43. doi: 10.1016/0076-6879(91)04004-8

Stopar, D., Spruijt, R. B., Wolfs, C. J., and Hemminga, M. A. (1998). Mimicking initial interactions of bacteriophage M13 coat protein disassembly in model membrane systems. *Biochemistry* 37, 10181–10187. doi: 10.1021/bi9718144

Stopar, D., Spruijt, R. B., Wolfs, C. J., and Hemminga, M. A. (2002). Structural characterization of bacteriophage M13 solubilization by amphiphiles. *Biochim. Biophys. Acta* 1594, 54–63. doi: 10.1016/S0167-4838(01)00281-3

Stopar, D., Spruijt, R. B., Wolfs, C. J., and Hemminga, M. A. (2003). Protein-lipid interactions of bacteriophage M13 major coat protein. *Biochim. Biophys. Acta* 1611, 5–15. doi: 10.1016/S0005-2736(03)00047-6

Vieira, J., and Messing, J. (1987). Production of single-stranded plasmid DNA. *Methods Enzymol.* 153, 3–11. doi: 10.1016/0076-6879(87)53044-0

Weller, M., Wiedemann, P., Heimann, K., and Zilles, K. (1988). Fibronectin quantification in plasma and vitreous by a non-competitive ELISA technique. *Doc. Ophthalmol.* 69, 341–351. doi: 10.1007/BF00162748

Zwick, M. G., Shen, J., and Scott, J. K. (1998). Phage-displayed peptide libraries. *Curr. Opin. Biotech.* 9, 427–436. doi: 10.1016/S0958-1669(98)80017-7

**Conflict of Interest Statement:** The authors declare that the research was conducted in the absence of any commercial or financial relationships that could be construed as a potential conflict of interest.

frontiers in
MICROBIOLOGY

MINI REVIEW ARTICLE
published: 23 December 2014
doi: 10.3389/fmicb.2014.00734

# Chemical strategies for the covalent modification of filamentous phage

***Jenna M. L. Bernard*** [1,2] ***and Matthew B. Francis*** [1,2] *******

[1] *Department of Chemistry, University of California at Berkeley, Berkeley, CA, USA*
[2] *Materials Sciences Division – Lawrence Berkeley National Laboratories, Berkeley, CA, USA*

***Edited by:***
*Jasna Rakonjac, Massey University, New Zealand*

***Reviewed by:***
*Ratmir Derda, University of Alberta, Canada*
*Itai Benhar, Tel Aviv University, Israel*

****Correspondence:***
*Matthew B. Francis, Department of Chemistry, University of California at Berkeley, Berkeley, CA 94720, USA*
*e-mail: mbfrancis@berkeley.edu*

Historically filamentous bacteriophage have been known to be the workhorse of phage display due to their ability to link genotype to phenotype. More recently, the filamentous phage scaffold has proven to be powerful outside the realm of phage display technology in fields such as molecular imaging, cancer research and materials, and vaccine development. The ability of the virion to serve as a platform for a variety of applications heavily relies on the functionalization of the phage coat proteins with a wide variety of functionalities. Genetic modification of the coat proteins has been the most widely used strategy for functionalizing the virion; however, complementary chemical modification strategies can help to diversify the range of materials that can be developed. This review emphasizes the recent advances that have been made in the chemical modification of filamentous phage as well as some of the challenges that are involved in functionalizing the virion.

**Keywords: filamentous phage, chemical modification, bioconjugation, protein modification, polymers, delivery**

## INTRODUCTION

The Ff group of filamentous bacteriophage are non-lytic viruses that infect bacteria by attachment to their F pili (Smith and Petrenko, 1997; Kehoe and Kay, 2005). M13, f1, and fd are the most well-characterized types of this virus and have a DNA sequence similarity up to 98.5% (Rakonjac et al., 2011). These viruses are known to be the workhorses of phage display, as they can be selected and evolved to identify novel binding activity through repeated cycles of mutation, selection, and amplification. This methodology allows for the production of phage constructs that can bind a variety of targets, including proteins, polymers, small molecules, and metal ions (Smith and Petrenko, 1997; Kehoe and Kay, 2005). In terms of structure, filamentous phage exist as long, thin tubes with a large aspect ratio (∼900 nm in length and 6 nm in width). The capsids comprise of five copies of each minor coat protein (pIII, pVI, pVII, and pIX) and a varying amount of the major coat protein (pVIII; Li et al., 2010). The interior of the virion contains a single-stranded deoxyribonucleic acid (ssDNA) genome that is protected by the cylindrical protein housing formed by the pVIII subunits. The minor coat proteins form caps at both ends of the assembly and are involved in host infection. The overall filamentous phage structure is shown in **Figure 1A**.

In addition to their important role in molecular evolution, filamentous phage have served as attractive platforms for a wide variety of applications due to their stability, ability to display peptides with strong affinities for their targets, and ease of production by propagation in bacteria. Moreover, the high number of repetitive coat proteins in the virion allow for multiple copies of a desired functionality to be displayed with well-defined spatial relationships. Reported applications include light-harvesting (Nam et al., 2010), nanoparticle nucleation (Mao et al., 2004), electrode templating (Lee et al., 2009), cell growth and differentiation (Merzlyak et al., 2009), bactericidal agents (Hagens and Blasi, 2003), molecular imaging (Hajitou et al., 2006; Chen et al., 2007; Li et al., 2010; Carrico et al., 2012; Ghosh et al., 2012), and drug delivery (Bar et al., 2008; Suthiwangcharoen et al., 2011; Ghosh et al., 2012).

The use of these virions in many applications requires the integration of targeting groups and/or cargo molecules that cannot be biosynthesized. For example, early work used phage display to evolve M13 phage coat proteins to bind semiconductors of varied compositions and geometries (Whaley et al., 2000). Continued work in this field has used similar techniques to develop phage-based scaffolds that can serve as improved anodes in lithium ion batteries, leading to enhanced storage capacity, improved conductivity, and the ability to produce thin flexible 2D arrays (Lee et al., 2002; Nam et al., 2006; Avery et al., 2009). In addition, applications in the fields of drug delivery and medical imaging have also relied heavily on the functionalization of filamentous phage particles with a range of synthetic molecules (Deutscher and Kelly, 2011).

In early work, the genetic manipulation of the phage coat proteins to incorporate peptides with novel function was the standard approach for filamentous phage modification (Willats, 2002). More recently, bioconjugation techniques have been exploited to allow a greater variety of synthetic molecules to be attached to the phage. The incorporation of these bioconjugation techniques has allowed for the production of a much more diverse set of constructs. As examples, the phage scaffold has been successfully modified with a variety of small organic molecules (Niu et al., 2008; Carrico et al., 2012), quantum dots (Merzlyak et al., 2009), fluorophores (Goldman et al., 2000; Hilderbrand et al., 2005, 2008; Carrico et al., 2012), and drugs (Yacoby et al., 2006; Bar et al., 2008). Despite these accomplishments, however, there still exist a limited number of chemical labeling strategies to modify the

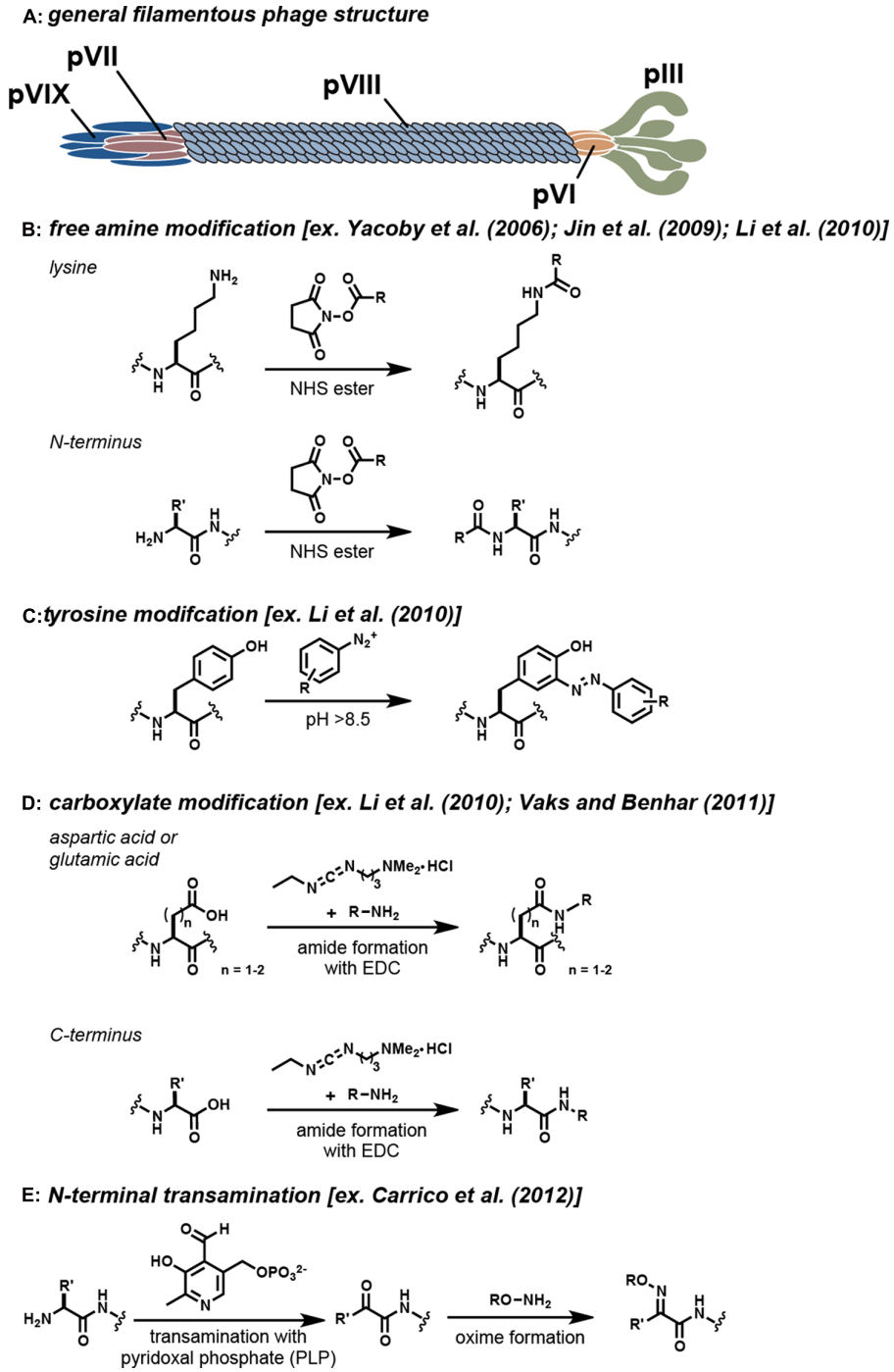


**FIGURE 1 | Covalent modification strategies for filamentous phage.** **(A)** The general locations of the coat proteins are shown. Note that actual phage have significantly more copies of the pVIII protein than are shown. Typical reactions that are used to modify specific functional groups on these proteins are shown in **(B–E)**. For each strategy, example references appear in the brackets.

filamentous phage coat proteins. The most widely used strategies rely on reagents that target reactive amino acid residues present in the sequences (i.e., the N-terminus, lysines, cysteines, tyrosines, aspartic acids, and glutamic acids). A summary of the strategies that have been frequently used to modify the virion is shown in **Figure 1**. As powerful as these modification strategies are, the majority of these techniques lack the high degree of specificity and control that is needed for many applications. The ideal bioconjugation reaction should be able to modify targets in a site-specific manner while still conserving the integrity of

the construct by operating in aqueous media under mild pH and temperature conditions.

With these considerations in mind, this review will focus on the recent chemical modification strategies that have been implemented on filamentous phage for materials construction. It should be noted that several detailed discussions regarding the use of filamentous phage in the context of phage display (Smith and Petrenko, 1997; Kehoe and Kay, 2005), gene therapy (Verma and Weitzman, 2005; Schaffer et al., 2008), and adjuvants for vaccines (Garcea and Gissmann, 2004) have appeared, and thus these applications will not be emphasized in this review. In addition, several in-depth reviews on the structure, replication cycle, and general applications of the filamentous phage have been also published elsewhere (Hemminga et al., 2010; Branston et al., 2011; Rakonjac et al., 2011).

## MAIN

### GENETIC MODIFICATION OF THE COAT PROTEINS

The most widely used strategy for functionalizing the phage scaffold has been the genetic incorporation of peptides that are engineered to associate with a novel target or serve as reactive handles (Rakonjac et al., 2011). It has been demonstrated that each type of coat protein present on the filamentous phage possesses the ability to display foreign proteins through genetic modification (Kwasnikowski et al., 2005; Smelyanski and Gershoni, 2011; Ghosh et al., 2012). The minor pIII coat protein is the most widely used to display protein motifs due to its ability to tolerate a high number and variety of amino acid insertions (Kwasnikowski et al., 2005). In applications where a large loading capacity is desired, such as drug delivery or imaging, it is common to label the major coat protein, pVIII, due to its high copy number (approximately 2700 monomers for M13 and f1, and 4,200 monomers for fd). However, it is important to note that genetic engineering of this major coat protein is less common because the pVIII monomers can only tolerate the incorporation of 6–8 amino acids (Popp et al., 2007; Hess et al., 2012).

With the incorporation of peptide sequences onto the phage scaffold comes the ability to modify the phage using either enzyme-based ligation techniques or chemoselective bioconjugation reactions. The genetic incorporation of enzymatic ligation handles has been demonstrated in several phage systems, including the biotin ligase (Chen et al., 2007; Smelyanski and Gershoni, 2011) and sortase A (Hess et al., 2012) systems. These methods are particularly useful in terms of their high degree of specificity compared to chemical approaches. Alternatively, several examples that use genetic modification to incorporate an amino acid that can act as a functional handle also exist. For example, genetically incorporated cysteine residues have been shown to be modified through native chemical ligation (Dwyer et al., 2000), thiol alkylation (Jespers et al., 2004; Heinis et al., 2009), and maleimide modification (Santoso et al., 2013). However, with these latter strategies, one has to take great care in the placement of the cysteine residues to limit problems with disulfide cross-linking between the closely packed phage coat proteins. Furthermore, the chemical modification of introduced cysteines can result in the unwanted labeling of endogenous solvent exposed cysteines found on the phage coat proteins (pVI, pVII, pIX; Soumillion et al., 1994; Pedersen et al., 1998). One way to circumvent these difficulties is to use immobilized tris(2-carboxyethyl)phosphine (iTCEP) to reduce only the sterically accessible cysteines on a peptide sequence displayed on the pIII coat protein of the phage (Jafari et al., 2014). Using this modification strategy, the Derda group was able to create a light-inhibited ligand system by alkylating and reducing two cysteines on the pIII that flank a randomized heptamer peptide sequence that was incorporated into the phage by phage display. Although the genetic incorporation of amino acids has proven to be a powerful tool for installing peptide motifs and natural amino acids as functional handles on the pIII protein, this strategy is limited to a low number of modifications on phage if the major coat protein cannot tolerate these genetic insertions following the signal sequence.

### FREE AMINE MODIFICATION

One of the most widely used strategies for the chemical modification of the filamentous phage relies on the non-specific modification of the free amine groups of the phage coat proteins. A number of strategies exist to target amines on proteins, including the use of isothiocyanates, isocyanates, acyl azides, and *N*-hydroxysuccinimide (NHS) esters (Hermanson, 2013). Of these, the acylation of amines using NHS esters has seen the most use. This reaction proceeds within an ideal pH range of 7.0–9.2 and results in the formation of a stable amide linkage following NHS release (**Figure 1B**; Mujumdar et al., 1993). Reports by several research groups have demonstrated that NHS ester chemistry is a reliable strategy for modifying the virion coat proteins (**Table 1**), although this approach can also lead to unwanted acylation of the lysine residues on protein fusions. For instance, Yacoby et al. (2006) demonstrated that both fd and M13 phage could serve as targeted drug carriers. In this interesting study, the phage scaffold was first modified genetically to include either a targeting peptide on the pVIII coat protein or a fUSE5-ZZ IgG binding domain on the pIII coat protein. Subsequently, the lysine residues were functionalized with chloramphenicol glutarate derivatives bearing additional NHS ester groups for phage attachment. It was then demonstrated that the phage-chloramphenicol constructs acted as prodrugs because they did not have cytotoxic activity until the labile ester linkages were released at the target site. Although the protein modification strategy proved to be successful overall, several complications arose upon using free amine modification to create this prodrug phage construct. First, the researchers had to take the precaution of selecting the targeting peptide displayed on pVIII such that it did not contain a free lysine in its motif. Additionally, the fuSE5-ZZ binding moiety displayed on the pIII protein had to be protected with human protein A-purified IgG prior to being conjugated with the chloramphenicol derivatives. Another difficulty that the researchers faced was that the high percentage of modification of the phage proteins caused them to become unstable and insoluble.

To gain an improved understanding of phage coat protein modification using NHS esters, Jin et al. (2009) developed an empirical kinetic model to predict the modification level of filamentous

**Table 1 | Functionalization of filamentous phage for application.**

| Application | Modification strategies [G]: Genetic [C]: Chemical | Functionalization | Reference |
|---|---|---|---|
| Protein engineering | [G] Peptide (pIII, pVIII) | Native chemical ligation | Dwyer et al. (2000) |
| Combinatorial library | [G] Yeast acceptor peptide (pIII) | Streptavidin-fluorophore | Chen et al. (2007) |
| Imaging | [G] Sortase motif (pIII, pVIII) | Single domain antibody, fluorescent peptide | Hess et al. (2012) |
| Immunoassays | [G] Antigen binding site (pIII)[C] Thiol alkylation | Fluorophore | Jespers et al. (2004) |
| Combinatorial library | [G] Peptide motif (pIII)[C] Thiol alkylation | Small molecule | Heinis et al. (2009) |
| Light-responsive ligands | [G] Cysteine containing peptide (pIII)[C] Alkylation/reduction | Photoresponsive azobenzene core | Jafari et al. (2014) |
| Targeted binding | [G] Cysteine containing peptide (pIII)[C] Maleimide | EGFR-binding peptide | Santoso et al. (2013) |
| Ligand identification | [G] N-terminal Ser/Thr (pIII)[C] Sodium periodate/oxime form. | Glycan | Ng et al. (2012) |
| Biosensor | [G] Targeting peptide (pIII)[C] NHS ester | Cy5 dye | Goldman et al. (2000) |
| Imaging application | [G] Targeting peptide (pIII, pVIII)[C] NHS ester | Fluorochromes | Hilderbrand et al. (2005) |
| Targeted drug delivery | [G] Targeting peptide (pIII, pVIII)[C] NHS ester | Chloramphenicol | Yacoby et al. (2006) |
| pH-responsive imaging | [C] NHS ester | pH responsive dye | Hilderbrand et al. (2008) |
| Composite fibers | [C] Lysine modification | Glutaric anhydride | Niu et al. (2008) |
| NHS kinetic study | [C] NHS ester | AF680 | Jin et al. (2009) |
| Cancer cell imaging | [C] NHS ester, diazonium coupling | Fluorescein, folate azide | Li et al. (2010) |
| Drug delivery | [C] NHS ester | Folic acid | Suthiwangcharoen et al. (2011) |
| Cancer cell imaging | [G] scFv (pIII)[C] N-terminal transamination | Small molecule, fluorophore | Carrico et al. (2012) |
| NMR biosensor | [G] scFv (pIII)[C] N-terminal transamination | $^{129}$Xe cryptophane-A | Palaniappan et al. (2013) |

phage under a wide range of reaction conditions. This study found that fifty percent of the phage maximum binding capacity to streptavidin was reached when approximately 0.03 biotins were attached per pVIII subunit. Such information can reduce the need for over modifying a targeting construct in future studies, perhaps allowing additional modifications to be used to append secondary cargo and/or solubilizing moieties.

Subsequent studies by Li et al. (2010) screened the reactivity of the amino groups of the virion by varying the concentration of *N*,*N*,*N*′,*N*′-tetramethylrhodamine (TMR) NHS ester in a 24 h reaction. Through use of UV-visible spectroscopy, it was found that 1600 rhodamine units could be attached to the M13 bacteriophage, but fluorescence quenching occurred when the phage particles bore more than 400 dyes each. In addition, the study elucidated that some of the six amines present on the M13 pVIII protein (N-terminal alanine 1 and lysines 8, 40, 43, 44, and 48) were more reactive than others. At low levels of modification, Ala-1 was primarily modified and at high modification levels both Ala-1 and Lys-8 were modified.

As another example of using NHS esters to functionalize phage, Li et al. (2010) created a construct for drug delivery using an M13 particle assembly. This structure was functionalized to bind cancer cells by using NHS ester chemistry to attach folic acid. The group was able to demonstrate that each pVIII subunit contained only one modification, and that these assemblies were amenable to loading with doxorubicin. Moreover, it was demonstrated that these constructs were stable under physiological conditions, but disassembled upon being delivered to the target site. This construct is just one of many examples that demonstrate that free amine modification utilizing NHS chemistry is a viable strategy for the creation of functionalized phage (See **Table 1**).

## TYROSINE MODIFICATION

Diazonium groups have long been known to react with a lysine, tyrosine, and histidine residues (Higgins and Harrington, 1959). These highly reactive diazonium groups can be used to modify tyrosine residues at pH values that are typically greater than 8.5 through an electrophilic attack on the active pi system of tyrosine (**Figure 1C**; Hermanson, 2013). The ability of diazonium salts to modify the phage major coat proteins was tested by Li et al. (2010). It was found that this strategy could append approximately 400 biotin groups per phage particle. Modifications occurred on the two tyrosine residues displayed on the pVIII major coat proteins (Tyr 21 and Tyr 24), whereas the lysine and histidine residues remained unmodified. This study is an important demonstration of a chemical modification strategy that can be used to complement the more commonly used lysine modification strategies. Experimental results from this study demonstrated that lower levels of modifications were achieved with the use of diazonium salt modification (400 molecules per phage) instead of NHS ester modification (1600 molecules per phage). It should be noted that this modification strategy non-specifically labels tyrosine moieties on the entire phage scaffold and therefore may not be ideal in scenarios in

which binding moieties contain tyrosines. The generation of diazonium salts with nitrous acid also places some limits on the functional groups that can be present on the group to be attached.

### CARBOXYLIC ACID MODIFICATION

Carbodiimide compounds, such as 1-ethyl-3-(-3-dimethylaminopropyl) carbodiimide hydrochloride (EDC) and *N*′,*N*′-dicyclohexyl carbodiimide (DCC), are common bioconjugation reagents used to activate carboxylic acid containing residues. These compounds react with aspartate and glutamate residues to form *O*-acylisourea intermediates, which subsequently react with primary amines to form stable amide bonds, **Figure 1D** (Hermanson, 2013). The reactivity of the carboxylic acid containing residues with carbodiimide chemistry was investigated by Li et al. (2010). In this study, varying concentrations of rhodamine B amine (RB), 1-ethyl-3-(3-dimethylaminopropyl) carbodiimide (EDC), and *N*-hydroxysulfosuccinimide (sulfo-NHS) were allowed to react with the phage coat proteins during a 12 h incubation period. It was found that the RB dye had a low degree of reactivity, and therefore a small molecule analog, propargylamine, was used to identify the reactive moieties. Of the four available carboxylic acid containing sites, only two sites (Glu-2 and Asp4/Asp5) on the pVIII monomers were found to be modified. The second modification site could not be distinguished between Asp4/Asp5 due to their close proximity.

Successive studies done by Vaks and Benhar (2011), demonstrated the capability of EDC coupling to functionalize the phage scaffold as an anti-microbial agent. In this study, the filamentous phage scaffold was covalently attached to chloramphenicol with an aminoglycoside linker using EDC coupling. These modified phage particles were shown to have prodrug qualities, longer circulation times, and lower immunogenicity compared to wild type phage.

The studies described above demonstrate that EDC coupling is a modification strategy that can be used effectively to target the carboxylic acid moieties on the phage scaffold to create new phage materials. As shown by Li et al. (2010), these carboxylic acid moieties are less chemically reactive than their lysine and tyrosine amino acid counterparts, and so are likely to result in lower percent modification of the phage scaffold. Because EDC coupling is not a site-specific chemical modification strategy, any carboxyl entity on a displayed protein is susceptible to modification.

### N-TERMINAL MODIFICATION

In an effort to move toward a site-selective modification approach, an N-terminal transamination modification strategy has been developed using pyridoxal 5′-phosphate (PLP) to functionalize the phage (Carrico et al., 2012). This method involves a two-step site-selective transamination/oxime-formation reaction, wherein the N-terminal amine is transformed into a pyruvamide group that is then converted into an oxime using alkoxyamine reagents (**Figure 1E**). Through this chemistry, 80% of the pVIII N-termini along the capsids could be converted to ketone functional groups, as determined by HPLC. The reaction was found to be selective for only solvent accessible N-terminal amines, with no participation from the ε-amine groups of lysine (Scheck et al., 2008). With this chemistry, fd phage bearing single-chain antibody fragment (scFv) groups previously determined to bind epidermal growth factor receptor (EGFR; Heitner et al., 2001) and human EGFR 2 (HER2; Poul et al., 2000) were modified with fluorophores and polyethylene glycol 2k (PEG2k) to create phage constructs that could distinguish breast cancer cell markers using fluorescence microscopy. Following this initial report, Palaniappan et al. (2013) further explored the versatility of this chemistry to create phage constructs for use as targeted $^{129}$Xe NMR biosensors. The use of N-terminal transamination/oxime-formation for the functionalization of the phage scaffold provides one of the first examples of a site-selective method that has been used to modify the phage coat proteins. This strategy provides a way to reach high levels of modification while preserving the binding capabilities of peptides that are displayed in other positions. Through the use of strategies such as these, well-defined constructs with multiple functionalities can be obtained.

As an alternative, serine and threonine residues have also been incorporated as latent N-terminal functional handles. The Derda group has demonstrated the functionalization of the virion through genetic introduction of a serine or threonine at the N-terminus of the minor coat pIII proteins (Ng et al., 2012). These phage were treated with sodium periodate to provide aldehydes, allowing for the incorporation of glycan moieties through oxime formation. Moreover, the Derda group further showed the power of genetic incorporation to serve as an N-terminal functional handle as they demonstrated that 2-amino benzamidoxime (ABAO) derivatives could react with oxidized N-terminal serines present on the pIII protein of the phage (Kitov et al., 2014). This latter strategy can be used to functionalize the pIII minor coat proteins directly.

## CONCLUSION AND FUTURE DIRECTIONS

The chemical modification strategies described in this review showcase the current methods that have been used to create promising constructs; however, they also highlight many of the challenges of this field. Genetic modifications have allowed for the introduction of peptide motifs and natural amino acids that can act as handles for phage functionalization. In addition to the genetic incorporation of natural amino acids, unnatural amino acids have also been shown to be incorporated (Chen et al., 2007; Liu et al., 2008). With the new functional groups that this technique introduces comes a substantially expanded range of reactions that can be used to functionalize the phage by targeting uniquely reactive moieties such as ketones, azides, and alkynes. This will undoubtedly yield many selective modification strategies in the future. However, one major hurdle in using genetic approaches such as these is that the successes of these strategies are highly dependent on the ability of the phage coat proteins to tolerate genetic modifications.

The bioconjugation toolbox for phage functionalization is still limited in its ability to modify the scaffold under reaction conditions that will keep the construct functional. Commonly used bioconjugation techniques, such as NHS ester, EDC, and diazonium chemistry, have limited degrees of site-selectivity and can be difficult to control in terms of the modification they can achieve. If high levels of modifications are to be attempted, these chemical modifications can result in over-modification of the scaffold,

rendering displayed peptides inactive and/or desolubilizing and destabilizing the construct. Site-selective bioconjugation strategies allow for the development of more well-defined constructs, which can obtain high levels of site-specific modification and still maintain function.

Although untested in the context of filamentous phage, a number functionalization strategies may prove to be effective tools in creating well-defined phage constructs. For example, enzymatic modifications such as those developed by Carrico et al. (2007) may allow for the incorporation of a chemical functional handle onto the phage scaffold. In addition to this, chemical strategies that target tyrosine residues could be applied, such as palladium pi-allyl chemistry (Tilley and Francis, 2006), Mannich reactions (Joshi et al., 2004), oxidative couplings (Seim et al., 2011), and a new tyrosine-click reaction (Ban et al., 2013). These strategies could expand the functional group tolerance beyond that of diazonium coupling reactions. Moreover, site-specific protein transamination using *N*-methylpyridinium-4-carboxaldehyde (Rapoport's Salt) to introduce a carbonyl can be seen as a promising chemical modification strategy for the filamentous phage as the major coat protein pVIII contains a glutamate-rich sequence that is predicted to be reactive for this reagent (Witus et al., 2013). This strategy shows potential for achieving higher levels of modifications of the pVIII coat proteins that may be advantageous for a number of applications.

Despite the advances that have been made in phage functionalization, it is still generally difficult to construct scaffolds that can be modified in multiple locations in a well-defined manner. Future advances in the development of phage constructs will most likely focus on the development of combined genetic and chemical strategies that will allow for site-specific incorporation of multiple functionalities onto the virion. Although genetic engineering approaches have been shown to be powerful tools to display peptide functionalities on the phage scaffold, complementary chemical modification strategies can offer simple and reliable methods for appending widely varying functionalities to provide access to a wider variety of multifunctional materials.

## ACKNOWLEDGMENTS

This work was generously supported by the DOD Breast Cancer Research Program (BC016995). The University of California Berkeley Chemical Biology Graduate Program (Training Grant 1 T32 GMO66698) is also acknowledged for their support of Jenna M. L. Bernard.

## REFERENCES

Avery, K. N., Schaak, J. E., and Schaak, R. E. (2009). M13 bacteriophage as a biological scaffold for magnetically-recoverable metal nanowire catalysts: combining specific and nonspecific interactions to design multifunctional nanocomposites. *Chem. Mater.* 21, 2176–2178. doi: 10.1021/cm900869u

Ban, H., Nagano, M., Gavrilyuk, J., Hakamata, W., Inokuma, T., and Barbas, C. F. (2013). Facile and stabile linkages through tyrosine: bioconjugation strategies with the tyrosine-click reaction. *Bioconjug. Chem.* 24, 520–532. doi: 10.1021/bc300665t

Bar, H., Yacoby, I., and Benhar, I. (2008). Killing cancer cells by targeted drug-carrying phage nanomedicines. *BMC Biotechnol.* 8:37. doi: 10.1186/1472-6750-8-37

Branston, S., Stanley, E., Ward, J., and Keshavarz-Moore, E. (2011). Study of robustness of filamentous bacteriophages for industrial applications. *Biotechnol. Bioeng.* 108, 1468–1472. doi: 10.1002/bit.23066

Carrico, I. S., Carlson, B. L., and Bertozzi, C. R. (2007). Introducing genetically encoded aldehydes into proteins. *Nat. Chem. Biol.* 3, 321–322. doi: 10.1038/nchembio878

Carrico, Z. M., Farkas, M. E., Zhou, Y., Hsiao, S. C., Marks, J. D., Chokhawala, H., et al. (2012). N-terminal labeling of filamentous phage to create cancer marker imaging agents. *ACS Nano* 6, 6675–6680. doi: 10.1021/nn301134z

Chen, I., Choi, Y.-A., and Ting, A. Y. (2007). Phage display evolution of a peptide substrate for yeast biotin ligase and application to two-color quantum dot labeling of cell surface proteins. *J. Am. Chem. Soc.* 129, 6619–6625. doi: 10.1021/ja071013g

Deutscher, S. L., and Kelly, K. A. (2011). "Imaging with bacteriophage-derived probes," in *Phage Nanobiotechnology,* Chap. 5, eds V. A. Petrenko and G. P. Smith (London: The Royal Society of Chemistry), 83–100.

Dwyer, M. A., Lu, W., Dwyer, J. J., and Kossiakoff, A. A. (2000). Biosynthetic phage display: a novel protein engineering tool combining chemical and genetic diversity. *Chem. Biol.* 7, 263–274. doi: 10.1016/S1074-5521(00)00102-2

Garcea, R. L., and Gissmann, L. (2004). Virus-like particles as vaccines and vessels for the delivery of small molecules. *Curr. Opin. Biotechnol.* 15, 513–517. doi: 10.1016/j.copbio.2004.10.002

Ghosh, D., Kohli, A. G., Moser, F., Endy, D., and Belcher, A. M. (2012). Refactored M13 bacteriophage as a platform for tumor cell imaging and drug delivery. *ACS Synth. Biol.* 1, 576–582. doi: 10.1021/sb300052u

Goldman, E. R., Pazirandeh, M. P., Mauro, J. M., King, K. D., Frey, J. C., and Anderson, G. P. (2000). Phage-displayed peptides as biosensor reagents. *J. Mol. Recognit.* 13, 382–387. doi: 10.1002/1099-1352(200011/12)13:6<382::AID-JMR511>3.0.CO;2-W

Hagens, S., and Blasi, U. (2003). Genetically modified filamentous phage as bactericidal agents: a pilot study. *Lett. Appl. Microbiol.* 37, 318–323. doi: 10.1046/j.1472-765X.2003.01400.x

Hajitou, A., Trepel, M., Lilley, C. E., Soghomonyan, S., Alauddin, M. M., Marini, F. C. III, et al. (2006). A hybrid vector for ligand-directed tumor targeting and molecular imaging. *Cell* 125, 385–398. doi: 10.1016/j.cell.2006.02.042

Heinis, C., Rutherford, T., Freund, S., and Winter, G. (2009). Phage-encoded combinatorial chemical libraries based on bicyclic peptides. *Nat. Chem. Biol.* 5, 502–507. doi: 10.1038/nchembio.184

Heitner, T., Moor, A., Garrison, J. L., Marks, C., Hasan, T., and Marks, J. D. (2001). Selection of cell binding and internalizing epidermal growth factor receptor antibodies from a phage display library. *J. Immunol. Methods* 248, 17–30. doi: 10.1016/S0022-1759(00)00340-9

Hemminga, M., Vos, W., Nazarov, P., Koehorst, R. M., Wolfs, C. A. M., Spruijt, R., et al. (2010). Viruses: incredible nanomachines. New advances with filamentous phages. *Eur. Biophys. J.* 39, 541–550. doi: 10.1007/s00249-009-0523-0

Hermanson, G. T. (2013). "The reactions of bioconjugation," in *Bioconjugate Techniques,* 3rd Edn, Chap. 3, ed. G. T. Hermanson (Boston: Academic Press), 229–258. doi: 10.1016/B978-0-12-382239-0.00003-0

Hess, G. T., Cragnolini, J. J., Popp, M. W., Allen, M. A., Dougan, S. K., Spooner, E., et al. (2012). M13 bacteriophage display framework that allows sortase-mediated modification of surface-accessible phage proteins. *Bioconjug. Chem.* 23, 1478–1487. doi: 10.1021/bc300130z

Higgins, H. G., and Harrington, K. J. (1959). Reaction of amino acids and proteins with diazonium compounds. II. Spectra of protein derivatives. *Arch. Biochem. Biophys.* 85, 409–425. doi: 10.1016/0003-9861(59)90506-5

Hilderbrand, S. A., Kelly, K. A., Niedre, M., and Weissleder, R. (2008). Near infrared fluorescence-based bacteriophage particles for ratiometric pH imaging. *Bioconjug. Chem.* 19, 1635–1639. doi: 10.1021/bc800188p

Hilderbrand, S. A., Kelly, K. A., Weissleder, R., and Tung, C.-H. (2005). Monofunctional near-infrared fluorochromes for imaging applications. *Bioconjug. Chem.* 16, 1275–1281. doi: 10.1021/bc0501799

Jafari, M. R., Deng, L., Kitov, P. I., Ng, S., Matochko, W. L., Tjhung, K. F., et al. (2014). Discovery of light-responsive ligands through screening of a light-responsive genetically encoded library. *ACS Chem. Biol.* 9, 443–450. doi: 10.1021/cb4006722

Jespers, L., Bonnert, T. P., and Winter, G. (2004). Selection of optical biosensors from chemisynthetic antibody libraries. *Protein Eng. Des. Sel.* 17, 709–713. doi: 10.1093/protein/gzh083

Jin, X., Newton, J. R., Montgomery-Smith, S., and Smith, G. (2009). A generalized kinetic model for amine modification of proteins with application to phage display. *Biotechniques* 46, 175–182. doi: 10.2144/000113074

Joshi, N. S., Whitaker, L. R., and Francis, M. B. (2004). A three-component mannich-type reaction for selective tyrosine bioconjugation. *J. Am. Chem. Soc.* 126, 15942–15943. doi: 10.1021/ja0439017

Kehoe, J. W., and Kay, B. K. (2005). Filamentous phage display in the new millennium. *Chem. Rev.* 105, 4056–4072. doi: 10.1021/cr000261r

Kitov, P. I., Vinals, D. F., Ng, S., Tjhung, K. F., and Derda, R. (2014). Rapid, hydrolytically stable modification of aldehyde-terminated proteins and phage libraries. *J. Am. Chem. Soc.* 136, 8149–8152. doi: 10.1021/ja5023909

Kwasnikowski, P., Kristensen, P., and Markiewicz, W. T. (2005). Multivalent display system on filamentous bacteriophage pVII minor coat protein. *J. Immunol. Methods* 307, 135–143. doi: 10.1016/j.jim.2005.10.002

Lee, S. W., Mao, C., Flynn, C. E., and Belcher, A. M. (2002). Ordering of quantum dots using genetically engineered viruses. *Science* 296, 892–895. doi: 10.1126/science.1068054

Lee, Y. J., Yi, H., Kim, W.-J., Kang, K., Yun, D. S., Strano, M. S., et al. (2009). Fabricating genetically engineered high-power lithium-ion batteries using multiple virus genes. *Science* 324, 1051–1055. doi: 10.1126/science.1171541

Li, K., Chen, Y., Li, S., Nguyen, H. G., Niu, Z., You, S., et al. (2010). Chemical modification of M13 bacteriophage and its application in cancer cell imaging. *Bioconjug. Chem.* 21, 1369–1377. doi: 10.1021/bc900405q

Liu, C. C., Mack, A. V., Tsao, M. L., Mills, J. H., Lee, H. S., Choe, H., et al. (2008). Protein evolution with an expanded genetic code. *Proc. Natl. Acad. Sci. U.S.A.* 105, 17688–17693. doi: 10.1073/pnas.0809543105

Mao, C., Solis, D. J., Reiss, B. D., Kottmann, S. T., Sweeney, R. Y., Hayhurst, A., et al. (2004). Virus-based toolkit for the directed synthesis of magnetic and semiconducting nanowires. *Science* 303, 213–217. doi: 10.1126/science.1092740

Merzlyak, A., Indrakanti, S., and Lee, S.-W. (2009). Genetically engineered nanofiber-like viruses for tissue regenerating materials. *Nano Lett.* 9, 846–852. doi: 10.1021/nl8036728

Mujumdar, R. B., Ernst, L. A., Mujumdar, S. R., Lewis, C. J., and Waggoner, A. S. (1993). Cyanine dye labeling reagents: sulfoindocyanine succinimidyl esters. *Bioconjug. Chem.* 4, 105–111. doi: 10.1021/bc00020a001

Nam, K. T., Kim, D.-W., Yoo, P. J., Chiang, C.-Y., Meethong, N., Hammond, P. T., et al. (2006). Virus-enabled synthesis and assembly of nanowires for lithium ion battery electrodes. *Science* 312, 885–888. doi: 10.1126/science.1122716

Nam, Y. S., Shin, T., Park, H., Magyar, A. P., Choi, K., Fantner, G., et al. (2010). Virus-templated assembly of porphyrins into light-harvesting nanoantennae. *J. Am. Chem. Soc.* 132, 1462–1463. doi: 10.1021/ja908812b

Ng, S., Jafari, M. R., Matochko, W. L., and Derda, R. (2012). Quantitative synthesis of genetically encoded glycopeptide libraries displayed on M13 phage. *ACS Chem. Biol.* 7, 1482–1487. doi: 10.1021/cb300187t

Niu, Z., Bruckman, M., Harp, B., Mello, C., and Wang, Q. (2008). Bacteriophage M13 as a scaffold for preparing conductive polymeric composite fibers. *Nano Res.* 1, 235–241. doi: 10.1007/s12274-008-8027-2

Palaniappan, K. K., Ramirez, R. M., Bajaj, V. S., Wemmer, D. E., Pines, A., and Francis, M. B. (2013). Molecular imaging of cancer cells using a bacteriophage-based 129Xe NMR biosensor. *Angew. Chem. Int. Ed. Engl.* 52, 4849–4853. doi: 10.1002/anie.201300170

Pedersen, H., Hölder, S., Sutherlin, D. P., Schwitter, U., King, D. S., and Schultz, P. G. (1998). A method for directed evolution and functional cloning of enzymes. *Proc. Natl. Acad. Sci. U.S.A.* 95, 10523–10528. doi: 10.1073/pnas.95.18.10523

Popp, M. W., Antos, J. M., Grotenbreg, G. M., Spooner, E., and Ploegh, H. L. (2007). Sortagging: a versatile method for protein labeling. *Nat. Chem. Biol.* 3, 707–708. doi: 10.1038/nchembio.2007.31

Poul, M.-A., Becerril, B., Nielsen, U. B., Morisson, P., and Marks, J. D. (2000). Selection of tumor-specific internalizing human antibodies from phage libraries. *J. Mol. Biol.* 301, 1149–1161. doi: 10.1016/S1074-5521(00)00102-2

Rakonjac, J., Bennett, N. J., Spagnuolo, J., Gagic, D., and Russel, M. (2011). Filamentous bacteriophage: biology, phage display and nanotechnology applications. *Curr. Issues Mol. Biol.* 13, 51–76. doi: 10.1002/9780470015902.a0000777

Santoso, B., Lam, S., Murray, B. W., and Chen, G. (2013). A simple and efficient maleimide-based approach for peptide extension with a cysteine-containing peptide phage library. *Bioorg. Med. Chem. Lett.* 23, 5680–5683. doi: 10.1016/j.bmcl.2013.08.032

Schaffer, D. V., Koerber, J. T., and Lim, K. I. (2008). Molecular engineering of viral gene delivery vehicles. *Annu. Rev. Biomed. Eng.* 10, 169–194. doi: 10.1146/annurev.bioeng.10.061807.160514

Scheck, R. A., Dedeo, M. T., Iavarone, A. T., and Francis, M. B. (2008). Optimization of a biomimetic transamination reaction. *J. Am. Chem. Soc.* 130, 11762–11770. doi: 10.1021/ja802495w

Seim, K. L., Obermeyer, A. C., and Francis, M. B. (2011). Oxidative modification of native protein residues using cerium(IV) ammonium nitrate. *J. Am. Chem. Soc.* 133, 16970–16976. doi: 10.1021/ja206324q

Smelyanski, L., and Gershoni, J. M. (2011). Site directed biotinylation of filamentous phage structural proteins. *Virol. J.* 8, 495. doi: 10.1186/1743-422X-8-495

Smith, G. P., and Petrenko, V. A. (1997). Phage display. *Chem. Rev.* 97, 391–410. doi: 10.1021/cr960065d

Soumillion, P., Jespers, L., Bouchet, M., Marchand-Brynaert, J., Winter, G., and Fastrez, J. (1994). Selection of β-lactamase on filamentous bacteriophage by catalytic activity. *J. Mol. Biol.* 237, 415–422. doi: 10.1006/jmbi.1994.1244

Suthiwangcharoen, N., Li, T., Li, K., Thompson, P., You, S., and Wang, Q. (2011). M13 bacteriophage-polymer nanoassemblies as drug delivery vehicles. *Nano Res.* 4, 483–493. doi: 10.1007/s12274-011-0104-2

Tilley, S. D., and Francis, M. B. (2006). Tyrosine-selective protein alkylation using π-allylpalladium complexes. *J. Am. Chem. Soc.* 128, 1080–1081. doi: 10.1021/ja057106k

Vaks, L., and Benhar, I. (2011). In vivo characteristics of targeted drug-carrying filamentous bacteriophage nanomedicines. *J. Nanobiotechnology* 9, 58. doi: 10.1186/1477-3155-9-58

Verma, I. M., and Weitzman, M. D. (2005). GENE THERAPY: twenty-first century medicine. *Annu. Rev. Biochem.* 74, 711–738. doi: 10.1146/annurev.biochem.74.050304.091637

Whaley, S. R., English, D. S., Hu, E. L., Barbara, P. F., and Belcher, A. M. (2000). Selection of peptides with semiconductor binding specificity for directed nanocrystal assembly. *Nature* 405, 665–668. doi: 10.1038/35015043

Willats, W. T. (2002). Phage display: practicalities and prospects. *Plant Mol. Biol.* 50, 837–854. doi: 10.1023/A:1021215516430

Witus, L. S., Netirojjanakul, C., Palla, K. S., Muehl, E. M., Weng, C.-H., Iavarone, A. T., et al. (2013). Site-specific protein transamination using N-methylpyridinium-4-carboxaldehyde. *J. Am. Chem. Soc.* 135, 17223–17229. doi: 10.1021/ja408868a

Yacoby, I., Shamis, M., Bar, H., Shabat, D., and Benhar, I. (2006). Targeting antibacterial agents by using drug-carrying filamentous bacteriophages. *Antimicrob. Agents Chemother.* 50, 2087–2097. doi: 10.1128/AAC.00169-06

**Conflict of Interest Statement:** The authors declare that the research was conducted in the absence of any commercial or financial relationships that could be construed as a potential conflict of interest.

*Received: 10 October 2014; paper pending published: 10 November 2014; accepted: 04 December 2014; published online: 23 December 2014.*

*Citation: Bernard JML and Francis MB (2014) Chemical strategies for the covalent modification of filamentous phage. Front. Microbiol.* ***5****:734. doi: 10.3389/fmicb.2014.00734*

frontiers in Microbiology

MINI REVIEW
published: 30 June 2016
doi: 10.3389/fmicb.2016.01013

# Filamentous Phages As a Model System in Soft Matter Physics

*Zvonimir Dogic* *

*Department of Physics, Brandeis University, Waltham, MA, USA*

Filamentous phages have unique physical properties, such as uniform particle lengths, that are not found in other model systems of rod-like colloidal particles. Consequently, suspensions of such phages provided powerful model systems that have advanced our understanding of soft matter physics in general and liquid crystals in particular. We described some of these advances. In particular we briefly summarize how suspensions of filamentous phages have provided valuable insight into the field of colloidal liquid crystals. We also describe recent experiments on filamentous phages that have elucidated a robust pathway for assembly of 2D membrane-like materials. Finally, we outline unique structural properties of filamentous phages that have so far remained largely unexplored yet have the potential to further advance soft matter physics and material science.

**Keywords: filamentous bacteriophages, soft matter physics, self-assembly, liquid crystals**

OPEN ACCESS

***Edited by:***
*Ratmir Derda,*
*University of Alberta, Canada*

***Reviewed by:***
*Ahmed Askora,*
*Zagazig University, Egypt*
*Dragana Gagic,*
*Massey University, New Zealand*

***Correspondence:**
*Zvonimir Dogic*
*zdogic@brandeis.edu*

***Specialty section:***
*This article was submitted to Virology, a section of the journal Frontiers in Microbiology*

***Received:*** *27 January 2016*
***Accepted:*** *14 June 2016*
***Published:*** *30 June 2016*

***Citation:***
*Dogic Z (2016) Filamentous Phages As a Model System in Soft Matter Physics. Front. Microbiol. 7:1013. doi: 10.3389/fmicb.2016.01013*

## INTRODUCTION

Nature is capable of assembling structures or remarkable complexity that frequently cannot be matched by materials synthesized in a laboratory setting. Filamentous phages are one example of such a material, where the knowledge of the fundamental biology has significantly advanced the seemingly unrelated fields of protein engineering and discovery, material science, nanotechnology and soft matter physics (Rakonjac et al., 2011). We review how filamentous phages have furthered our understanding of soft materials. Nature has engineered filamentous phages so that they are essentially identical to each other. Consequently properties of phage suspensions such as their length distribution are much narrower when compared to synthetic rodlike particles. This unique property has significantly impacted the field of soft matter physics directly leading to discovery of myriad structures, self-assembly pathways and previously unknown states of matter (Dogic and Fraden, 2006). We argue that the synergies and opportunities that emerge when filamentous phages are combined with soft matter physics have only been scratched and many exciting prospects lie ahead. The primary focus of this mini-review is on how filamentous phages have furthered our fundamental understanding of soft matter physics. Filamentous phages have also been used as a platform for developing materials with diverse practical applications ranging from biological

sensors, piezoelectric and photovoltaic devices and phage-based batteries. These technologically important advances have been reviewed elsewhere (Mao et al., 2009; Rakonjac et al., 2011; Farr et al., 2014).

## LIQUID CRYSTALLINE PHASES OF FILAMENTOUS PHAGES

Gels as well as suspensions of colloids, polymers, and amphiphiles are typical examples of soft materials. Liquid crystals, comprised from anisotropic rod-shaped molecules, are another technologically important example (de Gennes and Prost, 1995). At low concentrations, rod-like molecules are disordered and point in random directions. Such an arrangement of rod-like molecules is called an isotropic phase (**Figure 1A**). With increasing particle concentration an isotropic phase undergoes a discontinuous transition into a phase, in which all rods are aligned along one particular axis. Such an arrangement of molecules is called a nematic liquid crystal. Increasing the particle concentration further leads to more ordered phases. Of particular prominence is a smectic phase in which the molecules organize into one-rod-length thick liquid-like layers of aligned rods that are stacked on top of each other (**Figure 1A**). In the language of condensed matter physics smectic liquid crystals have a long-range orientational order and 1D quasi-long-range positional order.

In many ways filamentous viruses have catalyzed the development of the entire field of colloidal liquid crystals. In 1935, Wendell Meredith Stanley purified anisotropic rod-like Tobacco mosaic virus (TMV) (Stanley, 1935). Soon thereafter, John Bernal and his coworkers prepared TMV suspensions at high-enough concentrations to observe formation of a stable nematic phase (Bawden et al., 1936). Amongst others, these observations have inspired Lars Onsager to develop his seminal theory of the isotropic-nematic phase transition in colloidal liquid crystals (Onsager, 1949). However, TMV has a number of deficiencies including: long time required to grow tobacco plants and isolate the virus, the relative ease with which particles aggregate end-to-end yielding polydisperse suspensions, and the difficulty of introducing genetic modifications. For these reasons filamentous phages have supplanted TMV as a choice model system of rod-like particles.

While liquid crystalline behavior of filamentous bacteriophages has been known to structural biologists for a long time, the first detailed report describing these properties has been published by the group of Don Marvin (Lapointe and Marvin, 1973). Amongst other information this work reports direct visualization of smectic layers, a feat that precedes by many years the imaging revolution that has profoundly affected soft matter physics. Since these early advances the filamentous phages have become an important model system used to investigate liquid crystals. For example, filamentous bacteriophages enabled the first quantitative test of the Onsager theory. Specifically, once the virus flexibility and surface charge is taken into account, it was shown that the Onsager theory quantitatively explains the location and nature of the isotropic to nematic phase transition (**Figures 1B,C**; Tang and Fraden, 1995; Barry et al., 2009). Large aspect ratio and length uniformity were the two essential features that enabled quantitative comparison between experiments and theory.

While many biological and synthetic systems exhibit nematic ordering, observing a smectic phase has been a more formidable challenge. Since smectics are layered structures it is essential that the constituent rodlike molecules have uniform length. Until very recently, these conditions have been difficult to realize in synthetic systems (Kuijk et al., 2011). Therefore, smectic ordering in colloidal liquid crystals was first observed in TMV suspensions in the 1980's (Wen et al., 1989). Following upon this early work, phases with smectic-A, crystalline and columnar order have been more thoroughly characterized in suspensions of filamentous bacteriophages (**Figure 1D**; Dogic and Fraden, 1997; Grelet, 2008, 2014). Comparison between the rigid TMV rods, semi-flexible *fd* rods, theoretical models and computer simulations has demonstrated that even a slight flexibility pushes the nematic-to-smectic phase transition to higher particle concentrations and suppresses the formation of a smectic phase. Isolated filamentous phages can be visualized with optical microscopy, an advance that has provided important insight into the dynamics of the nematic, smectic, and columnar liquid crystals (Lettinga et al., 2005; Lettinga and Grelet, 2007; Pouget et al., 2011; Naderi et al., 2013).

## A MORE RECENT EXAMPLE—ASSEMBLY OF PHAGE BASED 2D COLLOIDAL MEMBRANES

So far we have described how the unique properties of filamentous bacteriophage suspensions have been used to test long-standing theoretical predictions related to bulk ordering of rod-like particles and thus advance the field of colloidal liquid crystals. More recent experiments, which again have relied on the unique properties of virus particles, have elucidated a fundamentally different pathway for assembly of virus particles into 1D and 2D materials. We discuss some of these advances and how they impacted our broader thinking about self-assembly of soft materials.

Virus particles are traditionally purified through a few cycles of differential centrifugation. In a first step a non-adsorbing polymer such as polyethylene glycol (PEG) is added to a dilute virus suspension. This induces filament attraction and their condensation, causing the suspension to acquire a cloudy appearance. This ubiquitous effect is know as depletion attraction in colloid science and macromolecular crowding in biology (**Figure 2A**; Asakura and Oosawa, 1954; Zhou et al., 2008). Recent work has shown that in purified virus suspensions the same effect leads to formation of myriad assemblages with surprisingly complex shapes (Dogic and Fraden, 2001; Dogic, 2003). At lowest depletant concentrations the viruses condense into spindle-shaped droplets (Dogic, 2003). Within the droplet the rod-like particles have nematic structure. Increasing the depletant concentration leads to a dramatic shape

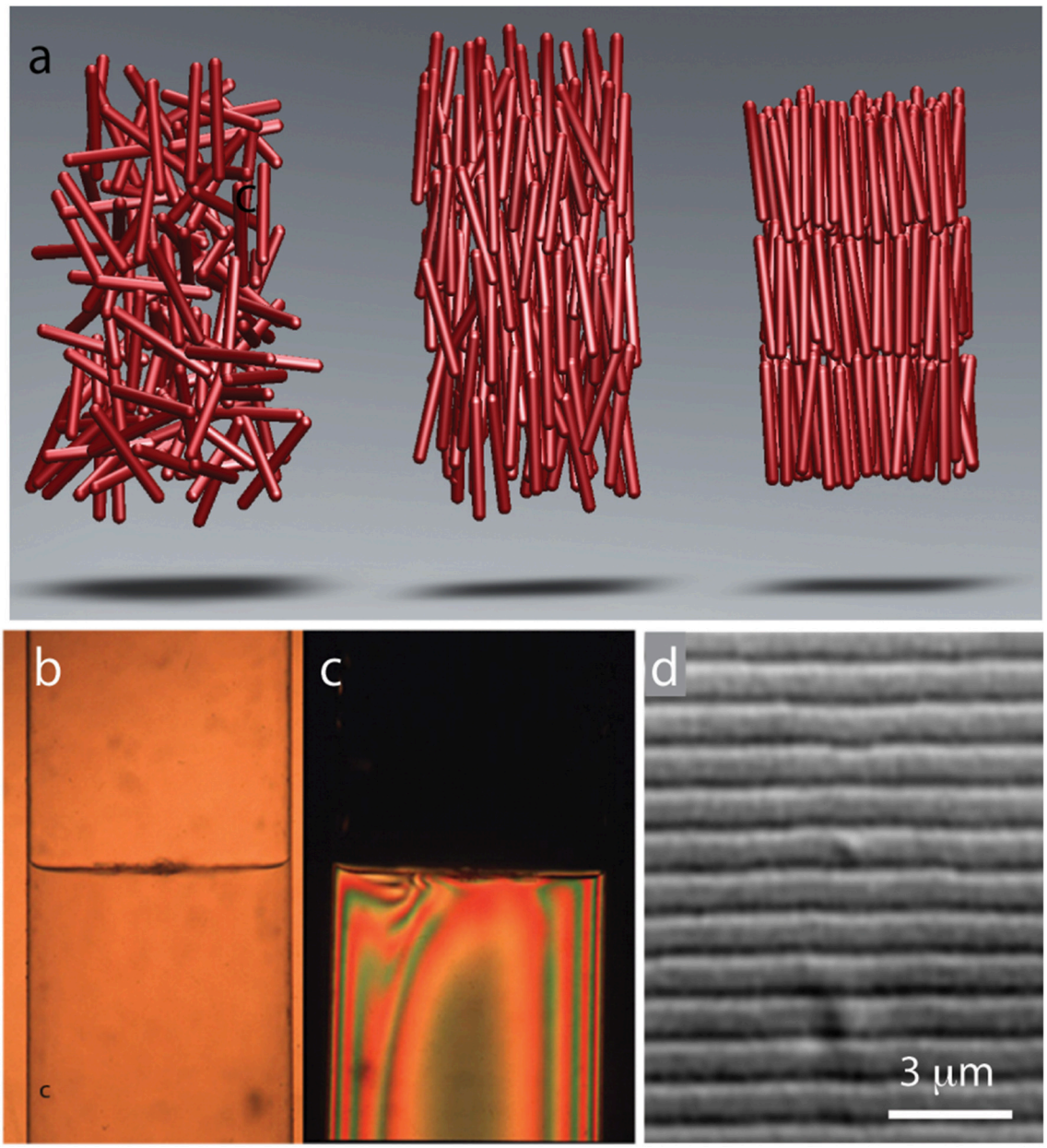


**FIGURE 1 | Common liquid crystalline phases observed in colloidal suspension of rodlike viruses. (A)** Schematic illustration of rods in an isotropic, nematic, and smectic liquid phase. **(B)** With increasing concentrations a suspension of TMV particles exhibits coexistence between an isotropic and a nematic phase. **(C)** Image of the same coexisting isotropic-nematic sample viewed under cross-polarizers. The birefringent nematic phase with higher density sediments to the bottom. **(D)** At high concentrations filamentous viruses form a smectic phase. High-resolution differential interference contrast (DIC) microscopy allows for direct visualization of one-rod-length long smectic layers. Here we illustrated the most common and important liquid crystalline phases. Filamentous phages exhibit a much richer phase diagram (for more details see Lettinga et al., 2005; Lettinga and Grelet, 2007; Pouget et al., 2011; Naderi et al., 2013).

change of the condensed droplet. In particular, at intermediate depletant concentrations the viruses associate laterally into a one rod-length thick monolayer membrane comprised from aligned rods (**Figures 2B,C**). The lateral size of these quasi-2D assemblages can be hundreds of microns (Barry and Dogic, 2010; Gibaud et al., 2012; Yang et al., 2012; Zakhary et al., 2014). Within each layer rods retain liquid-like dynamics. The properties of such 2D-assemblages are similar to those of conventional lipid bilayers, hence such structures are called colloidal membranes. Finally, at highest depletant concentrations the 2D colloidal membrane layers stack on top of each other, thus forming a bulk 3D condensate with smectic-like structure.

The discovery of colloidal membranes is important for several reasons. From a general perspective, it is possible to think of colloidal particles as giant atoms, and there is

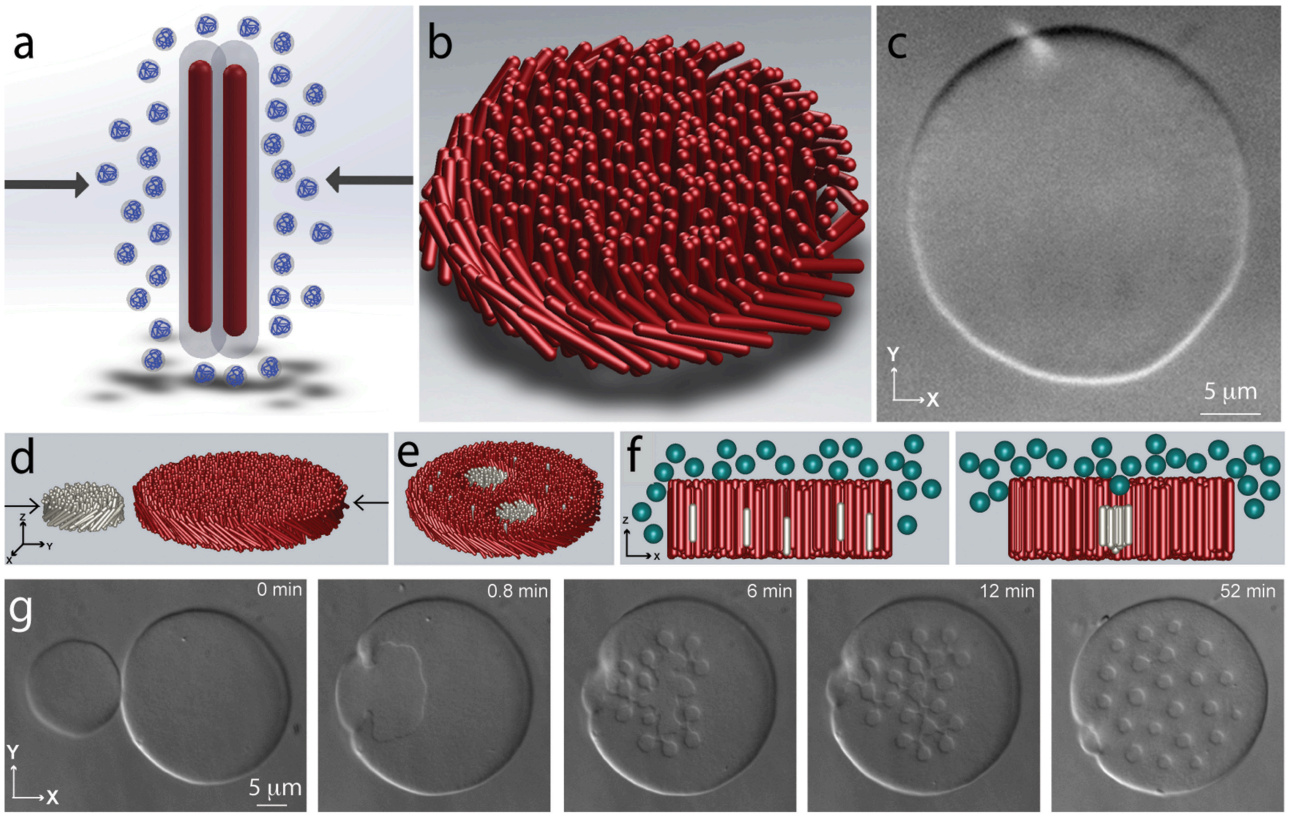


**FIGURE 2 | Assembly of filamentous phages into 2D colloidal membranes and rafts. (A)** Schematic illustration of the depletion interaction. Addition of non-adsorbing polymer leads to the imbalance of the osmotic pressure and effective attractive interactions between rod-like particles. **(B)** Depletion interactions lead to lateral condensation of rod-like particles and formation of 2D colloidal membranes that are enveloped by the depleting polymer suspension (not shown in the schematic). **(C)** DIC microscopy image of a colloidal membrane comprised from *fd-wt*. Rod-like particles point along the *z*-direction and the assemblage is comprised of millions of rod-like viruses. **(D)** Coalescence of two colloidal membranes leads to robust assembly of finite-sized colloidal rafts. Each membrane is comprised of filamentous phages of different length and chirality. Each monodisperse raft contains approximately 20,000 virus particles. **(E)** Schematic illustration of the coalescence experiments. **(F)** Lateral association of shorter rods dissolved within a colloidal membrane can be understood in terms of excluded volume. Inserting an isolated rod into a membrane creates additional volume at the ends of the filament that is inaccessible to the depleting polymer. Lateral association of shorter rods reduces the excluded volume and thus decreases the system free energy. **(G)** Lateral coalescence of short right-handed fd-Y21M and long left-handed M13KO7 membranes leads to the formation of finite-sized rafts.

a tradition of exploiting an analogy between colloidal and molecular systems. For example, with increasing concentration micron-sized spherical colloids spontaneously transition into 3D crystal (Pusey and Vanmegen, 1986). Many properties of such colloidal crystals bear resemblance to more conventional crystals built from molecular building blocks. However, in contrast to molecular crystals, optical microscopy enables visualization and tracking of all the constituent colloidal units as the crystal undergoes complex dynamical processes. Consequently, colloidal crystals have provided insight into universal processes in crystals that do not depend on the size of the constituent units, such as nucleation dynamics and glass formation (Gasser et al., 2001; Schall et al., 2004; Alsayed et al., 2005).

In a similar vein, although the microscopic interactions that drive their assembly are distinct, colloidal monolayers are micron-sized analogs of conventional lipid bilayers. Most importantly the same class of theories describe large-scale continuum deformations of both colloidal monolayers and lipid bilayers (Safran, 1994; Barry and Dogic, 2010). It follows that the studies of colloidal membranes could provide important insights into the universal aspects of membrane biophysics. For example, it has been suggested that lipid rafts, which are nanometer-sized clusters of certain lipids and other membrane soluble proteins, are the fundamental organizing principle of biological membranes (Lingwood and Simons, 2010). However, because of the size of the elemental units it is not possible to visualize lipid rafts and the subject remains controversial. From a more general perspective little is known about how membranes mediate effective interactions between various inclusions. We note that the important features of constituent viruses, namely their large and highly uniform length, endow colloidal membranes with their unique properties. Most importantly, colloidal membranes are easily visualized by optical microscopy offering a new system that might provide insight into the nature of ubiquitous membrane mediated interactions.

Recent experiments have explored the behavior of inclusions embedded within a colloidal monolayer membrane (Sharma et al., 2014). Specifically, colloidal membranes were doped with a low volume fraction of rods that were 30% shorter than the background rods. At low depletant concentrations the shorter rods where uniformly dispersed throughout the colloidal membrane, while at high osmotic pressure they bulk phase separated from the background membrane. Intriguingly, at intermediate depletant concentrations the shorter rods associated into robust, permanently stable, finite-sized clusters, comprised from approximately 20,000 rods (**Figures 2D–G**). The unique lengthscale of colloidal membranes have enabled characterization of colloidal rafts in great detail. For example, a combination of single-molecule tracking and FRAP techniques enabled direct measurement of $k_{on}$ and $k_{off}$, the kinetic rates at which individual rods associated with and dissociate from a colloidal raft. From here it is possible to measure the free energy landscape of colloidal rafts. Similar measurements are not feasible in analogous molecular systems. Using optical tweezers it was also possible to directly trap colloidal rafts and measure their membrane-mediated interactions. These experiments have shown that colloidal rafts have long-ranged repulsive interactions that can be many microns. Furthermore, it has been possible to relate these effective interactions to the distortions of the background membrane that can be visualized using specialized optical microscopy techniques. Again these experiments were only possible due to the unique properties of colloidal membranes.

It is intriguing to speculate about the possible broader relevance of such findings. For example, colloidal rafts demonstrate that all chiral inclusion in a colloidal membrane will acquire long-ranged repulsive interactions. Since these interactions depend only on the symmetries of the constituent particles, membrane-mediated chiral repulsions are universal and relevant for both lipid and colloidal membranes. Intriguingly, for conventional membranes, it is known that cholesterol is essential for assembly of lipid rafts. A possible and largely unexplored role of cholesterol might be to induce local twist, which would lead to raft-raft repulsions, and thus stabilize finite size assemblages. Intriguingly, from liquid crystal literature cholesterol is known to be an effective chiral dopant; hence chiral nematics are referred to as a cholesteric phase (de Gennes and Prost, 1995).

Self-assembly of membranes is a ubiquitous process in nature whose importance spans disparate scientific fields and many technological applications. The paramount example of lipid bilayers has inspired the synthesis of numerous other building blocks that assemble into 2D membrane-like structures (Discher et al., 1999; Antonietti and Forster, 2003; Park et al., 2004). The common feature shared by all these systems is the covalent link that holds together chemically incompatible moieties, such as a hydrophobic chain and a hydrophilic head. This irreversible bond introduces a molecular frustration that suppresses macroscopic bulk phase separation, and instead drives the formation of microphase-separated structures (Israelachvili, 2011). From this perspective, colloidal membranes are important for several reasons. First, they establish a new route for solution based self-assembly of 2D materials, one that does not rely on the established paradigm of amphiphilic assembly of chemically heterogeneous moieties, but rather on the geometrical properties of the constituent particles. Second, the formation of colloidal membranes is driven by universal hard-core repulsive interactions. Since such exclude volume interactions are relevant to all rod-like particles, experimental findings using filamentous bacteriophages should be widely applicable.

## OPPORTUNITIES AND CHALLENGES THAT LIE AHEAD

The uniformity of particle length has made filamentous bacteriophages an attractive model system in soft matter physics. However, there are other appealing features of filamentous phages that could also impact soft matter physics, but have not been utilized to nearly the same extent. Further advances will likely require a much tighter cooperation between biologist that can systematically modify various virus properties and physicist who can use these particles to assemble and characterize novel soft materials.

Filamentous phages afford almost arbitrary control over their contour length, which is another exciting feature. Because its length scales linearly with its genome size, filamentous phages have a unique ability to package very long or short DNA segments. Longer genomic DNA lead to longer viruses. Using molecular cloning techniques it has been possible to engineer viruses that are as short as 50 nm and as long as 8000 nm (Herrmann et al., 1980; Specthrie et al., 1992; Marchi et al., 2014; Brown et al., 2015; Sattarl et al., 2015). In principle, this makes it feasible to create monodisperse rods whose aspect ratio varies from anywhere between 10 and 1000. So far the filamentous phages with tunable lengths have been used in only a few studies, starting with the pioneering experiments that examined how rotational dynamics of rods in the isotropic phase scales with their length (Maguire et al., 1980). Subsequently, viruses have been used to examine the effect of rod length on the location of the isotropic-nematic phase transition as well as the stability of the smectic phase (Dogic and Fraden, 2001; Purdy and Fraden, 2004, 2007). Furthermore, studies on colloidal membranes have demonstrated dramatic effect that even slight changes in the rod lengths have on the stability of colloidal clusters (Sharma et al., 2014).

However, these studies have only scratched the surface of many experiments that become possible with a library of viruses of different lengths. Creating such a library requires expertise in molecular cloning that is not readily accessible to the physics community. A particular challenge is that longer phages have a tendency to delete the inserted DNA segments and thus revert back to the wild-type length. Since longer phages take longer to grow any particle that excises the extra DNA segment has shorter reproduction time and quickly overtakes the entire population. However, there are very few alternate model systems of rod-like particles with tunable length, and creating a library of filamentous phages of varying contour length that can be robustly grown would surely have a significant impact on soft matter physics.

Another attractive feature of the phages that has not received enough attention is the possibility of tuning the physical properties of the filaments by systematically changing the composition of the major coat protein. For example, structural biologists have studied fd-Y21M (a mutant virus in which the 21st amino acid of the major coat protein is changed from tyrosine to methionine) because it yielded higher quality diffraction patterns (Marvin et al., 1994). More recent work has demonstrated that Y21M mutation dramatically changes the physical properties of the virus (Barry et al., 2009). In particular, the persistence length of Y21M mutant is 9.9 μm in comparison to the wild-type phage that is only 2.4 μm. Furthermore, *fd-wt* forms a cholesteric liquid crystal with left-handed chirality, whereas Y21M mutant switches the handedness of the system. Needless to say the phase space of all possible mutations of the major coat protein is much larger, and so far there has been no attempts to systematically alter the coat protein structure and correlate this to coarse-grained properties of the filament. For example, it would be interesting to determine how the bending rigidity of filaments changes as the composition of the major coat protein varies from purely Y21M to wild-type protein. This might systematically change the bending rigidity and thus create filaments with tunable persistence length and chirality, a unique feature not present in any other model system. Using phage display technology it has proven possible to systematically change the composition of the coat proteins within a single virus (Rowitch et al., 1988).

Finally, another underused but attractive feature of filamentous bacteriophages is the structure of its ends. Specifically, a distinct set of proteins is associated with each virus end, thus raising the possibility of specifically labeling each virus end. There have been several notable efforts in this direction, although most of these have been restricted to studies at a single filament level instead of studying properties of macroscopic assemblages. In an important early step, phage display technology has been used to select for amino-acid sequences that specifically bind to inorganic surfaces (Whaley et al., 2000). This feature made it possible to assemble soft materials in which filamentous phages organize into smectic layers that are intercalated with layers of end-bound inorganic nanoparticles (Lee et al., 2002). It should be noted that there are alternate pathways toward assembly of such structures. In particular, similar lamellar structures can also robustly form in a simple mixture of hard rods and spheres that lack any specific link between spheres and rods (Adams et al., 1998; Dogic et al., 2000). In another notable study two ends of the virus have been labeled with distinct labels. In one case these molecules associated with each other, thus transforming linear bacteriophages into ring-like structures, while in another experiment similar end labels have been used for single-molecule experiments that have measured the mechanical properties of the virus using force-extension experiments (Nam et al., 2004; Khalil et al., 2007). Finally, in another study the end labeled viruses have been used to coat the surface of a micron-sized colloidal particle and thus create a unique star colloids with very long repulsive interactions (Huang et al., 2009). However, these are only a few of many applications that become possible using end labeled filaments. In particular, a chemical coupling scheme is needed that will allow for specific and robust attachment of diverse sets of chemicals, including dyes to either of the filaments ends. Such a scheme would enable a much wider range of experiments.

## AUTHOR CONTRIBUTIONS

The author confirms being the sole contributor of this work and approved it for publication.

## FUNDING

Research program on self-assembly of filamentous viruses is supported by the National Science Foundation grants no. DMR-MRSEC-1402382, DMR-1609742 and DMR-0955776.

## ACKNOWLEDGMENTS

I sincerely thank all the students and colleagues who have over the years contributed to our research on self-assembly of filamentous viruses, especially Seth Fraden, Robert Meyer, Pavlik Lettinga, Eric Grelet, Edward Barry, Thomas Gibaud, Prerna Sharma, and Mark Zakhary. Research program on self-assembly of filamentous viruses is supported by the National Science Foundation grants no. DMR-MRSEC-1420382 and DMR-0955776.

## REFERENCES

Adams, M., Dogic, Z., Keller, S. L., and Fraden, S. (1998). Entropically driven microphase transitions in mixtures of colloidal rods and spheres. *Nature* 393, 349–352. doi: 10.1038/30700

Alsayed, A. M., Islam, M. F., Zhang, J., Collings, P. J., and Yodh, A. G. (2005). Premelting at defects within bulk colloidal crystals. *Science* 309, 1207–1210. doi: 10.1126/science.1112399

Antonietti, M., and Forster, S. (2003). Vesicles and liposomes: a self-assembly principle beyond lipids. *Adv. Mater.* 15, 1323–1333. doi: 10.1002/adma.200300010

Asakura, S., and Oosawa, F. (1954). On interaction between 2 bodies immersed in a solution of macromolecules *J. Chem. Phys.* 22, 1255–1256. doi: 10.1063/1.1740347

Barry, E., Beller, D., and Dogic, Z. (2009). A model liquid crystalline system based on rodlike viruses with variable chirality and persistence length. *Soft Matter* 5, 2563–2570. doi: 10.1039/b822478a

Barry, E., and Dogic, Z. (2010). Entropy driven self-assembly of nonamphiphilic colloidal membranes. *Proc. Natl. Acad. Sci. U.S.A.* 107, 10348–10353. doi: 10.1073/pnas.1000406107

Bawden, F., Pirie, N., Bernal, J. D., and Fankuchen, I. (1936). Liquid crystalline substances from virus infected plants. *Nature* 138, 1051–1052. doi: 10.1038/1381051a0

Brown, S., Majikes, J., Martínez, A., Girón, T. M., Fennell, H., Samano, E. C., et al. (2015). An easy-to-prepare mini-scaffold for DNA origami. *Nanoscale* 7, 16621–16624. doi: 10.1039/C5NR04921K

de Gennes, P. G., and Prost, J. (1995). *The Physics of Liquid Crystals*. Oxford, UK: Oxford University Press. doi: 10.1063/1.2808028

Discher, B. M., Won Y. Y., Ege, D. S., Lee, J. C., Bates, F. S., Discher, D. E., et al. (1999). Polymersomes: tough vesicles made from diblock copolymers. *Science* 284, 1143–1146. doi: 10.1126/science.284.5417.1143

Dogic, Z. (2003). Surface freezing and a two-step pathway of the isotropic-smectic phase transition in colloidal rods. *Phys. Rev. Lett.* 91:165701. doi: 10.1103/physrevlett.91.165701

Dogic, Z., and Fraden, S. (1997). Smectic phase in a colloidal suspension of semiflexible virus particles. *Phys. Rev. Lett.* 78, 2417–2420. doi: 10.1103/PhysRevLett.78.2417

Dogic, Z., and Fraden, S. (2001). Development of model colloidal liquid crystals and the kinetics of the isotropic-smectic transition. *Philos. Trans. R. Soc. Math. Phys. Eng. Sci.* 359, 997–1014. doi: 10.1098/rsta.2000.0814

Dogic, Z., and Fraden, S. (2006). Ordered phases of filamentous viruses. *Curr. Opin. Colloid Interface Sci.* 11, 47–55. doi: 10.1016/j.cocis.2005.10.004

Dogic, Z., Frenkel, D., and Fraden, S. (2000). Enhanced stability of layered phases in parallel hard spherocylinders due to addition of hard spheres. *Phys. Rev. E* 62, 3925–3933. doi: 10.1103/PhysRevE.62.3925

Farr, R., Choi, D. S., and Lee, S. W. (2014). Phage-based nanomaterials for biomedical applications. *Acta Biomater.* 10, 1741–1750. doi: 10.1016/j.actbio.2013.06.037

Gasser, U., Weeks, E. R., Schofield, A., Pusey, P. N., and Weitz, D. A. (2001). Real-space imaging of nucleation and growth in colloidal crystallization. *Science* 292, 258–262. doi: 10.1126/science.1058457

Gibaud, T., Barry, E., Zakhary, M. J., Henglin, M., Ward, A., Yang, Y., et al. (2012). Reconfigurable self-assembly through chiral control of interfacial tension. *Nature* 481, 348–351. doi: 10.1038/nature10769

Grelet, E. (2008). Hexagonal order in crystalline and columnar phases of hard rods. *Phys. Rev. Lett.* 100:168301. doi: 10.1103/physrevlett.100.168301

Grelet, E. (2014). Hard-rod behavior in dense mesophases of semiflexible and rigid charged viruses. *Phys. Rev. X* 4:021053. doi: 10.1103/physrevx.4.021053

Herrmann, R., Neugebauer, K., Pirkl, E., Zentgraf, H., and Schaller, H. (1980). Conversion of bacteriophage-fd into an efficeint single-stranded DNA vectro system. *Mol. Gen. Genet.* 177, 231–242. doi: 10.1007/BF00267434

Huang, F., Addas, K., Ward, A., Flynn, N. T., Velasco, E., Hagan, M. F., et al. (2009). Pair potential of charged colloidal stars. *Phys. Rev. Lett.* 102:108302. doi: 10.1103/physrevlett.102.108302

Israelachvili, J. N. (2011). *Intermolecular and Surface Forces. Revised 3rd Edn*. Cambridge, MA: Academic Press.

Khalil, A. S., Ferrer, J. M., Brau, R. R., Kottmann, S. T., Noren, C. J., Lang, M. J., et al. (2007). Single M13 bacteriophage tethering and stretching. *Proc. Natl. Acad. Sci. U.S.A.* 104, 4892–4897. doi: 10.1073/pnas.0605727104

Kuijk, A., van Blaaderen, A., and Imhof, A. (2011). Synthesis of monodisperse, rodlike silica colloids with tunable aspect ratio. *J. Am. Chem. Soc.* 133, 2346–2349. doi: 10.1021/ja109524h

Lapointe, J., and Marvin, D. A. (1973). Filamentous bacterial viruses. 8. Liquid crystals of fd. *Mol. Cryst. Liquid Cryst.* 19, 269. doi: 10.1080/15421407308084657

Lee, S. W., Mao, C. B., Flynn, C. E., and Belcher, A. M. (2002). Ordering of quantum dots using genetically engineered viruses. *Science* 296, 892–895. doi: 10.1126/science.1068054

Lettinga, M. P., Barry, E., and Dogic, Z. (2005). Self-diffusion of rod-like viruses in the nematic phase. *Europhys. Lett.* 71, 692–698. doi: 10.1209/epl/i2005-10127-x

Lettinga, M. P., and Grelet, E. (2007). Self-diffusion of rodlike viruses through smectic layers. *Phys. Rev. Lett.* 99:197802. doi: 10.1103/physrevlett.99.197802

Lingwood, D., and Simons, K. (2010). Lipid rafts as a membrane-organizing principle. *Science* 327, 46–50. doi: 10.1126/science.1174621

Maguire, J. F., McTague, J. P., and Rondelez, F. (1980). Rotational diffusion of sterically interacting rodlike macromolecules. *Phys. Rev. Lett.* 45, 1891–1894. doi: 10.1103/PhysRevLett.45.1891

Mao, C. B., Liu, A. H., and Cao, B. R. (2009). Virus-based chemical and biological sensing. *Angew. Chem. Int. Ed.* 48, 6790–6810. doi: 10.1002/anie.200900231

Marchi, A. N., Saaem, I., Vogen, B. N., Brown, S., and LaBean, T. H. (2014). Toward larger DNA origami. *Nano Lett.* 14, 5740–5747. doi: 10.1021/nl502626s

Marvin, D., Hale, R., Nave, C., and Citterich, M. H. (1994). Molecular models and structural comparisons of native and mutant class I filamentous bacteriophages: Ff (fd, f1, M13), If1 and IKe. *J. Mol. Biol.* 235, 260–286. doi: 10.1016/S0022-2836(05)80032-4

Naderi, S., Pouget, E., Ballesta, P., van der Schoot, P., Grelet, E., and Lettinga, P. (2013). Fractional hoppinglike motion in columnar mesophases of semiflexible rodlike particles. *Phys. Rev. Lett.* 111:037801. doi: 10.1103/PhysRevLett.111.037801

Nam, K. T., Peelle, B. R., Lee, S. W., and Belcher, A. M. (2004). Genetically driven assembly of nanorings based on the M13 virus. *Nano Lett.* 4, 23–27. doi: 10.1021/nl0347536

Onsager, L. (1949). The effects of shape on the interaction of colloidal particles. *Ann. N. Y. Acad. Sci.* 51, 627–659. doi: 10.1111/j.1749-6632.1949.tb27296.x

Park, S., Lim, J. H., Chung, S. W., and Mirkin, C. A. (2004). Self-assembly of mesoscopic metal-polymer amphiphiles. *Science* 303, 348–351. doi: 10.1126/science.1093276

Pouget, E., Grelet, E., and Lettinga, M. P. (2011). Dynamics in the smectic phase of stiff viral rods. *Phys. Rev. E* 84:041704. doi: 10.1103/PhysRevE.84.041704

Purdy, K. R., and Fraden, S. (2004). Isotropic-cholesteric phase transition of filamentous virus suspensions as a function of rod length and charge. *Phys. Rev. E* 70:011705. doi: 10.1103/physreve.70.061703

Purdy, K. R., and Fraden, S. (2007). Influence of charge and flexibility on smectic phase formation in filamentous virus suspensions. *Phys. Rev. E* 76:061703. doi: 10.1103/physreve.76.011705

Pusey, P. N., and Vanmegen, W. (1986). Phase-behavior of concentrated suspension of nearly hard colloidal spheres. *Nature* 320, 340–342. doi: 10.1038/320340a0

Rakonjac, J., Bennett, N. J., Spagnuolo, J., Gagic, D., and Russel, M. (2011). Filamentous bacteriophage: biology, phage display and nanotechnology applications. *Curr. Issues Mol. Biol.* 13, 51–75. doi: 10.1002/9780470015902.a0000777

Rowitch, D. H., Hunter, G. J., and Perham, R. N. (1988). Variable electrostatic interaction between DNA and coat protein in filamentous bacteriophage assembly. *J. Mol. Biol.* 204, 663–674. doi: 10.1016/0022-2836(88)90363-4

Safran, S. A. (1994). *Statistical Thermodynamics of Surfaces, Interfaces, and Membranes. Vol. 90.* Boulder, CO: Perseus Books.

Sattarl, S., Bennett, N. J., Wen, W. X., Guthrie, J. M., Blackwell, L. F., Conway, J. F., et al. (2015). Ff-nano, short functionalized nanorods derived from Ff (f1, fd, or M13) filamentous bacteriophage. *Front. Microbiol.* 6:316. doi: 10.3389/fmicb.2015.00316

Schall, P., Cohen, I., Weitz, D. A., and Spaepen, F. (2004). Visualization of dislocation dynamics in colloidal crystals. *Science* 305, 1944–1948. doi: 10.1126/science.1102186

Sharma, P., Ward, A., Gibaud, T., Hagan, M. F., and Dogic, Z. (2014). Hierarchical organization of chiral rafts in colloidal membranes. *Nature* 513, 77. doi: 10.1038/nature13694

Specthrie, L., Bullitt, E., Horiuchi, K., Model, P., Russel, M., and Makowski, L. (1992). Construction of a microphage variant of filamentous bacteriophage. *J. Mol. Biol.* 228, 720–724. doi: 10.1016/0022-2836(92)90858-H

Stanley, W. M. (1935). Isolation of a crystalline protein possessing the properties of tobacco-mosaic virus. *Science* 81, 644–645. doi: 10.1126/science.81.2113.644

Tang, J. X., and Fraden, S. (1995). Isotropicp-cholesteric phase-transition in colloidal suspensions of filamentous bacteriophage-fd. *Liq. Cryst.* 19, 459–467. doi: 10.1080/02678299508032007

Wen, X., Meyer, R. B., and Caspar, D. L. D. (1989). Observation of smectic-A order in a solution of rigid-rod-like particles. *Phys. Rev. Lett.* 63, 2760–2763. doi: 10.1103/PhysRevLett.63.2760

Whaley, S. R., English, D. S., Hu, E. L., Barbara, P. F., and Belcher, A. M. (2000). Selection of peptides with semiconductor binding specificity for directed nanocrystal assembly. *Nature* 405, 665–668. doi: 10.1038/35015043

Yang, Y. S., Barry, E., Dogic, Z., and Hagan, M. F. (2012). Self-assembly of 2D membranes from mixtures of hard rods and depleting polymers. *Soft Matter* 8, 707–714. doi: 10.1039/C1SM06201H

Zakhary, M. J., Gibaud, T., Kaplan, C. N., Barry, E., Oldenbourg, R., Meyer, R. B., et al. (2014). Imprintable membranes from incomplete chiral coalescence. *Nat. Commun.* 5:3063. doi: 10.1038/ncomms4063

Zhou, H. X., Rivas, G. N., and Minton, A. P. (2008). Macromolecular crowding and confinement: biochemical, biophysical, and potential physiological consequences. *Ann. Rev. Biophys.* 37, 375–397. doi: 10.1146/annurev.biophys.37.032807.125817

**Conflict of Interest Statement:** The author declares that the research was conducted in the absence of any commercial or financial relationships that could be construed as a potential conflict of interest.

# Advantages of publishing in Frontiers

**OPEN ACCESS**
Articles are free to read, for greatest visibility

**COLLABORATIVE PEER-REVIEW**
Designed to be rigorous – yet also collaborative, fair and constructive

**FAST PUBLICATION**
Average 85 days from submission to publication (across all journals)

**COPYRIGHT TO AUTHORS**
No limit to article distribution and re-use

**TRANSPARENT**
Editors and reviewers acknowledged by name on published articles

**SUPPORT**
By our Swiss-based editorial team

**IMPACT METRICS**
Advanced metrics track your article's impact

**GLOBAL SPREAD**
5'100'000+ monthly article views and downloads

**LOOP RESEARCH NETWORK**
Our network increases readership for your article

**Frontiers**
EPFL Innovation Park, Building I • 1015 Lausanne • Switzerland
Tel +41 21 510 17 00 • Fax +41 21 510 17 01 • info@frontiersin.org
**www.frontiersin.org**

**Find us on**